



# Mineralogical and textural analysis of processing products, tailings and residues from Mid-European Kupferschiefer- type black shale ores

---

## Dissertation

zur Erlangung des akademischen Grades  
Doctor rerum naturalium (Dr. rer. nat.)

vorgelegt der

Naturwissenschaftliche Fakultät III – Agrar- und Ernährungswissenschaften,  
Geowissenschaften und Informatik

der

**Martin-Luther-Universität Halle-Wittenberg**

von

Andreas Kamradt  
geb. am 24.01.1974 in Crimmitschau

Gutachter:

Prof. Dr. Gregor Borg  
Prof. Dr. Beate Orberger

Tag der Verteidigung:

Halle/Saale, 18.11.2019

## DECLARATION

---

I declare that this thesis is my own work entirely and has been written without any help from other people. I used only the sources mentioned and included all the citations correctly both in word or content. All direct or indirect sources used are acknowledged as references.

Andreas Kamradt

## ACKNOWLEDGMENTS

---

First at all I want thank my supervisor Prof. Gregor Borg, who has encouraged me by his continuously motivation to finalized this thesis.

Juliane Schaefer is thanked for their persistent patience to answer my many questions regarding comminution and flotation in numerous meetings and telephone calls. She was mainly responsible to provide carefully prepared sample material of comminution and flotation tests.

Sabrina Hedrich and Prof. Axel Schippers from the Geomicrobiology group of the German Federal Institute from Geosciences and Natural Resources are thanked to provided sample material of bioleaching residues and raising my understanding for processes related to bioleaching by numerous, fruitful conversations. Sabine Willscher, who also expend time to enlarge my knowledge in the field of bioleaching by long discussions.

My French colleagues Françoise Bodenan and Anne-Gwenaelle Guezennec from the Water, Environment and Ecotechnologies Division of the Bureau de recherches géologiques et minières (BRGM) are thanked for the close cooperation as well in scientific concerns as in terms of hospitality and very well-organized meetings taken place at different locations within France.

Raymond Michels from the University of Lorraine in Nancy is thanked for unforgettable talks with good wine and underground field trips to the Rudna and Sangerhausen Mines. Deepened conversations about the role of organic matter related to black shale-hosted base metal mineralization widened my understanding in the formation of black shale deposits by his expertly knowledge in organic geochemistry and ore geology.

Sabine Walther is thanked for her continuously support in many kinds and especially in monitoring SEM-EDX-based mineral distribution analyses and revision of EDX-spectra.

My colleagues Tim Rödel, Nico Kropp, Nicolas Meyer and Johannes Mennicke, who helped a lot by managing sample preparation and SEM-imaging.

Finally, special thanks to my family, which has been always a reliable support for me, even in difficult times, and helped me a lot with extensive understanding. In particular Sandra and my parents, Brigitta and Dietrich, made it possible to finalize this work.

### Journal articles

Kamradt, A., Walther, S., Schaefer, J., Hedrich, S. & Schippers, A. (2018): Mineralogical distribution of base metal sulfides in processing products of black shale-hosted Kupferschiefer-type ore. *Minerals Engineering* 119: 23 – 30. [<https://doi.org/10.1016/j.mineng.2017.11.009>]

Kamradt, A., Schaefer, J., Schippers, A. & Hedrich, S. (2017): Comparative Bioleaching and Mineralogical Characterization of Black Shale-Hosted Ores and Corresponding Flotation Concentrates. *Solid State Phenomena* 262: 139-142. [doi:10.4028/www.scientific.net/SSP.262.139]

Kutschke, S., Guezennec, A.G., Hedrich, S., Schippers, A., Borg, G., Kamradt, A., Gouin, J., Giebner, F., Schopf, S., Schlömann, M., Rahfeld, A., Gutzmer, J., d'Hugues, P., Pollmann, K., Dirlich, S., Bodéan, F. (2015): Bioleaching of Kupferschiefer black shale – A review including perspectives of the Ecometals project. *Minerals Engineering*, 75: 116-125. [<http://dx.doi.org/10.1016/j.mineng.2014.09.015>]

Kamradt, A., Borg, G., Schaefer, J., Kruse, S., Fiedler, M., Romm, Ph., Schippers, A., Gorny, R., du Bois, M., Bielgk, Ch., Liebetrau, N., Nell, S., Friedrich, B., Morgenroth, H., Wotruba, H. & Merkel, Ch. (2012): An Integrated Process for Innovative Extraction of Metals from Kupferschiefer Mine Dumps, Germany. *Chemie Ingenieur Technik*, 84: 1694–1703. [<http://dx.doi.org/10.1002/cite.201200070>] [ISSN 0009-286 X]

### Publications (non-peer reviewed)

Borg, G., Scharfe F. and Kamradt, A. (2016): High-velocity comminution of massive sulphide ores by the VeRo Liberator® technology for more energy efficient size reduction and particle liberation. *World of Mining – Surface & Underground*, Vol. 68 (1), p No. 24-31.

Borg, G., Scharfe, F., Lempp, Ch. and Kamradt, A. (2015): Improved particle liberation of graphite and other complex ore minerals by high-velocity comminution – introducing the new VeRo Liberator®. *World of Mining – Surface and Underground*, Vol. 67 (3), 207-212.

Kamradt, A., Borg, G., du Bois, M., Fiedler, M., Friedrich, B., Gorny, R., Kruse, S., Morgenroth, H., Romm, Ph., Schaefer, J. & Wotruba, H. (2013): Innovative Gewinnung von Wertmetallen aus Kupferschiefer-Halden des ehemaligen Mansfelder Bergbaudistriktes, Sachsen-Anhalt. In: Woidasky, J., Ostertag, K. & Stier, Ch. (Hrsg.): *Innovative Technologien für Ressourceneffizienz in rohstoffintensiven Produktionsprozessen*. Fraunhofer Verlag, p. 52-67. [ISBN: 978-3-8396-0596-7]

### Conference proceedings

Kamradt, A. & Schaefer, J. (2017): Compositional analysis of copper flotation concentrates extracted from different Kupferschiefer-type black shale-hosted ores. In: *Proceedings of European Metallurgical Conference EMC 2017*, 25. - 28. June 2017, Leipzig, Germany, Vol.4, 1771-1784. [Refereed Conference Paper], [ISBN 978-3-940276-76-6]

Kamradt, A., Walther, S., Hedrich, S., Schaefer, J. and Schippers, A. (2017): Mineralogical distribution of base metal sulfides in processing products of black shale-hosted Kupferschiefer-type ore. *Process Mineralogy '17 Program*, 20. -22. March 2017, Cape Town, South Africa, pp. 1-13. [Non-Refereed Conference Paper]

## PUBLICATIONS

---

Kamradt, A., Hedrich, S., Schippers, A. and Guezennec, A.-G. (2016): Mineralogical characterization of copper sulfides in bioleaching residues derived from Kupferschiefer-type black shale ore and flotation concentrates. In: Proceedings of the 9th International Copper Conference Copper 2016, 13-16 November 2016, Kobe, Japan, p. 1695-1706. [Refereed Conference Paper]

Borg, G., Scharfe, F., Scharfe, O., Kamradt, A. and Lempp, C. (2016): Significantly improved energy consumption, particle liberation, and size reduction by VeRo Liberator® comminution. Conference Volume, Comminution '16, Cape Town, South Africa. [Non-Refereed Conference Paper]

Kamradt, A. (2015): Comminution as an economic efficient key for the improvement of metal recovery from low-grade Kupferschiefer-type black shale-hosted copper ore from the Mansfeld mining district, Germany. In: André-Mayer, A.S., Cathelineau, M., Muchez, Ph., Pirard, E., Sindern, S. (eds). Mineral resources in a sustainable world. Proceedings of the 13<sup>th</sup> Biennial SGA Meeting, 2015, Nancy, France, Vol. 4, p. 1373-1376. [Refereed Conference Paper]

Borg, G., Scharfe, F., Lempp, Ch. and Kamradt, A. (2015): Stretching the limits of comminution – improved size reduction and particle liberation by the new VeRo Liberator®. Conference Volume, Physical Separation 2015, Falmouth, Cornwall. [Non-Refereed Conference Paper]

Borg, G., Scharfe, O. and Kamradt, A. (2015): Breaking down comminution barriers - new dimensions of particle size reduction and liberation by VeRo Liberator®. ICC2015, St Luis Potosi, Mexico, p. 277-289. [ISBN 9781329013322] [Refereed Conference Paper]

Borg, G., Scharfe F. and Kamradt, A. (2015): Improved Particle Liberation by High-Velocity Comminution – the new VeRo Liberator® ICNOP2015, 27.-29.05.2015, Trzebieszowice, Poland, Conference Proceedings Volume. [Non-Refereed Conference Paper]

### **Conference abstracts (oral presentation)**

Guezennec, A.-G., Hedrich, S., Schippers, A., Kamradt, A., Matys, S., Michels, R., Jouliau, C., Bodéan, F. (2017): Bioleaching in stirred tank reactors to process Kupferschiefer- type ore: current status and perspectives. In: Livre des Résumés, 16<sup>ème</sup> Congrès de la Société Française de Génie des Procédés, 11. – 13. July 2017, Nancy, France, pp. 964 – 965.

Schaefer, J. und Kamradt, A. (2016): Flotation von Kupfererz der Lagerstätte Rudna. Tagungsband „Tagung Aufbereitung und Recycling“ – 9.-10. November 2016 – Freiberg, S. 8.

Borg, G., Kamradt, A., Lempp, Chr. and Scharfe, F. (2015): Improved particle liberation from a new, high-velocity impact crusher - the VeRo Liberator®. In Martens, P.N. (ed.): 5<sup>th</sup> International mining Symposia - Mineral Resources and Mine Development, RWTH Aachen University, Institute of Mining Engineering I, 27 -28 May 2015, Abstract volume, pp. 53-54.

Kamradt, A. and Liebetrau, N. (2012): In-situ weathering of low-grade Kupferschiefer ore dumps, Mansfeld mining district, Germany. In GeoHannover 2012: GeoRohstoffe für das 21. Jahrhundert. Kurzfassungen der Vorträge und Poster. Hrsg.: Kümpel, H.-J., Röhling, H.-G. & Steinbach, V., Schriftenreihe der Deutschen Gesellschaft für Geowissenschaften, 80: 51. [ISBN 978-3-510-49228-2]

## PUBLICATIONS

---

Kamradt, A. and Borg, G. (2010): Combined use of portable on-site exploration tools; application of handheld XRF-analyzer and shortwave infrared spectrometer on Kupferschiefer mine dumps, Mansfield District, Germany. In GeoDarmstadt 2010: geosciences secure the future. Kurzfassungen der Vorträge und Poster. Hrsg.: Hoppe, A., Röhling, H.-G., Schüth, Ch., Schriftenreihe der Deutschen Gesellschaft für Geowissenschaften, 68: 285. [ISBN 978-3-510-49219-0]

Fiedler, M., Kamradt, A. und Borg, G. (2010): Geochemische und mineralogische Charakterisierung von Halden des Kupferschieferbergbaues des Mansfelder Distriktes; erste Ergebnisse. In GeoDarmstadt 2010: Geosciences secure the future. Kurzfassungen der Vorträge und Poster. Hrsg.: Hoppe, A., Röhling, H.-G., Schüth, Ch., Schriftenreihe der Deutschen Gesellschaft für Geowissenschaften, 68: 168-169. [ISBN 978-3-510-49219-0]

### **Conference abstracts (poster presentation)**

Kamradt, A., Schaefer, J., Schippers, A. & Hedrich, S. (2017): Comparative Bioleaching and Mineralogical Characterization of Black Shale-Hosted Ores and Corresponding Flotation Concentrates. 22nd International Biohydrometallurgy Symposium, 24.-27. September 2017, TU Bergakademie Freiberg, Germany.

Kamradt, A., Guezennec, A.-G., Bodéan, F. and Bailly, L. (2017): The use of advanced characterization tools to perform mineralogical mass balances and to assess the efficiency of bioleaching processes for the treatment of complex ores. In: Livre des Résumés, 16ème Congrès de la Société Française de Génie des Procédés, 11. – 13. July 2017, Nancy, France, pp. 976-977.

Schiele, S., Kamradt, A. and Gossel, W. (2016): Characterization of organic compounds in Kupferschiefer-type black shales from the former Mansfeld-Sangerhausen mining district, Central Germany. In Ortner, H. [Ed.] (2016): Abstract Volume of GeoTirol2016 - Annual Meeting of DGGV and PAN-GEO Austria, 25-28. September 2016, Innsbruck, Austria, pp. 301.

Kropp, N. and Kamradt, A. (2016): Ore microscopy and cathodoluminescence studies on sandstone-hosted Kupferschiefer-type ore from the Wolfsberg Mine dump, Richelsdorf Mountains. In Ortner, H. [Ed.] (2016): Abstract Volume of GeoTirol2016 - Annual Meeting of DGGV and PAN-GEO Austria, 25-28. September 2016, Innsbruck, pp. 168.

Kamradt, A., Meyer, N. and Rahfeld, A. (2016): Potential advances in the comminution of Kupferschiefer-type black shale ore by the utilization of alternative impact crushing technology. Aachen International Mining Symposia (AIMS 2016), 1<sup>st</sup> International Conference "Mining in Europe", RWTH Aachen University, Institute of Mining Engineering I, 18-19 May 2016, ABSTRACTVOLUME, p. 89. [ISBN: 978-3-941277-27-4]

Bremerstein I., Schaefer, J. and Kamradt A. (2015): Recent investigations on flotation of black-shale hosted copper ores from Sangerhausen-Mansfeld mining district at UVR-FIA GmbH. Proceedings of the 7<sup>th</sup> International Flotation Conference 2015, Cape Town, South Africa.

Kamradt, A. (2015): Comparative particle analysis of mineral processing products of black shale-hosted Kupferschiefer-type ore. In: Wagner, J. and Elger, K. [Eds.] (2015): GeoBerlin 2015 - Dynamic Earth from Alfred Wegener to today and beyond - Abstracts. Annual Meeting of DGGV and DMG, 4-7 October 2015, Berlin: GFZ German Research Centre for Geosciences. <http://doi.org/10.2312/GFZ.LIS.2015.003>

## PUBLICATIONS

---

Kamradt, A. (2012): Hypogene emplacement and supergene alteration of the dolomite-hosted Chichaklou Zn-Pb deposit, Takab Province, NW Iran. In GeoHannover 2012: GeoRohstoffe für das 21. Jahrhundert. Kurzfassungen der Vorträge und Poster. Hrsg.: Kümpel, H.-J., Röhling, H.-G. & Steinbach, V., Schriftenreihe der Deutschen Gesellschaft für Geowissenschaften, 80: 51. [ISBN 978-3-510-49228-2]

### **other**

Kuhn, K., Kamradt, A. and Büttner, Ph. (2015): Foresight Study - Economic Potential of Mine Wastes in Germany. In: Kiss, J., Horváth, Z., Kuhn, K., Kamradt, A., Büttner, Ph., de Oliveira, D., Quenta, L., Lopes, C., Wilts, H., Espinoza, L.T. and Wittmer, D. Thematic Report IV Secondary Raw Materials Report for WP6 in Minerals4EU project - Minerals Intelligence Network for Europe. [http://minerals4eu.brgm-rec.fr/sites/default/files/Minerals4EU\\_Foresight-Study\\_Thematic-Report-IV\\_Secondary-raw-materials.pdf](http://minerals4eu.brgm-rec.fr/sites/default/files/Minerals4EU_Foresight-Study_Thematic-Report-IV_Secondary-raw-materials.pdf), p. 36-62.

Kamradt, A. (2014): Innovative Ansätze zur Aufbereitung von Mansfelder Kupferschieferhalden. In: Vom Perm bis zum Quartär im südöstlichen Harzvorland - Tagungsband. Hrsg.: Thüringer Geologischen Verein, Jahreshauptversammlung, 13.-15. Juni 2014, Sangerhausen.

Schippers, A., Borg, G., Glombitza, F., Kalin, M., Kamradt, A., Kassahun, A., Sand, W. und Willscher, S. (2013): Bergbauhalden – Sanierung oder Wertstoffdepot?. In: Geobiotechnologie-Stand und Perspektiven, DECHEMA Gesellschaft für Chemische Technik und Biotechnologie e.V., S. 10-14.

## ABSTRACT

---

Black shale-hosted base metal deposits occur globally and represent partially world-class deposits with significant reserves of copper. Kupferschiefer-type deposits of Central Europe contain considerable base metal reserves partly associated with increased contents of precious metals (including Cu, Pb, Zn, Ag, Au, Co, Ni, Mo, V, Pt, and Pd) that potentially represent strategic and critical raw materials for Europe. The ore mineralization is polymetallic and characterized by the presence of base metal sulphides complexly and intimately intergrown. Two major difficulties restrict the exploitation of Kupferschiefer-type ores. Firstly, the low efficiency in the recovery of valuable metals by conventional mineral dressing techniques from comminution to metallurgical processes and secondly, their environmental impact by high energy consumption. Additionally, the increased content of organic carbon associated with black shales represents a main challenge in the processing of the ore and causes markedly declining copper grades in concentrates extracted currently in Polish Kupferschiefer-type mining operations.

This study aims to the detailed mineralogical characterization of processing products and residues from mineral processing methods comprising comminution, sulphide flotation and bioleaching applied to black shale-hosted Kupferschiefer-type ores from different Mid-European deposits. The main objectives of this study are to highlight improvements achieved by alternative and advanced mineral processing methods of black shale ores by impact crushing as well as refined sulphide flotation and bioleaching and to define process efficiency of value minerals and commodities prior to upscaling. In this thesis, a combined approach for the detailed mineralogical characterization of comminution products, flotation concentrates and tailings as well as bioleaching residues comprise granulometry, mineral distribution and liberation analysis as well as microscopy with a special focus to copper sulphides. The advanced characterization revealed textural features and mineralogical relationships, by which decisive information were obtained to assess process-related parameters such as recoverability.

The investigations revealed that black shales originating from three important Mid-European mining locations (Mansfeld, Rudna, Sangerhausen) were different in composition, metal content and ore association. Comminution of these black shale ores yield in varying degree of liberation of copper sulphides depending on the grain size distribution in the comminution products and the style of mineralization in the feed. Considerably increased liberation was partially achieved by the novel VeRo Liberator® impact crushing technology promoted by preferential breakage on grain boundaries of gangue and sulphide minerals. Flotation tests with ball mill products of Sangerhausen and Rudna black shale showed that flotation using dextrin was highly selective in terms of copper sulphide recovery into concentrates. However, flotation with dextrin and ethanol pre-treated feed achieved considerably increased copper recovery (75%) at significantly lower mass recovery (30%) compared to standard sulphide flotation, which is mainly caused by the enhanced entrainment of partly liberated (middlings) and locked copper sulphides into the froth products showing significantly increased copper contents (Rudna feed: 10.0%, Sangerhausen feed: 14.4%). While the usage of dextrin promotes the selectivity to depress pyrite, galena and organic matter into the tailings, ethanol pre-treatment of the feed causes enhanced flotability of copper sulphides by improved wettability of particle surfaces favouring the interaction with flotation agents as well as the attachment of nanobubbles. This is a crucial prerequisite to an enhanced attachment on larger air bubbles that entrain hydrophobic sulphides increasingly. A more advanced copper recovery was mainly permitted by the restricted liberation of copper sulphides in the feed. Bioleaching was applied to different black shales, industrial concentrates from Lubin, Poland, and concentrates gained from the flotation using dextrin and ethanol pre-treated feed. The recovery of Cu was vastly enhanced by bioleaching compared to sterile control leaching, but 80-90%

## ABSTRACT

---

copper recovery indicate incomplete dissolution exclusively attribute to chalcopyrite. Investigations on bioleaching residues revealed that bornite and chalcocite were dissolved completely, mainly during the first 4 days, whereas considerable amounts of chalcopyrite remained in the final residues. The restricted dissolution of chalcopyrite was caused by coatings of secondary formed metal sulphates, mainly anglesite-like Pb sulphate, and thin layers of Cu-sulphate onto chalcopyrite grains.

This study has shown that energy-saving alternative mineral processing methods comprising impact crusher comminution and improved approaches in flotation and bioleaching can substantially contribute to the economically and environmentally improved recovery of copper and byproducts and their implementation can raise the potential for the processing of complex organic-rich ores.

## LIST OF ABBREVIATIONS

---

### General

µm	micrometres
ALS	ALS Geochemistry, Loughrea, Ireland
BRGM	Bureau de Recherches Géologiques et Minières
BSE	Back-Scattered Electron
EDS	Energy-Dispersive Spectrometry
HIF	Helmholtz Institute Freiberg for Resource Technology
KGHM	Kombinat Górniczo-Hutniczy Miedzi Polska Miedź S.A.
MLA	Mineral Liberation Analysis
MLU	Martin Luther University, Economic Geology and Petrology Research Unit
PGE	Platinum Group Elements
PSD	Particle Size Distribution
SE	Secondary Electron
SEM	Scanning Electron Microscope
TUBAF	Technical University (BergAkademie) Freiberg
UVR-FIA	Umweltschutztechnik Verfahrensentwicklung Recycling – Forschungsinstitut für Aufbereitung GmbH

### Minerals

Bn	bornite
BrT	barite
Cal	calcite
Cct	chalcocite
Ccp	chalcopyrite
Cv	covellite
Dol	dolomite
Gn	galena
Py	pyrite
fPy	framboidal pyrite
Ida	idaite
Sp	sphalerite

# TABLE OF CONTENTS

---

<b>DECLARATION</b> .....	<b>I</b>
<b>ACKNOWLEDGMENTS</b> .....	<b>II</b>
<b>PUBLICATIONS</b> .....	<b>III</b>
<b>ABSTRACT</b> .....	<b>VII</b>
<b>LIST OF ABBREVIATIONS</b> .....	<b>IX</b>
<b>TABLE OF CONTENTS</b> .....	<b>X</b>
<b>LIST OF FIGURES</b> .....	<b>XIV</b>
<b>LIST OF TABLES</b> .....	<b>XXIII</b>
<b>CHAPTER 1 INTRODUCTION</b> .....	<b>1</b>
<b>1.1 SCOPE OF THIS STUDY</b> .....	<b>1</b>
<b>1.2 SIGNIFICANCE OF BLACK SHALE-HOSTED KUPFERSCHIEFER-TYPE DEPOSITS</b> .....	<b>2</b>
1.2.1 GLOBAL DISTRIBUTION .....	2
1.2.2 OCCURRENCE OF BASE AND CRITICAL METALS IN BLACK SHALE-HOSTED KUPFERSCHIEFER-TYPE MINERALIZATION .....	3
1.2.3 MINING OF KUPFERSCHIEFER-TYPE DEPOSITS.....	4
<b>1.3 MINERAL PROCESSING METHODS – PAST AND PRESENT</b> .....	<b>6</b>
1.3.1 COMMINUTION .....	7
1.3.2 FLOTATION .....	8
1.3.3 BIOLEACHING.....	10
<b>1.4 GENERAL ASPECTS OF BLACK SHALE-HOSTED KUPFERSCHIEFER-TYPE MINERALIZATION</b> .....	<b>12</b>
1.4.1 STYLES AND TEXTURES OF SULPHIDES IN BLACK SHALES OF THE KUPFERSCHIEFER-TYPE MINERALIZATION .....	14
<b>CHAPTER 2 METHODS</b> .....	<b>18</b>
<b>2.1 FEED SAMPLES</b> .....	<b>18</b>
<b>2.2 TEST WORK</b> .....	<b>19</b>
2.2.1 COMMINUTION .....	19
2.2.1.1 BALL MILLING.....	19
2.2.1.2 VeRO LIBERATOR® IMPACT CRUSHER.....	21
2.2.2 FLOTATION TESTS.....	22
2.2.3 BIOLEACHING TESTS .....	23
<b>2.3 GRANULOMETRY</b> .....	<b>24</b>
2.3.1 SIEVING ANALYSES .....	24
2.3.2 LASER GRANULOMETRY .....	24
<b>2.4 GEOCHEMICAL ANALYSIS</b> .....	<b>24</b>
<b>2.5 MICROSCOPY</b> .....	<b>25</b>
2.5.1 SAMPLE PREPARATION .....	25
2.5.2 EQUIPMENT.....	25
<b>2.6 AUTOMATED MINERALOGY</b> .....	<b>26</b>
2.6.1 MINERAL DISTRIBUTION ANALYSIS USING BRUKER ESPRIT 2.1 FEATURE .....	26
2.6.2 MINERAL LIBERATION ANALYSIS (MLA).....	26
2.6.2.1 MINERAL LIBERATION ANALYSER FEI MLA 650F .....	26

# TABLE OF CONTENTS

---

2.6.2.2 ZEISS MINERALOGIC MINING- SYSTEM .....	27
2.6.3 GENERAL CONSIDERATIONS ON THE AUTOMATED MINERAL ANALYSIS OF PROCESSED KUPFERSCHIEFER-TYPE BLACK SHALE ORE .....	27
<b>CHAPTER 3 RESULTS .....</b>	<b>29</b>
<b>3.1 MINERALOGICAL AND GEOCHEMICAL CHARACTERIZATION OF BLACK SHALE COMMINUTION PRODUCTS .....</b>	<b>29</b>
3.1.1 PARTICLE SIZE DISTRIBUTION OF COMMINUTED BLACK SHALE ORES .....	29
3.1.1.1 BALL MILL PRODUCTS OF DIFFERENT BLACK SHALE ORES .....	29
3.1.1.2 PARTICLE SIZE DISTRIBUTION OF COMMINUTED BLACK SHALE ORES USING AN INNOVATIVE IMPACT CRUSHING TECHNOLOGY (VeRO LIBERATOR®).....	30
3.1.1.2.1 COMPARISON WITH CONVENTIONAL CRUSHER UNITS .....	30
3.1.1.2.2 GRANULOMETRIC DISTRIBUTION OF VeRO LIBERATOR® IMPACT CRUSHER PRODUCTS.....	31
3.1.1.2.3 COMPARISON OF PARTICLE SIZE DISTRIBUTION OF IMPACT CRUSHER PRODUCTS WITH BALL MILL PRODUCT IN THE - 100 µM GRAIN SIZE RANGE.....	33
3.1.2 MINERALOGICAL AND GEOCHEMICAL CHARACTERIZATION OF COMMINUTED BLACK SHALE ORES.....	36
3.1.2.1 MINERAL DISTRIBUTION ANALYSIS .....	38
3.1.2.2 GEOCHEMICAL DISTRIBUTION OF METALS IN BLACK SHALE COMMINUTION PRODUCTS .....	41
3.1.3 LIBERATION ANALYSIS OF BLACK SHALE COMMINUTION PRODUCTS .....	42
3.1.3.1 GRAIN SIZE DISTRIBUTION OF COPPER SULPHIDES IN BLACK SHALE BALL MILL PRODUCTS .....	42
3.1.3.2 LIBERATION OF COPPER SULPHIDES IN BLACK SHALE BALL MILL PRODUCTS.....	44
3.1.3.2.1 COPPER SULPHIDE LIBERATION BY PARTICLE SIZE CLASSES .....	47
3.1.3.3 MINERAL LOCKING IN BALL MILL PRODUCTS OF DIFFERENT BLACK SHALE ORES .....	51
3.1.3.3.1 MINERAL DISTRIBUTION OF LOCKING ASSOCIATIONS FOR COPPER SULPHIDES IN BLACK SHALE BALL MILL PRODUCTS.....	54
3.1.3.4 GRAIN SIZE DISTRIBUTION OF COPPER SULPHIDES IN VeRO LIBERATOR® IMPACT CRUSHER PRODUCTS .....	60
3.1.3.5 LIBERATION OF COPPER SULPHIDES IN VeRO LIBERATOR® IMPACT CRUSHER PRODUCTS .....	62
3.1.3.5.1 COPPER SULPHIDE LIBERATION IN VeRO LIBERATOR® PRODUCTS BY PARTICLE SIZE CLASSES .....	66
3.1.3.6 MINERAL LOCKING OF COPPER SULPHIDES IN VeRO LIBERATOR® PRODUCTS OF DIFFERENT BLACK SHALE ORES.....	70
3.1.3.7 MINERAL DISTRIBUTION OF LOCKING ASSOCIATIONS FOR COPPER SULPHIDES IN VeRO LIBERATOR® IMPACT CRUSHER PRODUCTS .....	74
3.1.3.7.1 MANSFELD BLACK SHALE ORE.....	74
3.1.3.7.2 RUDNA BLACK SHALE ORE.....	76
3.1.4 SUMMARY.....	81
<b>3.2 MINERALOGICAL AND GEOCHEMICAL ANALYSIS OF FLOTATION PRODUCTS AND TAILINGS GENERATED FROM BLACK SHALE ORES .....</b>	<b>85</b>
3.2.1 MASS AND COPPER RECOVERY BALANCE .....	85
3.2.2 PARTICLE SIZE DISTRIBUTION .....	86
3.2.3 SULPHIDES IN CONCENTRATES AND TAILINGS FROM BLACK SHALE FEED .....	89
3.2.4 CONCENTRATES AND TAILINGS FROM FLOTATION TESTS WITH RUDNA MINE BLACK SHALE .....	91
3.2.4.1 MINERAL DISTRIBUTION OF FLOTATION PRODUCTS FROM RUDNA BLACK SHALE FEED.....	91
3.2.4.2 MINERAL DISTRIBUTION OF TAILINGS FROM FLOTATION TESTS ON RUDNA BLACK SHALE FEED .....	94
3.2.4.3 CONTENT OF BASE AND TRACE METALS IN CONCENTRATES AND TAILINGS FROM THE FLOTATION OF RUDNA BLACK SHALE .....	96
3.2.5 CONCENTRATES AND TAILINGS FROM FLOTATION TESTS WITH SANGERHAUSEN BLACK SHALE .....	98
3.2.5.1 MINERAL DISTRIBUTION OF FLOTATION PRODUCTS FROM SANGERHAUSEN BLACK SHALE FEED .....	98
3.2.5.2 MINERAL DISTRIBUTION OF TAILINGS FROM FLOTATION TESTS ON SANGERHAUSEN BLACK SHALE FEED .....	100
3.2.5.3 CONTENT OF BASE AND TRACE METALS IN CONCENTRATES AND TAILINGS FROM THE FLOTATION OF SANGERHAUSEN BLACK SHALE .....	103

# TABLE OF CONTENTS

---

3.2.6 LIBERATION ANALYSIS OF COPPER SULPHIDES IN FLOTATION CONCENTRATES AND TAILINGS .....	104
3.2.6.1 LIBERATION OF COPPER SULPHIDES IN FLOTATION CONCENTRATES AND TAILINGS .....	104
3.2.6.2 GRAIN SIZE DISTRIBUTION OF COPPER SULPHIDES IN CONCENTRATES FROM RUDNA AND SANGERHAUSEN BLACK SHALE FEED.....	106
3.2.6.3 LIBERATION AND LOCKING ASSOCIATION OF COPPER SULPHIDES IN SELECTED FLOTATION CONCENTRATES FROM RUDNA AND SANGERHAUSEN BLACK SHALE FEED.....	108
3.2.6.3.1 CHALCOCITE IN FLOTATION CONCENTRATES FROM RUDNA BLACK SHALE ORE .....	108
3.2.6.3.2 BORNITE IN FLOTATION CONCENTRATES FROM RUDNA BLACK SHALE ORE .....	111
3.2.6.3.3 BORNITE IN FLOTATION CONCENTRATES FROM SANGERHAUSEN BLACK SHALE ORE .....	114
3.2.6.3.4 CHALCOPYRITE IN FLOTATION CONCENTRATES FROM SANGERHAUSEN BLACK SHALE ORE .....	117
3.2.7 COPPER DEPARTMENT IN CONCENTRATES AND TAILINGS FROM BLACK SHALE FEED .....	120
3.2.8 MINERALOGY AND METAL CONTENT OF COPPER CONCENTRATES FROM LUBIN, POLAND.....	122
3.2.8.1 MINERAL DISTRIBUTION OF LUBIN CONCENTRATES .....	122
3.2.8.2 METAL CONTENT IN LUBIN COPPER CONCENTRATES .....	125
3.2.9 SUMMARY.....	126
<b>3.3 MINERALOGY AND GEOCHEMISTRY OF BIOLEACHING RESIDUES .....</b>	<b>129</b>
3.3.1 INTRODUCTION .....	129
3.3.2 GENERAL MINERALOGICAL COMPOSITION OF BIOLEACHING RESIDUES FROM BLACK SHALE ORES AND RELATED FLOTATION CONCENTRATES .....	129
3.3.3 PARTICLE PROPERTIES IN (BIO)-LEACHING RESIDUES .....	131
3.3.4 RESULTS .....	136
3.3.4.1 BIOLEACHING RESIDUES DERIVED FROM BLACK SHALE ORES .....	136
3.3.4.1.1 BIOLEACHING RESIDUES OF BLACK SHALE- AS WELL AS LIMESTONE-HOSTED LOW-GRADE ORE, MANSFELD DISTRICT, CENTRAL GERMANY .....	136
3.3.4.1.1.1 METAL CONTENT AND RECOVERY .....	136
3.3.4.1.2 BIOLEACHING RESIDUES OF SANGERHAUSEN BLACK SHALE-HOSTED ORE.....	137
3.3.4.1.2.1 MINERAL DISTRIBUTION .....	137
3.3.4.1.2.2 METAL CONTENT AND RECOVERY .....	139
3.3.4.2 BIOLEACHING RESIDUES FROM COPPER FLOTATION CONCENTRATES.....	141
3.3.4.2.1 BIOLEACHING RESIDUES OF FLOTATION CONCENTRATE EXTRACTED FROM SANGERHAUSEN BLACK SHALE ORE .....	141
3.3.4.2.1.1 MINERAL DISTRIBUTION .....	141
3.3.4.2.1.2 METAL CONTENT, METAL AND MINERAL RECOVERY .....	143
3.3.4.2.2 BIOLEACHING RESIDUES OF THE FLOTATION CONCENTRATE FROM RUDNA BLACK SHALE ORE .....	145
3.3.4.2.2.1 MINERAL DISTRIBUTION .....	145
3.3.4.2.2.2 GEOCHEMICAL COMPOSITION, MINERAL AND METAL RECOVERY .....	147
3.3.4.2.3 BIOLEACHING RESIDUES OF LUBIN CONCENTRATE LC15A .....	148
3.3.4.2.3.1 MINERAL DISTRIBUTION .....	148
3.3.4.2.3.2 METAL CONTENT, METAL AND MINERAL RECOVERY .....	150
3.3.4.2.4 BIOLEACHING RESIDUES OF FLOTATION CONCENTRATE LCA06, LUBIN, POLAND.....	152
3.3.4.2.4.1 MINERAL DISTRIBUTION .....	152
3.3.4.2.4.2 GEOCHEMICAL COMPOSITION, MINERAL/ELEMENTAL RECOVERY.....	154
3.3.4.2.5 ANALYSIS OF RESIDUES FROM BIOLEACHING TESTS WITH INCREASING RETENTION TIMES ON FLOTATION CONCENTRATE LC15B .....	155
3.3.4.2.5.1 MINERAL DISTRIBUTION .....	155
3.3.4.2.5.2 GEOCHEMICAL COMPOSITION, METAL AND SULPHIDE RECOVERY.....	156
3.3.5 SUMMARY.....	159
<b>CHAPTER 4 DISCUSSION .....</b>	<b>161</b>
<b>4.1 COMMINATION .....</b>	<b>161</b>

# TABLE OF CONTENTS

---

4.1.1 BALL MILLING.....	161
4.1.1.1 MINERAL SPECIFIC PARAMETERS AFFECTING THE GRAIN SIZE DISTRIBUTION AND ENERGY CONSUMPTION OF BALL MILL PRODUCTS FROM BLACK SHALE ORES.....	161
4.1.1.2 TEXTURAL PROPERTIES AND MINERALOGICAL ASSOCIATIONS OF COPPER SULPHIDES IN BALL MILL PRODUCTS OF BLACK SHALE ORES .....	167
4.1.1.2.1 LIBERATION OF COPPER SULPHIDES.....	167
4.1.1.2.2 RELATIONSHIP OF LOCKING MODE AND THE DEGREE OF LIBERATION .....	169
4.1.1.3 INFLUENCE OF THE MINERALIZATION STYLE TO GRAIN SIZE AND LIBERATION OF SULPHIDES IN BALL MILL PRODUCTS OF BLACK SHALE ORES .....	172
4.1.2 BLACK SHALE COMMINUTION USING THE VeRO LIBERATOR® IMPACT CRUSHER .....	175
4.1.2.1 COMPARISON OF TEXTURAL PROPERTIES OF COPPER SULPHIDES IN VeRO LIBERATOR® IMPACT CRUSHER PRODUCTS.....	177
4.1.2.1.1 GRAIN SIZE OF COPPER SULPHIDES.....	177
4.1.2.1.2 LIBERATION OF COPPER SULPHIDES.....	177
4.1.2.1.3 LOCKING MODES OF COPPER SULPHIDES .....	179
<b>4.2 FLOTATION .....</b>	<b>187</b>
4.2.1 RECOVERY OF COPPER SULPHIDES BY FLOTATION OF RUDNA AND SANGERHAUSEN BLACK SHALE ORE .....	187
4.2.1.1 TEXTURAL PROPERTIES OF COPPER SULPHIDES AFFECTING RECOVERABILITY .....	189
4.2.1.2 INFLUENCE OF DEXTRIN AND ETHANOL PRE-TREATMENT REGARDING THE FLOTABILITY AND RECOVERY OF SULPHIDES .....	193
4.2.2 CONTENT OF COPPER AND ASSOCIATED METALS IN CONCENTRATES FROM KUPFERSCHIEFER-TYPE ORE .....	195
<b>4.3 BIOLEACHING .....</b>	<b>199</b>
4.3.1 LEACHING PERFORMANCE OF COPPER SULPHIDES AND COPPER RECOVERY BY BIOLEACHING OF DIFFERENT BLACK SHALE RELATED FEED .....	199
4.3.2 RECOVERABILITY OF TRACE METALS CONCERNING DISSOLUTION OF SULPHIDES IN BIOLEACHING PROCESSES .....	202
4.3.3 MINERALOGICAL FACTORS CONTROLLING THE RESTRICTED DISSOLUTION OF CHALCOPYRITE.....	204
<b>CHAPTER 5 SYNOPSIS .....</b>	<b>211</b>
<b>REFERENCES .....</b>	<b>216</b>
<b>APPENDIX A - COMMINUTION .....</b>	<b>226</b>
<b>APPENDIX B - FLOTATION.....</b>	<b>230</b>
<b>APPENDIX C - BIOLEACHING .....</b>	<b>243</b>
<b>APPENDIX D – DIGITAL .....</b>	<b>253</b>

## LIST OF FIGURES

---

<b>FIGURE 1.2.1:</b> GLOBAL DISTRIBUTION OF SEDIMENT-HOSTED COPPER DEPOSITS (SHCD) SUBDIVIDED IN BLACK SHALE, METAMORPHIC BLACK SHALE, SANDSTONE/CARBONATE AND METAMORPHIC SHCD. IMPORTANT BLACK SHALE-HOSTED DEPOSITS OR MINING DISTRICTS ARE INDICATED BY THEIR NAMES (COX ET AL., 2003; MUDD ET AL., 2013). .....	3
<b>FIGURE 1.2.2:</b> ACTIVE AND CEASED BLACK SHALE-HOSTED KUPFERSCHIEFER-TYPE DEPOSITS AND EXPLORATION TARGETS IN CENTRAL EUROPE LOCATED AT THE SOUTHERN MARGIN OF THE ZECHSTEIN BASIN. MINING LOCATIONS FROM WHICH SAMPLE MATERIAL WAS OBTAINED FOR THIS STUDY ARE INDICATED IN RED (AFTER BORG ET AL., 2012). .....	5
<b>FIGURE 1.3.1:</b> SIMPLIFIED FLOW SHEET OF FLOTATION CIRCUITS OPERATED IN THE LUBIN CONCENTRATOR, POLAND (LUSZCZKIEWICZ AND CHMIELEWSKI, 2008). .....	9
<b>FIGURE 1.3.2:</b> PROCESS FLOW FOR BIOLEACHING OF LUBIN CONCENTRATE DEVELOPED WITHIN THE “BIOSHALE” PROJECT (D’HUGUES ET AL., 2007). .....	11
<b>FIGURE 1.4.1:</b> STRATIGRAPHIC COLUMN AND MEMBERS OF THE LOWER PERMIAN THAT FORM THE HOST ROCKS OF KUPFERSCHIEFER-TYPE MINERALIZATION INDICATED BY RED DASHED LINES ON THE ADJOINING PHOTOGRAPH FROM A STOPE OF THE RUDNA UNDERGROUND MINE IN THE POLISH LUBIN-SIEROSZOWICE MINING DISTRICT. ....	12
<b>FIGURE 1.4.2:</b> REFLECTED-LIGHT-IMAGE OF A POLISHED SECTION SHOWS THE VARIABLE DISTRIBUTION OF SULPHIDE ORE MINERALS WITHIN THE BLACK SHALE. SULPHIDES RANDOMLY DISTRIBUTED CHARACTERIZE THE DISSEMINATED FRACTION, OTHERWISE THEY FORM BEDDING-PARALLEL FILLINGS CLEARLY DELIMITED BY ORGANIC MATTER-CLAY BANDS.....	13
<b>FIGURE 1.4.3:</b> TYPICAL ORE TEXTURES IN KUPFERSCHIEFER-TYPE BLACK SHALES. THE SULPHIDE PARTICLES OCCUR FINELY DISPERSED WITHIN THE FINELY LAMINATED ROCK MATRIX OR FORM INTRICATELY INTERGROWTHS OF SEVERAL SULPHIDES OR GANGUE. (BN= BORNITE (BRIGHTER), CCP= CHALCOPYRITE (MORE GREYISH); POLISHED SECTION, BSE-SEM-IMAGE) .....	15
<b>FIGURE 1.4.4:</b> DISSEMINATED COPPER ORE PARTICLES IN THE BLACK SHALE CHARACTERIZED BY A PATCHY COPPER SULPHIDE-SILVER-ASSEMBLAGE CONSISTING OF BORNITE (BN), CHALCOPYRITE (CCP) AND CHALCOCITE (CC) AS WELL AS SILVER (AG). (MANSFELD DISTRICT, REFLECTED LIGHT).....	16
<b>FIGURE 1.4.5:</b> LENSOID REPLACEMENT CONSISTING OF CHALCOCITE INTERGROWN WITH SUBEHDRAL CALCITE CRYSTALS SURROUNDED BY MOSTLY IRREGULAR SHAPED CHALCOCITE PARTICLES EMBEDDED WITHIN THE BLACK SHALE BEDDING. (MANSFELD DISTRICT, REFLECTED LIGHT).....	16
<b>FIGURE 1.4.6:</b> LENTICULAR, BAND-LIKE ALIGNMENTS OF BORNITE (BN) AND CHALCOPYRITE (CCP) AGGREGATES ORIENTED WITHIN THE STRATIFICATION OF THE BLACK SHALE. (SANGERHAUSEN DISTRICT, REFLECTED LIGHT) .....	16
<b>FIGURE 1.4.7:</b> ELONGATED AGGREGATES OF CHALCOPYRITE (CCP) ORIENTED WITHIN THE STRATIFICATION OF THE BLACK SHALE SURROUNDED BY THIN BANDS AND STREAKS OF BORNITE. (SANGERHAUSEN DISTRICT, REFLECTED LIGHT).....	16
<b>FIGURE 1.4.8:</b> CROSS-CUTTING VEIN CONSISTS OF INTERGROWTHS OF BORNITE, CHALCOCITE AND CALCITE SHOWING SUBHEDRAL TO ANHEDRAL CRYSTALS. (SANGERHAUSEN DISTRICT, REFLECTED LIGHT) .....	17
<b>FIGURE 1.4.9:</b> MASSIVE CROSS-CUTTING VEIN FILLED WITH CHALCOPYRITE PARTLY INTERGROWN AND LINED BY CHALCOCITE AND CARBONATE MINERALS. IRREGULAR DISTRIBUTED SMALL YELLOW DOTS INDICATE $\mu\text{M}$ -SCALED SULPHIDE FRAMBOIDS (SANGERHAUSEN DISTRICT, REFLECTED LIGHT).....	17
<b>FIGURE 1.4.10:</b> MICROPHOTOGRAPH SHOWING REPLACEMENT OF CALCAREOUS FOSSIL SHELLS AS WELL AS IRREGULAR ELONGATED FILLINGS BY CHALCOCITE. SLIGHTLY UNDULATING CALCITE BANDS OCCUR COMMONLY WITHIN THE STRATIFICATION OF THE BLACK SHALE. (MANSFELD DISTRICT, REFLECTED LIGHT).....	17
<b>FIGURE 1.4.11:</b> IRREGULAR INTERGROWTH OF CHALCOPYRITE AND CHALCOCITE REPLACING A FOSSIL REMNANT. (RUDNA MINE, REFLECTED LIGHT).....	17
<b>FIGURE 2.2.1:</b> FLOW CHART ILLUSTRATING THE COMMINUTION LINE PRODUCING A FINAL BALL MILL PRODUCT FROM MANSFELD AND RUDNA BLACK SHALE BULK SAMPLES. WEIGHT DATA REFERS TO SAMPLE SIZE. ....	20
<b>FIGURE 2.2.2:</b> FLOW CHART OF THE COMMINUTION OF SANGERHAUSEN BLACK SHALE ORE TO A FINAL BALL MILL PRODUCT < 100 $\mu\text{M}$ . .....	21
<b>FIGURE 2.2.3:</b> PHOTOGRAPH SHOWING THE VeRo LIBERATOR <sup>®</sup> IN DEVELOPMENT STAGE VR-03-I, FRONT LEFT, WITH OPTIONAL SORTING SYSTEM (MIDDLE) AND ULTRA-CLEAN FILTER SYSTEM (BACK RIGHT). (FROM BORG ET AL., 2015) .....	21
<b>FIGURE 2.2.4:</b> GRADE-RECOVERY DIAGRAM FOR FLOTATION TESTS CARRIED OUT ON MILLED BLACK SHALE ORE WITH OR WITHOUT ADDITION OF DEXTRIN AS WELL AS PRE-TREATMENT (PT) WITH ETHANOL (ETOH). .....	22
<b>FIGURE 2.2.5:</b> SCHEMATIC EXPERIMENTAL SET-UP OF BIOLEACHING APPROACHES CARRIED OUT WITH LUBIN CONCENTRATE LC15B, WHICH WAS SUBJECTED TO DIFFERENT LEACHING RETENTION TIMES. ....	23
<b>FIGURE 3.1.1:</b> LASER-GRANULOMETRIC PARTICLE SIZE DISTRIBUTION SHOWING BALL MILL PRODUCTS OF THREE DIFFERENT BLACK SHALE ORES. (DATA. UVR-FIA) .....	29

## LIST OF FIGURES

---

<b>FIGURE 3.1.2:</b> GRAIN-SIZE DISTRIBUTION OF EXEMPLARILY COMMINUTION TESTS OF BLACK SHALE ORE FROM SANGERHAUSEN DISTRICT CARRIED OUT WITH DIFFERENT CRUSHING UNITS. DATA REPRESENTING SIEVE ANALYSES ACCORDING TO DIN ISO 3310, DIN 4188 AND DIN 4187 (GERMAN INSTITUTE FOR STANDARDIZATION). (DATA: UVR-FIA) .....	31
<b>FIGURE 3.1.3:</b> PARTICLE SIZE CURVES REPRESENT SIEVE ANALYSES OF RUN OF-MINE, LOW GRADE ORE CONSISTING OF BLACK SHALE AS WELL AS HANGING WALL LIMESTONE FROM MANSFELD COMMINUTED BY THE VeRo LIBERATOR® IMPACT CRUSHER. DATA REPRESENTING SIEVE ANALYSES ACCORDING TO DIN ISO 3310, DIN 4188 AND DIN 4187 (GERMAN INSTITUTE FOR STANDARDISATION). (DATA: UVR-FIA) .....	32
<b>FIGURE 3.1.4:</b> SIEVE CURVES FOR VeRo LIBERATOR® IMPACT CRUSHER PRODUCTS DISPLAYING SLIGHT DIFFERENCES BETWEEN THE DEPLOYMENT OF ANGULAR AND ROUND (R) HAMMER TOOLS. (DATA: UVR-FIA, ACCORDING TO DIN 66165 (GERMAN INSTITUTE FOR STANDARDIZATION). .....	33
<b>FIGURE 3.1.5:</b> LASER GRANULOMETRIC DATA FOR BALL MILL PRODUCTS AND CORRESPONDING FRACTION OF VeRo LIBERATOR® IMPACT CRUSHER PRODUCTS FROM MANSFELD AS WELL AS RUDNA BLACK SHALE ORE. (RUDNA IMPACT CRUSHER PRODUCT 62.5% < 100 µm, MANSFELD 63.7% < 90 µm; DATA: UVR-FIA).....	34
<b>FIGURE 3.1.6:</b> SEM-IMAGE DISPLAYS PARTICLES IN A BALL MILL PRODUCT THAT EXHIBITING VARIOUS GRAIN SHAPES AND INTERGROWTH TEXTURES. (MANSFELD BALL MILL PRODUCT, SEM-BSE).....	36
<b>FIGURE 3.1.7:</b> MICROGRAPH OF PREDOMINANTLY IRREGULAR SHAPED PARTICLES CONTAINING INTERGROWTHS OF GANGUE AND ORE MINERALS AT DIFFERENT LEVELS OF LIBERATION. (MANSFELD BALL MILL PRODUCT, SEM-BSE).....	36
<b>FIGURE 3.1.8:</b> MORE COARSE-GRAINED SULPHIDES PARTLY LIBERATED AS WELL AS INTERGROWN WITH GANGUE MINERALS ACCOMPANIED BY BARITE. (SANGERHAUSEN BALL MILL PRODUCT, SEM-BSE).....	36
<b>FIGURE 3.1.9:</b> PARTICLES SHOWING INTIMATELY INTERGROWTHS OF GANGUE MINERALS (CAL=CALCITE, ILT=ILLITE, QZ=QUARTZ) WITH BORNITE (BN) AND GALENA (GN). BARITE (BRT) AND FRAMBOIDAL PYRITE ARE COMMON. (SANGERHAUSEN BALL MILL PRODUCT, SEM-BSE).....	36
<b>FIGURE 3.1.10:</b> GENERAL VIEW ON A VeRo LIBERATOR® IMPACT CRUSHER PRODUCT DISPLAYS THE VAST HETEROGENEITY OF THE PARTICLE SIZE AND VARIABILITY OF PARTICLE SHAPES. (MANSFELD BLACK SHALE, SEM-BSE).....	37
<b>FIGURE 3.1.11:</b> VeRo LIBERATOR® IMPACT CRUSHER PRODUCTS HOSTED BOTH, COMPLETE LIBERATED (BN=BORNITE, GN=GALENA, SP=SPHALERITE) UP TO COMPLETE LOCKED (CCT=CHALCOCITE, PY=PYRITE) SULPHIDE GRAINS (MANSFELD BLACK SHALE, SEM-BSE).....	37
<b>FIGURE 3.1.12:</b> IMAGE DEPICTING A LARGER PARTICLE IN A VeRo LIBERATOR® PRODUCT THAT CONTAINS PREDOMINANTLY INTERGROWTHS OF GANGUE MINERALS (AP=APATITE, FSP=FELDSPAR, ILT=ILLITE, QZ=QUARTZ) AND BORNITE (BN) GRAINS AT THE PARTICLE MARGINS PARTLY ENCLOSED BY SILVER. (MANSFELD BLACK SHALE, SEM-BSE) .....	37
<b>FIGURE 3.1.13:</b> VeRo LIBERATOR® PRODUCT SHOWING MAINLY COMPLETE LIBERATED GRAINS OF BORNITE (BN) AS WELL AS PARTICLES CONSISTING OF INTERGROWTHS OF GANGUE MINERALS (QZ=QUARTZ, DOL=DOLOMITE, ILT=ILLITE) PARTLY WITH BORNITE AND GALENA (GN). (MANSFELD BLACK SHALE, SEM-BSE) .....	37
<b>FIGURE 3.1.14:</b> MINERAL DISTRIBUTION DIAGRAM PRESENTING THE MAIN MINERAL PHASES AND MINERAL CLASSES OF DIFFERENT BLACK SHALE COMMINUTION PRODUCTS AS WELL AS THEIR CONTENT OF BASE METAL SULPHIDES. BESIDES DIFFERENCES EXISTING IN THE PROPORTION OF CARBONATES, ILLITE AND QUARTZ, THE DISTRIBUTION OF BASE METAL SULPHIDES AMONGST THE COMMINUTED BLACK SHALES WAS PARTLY VARYING. (DATA: MLU) .....	39
<b>FIGURE 3.1.15:</b> CUMULATIVE GRAIN SIZE DISTRIBUTION OF COPPER SULPHIDES IN BALL MILL PRODUCTS OF DIFFERENT BLACK SHALE ORES. (DATA: MLA-HIF) .....	43
<b>FIGURE 3.1.16:</b> DISTRIBUTION CURVES OF BORNITE ACCORDING TO FREE SURFACE LIBERATION FOR BALL MILL PRODUCTS FROM THREE DIFFERENT BLACK SHALE ORES. NOTE THAT BORNITE IN THE MANSFELD BALL MILL PRODUCT WAS SIGNIFICANTLY BETTER LIBERATED THAN IN THE RUDNA BALL MILL PRODUCT. (DATA: MLA-HIF).....	45
<b>FIGURE 3.1.17:</b> CUMULATIVE DISTRIBUTION OF CHALCOCITE PARTICLES IN RELATION TO THE PERCENTAGE OF LIBERATION FOR BALL MILL PRODUCTS FROM DIFFERENT BLACK SHALE ORES. (DATA: MLA-HIF) .....	46
<b>FIGURE 3.1.18:</b> CHALCOPYRITE LIBERATION CURVES FOR BLACK SHALE ORES FROM DIFFERENT DEPOSITS. (DATA: MLA-HIF) .....	47
<b>FIGURE 3.1.19:</b> DISTRIBUTION OF LIBERATION CLASSES FOR BORNITE IN BALL MILL PRODUCTS FROM DIFFERENT BLACK SHALE DEPOSITS ACCORDING TO PARTICLE SIZE CLASSES IN THE RANGE -100 MICRON. (DATA: MLA-HIF).....	48
<b>FIGURE 3.1.20:</b> STACKED COLUMN PLOTS FOR THE DISTRIBUTION OF CHALCOCITE LIBERATION CLASSES ACCORDING TO PARTICLE SIZE CLASSES IN THE BALL MILL PRODUCTS OF DIFFERENT BLACK SHALE ORES. (DATA: MLA-HIF).....	50
<b>FIGURE 3.1.21:</b> LIBERATION CLASSES OF CHALCOPYRITE BASED ON FREE SURFACE AREA AND THEIR PERCENTUAL OCCURRENCE IN PARTICLE SIZE CLASSES IN BALL MILL PRODUCTS OF DIFFERENT BLACK SHALE ORES. (DATA: MLA-HIF).....	51

## LIST OF FIGURES

---

<b>FIGURE 3.1.22:</b> STACKED COLUMN PLOTS SHOWING CUMULATIVE DISTRIBUTION DATA OF LOCKING MODES BASED ON WEIGHT % FOR BORNITE, CHALCOCITE AND CHALCOPYRITE IN BALL MILL PRODUCTS OF DIFFERENT BLACK SHALE ORES. (DATA: MLA-HIF) .....	52
<b>FIGURE 3.1.23:</b> COMPILATION OF STACKED COLUMN CHARTS DISPLAYING THE PERCENTUAL PROPORTION OF MINERALS ASSOCIATED WITH BINARY AND TERNARY+ (STRIATED SHADING) LOCKED BORNITE FOR THE TOTAL SAMPLE (LEFT SIDE) AND ACCORDING TO PARTICLE SIZE CLASSES IN THE BALL MILL PRODUCTS OF BLACK SHALES FROM MANSFELD, RUDNA AND SANGERHAUSEN. (DATA: MLA-HIF).....	55
<b>FIGURE 3.1.24:</b> COMPILATION OF STACKED COLUMN CHARTS DISPLAYING THE PERCENTUAL PROPORTION OF MINERALS ASSOCIATED WITH BINARY AND TERNARY+ (STRIATED SHADING) LOCKED CHALCOCITE FOR THE TOTAL SAMPLE (LEFT SIDE) AND ACCORDING TO PARTICLE SIZE CLASSES IN BALL MILL PRODUCTS OF BLACK SHALES FROM MANSFELD, RUDNA AND SANGERHAUSEN. (DATA: MLA-HIF).....	57
<b>FIGURE 3.1.25:</b> COMPILATION OF STACKED COLUMN CHARTS DISPLAYING THE PERCENTUAL PROPORTION OF MINERALS ASSOCIATED WITH BINARY AND TERNARY+ (STRIATED SHADING) LOCKED CHALCOPYRITE FOR THE TOTAL SAMPLE (LEFT SIDE) AND ACCORDING TO PARTICLE SIZE CLASSES IN BALL MILL PRODUCTS OF BLACK SHALES FROM MANSFELD, RUDNA AND SANGERHAUSEN. (DATA: MLA-HIF).....	58
<b>FIGURE 3.1.26:</b> GRAIN SIZE DISTRIBUTION CURVES OF BORNITE, CHALCOCITE AND CHALCOPYRITE IN THE PARTICLE SIZE FRACTION < 100 VeRO LIBERATOR® PRODUCTS OF MANSFELD AND RUDNA BLACK SHALE AND FOR COMPARISON IN THE RESPECTIVE BALL MILL PRODUCTS. (VeRO LIBERATOR®_R = ROUND HAMMER TOOLS, DATA: MLA-HIF) .....	60
<b>FIGURE 3.1.27:</b> LIBERATION CURVES OF BORNITE (IN WT. %) IN VARIOUS COMMUNITION PRODUCTS OF RUDNA (BLUE) AND MANSFELD (GREY) BLACK SHALE. TESTS WITH THE VeRO LIBERATOR® IMPACT CRUSHER WERE PERFORMED USING DIFFERENT TOOL DEPLOYMENT. (R=ROUND TOOLS; DATA: MLA-HIF) .....	63
<b>FIGURE 3.1.28:</b> LIBERATION CURVES OF CHALCOCITE (IN WT. %) IN VeRO LIBERATOR® BALL MILL PRODUCTS OF RUDNA (BLUE) AND MANSFELD (GREY) BLACK SHALE. TESTS WITH THE VeRO LIBERATOR® IMPACT CRUSHER WERE PERFORMED USING DIFFERENT TOOL CHARGES. (R=ROUND TOOLS; DATA: MLA-HIF) .....	64
<b>FIGURE 3.1.29:</b> LIBERATION CURVES OF CHALCOPYRITE (IN WT. %) IN VeRO LIBERATOR® PRODUCTS OF RUDNA (BLUE) AND MANSFELD (GREY) BLACK SHALE IN COMPARISON TO BALL MILL PRODUCTS. TESTS WITH THE VeRO LIBERATOR® IMPACT CRUSHER WERE PERFORMED USING DIFFERENT TOOL DEPLOYMENT. (R=ROUND TOOLS; DATA: MLA-HIF) .....	65
<b>FIGURE 3.1.30:</b> COLUMN PLOTS DISPLAYING PROPORTIONS OF LIBERATION CLASSES OF BORNITE IN PARTICLE SIZE CLASSES OF VeRO LIBERATOR® AND BALL MILL PRODUCTS FROM RUDNA AND MANSFELD BLACK SHALE. (DATA: MLA-HIF).....	66
<b>FIGURE 3.1.31:</b> COLUMN PLOTS DISPLAYING PROPORTIONS OF LIBERATION CLASSES OF CHALCOCITE IN PARTICLE SIZE CLASSES OF VeRO LIBERATOR® AND BALL MILL PRODUCTS FROM RUDNA AND MANSFELD BLACK SHALE. (DATA: MLA-HIF).....	68
<b>FIGURE 3.1.32:</b> COLUMN PLOTS DISPLAYING PROPORTIONS OF LIBERATION CLASSES OF CHALCOPYRITE IN PARTICLE SIZE CLASSES OF VeRO LIBERATOR® AND BALL MILL PRODUCTS FROM RUDNA AND MANSFELD BLACK SHALE. (DATA: MLA-HIF) .....	69
<b>FIGURE 3.1.33:</b> STACKED COLUMN PLOTS OF LOCKING MODES FOR BORNITE, CHALCOCITE AND CHALCOPYRITE IN THE TOTAL VeRO LIBERATOR® (< 100 µm FRACTION) AS WELL AS BALL MILL PRODUCT FROM MANSFELD BLACK SHALE AND THE DISTRIBUTION IN THE RESPECTIVE PARTICLE SIZE CLASSES OF BOTH COMMUNITION PRODUCTS. (DATA: MLA-HIF) .....	71
<b>FIGURE 3.1.34:</b> STACKED COLUMN PLOTS OF LOCKING MODES FOR BORNITE, CHALCOCITE AND CHALCOPYRITE IN THE TOTAL VeRO LIBERATOR® (< 100 µm FRACTION) AS WELL AS BALL MILL PRODUCT FROM RUDNA BLACK SHALE AND THE DISTRIBUTION IN THE RESPECTIVE PARTICLE SIZE CLASSES OF BOTH COMMUNITION PRODUCTS. (DATA: MLA-HIF) .....	73
<b>FIGURE 3.1.35:</b> STACKED COLUMN PLOTS ILLUSTRATING THE DISTRIBUTION OF MINERALS ASSOCIATED WITH BINARY AND TERNARY+ LOCKED BORNITE IN PARTICLE SIZE CLASSES AND IN THE TOTAL VeRO LIBERATOR® AS WELL AS BALL MILL PRODUCT FROM MANSFELD BLACK SHALE. (DATA: MLA-HIF) .....	74
<b>FIGURE 3.1.36:</b> STACKED COLUMN PLOTS ILLUSTRATING THE DISTRIBUTION OF MINERALS ASSOCIATED WITH BINARY AND TERNARY+ LOCKED CHALCOCITE IN PARTICLE SIZE CLASSES AND IN THE TOTAL VeRO LIBERATOR® AS WELL AS BALL MILL PRODUCT FROM MANSFELD BLACK SHALE. (DATA: MLA-HIF) .....	75
<b>FIGURE 3.1.37:</b> STACKED COLUMN PLOTS ILLUSTRATING THE DISTRIBUTION OF MINERALS ASSOCIATED WITH BINARY AND TERNARY+ LOCKED CHALCOPYRITE IN PARTICLE SIZE CLASSES AND THE TOTAL VeRO LIBERATOR® AS WELL AS BALL MILL PRODUCT FROM MANSFELD BLACK SHALE. (DATA: MLA-HIF) .....	76
<b>FIGURE 3.1.38:</b> STACKED COLUMN PLOTS ILLUSTRATING THE DISTRIBUTION OF MINERALS ASSOCIATED WITH BINARY AND TERNARY+ LOCKED BORNITE IN PARTICLE SIZE CLASSES AND THE TOTAL VeRO LIBERATOR® PRODUCTS (ANGULAR/ ROUND TOOLS) AS WELL AS BALL MILL PRODUCT FROM MANSFELD BLACK SHALE. (VeRO LIBERATOR®_R=ROUND TOOLS, DATA: MLA-HIF) .....	77

## LIST OF FIGURES

---

<b>FIGURE 3.1.39:</b> STACKED COLUMN PLOTS ILLUSTRATING THE DISTRIBUTION OF MINERALS ASSOCIATED WITH BINARY AND TERNARY+ LOCKED BORNITE IN PARTICLE SIZE CLASSES AND THE TOTAL VeRO LIBERATOR® PRODUCTS (ANGULAR/ ROUND TOOLS) AS WELL AS BALL MILL PRODUCT FROM MANSFELD BLACK SHALE. (VeRO LIBERATOR® _R=ROUND TOOLS, DATA: MLA-HIF) .....	79
<b>FIGURE 3.1.40:</b> STACKED COLUMN PLOTS ILLUSTRATING THE DISTRIBUTION OF MINERALS ASSOCIATED WITH BINARY AND TERNARY+ LOCKED BORNITE IN PARTICLE SIZE CLASSES AND THE TOTAL VeRO LIBERATOR® PRODUCTS (ANGULAR/ ROUND TOOLS) AS WELL AS BALL MILL PRODUCT FROM MANSFELD BLACK SHALE. (VeRO LIBERATOR® _R=ROUND TOOLS, DATA: MLA-HIF) .....	80
<b>FIGURE 3.2.1:</b> PARTICLE SIZE DISTRIBUTION CURVES OF FLOTATION CONCENTRATES AND TAILINGS GENERATED FROM RUDNA BLACK SHALE FEED. (DATA: MLU) .....	86
<b>FIGURE 3.2.2:</b> PARTICLE SIZE DISTRIBUTION CURVES OF FLOTATION CONCENTRATES AND TAILINGS GENERATED FROM SANGERHAUSEN BLACK SHALE FEED. (DATA: MLU) .....	88
<b>FIGURE 3.2.3:</b> MICROPHOTOGRAPH SHOWS THE INCREASED OCCURRENCE OF SULPHIDES EXHIBITING NUMEROUS GRAIN SHAPES IN A FLOTATION CONCENTRATE, WHICH CONTAINED MAINLY BORNITE (BROWNISH), CHALCOCITE (BLUISH GREY), CHALCOPYRITE (YELLOW) AND SOME COVELLITE (BRIGHTER BLUE). (LUBIN CONCENTRATE LC15A, REFLECTED LIGHT) .....	89
<b>FIGURE 3.2.4:</b> OVERVIEW IMAGE OF TAILINGS DISPLAYING THE DECREASED CONTENT OF SULPHIDES. BESIDES SOME LARGER SULPHIDE PARTICLES MARKED BY INTERGROWTHS THAT CONSISTS OF PREDOMINANTLY BORNITE (LIGHT PURPLE) AND MINOR CHALCOPYRITE (YELLOW), TAILINGS CONTAINED PARTICULARLY FINE-GRAINED SULPHIDES. (TAILINGS FROMH SANGERHAUSEN BLACK SHALE FEED, REFLECTED LIGHT).....	89
<b>FIGURE 3.2.5:</b> COMPLEXLY INTERGROWTHS IN A PARTICLE EXHIBITING THE INTIMATELY INTERLOCKING OF AS WELL SULPHIDES AS SULPHIDES WITH A EUHEDRAL DOLOMITE CRYSTAL. BORNITE (BROWNISH), CHALCOCITE (GREY) AND CHALCOPYRITE (YELLOW) FORM MINUTE AND IRREGULAR INTERGROWTH ASSOCIATIONS. (PRODUCT, DEXTRIN-FLOTATION USING ETHANOL PRE-TREATED SANGERHAUSEN FEED, REFLECTED LIGHT) .....	90
<b>FIGURE 3.2.6:</b> LARGER PARTICLE FOUND IN TAILINGS MARKED BY INTERGROWTH OF CHALCOPYRITE (YELLOW), BORNITE (BROWNISH), GANGUE (DARK GREY) AND SOME SMALL GRAINS OF CHALCOCITE (LIGHT GREY BLOBS). CHALCOPYRITE GRAIN IN THE CENTER AS WELL AS BORNITE ARE LARGELY TO COMPLETELY LOCKED. BORNITE SHOWS SLIGHT ALTERATION TO COVELLITE AND TINY INCLUSIONS OF CHALCOPYRITE AND CHALCOCITE. (TAILINGS, DEXTRIN-FLOTATION USING ETHANOL PRE-TREATED SANGERHAUSEN FEED, REFLECTED LIGHT).....	90
<b>FIGURE 3.2.7:</b> OVERVIEW SEM-IMAGE SHOWS CLEARLY THE COMMON INTERLOCKING OF SULPHIDES (BRIGHT PHASES) WITH GANGUE MINERALS (GREY) IN PARTICLES OF CONCENTRATES. (PRODUCT FROM FLOTATION USING DEXTRIN AND ETHANOL PRE-TREATED RUDNA FEED, SEM-BSE IMAGE).....	90
<b>FIGURE 3.2.8:</b> EXAMPLES OF EXTREMELY FINE-GRAINED INTERGROWTHS OF GALENA (GN) WITH BORNITE (BN) AS WELL AS GALENA WITH PYRITE (PY). IN ADDITION, SULPHIDES, ALSO SOME CHALCOCITE (CCT), ARE INTERGROWN WITH MAINLY CALCITE (CAL). (ILL=ILLITE; PRODUCT FROM FLOTATION USING DEXTRIN AND ETHANOL PRE-TREATED RUDNA FEED, SEM-BSE IMAGE) .....	90
<b>FIGURE 3.2.9:</b> OVERVIEW SEM-IMAGE OF TAILINGS SHOWS SULPHIDES OFTEN COMPLETELY LOCKED BY GANGUE MINERALS, BUT ALSO SULPHIDES CONSIDERABLY LIBERATED. (TAILINGS FROM THE FLOTATION OF RUDNA BLACK SHALE FEED, SEM-BSE IMAGE).....	91
<b>FIGURE 3.2.10:</b> LARGE-SIZED PARTICLES IN TAILINGS MARKED BY BORNITE (BN), CHALCOCITE (CCT) AND SPHALERITE (SP) MOSTLY COMPLETE LOCKED BY GANGUE MINERALS. (TAILINGS FROM THE FLOTATION OF RUDNA BLACK SHALE FEED, SEM-BSE IMAGE).....	91
<b>FIGURE 3.2.11:</b> PIE CHARTS REPRESENTING THE PROPORTION OF GANGUE AND SULPHIDE MINERALS IN RUDNA BLACK SHALE FEED AND RELATED COPPER FLOTATION CONCENTRATES. (DATA: MLU) .....	91
<b>FIGURE 3.2.12:</b> COMPILATION OF MINERAL DISTRIBUTION ANALYSES FOR RUDNA BLACK SHALE FEED AND RELATED FLOTATION CONCENTRATES SHOWING PROPORTION OF SULPHIDES (UPPER SECTION) AS WELL AS GANGUE MINERALS (LOWER SECTION). (DATA: MLU) .....	92
<b>FIGURE 3.2.13:</b> PIE CHARTS DISPLAYING THE PROPORTION OF SULPHIDES AND GANGUE MINERALS IN RUDNA BLACK SHALE FEED AND TAILINGS FROM DIFFERENT FLOTATION TESTS. (DATA: MLU) .....	94
<b>FIGURE 3.2.14:</b> MINERAL DISTRIBUTION OF RUDNA BLACK SHALE FEED AND TAILINGS FROM DIFFERENT FLOTATION TESTS. (DATA: MLU) .....	95
<b>FIGURE 3.2.15:</b> PROPORTIONS OF SULPHIDES AND GANGUE MINERALS IN DIFFERENT FLOTATION CONCENTRATES AND SANGERHAUSEN BLACK SHALE FEED. (DATA: MLU) .....	98
<b>FIGURE 3.2.16:</b> MINERAL DISTRIBUTION FOR SANGERHAUSEN BLACK SHALE FEED AND RELATED FLOTATION CONCENTRATES SHOWING THE PROPORTION OF SULPHIDES (UPPER SECTION) AS WELL AS GANGUE MINERALS (LOWER SECTION). (DATA: MLU).....	99
<b>FIGURE 3.2.17:</b> PIE CHARTS INDICATING THE PROPORTION OF SULPHIDES AND GANGUE MINERALS IN FLOTATION TAILINGS FROM DIFFERENT FLOTATION TESTS PERFORMED ON SANGERHAUSEN BLACK SHALE FEED. (DATA: MLU) .....	101

## LIST OF FIGURES

---

<b>FIGURE 3.2.18:</b> MINERAL DISTRIBUTION SHOWING THE PROPORTIONS OF PARTICULAR SULPHIDE (UPPER PART) AND GANGUE MINERALS AS WELL AS TOTAL ORGANIC MATTER CONTENT (TOC) IN SANGERHAUSEN BLACK SHALE FEED AND RELATED TAILINGS FROM DIFFERENT FLOTATION TESTS. (DATA: MLU) .....	102
<b>FIGURE 3.2.19:</b> DISTRIBUTION OF LIBERATION CLASSES, ACCORDING TO FREE PERIMETER OF THE TARGET MINERAL, FOR BORNITE, CHALCOCITE AND CHALCOPYRITE IN CONCENTRATES OF DIFFERENT FLOTATION TEST SERIES WITH SANGERHAUSEN AS WELL AS RUDNA BLACK SHALE FEED. (FL_CONC=CONCENTRATE STANDARD FLOTATION, FL_DX_CONC=CONCENTRATE FLOTATION WITH DEXTRIN, FL_DX_ET_CONC=CONCENTRATE FLOTATION WITH DEXTRIN AND ETHANOL PRE-TREATED FEED; DATA: PETROLAB) .....	105
<b>FIGURE 3.2.20:</b> STACKED BAR CHART DISPLAYING THE DISTRIBUTION OF LIBERATION CLASSES, ACCORDING TO FREE PERIMETER OF THE TARGET MINERAL, FOR BORNITE, CHALCOCITE AND CHALCOPYRITE IN CONCENTRATES OF DIFFERENT FLOTATION TEST SERIES WITH SANGERHAUSEN AS WELL AS RUDNA BLACK SHALE FEED. (RD=RUDNA, SA=SANGERHAUSEN, FL_TAIL=TAILINGS STANDARD FLOTATION, FL_DX_TAIL=TAILINGS FLOTATION WITH DEXTRIN, FL_DX_ET_TAIL=TAILINGS FLOTATION WITH DEXTRIN AND ETHANOL PRE-TREATED FEED; DATA: PETROLAB) .....	106
<b>FIGURE 3.2.21:</b> GRAIN SIZE DISTRIBUTION OF BORNITE, CHALCOCITE AND CHALCOPYRITE IN SANGERHAUSEN AS WELL AS RUDNA FEED AND RELATED CONCENTRATES EXTRACTED BY FLOTATION USING DEXTRIN. (FL_DX_CONC=CONCENTRATE FLOTATION WITH DEXTRIN, FL_DX_ET_CONC=CONCENTRATE FLOTATION WITH DEXTRIN AND ETHANOL PRE-TREATED FEED; DATA: PETROLAB) .....	107
<b>FIGURE 3.2.22:</b> DISTRIBUTION OF LIBERATION CLASSES FOR CHALCOCITE REGARDING TO PARTICLE SIZE CLASSES IN THE CONCENTRATE EXTRACTED BY FLOTATION USING DEXTRIN FROM RUDNA BLACK SHALE FEED. BLACK LINE GRAPH SHOWS THE RECOVERY CURVE OF CHALCOCITE. (DATA: PETROLAB).....	109
<b>FIGURE 3.2.23:</b> LIBERATION MODES OF CHALCOCITE IN PARTICLE SIZE CLASSES OF THE CONCENTRATE EXTRACTED BY FLOTATION USING DEXTRIN FROM ETHANOL PRE-TREATED RUDNA BLACK SHALE FEED. BLACK LINE GRAPH INDICATES THE CHALCOCITE RECOVERY CURVE. (DATA: PETROLAB) .....	110
<b>FIGURE 3.2.24:</b> DISTRIBUTION OF LIBERATION MODES OF BORNITE IN PARTICLE SIZE CLASSES OF THE CONCENTRATE EXTRACTED BY FLOTATION USING DEXTRIN FROM RUDNA BLACK SHALE FEED. BLACK LINE GRAPH REPRESENTS THE RECOVERY CURVE FOR BORNITE. (DATA: PETROLAB).....	112
<b>FIGURE 3.2.25:</b> STACKED COLUMN PLOT FOR LIBERATION MODES OF BORNITE IN PARTICLE SIZE CLASSES OF THE CONCENTRATE GENERATED BY FLOTATION USING DEXTRIN AND ETHANOL PRE-TREATED RUDNA BLACK SHALE FEED. (DATA: PETROLAB) .....	113
<b>FIGURE 3.2.26:</b> STACKED COLUMN DIAGRAM REPRESENTING PROPORTIONS FOR LIBERATION MODES OF BORNITE IN THE CONCENTRATE GAINED BY FLOTATION USING DEXTRIN FROM SANGERHAUSEN BLACK SHALE FEED. BLACK LINE GRAPH INDICATES THE THEORETICAL RECOVERY CURVE FOR BORNITE. (DATA: PETROLAB) .....	115
<b>FIGURE 3.2.27:</b> STACKED COLUMN DIAGRAM REPRESENTING PROPORTIONS FOR LIBERATION MODES OF BORNITE IN THE CONCENTRATE GAINED BY FLOTATION USING DEXTRIN AND ETHANOL PRE-TREATED SANGERHAUSEN BLACK SHALE FEED. BLACK LINE GRAPH INDICATES THE THEORETICAL RECOVERY CURVE FOR BORNITE. (DATA: PETROLAB) .....	116
<b>FIGURE 3.2.28:</b> LIBERATION MODES OF CHALCOPYRITE IN PARTICLE SIZE CLASSES OF THE CONCENTRATE EXTRACTED BY FLOTATION USING DEXTRIN FROM SANGERHAUSEN BLACK SHALE FEED. BLACK LINE GRAPH INDICATES THE CHALCOCITE RECOVERY CURVE. (DATA: PETROLAB) .....	118
<b>FIGURE 3.2.29:</b> STACKED COLUMN PLOT SHOWING LIBERATION MODES OF CHALCOPYRITE IN PARTICLE SIZE CLASSES OF THE CONCENTRATE GENERATED BY FLOTATION USING DEXTRIN AND ETHANOL PRE-TREATED SANGERHAUSEN BLACK SHALE FEED. BLACK LINE GRAPH SHOWS THE RECOVERY CURVE OF CHALCOPYRITE (DATA: PETROLAB).....	119
<b>FIGURE 3.2.30:</b> STACKED COLUMN PLOT INDICATING THE DEPARTMENT OF CU IN CONCENTRATES AND TAILINGS FROM DIFFERENT FLOTATION TESTS CARRIED OUT WITH RUDNA BLACK SHALE FEED. (DATA: MLU) .....	121
<b>FIGURE 3.2.31:</b> STACKED COLUMN PLOT INDICATING THE DEPARTMENT OF CU IN THE MAIN THREE COPPER-BEARING SULPHIDES IN CONCENTRATES AND TAILINGS FROM DIFFERENT FLOTATION TESTS CARRIED OUT WITH SANGERHAUSEN BLACK SHALE FEED. (DATA: MLU) .....	122
<b>FIGURE 3.2.32:</b> PROPORTIONS OF SULPHIDES AND GANGUE MINERALS IN CONCENTRATES PRODUCED BY THE LUBIN CONCENTRATOR, POLAND. (DATA: MLU) .....	123
<b>FIGURE 3.2.33:</b> MINERAL DISTRIBUTION SHOWING THE PROPORTIONS OF PARTICULAR SULPHIDE (UPPER PART) AND GANGUE MINERALS AS WELL AS TOTAL ORGANIC MATTER CONTENT (TOC) IN LUBIN CONCENTRATES LCA06, LC15A, LC15B. (DATA: MLU) .....	124

## LIST OF FIGURES

---

<b>FIGURE 3.3.1:</b> SEM-IMAGE OF HIGHLY ALTERED SILICATE PARTICLES IN THE LOWER PART EXHIBITING DISSOLUTION FEATURES SUCH AS EMBAYMENT AND BOXWORK-LIKE TEXTURES OF DISSOLVED MINERAL PHASES (CARBONATES AND SULPHIDES). THE LARGE ELONGATED PARTICLE IN THE UPPER PART CONSISTED SUBSTANTIALLY OF ORGANIC MATTER-CLAY INTERGROWTHS THAT HINDERED THE DISSOLUTION OF ENCLOSED SOLUBLE MINERAL GRAINS SUCH AS PYRITE (PY) AND SPHALERITE (SP). (BIOLEACHING RESIDUE OF MANSFELD BLACK SHALE, SEM-BSE).....	130
<b>FIGURE 3.3.2:</b> LARGE PARTICLE SHOWING SMALL REMNANTS OF CHALCOPYRITE (BRIGHT YELLOW) ALMOST COMPLETE REPLACED BY COVELLITE (BLUISH TO DEEP PURPLE). A FURTHER SMALLER CHALCOPYRITE PARTICLE (BELOW LEFT) SHOWS NEARLY NO INDICATION OF ALTERATION. (BIOLEACHING RESIDUE OF LCA06, REFLECTED LIGHT) .....	131
<b>FIGURE 3.3.3:</b> GALENA SHOWING DISSOLUTION FEATURES AT THE GRAIN EDGE AND THIN COATINGS OF COVELLITE THAT IS OVERGROWN BY ANGLSITE. (BIOLEACHING RESIDUE OF LCA06, REFLECTED LIGHT).....	131
<b>FIGURE 3.3.4:</b> GRAIN SIZE DISTRIBUTION CURVES FOR SANGERHAUSEN AND RUDNA CONCENTRATE AND RELATED BIOLEACHING RESIDUES. (DATA: MLU) .....	132
<b>FIGURE 3.3.5:</b> SEM-IMAGE OF A PARTICLE ILLUSTRATING COMMON INTERGROWTHS CONSISTING OF ILLITE (ILT) AND CHALCOPYRITE (CCP) AS FOUND IN BIOLEACHING RESIDUES OF LUBIN CONCENTRATE LCA06. (SEM-BSE).....	133
<b>FIGURE 3.3.6:</b> CHALCOPYRITE PARTICLE EXHIBITING ISOLATED BACTERIAL CORROSION PITS (ARROWS) AS CATEGORIZED BY BENNETT AND TRIBUTSCH (1978) DETECTED IN THE BIOLEACHING RESIDUES OF SANGERHAUSEN BLACK SHALE FEED. (SEM-SE).....	133
<b>FIGURE 3.3.7:</b> SURFACE OF A CHALCOPYRITE PARTICLE IN THE CHEMICAL CONTROL EXHIBITING AREAS MARKED BY CRYSTAL PLANE CLEAVAGE (ETCHING STRUCTURE) AND IRREGULAR FORMS OF ALTERED MINERAL SURFACE. (SEM-SE) .....	133
<b>FIGURE 3.3.8:</b> DETAIL IMAGE OF SECONDARY FORMED COATINGS OF COPPER SULFATE OCCUPYING A PREVIOUSLY CORRODED CHALCOPYRITE PARTICLE. (SEM-SE) .....	133
<b>FIGURE 3.3.9:</b> OVERVIEW IMAGE OF PARTICLES IN BIOLEACHING RESIDUES OF THE SANGERHAUSEN BLACK SHALE FEED DEMONSTRATES THE ABUNDANT OCCURRENCE OF UNDISSOLVED SULFIDES (CCP-CHALCOPYRITE, GN-GALENA, SPH-SPHALERITE), BARITE (BRT) AND ANGLSITE (ANG). (SEM-BSE).....	134
<b>FIGURE 3.3.10:</b> THE WIDESPREAD FORMATION OF SECONDARY LEAD SULFATE DEVELOPED AS MICROCRYSTALLINE ANGLSITE (ANG) ENVELOPES OF GALENA (GN) OR BARITE (BRT) PARTICLES OFTEN REPRESENTS AN COMMON IN-SITU REPLACEMENT IN LEACHING RESIDUES. (SEM-BSE).....	134
<b>FIGURE 3.3.11:</b> PARTICLE CONSISTING OF GALENA (GN) AND CHALCOPYRITE (CCP) SHOWS LEAD SULFATE FORMATION AT THE RIMS OF THE GALENA AREA. THE OUTER CHALCOPYRITE EDGES EXHIBIT INDEED NO ALTERATION RIM. (SEM-BSE).....	134
<b>FIGURE 3.3.12:</b> IMAGE OF NEARLY COMPLETELY DISSOLVED GALENA (GN) GRAIN REPLACED EXTENSIVE BY MASSIVE TO CELLULAR ANGLSITE (ANG), WHICH WAS AN COMMON REPLACEMENT TEXTURE DETECTED IN BIOLEACHING AS WELL AS STERILE CONTROL RESIDUE.(SEM-BSE).....	134
<b>FIGURE 3.3.13:</b> CHALCOPYRITE (CCP) GRAINS EXHIBITED VERY DIFFERENT SHAPES IN BIOLEACHING RESIDUES. THEY WERE EITHER SMOOTH AND ANGULAR SHOWING HARDLY ANY INDICATIONS OF ALTERATION OR STRONGLY CORRODED PARTICLE MARKED BY ROUGHENED AND PITTED SURFACES. IMAGE SHOWS ALSO PARTIAL DISSOLVED SPHALERITE (SP) AND PRECIPITATES OF ANGLSITE (ANG). (SEM-SE) .....	135
<b>FIGURE 3.3.14:</b> DISSOLUTION PATTERN TRANSECTING A CHALCOPYRITE PARTICLE DOCUMENTS THE ADVANCED BUT NOT COMPLETE DISINTEGRATION COMMON IN BIOLEACHING RESIDUES. (SEM-SE).....	135
<b>FIGURE 3.3.15:</b> EXAMPLE OF CHALCOPYRITE (CCP) PARTICLES IN BIOLEACHING RESIDUES DISPLAYS IRON AND COPPER-BEARING SULFATE (FeCuSO) ON THE GRAIN SURFACE AS WELL AS WITHIN INTERSTICES (BSE-SEM-IMAGE). .....	135
<b>FIGURE 3.3.16:</b> GENERAL PROPORTIONS OF GANGUE AND MINERALS INDICATION THE MORE ADVANCED DISSOLUTION OF SULPHIDES IN THE BIOLEACHING RESIDUES OF THE SANGERHAUSEN BLACK SHALE FEED. (DATA: MLU).....	137
<b>FIGURE 3.3.17:</b> MINERAL DISTRIBUTION OF SANGERHAUSEN BLACK SHALE FEED, BIOLEACHING AS WELL AS STERILE CONTROL LEACHING RESIDUES. (DATA: MLU) .....	138
<b>FIGURE 3.3.18:</b> PROPORTION OF GANGUE MINERALS AND SULPHIDES IN THE SANGERHAUSEN CONCENTRATE FEED AND RELATED BIOLEACHING AND STERILE CONTROL LEACHING RESIDUES. (DATA: MLU) .....	141
<b>FIGURE 3.3.19:</b> MINERAL DISTRIBUTION DIAGRAM FOR SANGERHAUSEN COPPER CONCENTRATE FEED AS WELL AS BIOLEACHING AND STERILE LEACHING RESIDUES. (DATA: MLU) .....	142
<b>FIGURE 3.3.20:</b> PIE CHARTS FOR RUDNA CONCENTRATE FEED AND RELATED BIOLEACHING AS WELL AS STERILE CONTROL LEACHING RESIDUES SHOWING THE PROPORTION OF SULPHIDES AND GANGUE MINERALS. (DATA: MLU .....	145
<b>FIGURE 3.3.21:</b> BAR CHART DISPLAYING THE DISTRIBUTION OF SULPHIDES AS WELL AS GANGUE-TYPE MINERALS AND MINERAL GROUPS IN THE RUDNA COPPER CONCENTRATE AND ITS BIOLEACHING AND STERILE CONTROL LEACHING RESIDUES. (DATA: MLU).....	146

## LIST OF FIGURES

---

<b>FIGURE 3.3.22:</b> PIE CHARTS INDICATING THE PROPORTION OF SULPHIDES AND GANGUE MINERALS IN LUBIN CONCENTRATE LC15A AND RELATED LEACHING RESIDUES. (DATA: MLU) .....	148
<b>FIGURE 3.3.23:</b> DISTRIBUTION OF SULPHIDES, SULPHATES AND GANGUE MINERALS IN THE LUBIN CONCENTRATE LC15A IN COMPARISON WITH THE BIOLEACHING AS WELL AS STERILE CONTROL LEACHING RESIDUES. ....	149
<b>FIGURE 3.3.24:</b> PROPORTION OF SULPHIDES AND GANGUE MINERALS IN LUBIN CONCENTRATE LCA06 AND RELATED BIOLEACHING RESIDUES. (DATA: MLU) .....	152
<b>FIGURE 3.3.25:</b> MINERAL DISTRIBUTION OF LUBIN CONCENTRATE LCA06 IN COMPARISON TO THE BIOLEACHING RESIDUE. (DATA: MLU) .....	153
<b>FIGURE 3.3.26:</b> STACKED COLUMN PLOT ILLUSTRATING THE SHIFT OF THE MASS BALANCE OF MINERAL FROM THE LC15B CONCENTRATE FEED OVER BIOLEACHING RESIDUES TAKEN ON DISTINCT RETENTION TIMES DURING AND AFTER THE BIOLEACHING TEST. IN PARTICULAR, PROPORTIONAL CHANGES FOR CHALCOCITE, CHALCOPYRITE, PYRITE, CARBONATES AND MINERALS OF THE FELDSPAR-CLAY GROUP ARE VERY OBVIOUS. FOR DETAILED EXPLANATION SEE TEXT. (DATA: MLU) .....	156
<b>FIGURE 3.3.27:</b> GRADUAL CHANGE OF BASE METAL CONTENT IN BIOLEACHING RESIDUES AFTER PROGRESSIVELY INCREASING RETENTION TIMES IN THE PROCESS SOLUTION. (DATA: ALS) .....	157
<b>FIGURE 4.1.1:</b> COMMON ROCK FABRIC OF BLACK SHALES FEATURING ELONGATED MINERAL AGGREGATES THAT CONSIST MAINLY OF ANHEDRAL CARBONATES, QUARTZ AND FELDSPAR GRAINS, WHICH ARE ENCLOSED BY DIFFERENTLY THICK, SCHLIEREN-LIKED ASSOCIATION OF INTIMATELY INTERGROWN ILLITE-ORGANIC MATTER BANDS. (MANSFELD BLACK SHALE, THIN SECTION, PLANE PLANAR POLARISATION) .....	163
<b>FIGURE 4.1.2:</b> DISTRIBUTION OF BRITTLE AND ELASTIC MINERALS (A-C) AS WELL AS DISTRIBUTION OF HARDNESS CLASSES ACCORDING TO MINERAL HARDNESS (D) IN BALL MILL PRODUCTS OF DIFFERENT BLACK SHALE ORES. ....	166
<b>FIGURE 4.1.3:</b> COLUMN CHART ILLUSTRATING THE PROPORTIONS OF LIBERATED BORNITE, CHALCOCITE AND CHALCOPYRITE AND THEIR MIDDINGS IN BALL MILL PRODUCTS OF DIFFERENT BLACK SHALE ORES. ....	167
<b>FIGURE 4.1.4:</b> SCATTERED PLOT SHOWING THE CONTENT OF MIDDINGS IN RELATION TO THE CONTENT OF BINARY LOCKING FOR COPPER SULPHIDES. THE DISTRIBUTION INDICATING THAT COPPER SULPHIDE MIDDINGS ARE OFTEN BINARY LOCKED. ....	170
<b>FIGURE 4.1.5:</b> RELATIONSHIP BETWEEN COPPER SULPHIDE MIDDINGS (30-80% LIBERATED) AND BINARY AND TERNARY+ LOCKED COPPER SULPHIDES. IT SHOWS THAT COPPER SULPHIDES ARE MAINLY TERNARY+ LOCKED BUT IN PARTICULAR FOR BALL MILL PRODUCTS OF MANSFELD AND RUDNA BLACK SHALE IT IS APPARENT THAT THE OCCURRENCE OF COPPER SULPHIDE MIDDLING COINCIDE WITH BINARY LOCKING. ....	171
<b>FIGURE 4.1.6:</b> DIAGRAM ILLUSTRATES THE DEPENDENCY OF THE $D_{80}$ GRAIN SIZE OF THE TOTAL BALL MILL PRODUCTS AND OF COPPER SULPHIDES IN REGARDS TO THE DISTRIBUTION OF LIBERATED COPPER SULPHIDES AND PARTLY LIBERATED MIDDINGS (30-80% FREE SURFACE) .....	174
<b>FIGURE 4.1.7:</b> SCHEMATIC ILLUSTRATION OF THE PROPOSED WORKING PRINCIPLE OF VeRo LIBERATOR® IMPACT CRUSHING TECHNOLOGY FROM BORG ET AL. (2015B). A) IMPACTING ENERGY INFLICTED ON INHOMOGENEOUS MATERIAL BY HAMMER TOOLS SEND THROUGH THE MATERIAL. B) THE VARIOUS PARTICLES REACT DIFFERENTLY TO SHOCK WAVES ACCORDING TO THEIR SPECIFIC COMPRESSIBILITY AND ELASTICITY MODULI UNDER HIGH-FREQUENCY STIMULATION. C) TENSIONAL AND/OR SHEAR STRESS IS ACCUMULATED AT GRAIN BOUNDARIES BETWEEN DIFFERENT MINERALS OR ALONG WEAK INTRA-MINERAL CRYSTAL ZONES (CLEAVAGE) AND EVENTUALLY CAUSING BREAKAGE BY SHEARING. D) PREDOMINANCE OF INTER-GRANULAR, RATHER THAN INTRA- OR CROSS-GRANULAR FRACTURING. ....	175
<b>FIGURE 4.1.8:</b> COMPARISON OF THE REPRESENTATIVE MAXIMUM GRAIN SIZE OF COPPER SULPHIDES IN VeRo LIBERATOR® AND BALL MILL PRODUCTS INDICATING LARGELY COINCIDENT GRAIN SIZES FOR CHALCOPYRITE AND CHALCOCITE. BORNITE IS FINER-GRAINED IN RUDNA VeRo LIBERATOR® PRODUCTS AND COARSER-GRAINED THE BALL MILL PRODUCT OF MANSFELD BLACK SHALE. (VeRo LIBERATOR®_R= ROUND HAMMER TOOLS) .....	178
<b>FIGURE 4.1.9:</b> COMPARISON OF THE PROPORTIONS OF LIBERATED COPPER SULPHIDES AND MIDDINGS IN VeRo LIBERATOR® PRODUCTS FROM MANSFELD AND RUDNA BLACK SHALE IN RESPECT TO BALL MILL PRODUCTS. ....	179
<b>FIGURE 4.1.10:</b> COLUMN CHART ILLUSTRATING THE LOCKING MODE OF COPPER SULPHIDES IN THE VeRo LIBERATOR® PRODUCT COMPARED TO THE BALL MILL PRODUCT OF MANSFELD BLACK SHALE. THE PROPORTION OF LIBERATED COPPER SULPHIDES AND ALSO BINARY LOCKED COPPER SULPHIDES IS COMMONLY INCREASED IN THE BALL MILL PRODUCT .....	180
<b>FIGURE 4.1.11:</b> COMPILATION OF LOCKING ASSOCIATIONS OF COPPER SULPHIDES IN VeRo LIBERATOR® PRODUCTS OF RUDNA BLACK SHALE IN COMPARISON TO THE RESPECTIVE BALL MILL PRODUCT. COPPER SULPHIDES IN VeRo LIBERATOR® PRODUCTS ARE MORE LIBERATED AND BINARY LOCKED THAN IN THE BALL MILL PRODUCT, IN PARTICULAR IN THE VeRo LIBERATOR® PRODUCT GENERATED BY ROUND HAMMER TOOLS. ....	182

## LIST OF FIGURES

---

<b>FIGURE 4.1.12:</b> COMPARISON OF THE PROPORTION OF BRITTLE AND ELASTIC-ACTING MINERAL CONSTITUENTS IN VeRO LIBERATOR® AND BALL MILL PRODUCTS OF MANSFELD (A) AND RUDNA BLACK SHALE (B). THE DISTRIBUTION OF ROCK-FORMING MINERALS ACCORDING TO THEIR AFFINITY TO DIFFERENT HARDNESS CLASSES (C) SHOWS THAT MANSFELD BLACK SHALE CONTAINS A GENERALLY INCREASED AMOUNT OF MINERALS WITH HARDNESS > 6 THAT ARE OBVIOUSLY MOST INCREASED IN THE VeRO LIBERATOR® PRODUCT.....	184
<b>FIGURE 4.1.13:</b> PROPORTION OF CARBONATES IN BINARY AND TERNARY+ LOCKED COPPER SULPHIDES IN VeRO LIBERATOR® PRODUCTS COMPARED TO BALL MILL PRODUCTS. BALL MILL PRODUCTS CONTAIN GENERALLY INCREASED PROPORTIONS OF CARBONATES INTERLOCKED WITH COPPER SULPHIDES. ....	185
<b>FIGURE 4.2.1:</b> RECOVERY RATES OF COPPER SULPHIDES BY DIFFERENT FLOTATION TESTS INDICATING THAT THE FLOTATION WITH DEXTRIN WITHOUT ETHANOL PRE-TREATMENT OF THE FEED ACHIEVES GENERALLY LOW RECOVERY, FLOTATION WITH DEXTRIN AND ETHANOL PRE-TREATED FEED GENERATES FLOTATION PRODUCTS MARKED BY RECOVERY RATES SIMILAR TO THE STANDARD FLOTATION AT REDUCED MASS RECOVERY. ....	188
<b>FIGURE 4.2.2:</b> COMPILATION OF THE PROPORTION OF LIBERATED COPPER SULPHIDES AND MIDDINGS IN FEED AND DIFFERENT CONCENTRATES. THE COMPARATIVELY INCREASED RECOVERY IN GENERAL FOR COPPER SULPHIDES BY FLOTATION USING DEXTRIN AND ETHANOL PRE-TREATED FEED IS CAUSED BY COMMONLY INCREASED PORTIONS OF LIBERATED AND PARTLY LIBERATED COPPER SULPHIDE GRAINS THAT HAVE BEEN INTENSIFIED ENTRAINED IN THE FLOTATION PRODUCT AFFECTING RECOVERY RATES. (FL_ST=STANDARD FLOTATION, FL_DX=FLOTATION WITH DEXTRIN, FL_DX+ET=FLOTATION WITH DEXTRIN AND ETHANOL PRE-TREATED FEED) .....	190
<b>FIGURE 4.2.3:</b> COMPARISON OF THE D <sub>80</sub> -GRAIN SIZE OF COPPER SULPHIDES IN RUDNA AND SANGERHAUSEN FEED AS WELL AS RELATED CONCENTRATES GAINED BY FLOTATION USING DEXTRIN (+ DEXTRIN) AND CONCENTRATES FROM FLOTATION WITH DEXTRIN AND ETHANOL -PRE-TREATMENT (EtOH PRE-TREAT + DEXTRIN) OF THE FEED. THE GRAIN SIZE OF EXTRACTED COPPER SULPHIDES IS PARTLY FINER-IN THE CONCENTRATES FROM FLOTATION USING ETHANOL PRE-TREATED FEED OR COINCIDING WITH CONCENTRATED FROM FLOTATION USING ONLY DEXTRIN. ....	191
<b>FIGURE 4.2.4:</b> RECOVERY PROPORTIONS OF SELECTED TRACE METALS ASSOCIATED WITH KUPFERSCHIEFER-TYPE MINERALIZATION. ACCORDING TO THE LOW AND SELECTIVE RECOVERY OF COPPER SULPHIDES AS WELL AS OTHER SULPHIDES (E.G. PYRITE) BY FLOTATION USING DEXTRIN, TRACE METAL RECOVERY IS EXTREMELY LOW. SIMILAR INCREASED RECOVERY RATES FOR AG ARE DISPLAYED FOR STANDARD FLOTATION AND FLOTATION WITH DEXTRIN AND ETHANOL PRE-TREATED FEED. LOW RECOVERY OF Co, Mo, Ni, V ARE MAINLY CAUSED BY DEPRESSION OF PYRITE AND ORGANIC MATTER BY FLOTATION USING DEXTRIN. MODERATE RECOVERY RATES WERE ACHIEVED BY FLOTATION USING DEXTRIN AND ETHANOL PRE-TREATED FEED. ....	196
<b>FIGURE 4.2.5:</b> EXTREMELY GOOD CORRELATION OF CU AND AG IN RUDNA CONCENTRATES AND TAILINGS INDICATING THAT CHALCOHITE HOSTS SIGNIFICANT AMOUNTS OF AG. ....	197
<b>FIGURE 4.2.6:</b> THE CORRELATION OF AS AND Co WITH Fe IN RUDNA CONCENTRATES AND TAILINGS REVEAL THE ASSOCIATION WITH PYRITE. ....	197
<b>FIGURE 4.2.7:</b> CORRELATION OF Mo AND Fe IN SANGERHAUSEN CONCENTRATES AND TAILINGS INDICATE THAT OCCURRENCE OF Mo IS RELATED TO PYRITE. ....	198
<b>FIGURE 4.2.8:</b> ADDITIONAL CORRELATION OF Mo WITH AS, Co AND Ni IMPLIES THAT Mo COULD ALSO ASSOCIATED TO COBALTITE OR GERSDORFFITE. ....	198
<b>FIGURE 4.3.1:</b> COMPARISON OF THE RECOVERY OF Cu, Co AND Mo BY BIOLEACHING TESTS OF DIFFERENT COPPER FLOTATION CONCENTRATES. BIOLEACHING YIELDED GENERALLY IN CONSIDERABLY INCREASE RECOVERY, RECOVERY RATES FOR BIOLEACHING OF RUDNA AND LUBIN CONCENTRATE LC15A WERE ESPECIALLY INCREASED. ....	200
<b>FIGURE 4.3.2:</b> RELATIONSHIP OF CHALCOPYRITE (CCP) CONTENT IN FEED AND THE PORTION AMONG COPPER SULPHIDES IN REGARDS TO THE DISSOLUTION CAPACITY (RECOVERY) OF CHALCOPYRITE AND TO THE TOTAL Cu-RECOVERY. THE AMOUNT OF CHALCOPYRITE IN THE FEED IS NOT DECISIVE FOR DISSOLUTION CAPACITY BY BIOLEACHING BUT ITS PORTION OF COPPER SULPHIDES AND THE RATE OF DISSOLUTION AFFECT OBVIOUSLY THE Cu-RECOVERY.....	201
<b>FIGURE 4.3.3:</b> BINARY PLOT ILLUSTRATING THE RELATIONSHIP OF RECOVERED Co IN RESPECT TO DISSOLUTION OF PYRITE. IT SEEMS THAT COBALT IN LUBIN CONCENTRATES IS MORE ASSOCIATED WITH COBALTITE. IN SANGERHAUSEN FEED Co IS MORE RELATED TO PYRITE.....	203
<b>FIGURE 4.3.4:</b> CORRELATION OF THE DISSOLUTION CAPACITY OF PYRITE WITH RECOVERY RATES OF Mo, WHICH APPLIES FOR MOST OF THE BIOLEACHING TESTS. ONLY BIOLEACHING OF LUBIN CONCENTRATE LCA06 SHOWED NO ASSOCIATION WITH PYRITE AT ALL. ....	203

## LIST OF FIGURES

---

<b>FIGURE 4.3.5:</b> DISSOLUTION RATES OF Co, Mo AND Ni IN RELATION TO PYRITE SHOWING CONTINUOUSLY INCREASING RECOVERY UP TO DAY 4 IN THE BIOLEACHING EXPERIMENT WITH LUBIN CONCENTRATE LC15B, WHICH IS PARTLY CONGRUENT WITH THE DISSOLUTION OF PYRITE. BUT THE CONSIDERABLE RECOVERY OF PYRITE FROM DAY 4 TO DAY 10 SEEMS TO AFFECT RECOVERY RATES OF Co, Mo AND Ni INSIGNIFICANTLY.....	204
<b>FIGURE 4.3.6:</b> RECOVERY RATES OF COPPER SULPHIDES AS WELL AS PYRITE, SPHALERITE AND GALENA WITHIN THE BIOLEACHING TESTS OF LUBIN CONCENTRATE LC15B. CHALCOCITE IS LARGELY DISSOLVED AND BORNITE IS MODERATELY DISSOLVED AT THE BEGINNING OF THE EXPERIMENT BUT BOTH ARE COMPLETELY DISSOLVED AT THE END. CHALCOPYRITE AND PYRITE SHOW LOW DISSOLUTION AT THE BEGINNING, WHICH IS CONSTANTLY INCREASING TO THE END FOR PYRITE. CHALCOPYRITE DISSOLUTION IS CONSISTENT TO PYRITE UP TO DAY 4, WHERE IT STOPS AND A FURTHER DISSOLUTION AT PROGRESSIVE LEACHING TIME IS OBVIOUSLY HINDERED. SPHALERITE AND GALENA DISSOLVE MODERATELY AT THE BEGINNING, WHEREAS SPHALERITE IS CONTINUOUSLY DISSOLVED TO THE END, GALENA IS NOT DISSOLVED IN THE FOLLOWING COURSE OF THE BIOLEACHING TESTS AND REMAINS RELATIVELY ENRICHED IN THE RESIDUES. ....	207
<b>FIGURE 4.3.7:</b> CONTENT OF SECONDARY FORMED SULPHATE SPECIES IN BIOLEACHING RESIDUES SAMPLED AFTER CONSECUTIVE RETENTION TIMES WITHIN THE BIOLEACHING OF LUBIN CONCENTRATE LC15B IN RELATION TO CHALCOPYRITE RECOVERY. Pb SULPHATE IS FORMED MAINLY AT THE BEGINNING OF THE BIOLEACHING TEST BUT ADDITIONALLY IN THE PERIOD FROM DAY 2 TO DAY 7. INCREASED AMOUNTS OF SULPHATES FROM DAY 4 TO DAY 10 SEEM TO AFFECT THE DISSOLUTION OF CHALCOPYRITE BY FLATTENING THE SLOPE OF THE CHALCOPYRITE RECOVERY CURVE.....	208
<b>FIGURE 4.3.8:</b> COMPARISON OF CHALCOPYRITE PARTICLES AT DIFFERENT STAGES OF THE LEACHING TEST. LITTLE AFFECTED BY BIOLEACHING (LEFT COLUMN) AND EXHIBITING DISSOLUTION FEATURES WITH VARYING EXTEND (RIGHT COLUMN). (SE-SEM-IMAGES; ANG=ANGLESITE, CCP=CHALCOPYRITE, PY=PYRITE).....	209
<b>FIGURE 5.1:</b> PROCESSING SCHEME FOR THE PROCESSING OF RUDNA AND SANGERHAUSEN BLACK SHALE AS APPLIED IN THE FRAME OF THIS STUDY. ....	215

## LIST OF TABLES

---

<b>TABLE 1.4.1:</b> COMPILATION OF COMMON BASE METAL SULPHIDES AND SOME MINOR AND RARE METAL SULPHIDES AND ALLOYS ASSOCIATED WITH KUPFERSCHIEFER-TYPE MINERALIZATION AND THEIR INVENTORY OF TRACE METALS. ....	14
<b>TABLE 2.4.1:</b> ANALYTICAL METHODS USED FOR GEOCHEMICAL ASSAYS OF DIFFERENT PROCESSING SAMPLES AS COMMISSIONED AT ALS GEOCHEMISTRY, LOUGHREA, IRLAND. ....	25
<b>TABLE 3.1.1:</b> COMPARISON OF PARTICLE SIZES ACHIEVED BY BALL MILLING AT DEFINED PASSING FRACTIONS (20%, 50% AND 80%). (DATA: UVR-FIA).....	30
<b>TABLE 3.1.2:</b> COMPARISON OF PARTICLE SIZES IN BALL MILL AND IMPACT CRUSHER COMMINUTION PRODUCTS OF MANSFELD AND RUDNA BLACK SHALE AT DEFINED PASSING FRACTIONS (20%, 50% AND 80%). (DATA: UVR-FIA) .....	34
<b>TABLE 3.1.3:</b> METAL CONTENTS OF THE DIFFERENT BLACK SHALE COMMINUTION PRODUCTS EXTRACTED FROM GEOCHEMICAL ANALYSES. (DATA: ALS) .....	41
<b>TABLE 3.1.4:</b> COMPARISON OF GRAIN SIZES OF COPPER SULPHIDES IN BALL MILL PRODUCTS OF BLACK SHALES AT DEFINED PASSING FRACTIONS (20%, 50% AND 80%). (M=MANSFELD, R=RUDNA, S=SANGERHAUSEN; DATA: MLA-HIF) .....	44
<b>TABLE 3.1.5:</b> LIBERATION CLASSES OF BORNITE IN BLACK SHALE BALL MILL PRODUCTS. (DATA: MLA-HIF).....	45
<b>TABLE 3.1.6:</b> LIBERATION CLASSES OF CHALCOCITE IN BLACK SHALE BALL MILL PRODUCTS. (DATA: MLA-HIF) .....	46
<b>TABLE 3.1.7:</b> DISTRIBUTION OF CHALCOPYRITE IN BALL MILL PRODUCTS OF BLACK SHALE ORES GROUPED TO LIBERATION CLASSES. (DATA: MLA-HIF) .....	47
<b>TABLE 3.1.8:</b> COMPARISON OF GRAIN SIZES OF COPPER SULPHIDES IN VeRo VeRo LIBERATOR <sup>®</sup> AND BALL MILL PRODUCTS OF BLACK SHALES ORES AT DEFINED PASSING FRACTIONS (20%, 50% AND 80%). (VeRo LIBERATOR <sup>®</sup> _R = ROUND HAMMER TOOLS; DATA: MLA-HIF) .....	61
<b>TABLE 3.1.9:</b> LIBERATION CLASSES FOR BORNITE IN VARIOUS COMMINUTION PRODUCTS. (DATA: MLA-HIF) .....	63
<b>TABLE 3.1.10:</b> DISTRIBUTION OF LIBERATION CLASSES FOR CHALCOCITE IN VARIOUS COMMINUTION PRODUCTS. (DATA: MLA-HIF) .....	64
<b>TABLE 3.1.11:</b> DISTRIBUTION OF LIBERATION CLASSES FOR CHALCOPYRITE IN VARIOUS COMMINUTION PRODUCTS. (DATA: MLA-HIF) .....	65
<b>TABLE 3.1.12:</b> COMPILATION OF RECOVERY DATA FOR CONCENTRATES AND TAILINGS EXTRACTED BY DIFFERENT FROTH FLOTATION APPROACHES FROM RUDNA AND SANGERHAUSEN BLACK SHALE FEED.....	85
<b>TABLE 3.2.1:</b> COMPARISON OF PARTICLE SIZES OF VARIOUS FLOTATION PRODUCTS AND TAILINGS GAINED FROM RUDNA AS WELL AS SANGERHAUSEN BLACK SHALE AT DEFINED PASSING FRACTIONS (20%, 50% AND 80%). (R <sub>M</sub> = MASS RECOVERY). (DATA: MLU) .....	87
<b>TABLE 3.2.2:</b> CONTENT OF BASE METALS AND TRACE METALS IN CONCENTRATES AND TAILINGS GENERATED FROM RUDNA BLACK SHALE FEED. (DATA: ALS).....	97
<b>TABLE 3.2.3:</b> CONTENT OF BASE AND ASSOCIATED TRACE METALS IN CONCENTRATES AND TAILINGS FROM DIFFERENT FLOTATION TESTS USING SANGERHAUSEN BLACK SHALE FEED. (DATA: ALS) .....	103
<b>TABLE 3.2.4:</b> LOCK TYPES OF CHALCOCITE IN FLOTATION CONCENTRATES FROM RUDNA BLACK SHALE FEED. (DATA: PETROLAB)....	110
<b>TABLE 3.2.5:</b> MINERAL ASSOCIATION OF LOCKED CHALCOCITE IN FLOTATION CONCENTRATES EXTRACTED FROM RUDNA BLACK SHALE FEED. (DATA: PETROLAB).....	111
<b>TABLE 3.2.6:</b> LOCK TYPES OF CHALCOCITE IN FLOTATION CONCENTRATES FROM RUDNA BLACK SHALE FEED. (DATA: PETROLAB)....	113
<b>TABLE 3.2.7:</b> DISTRIBUTION OF MINERALS ASSOCIATED WITH LOCKED BORNITE IN FLOTATION CONCENTRATES EXTRACTED FROM RUDNA BLACK SHALE FEED. (DATA: PETROLAB) .....	114
<b>TABLE 3.2.8:</b> LOCK TYPES OF BORNITE IN CONCENTRATES FROM SANGERHAUSEN BLACK SHALE FEED. (DATA: PETROLAB) .....	116
<b>TABLE 3.2.9:</b> PROPORTIONS OF MINERALS ASSOCIATED IN LOCKING ASSOCIATION WITH BORNITE IN CONCENTRATES FROM SANGERHAUSEN BLACK SHALE FEED. (DATA: PETROLAB) .....	117
<b>TABLE 3.2.10:</b> LOCK TYPES OF CHALCOPYRITE IN FLOTATION CONCENTRATES FROM SANGERHAUSEN BLACK SHALE FEED. (DATA: PETROLAB).....	119
<b>TABLE 3.2.11:</b> MINERAL ASSOCIATION OF LOCKED CHALCOPYRITE IN FLOTATION CONCENTRATES EXTRACTED FROM SANGERHAUSEN BLACK SHALE FEED. (DATA: PETROLAB) .....	120
<b>TABLE 3.2.12:</b> BASE METAL CONCENTRATIONS AND CONTENT OF SELECTED TRACE METALS IN DIFFERENT COPPER FLOTATION CONCENTRATES FROM THE LUBIN PROCESSING PLANT, POLAND. (DATA: ALS).....	125
<b>TABLE 3.3.1:</b> CONTENTS OF BASE METALS AND TRACE METAL IN THE MANSFELD BLACK SHALE LOW-GRADE ORE AS WELL AS BIOLEACHING AND STERILE LEACHING RESIDUES. (DATA: BGR) .....	136

## LIST OF TABLES

---

<b>TABLE 3.3.2:</b> COMPARISON OF THE RECOVERY PERFORMANCE FOR SELECTED METALS BY BIOLEACHING AND STERILE CHEMICAL LEACHING OF BLACK SHALE LOW-GRADE ORE FROM MANSFELD, GERMANY. (NOTE: NEGATIVE VALUES REPRESENTED RELATIVE ENRICHMENT IN THE LEACHING RESIDUES) .....	137
<b>TABLE 3.3.3:</b> GEOCHEMICAL DATA OF SELECTED BASE AND TRACE METALS CONTAINED IN THE SANGERHAUSEN BLACK SHALE ORE FEED AND ITS BIOLEACHING AND STERILE CONTROL LEACHING RESIDUES. (DATA: BGR).....	139
<b>TABLE 3.3.4:</b> LEACHING YIELDS FOR BASE AND TRACE METALS ACHIEVED BY BIOLEACHING AND CHEMICAL CONTROL LEACHING OF SANGERHAUSEN BLACK SHALE ORE. (NOTE: NEGATIVE VALUES FOR Pb AND Ag INDICATE A RELATIVE ENRICHMENT IN THE RESIDUES) .....	140
<b>TABLE 3.3.5:</b> MINERAL LEACHING RECOVERY FOR BASE METAL SULPHIDES AS DETERMINED BY MINERAL DISTRIBUTION ANALYSES. (NEGATIVE PERCENTAGES REPRESENT RELATIVE ENRICHMENT) (DATA: MLU) .....	140
<b>TABLE 3.3.6:</b> GEOCHEMICAL DATA OF SOME SELECTED ELEMENTS COMPRISING BASE AND TRACE METAL CONTENTS IN THE SANGERHAUSEN FLOTATION CONCENTRATE, BIOLEACHING AND STERILE CONTROL LEACHING RESIDUES.(DATA: ALS) .....	143
<b>TABLE 3.3.7:</b> RECOVERY RATES OF SELECTED METALS FOR BIOLEACHING AS WELL AS STERILE CONTROL LEACHING TESTS OF SANGERHAUSEN BLACK SHALE ORE FLOTATION CONCENTRATE. ....	144
<b>TABLE 3.3.8:</b> RECOVERY RATES FOR SULPHIDES ACCORDING THE MINERAL DISTRIBUTION ANALYSES OF SANGERHAUSEN COPPER CONCENTRATE FEED, BIOLEACHING AND STERILE CONTROL LEACHING RESIDUES.....	144
<b>TABLE 3.3.9:</b> BASE METAL AND TRACE METAL CONTENT IN THE RUDNA COPPER CONCENTRATE AS WELL AS IN THE RESIDUES OF THE BIOLEACHING AND STERILE CONTROL LEACHING EXPERIMENTS. (DATA: ALS) .....	147
<b>TABLE 3.3.10:</b> RECOVERY RATES OF SELECTED METALS BY STERILE CONTROL LEACHING AND BIOLEACHING TESTS. ....	148
<b>TABLE 3.3.11:</b> LEACHING RECOVERY PROPORTION OF BASE METAL SULFIDES DISSOLVED BY BIOLEACHING AS WELL AS STERILE CONTROL LEACHING TESTS. (DATA: MLU) .....	148
<b>TABLE 3.3.12:</b> ELEMENT CONCENTRATION OF BASE METALS AND SELECTED TRACE METALS IN THE COPPER CONCENTRATE LC15A AS WELL AS THE RESIDUES OF BIOLEACHING AND STERILE CONTROL LEACHING TESTS. (DATA: ALS).....	151
<b>TABLE 3.3.13:</b> COMPARISON OF METAL RECOVERY RATES GENERATED BY STERILE CONTROL LEACHING AND BIOLEACHING OF LC15A.. .....	151
<b>TABLE 3.3.14:</b> PERCENTUAL RECOVERY OF COMMON METAL SULPHIDES BY STERILE CHEMICAL LEACHING AND BIOLEACHING OF LUBIN COPPER CONCENTRATE LC15A. (DATA: MLU).....	152
<b>TABLE 3.3.15:</b> SELECTED METAL ELEMENTS IN THE LUBIN CONCENTRATE LCA06 AND THE CORRESPONDING BIOLEACHING RESIDUES. (DATA: ALS) .....	154
<b>TABLE 3.3.16:</b> METAL RECOVERY BY BIOLEACHING OF LUBIN CONCENTRATE LCA06. ....	154
<b>TABLE 3.3.17:</b> RECOVERY RATES FOR SULPHIDES ATTAINED BY BIOLEACHING EXPERIMENTS ON COPPER CONCENTRATE LCA06. (DATA: MLU) .....	154
<b>TABLE 3.3.18:</b> BASE AND TRACE METAL CONTENTS IN THE FEED CONCENTRATE LC15B AND BIOLEACHING RESIDUES SAMPLED AFTER INCREASING RETENTION TIMES. (DATA: ALS) .....	158
<b>TABLE 3.3.19:</b> LEACHING RECOVERY RATES FOR BIOLEACHING RESIDUES AFTER DEFINED RETENTION TIMES ACHIEVED OF THE CONCENTRATE LA15B. ....	158
<b>TABLE 3.3.20:</b> RECOVERY RATES OF COPPER-BEARING AND ASSOCIATED SULPHIDES BY BIOLEACHING OF COPPER CONCENTRATE LC15B, DETERMINED ACCORDING TO THE MINERAL DISTRIBUTION ANALYSES. (DATA: MLU) .....	159
<b>TABLE 4.1.1:</b> COMPARISON OF COMPOSITIONAL FEATURES AND GRAIN SIZE AS WELL AS ENERGY CONSUMPTION OF BALL MILL PRODUCT FROM DIFFERENT BLACK SHALE DEPOSITS.....	162
<b>TABLE 4.1.2:</b> BOND INDICES FOR DIFFERENT STANDARD MATERIALS WIDELY OCCUR IN BLACK SHALES (FROM WILLS AND NAPIER-MUNN, 2007). ....	164
<b>TABLE 4.1.3:</b> PREDOMINANT MINERAL PHASES ASSOCIATED WITH BINARY AND TERNARY+ LOCKED COPPER SULPHIDES IN BALL MILL PRODUCTS OF DIFFERENT BLACK SHALE FEEDS IN ORDER OF ABUNDANCE.(BN=BORNITE, CARB=CARBONATES, CCT=CHALCOCITE, ILL=ILLITE, PY=PYRITE; DOMINANT MINERALS ARE UNDERLINED) .....	171
<b>TABLE 4.1.4:</b> PREDOMINANT MINERAL PHASES ASSOCIATED WITH BINARY AND TERNARY+ LOCKED COPPER SULPHIDES IN THE VERO LIBERATOR® PRODUCT AND RELATED BALL MILL PRODUCT FROM MANSFELD BLACK SHALE FEED.(BN=BORNITE, CARB=CARBONATES, CCT=CHALCOCITE, ILL=ILLITE, PY=PYRITE, QTZ=QUARTZ; DOMINANT MINERALS ARE UNDERLINED).....	181
<b>TABLE 4.1.5:</b> PREDOMINANT MINERAL PHASES ASSOCIATED WITH BINARY AND TERNARY+ LOCKED COPPER SULPHIDES IN VERO LIBERATOR® PRODUCTS AND BALL MILL PRODUCT OF RUDNA BLACK SHALE.(BN=BORNITE, CARB=CARBONATES, CCT=CHALCOCITE, ILL=ILLITE, PY=PYRITE; DOMINANT MINERALS ARE UNDERLINED) .....	182

LIST OF TABLES

---

**TABLE 4.2.1:** CONCENTRATIONS OF BASE METALS AND ASSOCIATED TRACE METALS IN DIFFERENT COPPER CONCENTRATES PRODUCED FROM DIFFERENT FEEDS. (<sup>A</sup> BLACK SHALE FEED, KGHM; <sup>B</sup> MIXED ORE FEED, KGHM, DATA FROM CHMIELEWSKI (2015) AND CHMIELEWSKI ET AL. (2014A); <sup>C</sup> MIXED ORE FEED, KGHM; <sup>D</sup> BLACK SHALE FEED, UVR-FIA, FLOTATION WITH DEXTRIN AND ETHANOL PRE-TREATMENT OF THE FEED. (GREY BACKGROUND=THIS THESIS)) ..... 195

# Chapter 1 Introduction

## 1.1 Scope of this study

This study aims to the detailed mineralogical characterization of processing products and residues from mineral processing methods comprising comminution, sulphide flotation and bioleaching applied to black shale-hosted Kupferschiefer-type ores from different Mid-European deposits. Numerous studies covering geological and mineralogical features of Permian Kupferschiefer-type black shale rocks have been published to date but spanned investigations of mineral processing products originating from different characteristic black shale deposits are hardly to not available. Studies of processing products are at most directed to technical and operational issues and addresses mainly single upgrading aspects within a process line. Advanced and detailed studies focused on mineralogical features of processing products and residues related to black shale ores provide an important basis for the comprehensive understanding of the behaviour of target minerals affected by physico-chemical treatment methods. Cross-cutting investigations addressing several processing steps within a process chain of a certain ore-type are generally not common. However, a well-established combination of analysis methods coupled with advanced knowledge-based mineralogical information regarding a distinct type of ore deposits applied to related mineral extraction techniques allow conclusions feasible for the problem recognition and represents an interdisciplinary contribution advantageous for engineering tasks.

Advanced mineralogical investigations using granulometry, mineral distribution and liberation analysis as well as microscopy are combined in order to disclose mineralogical and textural attributes focused to copper sulphides, which represent an economically vital copper source in Kupferschiefer-type black shale ores. Quantified mineralogical and textural features were used to delineate the variable behaviour of minerals of interest caused by mineral processing techniques and to assess process-related efficiency in regards to their recoverability by metal and mineralogical mass balances. Investigations in the frame of this study were mainly directed to the following issues:

- distribution of copper sulphides and their liberation state in comminution products generated by different working principles (ball milling vs. impact crushing),
- textural features of copper sulphides in comminution products influencing the recoverability by extractive processing methods,
- recoverability of copper sulphides by different flotation approaches and determination of mineralogical-textural features related to process behaviour,
- dissolution rates of copper and base metal sulphides in bioleaching tests of various black shale-related feed materials and related metal recovery,
- mineralogical composition of bioleaching residues with respect to the quantification of secondary formed mineralic compounds and their influence to the dissolution of copper sulphides.

The main objectives of this study are to highlight improvements by alternative and advanced mineral processing methods of black shale ores, such as impact crushing and refined extraction techniques comprising sulphide flotation and bioleaching, and to define process efficiency prior to

upscaling. Thus, a comprehensive and integrated investigation mainly conducted by SEM-based automated mineralogy of mineral processing products, tailings and residues revealed mineralogical relationships momentous for the assessment of mineral recovery and intended as a contribution to a more energy-saving and efficient metal extraction from black shale ores.

## 1.2 Significance of black shale-hosted Kupferschiefer-type deposits

### 1.2.1 Global distribution

Kupferschiefer-type deposits, first named by Kirkham (1989), are characterized by Cu-Pb-Zn mineralization and are generally assigned to sediment-hosted copper deposits, in which black shale represent a subtype of host rocks sedimented under reduced facies condition (Cox et al., 2003; Kirkham, 1989). Sediment-hosted copper represents the second most common copper resource worldwide, behind largely dominating porphyry copper (69%), and covers currently 12% of the known deposits (Singer, 2017). Sediment-hosted stratiform copper deposits ranging in size from supergiant to small deposits containing a total reserve of 165.48 Mt Cu (Hitzman et al., 2010; Singer, 2017).

Supergiant sediment-hosted deposits occur on several continents, namely in the Zambian (or Katangan) Copper belt, the Kodaro-Udokan Basin of Siberia and the Permian Zechstein Basin of central Europe, the latter hosting black shale associated Kupferschiefer-type mineralization (Hitzman et al., 2005, 2010). Amongst the largest sediment-hosted copper deposits, the Lubin-Sieroszowice mining district in western Poland and the Mansfeld-Sangerhausen mining district in central Germany occupying the second place behind the huge deposits of the Central African Copperbelt. While most of the sediment-hosted deposits are chronologically associated, in terms of geological ages, with Proterozoic rock sequences, the Kupferschiefer-type deposits in northern central Europe are hosted in substantially younger sediments of the Palaeozoic Permian Zechstein (Borg et al., 2012; Cox et al., 2003).

Sediment-hosted deposits associated with black shale are globally distributed as shown in Figure 1.2.1 and include, besides the before mentioned Polish and German Kupferschiefer-type mining districts, renowned deposits, such as White Pine (USA), Nifty Mine (Australia), Tenke Fungurume (DR Congo), Witvlei (Namibia) and Qaleh Zari (Iran).

The economic importance of sediment-hosted deposits illustrates the ranking of the copper resource contained in the Polish Kupferschiefer-type deposits of the Lubin Sieroszowice mining district that represents the fourth copper (26.4 Mt Cu) and first silver (0.11 Mt) resource worldwide, whereas 2.6 Mt of 3.4 Mt Cu and 0.14 Mt of 0.18 Mt Ag, respectively, were extracted by long lasting mining in the former Mansfeld-Sangerhausen until the mine closure in 1990 (Borg et al., 2012; Knitzschke, 1995; Mudd et al., 2013).

Extensive industrial mining of sediment-hosted copper and particular black shale-hosted copper deposits has been taken place over the last 150 years in the Sangerhausen-Mansfeld mining district and 100 years in the Central African Copperbelt, which has remained huge amounts of waste dumps, partially considered at the time of deposition to be low-grade ore economically not exploitable. In recent times the low mineralized material of black shale associated deposits represents copper resources often exceeding the cut-off grade of recent copper mining operations. However, these low-grade ores consist predominantly of fine-grained, organic carbon-rich black shale with extremely fine-grained disseminated base metal sulphide mineralization, which has proven to be extremely difficult

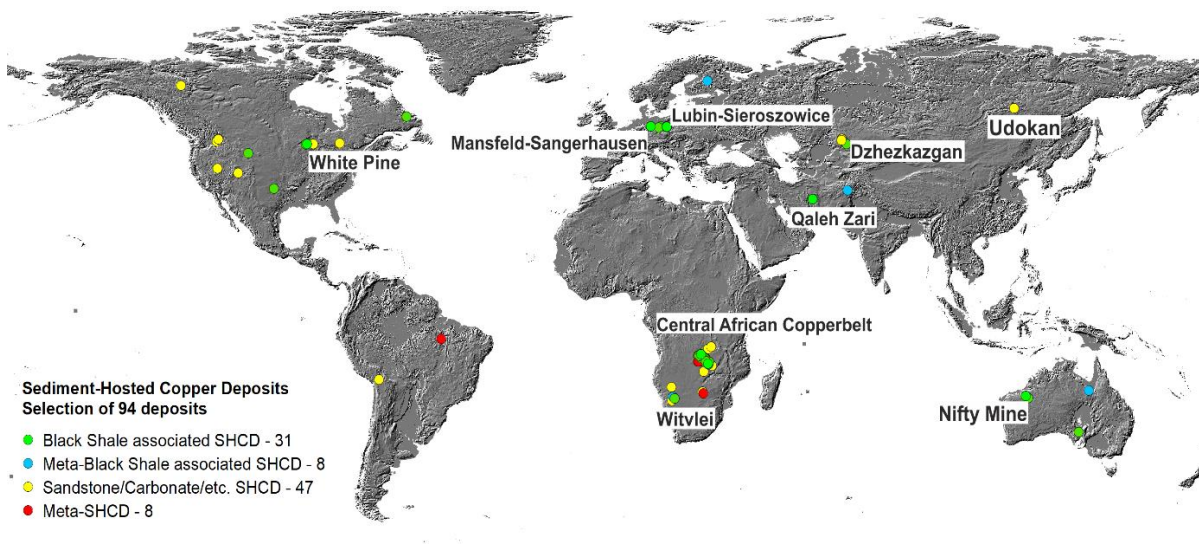


**Figure 1.2.1:** Global distribution of sediment-hosted copper deposits (SHCD) subdivided in black shale, metamorphic black shale, sandstone/carbonate and metamorphic SHCD. Important black shale-hosted deposits or mining districts are indicated by their names (Cox et al., 2003; Mudd et al., 2013).

to process. This is one of the main reasons for the material to still exist as mine dumps. Similar subeconomic low-grade ore and mineralized waste dumps of black shale-hosted copper ores can be found worldwide, e.g., the Polish Kupferschiefer district around Lubin, the African Copperbelt of Zambia and Zaire, and the deposits of Dzhezkazgan, Central Kazakhstan (Bellenfant et al., 2013; Kamradt et al., 2012; Magwaneng, 2019).

### 1.2.2 Occurrence of base and critical metals in black shale-hosted Kupferschiefer-type mineralization

Copper is one of the most demand metals in the industry. It plays a crucial role in the growth of the modern society including technology, infrastructure and building industry. The past decade has seen an increased awareness of both political decision makers and industry alike of the significance of a reliable mineral resource supply. Specifically, the so-called high-tech metals, e.g., copper, platinum, or rare earth elements, are necessary raw materials for numerous technical uses and solutions.

It is widely known that black shales contain commonly increased contents of base and trace metals compared to other sedimentary rocks, even if large areas of black shale formations are not sufficient enriched in metals to be exploitable (Wedepohl, 1964). However, geological features such as tectonic setting, basin position, structurally controlled pathways for metal-bearing fluids as well as redox-sensitive metal trapes of host rocks (clastic sediments, organic-rich shales, limestones) provide, as far as understood by numerous researchers, metal enriched zones within the host rock lithology partly containing economic resources of predominantly copper, lead and zinc and subordinately silver, cobalt, vanadium, nickel, molybdenum, rhenium, selenium and niobium (Borg, 1991; Borg et al., 2012; Hofmann, 2013; Paul, 2006; Rentzsch et al., 1997; Wodzicki and Piestrzyński, 1994)

Generally, copper is the main commodity in black shale associated Kupferschiefer-type deposits, but Zn, Pb, Ag and Co often accompanying the mineralization with economic grades so that these metals are winnable as by-products. However, decreasing copper content of mined ore in deposits of the Lubin-Sieroszowice district is notably striking by Cu grades between 1.4% and 2.6% Cu accompanied

by 44-81 g/t Ag in the ores mined before 2000 (Suchan, 2001) and a decrease over the last decade to current contents of 1.0-1.8% Cu accompanied by 35-51 g/t Ag (Malewski, 2016).

A similar decline of the copper content in the mined ore, but 70 years before, took place at the ore production in the Mansfeld district, in which the ore had 3% Cu initially, but dropped around 1935 generally to 2.5% Cu as well as 0.3–2% Zn and 170 g/t Ag (Gillitzer, 1935). Nearly 50 years later, in the 1980's, the average Cu content of mined ore in the Sangerhausen area decreased to 1.8% Cu and triggered the end of mining operations in 1990. During that period, additional purchased copper scrap feed was necessary to maintain the pyrometallurgical process (Langluettich et al., 1999).

The concentration of U, Au or PGE is partly increased but in sub economic quantities. Especially enrichments of Au and PGE are closely related to the chemically reducing formation conditions of black shales, in which the bottommost layers contain increased amounts of noble metals erratic distributed, as well as to a oxidized hematite-rich facies (miner's term: Rote Fäule) that occur, if present, in spatially proximity basal to the black shale in the footwall Weissliegend sandstone or hanging wall in the dolomite/limestone sequence (Borg et al., 2005; Piestrzyński and Wodzicki, 2000; Wodzicki and Piestrzyński, 1994). Reported anomalously values of noble metals in the Mansfeld-Sangerhausen and Lubin-Sieroszowice mining district ranging between 0.3-1.5 g/t Au and 0.01-0.3 g/t for Pt as well as Pd (Bechtel et al., 2001; Borg et al., 2005; Kamradt et al., 2012; Piestrzyński and Sawlowicz, 1999; Piestrzyński and Wodzicki, 2000). Enormous enrichment of noble metals is closely linked to the clay-organic matrix and bitumen-rich, lenticular thucholite aggregates within black shale (Kucha and Przyłowicz, 1999).

Economic significant sediment layers in the Central African Copperbelt showing mineralization between 3 and 30 metres thickness and contain Cu associated with Co, Ag, Pb, Zn, Pt and Pd with copper grades of 1–3%. The stratiform mineralization is very continuous, which results in partly high tonnages. Generally, value minerals are represented by fine-grained disseminated sulphides, comprising largely of chalcopyrite, bornite, chalcocite, and digenite. Additionally, copper oxides are often enriched in supergene caps that also host economically amounts of cobalt (Hitzman et al., 2012).

### 1.2.3 Mining of Kupferschiefer-type deposits

The mining of the Kupferschiefer-type black shale-hosted copper ore over a timespan of nearly 800 years has formed significant legacies of mining and processing residues within the landscape of the Mansfeld-Sangerhausen mining district. Until the closure of the last mining shaft, 109 Mt of Kupferschiefer ore were mined and processed with an entirely extraction of 2.63 Mt of copper and 14,000 t of silver, as well as byproducts as zinc, lead, cobalt, nickel, rhenium and gold (Knitzschke, 1995; Rappsilber et al., 2008). Mining legacies caused by the mining of ore and subsequent extraction of metal commodities comprise numerous historic small-scaled dumps, tabular dumps piled up from the beginning of the industrial mining age and huge conical dumps, which mark the youngest remnants of the local mining history in the socialistic era as well as tailing ponds of process residues.

Artisanal mining trace the northern boundaries of both districts, where the Kupferschiefer bed outcrops, but can be tracked equally on the western rim of the Mansfeld basin. These small-scale mining shafts reached only few meters depth and left unexceptional wall rocks heaps of 10 to 20 meters, because of the very selective mining during the Middle Age (1200-1600). With increasing quantities of mined Kupferschiefer ore, the new shafts were sunk further basin inwards corresponding with increasing mining depths and volumes of waste rocks deposited on increasing larger heaps/dumps

(mining period 1600-1800). Improvement of mining and extraction techniques led to the mining depths reached over 100 meters with appropriate volumes of wall rocks that has to excavate by the sinking of the deeper shafts.

From about 1850 a new era of mining in the Mansfeld district took place and marks the change to the application of industrial mining methods. In consequence, the mining depths and the size of the dumps rose up further, inherent with increasing stoping heights and extraction of thicker portions of the Kupferschiefer bed towards the hanging wall limestone. Low-grade ore, uneconomic at that time, was stored mostly at a certain part at the top of the tabular dumps and represent nowadays an easily accessible resource. Large scale mining of Kupferschiefer starting from the technology jump after second world war and resulting in large conical dumps in both, the Mansfeld and Sangerhausen district, with heights of up to 150 meters with 300 m diameter, piled up in the Mansfeld area on top of tabular dumps from the former mining era.

Figure 1.2.2 shows an overview of mines extracting Kupferschiefer-type ore recently and in the past as well as occurrences of Kupferschiefer-type related ore explored so far. Mining in the Mansfeld-Sangerhausen district was generally marked by winning of the Permian stratiform black shale-hosted ore, but also stratigraphic adjacent lithotypes, namely the hanging wall Werra limestone/dolomite and footwall Rotliegend sandstone have been mined in several Mid-European Kupferschiefer-type deposits (Richelsdorf, Lower Silesia/SW Poland, Lower Rhine Basin) and are extensively extracted in the Polish Kupferschiefer-type deposits of the Lubin-Sierszowice mining district. Mining of black shale ore in the Mansfeld-Sangerhausen area was exclusively aimed to the processing to recover copper and byproducts in the pyrometallurgical route, which has produced both huge amounts of waste rocks and tailings. The more complete utilization of previously mined waste rocks particularly the black shale-dominated part was the main aspect that has been the focus of research to investigate a feasible



**Figure 1.2.2:** Active and ceased black shale-hosted Kupferschiefer-type deposits and exploration targets in central Europe located at the southern margin of the Zechstein basin. Mining locations from which sample material was obtained for this study are indicated in red (after Borg et al., 2012).

extraction of remaining metals from low-grade copper ores of the Kupferschiefer mining district of Mansfeld in Central Germany (Kamradt et al., 2013, 2012).

Old artisanal mining activities have been also traced in Central African Copperbelt, where copper mining and extraction were proven up to 2000 years before. However, modern industrial mining commenced by instigation of the British administration in 1913. For example, mining in the Zambian Copperbelt has reached the copper production peak in 1969 with 769,000 t of extracted Cu. Shortly later, the mining sector was nationalized in 1973 and production declined reaching the lowest level in 2000, in which just a third of the peak production was extracted (250,000 t Cu). Privatization after 2000 led to a renewed production peak in 2013 with 763,000 t of extracted Cu (Sikamo et al., 2016).

Comparatively much younger mining history is related to the deposits of the Lubin-Sieroszowice mining district that were discovered in the 1960's and comprise currently of four mining operations: Lubin, Polkowice, Rudna and Sieroszowice. The first mine sites were discovered in 1957 during an exploration drilling campaign in the vicinity of the town Lubin and Polkowice followed by the establishment of the shaft constructions in 1960 and completion of the Lubin ore processing facilities as well as the "Głogów" copper smelter in 1968. The largest mine in the Lubin-Sieroszowice mining district represents the Rudna mine, where production started in 1974. Currently, the operating company KGHM Polska Miedź S.A. completed the planning approval program of a new mine site ("Deep Głogów"- Głogów Głęboki – Przemysłowy) in the southern extension to the Rudna and Polkowice Mines, in which the mining depth exceeds 1200 m (Adach-Pawelus et al., 2018; Malewski, 2017, 2016)

### 1.3 Mineral processing methods – past and present

Kupferschiefer-type deposits of Central Europe contain considerable base metal reserves partly associated with increased contents of precious metals (including Cu, Ni, Zn, Pb, Ag, Au, Pt, and Pd) that potentially represent strategic and critical raw materials for Europe. The occurrence of economic potential Kupferschiefer-type ore is linked to sediment-hosted copper deposits of Permian age, in which enrichment zones of ore minerals occur in varying extend over three lithological layers comprising black shale (Kupferschiefer) as well as footwall sandstone and hanging wall carbonate rock. Significant ore mineralization accompanied with increased contents of trace and precious metals are typically for black shale ore. Kupferschiefer-type ore mineralization is polymetallic and characterized by the presence of base metal and complex sulphides variable in the spatial distribution within the stratigraphic horizons as well as concerning their relative proportion. A striking feature of the black shale is the high organic carbon content that exceeds at least 0.5 wt.% and usually varies from 2 to 15 wt.%. The metal-bearing sulphides either occur dispersed as small-sized particles or form stratiform, up to mm-sized layers. Two major difficulties restrict the exploitation of Kupferschiefer-type ores. Firstly, the low efficiency in the recovery of valuable metals by traditional mineral dressing techniques from mining extraction over comminution to metallurgical processes and secondly, their environmental impact. The beneficiation process of copper and by-products was aimed historically and recently to the pyrometallurgical extraction. Since the production costs arise by this energy-intensive processing route paired with the low efficiency in the recovery, alternative mineral processing techniques are required to economically and sustainably improve the recovery rates.

### 1.3.1 Comminution

Generally, the challenge in the processing of ores starts with the reduction of the grain sizes to a liberation degree, in which the desired mineral can be extracted (e.g. flotation, leaching or gravity concentration). A well-established and applied comminution of sulphide ore is a multi-stage process of crushing and grinding, in which the raw ore is fed initially to a primary jaw crusher and subsequently processed by a secondary cone crusher in order to produce a pre-crushed, several mm-sized product, which is in the most cases too coarse-grained for the following extraction process. The required fineness of the comminuted ore is commonly achieved by grinding with ball mills.

Comminution of fine-grained complex ores represents a special challenge in terms of cost-effective particle size reduction and ore liberation in the beneficiation process of metal commodities. The Cu-Pb-Zn-mineralization of Kupferschiefer-type black shale-hosted deposits is largely characterized by minute finely disseminated ore particles and complex intergrowths of base metal sulphides forming microscopic to mesoscopic, bedding parallel linear replacement fillings.

Ball mill grinding has to struggle with potentially serious issues to unlock target minerals. Most prominent and known is the overgrinding effect, in which an undesirable part of the comminution product has been crushed to very fine particles  $< 5 \mu\text{m}$  that are usually not recoverable by e.g. froth flotation. Economically, a considerable portion of the feed material can be lost, because the mass of the particles becomes very low at simultaneous enlargement of specific particle surface and thus, particles are not accessible to be trapped by air bubbles (Chander, 1978). Moreover, fine-grained particles below  $10 \mu\text{m}$  tend to stick together due to adhesive forces, in particular when the feed contains clays or micas. Agglomerated particles, particularly if built up by a mix of gangue and sulphides, will be lost for subsequent processing too, because sulphide particles are shielded by gangue particles, unable to attach to air bubbles in the flotation pulp.

Grain size distribution curves of ball mill products from shale-hosted ore show often that more than 50% of the comminution product ranges below  $20 \mu\text{m}$ . It is questionable; if such fine-grained material can be processed satisfactorily in conventional flotation cells, especially if one has to consider that a part of sulphides was not liberated. Significant lower grain sizes in the final product though can be achieved by the usage of an Isamill, a stirred-medium grinding mill producing ultra-fine products with  $P_{80} < 15 \mu\text{m}$  (Pease et al., 2010).

While copper extraction in the former Mansfeld-Sangerhausen district was exclusively developed to a pyrometallurgical processing scheme, in which elaborative comminution lines were not planned due to the untreated feed of lumpy ore to the first smelter stage (raw copper), the comminution facilities used in mineral processing plants of the Central African Copperbelt and the Polish copper district were designed with energy intense crushing and milling stages. Thus, ball and rod mill circuits as well as recently semi-autogenous grinding (SAG) mills, are commonly set up downstream to primary crusher stages mainly jaw crushers (Simubali and Chileshe, 2013; Whyte et al., 2001; Wieniewski and Skorupska, 2016).

A main issue of comminution units of the three concentrator plants (Lubin, Rudna, Polkowice) in the Lubin-Sieroszowice mining district represent the varying grain size of sulphides in different feed lithotypes that requires special grinding treatment for sandstone ( $\sim 100 \mu\text{m}$ ), black shale ( $\sim 35 \mu\text{m}$ ) and dolomite ( $\sim 45 \mu\text{m}$ ) in order to improve the restricted liberation of copper sulphides (pers. comm. Kajetan Witecki, CUPRUM). In particular, the black shale fraction in the mixed copper ore fed to the flotation plant suffers on low liberation of copper sulphides and cause recovery difficulties in the

flotation products (Luszczkiewicz and Chmielewski, 2008; Wieniewski and Skorupska, 2016). Increasing portion of black shale-hosted ore in the feed to the copper concentrators has nearly doubled in the last 20 years and reached maximum proportions (up to 27 %) in the feed to the Lubin processing facilities (Luszczkiewicz et al., 2012)

Comminution in mineral processing plants of the Central African Copperbelt is subdivided in comminution units that on the one hand treat oxidized ore by several rod and ball mills stages and on the other hand comminute sulphide ore by several parallel closed ball mill circuits. However, a replacement since the 2000's by comminution lines consisting of semi-autogenous grinding mills coupled with ball mill-cyclones circuit were implemented at several large mine operations in the Central African Copperbelt (Barry Wills, 2012, MEI Blog 13.08.2012; Simubali and Chileshe, 2013).

New developments of alternative comminution techniques to be implemented in crushing and milling circuits are desired, even if energy costs rises due to decreasing ore grades simultaneous with more complex and finer mineralization in the feed. Thus, comminution lines provided with significantly lower specific power consumption at enhanced liberation of the sulphide ore are requested and the application of alternative comminution methods can offer a substantial cost and energy-saving contribution for an additionally improved extraction of complex sulphide ores.

### 1.3.2 Flotation

The recovery of copper from black shale-hosted ore was extensively practised pyrometallurgically in the former Kupferschiefer mining district of Central Germany. Although efforts to implement flotation for black shale feed < 5 mm (losses from the mine input) were approached, it was never realized on production level. Flotation represents the main copper winning technology of recently mined black shale-hosted ores in the Polish and Central African copper mining districts. Volatile price developments on the metal markets and increasing production cost at currently decreasing copper content in the ore (Chmielewski, 2015) require more efficiency in the established process chain or the introduction of alternative energy- and resource efficient processing technologies. Such new processing options either aim to the adaption and improvement of existing process protocols, e.g., for froth flotation, or to the substitution of an uneconomic process unit, e.g. pyrometallurgy by (bio)-hydrometallurgy.

However, the flotability of copper sulphides in black shale ores is a challenge due to its fine-grained intergrowth of valuable minerals and special carbonaceous and argillaceous composition. With regard to achieve improvements in the recovery of copper by froth flotation, numerous tests were carried out in the past and recent decades. In 1932, Aletan investigated the flotation of black shale ore from Niedermarsberg and Mansfeld mines. He already described that the high content of organic compounds impairs a selective flotation of copper minerals. Babiński et al. (1978) and Kleiner et al. (1987) reported a setback in the approach to increase the recovery of sulphides by flotation caused by the abundance of clay minerals and elevated organic carbon contents. Hammami (1980) paid close attention to eliminate or passivate the organic carbon in the flotation of black shale ore. For example, he tried to extract the bituminous components with solvents of the coal and oil shale extraction industry, but only reached low recovery yields.

Black shale is also considered to be a hard-to-treat feed in the mineral processing plants of the Polish Kupferschiefer-type deposits (Chmielewski and Luszczkiewicz, 2010). Generally, flotation circuits designed for the extraction of copper-bearing sulphides from mixed ore feed (sandstone, black shale, dolomite) in the three Concentrator plants consist of a rougher-scavenger stage and a downstream

multistage cleaning flotation (Figure 1.3.1). Middlings containing often intergrowths with very fine-grained sulphides cannot be extracted satisfactorily and are fed back to a hydrocyclone-ball mill stage in order to feed again in the flotation circuit (Chmielewski and Luszczkiewicz, 2010). Concentrates extracted in the flotation units of the Concentrator plants are dried and contributed directly to the copper smelters located in Legnica and Głogów.

The increasing amount of black shale in feed of Polish copper concentrators in the Lubin-Sieroszowice mining district causes decreasing Cu recovery yields accompanied by shrinking Cu content in concentrates, which also affects the recoverability of Ag. Copper concentrates gained from porphyry copper ore show usually a recovery yield of 90% at 25% Cu. Copper extraction was generally less efficient in the flotation of mixed ore processed in Polish flotation plants, where produced copper concentrates contain usually 17-20% Cu at 90% Cu recovery. The increasing black shale portion in recent years, for instance 8% in the 1990's vs. 15% in 2004 in the feed for the Lubin Concentrator, causes losses in the Cu recovery and declines the copper content in the concentrates notably (86% recovery @ 14% Cu, Lubin concentrate in 2004) (Chmielewski, 2015; Chmielewski and Kaleta, 2011). A further decline of the copper content in the concentrate in the actual production demonstrates the deterioration of the copper sulphide recovery mainly associated with the extremely fine-grained nature of the mineralization hosted in black shale feed. This is particularly disadvantageous if it is considered that nearly 25% of the Cu resource and the main portion of associated metals is hosted in black shale layers of the Lubin-Sieroszowice mining district (Chmielewski et al., 2008).

To raise the recovery of copper sulphides by flotation of black shale ore generally, it demands finer grinding but it is additionally questionable; sufficient grinding and liberation is provided, if such fine-grained material can be processed satisfactorily in conventional flotation cells, especially if one has to

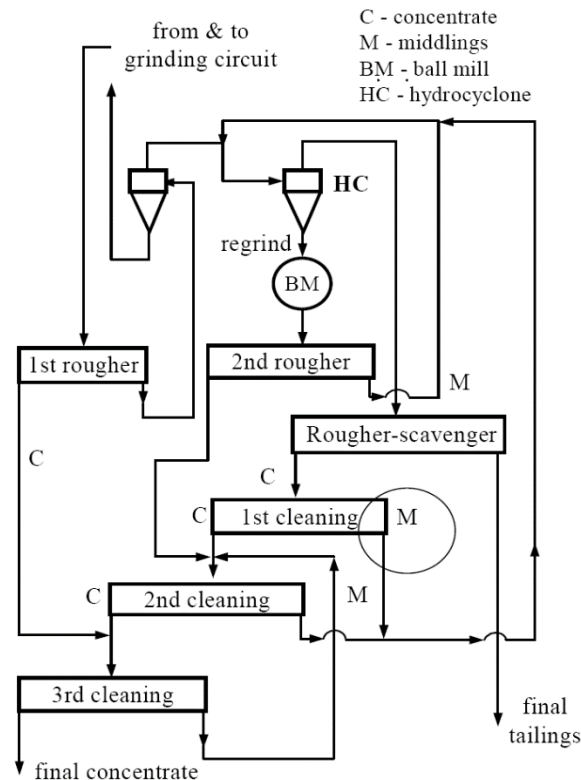


**Figure 1.3.1:** Simplified flow sheet of flotation circuits operated in the Lubin Concentrator, Poland (Luszczkiewicz and Chmielewski, 2008).

consider that a part of the sulphides were not liberated. Otherwise, with the slowly established column flotation it is economically possible to increase the recovery of fine particles by flotation (Abd El-Rahiem, 2014). Recent flotation tests of the UVR-FIA GmbH (Freiberg, Germany) with black shale ore promised a high copper recovery in combination with high copper content using a new pre-treatment method for flotation tests, from which concentrates and tailings are detailed investigated in this study.

Ore feed from the copper mines in the Central African Copperbelt is processed separately. While oxide ore from open pits is dressed by acid leaching in leach plants, the sulphide ore mined in underground mines is partly processed by scavenger flotation on site and subsequently fed to rougher flotation units in the Concentrator plant reaching a concentrate with 15-20% Cu, which is further processed by column flotation achieving a high-grade copper concentrate (38-45% Cu). Tailings from the column flotation are pumped back to scavenger flotation, from which tailings are treated subsequently in the tailing leach plant in order to recover acid soluble copper, The copper-rich concentrates are commonly blended with iron-rich concentrates from other mines of the mining district in order to feed the mixed concentrate to the Nkana smelter at Kitwe or the Mufulira smelter (Mpongo and Siame, 2011).

### 1.3.3 Bioleaching

In the last decade several research projects were dedicated to the development of bioleaching processes for the treatment of black shale ores. Due to the presence of significant amounts of carbonate in the ores, bioleaching in stirred tank reactors was proven to be more efficient than by heap leaching that is more uneconomic due to operational aspects, such as carbonate and clay contents as well as related acid consumption (Brierley, 2008). However, the influence of the operating parameters on leaching kinetics and metal yields is often difficult to interpret due to the complexity of the ore mineralogy. In particular, metal mass balances commonly used to assess bioleaching efficiency are not enough to identify the leaching limitations (Kutschke et al., 2015).

As conventional copper extraction via smelting has been extremely energy-consuming, (bio)-hydrometallurgy in combination with electrowinning represents a low-cost and environmental-friendly and energy-saving extractive method to win copper products. Studies on the processing of low-grade Kupferschiefer ore and dump material by bioleaching started in the 1970s in laboratory and pilot scale percolator experiments to simulate heap bioleaching and has been relaunched recently (Kamradt et al., 2012). Further experimental work within the European project “Bioshale” (d’Hugues et al., 2007) lead from bench scale to pilot scale for bioleaching of a copper concentrate from KGHM Lubin mine in Poland. This was produced from an organic-rich ore by flotation. This carbonate-rich, multi-element (Cu, Ag) and polymineral concentrate contained chalcocite, bornite, chalcopyrite and covellite. Given the fine nature of the concentrate and its carbonate content, stirred tank bioleaching was applied instead of heap leaching. The best copper recovery obtained in the continuous operation was 92% within 6.6 days at 15% solids content in 60 L operating volume in three consecutive bioreactors, and hot brine leaching of the bioleaching residue (PLINT Process) permitted the recovery of 92% of the silver. Copper recovery seemed to be limited by incomplete chalcopyrite dissolution. Final copper recovery was higher in batch cultures (> 95%) than in continuous mode (Spolaore et al., 2011, 2009). Further experimental work on testing a higher solid load was done within the European project “Promine” (<http://promine.gtk.fi/>). The bioleaching performances at 25% solids were similar to those obtained in “Bioshale” with 15% solids at the same operating conditions. However, the incomplete dissolution of chalcopyrite was confirmed which remains a key issue for copper ore

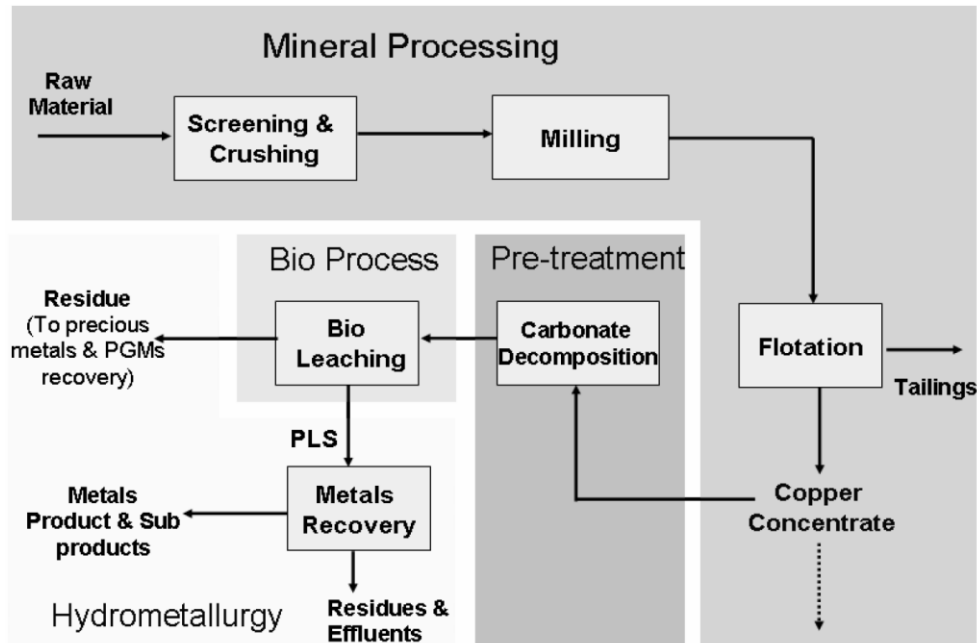


**Figure 1.3.2:** Process flow for bioleaching of Lubin concentrate developed within the “Bioshale” project (d’Hugues et al., 2007).

bioleaching improvement (Ahmadi et al., 2011; Schippers et al., 2013; Watling, 2014, 2006). Improvement required further investigations which are partly presented here in order to ensure an optimal control of the process for upscaling in the German-French project “Ecometals” (Kutschke et al., 2015).

Recent approaches to implement bioleaching as alternative in-situ technology was aimed to deep lying deposits of more than 1000 m depth, where in-situ leaching coupled with bioleaching was applied to copper ore (mainly sandstone) at three underground tests sites of KGHM owned Rudna Mine in the frame of the European research consortium “BioMore” (Filippov et al., 2017; Pakostova et al., 2017).

Further considerations to implement as well acid leaching as bioleaching units at Concentrator plants in the Lubin-Sieroszowice mining district were directed to improve the recovery of middlings arise from flotation circuits (Chmielewski, 2015).

## 1.4 General aspects of black shale-hosted Kupferschiefer-type mineralization

The Permian black shale that represents the base unit of the Central European Zechstein basin is one of the world's largest sediment-hosted copper deposit (Borg et al., 2012; Cox et al., 2003) and widely known as Kupferschiefer-type ore. Base metal enrichments are located at the southern edge of the Permian Basin (Germany & Poland) and they are spatially related to northeast-southwest trending faults (Borg, 1991). However, black shale and its adjacent lithological units contain no significant enrichment of base metals over wide areas of the Zechstein basin, in which only syndimentary pyrite occurs associated with black shale (Oszczepalski, 1999). The ore-bearing mineralization is locally distributed over several sedimentary units, comprising of Permian sandstone overlain by the basal black shale (T1) as well as limestone/dolomite (Ca1) of the marine Werra carbonate and evaporite cycle (Z1) (see Figure 1.4.1). Commonly, the black shale unit contains the most significant ore grades. Variations on the ore distribution is displayed by different grades of base metal sulphides in the footwall as well as hanging sequence. In particular parts of the Polish Lubin-Sieroszowice district, but also the former Richelsdorf mining district, are characterized by an economically relevant occurrence of copper sulphides in the footwall sandstone and hanging wall dolomite. Ore mineralization, if present, varies strongly in quantity and stratigraphic position so that the thickness of the ore zone can reach from centimetres up to several meters (Kopp et al., 2008; Vaughan et al., 1989).

The occurrence of significant ore grades in the Sangerhausen mining district is mainly limited to the thin black shale layer (< 20 cm), whereas in the neighbouring Mansfeld district markedly enrichments

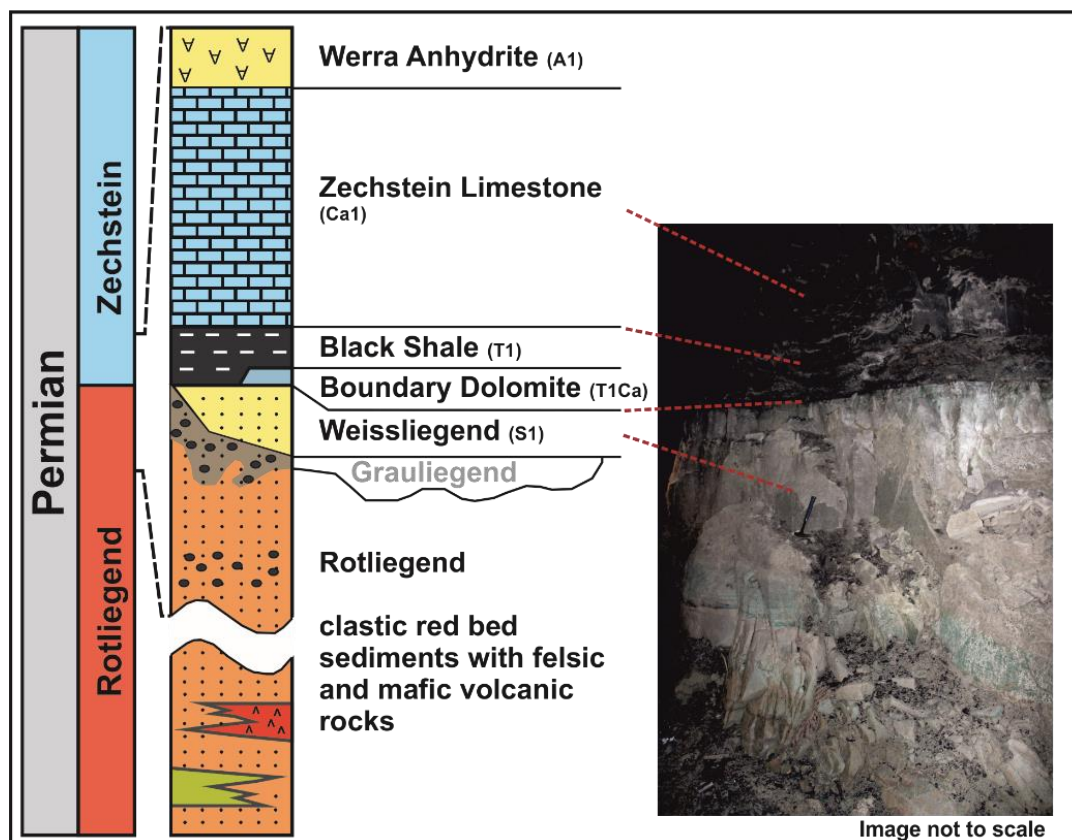


**Figure 1.4.1:** Stratigraphic column and members of the Lower Permian that form the host rocks of Kupferschiefer-type mineralization indicated by red dashed lines on the adjoining photograph from a stope of the Rudna underground mine in the Polish Lubin-Sieroszowice mining district.

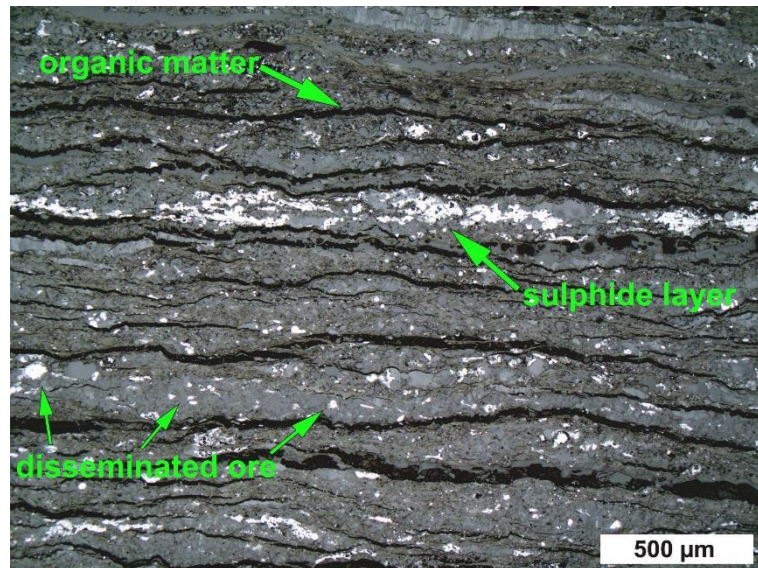


**Figure 1.4.2:** Reflected-light-image of a polished section shows the variable distribution of sulphide ore minerals within the black shale. Sulphides randomly distributed characterize the disseminated fraction, otherwise they form bedding-parallel fillings clearly delimited by organic matter-clay bands.

of base metal sulphides extends from the contact zone of footwall sandstone, stratigraphically determined as Weissliegend, to the black shale up to decimetre into the Werra limestone. The Polish Kupferschiefer-type deposits of the Lubin-Sierszowice mining district host substantial parts of the ore mineralization associated with the footwall sandstone, where ore zones can reach several meters thickness, passing into black shale interfingered with the Boundary dolomite unit and further into the hanging wall dolomite (Borg et al., 2012; Oszczepalski, 1989; Piestrzyński and Wodzicki, 2000).

Lithologically, black shale is a finely laminated carbonaceous marl, mainly composed of quartz, carbonates (calcite/dolomite), feldspars, clays (mainly illite), organic matter (kerogen type II) and varying portions of Cu-, Pb-, Zn- and Fe-sulphides, depending on the ore zone. The grade of base metal sulphides can change in short intervals from barren to highly enriched within lateral sections of the black shale layer. Additionally, the base metal mineralization occurs lithologically layer-overlapping by transitional enrichment zones of sulphides in the footwall sandstone as well as in the hanging wall limestone sequence.

Black shale shows a typical layering and is dark anthracite to dark grey due to the high portion of organic matter. Besides the layered rock fabric, black shale ore is partly characterized by crosscutting veins hosting barite and various carbonate minerals as well as sulphides. More common are bedding parallel vein fillings of up to several millimetres thickness and mostly associated with replacement of base metal sulphides. The sulphide assemblage associated with Kupferschiefer-type mineralization contains chiefly bornite, chalcopyrite, chalcocite, galena, sphalerite and pyrite (see Table 1.4.1). Besides these economically important ore minerals, Ni-Co-arsenides (cobaltite-gersdorffite), covellite, idaite, tetraedrite-tennantite and others occur subordinate and sporadically in individual deposits. Cu-Ag-sulphides (e.g. stromeyerite) and silver minerals as well copper-bearing sulfosalts (bournonite or famatinite) as native silver represent metal mineral species that exist rarely in Kupferschiefer-type deposits. However, minor sulphides and rare copper-bearing sulphides as well as metal phases contribute to a considerable part to the content of trace metals associated with black shale ore.

**Table 1.4.1:** Compilation of common base metal sulphides and some minor and rare metal sulphides and alloys associated with Kupferschiefer-type mineralization and their inventory of trace metals.

	<b>Mineral</b>	<b>Formula</b>	<b>Trace element</b>
<b>Main sulphides</b>	bornite	Cu <sub>5</sub> FeS <sub>4</sub>	Zn, As, Co, Ni, Ag
	chalcocite	Cu <sub>2</sub> S	Fe, Ag
	chalcopyrite	CuFeS <sub>2</sub>	Pb, As
	galena	PbS	Zn, Cu, Fe, Ag, Se
	pyrite	FeS <sub>2</sub>	Zn, Cu, As, Co, Ni
	sphalerite	ZnS	Cu, Fe, Cd
<b>Minor sulphides</b>	cobaltite	CoAsS	Ni, Cu, Fe
	covellite	CuS	Fe, Se, Ag, Pb
	enargite	Cu <sub>3</sub> AsS <sub>4</sub>	Sb, Fe, Pb, Zn, Ag, Ge
	gersdorffite	(Ni,Co)AsS	Cu, Fe, Ag
	idaite	Cu <sub>5</sub> FeS <sub>6</sub>	
	tennantite	Cu <sub>6</sub> [Cu <sub>4</sub> (Fe,Zn) <sub>2</sub> ]As <sub>4</sub> S <sub>13</sub>	Zn, Co, Ni, Ag
	tetraedrite	Cu <sub>6</sub> [Cu <sub>4</sub> (Fe,Zn) <sub>2</sub> ]Sb <sub>4</sub> S <sub>13</sub>	Sb, Bi, Pb
<b>Rare metal phases</b>	acanthite	Ag <sub>2</sub> S	Se
	bournonite	PbCuSbS <sub>3</sub>	As, Ag, Fe, Zn, Mn, Ni
	eugenite	Ag <sub>11</sub> Hg <sub>2</sub>	Cu
	famatinite	Cu <sub>3</sub> SbS <sub>4</sub>	Zn, As, Fe
	native silver	Ag	Cu
	roxbyite	Cu <sub>9</sub> S <sub>5</sub>	Fe
	stromeyerite	AgCuS	Pb, Fe

### 1.4.1 Styles and textures of sulphides in black shales of the Kupferschiefer-type mineralization

The main part of the ore mineralization occurs as fine disseminated sulphide particles within the layered rock fabric, which often consists of intimately intergrowths of several sulphides or sulphides with gangue minerals (Figure 1.4.3). Another ore texture that can be observed in the black shale ore is indicated by bedding-parallel replacement fillings marked by more massive, up to several mm thick sulphides layers, in which the sulphides are partially intergrown more coarse-grained chiefly with carbonate minerals.

The grain size of sulphide particles ranges commonly from few to hundred micrometres (µm), but the majority of ore particles covers the grain size range between 30 and 70 µm. However, ore particles can partly exceed hundreds of microns especially in the vein-type associated ore.

The disseminated ore displays different textural features, of which lenticular shaped sulphide particles mostly elongated within the stratified rock fabric represent a common pattern (Figure 1.4.4 & Figure 1.4.5). Additionally, band-like streaky sulphides occur closely intergrown with illite-kerogen associations and were presumably formed by replacement of carbonate clasts (Figure 1.4.6 & Figure 1.4.7). A striking feature between primary and secondary carbonates occurring within the stratification of the black shale represents the state of conservation. Primary, sedimentary carbonate particles show commonly corroded particle rims often thinly coated with iron oxyhydroxide, whereas secondary

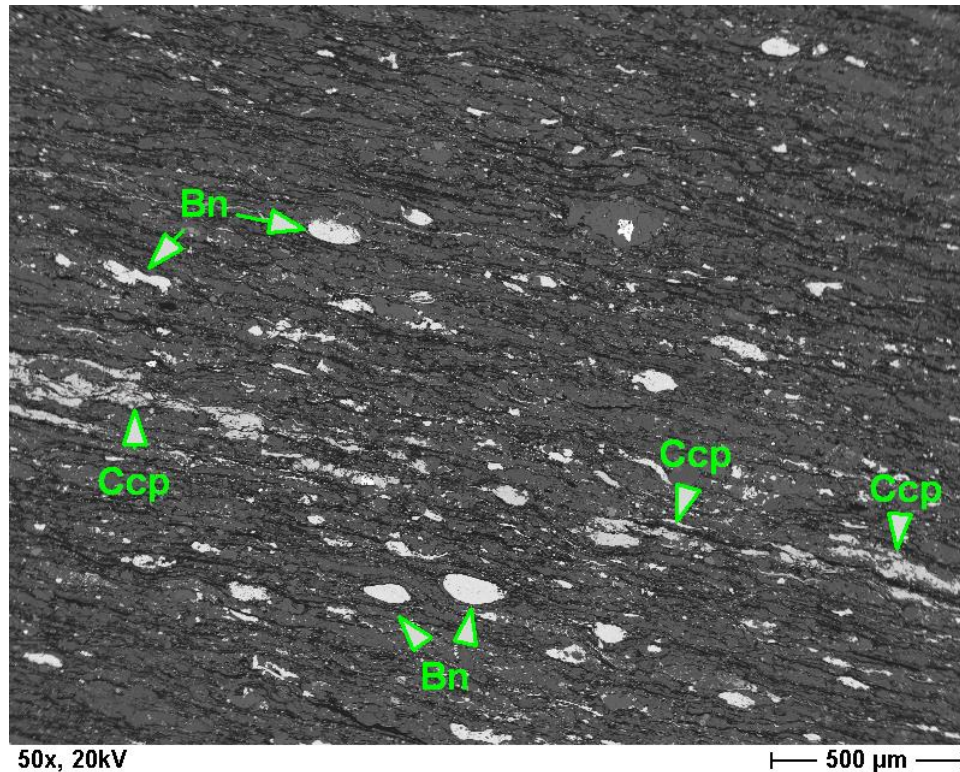


**Figure 1.4.3:** Typical ore textures in Kupferschiefer-type black shales. The sulphide particles occur finely dispersed within the finely laminated rock matrix or form intricately intergrowths of several sulphides or gangue. (Bn= bornite (brighter), Ccp= chalcopyrite (more greyish); polished section, BSE-SEM-image)

carbonate particles formed by a later hydrothermal stage display fresh, unaltered crystal shapes. Partly euhedral sulphide crystals occur mainly associated with secondary carbonate minerals in veins fillings or as replacement of pores or interstices. The latter resulted by dissolution of the carbonatic-clayey cement of the initial rock fabric and provided voids, in which irregular aggregates comprising intimately intergrowth of several sulphides and carbonate minerals are located. In parts where this replacement type dominates, network-like aggregates of intensely intergrown sulphides forming complex ore textures occur commonly. Sedimentary formed pyrite framboids are very common and irregularly distributed within the black shale stratification. The size of framboids exceeds 5 microns rarely and framboids larger than 20 microns occur exemplarily. In mineralized zones, the initial pyrite framboids are partially to completely replaced by other base metal sulphides. Moreover, framboidal pyrite seems to be serve as nucleus of a later stage of sulphide formations that overgrow pyrite crystals of framboids without replacing them.

The most prominent feature of vein-type mineralization in Kupferschiefer-type black shale are several millimetres thick sulphide layers embedded along the black shale stratification consisting of a particular sulphide, usually bornite or chalcopyrite, or containing rather coarse-grained intergrowths of both sulphides. The proportion of intergrowths of sulphides and gangue minerals (illite, dolomite, quartz) increases markedly in less massive and consistent sulphide layers, which also exhibit more irregular crystal shapes of sulphides.

Cross-cutting veins as shown in Figure 1.4.8 and Figure 1.4.9 are less common and characterized by fillings either of massive sulphides or carbonate (calcite, ankerite) and barite dominated intergrowth with base metals such as chalcopryrite, bornite or chalcocite. In this association partly euhedral sulphide crystals are interlocked with rhombohedral carbonate minerals or grainy to tabular barite.

A further ore texture is closely linked with the occurrence of fossil remnants (Figure 1.4.10 & Figure 1.4.11). Partly to complete replacements of predominantly mollusc shells can be found rather rarely with the stratification layers of the black shale. Sulphide associated with lensoidal apatite of biogenic origin occur occasionally and form linings or fill cavities.

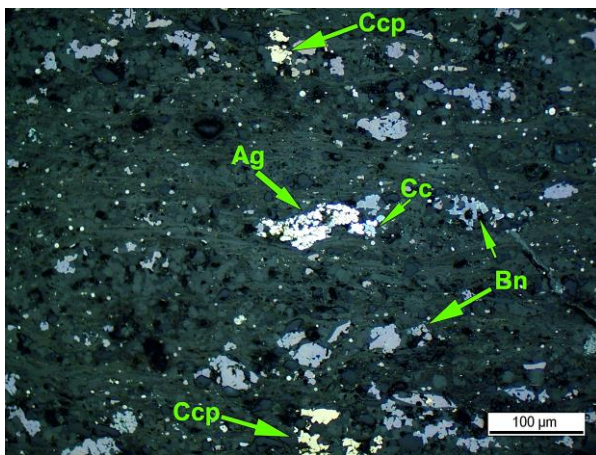


**Figure 1.4.4:** Disseminated copper ore particles in the black shale characterized by a patchy copper sulphide-silver-assemblage consisting of bornite (Bn), chalcopryrite (Ccp) and chalcocite (Cc) as well as silver (Ag). (Mansfeld district, reflected light)

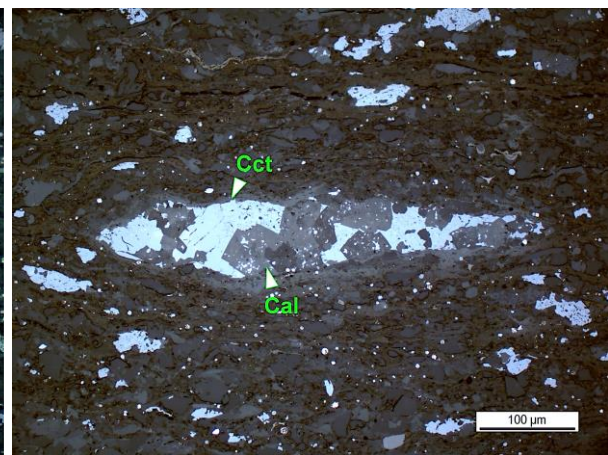


**Figure 1.4.5:** Lensoid replacement consisting of chalcocite intergrown with subeuhedral calcite crystals surrounded by mostly irregular shaped chalcocite particles embedded within the black shale bedding. (Mansfeld district, reflected light)

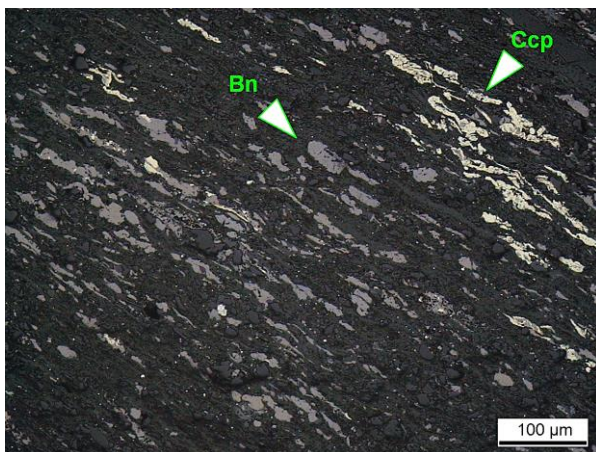


**Figure 1.4.6:** Lenticular, band-like alignments of bornite (Bn) and chalcopryrite (Ccp) aggregates oriented within the stratification of the black shale. (Sangerhausen district, reflected light)

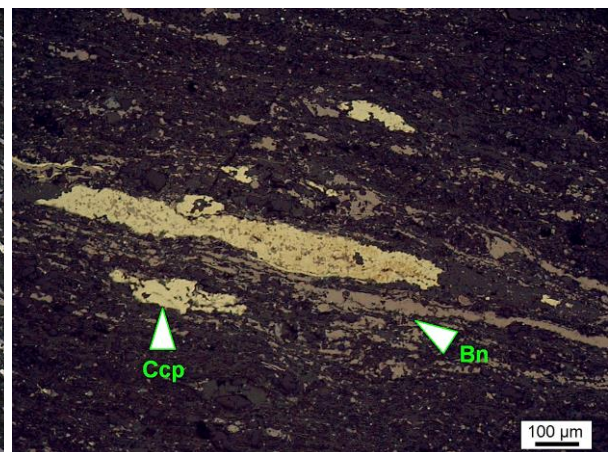


**Figure 1.4.7:** Elongated aggregates of chalcopryrite (Ccp) oriented within the stratification of the black shale surrounded by thin bands and streaks of bornite. (Sangerhausen district, reflected light)

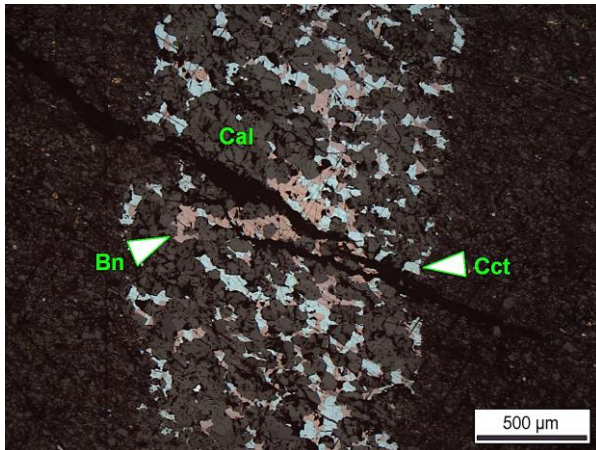


**Figure 1.4.8:** Cross-cutting vein consists of intergrowths of bornite, chalcocite and calcite showing subhedral to anhedral crystals. (Sangerhausen district, reflected light)

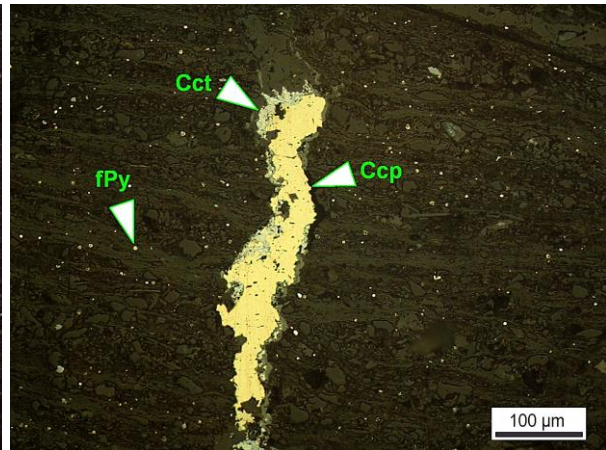


**Figure 1.4.9:** Massive cross-cutting vein filled with chalcopyrite partly intergrown and lined by chalcocite and carbonate minerals. Irregularly distributed small yellow dots indicate μm-scaled sulphide framboids (Sangerhausen district, reflected light)

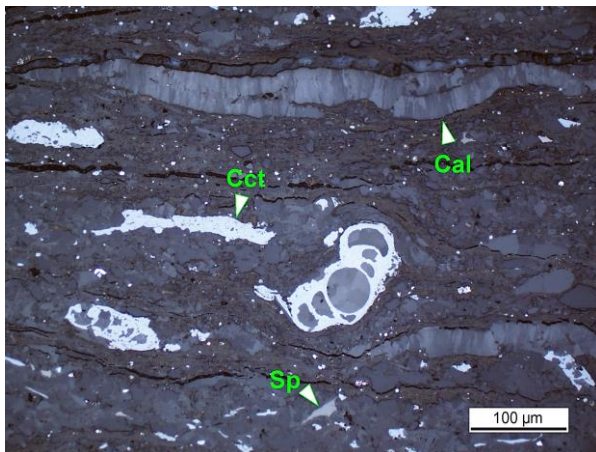


**Figure 1.4.10:** Microphotograph showing replacement of calcareous fossil shells as well as irregular elongated fillings by chalcocite. Slightly undulating calcite bands occur commonly within the stratification of the black shale. (Mansfeld district, reflected light)

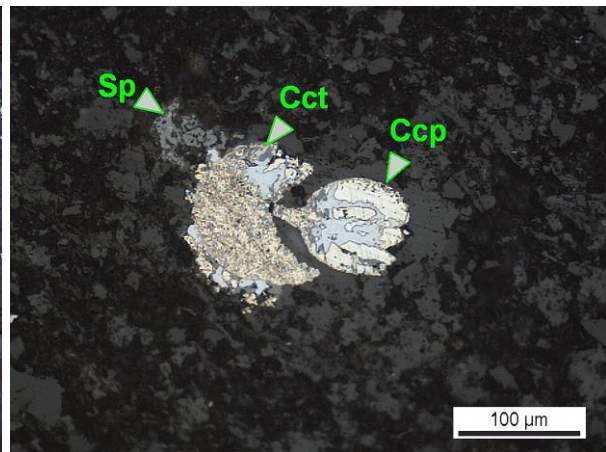


**Figure 1.4.11:** Irregular intergrowth of chalcopyrite and chalcocite replacing a fossil remnant. (Rudna mine, reflected light)

## Chapter 2 Methods

### 2.1 Feed samples

#### Mansfeld black shale

A large-scaled sampling by the usage of an excavator was carried out on the tabular dump part of the dump complex of the former Fortschritt-(I)-Shaft-Mine, which is located in the north-eastern vicinity of the town Eisleben, Mansfeld-District, Germany. Blocky black shale low-grade ore, not subjected to further processing at the time of deposition (1923-1949), represented an upper layer on top of the dump reaching a thickness up to 7 m determined by drill holes (Knobloch, 2015). During the sampling campaign in 2007, the uppermost layer (1 m) was removed and approximately 250 tons of not weathered material from deeper levels of the dump were extracted in technical scale using an excavator and stored in Helbra. Later in 2014, a bulk sample of 950 kg was separated and shipped to the UVR-FIA GmbH, Freiberg/Saxony (UVR-FIA) in order to be comminuted for mineral processing test works. Hand specimen for mineralogical investigation were taken individually from the dump as well as the separated bulk sample and used for geochemical and mineralogical investigations.

#### Sangerhausen black shale

A further black shale bulk sample from central Germany of about 200 kg was provided by an underground drilling campaign in a ventilation tunnel (level 1 in 238 m depth) of the “Roehrig” shaft, part of the Thomas Muentzer Mine in the former Sangerhausen mining district, Germany. 17 drill cores with 10-cm diameter and more than 1m length of fresh, not oxidized sample material were extracted bedding-parallel and along the lower black shale base from a 15 meter wide area of the tunnel.

Drill cores were subjected to a geochemical screening using a portable XRF-Analyzer (Niton XL3t 900 He, Thermo Scientific) and subsequent selected according to increased copper contents. The selected sample material was shipped to UVR-FIA in order to be comminuted for mineral processing test works. Individual parts of the copper-rich as well as remaining drill cores were sampled small-scaled to carry out mineralogical investigations.

#### Rudna black shale

A third bulk sample of black shale ore was provided from KGHM Polska Miedź S.A. (KGHM) in 2015 and was extracted from the active part of the Rudna I Mine in Polkowice located 15 km NNW of Lubin, western Poland. The bulk samples, also sandstone and dolomite sample were provided in the frame of the sampling campaign, were extracted at a mine level of 1100 m depth. Desired sample material was blasted from the stope wall, sorted after lithotypes and packed into big bags by mine staff of KGHM. Additionally, hand specimen for geochemical and mineralogical investigations were collected from the heaps of blasted material. The bulk samples were shipped for further processing to UVR-FIA for crushing, splitting and milling.

#### Lubin concentrates

Copper flotation concentrates exclusively used for bioleaching tests originated from the KGHM-owned mineral processing facilities in Lubin, western Poland. Generally, the copper concentrate is produced by flotation of various feed-types representing a mix of ore-bearing run-of-mine lithotypes (sandstone, black shale, dolomite) from the Lubin Mine of the Lubin-Sieroszowice mining district, SW Poland.

Commonly, the feed is dominated by sandstone ore (60%), but varies in respect to the black shale portion (15–25 %) (Chmielewski, 2015). Thus, the composition of the Lubin concentrate can vary, which can be attributed to changing portions of feed material and production period.

In this study, two different samples of Lubin copper concentrate were investigated in relation to residues of bioleaching test series. A concentrate (LCA06) produced in 2006 from mainly organic-rich ore feed was used for bioleaching tests conducted in the mineral processing pilot plant of the French Geological Survey (Bureau de Recherches Géologiques et Minières, BRGM) in Orleans, France, in the frame of the “Bioshale” research project (2004-2008; d’Hugues et al., 2007). This concentrate was subjected to a pre-treatment (acidification) by sulfuric acid to remove the carbonate mineral fraction prior to subsequent bioleaching experiments.

A further concentrate (LC15) provided by KGHM in 2015 represented the feed material for bioleaching tests conducted by the Geomicrobiology group of the Federal Institute for Geosciences and Natural Resources (BGR) in Hannover, Germany, and BRGM in the frame of the French-German research project “Ecometals” (2013-2017; Kutschke et al., 2015). Two splits (LC15a and LC15b) of concentrate LC15 existed and were mainly used for extractive metallurgy tests. The main batch (LC15b, 3.8 t) was delivered to BRGM for distribution to French project partners, whereas a small split (LC15a, 10 kg) was shipped to UVR-FIA in order to be split and redistributed to German project partners.

## 2.2 Test work

Black shale bulk samples were mainly comminuted using a multi-stage comminution line equipped with conventional technique set-up. Additionally, selected bulk samples were comminuted by a VeRo Liberator® impact crusher in single throughput mode. The milled ore was mainly used to perform flotation tests in order to generate copper pre-concentrates. The copper concentrates in turn were utilized for bioleaching batch tests. Comminuted black shale ore, flotation product and tailings as well as residues from bioleaching and sterile control tests were investigated in this study.

### 2.2.1 Comminution

#### 2.2.1.1 Ball milling

Comminution as well as comminution tests producing final ball mill products were exclusively carried out in the pilot plant facilities of the UVR-FIA GmbH, Freiberg/Saxony, Germany. Bulk samples from three sample locations were treated by different comminution lines. Equipment used comprised in general a primary jaw crusher (Pulverisette 1, model II, Fritsch GmbH, Germany), a cone crusher (type Symons, size 1, FIA Freiberg, Germany) and a screening ball mill (SKM 400, FIA Freiberg, Germany), furthermore vibrating screens and riffle splitter. The screening ball mill delivered commonly a final comminution product with a grain size of < 100 µm.

A bulk sample of 950 kg run-off-mine ore (avg. 12 cm size) from the shaft “Fortschritt” dump (Mansfeld mining district) was stepwise comminuted. Figure 2.2.1 shows the multi-stage comminution line. The feed was pre-crushed using two cone crushers (gap size 1: 2 cm and gap size 2: 5 mm), the first interposed by a vibrating screen of 12 mm. The final grain size of the product was achieved by two-stage milling using a screening ball mill (screen size: 3.15 mm and 100 µm).

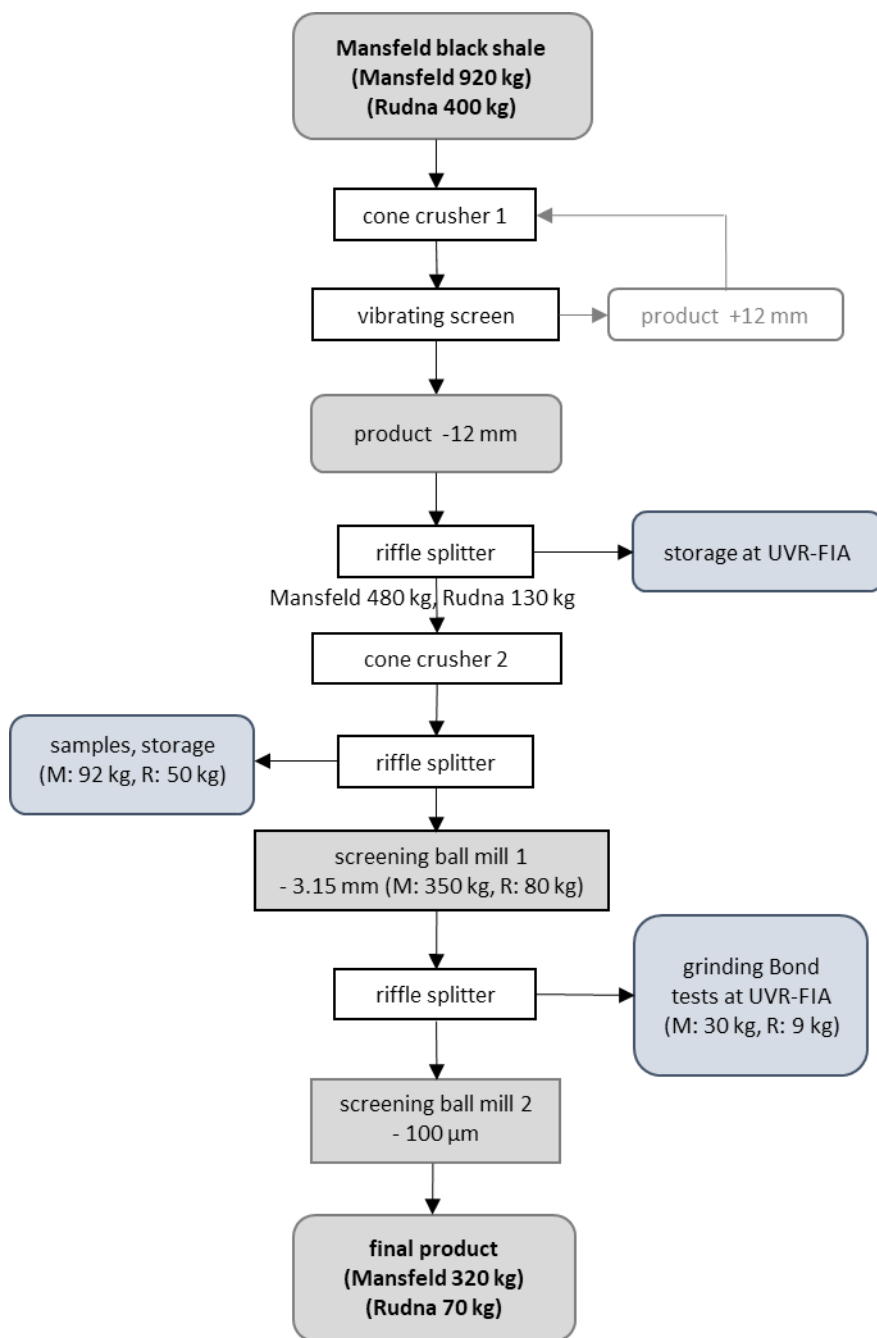


**Figure 2.2.1:** Flow chart illustrating the comminution line producing a final ball mill product from Mansfeld and Rudna black shale bulk samples. Weight data refers to sample size.

Black shale from the Rudna mine was delivered by KGHM as run-off-mine ore. The complete comminution line for the bulk sample of Rudna black shale, identical to Mansfeld black shale, is shown in Figure 2.2.1. After splitting from the whole bulk sample (2.64 t), 400 kg were fed to a two-stage cone crusher set-up followed by two-stage screening ball mill to achieve total volume of 70 kg with the final product grain size of < 100 μm.

Sample material from the shaft “Roehrig” in the vicinity to Sangerhausen was extracted by drilling. Due to the layered fabric of the black shale, the drilled material was mainly broken in medium-sized pieces (avg. 10 cm). 130 kg of drilled material was mainly treated using a jaw crusher in two stages

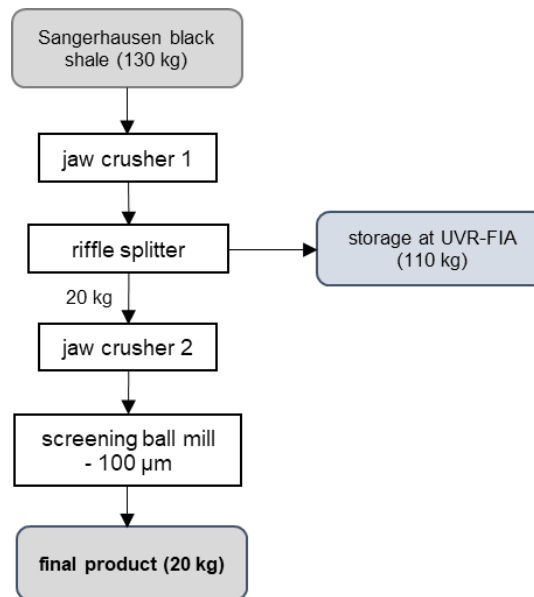


**Figure 2.2.2:** Flow chart of the comminution of Sangerhausen black shale ore to a final ball mill product < 100 μm.

(gap size 1: 4.5 mm, gap size 2: 1 mm). The product was fed to a screening ball mill to produce a final comminution product with a grain size < 100 μm (see Figure 2.2.2).

#### 2.2.1.2 VeRo Liberator® impact crusher

Comminution tests using the VeRo Liberator® comminution system were performed at the test facility of PMS GmbH in Stade in the vicinity to Hamburg, northern Germany. The VeRo Liberator® is a newly developed, vertical axle-in-axle impact crusher, which is equipped with hammer tools mounted on three different levels in a cylindrical comminution chamber. Comminution tests of Mansfeld black



**Figure 2.2.3:** Photograph showing the VeRo Liberator® in development stage VR-03-i, front left, with optional sorting system (middle) and ultra-clean filter system (back right). (from Borg et al., 2015)

shale and carbonaceous limestone as well as Rudna black shale were carried out in 2016, in which the impact crusher had attained a development stage to an industrial-scale comminution system (see Figure 2.2.3; model revision VR-03-i; Borg et al., 2017). The test runs comprised the comminution of run-of-mine feed (< 12 cm) as well as pre-crushed (< 3.15 cm) material and were conducted in a dry, single throughput of each bulk sample that had a mass between 20 and 70 kg. The comminution products were filled into sample bags and shipped to UVR-FIA for granulometric analyses and following flotation tests.

### 2.2.2 Flotation tests

The flotation was carried out at the technical centre of the UVR-FIA using a lab-scale DENVER flotation machine (1.2-liter-cell) with a solid content in the flotation feed of about 30 %. The pH value 10 was adjusted with sodium hydroxide, as dispersing agent 150 g/t polyacrylate was added. Dextrin (1500 g/t) was applied to diminish the organic carbon content in the flotation concentrate. The depressing mechanism of dextrin is described by (Liu et al., 2000).

300 g/t of xanthate was added as sulfide mineral collector. The applied frother is similar to the one used in commercial copper shale ore flotation. A mixture of alcohol and polyethylene glycol ether (150 g/t) acted as the frother. The duration of each flotation test was five minutes. The flotation tests were carried out once with a pre-treatment with 30 % ethanol and once without the pre-treatment stage in advance to the flotation conditioning.

The grade-recovery diagram depicted in Figure 2.2.4 shows that the single addition of dextrin leads to a very low Cu recovery, whereas the additional pre-treatment (PT) with ethanol caused an increase of the recovery. The omission of dextrin whilst retaining the pre-treatment resulted in a high Cu recovery connected to a very low Cu content. It has to be mentioned, that at the described stage of the project, the aim of the flotation work was not the optimization but showing maximum achievable

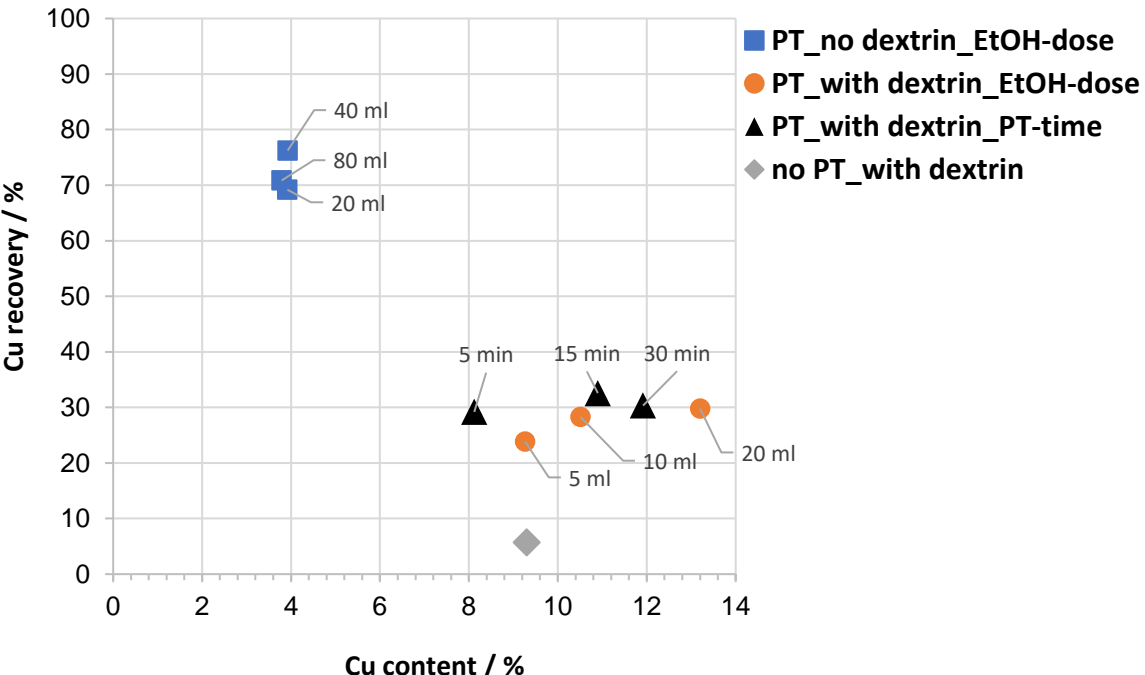


**Figure 2.2.4:** Grade-recovery diagram for flotation tests carried out on milled black shale ore with or without addition of dextrin as well as pre-treatment (PT) with ethanol (EtOH).

values concerning the Cu content. After the flotation tests the products were filtered, dried at 120 °C and weighed.

### 2.2.3 Bioleaching tests

A series of bioleaching experiments, from which residues have been partly investigated in the frame of this study, were carried out at the laboratory of the Geomicrobiology group of the BGR. Bioleaching tests were executed on milled black shale splits of bulk samples from Mansfeld and Sangerhausen ore as well as on several flotation concentrates extracted from Sangerhausen and Rudna black shale as well as on Lubin concentrate LC15a. The bioleaching tests were conducted in 2L stirred batch bioreactors at 42°C with 10% (w/v) solids load using a consortium of acidophilic, autotrophic mineral-oxidizing bacteria kept in basal salt medium (Hedrich et al., 2016). In a first step, the pH of the suspension was adjusted by adding H<sub>2</sub>SO<sub>4</sub> until the pH stayed below 1.8. The bioreactors were sparged with air at 120 l/h. Each experiment was carried out in triplicate. Chemical control experiments were carried out with the same set up but under sterile conditions.

Other bioleaching residues investigated within this study were sampled after increasing reaction/retention times (1,2,4,7 and 10 days, see Figure 2.2.5) and stem from bioleaching tests carried out with Lubin concentrate LC15b. Batch experiments were conducted at the BRGM technical centre in 2 L agitated laboratory-scale glass reactors thermostated at 42 °C with 10% solid. The pH was maintained under 1.7 by addition of H<sub>2</sub>SO<sub>4</sub> (20% v/v) when necessary. Air (120 L h<sup>-1</sup>) enriched in CO<sub>2</sub> (1%) was injected beneath a turbine (impeller rotation speed at 400 rpm) at the bottom of the reactor via a stainless-steel pipe. Acidophilic and autotrophic micro-organisms of the consortium “BioShale-BRGM” was used; it is co-dominated by *Acidithiobacillus* (At.) *caldus* and *Leptospirillum* (L.) *ferriphilum*. The species *Sulfobacillus* (Sb.) *benefaciens* BRGM2 and *Sb. thermosulfidooxidans* are also present in lower ratios. The culture was grown in a nutrient medium “OK” of standard composition standard composition: (NH<sub>4</sub>)<sub>2</sub>SO<sub>4</sub>, 3.70 g L<sup>-1</sup>; H<sub>3</sub>PO<sub>4</sub>, 0.80 g L<sup>-1</sup>; MgSO<sub>4</sub>·7H<sub>2</sub>O, 0.52 g L<sup>-1</sup> and KOH, 0.48 g L<sup>-1</sup>. Leached pulps were sampled at regular intervals (Figure 2.6) and filtered with a Büchner funnel to separate liquid and solid phases. The filtered solid material was then rinsed with a sulfuric acid solution at pH 1.8 and dried before analyses.

Further bioleaching experiments (BRGM, unpublished “Ecometals”-project results) conducted at the technical centre of the BRGM in 2014 with Lubin concentrate LCA06 delivered a bioleaching residue examined mineralogically in this study. The experimental protocol used for the bioleaching tests was identically to the bioleaching of LC15b described above.

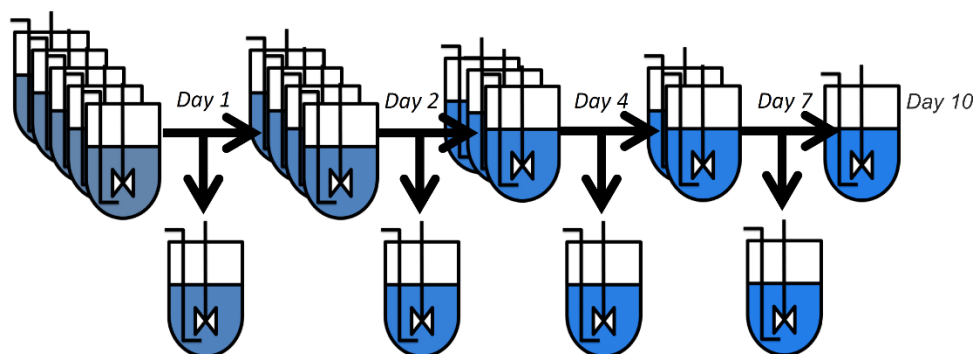


**Figure 2.2.5:** Schematic experimental set-up of bioleaching approaches carried out with Lubin concentrate LC15b, which was subjected to different leaching retention times.

## 2.3 Granulometry

### 2.3.1 Sieving analyses

Particle size distribution of crusher and VeRo Liberator® products from comminution tests were analysed using a vibrating screen machine from Retsch type AS 200 in the laboratories of the UVR-FIA GmbH. Subsamples were achieved by dividing cross and riffle splitter. Sample splits of approx. 250 g were dry sieved in air jet mode using a sieve stack according to DIN ISO 3310-1, DIN 4188, DIN 4187. The termination condition was set within one minute to 0.1 % of the mass change based on the feed mass. Round screen cuts used for these investigations were 63 µm, 125 µm, 250 µm, 500 µm, 1 mm, 2 mm, 4 mm, 8 mm and 16 mm.

### 2.3.2 Laser granulometry

Particle size distribution of comminution products, flotation concentrates and tailings as well as partly bioleaching residues were determined by laser granulometry.

Granulometric data of ball mill products and VeRo Liberator® products in the grain size range  $\leq 100$  µm were measured at the technical centre of the UVR-FIA GmbH using a Laser diffraction granulometer SYMPATEC type HELOS H2023 (Clausthal-Zellerfeld, Germany) in airstream mode RODOS, which prevent the introduction of agglomerated particles into the measurement chamber by a pressurized airstream that abruptly decreases at the discharge of the sample from the nozzle in the measuring chamber. Measuring range was 1.8-350 µm at 30 s measuring time, 1-2 bar airstream pressure and 75-100 mbar in the measuring cell.

The determination of particle size distribution of flotation samples and selected bioleaching residues was performed using a laser granulometer CILAS 920 (CILAS, Orléans, France). Laser diffraction measurements were carried out in wet dispersion. Therefore, approximately 400 ml of isopropanol was added to the cytofunnel chamber and a calibration measurement was carried out first. Thereafter, 0.15 g sample material was added to the feeding chamber filled with isopropanol and the actual measurement was implemented. The detection range of the laser granulometer was from 0.7 to 400 µm. Three measurements per one dispersed sample charge were recorded and repeated three times. Output data for each sample were averaged.

Granulometric data are presented in tables and particle size distribution diagrams displaying particle size vs. cumulative particle distribution in percentages.

## 2.4 Geochemical analysis

Determination of elemental concentration in bulk rock and processing samples was carried out by geochemical analyses, for which the certificated laboratory ALS in Ireland was commissioned. The following analytical methods, ALS method codes in brackets, were applied:

- four acid digestion with ICP-MS finish (ME-ICP61) for flotation concentrates,
- fused bead, acid digestion with ICP-AES (ME-ICP06) + aqua regia digestion with ICP-MS (ME-ICP41a) for comminution samples and flotation tailings,
- aqua regia digestion with ICP-MS (ME-MS41) for bioleaching residues.

Elevated concentrations, overlimits, were separately analysed with methods:

- lithium borate fusion with strongly oxidizing agents and XRF finish (ME-XRF15c),
- aqua regia overlimit method with ICP-AES finish (ME-OG46) especially for flotation concentrates, but also for comminution samples as well as bioleaching residues.

Table 2.4.1 summarizes the analytical packages applied to different sample types.

**Table 2.4.1:** Analytical methods used for geochemical assays of different processing samples as commissioned at ALS Geochemistry, Loughrea, Ireland.

ALS method code	Comminution products	Flotation concentrates	Flotation tailings	Bioleaching residues
ME-ICP06 + ME-ICP41a	X		X	
ME-MS41				
ME-ICP61		X		X
ME-XRF15c	X	X		X
ME-OG46	X	X		X

## 2.5 Microscopy

### 2.5.1 Sample preparation

Strewn slides were mainly prepared as thick sections (28 x 48 mm, approx. 300 µm sample thickness) and partly embedded in round polished resin blocks (diameter 25 mm). For characterization of the feed materials, rock samples were prepared in thick as well as thin sections. Embedding media mainly used for the preparation of strewn slides was Araldite 2020 (Huntsman, Switzerland). Polished thick sections of bioleaching residues were predominantly produced by embedding in “EpoFix Resin” (Struers, Denmark). The sections were prepared using an “Accutom-100” precision grinding machine and a polishing machine “PM5” (both Logitech, Great Britain).

### 2.5.2 Equipment

Reflected light microscopy for the identification of sulphide minerals was carried out with a Carl Zeiss Axiophot polarisation microscope, combined with a Nikon Digital Sight DS-Fi2/ DS-U3 analogue-to-digital converter.

Scanning electron microscopy of carbon-coated polished sections and gold-coated grain samples mounted onto carbon adhesive pads was conducted on a JEOL JSM 6300 SEM equipped with an EDX-detector (XFlash 5010, Bruker, USA). Images to depict mineralogic relationships and grain properties were taken in back scattered electron (BSE) as well as secondary electron (SE) mode. Mineral abbreviations used to indicate mineral phases in figures follow the listing and recommendations of Whitney and Evans (2010).

## 2.6 Automated mineralogy

### 2.6.1 Mineral distribution analysis using Bruker Esprit 2.1 Feature

Representative aliquots of the black shale ore, flotation products and tailings as well as residues from bioleaching and sterile control tests were prepared as polished grain mounts. For investigations carried out on a scanning electron microscope (SEM) the grain mounts were carbon-coated. The determination of the mineral distribution in the samples was conducted with the “Feature”-tool, which is part of the “Esprit 2” microanalysis software of the Bruker Quantax EDS System.

Suitable areas for the particle analysis were first captured in the BSE-mode and detected particles were grouped into binarization classes according to their grey values in order to separate individual minerals associated with intergrowths. Image filters were used to improve the particle detection. At least 3000 accepted grains with an area of at least 25  $\mu\text{m}^2$  were measured automatically using an energy-dispersive X-ray detector (Bruker X-Flash 5010, 123 eV) at 20 kV. Acquisition time of an EDS spectra was 3 s with 2500-6000 counts per grain depending on the composition. Particle EDS-spectra were assigned to a specific mineral database adapted to the sample type. Output data were recalculated to weight percent (wt.%) and corrected regarding the total organic carbon (TOC) content. Some minerals in particular gangue-type minerals were grouped according to their chemical similarity, in particular carbonate minerals as well as feldspar and clays.

Geochemical data were used to validate the analysed mineral content, in particular for copper sulfides. Therefore, the elemental copper content was recalculated by the stoichiometric portion in related mineral phases and their content as detected by automated mineral distribution analysis.

### 2.6.2 Mineral liberation analysis (MLA)

#### 2.6.2.1 Mineral liberation analyser FEI MLA 650F

MLA measurements on comminution samples and selected flotation products were carried out in the frame of the research project “Ecometals” at the Geometallurgy Laboratory of the Technical University Freiberg (TUBAF).

Quantitative mineralogical analysis using MLA was performed on polished and carbon-coated grain mounts. The grain mounts produced from a mixture of 3 g sample material with 2 g epoxy resin were measured on a FEI MLA 650F system comprising a scanning electron microscope (FEI Quanta 650 FEG) equipped with two Bruker Quantax X-Flash 5030 energy-dispersive X-ray spectrometers. Automated acquisition of data and its evaluation was realized using MLA software Suite 3.1.4. Measurements conducted in grain-based X-ray mapping (GXMAP) mode with a pixel grid size of 1  $\mu\text{m}$  and in a pre-set BSE grey-scale range. EDS spectra acquisition time was 7 s and resulted in about 2000–4000 counts per pixel depending on the measured mineral phase. Measurements examined in this study were conducted with 25 kV electron beam acceleration voltage, which delivered the more accurate identification, in particular of bornite and chalcopyrite, whereas measurements with 15 kV resulted in better detection of gangue minerals (silicates, carbonates) due to lower excitation volume (Rahfeld et al., 2018). The evaluation of MLA data sets used in this study was edited with the FEI-distributed application “Dataview 3.1.4”.

### 2.6.2.2 ZEISS Mineralogic Mining- System

Further mineral liberation analyses were performed on a ZEISS Mineralogic Mining, a product for automated mineral characterisation based on scanning electron microscopy. Petrolab Ltd (Redruth, Cornwall, UK) was commissioned to analyse mineral liberation of comminution products, flotation concentrates and tailings.

Polished blocks were prepared from each of the submitted sample/ fractions and carbon coated to a thickness of 10 nm. Each block was analysed using a ZEISS EVO MA 25 scanning electron microscope (SEM) fitted with a Bruker xFlash 6|60 x-ray detector for energy-dispersive X-ray spectroscopy (EDX) analysis. The Mineralogic Mining 1.4 software controlled the SEM and acquired morphology and X-ray data. A phase classification scheme was developed using the Mineralogic Mining software.

Liberation mapping mode was utilized, as analysis was undertaken to determine the overall abundance of major/minor phases, grain/particle sizes and locking characteristics. The mineral liberation mode was performed with 1  $\mu\text{m}$  mapping resolution at 10  $\mu\text{m}^2$  grain size limit. Data extracted from the measurements comprised cumulative liberation yields for selected target minerals (sulphides), their liberation mode and locking association.

### 2.6.3 General considerations on the automated mineral analysis of processed Kupferschiefer-type black shale ore

Mineral identification by automated particle analysis was performed by using semi-quantitative EDS-analysis, which is in general an error-prone method. To reduce incorrect particle identifications, definitions of element contents in the specified mineral database were widely defined, which in some analysis might be lead to overlapping definitions. Here, the software helped by weighing minerals in order of their listed position within the database, so that more probable minerals were preferentially matched with the chemical assay of a grain spectrum. However, the clear distinction between alkali feldspar and the illite group clay minerals poses difficulties because of the similar chemical composition and thus, the content of alkali feldspar could be overemphasized in the analyses.

In the EDS-based particle analysis the common interaction volume of the electron beam was 1 to 5  $\mu\text{m}$ . For sample material which was predominantly fine-grained, EDS-measurements were influenced by several disturbing effects, such as the electron beam interaction of particle rim and resin or simultaneous analysis of minute particles (< 5  $\mu\text{m}$ ) in the immediate proximity. The black shale ore and its processing products investigated in this study consisted mainly of very fine particles that had either a mono-mineralic composition or complex intergrowths consisting of several minute minerals, reflecting a typical ore texture in Kupferschiefer-type black shales. Thus, EDS-spectra of fine particles could characterize a single mineral phase or a mixture of minerals. To avoid a false classification of minute intergrowths, especially of sulfides and gangue minerals, the matching mineral database needed to be adapted and the grain spectra should be verified. Further, a portion of grains remained unclassified, because of missing assignment of the chemical composition defined by EDS-spectra to the database. In both cases, a manually input of the user to improve the accuracy of the analysis is indispensable, which represents a time-consuming procedure.

Particle analyses carried out on black shale-hosted ore and related flotation product and tailings required a minimum on user input for the above-mentioned analytical issues. Regarding the automated particle analysis of bioleaching as well as abiotic leaching residues, an intervention of the user was an absolute necessity. Especially in bioleaching products of black shale hosted ores, large

amounts of particles showed grain sizes of  $< 10 \mu\text{m}$ . The increased probability that the electron beam has hit particle edges resulted in spectra marked by weak detection counts, which led to incorrect determination of minerals in comparison with the database. Moreover, the fine-grained intergrowth of ore and gangue minerals resulted in a mixed spectrum, which could not clearly be associated with one distinct mineral phase in the database and caused erroneous content of minerals in the sample. The definition of mixed mineral classes in the database could reduce this incorrect assignment.

Additionally, mineral identification was also affected by the kind of treatment/processing of samples to be analysed. Especially the usage of acids (hydrochloric acid and/or sulfuric acid) in flotation and bioleaching processes led to additional chlorine and/or sulphur input that seemed to be adsorbed onto particles and thus interfered with EDS-spectra of particularly very fine-grained particles. Generally, particle EDS-data from bioleaching residues should be revised, because non-reviewed data often contain a strongly overemphasized number of mixed spectra of pyrite and gangue minerals and gypsum and/or anhydrite.

## Chapter 3 Results

This chapter is subdivided into three parts, comminution, flotation, bioleaching and contains mainly granulometric and mineralogical analyses partly previously published in Kamradt et al. (2017) and Kamradt et al. (2018). These publications have been drawn as project-related outcomes containing results according to the processing state at that time. Due to adaption of further developments of software-based data evaluation, some of these results are slightly different to data present hereinafter.

### 3.1 Mineralogical and geochemical characterization of black shale comminution products

#### 3.1.1 Particle size distribution of comminuted black shale ores

##### 3.1.1.1 Ball mill products of different black shale ores

Bulk samples of black shale ore from different central European mining location were comminuted by a multi-stage crushing and grinding line in the technical centre of UVR-FIA GmbH, Freiberg, Germany. Crusher and grinding machines used for the comminution tests represented laboratory-scale devices comprising a primary jaw crusher, cone crusher and finally a screening ball mill, which delivered a comminution product with a final grain size of  $< 100 \mu\text{m}$  (for details see Chapter 2.2.1.1). Black shales comminution products were preferentially used for flotation tests in order to gain flotation concentrates enriched with copper-bearing sulphides.

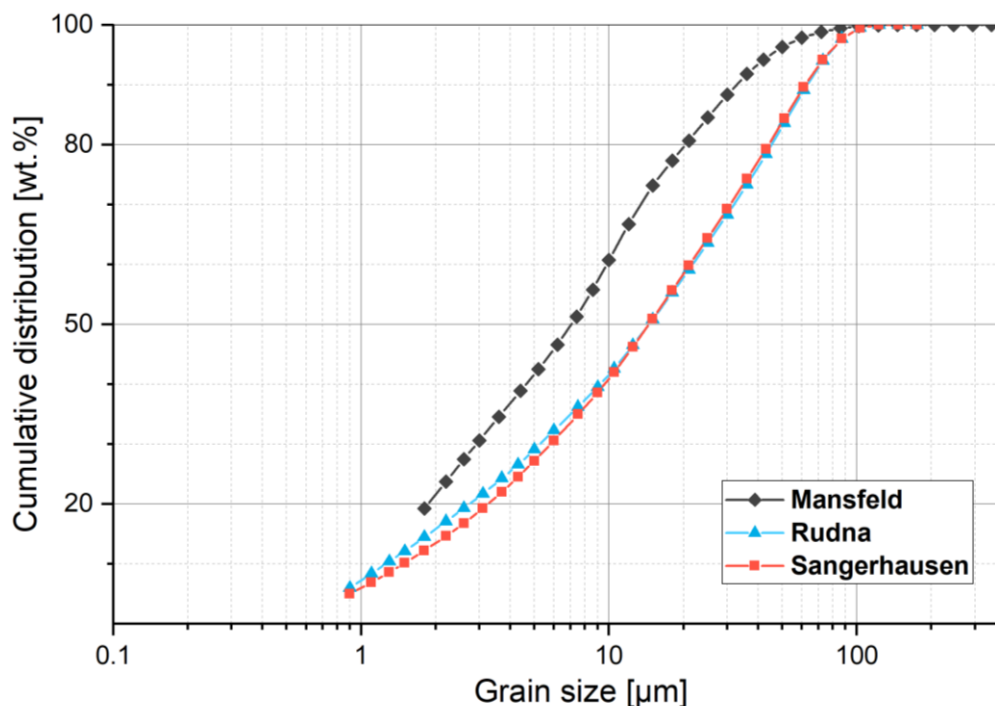


**Figure 3.1.1:** Laser-granulometric particle size distribution showing ball mill products of three different black shale ores. (Data. UVR-FIA)

**Table 3.1.1:** Comparison of particle sizes achieved by ball milling at defined passing fractions (20%, 50% and 80%). (Data: UVR-FIA)

Passing fraction	Particle size [ $\mu\text{m}$ ]		
	Mansfeld	Rudna	Sangerhausen
<b>D20</b>	1.8	2.6	3.2
<b>D50</b>	7.1	14.8	14.8
<b>D80</b>	20.4	44.6	45.2

The particle size distribution (PSD) for ball mill products from three different Mid-European black shale ore occurrences (see Chapter 2.1) is depicted in Figure 3.1.1. The PSD-curves revealed that ball mill products of black shale ore from Rudna and Sangerhausen contained a similar grain size distribution, whereas the final comminution product of the Mansfeld black shale low-grade ore achieved by ball milling was decidedly finer. Particle size distribution curves for black shale ball mill products from Rudna and Sangerhausen ore deviated marginally in the particle size range below 10  $\mu\text{m}$ , in which the ball mill product of Rudna black shale ore contained a slightly higher proportion of particles. The deviation of PSD-curves in the particle size range from 20 to 70  $\mu\text{m}$  is even lower, but showed marginally finer-grained particles in the Sangerhausen ball mill product.

Specific product particles sizes are conventional used to describe granulometric data and are determined at 50 % cumulative weight passing (frequency), which indicates the mean particle size, and 80 % cumulative passing that is considered as the representative maximum particle size of the overall particle size distribution of a sample, whereas  $D_{20}$  represents the characteristic minimum particle size. Therefore,  $D_{80}$ ,  $D_{50}$  and  $D_{20}$  are used to characterize comminution products by specific particle sizes at a defined weight fraction of a sample.

According to the PSD, ball mill products of Rudna as well as Sangerhausen black shale ore had a median particle size ( $D_{50}$ ) of 14.8  $\mu\text{m}$ . As shown in Table 3.1.1, the median particle size of milled Mansfeld black shale was substantially lower (7.1  $\mu\text{m}$ ). The general fine-grained particle size in the ball mill product of the Mansfeld black shale was also reflected in the 20% passing fraction ( $D_{20}$ ), in which particles occurred up to 1.8  $\mu\text{m}$ . The characteristic minimum particle size was more coarse-grained in ball mill products of Rudna ( $D_{20}=2.6$   $\mu\text{m}$ ) and Sangerhausen ( $D_{20}=3.2$   $\mu\text{m}$ ) black shale. Additionally, the maximum particle size in the 80% cumulative fraction of milled Rudna and Sangerhausen black shale was quite similar ( $D_{80}= 45$   $\mu\text{m}$ ), while the representative particle size in the ball mill product of the Mansfeld black shale was significantly lower, consisting of particles up to 20  $\mu\text{m}$ .

### 3.1.1.2 Particle size distribution of comminuted black shale ores using an innovative impact crushing technology (VeRo Liberator®)

#### 3.1.1.2.1 Comparison with conventional crusher units

The VeRo Liberator® represents a comminution system that applies a vertical impact crusher equipped with hammer tools on three vertical separate levels (for details see Chapter 2.2.1.2). In order to determine the performance of the VeRo Liberator®, particle size distribution (PSD) data of crushing tests were compared with PSD-data from tests carried out with other conventional crusher types. These tests were performed with black shale ore from the shaft "Fortschritt I" tabular dump in the

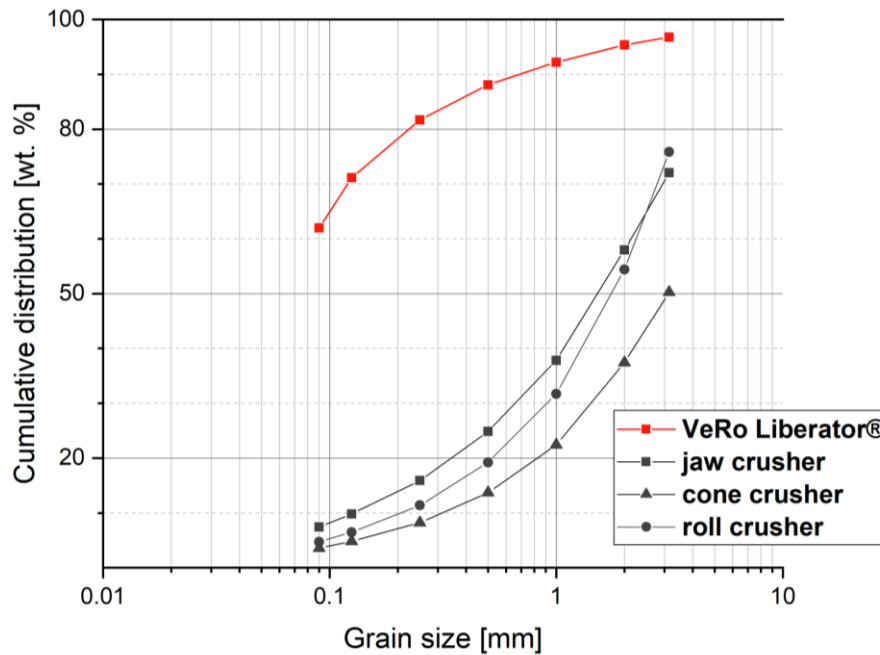


**Figure 3.1.2:** Grain-size distribution of exemplarily comminution tests of black shale ore from Sangerhausen district carried out with different crushing units. Data representing sieve analyses according to DIN ISO 3310, DIN 4188 and DIN 4187 (German Institute for Standardization). (Data: UVR-FIA)

Mansfeld district and comprised crushing tests with a jaw crusher (gap size: 1 mm), a cone crusher (gap size: 2 mm) and a roll crusher (gap size: 2mm).

Figure 3.1.2 illustrates PSD-curves determined from standardized sieve analyses for crushed black shale ore. By comparison, two main deviating features were especially remarkably. Firstly, the proportion of particles covering the particle size range was noticeably lower in crushing products of jaw, cone and roll crusher. Thus, a significant fraction of more than 25% of the whole sample consisted of particles > 3.15 mm in products of jaw and roll crusher, whereas the cone crusher achieved a product, in which just 50% of the sample was comminuted to a particle size < 3.15 mm. Contrary to that, the product of the impact crusher is characterized by a particle size distribution that was nearly 100% below 3.15 mm. Furthermore, the curve shape of the impact crusher product is convex, while products of other crushers show concave curves, which indicates the rapid decrease of the sample volume towards finer particle sizes. The coarse-grained nature of jaw, cone and roll crusher products is also expressed by  $D_{80} \gg 3.15$  mm, whereas the impact crusher product mainly consisted of particles  $D_{80} < 225$   $\mu$ m. Furthermore, the difference of the proportion of particles < 90  $\mu$ m in the impact crusher product is impressive. 62% of the impact crusher product was in the particle size range < 90  $\mu$ m, whereas other crusher products contained lower than 10 % of particles < 90  $\mu$ m.

#### 3.1.1.2.2 Granulometric distribution of VeRo Liberator® impact crusher products

A further test run to investigate the capability of particle size reduction of the impact crusher was carried out on low-grade black shale as well as limestone ore from the Mansfeld district. The approach followed by these comminution tests was to determine changes of the crusher product depending on different feed sizes. Therefore, pre-crushed bulk samples (particle size < 12 mm) and run-of-mine rock pieces (< 120 mm) of black shale as well as limestone were comminuted by a single pass crushing test.

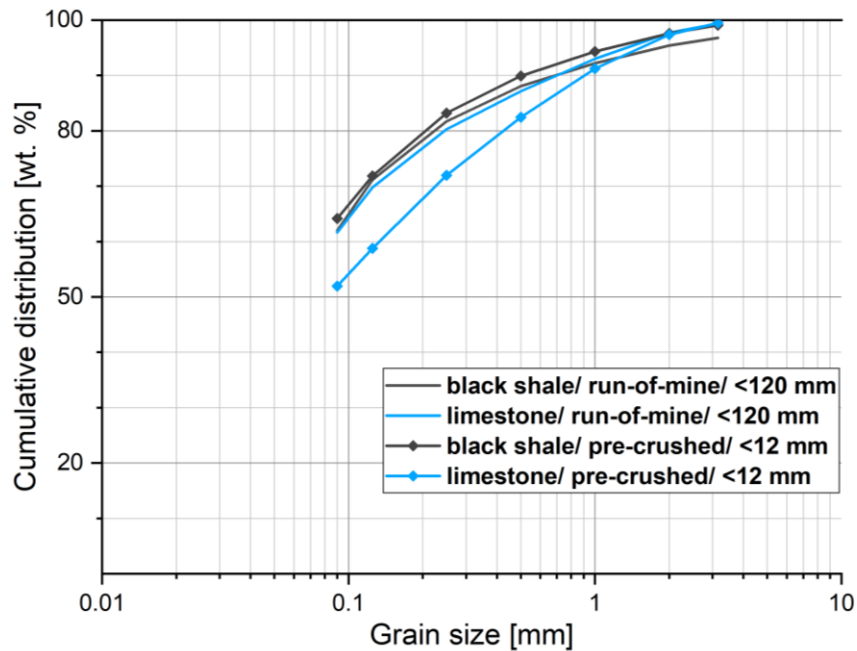


**Figure 3.1.3:** Particle size curves represent sieve analyses of run of-mine, low grade ore consisting of black shale as well as hanging wall limestone from Mansfeld comminuted by the VeRo Liberator® impact crusher. Data representing sieve analyses according to DIN ISO 3310, DIN 4188 and DIN 4187 (German Institute for Standardisation). (Data: UVR-FIA)

The mass volumes used for this test series were 70 kg of run-of-mine and 27 kg of pre-crushed black shale as well as 24 kg of run-of-mine and 22 kg of pre-crushed limestone.

The PSD of the impact crusher products shows Figure 3.1.3. The diagram revealed that PSD-curves of three crusher products were generally similar in terms of the grain size range, whereas the impact crusher comminution of pre-crushed limestone sample yielded a coarser product. Minor differences of the particle size distribution were detected for black shale samples. The pre-crushed sample showed the most fine-grained product, in which  $D_{80}$  was 210  $\mu\text{m}$  and 64.2% of the sample consisted of particles < 90  $\mu\text{m}$ . The impact crusher product of the run-of-mine black shale sample was characterized by  $D_{80}$  at 225  $\mu\text{m}$  and by 62.0% of the total crusher product covering the grain size range < 90  $\mu\text{m}$ . Only the test run carried out on pre-crushed limestone showed a more deviant particle size distribution, in which the  $D_{80}$ -fraction correspond to a grain size of 425  $\mu\text{m}$  and the portion of particles < 90  $\mu\text{m}$  was significantly lower at 52% of the cumulative sample volume.

Additional tests regarding the particle size distribution of VeRo Liberator® impact crusher products were carried out with the deployment of differently-shaped hammer tools. For this purpose, run-of-mine black shale bulk samples from the Rudna mine and Mansfeld were comminuted by the impact crusher equipped completely with angular-shaped, rod-like hammer tools, while in further crushing tests the impact crusher was operated with round, rod-like hammer tools.

Particle size distribution curves in Figure 3.1.4 illustrate that the test performed with round hammer tools achieved slightly finer crushing products. However, minor differences in impact crusher products of black shale feed were notable, because these comminution tests delivered generally finer-grained products in comparison to Rudna black shale feed. Sieve analyses showed that the  $D_{80}$ -product grain size generated with round hammer tool was nearly equal in the Mansfeld ( $D_{80}=220 \mu\text{m}$ ) and Rudna

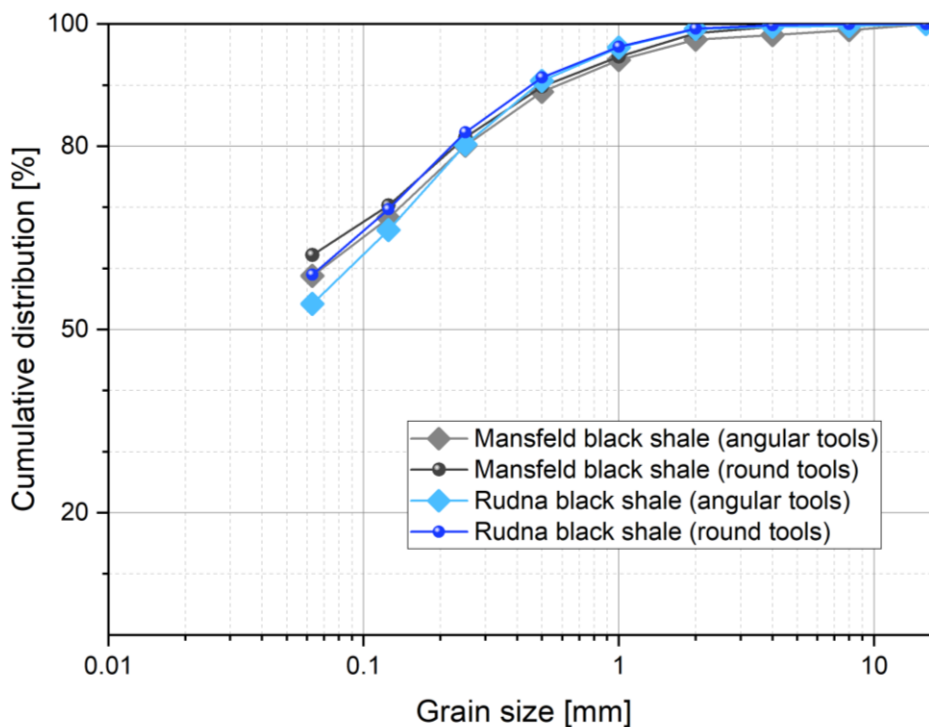


**Figure 3.1.4:** Sieve curves for VeRo Liberator® impact crusher products displaying slight differences between the deployment of angular and round (R) hammer tools. (Data: UVR-FIA, according to DIN 66165 (German Institute for Standardization)).

( $D_{80}=225 \mu\text{m}$ ) black shale sample, whereas  $D_{80}$  of both samples comminuted by angular hammer tools was identical at  $250 \mu\text{m}$ . Greater differences of the particle size distribution existed in the finer grain size range, which is especially pronounced in the passing fraction at  $63 \mu\text{m}$ . Here, the differences between both feed samples and the type of hammer tools used for the comminution tests were obvious. Impact crusher products of Mansfeld black shale contained higher proportions of particles  $< 63 \mu\text{m}$ . The comminution product generated by round hammer tools had the most increased passing fraction with 62.2% followed by 58.8% passing volume in the  $< 63 \mu\text{m}$  grain size range for the impact crusher product achieved with angular hammer tools. Impact crusher products from Rudna black shale showed a similar difference in the proportion of  $< 63 \mu\text{m}$ -fraction, though the passing volume for this grain size range was generally lower. While the crushing test implemented with round hammer tools reached a  $< 63 \mu\text{m}$ -fraction of 59.0%, the test performed on Rudna black shale with angular hammer tools achieved the lowest proportion of particles in the  $< 63 \mu\text{m}$  range with 54.2% passing volume.

#### 3.1.1.2.3 Comparison of particle size distribution of impact crusher products with ball mill product in the $- 100 \mu\text{m}$ grain size range

As shown in the previous subchapter, the main part of black shale impact crusher products consisted of particles in the size range  $< 100 \mu\text{m}$ . Impact crusher comminution tests achieved a proportion of 65% for the crushed Mansfeld black shale and 62% for the Rudna black shale in the grain size range  $< 100 \mu\text{m}$ . Thus, a comparison of impact crusher products with ball mill products within the same particle size range can be executed.

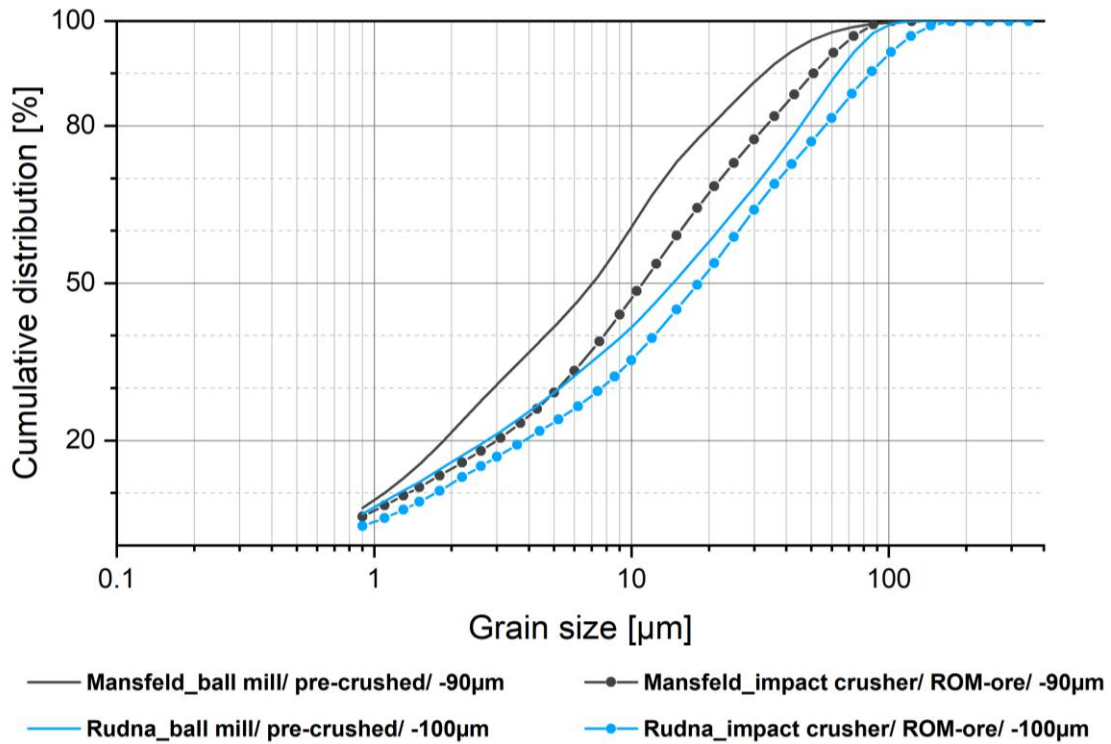


**Figure 3.1.5:** Laser granulometric data for ball mill products and corresponding fraction of VeRo Liberator® impact crusher products from Mansfeld as well as Rudna black shale ore. (Rudna impact crusher product 62.5% < 100 µm, Mansfeld 63.7% < 90 µm; Data: UVR-FIA)

Figure 3.1.5 shows the particle size distribution of impact crusher and ball mill products of comminuted Mansfeld and Rudna black shale samples. Generally, ball mill products of both black shales are characterized by a finer grain size distribution. However, the graphs show that a difference in the particle size distribution between ball mill and impact crusher products regarding the black shale feed type is obvious. While the particle size distribution of Rudna black shale products from ball mill and impact crusher differed lesser, the deviation for the Mansfeld black shale was more striking.

Table 3.1.2 summarizes the particles sizes at characteristic cumulative proportions ( $D_{80}$ ,  $D_{50}$ ,  $D_{20}$ ) of comminution products. Under the consideration that the impact crusher product < 100 µm represents the final product and oversized particles would be recharged into the crusher feed, impact crusher and ball mill products can be compared directly. Hence, Table 3.1.2 contains particle sizes at representative cumulative passing volume for the < 100 µm-fraction of total impact crusher products. The comparison

**Table 3.1.2:** Comparison of particle sizes in ball mill and impact crusher comminution products of Mansfeld and Rudna black shale at defined passing fractions (20%, 50% and 80%). (Data: UVR-FIA)

Passing fraction	Particle size [µm]					
	Ball mill product		Impact crusher product			
	Mansfeld	Rudna	Mansfeld < 100 µm	Mansfeld total	Rudna < 100 µm	Rudna total
<b>D20</b>	1.8	2.6	3.0	5.4	3.9	7.4
<b>D50</b>	7.1	14.8	11.5	29.8	18.3	45.6
<b>D80</b>	20.4	44.6	34.5	220.0	56.0	250.0

indicates as well for the ball mill as for the impact crusher that the comminuted Mansfeld black shale consisted of substantially finer grain sizes independently from the comminution method. However, particle sizes of impact crusher products from Mansfeld black shale were 60-70% coarser-grained as in the corresponding ball mill product, whereas particle size in the impact crusher product of Rudna black shale was 50% coarser-grained at  $D_{20}$  as well as 25% coarser-grained at  $D_{50}$  and  $D_{80}$ , respectively, to the ball mill product. This is also manifested by closer curve progression of particle size distribution curves in Figure 3.1.5. Although apparently differences between ball mill and impact crusher products were documented, the particle size distribution of impact crusher products can be considered as feed material for following mineral processing steps (e.g. flotation, gravity separation). Especially, if the particle size distribution meets grain size ranges of valuable minerals (in this case base metal sulphides), which demand a comminution to a grain size range below 60  $\mu\text{m}$  in order to be potentially liberated and thus, to be winnable by suitable extraction techniques.

### 3.1.2 Mineralogical and geochemical characterization of comminuted black shale ores

Comminution products of black shale ore were marked by a particle association in a certain grain size range. As shown in Chapter 3.1.1, ball milling generates black shale comminution products with mean particle sizes of usually < 15 µm and finer-grained. Products from VeRo Liberator® comminution were more deviating in terms of particle size distribution but still contained mean particle sizes < 50 µm in the total product and < 20 µm in the fraction < 100 µm. Thus, comminution products investigated in this study can be considered to be fine-grained, which is a necessary feature in order to liberate the sulphide association in the feed.

Particles of ball mill products featured generally irregular particle shapes, from grainy to angular to elongated, and from smooth to highly sutured particle rims. Particles were often marked by intricately intergrowths among gangue minerals as well as gangue with sulphide minerals and among sulphides.

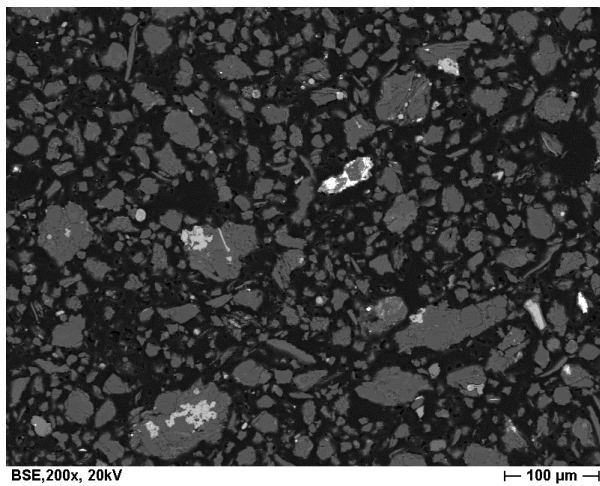


**Figure 3.1.6:** SEM-image displays particles in a ball mill product that exhibiting various grain shapes and intergrowth textures. (Mansfeld ball mill product, SEM-BSE)

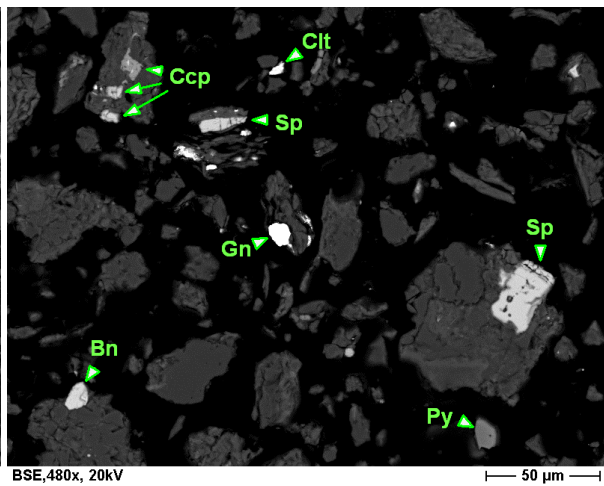


**Figure 3.1.7:** Micrograph of predominantly irregular shaped particles containing intergrowths of gangue and ore minerals at different levels of liberation. (Mansfeld ball mill product, SEM-BSE)

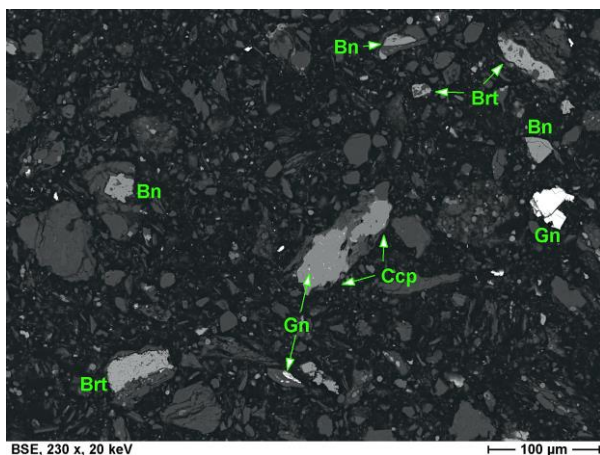


**Figure 3.1.8:** More coarse-grained sulphides partly liberated as well as intergrown with gangue minerals accompanied by barite. (Sangerhausen ball mill product, SEM-BSE)

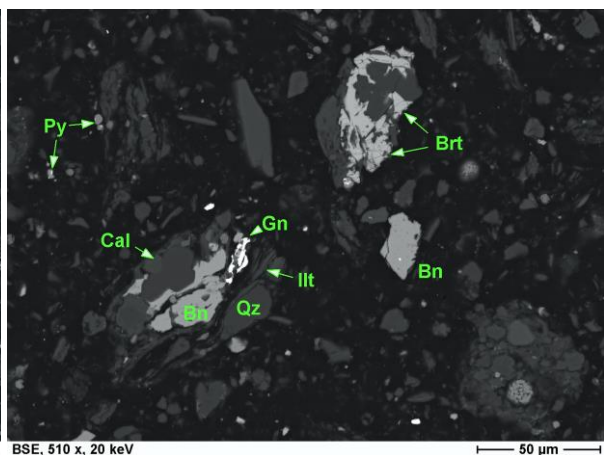


**Figure 3.1.9:** Particles showing intimately intergrowths of gangue minerals (Cal=calcite, Illt=illite, Qz=quartz) with bornite (Bn) and galena (Gn). Barite (Brt) and framboidal pyrite are common. (Sangerhausen ball mill product, SEM-BSE)

Particles in VeRo Liberator® products covered a more widespread particle size range. Usually they showed grainy, irregular particles shapes and intraparticle cracks and fissures predominantly on outer areas of particles that often featured straight to curved break lines, which can transect mineral grains or whole particles and run along mineral grain boundaries.

According to general rheological properties of the black shale, elongated to platy mineral fragments were observed besides the common grainy appearance of particles and were formed by brittle fracturing along sedimentary stratification layers of the black shale. Small-scaled intergrowths of organic matter and clay minerals were mainly located in band-like zones, alternating in mesoscopic range with layers rich in carbonate minerals. Predefined breakage occurred apparently more in rigid layers, in which carbonates as well as quartz and feldspar were present, and less in elastic clay-rich bands, which resulted in presence of elongated particles in VeRo Liberator® comminution products.

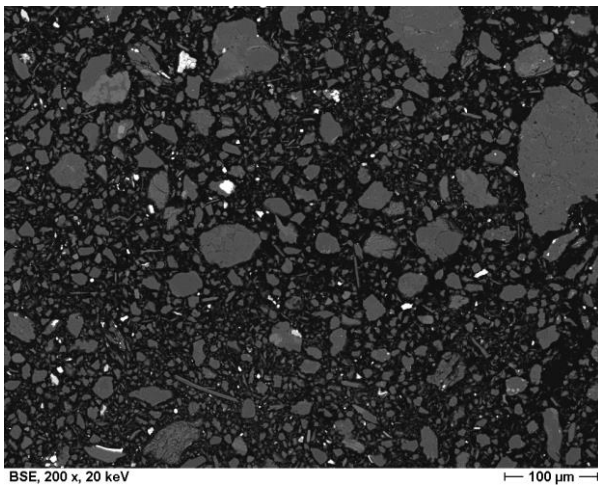


**Figure 3.1.10:** General view on a VeRo Liberator® impact crusher product displays the vast heterogeneity of the particle size and variability of particle shapes. (Mansfeld black shale, SEM-BSE)

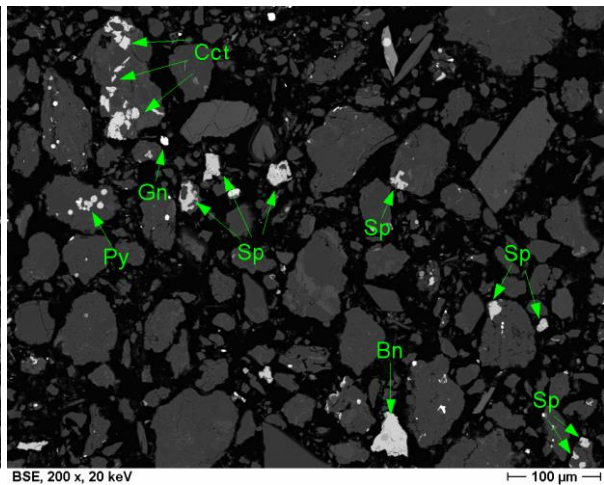


**Figure 3.1.11:** VeRo Liberator® impact crusher products hosted both, complete liberated (Bn=bornite, Gn=galena, Sp=sphalerite) up to complete locked (Cct=chalcocite, Py=pyrite) sulphide grains (Mansfeld black shale, SEM-BSE)

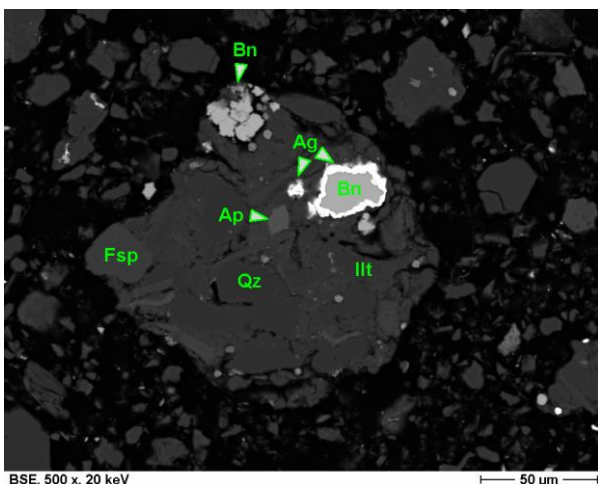


**Figure 3.1.12:** Image depicting a larger particle in a VeRo Liberator® product that contains predominantly intergrowths of gangue minerals (Ap=apatite, Fsp=feldspar, Illt=illite, Qz=quartz) and bornite (Bn) grains at the particle margins partly enclosed by silver. (Mansfeld black shale, SEM-BSE)

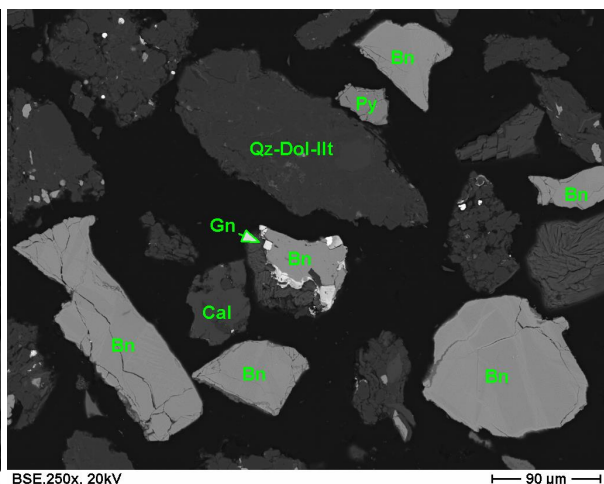


**Figure 3.1.13:** VeRo Liberator® product showing mainly complete liberated grains of bornite (Bn) as well as particles consisting of intergrowths of gangue minerals (Qz=quartz, Dol=dolomite, Illt=illite) partly with bornite and galena (Gn). (Mansfeld black shale, SEM-BSE)

### 3.1.2.1 Mineral distribution analysis

The identification of mineral phases and their distribution represent important prerequisites for a successful application of mineral dressing methods. Black shales from different Kupferschiefer-type deposits are characterized by varying contents of as well sulphides as rock-forming (gangue) minerals. Additionally, the proportion and type of organic matter change within the basal Zechstein black shale sediment laterally and vertically. Thus, mineral processing of black shale ores can have various challenges concerning the composition of the sulphide assemblage as well as the predominant gangue minerals.

In this study, black shale ores from three mining districts have been investigated in detail. Generally, the test material represents bulk samples. While black shale bulk samples from the Sangerhausen and Lubin-Sieroszowice (Rudna) mining district were provided by extraction from underground mines, the Mansfeld black shale bulk sample represents a low-grade ore, which was deposited on dumps during former mining activities (for details see Chapter 2.1).

Sample splits of ball mill products generated from bulk samples were characterized by SEM EDX-based mineral distribution analysis. Additionally, impact crusher products of Rudna and Mansfeld black shale were analysed in the grain size range  $< 100 \mu\text{m}$ . The feed (run-of-mine ore,  $< 120\text{mm}$ ) of the impact crusher test was hand-picked from bulk samples, by which slight differences in the mineral composition between ball mill and impact crusher products can be caused. For example, 950 kg of Mansfeld black shale (run-of-mine,  $< 120 \text{ mm}$ ) were pre-treated by cone crusher to achieve a grain size of  $< 12 \text{ mm}$ . A split of 500 kg was treated by a secondary cone crusher to a product with a final grain size of  $< 3.15 \text{ mm}$ , which was fed to a first screening ball mill. 350 kg of the first screening ball mill were ultimately milled by a second ball mill to the final product. During this multi-stage comminution process, the initial blocky black shale was sufficient homogenized. In contrast, the hand-picked split from the Mansfeld bulk sample used for impact crushing was by orders of magnitude smaller (70 kg) and thus, can deviate compositionally from the by far larger sample comminuted by the conventional crusher and mills. Similar effects can be assumed for the bulk sample from the Rudna mine, which had a total weight of over 3 tons and was treated by a similar comminution line in order to get the final ball mill product. For comparison, the sample weights of Rudna black shale comminuted by the VeRo Liberator® impact crusher were 63 kg run-of-mine feed and 87 kg pre-crushed ( $-12 \text{ mm}$ ) feed.

Mineralogically, investigated black shale comminution products are generally dominated by carbonates, silicates and clay minerals. Figure 3.1.14 shows the percentage composition of the main rock-forming minerals and additional mineral groups as well as the content of individual sulphides. The main difference in the composition of black shale samples from three different locations were the prevalent gangue-type minerals. Mansfeld and Rudna black shale comminution products were rich in carbonates, mainly dolomite, whereas Sangerhausen black shale was dominated by illite (26.4%) and quartz (21.4%). Furthermore, it contained moderate amounts of potassium feldspar (5.3%) and plagioclase (7.1%), while the carbonate content (6.9%; dolomite: 4.8%, calcite: 1.9%) was decidedly lower than in comminution products of Mansfeld and Rudna black shale. Quartz represented also a main constituent in Mansfeld black shale, which contained 23.8% in the ball mill product and 29.2% in the impact crusher product. Both comminution products show similar amounts of potassium feldspar (8.0%) and plagioclase (12.5%), while the proportion of illite differed moderately with 17.7% in the ball mill product and 12.9% in the impact crusher product.

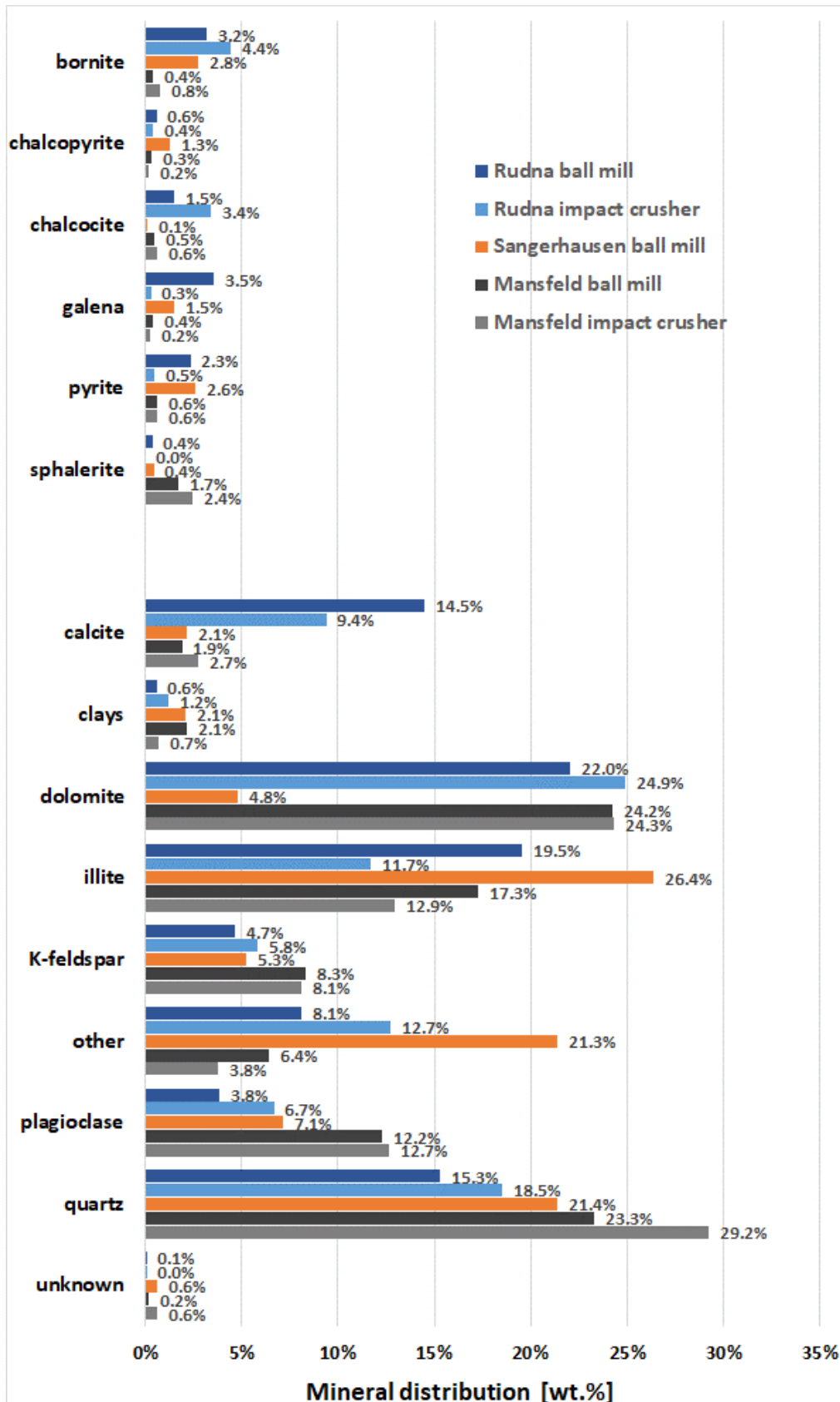


**Figure 3.1.14:** Mineral distribution diagram presenting the main mineral phases and mineral classes of different black shale comminution products as well as their content of base metal sulphides. Besides differences existing in the proportion of carbonates, illite and quartz, the distribution of base metal sulphides amongst the comminuted black shales was partly varying. (Data: MLU)

The carbonate content of Mansfeld black shale comminution products was also coequal with 27% and clearly dominated by dolomite (24.5%). The dominance of carbonates in Rudna black shale can be chiefly attributed to dolomite, which occurred with similar contents in both comminution products (ball mill: 22.0%, impact crusher: 24.9%). Calcite was distributed more heterogeneous, whereas the ball mill product of Rudna black shale hosted substantially more calcite (14.5%) compared to the content in the corresponding impact crusher product (9.4%). Rudna black shale comminution products contained generally the lowest quartz content among the investigated samples.

The distribution of sulphides in black shales was heterogeneous. The main copper-bearing sulphides, variously enriched in the individual black shales, were bornite, chalcopyrite and chalcocite. Additionally, galena, pyrite and sphalerite occurred in different amounts. A further difference represented the total amount of sulphides, which was increased in Sangerhausen and Rudna black shale, while Mansfeld black shale contained a significantly lower portion.

As mentioned above, sample charges for ball mill and impact crusher tests were different, whereby different contents of sulphides were detected in comminution products from the same black shale feed type. The sulphide association of Rudna black shale comminution products was dominated by bornite and chalcocite. The ball mill product contained 3.2% bornite, 1.5% chalcocite and 0.6% chalcopyrite. It also had an increased amount of galena (3.5%) and pyrite (2.3%) as well as a low portion of sphalerite (0.4%). The impact crusher product is characterized by higher concentrations of bornite (4.4%) and chalcocite (3.4%), while the content of chalcopyrite (0.4%), galena (0.3%), pyrite (0.5%) and sphalerite (0.0%) was partly distinctly lower compared to the ball mill product.

Compared to the Rudna ball mill product, the Sangerhausen ball mill product contained a similar increased content of bornite (2.8%), but hosted additionally more chalcopyrite (1.3%), though just traces of chalcocite (0.1%). Furthermore, the contents of galena (1.5%) and pyrite (2.6%) was more increased, whereas the sphalerite content (0.4%) was comparable to the Rudna ball mill product.

Regarding the copper content, the Mansfeld black shale sample represents a low-grade ore. Thus, the amount of copper-bearing sulphides was decidedly lower, so that they occurred virtually as trace minerals.

A slight difference in the distribution of sulphides between ball mill and impact crusher product was ascertainable. Copper-bearing sulphides in the comminution products of Mansfeld black shale were bornite (ball mill: 0.4%, impact crusher: 0.8%) chalcocite (ball mill: 0.5%, impact crusher: 0.6%) and chalcopyrite (ball mill: 0.3%, impact crusher: 0.2%). The amount of sphalerite was substantially increased (ball mill: 1.7%, impact crusher: 2.4%), whereas pyrite contents (0.6%) were equally low in both comminution products and galena (ball mill: 0.4%, impact crusher: 0.2%) had similar low concentrations as the copper sulphides.

The mineral class "other" in Figure 3.1.14 includes the content of organic matter (determined separately) as well as accessory mineral phases. The main portion in this class can be attributed to organic matter, which was high in the Sangerhausen black shale sample (14.4%), while Rudna black shale contained a moderate (7.3%) and Mansfeld black shale the lowest amount (2.4%) of total organic carbon. Thus, the portion of the "other" class was significantly high in the ball mill product of the Sangerhausen black shale. It consisted additionally an increased amount of barite (4.3%) and some apatite (1.0%). Accessory minerals were mainly anhydrite and traces of rutile, anglesite, ankerite, zircon, iron oxyhydroxides as well as iron and copper sulphates.

Besides the organic matter (7.3%), comminution products of Rudna black shale contained different portions of minor and accessory minerals. While in the ball mill product just traces (< 0.5%) of apatite and rutile were detected, Rudna black shale feed for the impact crusher test featured an increased amount of minor minerals, especially presented by anhydrite (2.7%), rutile (1.0 %) and apatite (0.7%). Additionally, traces of ankerite, iron oxyhydroxides and zircon occurred in the impact crusher product of Rudna black shale.

The content of minor and accessory minerals in comminution products of Mansfeld black shale was differently. Generally, the Mansfeld black shale had a low content of organic matter (2.4%). The ball mill product hosted 4.0% of minor mineral phases, whereas the impact crusher product contained just 1.4%. The main part of minor minerals in the ball mill product constituted anhydrite (1.6%), whereas additionally traces of ankerite, iron oxyhydroxides and rutile occurred. A similar association of minor minerals, but with lower quantities, was detected in the impact crusher product of Mansfeld black shale comprising mainly anhydrite (0.6 %) as well as traces of ankerite, apatite and rutile.

### 3.1.2.2 Geochemical distribution of metals in black shale comminution products

The mineral distribution analysis in Chapter 3.1.2.1 has shown that different black shale comminution products contained varying amounts of metal sulphides. Table 3.1.3 displays concentrations for base metals as well as accompanying metals of economic interest. Amongst comminution products, the Rudna black shale sample are characterized by an increased content of Cu, which was 3.65% in the ball mill product and particular high in the impact crusher product containing 5.51% Cu. While the Cu content was moderately in the Sangerhausen ball mill product (2.54%), Mansfeld black shale comminution products were characterized by the lowest Cu contents (ball mill: 0.60%, impact crusher: 0.83%)

Rudna comminution products were marked by strongly different Pb contents, which is mainly attributed to the circumstance that the sample used for the impact crusher test represented a hand-picked sub sample of the Rudna black shale bulk sample. Thus, variations in the metal content were also ascertainable for comminution products from Mansfeld black shale. The Rudna ball mill product contained an increased Pb content of 4.15%, but in the impact crusher product Pb was insignificant (0.48%). The content of Zn and Fe in both Rudna comminution products indicated just slight variation, but Zn was negligible low. The Sangerhausen ball mill product contained 1.02% Pb and a low Zn

**Table 3.1.3:** Metal contents of the different black shale comminution products extracted from geochemical analyses. (Data: ALS)

	Cu [%]	Pb [%]	Zn [%]	Fe [%]	Ag [ppm]	As [ppm]	Co [ppm]	Mo [ppm]	Ni [ppm]	V [ppm]
<b>Mansfeld ball mill</b>	0.60	0.84	1.04	1.56	227	40	48	95	109	159
<b>Mansfeld impact crusher</b>	0.83	0.90	1.35	1.56	70	40	54	129	129	203
<b>Sangerhausen ball mill</b>	2.54	1.02	0.13	2.40	73	400	743	368	250	739
<b>Rudna ball mill</b>	3.65	4.15	0.04	1.75	226	120	137	300	196	462
<b>Rudna impact crusher</b>	5.51	0.48	0.02	1.43	246	60	88	204	146	308

concentration, while Mansfeld black shale featured slightly increased contents of Pb (ball mill: 0.84%, impact crusher: 0.90%) and Zn (ball mill: 1.04%, impact crusher: 1.35%).

The Sangerhausen ball mill product was also enriched regarding contents of accompanying minor metals. Except for Ag, it hosted the highest amounts, in particular for As (400 ppm), Co (743 ppm) and V (739 ppm). An increased content of Mo was analysed also in the Sangerhausen (338 ppm) as well as in the Rudna (300 ppm) ball mill product. The latter as well as the Rudna impact crusher product were additionally marked by increased Ag contents (ball mill: 226 ppm, impact crusher: 246 ppm) similar to the ball mill product from Mansfeld black shale (227 ppm Ag).

### 3.1.3 Liberation analysis of black shale comminution products

An important factor for the extraction of valuable minerals especially by mineral processing methods are the characteristics of grain properties, such as grain size, shape and mineral association, in the comminution product. Thus, the analysis of the grain properties of minerals subjected to be won by extraction techniques reveals knowledge about the optimization of the recovery yields.

In this study, comminution products generated by ball mill and VeRo Liberator® impact crushing were analysed by datasets provided by the Mineral Liberation Analyzer (MLA) technique (see details in Chapter 2.6.2.1). MLA-data comprise textural grain-based information, but also information about grain constituents, assigned as particle-based information comprising geometrical relation and EDX-spectra. On basis of the latter, particle can be classified mineralogically according to a mineral database. One of the main features extractable from MLA-data is liberation of particles, which can be described as the percentual free surface of a particle along its perimeter. Furthermore, interlockings with other adjacent particles are quantifiable. Commonly, the degree to which a particle is liberated is assigned to liberation classes. Thus, it is widely appointed that four classes describe the liberation of a particle: 0% liberation indicates that the surface of a particle is not exposed. 0% to < 30% free surface corresponds with particles, which are predominantly locked by at least one other grain in a particle. 30% to < 80% free surface expresses moderate liberation, usually designated as middlings, while 80 to 100% free surface is used for liberated particles.

The economic most important minerals in Kupferschiefer-type black shale ores are copper-bearing sulphides. As shown in Chapter 3.1.2.1, bornite, chalcopyrite and chalcocite represented the most prevalent copper minerals in the black shales investigated in this study. Thus, particle size distribution and liberation analysis were restricted to these three copper sulphides.

#### 3.1.3.1 Grain size distribution of copper sulphides in black shale ball mill products

Ball mill products of black shales from three localities contained generally bornite, chalcopyrite and chalcocite. However, mineral distribution analyses showed that the content of each main copper sulphide was varying. Generally, can be stated that the copper-bearing phases in ball mill products of Rudna and Mansfeld black shale were dominated by bornite and chalcocite, whereas the copper sulphide association in Sangerhausen black shale was characterized by increased amounts of bornite and chalcopyrite.

Figure 3.1.15 shows the grain size distribution for bornite, chalcopyrite and chalcocite independently from the state of liberation. The distribution curves indicate that bornite grains in ball mill products occurred within a similar grain size range, whereas the grain size distribution for chalcocite and especially for chalcopyrite varied more.

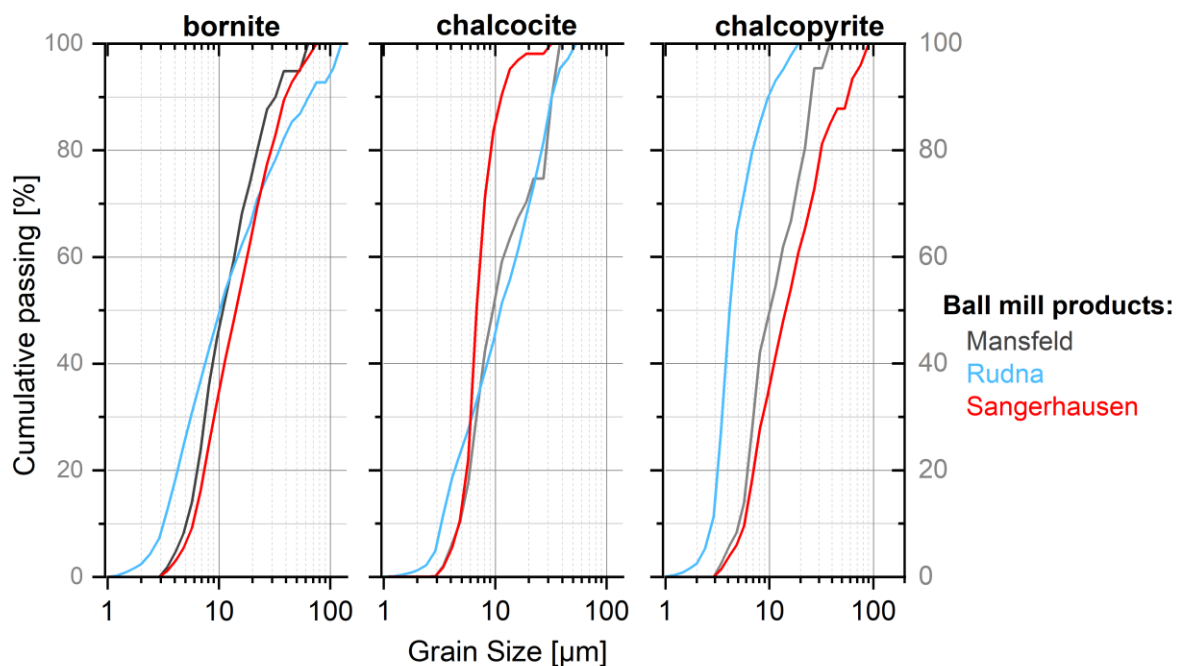


**Figure 3.1.15:** Cumulative grain size distribution of copper sulphides in ball mill products of different black shale ores. (Data: MLA-HIF)

In order to demonstrate differences of the grain size distribution for copper sulphides in ball mill products of black shales from Mansfeld, Rudna and Sangerhausen, the maximum particle sizes for bornite, chalcocite and chalcopyrite at significant volume fractions ( $D_{20}$ ,  $D_{50}$ ,  $D_{80}$ ) were compiled in Table 3.1.4.

As grain size distribution curves for bornite indicated, slight differences regarding the size of bornite grains existed for the mean diameter ( $D_{50}$ ) as well as for the representative particle size ( $D_{80}$ ) within the milled black shale ores. While  $D_{50}$  for bornite in Mansfeld and Rudna ball mill products was nearly equivalent (approx. 10 µm), bornite in milled Sangerhausen black shale was slightly coarser ( $D_{50}$ =14 microns). However, at  $D_{80}$  the ball mill product of Rudna black shale contained bornite grains up to 35 µm, otherwise bornite was more fine-grained in the ball mill products of Mansfeld ( $D_{80}$ =22 µm) and Sangerhausen ( $D_{80}$ =29.5 µm) black shale.

Chalcocite occurred mainly in ball mill products of Mansfeld and Rudna black shale, but in the Sangerhausen black shale it was just present in traces. As the data in Table 3.1.4 show, chalcocite in milled Sangerhausen black shale ore is generally fine-grained below 10 microns even in the fraction of the representative particle size ( $D_{80}$ ). For ball mill products of Mansfeld and Rudna ore, grain sizes of chalcocite in the  $D_{20}$ -fraction were comparably (Mansfeld=5.9 µm, Rudna=4.3 µm) and in the same range as bornite. Generally, the chalcocite grain size was quite similar, at  $D_{50}$  marginally coarser in the Rudna ball mill product (Mansfeld=9.5 µm, Rudna=11.1 µm) and at  $D_{80}$  minor increased in the milled Mansfeld black shale (28.6 µm) in comparison to the Rudna ball mill product (26.6 µm).

Chalcopyrite was a dominant constituent of the sulphide assemblage in the Sangerhausen ball mill product, but in the Rudna ball mill product it represented an accessory mineral, whereas in the Mansfeld ball mill product it occurred just in traces. The grain size distribution of chalcopyrite in Table 3.1.4 reveals very fine grain sizes in the ball mill product of the Rudna black shale ( $D_{80}$ =6.9 µm).

**Table 3.1.4:** Comparison of grain sizes of copper sulphides in ball mill products of black shales at defined passing fractions (20%, 50% and 80%). (M=Mansfeld, R=Rudna, S=Sangerhausen; Data: MLA-HIF)

Passing fraction	Grain size [ $\mu\text{m}$ ]								
	bornite			chalcocite			chalcopyrite		
	M	R	S	M	R	S	M	R	S
<b>D20</b>	6.4	4.3	7.3	5.9	4.3	5.6	6.1	3.2	7.1
<b>D50</b>	10.6	10.1	14.2	9.5	11.1	6.8	10.0	4.2	13.8
<b>D80</b>	22.0	35.0	29.5	28.6	26.6	9.2	22.0	6.9	31.5

It is noticeable that the grain size distribution of chalcopyrite is nearly analogous to bornite for the Mansfeld and Sangerhausen ball mill product, which indicates that the Sangerhausen ball mill product contained generally coarser grains of bornite and chalcopyrite. The Rudna ball mill product in turn contained the coarsest grains of bornite as well as slightly smaller grains of chalcocite as occurring in the Mansfeld ball mill product. The latter contained to most balanced grain size ranges for the examined copper sulphides,  $D_{80}$  was generally  $> 20 \mu\text{m}$  and the mean diameter ( $D_{50}$ ) was nearly at  $10 \mu\text{m}$ .

### 3.1.3.2 Liberation of copper sulphides in black shale ball mill products

Ball mill products of black shale ores were analysed according the liberation of copper sulphides. As mentioned in Chapter 3.1.3, the percentage of free grain surface commonly designated as liberation is differentiated into four classes: not exposed, locked, middlings and liberated. Liberation data for the main copper sulphides are presented hereinafter individually.

#### *Bornite*

Bornite was the most common copper-bearing sulphide determined in the black shale ores investigated in the frame of this study (see Chapter 3.1.2.1), its physical state (grain size, interlockings, free surface) regarding the recoverability is of immense importance for the mineral processing of black shale-hosted ores and even for further types of deposits. Figure 3.1.16 shows liberation curves of bornite for the examined black shale ball mill products. Table 3.1.5 indicates additionally percentages of bornite regarding the four liberation classes. Generally, the portion of liberated bornite grains was overall low and the best liberation yield, achieved for the Mansfeld black shale, was nearly a quarter (23.7%) of liberated bornite from total bornite. While the Mansfeld ball mill product contained a low portion of bornite, ball mill products of Sangerhausen and Rudna black shale were enriched in bornite, and thus the significance of the recoverability is especially crucial for an economic beneficiation. However, the proportion of liberated bornite in both ball mill products was low with 15.0% for the Sangerhausen and 11.8% for the Rudna black shale. Additionally, recoverable bornite grains represent middlings ( $30\% < \text{liberation} \leq 80\%$ ), which were consistent distributed over all within the investigated ball mill products with average 32% of the total bornite. Especially increased proportions of locked ( $< 30\%$  liberation) and not exposed bornite was determined for the Rudna ball mill product (56.5%). Also, in the ball mill product of Sangerhausen black shale, bornite remained largely locked or not exposed (52.0%). The lowest proportion of non- as well as hardly-recoverable bornite (44.3%) contained the ball mill product of Mansfeld black shale low-grade ore.

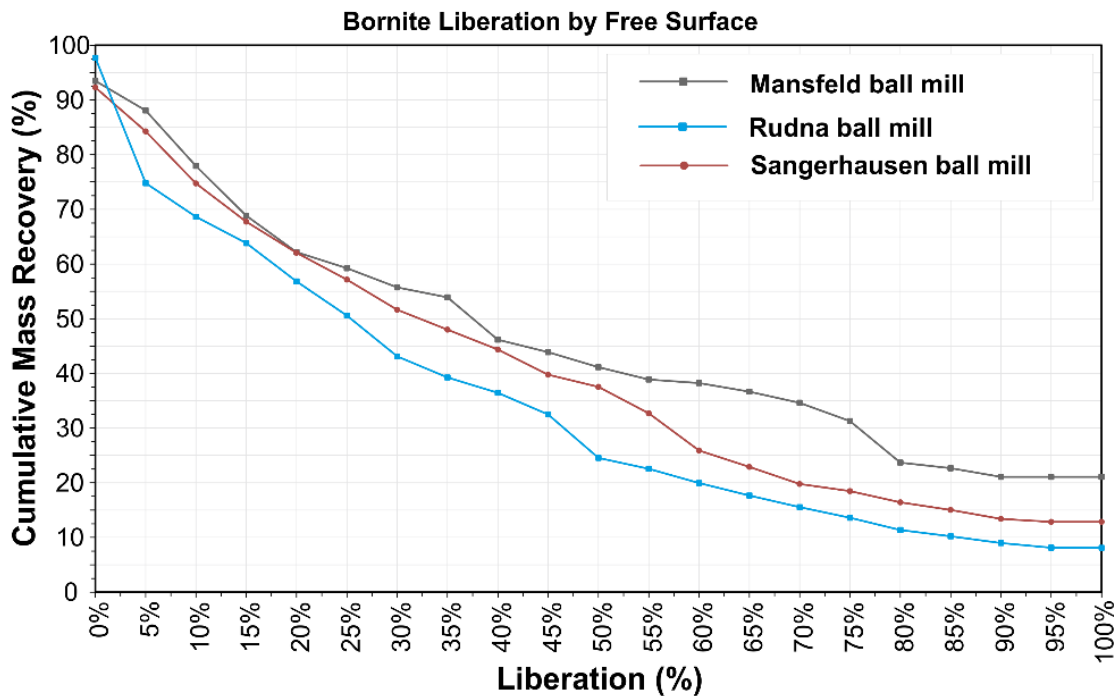


**Figure 3.1.16:** Distribution curves of bornite according to free surface liberation for ball mill products from three different black shale ores. Note that bornite in the Mansfeld ball mill product was significantly better liberated than in the Rudna ball mill product. (Data: MLA-HIF)

**Table 3.1.5:** Liberation classes of bornite in black shale ball mill products. (Data: MLA-HIF)

	Liberation			
	0% not exposed	0% < x ≤ 30% locked	30% < x ≤ 80% middlings	80% < x ≤ 100% liberated
bornite Mansfeld (n=1093)	6.50	37.77	32.05	23.68
bornite Rudna (n=12718)	1.83	54.62	31.74	11.82
bornite Sangerhausen (n=6345)	7.70	44.31	32.97	15.03

### Chalcocite

The limited liberation as recognized for bornite was far more pronounced in respect to chalcocite. Liberation curves for chalcocite in Figure 3.1.17 indicate wider variations regarding the liberation state of chalcocite amongst the different black shale ball mill products. Generally, the liberation is even lower as recognized for bornite. As Table 3.1.6 shows, extremely bad liberation was noticed for chalcocite in the ball mill product of Rudna black shale, just 3.4% were liberated and 12.1% represented middlings, so that almost 85% of the total chalcocite have to be considered to be potentially not recoverable because of the lack of sufficient exhibited grain surface. Similar low liberation was detected for chalcocite occurring in the ball mill product of Sangerhausen black shale ore. However, the proportion of liberated chalcocite grains (12.1%) was significantly increased, but the content of middlings (10.7%) is comparable to the Rudna ball mill product. Thus, still 77.2% of total chalcocite in the Sangerhausen ball mill product remained locked or not exposed. Better liberation data were determined for the ball mill product of Mansfeld black shale. Although the proportion of liberated chalcocite grains (11.7%) was similar low as for the Sangerhausen ball mill product, it contained a higher proportion of middlings (30.0%), but still 49.7% of locked and 8.6% of not exposed chalcocite.

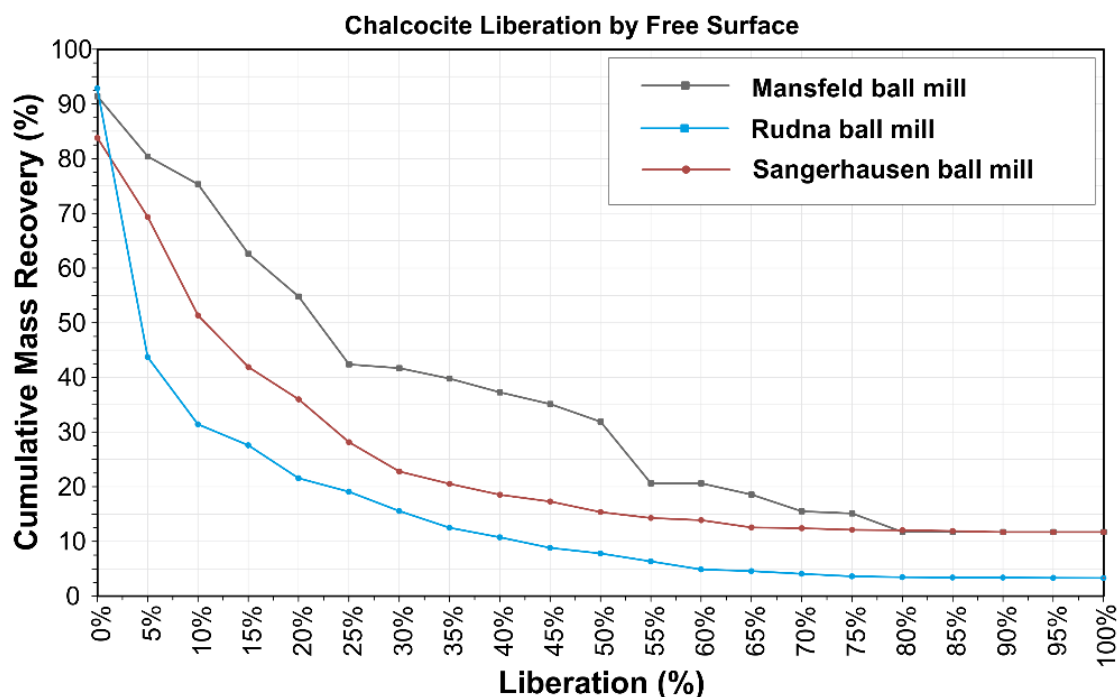


**Figure 3.1.17:** Cumulative distribution of chalcocite particles in relation to the percentage of liberation for ball mill products from different black shale ores. (Data: MLA-HIF)

**Table 3.1.6:** Liberation classes of chalcocite in black shale ball mill products. (Data: MLA-HIF)

	Liberation			
	0% not exposed	0% < x < 30% locked	30% < x ≤ 80% middlings	80% < x ≤ 100% liberated
chalcocite Mansfeld (n=184)	8.61	49.70	29.97	11.72
chalcocite Rudna (n=3061)	7.20	77.30	12.11	3.39
chalcocite Sangerhausen (n=1224)	16.21	61.00	10.74	12.05

### Chalcopyrite

The grain size distribution of chalcopyrite in Figure 3.1.18 revealed a wide range of chalcopyrite grains within the investigated black shale ball mill products. Besides the extremely fine-grained presence of chalcopyrite, its content was very low in the ball mill product of Rudna black shale. Opposed to that, the Sangerhausen ball mill product hosted substantially more chalcopyrite, from which the grains were much coarser and as similar as in the Mansfeld ball mill product. Chalcopyrite liberation data of the milled black shale ores, depicted in Figure 3.1.18 and listed in Table 3.1.7, show generally an increase of the liberation compared to chalcocite. Thus, chalcopyrite in the Sangerhausen ball mill product was marked by the highest proportion of liberated grains (19.3%), whereas the ball mill product of Mansfeld black shale contained a lower amount of liberated chalcopyrite (12.4%) followed by a very low proportion in the Rudna ball mill product (6.4%).

A similar relationship was determined for middlings. Moderately liberated chalcopyrite grains occurred in larger extent in the Sangerhausen ball mill product, whereas the ball mill product of the Mansfeld black shale had a substantially lower fraction of chalcopyrite middlings (23.4%). Similar to the portion of liberated particles, the Rudna ball mill product was characterized by an exceptionally low amount of partly liberated chalcopyrite (10.0%). According to the low proportion of middlings and liberated chalcopyrite, it features most prominent locked and not exposed chalcopyrite grains (83.6%).

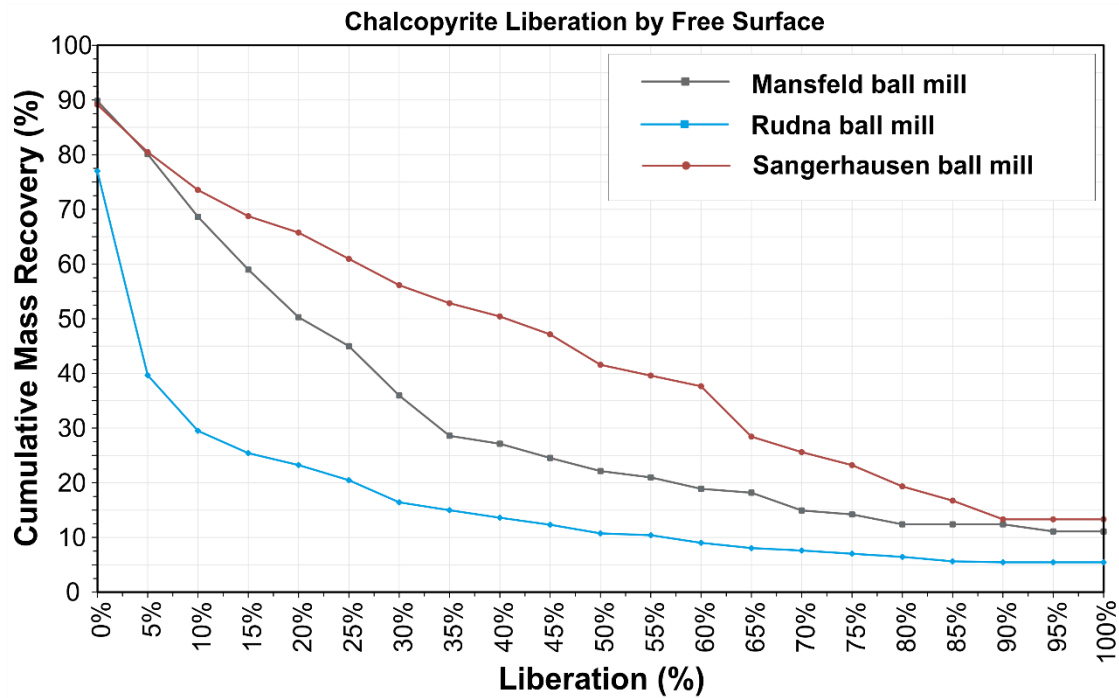


Figure 3.1.18: Chalcopyrite liberation curves for black shale ores from different deposits. (Data: MLA-HIF)

Table 3.1.7: Distribution of chalcopyrite in ball mill products of black shale ores grouped to liberation classes. (Data: MLA-HIF)

	Liberation			
	0% not exposed	0% < x < 30% locked	30% < x ≤ 80% middlings	80% < x ≤ 100% liberated
chalcopyrite Mansfeld (n=464)	10.16	53.90	23.54	12.40
chalcopyrite Rudna (n=1090)	23.01	60.58	9.97	6.44
chalcopyrite Sangerhausen (n=2010)	10.86	33.01	36.82	19.32

For the Mansfeld ball mill product, the percentage of extensive locked and not exposed chalcopyrite grains was significantly lower (64.1%). A far more decreased proportion of predominantly locked as well as not exposed chalcopyrite showed the Sangerhausen ball mill product, in which 43.9% of the total chalcopyrite occurred in a poorly liberation state.

### 3.1.3.2.1 Copper sulphide liberation by particle size classes

In the previous subchapter, liberation data of copper sulphides were presented in general. In order to emphasize the link between the general particle size in the ball mill products and the state of liberation of the value mineral (grain), liberation data were filtered accordingly to particle size classes of the ball mill products, considering the 0-100 µm size range at 10 µm steps each class. Therefore, liberation data representing free surface percentages of copper sulphides were summarized and defined according to common liberation classes (0%=not exposed, ≤ 30% mainly locked surface, ≤ 80% partially liberated surface, > 80% mainly liberated surface). Columns within the particle size class are stacked according to these liberation classes.

*Bornite*

Figure 3.1.19 contains the comparison of bornite liberation vs. general particle size class in ball mill products of Mansfeld, Rudna and Sangerhausen black shale ores. Generally, liberated bornite grains existed mainly in the lower particle size classes. Exceptional good liberation of bornite was detected in the particle size class < 10 micron, in which liberated bornite occurred up to 83%. In this particle size class, ball mill products of Mansfeld and Sangerhausen black shale showed very similar distribution of liberated and partially liberated (middlings) bornite grains. For these ball mill products, the distribution of bornite liberation was comparable also in coarser particle size classes up to the < 40 micron class, in which the proportion of liberated bornite grains decreased continuously and the proportion of middlings increased rapidly.

While the proportion of locked and not exposed bornite grains in the particle size range < 20 micron is low, it expanded to more than 50% in the particle size range > 40 microns. However, the Sangerhausen ball mill product contained a significantly portion of bornite middlings up to the particle size < 90 micron, while bornite in the Mansfeld ball mill product was chiefly hosted as middlings in the

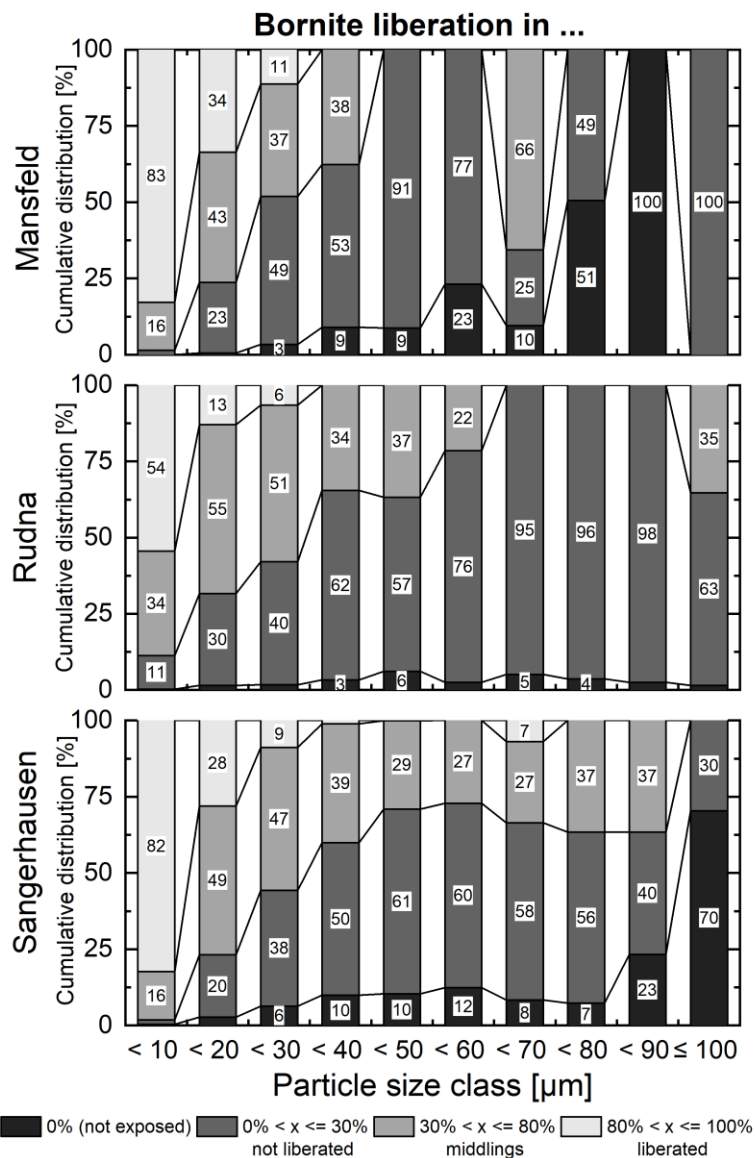


**Figure 3.1.19:** Distribution of liberation classes for bornite in ball mill products from different black shale deposits according to particle size classes in the range -100 micron. (Data: MLA-HIF)

particle size classes  $< 40 \mu\text{m}$  and additionally in the  $60\text{-}70 \mu\text{m}$ -class. Generally, bornite grains were mainly locked in the particle size classes  $\geq 40 \mu\text{m}$  and the proportion of not exposed bornite rose increasing to coarser particle size classes, which is notable from the  $50\text{-}60 \mu\text{m}$  class for the Mansfeld ball mill product, but also concerned bornite grains in the Sangerhausen ball mill product in the particle size range  $> 80 \mu\text{m}$ .

The distribution of liberation for bornite in the Rudna ball mill product was comparable to other ball mill products, but it had generally higher proportions of middlings and locked bornite grains in lower particle size classes ( $< 30 \mu\text{m}$ ). However, it contains a remarkable portion ( $22\% \leq x \leq 37\%$ ) of bornite middlings in the particle size fraction  $30\text{-}60 \mu\text{m}$  and showed the lowest content of not exposed bornite grains amongst ball mill products within the considered particle size range. Further, the Rudna ball mill product contained a comparatively increased amount of low liberated bornite grains over the entire particle size range.

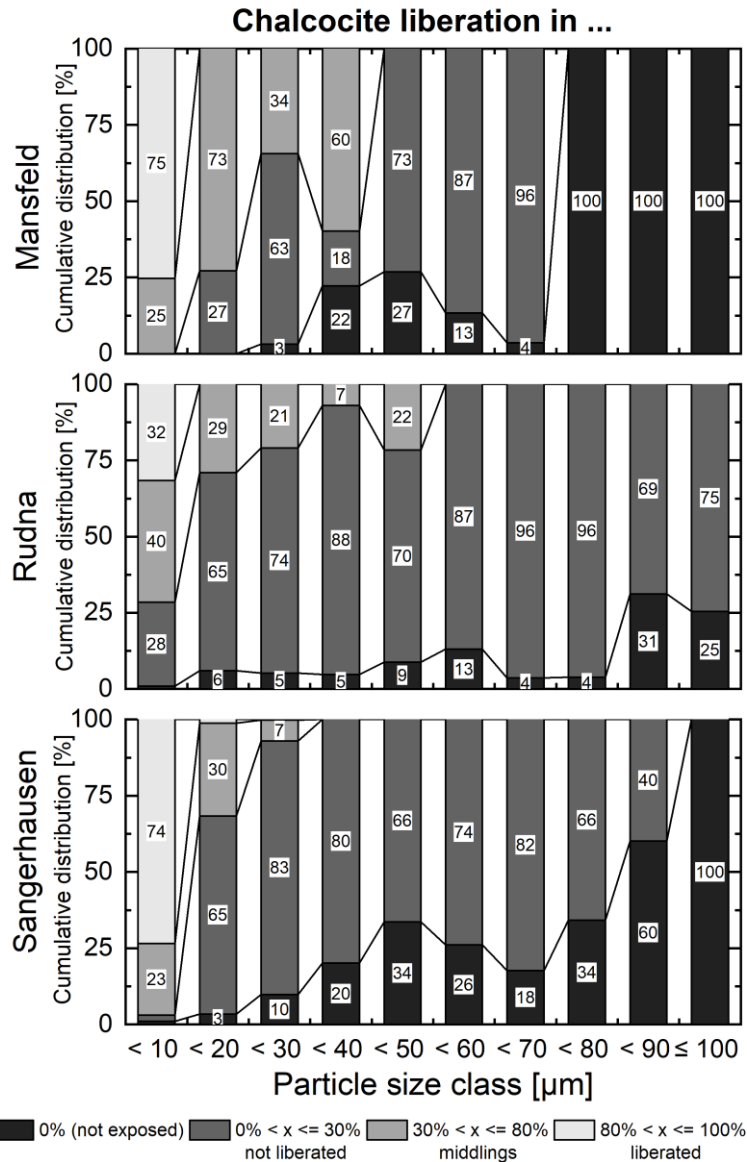
#### *Chalcocite*

Figure 3.1.20 depicts the liberation classification for chalcocite grains according to particle size classes up to 100 microns in black shale ball mill products. Liberated chalcocite was independently from the origin of the black shale ore only detected in the particle size class  $< 10 \mu\text{m}$ . While the Mansfeld ball mill product contained appreciable amounts of partly liberated (middlings) chalcocite grains in particle size classes  $< 40 \mu\text{m}$ , ball mill products from Sangerhausen and Rudna black shale showed much less proportions of middlings in the same particle size range. Especially, the Sangerhausen ball mill product featured chalcocite middlings just up to the  $< 30 \mu\text{m}$  particle size range. In the particle size range  $> 30$  microns, it contained exclusively chalcocite grains, which were predominantly locked or not exposed. The proportion of not exposed chalcocite was notably increased in the Sangerhausen ball mill product generally over the whole particle spectrum. However, the Mansfeld ball mill product was characterized by solely not exposed chalcocite in the  $< 80$  to  $100 \mu\text{m}$  fraction. Generally can be stated that the liberation of chalcocite in ball mill products was poor.

#### *Chalcopyrite*

The distribution of liberation modes for chalcopyrite according to particle size classes of ball mill products in Figure 3.1.21 revealed the most pronounced heterogeneity within the investigated black shale ball mill products. Very low liberation of chalcopyrite was detected for the Rudna ball mill product, in which liberation for chalcopyrite mainly in the  $< 10 \mu\text{m}$  class (26%) and subordinately in the  $< 20 \mu\text{m}$  class (4%) occurred. Additionally, the proportion of chalcopyrite middlings was restricted to a wider extent in the finest particle size class (43%) and decreased vastly in the  $< 20 \mu\text{m}$  class to few percent. Thus, chalcopyrite grains in the Rudna ball mill product were mostly locked (low liberation) as well as to a lesser extent not exposed over the examined particle size range. The liberation of chalcopyrite in the Mansfeld ball mill product was comparatively increased. It contained 72% liberated chalcopyrite grains in the  $< 10 \mu\text{m}$  particle size class but a significant lower proportion in the particle size class  $< 20 \mu\text{m}$  (14%). Partially liberated chalcopyrite middlings were especially present in the  $< 20 \mu\text{m}$  (48%) and  $< 60 \mu\text{m}$  (54%) particle size class. The proportion of locked to low liberated chalcopyrite grains increased constantly up to the  $< 50 \mu\text{m}$  particle size class, in which 95% of chalcopyrite was locked and 5% occurred not exposed. Chalcopyrite grains within the particle size range  $60\text{-}100 \mu\text{m}$  were either locked or not exposed in the ball mill product of the Mansfeld black shale.

Amongst ball mill products, the Sangerhausen black shale hosted the most increased liberation for chalcopyrite. Chalcopyrite in the particle size class  $< 10 \mu\text{m}$  was largely liberated (83%) or occurred in



**Figure 3.1.20:** Stacked column plots for the distribution of chalcocite liberation classes according to particle size classes in the ball mill products of different black shale ores. (Data: MLA-HIF)

partially liberated middlings (16%). The proportion of liberated chalcocite decreased substantially with increasing particle size, so that just 25% in the < 20 μm and 12% in the < 30 μm particle size class were liberated chalcocite grains. Although, a considerable percentage (44%) of liberated chalcocite were present in the < 60 μm particle size class. Furthermore, chalcocite middlings represented a considerable proportion in the particle size range from 10 to < 60 μm (37-51%) in the Sangerhausen ball mill product. While, the amount was significantly lower for chalcocite in the < 70 μm particle size class, chalcocite middlings were not detected in the < 80 μm class, but represented the major liberation state in < 90 μm particle size class (79%). The proportion of locked chalcocite grains in the ball mill product of Sangerhausen black shale increased nearly constantly from the < 20 μm to < 70 μm particle size class and decreased rapidly in the particle size range from 70 to < 90 μm range. The coarsest particle size class in turn consisted largely of locked chalcocite grains (96%).

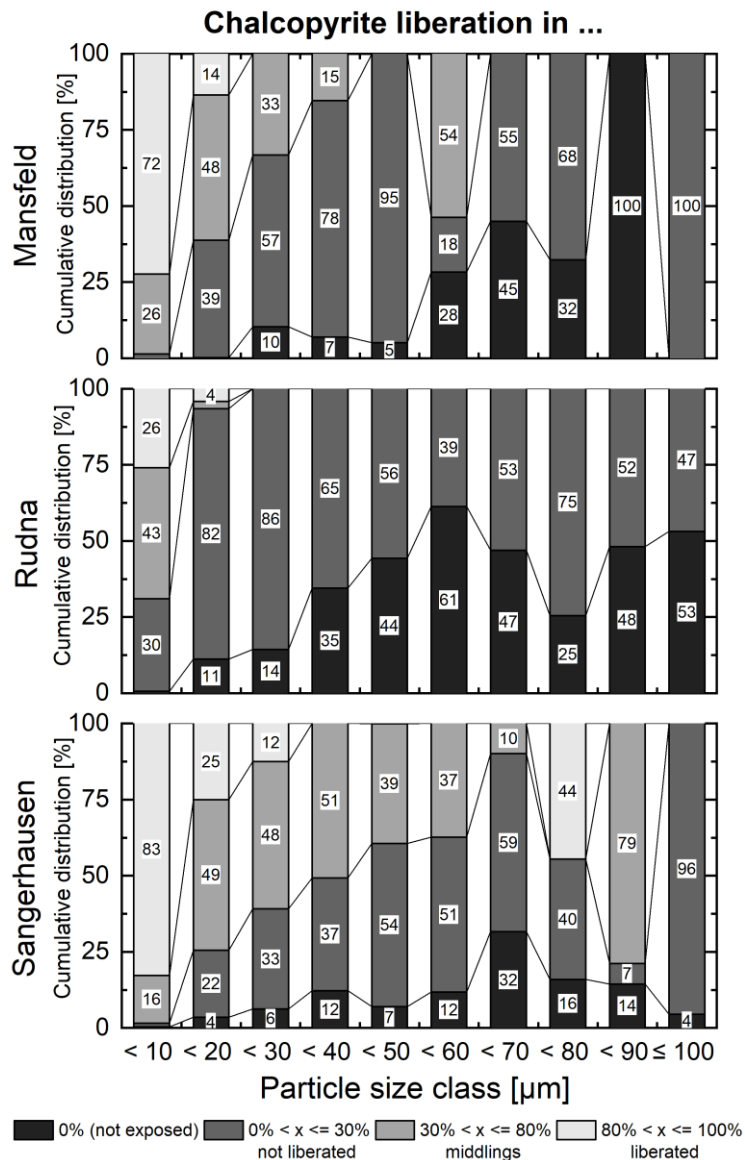


**Figure 3.1.21:** Liberation classes of chalcopyrite based on free surface area and their percentual occurrence in particle size classes in ball mill products of different black shale ores. (Data: MLA-HIF)

Generally, the Sangerhausen ball mill product showed the lowest proportion of not exposed chalcopyrite grains. The proportion in the particle size classes was mostly below 20% or even 10%, but reached exceptionally 32% in the < 70 μm particle size class. All in all, chalcopyrite in the ball mill product of Sangerhausen black shale showed the most increased liberation for chalcopyrite.

### 3.1.3.3 Mineral locking in ball mill products of different black shale ores

Additional relevant information of comminuted ores in respect to their processability indicate the mineralogical association of a certain value mineral intergrown with other minerals in a particle. Thus, locking associations of a mineral can be assigned to binary locked if second mineral phase occurs interlocked with the target mineral and form a particle. More complex intergrowth associations are described by ternary locking, which describes the interlocking of a mineral grain of interest adjoining with at least two other mineral phases within a particle.

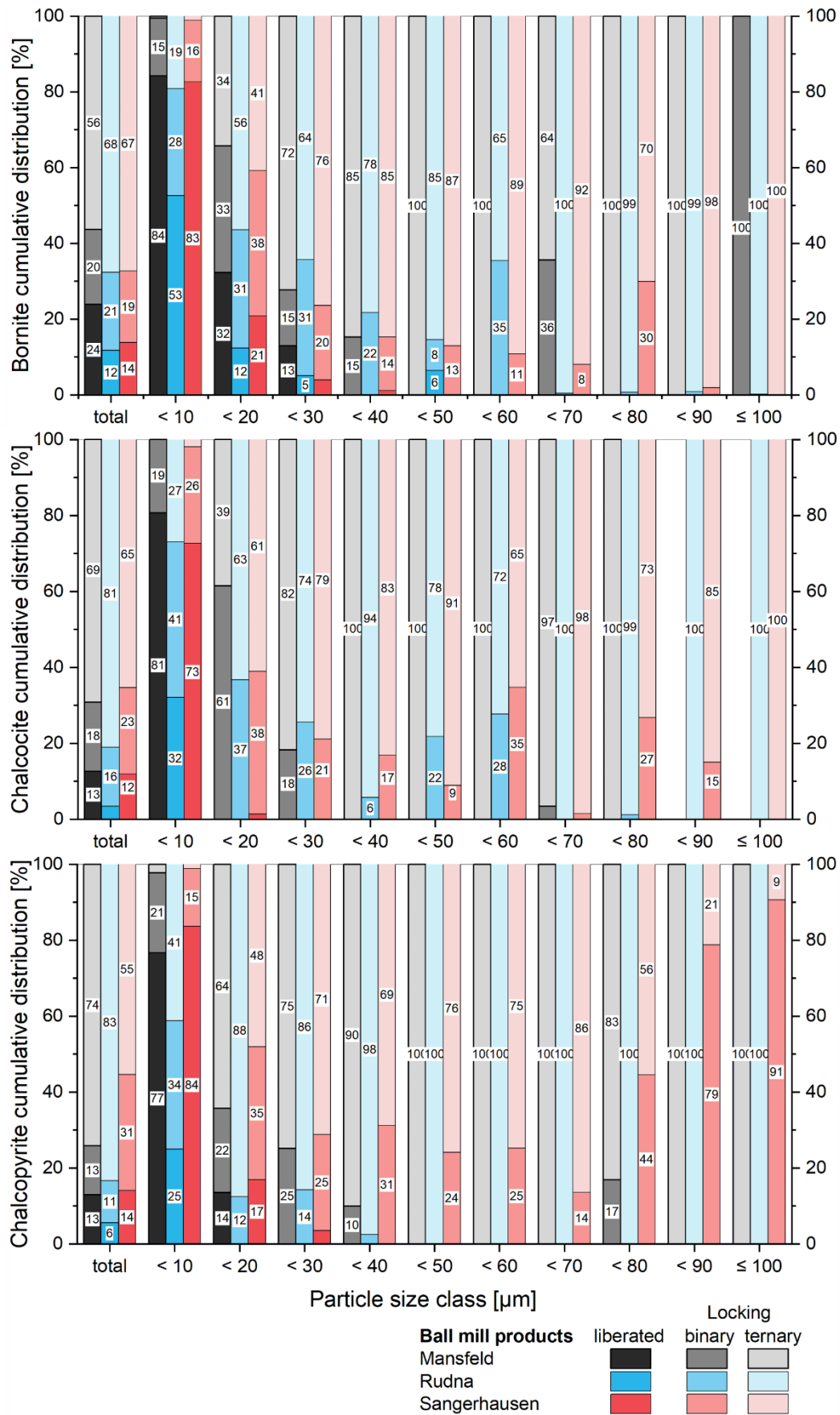


**Figure 3.1.22:** Stacked column plots showing cumulative distribution data of locking modes based on weight % for bornite, chalcocite and chalcopyrite in ball mill products of different black shale ores. (Data: MLA-HIF)

As the previous subchapter has shown, the liberation of copper sulphides in ball mill products of different black shale ores was largely remarkable low. According to that, the majority of copper sulphide grains in ball mill products were hosted in particles characterized by a mineral assemblage. Figure 3.1.22 shows a compilation of stacked column plots of the locking state of bornite, chalcocite and chalcopyrite according to particle size classes.

Generally, the locking association for bornite in all ball mill products was similar, in particular the proportion of the locking mode in Rudna and Sangerhausen ball mill products were almost identical (see Figure 3.1.22 left columns for the total particle size range). Thus, a low portion of bornite grains occurred liberated, but approximately two third of bornite grains were hosted in complexly intergrown particles (ternary+) and another 20% occurred binary locked. The Mansfeld ball mill product contained a significantly higher portion of liberated bornite grains (24%), the same amount of binary locked bornite grains and slightly more than 50% of ternary locked bornite.

The investigation of the locking mode regarding individual particle size classes of the ball mill products revealed a strong variability. While bornite grains in the particle size class < 10 microns of the Mansfeld and Sangerhausen ball mill were mainly liberated and low binary locked, the Rudna ball mill product deviated by markedly increased concentration of binary (28%) as well as additionally ternary (19%) locked bornite grains. The complexity of the locking association increases generally towards coarser particle size classes, whereas the amount of liberated bornite grains shrunk rapidly up to the particle size class < 40 micron in all ball mill products accompanied by a substantial increase of ternary locked bornite grains. Only the Rudna ball mill product contained a low portion (6%) of liberated bornite grains in the < 60 particle size class. Bornite binary locked occurred erratic in terms of distribution and content within the particle size range from 40 to 100 microns and represented seldom more than a third in a single particle size class, whereas the < 90 micron particle size class of the Mansfeld ball mill product consisted completely of binary locked bornite, although all other particle size classes + 40 microns contained bornite grains, which were ternary or more interlocked with other mineral phases.

The sole occurrence of ternary locking applied also to chalcocite grains from the + 30 microns particle size range in the Mansfeld ball mill product. While liberated chalcocite grains were nearly restricted to the < 10 micron particle size class of all ball mill products, binary locked chalcocite occurred in varying proportions most extensive in the Sangerhausen ball mill product up to the < 80 micron particle size class. Binary locked chalcocite was lower distributed in the Rudna ball mill product, in which it notably occurred up to the < 60 micron particle size class.

A general observation is that chalcocite grains were mostly ternary and more locked from the +20 micron particle size range in both, the Rudna and Sangerhausen ball mill products. Thus, the locking mode was generally dominated by ternary+ locked chalcocite over the whole particle size range in ball mill products and was exceedingly high in the Rudna ball mill product (81%), which also showed the lowest proportion of binary locked (16%) as well as liberated (4%) chalcocite grains. The distribution of the locking mode of chalcocite in the Mansfeld and Sangerhausen ball mill product was quite similar, but was also dominated by ternary locked chalcocite (Mansfeld: 69%, Sangerhausen: 65%). The latter hosted further similar quantities of binary locked chalcocite (Mansfeld: 16%, Sangerhausen: 23%) as well as liberated chalcocite grains (Mansfeld: 13%, Sangerhausen: 12%).

The locking association for chalcopyrite grains in the investigated ball mill products was commonly marked by ternary locking. In particular, the Rudna ball mill product showed an extensively high

proportion of ternary locked chalcopyrite (83%) as well as low portions of binary locked (11%) and liberated (6%) chalcopyrite grains. While the Mansfeld ball mill product contained some more binary locked chalcopyrite (13%), the proportion was significantly higher in the Sangerhausen ball mill product (31%), but ternary locked chalcopyrite represented the main locking mode (Mansfeld: 74%, Sangerhausen: 55%).

Liberated chalcopyrite grains occurred mainly in the < 10 microns particle size class, in which the proportion was markedly high in the Mansfeld (84%) and Sangerhausen (83%) ball mill products. In the same particle size class, the sum of binary and ternary locked chalcopyrite was decidedly increased in the Rudna ball mill product. Especially for the Mansfeld and Rudna ball mill products, the amount of binary locked chalcopyrite grains decreased rapidly up to the < 40 micron particle size class and ternary locked chalcopyrite occurred in the particle size range beyond. In contrast, the Sangerhausen ball mill product showed substantial amounts of binary locked chalcopyrite grains over the entire particle size spectrum, in which the content of binary locked chalcopyrite increased strongly up to 91% in the ≤ 100 particle size class.

#### 3.1.3.3.1 Mineral distribution of locking associations for copper sulphides in black shale ball mill products

Further investigation targeting the mode of locking in combination to mineral species interlocked were carried out on particle size classes of ball mill products. Copper sulphides, the main economic valuable minerals, and their binary and ternary+ locking mode combined with the mineral association in regards to the total comminution products but also in discrete particle size classes opens insights to the recoverability or even failed extraction yields. Thus, the determination of mineral associations of binary or more complexly locked copper sulphides was carried out for total ball mill products and in 10 micron particle size classes in the range up to 100 µm.

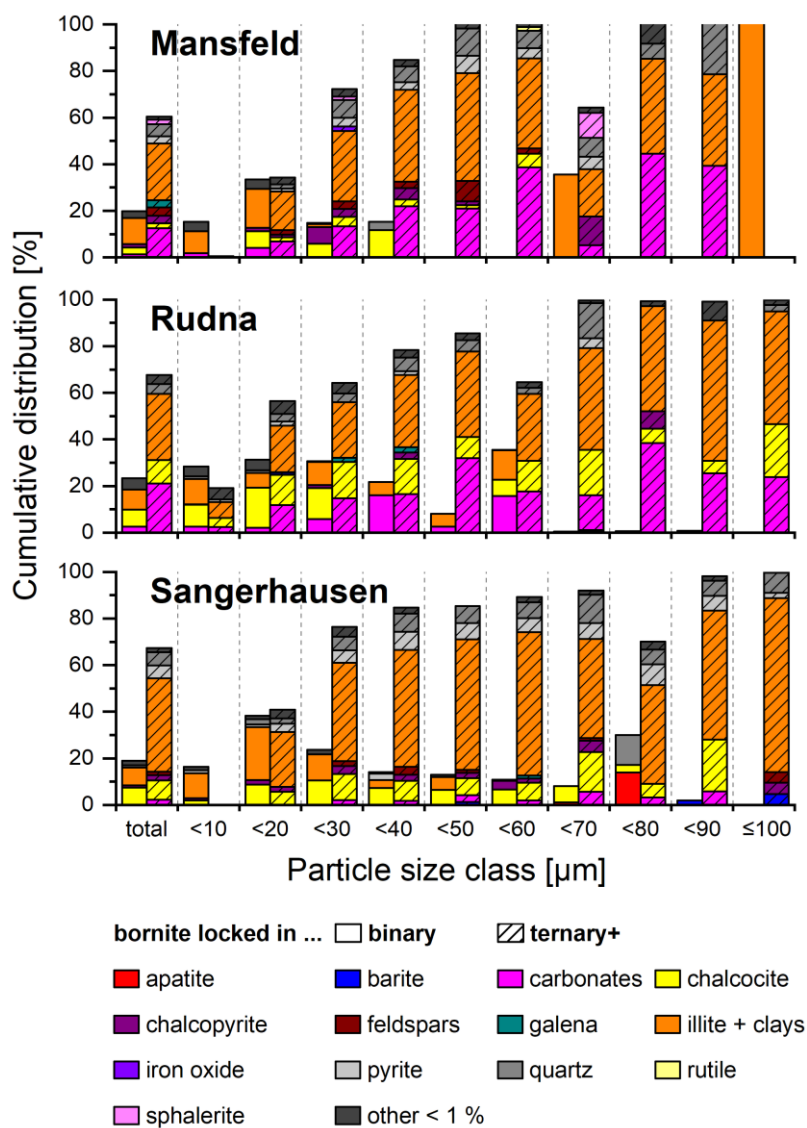
##### *Bornite*

Figure 3.1.23 shows the mineral distribution for binary as well as complexly (ternary+) locked bornite. Generally, main minerals interlocked with bornite represented carbonates (predominantly dolomite), illite-clay minerals as well as to a lower extend quartz, chalcocite, chalcopyrite and pyrite, especially in ball mill products of Mansfeld and Sangerhausen black shale ore. The ratio of binary and ternary+ locked bornite in total ball mill products was quite similar but the distribution of mineral species interlocked with bornite showed as well similarities as divergences. Binary locked bornite was predominantly intergrown with chalcocite or illite and subordinately with quartz in ball mill products of Rudna and Sangerhausen black shale, while in the ball mill product of Mansfeld black shale bornite was mainly interlocked with illite and to a lesser extend with chalcocite and chalcopyrite.

The mineral distribution of mineral phases intergrown with ternary+ locked bornite revealed the complexity of intergrowth textures in the examined black shale ores, especially regarding the Mansfeld ball mill product. While the number of interlocked mineral phases for ternary+ locked bornite in the Rudna ball mill product was significantly lower, ternary+ locked bornite in the Sangerhausen and Mansfeld ball mill products was more complexly intergrown, which is indicated by an increasing number of minerals interlocked with bornite. Basically, ternary+ locked bornite is intergrown mostly with illite/clays in the studied ball mill products, while appreciable proportions of interlocking with carbonates occurred only in Rudna and Mansfeld ball mill products. Complexly intergrowth of bornite with other sulphides varied amongst ball mill products. Chalcocite was more common in bornite

intergrowths in Rudna and Sangerhausen ball mill products, whereas chalcopyrite and pyrite but with lower proportions, were constituents of complex bornite intergrowth in milled Sangerhausen and Mansfeld black shales. In ball mill product of the latter, sphalerite was additionally part of the complex intergrowth association with bornite.

Binary locked bornite occurred mainly in the lower particle size range of the studied ball mill products and was mainly associated with illite as well as chalcocite. While illite dominated the binary intergrowth in the finer particle size fraction (up to 20  $\mu\text{m}$ ) of Mansfeld and Sangerhausen ball mill products, chalcocite was the more common mineral interlocked with bornite in the Rudna ball mill product and contained increasingly proportions of interlockings with carbonates towards coarser particle size classes. However, chalcocite was also mainly associated with binary locked bornite over nearly all particle size classes in Mansfeld and Sangerhausen ball mill products, exceptions were determined for the upper particle size range, in which binary locked bornite occurred. Here, bornite is



**Figure 3.1.23:** Compilation of stacked column charts displaying the percentual proportion of minerals associated with binary and ternary+ (striated shading) locked bornite for the total sample (left side) and according to particle size classes in the ball mill products of black shales from Mansfeld, Rudna and Sangerhausen. (Data: MLA-HIF)

intergrown exclusively with illite/clays in the Mansfeld ball mill product. Apatite and quartz were predominant minerals interlocked with bornite in coarser particles of the Sangerhausen ball mill product.

The distribution of mineral phases related to complex (ternary+) locked bornite within particle size classes of ball mill products was generally dominated by illite/clays. A fairly constant ratio of minerals involved to ternary+ locked bornite was ascertained for the Rudna ball mill product, in which, at increasing amount of ternary locking towards coarser particle grain size, illite/clay was the dominant mineral group intergrown with bornite accompanied by moderate proportions of locking with carbonates as well as chalcocite, subordinately quartz and chalcopyrite.

Generally, the proportion of illite/clay ternary+ locked with bornite was significantly higher over the entire particle size classes in the Sangerhausen ball mill product. It also contained slightly increased ternary+ interlockings of bornite with chalcopyrite, pyrite and quartz. Ternary intergrowths of bornite in the Mansfeld ball mill product contained mainly illite, but also increasing proportions of carbonate minerals towards coarser particle size fractions. There was additionally a perceptible amount of ternary+ locked bornite associated with feldspars, quartz as well as sulphides such as pyrite, chalcopyrite and chalcocite. Especially, ternary+ locked bornite in the <70 micron particle size class was intergrown with increased proportions of chalcopyrite and sphalerite. However, the coarse-grained particle size classes of the Mansfeld ball mill product contained ternary locked bornite intergrown to an equal extent with carbonates and illite/clays as well as some quartz.

#### *Chalcocite*

The distribution of minerals locked with chalcocite in Figure 3.1.24 shows clearly that chalcocite and bornite occurred strongly intergrown over the entire particle size range of the ball mill products. In particular binary locked chalcocite was almost exclusively intergrown with bornite. The only exception represented the < 10 micron particle size class of the investigated ball mill products, in which additional primarily illite/clays was binary locked with chalcocite. Low proportions of carbonate and feldspar minerals were interlocked binary with chalcocite in the lowest particle size class of the Mansfeld ball mill product.

Ternary+ locked chalcocite was in particular intergrown with bornite over a wide range of particle size classes in Rudna and Sangerhausen ball mill products. Commonly, interlocking of chalcocite with bornite represented more than 50% of the mineral associations within each particle size class, particularly up to the < 70 micron particle size range of ball mill products from Rudna and Sangerhausen black shale. Ternary intergrowths of illite/clays with chalcocite were the second most mineral association in particle size classes of the Sangerhausen ball mill product, whereas low proportions of chalcopyrite, pyrite, carbonates, feldspar and quartz were accompanying mineral phases interlocked ternary+ with chalcocite in the particle size range up to the < 70 micron class. In coarser particles in which chalcocite occurred, the proportion of intergrowths with in particular illite /clays and partly pyrite and quartz increased. Ternary+ locked chalcocite in the Rudna ball mill product was, besides bornite, associated mainly with illite/clays and carbonate minerals. Silver-bearing chalcocite was detected in association with chalcocite in the particle size range 10 to < 60 micron. The particle size classes < 80 and < 90 micron of the Rudna ball mill product contained ternary+ locked chalcocite mainly intergrown with illite/clay, carbonates and feldspars accompanied by the lowest proportion of bornite in the entire particle size range. But in the  $\leq 100$  micron particle size class bornite was again the dominating mineral interlocked with chalcocite.

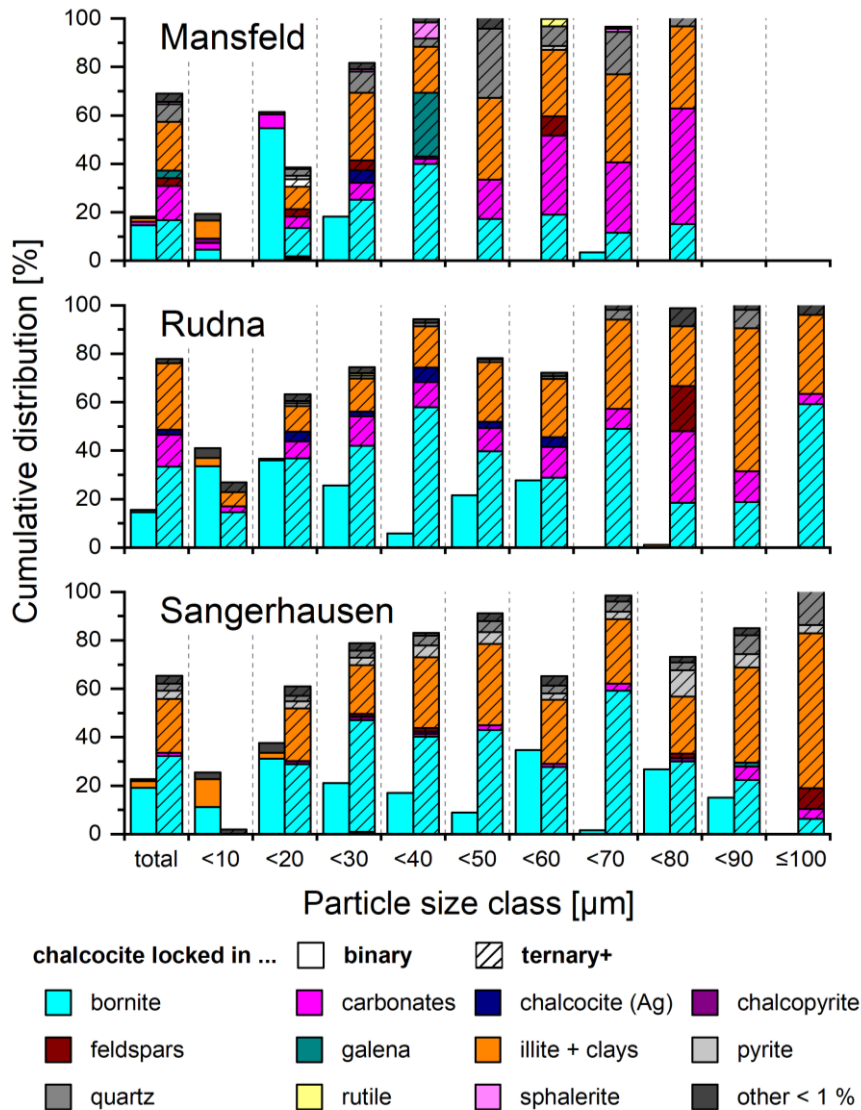


**Figure 3.1.24:** Compilation of stacked column charts displaying the percentual proportion of minerals associated with binary and ternary+ (striated shading) locked chalcocite for the total sample (left side) and according to particle size classes in ball mill products of black shales from Mansfeld, Rudna and Sangerhausen. (Data: MLA-HIF)

A quite heterogeneous distribution of minerals ternary+ interlocked with chalcocite was present in the particle size classes of the Mansfeld ball mill product. While the finest particle size class contained no ternary+ locked chalcocite, the < 20 micron class was marked by complex intergrowth comprising numerous minerals, mainly bornite and illite/clays and subordinately carbonates, feldspar, and quartz as well as cobaltite and pyrite. This heterogeneity continued until < 40 micron particle size, so that, besides the before mentioned minerals, also markedly proportion of silver-bearing chalcocite, but also galena and sphalerite were associated with ternary+ locked chalcocite. Above the < 40 micron particle size class the proportion of bornite interlocked with chalcocite decreased significantly and illite/clays, carbonates as well as quartz represented the main mineral phases intergrown complexly with chalcocite in the Mansfeld ball mill product.

## Chalcopyrite

The locking of chalcopyrite with mineral phases for the studied ball mill products is depicted in Figure 3.1.25. Generally, intergrowths of chalcopyrite were more complicated in Mansfeld and Sangerhausen ball mill products. Despite of that, chalcopyrite locking in the total Rudna ball mill product was mainly limited to illite/clay, carbonates and bornite as well as to much lower extend to pyrite, quartz and chalcocite. Binary locked chalcopyrite was mainly associated with bornite. In the total ball mill product of Mansfeld black shale binary locked chalcopyrite was mainly intergrown with bornite and pyrite at similar proportions. Ternary+ locked chalcopyrite in the total Mansfeld ball mill product was associated with an increased number of mineral phases. Intergrowths with chalcopyrite occurred mainly with illite/clays, pyrite, bornite and carbonates. Additionally, low amounts of pyrite, sphalerite as well as iron oxide and quartz constituted complex intergrowths with chalcopyrite. The highest amount of binary locked chalcopyrite in the total sample existed in the ball mill product of Sangerhausen black

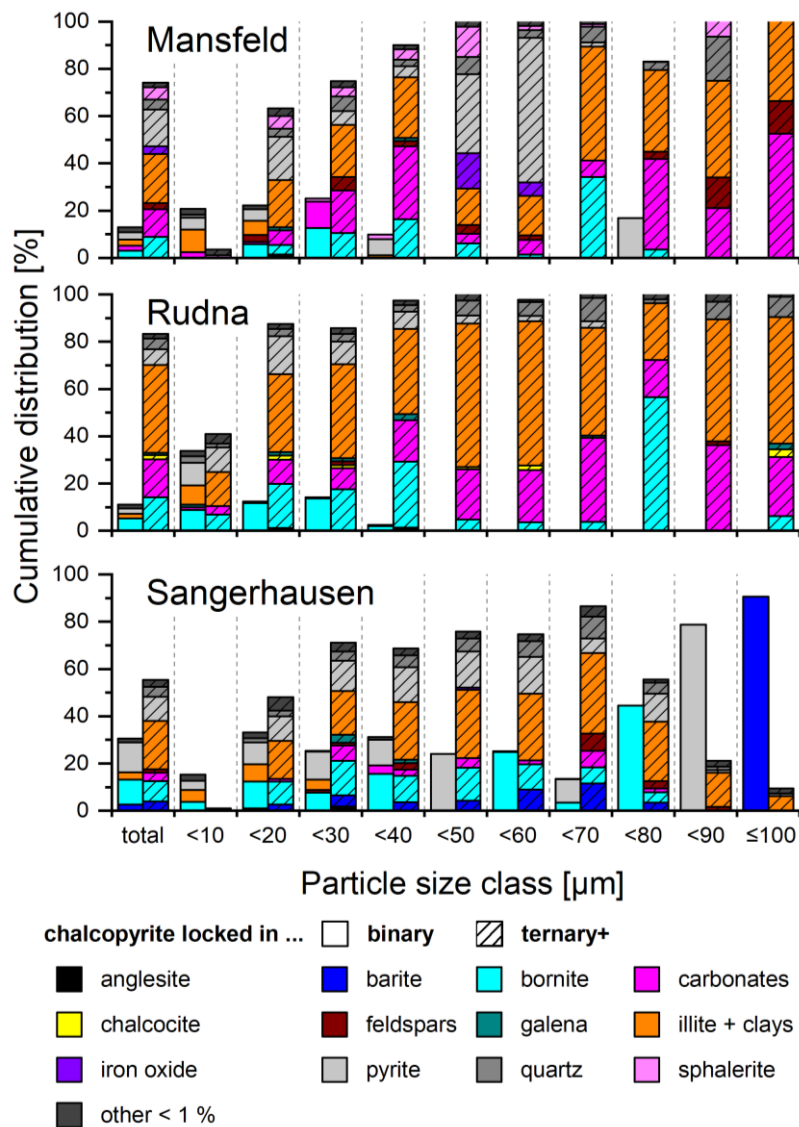


**Figure 3.1.25:** Compilation of stacked column charts displaying the percentual proportion of minerals associated with binary and ternary+ (striated shading) locked chalcopyrite for the total sample (left side) and according to particle size classes in ball mill products of black shales from Mansfeld, Rudna and Sangerhausen. (Data: MLA-HIF)

shale, where mainly interlocking of chalcopyrite with bornite and pyrite occurred. More complex intergrowth (ternary+) of chalcopyrite comprised locking associations with mainly illite/clays, pyrite and bornite.

The proportion of binary locked chalcopyrite was especially low within the particle size classes of ball products from Mansfeld and Rudna black shale. Both showed binary locked chalcopyrite predominantly in the lower particle size range, up to the < 40 micron. For the Rudna ball mill product, binary locked chalcopyrite was associated with several minerals (bornite, pyrite, illite/clays) in the lowest particle size class, but in remaining coarser classes only bornite was binary locked with chalcopyrite. The Mansfeld ball mill product in turn contained binary locked chalcopyrite with changing mineral associations in the individual particle size classes. In the fine particle size fraction, pyrite, illite/clays and bornite were binary locked with chalcopyrite, whereas in coarser particle size classes pyrite, bornite and carbonates were binary intergrown with chalcopyrite.

Ternary+ locked chalcopyrite in the Mansfeld ball mill product was gradually increasing intergrown with pyrite up to the < 60 micron particle size class. Additionally, complex chalcopyrite intergrowths contained moderate proportions of illite/clays, which increased significantly in particles in the range from 60 to 100 microns similar to intergrowths with carbonates. The latter had a quite heterogeneous distribution regarding their proportion in the individual particle size classes that showed low to moderate amounts in the particle size range up to the < 70 micron particle size class in order to raise significantly in the upper particle size range. Further mineral constituents of complex intergrowths with chalcopyrite in the Mansfeld ball mill product were iron oxide, sphalerite, feldspars and quartz at discontinuous occurrence.

Locking associations of ternary locked chalcopyrite within the particle classes of the Rudna ball mill product were comparatively simply marked by intergrowths with mainly illite/clays, bornite and carbonates as well as low amounts of pyrite and quartz as well as traces of other mineral phases. The proportion of bornite in complex intergrowth with chalcopyrite decreased towards coarser particle size classes, but was exceptionally high in the < 80 micron particle size class.

The Sangerhausen ball mill product contained binary locked chalcopyrite over the whole particle size classes. In the lower particle size range (up to the < 40 micron class), binary intergrowths with chalcopyrite were mainly marked by locking with bornite, illite/clays and pyrite. While in the coarser particle size range of the Sangerhausen ball mill product chalcopyrite was binary locked either with pyrite or bornite. An exception represented the  $\leq 100$  micron particle size class, in which chalcopyrite was completely intergrown with barite. Binary intergrowth of chalcopyrite increased significantly in the upper two particle size classes. The proportion of ternary+ locked chalcopyrite increased generally up to the < 70 micron particle size class. The mineral association binary locked with chalcopyrite was similar over a wide particle size range and was dominated by illite/clays, bornite and pyrite. Subordinately were barite, carbonates, quartz, partly galena and feldspar constituents of complex intergrowths with chalcopyrite.

3.1.3.4 Grain size distribution of copper sulphides in VeRo Liberator® impact crusher products

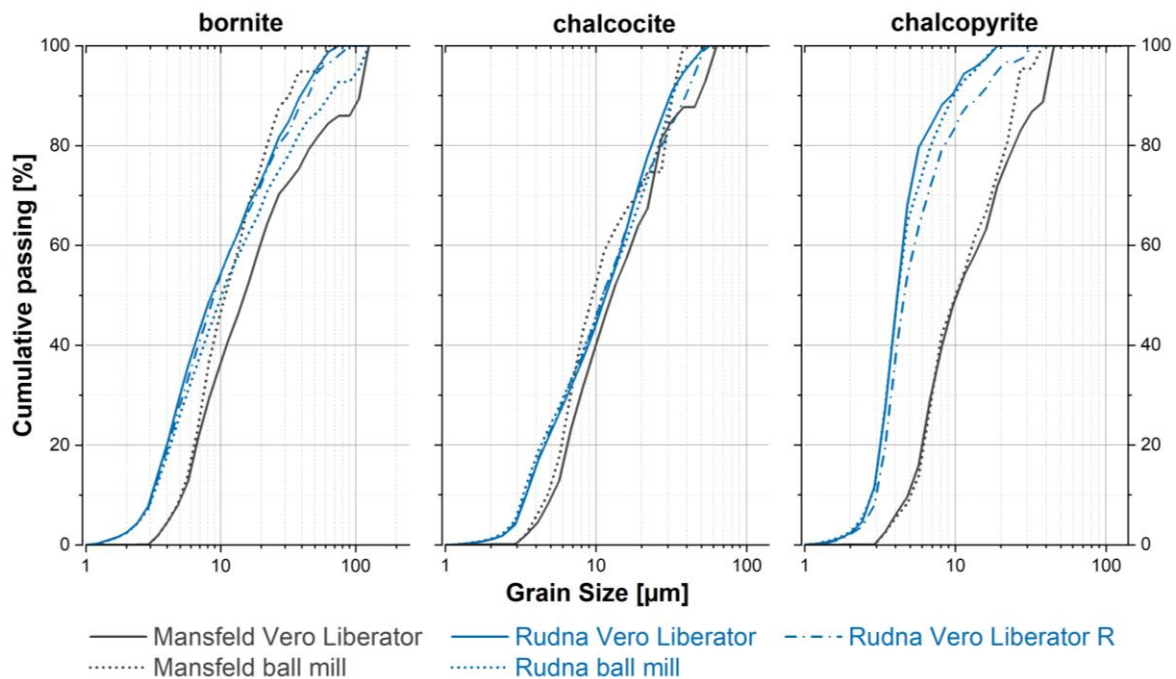
Comminution tests on two types of black shale ore were carried out with the VeRo Liberator® impact crusher, which delivered products that had a significantly proportion of particles  $\leq 100$  microns, 65% for Mansfeld black shale and 62% for Rudna black shale. Main copper sulphides determined in both black shale ores were bornite and chalcocite with increased amounts in Rudna black shale ore, whereas chalcopyrite generally represented the lowest quantities amongst the major copper sulphides in Rudna and Mansfeld bulk samples comminuted by the VeRo Liberator® (see Chapter 3.1.2.1).

Figure 3.1.26 depicts the grain size distribution of bornite, chalcocite and chalcopyrite for the VeRo Liberator® impact crusher products and additionally for a Rudna black shale product formed by the VeRo Liberator® using round hammer tools. For comparison, the particle size distribution of each copper sulphide in the ball mill products is also displayed.

The grain size distribution of copper sulphides in the  $\leq 100$  micron fraction of VeRo Liberator® products showed generally deviations to ball mill products. Grain size curves of bornite describe slightly finer bornite grains in the impact crusher product of Rudna black shale compared to the ball mill product, whereas the grain size distribution for bornite deviated substantially between ball mill and VeRo Liberator® product of Mansfeld black shale, in which bornite is notably coarser above the 20% passing fraction.

A comparable deviation of chalcocite grain size distribution curves for Mansfeld black shale comminution products showed that chalcocite was commonly finer up to 75% passing fraction in the ball mill product. In a short interval, up to 81% cumulative passing, the chalcocite grain size was similar but the deviation increased significantly towards 100% chalcocite cumulative passing.

The course of the chalcocite grain size distribution for Rudna black shale VeRo Liberator® and ball mill products is nearly identical, low deviations were only detected in the range between 60 and 90%



**Figure 3.1.26:** Grain size distribution curves of bornite, chalcocite and chalcopyrite in the particle size fraction  $< 100$  VeRo Liberator® products of Mansfeld and Rudna black shale and for comparison in the respective ball mill products. (VeRo Liberator®\_R = round hammer tools, Data: MLA-HIF)

**Table 3.1.8:** Comparison of grain sizes of copper sulphides in VeRo VeRo Liberator® and ball mill products of black shales ores at defined passing fractions (20%, 50% and 80%). (VeRo Liberator®\_R = round hammer tools; Data: MLA-HIF)

	Mineral	Sample	Product	Passing fraction		
				D20	D50	D80
Particle size [µm]	bornite	Mansfeld	ball mill	6.4	10.9	22.0
			VeRo Liberator®	6.6	15.0	47.2
		Rudna	ball mill	4.3	10.2	34.6
			VeRo Liberator®	4.0	8.6	25.6
			VeRo Liberator®_R	4.1	8.9	26.8
		chalcocite	Mansfeld	ball mill	5.9	9.5
	VeRo Liberator®			6.5	12.8	26.5
	Rudna		ball mill	4.3	11.1	26.1
			VeRo Liberator®	4.6	11.6	23.4
			VeRo Liberator®_R	4.5	11.1	27.5
	chalcopyrite		Mansfeld	ball mill	6.2	10.1
		VeRo Liberator®		6.0	10.2	24.6
		Rudna	ball mill	3.2	4.1	6.9
			VeRo Liberator®	3.2	4.1	5.8
			VeRo Liberator®_R	3.4	4.6	8.5

cumulative passing, in which the ball mill product contained slightly coarser chalcocite grains compared to the impact crusher product. The chalcocite grain size distribution between impact crusher products of Rudna black shale ore were coincident up to 70% passing fraction, but in the upper grain size range, the comminution product originated by the impact crusher equipped with round hammer tools hosted coarser chalcocite grains with up to 10 microns difference.

Chalcopyrite in Mansfeld black shale comminution products was substantially more coarse-grained. Generally, ball mill and impact crusher products of as well Rudna as Mansfeld black shale ore deviated weakly. For the comminuted Rudna black shale, the impact crusher with round hammer tools contained slightly coarser chalcopyrite compared to the VeRo Liberator® product generated with angular tools. Significantly coarser chalcopyrite grains were also detected in the upper grain size range (+80% cumulative passing) for the ball mill product from Mansfeld black shale ore that contained chalcopyrite grains up to 15 microns finer compared to the impact crusher product.

Table 3.1.8 summarizes and lists the grain sizes of bornite, chalcocite and chalcopyrite at standard cumulative passing fraction for VeRo Liberator® and ball mill products generated from Mansfeld and Rudna black shale bulk samples (see Chapter 3.1.3.1).

The grain size of bornite in comminution products of both, Mansfeld and Rudna black shale, was generally characterized by low deviation at the 20% passing fraction, although bornite was more than

2 µm finer in the comminuted Mansfeld ore. The average grain size ( $D_{50}$ ) of bornite was moderately coarser (15.0 µm) for the Mansfeld black shale impact crusher product than in the ball mill product (10.9 µm). Far more deviation showed representative fractions of Mansfeld black shale comminution products, in which the grain size of bornite was 22 µm in the ball mill product and more than twice the size in the VeRo Liberator® product ( $D_{80}=47$  µm). Contrary to that, the average bornite grain size in the ball mill product of Rudna black shale was slightly coarser than in VeRo Liberator® products, which showed independently from the hammer tool design similar bornite grain sizes at  $D_{50}$ . At  $D_{80}$ , the Rudna ball mill product hosted larger bornite grains (34.5 µm), whereas VeRo Liberator® products contained an average size of bornite up to 26.2 µm.

Low differences existed for chalcocite between ball mill and VeRo Liberator® products, even among the two black shale ores. The grain size for chalcopyrite generally differed in comminution products regarding the black shale ore so that Rudna comminution products contain generally much finer chalcopyrite grains. However, differences within the passing fractions were low.

#### 3.1.3.5 Liberation of copper sulphides in VeRo Liberator® impact crusher products

Mineral liberation data of VeRo Liberator® impact crusher products were detailed investigated for copper sulphides and compared with liberation data of respective ball mill products. Liberation data express the percentage of free particle surface and are commonly classified and designated as not exposed, locked, middlings and liberated.

##### *Bornite*

Bornite liberation data for VeRo Liberator® products are displayed in Figure 3.1.27 and Table 3.1.9. Generally, the liberation efficiency of the VeRo Liberator® impact crusher for the two types of black shale ore was quite different. While the complete liberation of bornite grains was achieved at a similar level, between 7 to 10% of total bornite, the distribution of partially liberated bornite grains was decidedly different. Very low bornite liberation was detected for VeRo Liberator® impact crushing of Mansfeld black shale ore. It contained nearly 80% of bornite grains, which were either not exposed (6.7%) or predominantly little liberated (73.4% < 30% free grain surface). A far better liberation yield for bornite was achieved in the ball mill product of Mansfeld black shale ore, in which 22.7% of bornite was liberated and 32.1% represented bornite middlings.

Bornite liberation yields for comminuted Rudna black shale were otherwise different. Generally, the VeRo Liberator® impact crusher delivered far better liberation of bornite. While the discrepancy between impact crusher and ball mill products in respect to complete liberated bornite was insignificant, the proportions of partly liberated bornite grains and middlings were essentially increased in impact crusher products. At 50% liberation, VeRo Liberator® products contained either 15% more (equipped with regular tools) or 20% more (round tools) liberated bornite in comparison to the ball mill product. Additionally, the impact crusher product generated with round hammer tools showed the best liberation for bornite by constantly increased proportions of liberated bornite and middlings compared to the regular VeRo Liberator® product.

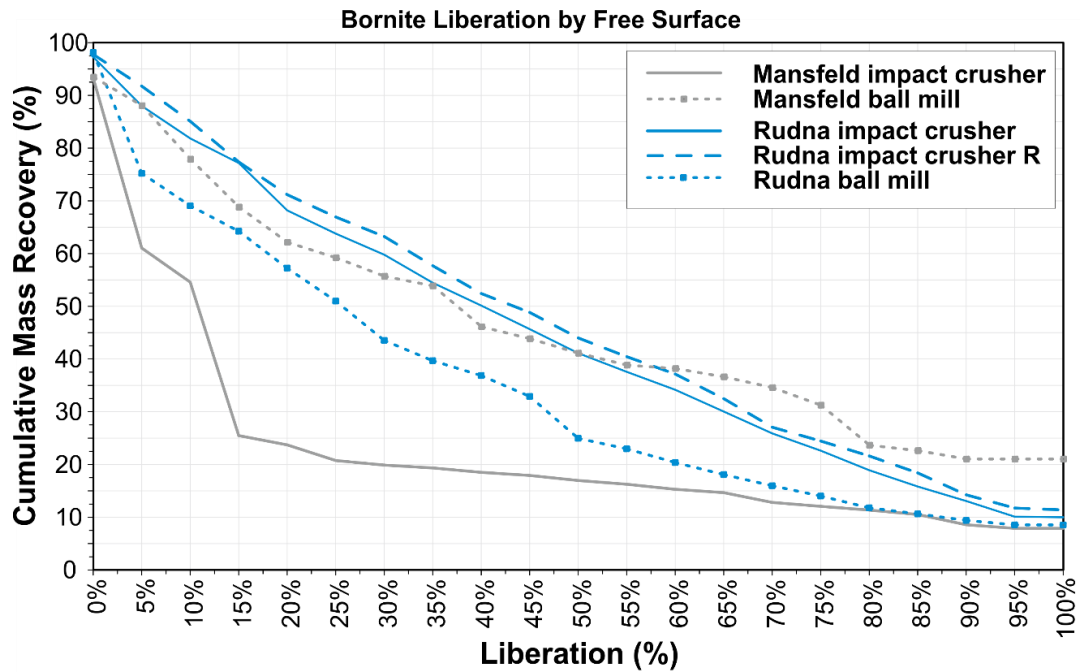


**Figure 3.1.27:** Liberation curves of bornite (in wt. %) in various comminution products of Rudna (blue) and Mansfeld (grey) black shale. Tests with the VeRo Liberator® impact crusher were performed using different tool deployment. (R=round tools; Data: MLA-HIF)

**Table 3.1.9:** Liberation classes for bornite in various comminution products. (Data: MLA-HIF)

	Liberation			
	0% not exposed	0% < x < 30% locked	30% < x ≤ 80% middlings	80% < x ≤ 100% liberated
Mansfeld impact crusher (n=3639)	6.70	73.42	8.52	11.35
Mansfeld ball mill (n=1093)	6.50	37.77	32.05	23.68
Rudna impact crusher (n=15598)	2.73	37.50	40.87	18.90
Rudna impact crusher R (n=13130)	2.25	34.53	41.62	21.60
Rudna ball mill (n=12718)	1.83	54.62	31.74	11.82

### Chalcocite

In Figure 3.1.28 and Table 3.1.10, the liberation of chalcocite is displayed for VeRo Liberator® impact crusher and ball mill products of black shale ores from Rudna and Mansfeld. Generally, the liberation of chalcocite grains was more advanced for comminution products of Mansfeld black shale, though the proportion of liberated chalcocite grains was low. The best liberation of chalcocite was achieved by ball milling (11.7% of total bornite), while the VeRo Liberator® product contained slightly lower amount of liberated chalcocite (7.6%). Generally, the ball mill product showed more increased liberation as the VeRo Liberator® product, although the amount of chalcocite with a free surface from 55 to 70% was nearly coincident in both products of Mansfeld black shale.

The liberation data of comminuted Rudna black shale ore revealed higher proportions of partially liberated chalcocite grains in VeRo Liberator® products, especially for chalcocite grains exhibiting lower than 75% free surface. The amount of liberated chalcocite had low deviations amongst Rudna black shale comminution products, from 3.4% in the ball mill product to 4.7% in the VeRo Liberator® product with regular tools. But significant higher portions of chalcocite middlings occurred predominantly in impact crusher products and were most increased in the VeRo Liberator® product generated with regular tools (31.0%) followed by 24.2% chalcocite middlings in the VeRo Liberator® product generated

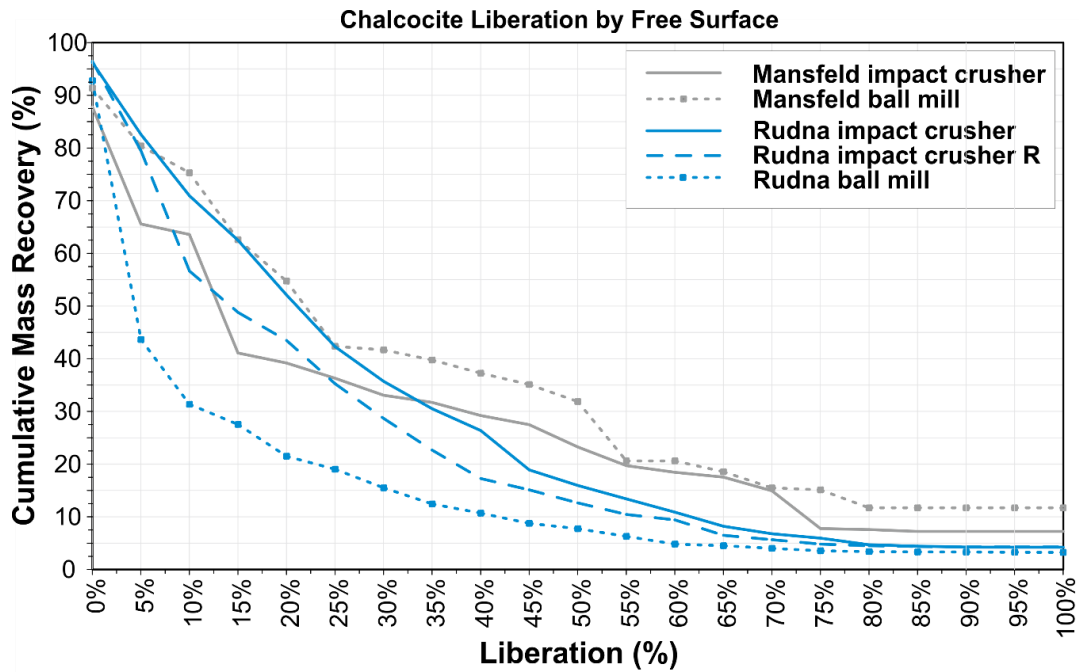


**Figure 3.1.28:** Liberation curves of chalcocite (in wt. %) in VeRo Liberator® ball mill products of Rudna (blue) and Mansfeld (grey) black shale. Tests with the VeRo Liberator® impact crusher were performed using different tool charges. (R=round tools; Data: MLA-HIF)

**Table 3.1.10:** Distribution of liberation classes for chalcocite in various comminution products. (Data: MLA-HIF)

	Liberation			
	0% not exposed	0% < x < 30% locked	30% < x ≤ 80% middlings	80% < x ≤ 100% liberated
Mansfeld impact crusher (n=630)	12.20	54.72	25.50	7.59
Mansfeld ball mill (n=184)	8.61	49.70	29.97	11.72
Rudna impact crusher (n=4988)	3.76	60.53	31.01	4.70
Rudna impact crusher R (n=3797)	3.56	67.75	24.17	4.51
Rudna ball mill (n=3061)	7.20	77.30	12.11	3.39

with round tools. Compared to that, the ball mill product just contained 12.1% chalcocite middlings and was additionally marked by high proportions of locked (77.3%) and not exposed (7.2%) chalcocite grains.

### Chalcopyrite

Chalcopyrite was similar to other copper sulphides differently well liberated depending on ore type as Figure 3.1.29 and Table 3.1.11 display. While the better chalcopyrite liberation was achieved for Mansfeld black shale by ball milling, a far advanced liberation for chalcopyrite in Rudna black shale ore was ascertained in the VeRo Liberator® product formed with regular tools. The latter excelled also the liberation of chalcopyrite in the Mansfeld ball mill product. Generally, the ball mill product of Mansfeld black shale contained the more advanced liberation of chalcopyrite in comparison to the VeRo Liberator® product. However, the portion of liberated chalcopyrite grains in both comminution products was low (ball mill: 12.4%; VeRo Liberator®: 9.0%), but was increased compared to liberated chalcocite. More striking was the content of chalcopyrite middlings in the ball mill product (23.5%), while the VeRo Liberator® product of Mansfeld black shale just contained 10.5% middlings from the total amount of chalcopyrite. Also, the portion of predominantly locked (46.0%) and not exposed

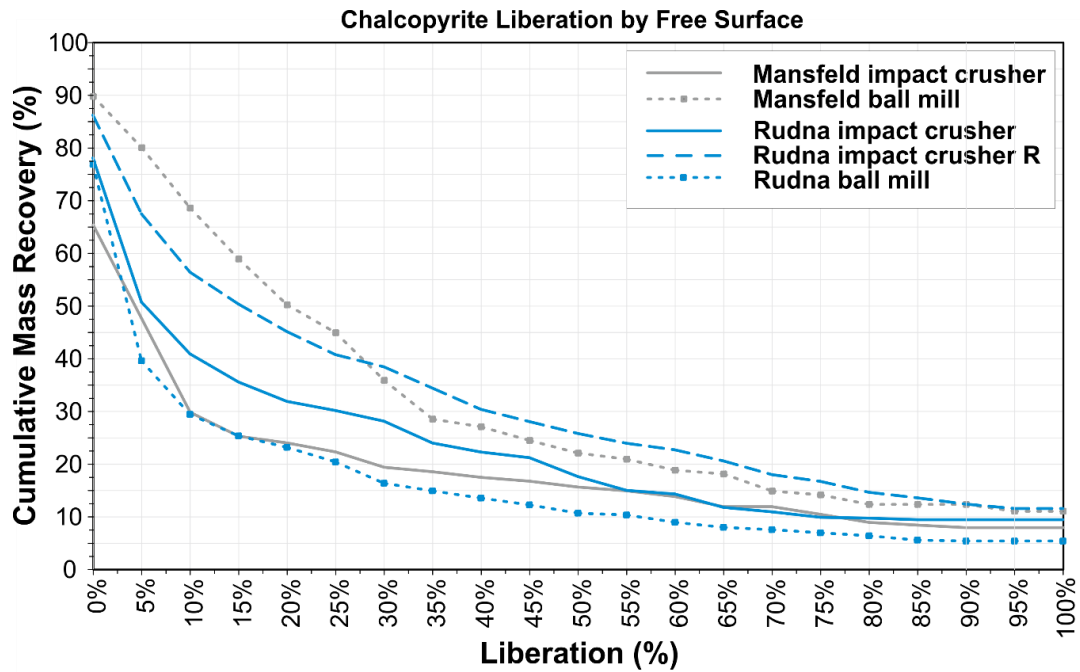


**Figure 3.1.29:** Liberation curves of chalcopyrite (in wt. %) in VeRo Liberator® products of Rudna (blue) and Mansfeld (grey) black shale in comparison to ball mill products. Tests with the VeRo Liberator® impact crusher were performed using different tool deployment. (R=round tools; Data: MLA-HIF)

**Table 3.1.11:** Distribution of liberation classes for chalcopyrite in various comminution products. (Data: MLA-HIF)

	Liberation			
	0% not exposed	0% < x < 30% locked	30% < x ≤ 80% middlings	80% < x ≤ 100% liberated
Mansfeld impact crusher (n=1085)	34.60	45.96	10.47	8.97
Mansfeld ball mill (n=464)	10.16	53.90	23.54	12.40
Rudna impact crusher (n=985)	21.84	49.97	18.40	9.79
Rudna impact crusher R (n=1334)	13.73	47.77	23.80	14.70
Rudna ball mill (n=1090)	23.01	60.58	9.97	6.44

(34.6%) chalcopyrite grains pointed to the low liberation state of chalcopyrite in the VeRo Liberator® product of Mansfeld black shale. Contrary to that the liberation of chalcopyrite was more advanced in VeRo Liberator® products of Rudna black shale ore. The ball mill product hosted a low amount of liberated chalcopyrite grains (6.4%), but VeRo Liberator® products were marked by increased proportions (VeRo Liberator® regular tools: 9.8%; VeRo Liberator® round tools: 14.7%). Especially, the impact crusher product achieved by the usage of round hammer tools provided the most advanced liberation of chalcopyrite grains. Thus, it contained the highest proportion of chalcopyrite middlings (23.8%) followed by the VeRo Liberator® product with regular hammer tools (18.4%), while the amount of chalcopyrite middlings in the ball mill product was low (10.0%). Additionally, the ball mill product of Rudna black shale ore contained high proportions of locked (60.6%) and not exposed (23.0%) chalcopyrite grains, and also VeRo Liberator® products were marked by high portions of locked and not exposed chalcopyrite.

### 3.1.3.5.1 Copper sulphide liberation in VeRo Liberator® products by particle size classes

In order to delineate the liberation of sulphides grains in VeRo Liberator® products, liberation data of sulphide grains were filtered according to 10 micron-particle size classes stretching over the whole particle size range of comminution products. Liberation data (free surface as free perimeter percentages) of copper sulphides were summarized and defined according to commonly used liberation classes (0%= not exposed,  $\leq 30\%$  mainly locked surface,  $\leq 80\%$  partially liberated surface,  $> 80\%$  mainly liberated surface). Proportions of these liberation ranges were plotted in columns indicating the proportion of the liberation state of the respective sulphides in a distinct particle size class of the comminution product.

#### Bornite

The liberation of bornite grains according to particle size classes of the comminution products is displayed for VeRo Liberator® and ball mill products of Mansfeld and Rudna black shale ore in Figure 3.1.30. Liberated Bornite grains in the VeRo Liberator® product of Mansfeld black shale ore occurred predominately in particles  $< 10$  microns (83%) and additionally to a much lower amount (13%) in the

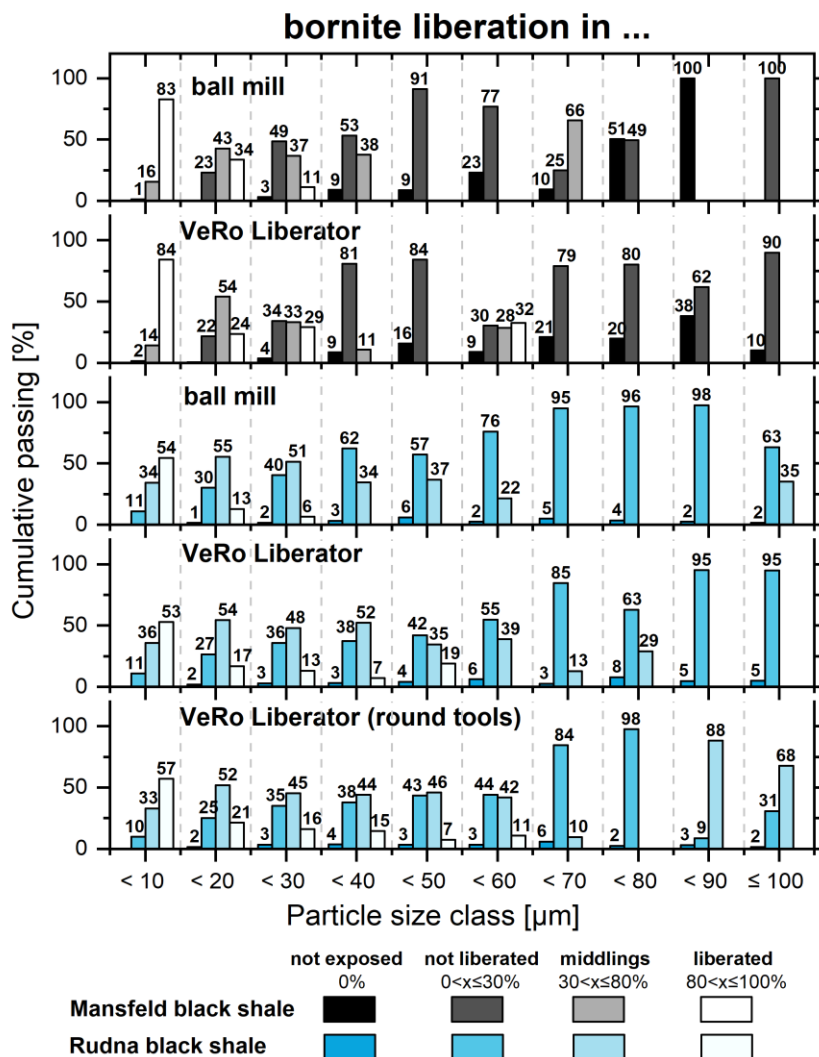


**Figure 3.1.30:** Column plots displaying proportions of liberation classes of bornite in particle size classes of VeRo Liberator® and ball mill products from Rudna and Mansfeld black shale. (Data: MLA-HIF)

particle size class < 20 microns. It also contained bornite middlings with increasing proportions up to particle sizes < 30 microns. Bornite grains in coarser particles of the impact crusher product remained either not liberated (low free surface) or not exposed, whereas the proportion of not exposed bornite grains was mostly much lower in the individual particle size classes, except in the classes < 50 and < 70 microns. In comparison, the ball mill product showed increased portion of liberated bornite grains up to the < 30 microns particle size class and moderate portions of bornite middlings (33-38%) up to particle size class < 40 microns as well as significantly increase (66%) in the < 70 microns particle size class. But also here, not liberated and exposed bornite grains occurred commonly in the particle size range from 40 to 100 microns.

Generally, lower liberation of bornite in the particle spectrum of comminuted Rudna black shale was detected as well for VeRo Liberator® products as ball mill product. Additionally, liberated bornite grains occurred only in the < 10 micron particle size class of the VeRo Liberator® products. In this class, bornite middlings (VL=VeRo Liberator®: 42%; VL\_R= VeRo Liberator® round tools: 44%) and liberated (VL: 32%; VL\_R: 38%) bornite grains represented the most common modes of bornite grains in both VeRo Liberator® products with slightly increased proportions in the VeRo Liberator® product generated with round hammer tools. Additionally, the < 10 micron particle size class contained moderate proportions (VL: 26%; VL\_R: 18%) of not liberated bornite grains. A low portion of liberated bornite grains occurred also in the < 20 particle size class of the VeRo Liberator® product created with round hammer tools. The latter showed lower contents of bornite middlings just up to < 30 micron particle size, whereas the VeRo Liberator® product with regular hammer tools had similar low quantities of bornite middlings in particle size classes < 20 and < 40 microns. In the remaining particle size range (40-100 microns) mainly low liberated as well as not exposed bornite grains were detected in both VeRo Liberator® products of Rudna black shale ore. The ball mill product showed comparably a wider particle size range (up to < 30 microns), in which liberated bornite grains occurred strongly decreasing. It also contained moderate to elevated amounts of bornite middlings (22-55%) up to the < 60 microns particle size class.

### *Chalcocite*

Liberation of chalcocite over the particle size classes of the VeRo Liberator® product from Mansfeld black shale was more advanced. As Figure 3.1.31 shows, it contained a substantial amount (72%) of liberated chalcocite in the < 10micron particle size class, which was likely the same in the ball mill product, and additionally, but to a lower extend (17%), in the < 20 microns particle size class.

Chalcocite middlings generally occurred at increased proportions (up to 63%) in particle size classes up to < 40 micron and furthermore in the < 60 micron particle size class on the VeRo Liberator® product. Chalcocite grains, which were not liberated or not exposed, occurred irregularly distributed in the < 50 micron particle size class as well as in the particle size range from 70 to 100 microns. VeRo Liberator® products from Rudna black shale showed moderate amounts of liberated chalcocite (VL: 31%; VL\_R: 33%) grains nearly exceptionally in the < 10 micron particle size class that also contained increased amounts of chalcocite middlings (VL: 51%; VL\_R: 46%) as well as lower proportions of not liberated chalcocite grains. Generally, the liberation of chalcocite within the grain size classes of both VeRo Liberator® products is commonly similar, even the proportion of chalcocite middlings varied partly in individual particle size classes. Apparently, the distribution of liberation modes for chalcocite over the particle size classes resembled that of the ball mill product, which had just higher proportions of not exposed chalcocite in the particle size range 80 to 100 micron. Additionally, VeRo Liberator® products showed increased amounts of chalcocite middlings up to the < 50 micron particle size class.

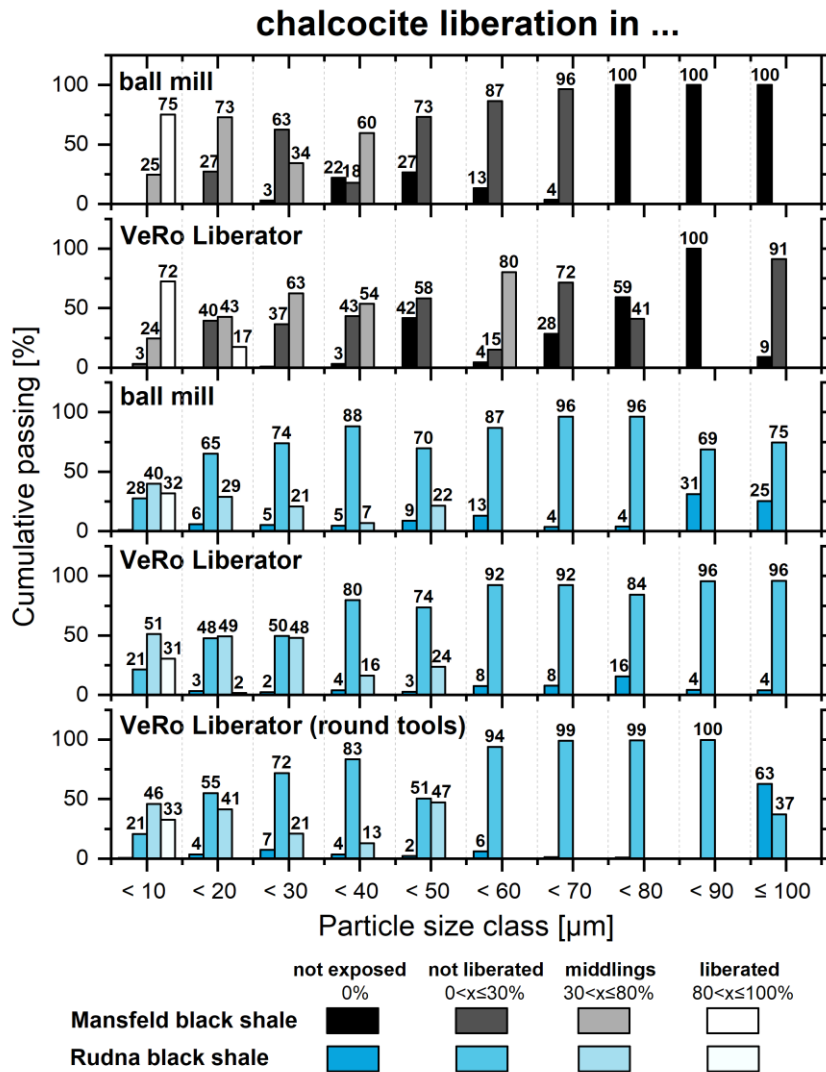


**Figure 3.1.31:** Column plots displaying proportions of liberation classes of chalcocite in particle size classes of VeRo Liberator® and ball mill products from Rudna and Mansfeld black shale. (Data: MLA-HIF)

### Chalcopyrite

Figure 3.1.32 displays the liberation of chalcopyrite in VeRo Liberator® products and for comparison in ball mill products of Mansfeld as well as Rudna black shale ore. The distribution of liberation modes for chalcopyrite in the VeRo Liberator® product was comparable to the ball mill product in the particle size range < 20 micron. The < 10 micron particle size class contained high amounts of liberated chalcopyrite grains (82%) and subordinately chalcopyrite middlings, whereas the proportion of the latter was increased as well as the content of liberated chalcopyrite decreased significantly (13%) in the < 20 micron particle size class, which also hosted elevated amounts of not liberated chalcopyrite particles. The occurrence of chalcopyrite middlings in the VeRo Liberator® product of Mansfeld black shale ore was restricted to particles < 30 µm showing constantly increasing amounts towards coarser particles within this particle size range. Chalcopyrite within the range 30-100 µm contained not liberated or not exposed in varying proportions. The ball mill product of Mansfeld black shale showed generally lower amounts of chalcopyrite middlings but slightly more coarse-grained up to < 40 micron particle size and additionally with a increased amount (54%) in the < 60 micron particle size class.

VeRo Liberator® products of Rudna black shale ore contained moderate concentrations of liberated chalcopyrite in the < 10 micron particle size class (VL: 32%; VL\_R: 38%) accompanied by similar contents of chalcopyrite middlings (VL: 42%; VL\_R: 44%) and low amounts of not liberated chalcopyrite. The VeRo Liberator® product generated with round hammer tools showed also low percentages of liberated chalcopyrite (8%) in the < 20 micron particle size class, in which it hosted further a moderate content of chalcopyrite middlings and a low portion of not liberated chalcopyrite. The proportion of chalcopyrite middlings in this particle size class was lower in the VeRo Liberator® product achieved with regular hammer tools, which was marked by higher amounts of not liberated and not exposed chalcopyrite compared to the VeRo Liberator® product generated with round hammer tools. While the < 30 micron particle size class hosted moderately amounts of chalcopyrite middlings in the VeRo Liberator® product generated with round hammer tools, chalcopyrite middlings occurred additionally in the < 40 micron particle size class of the VeRo Liberator® product generated with round hammer tools. The liberation of chalcopyrite in coarser particle size classes of both VeRo

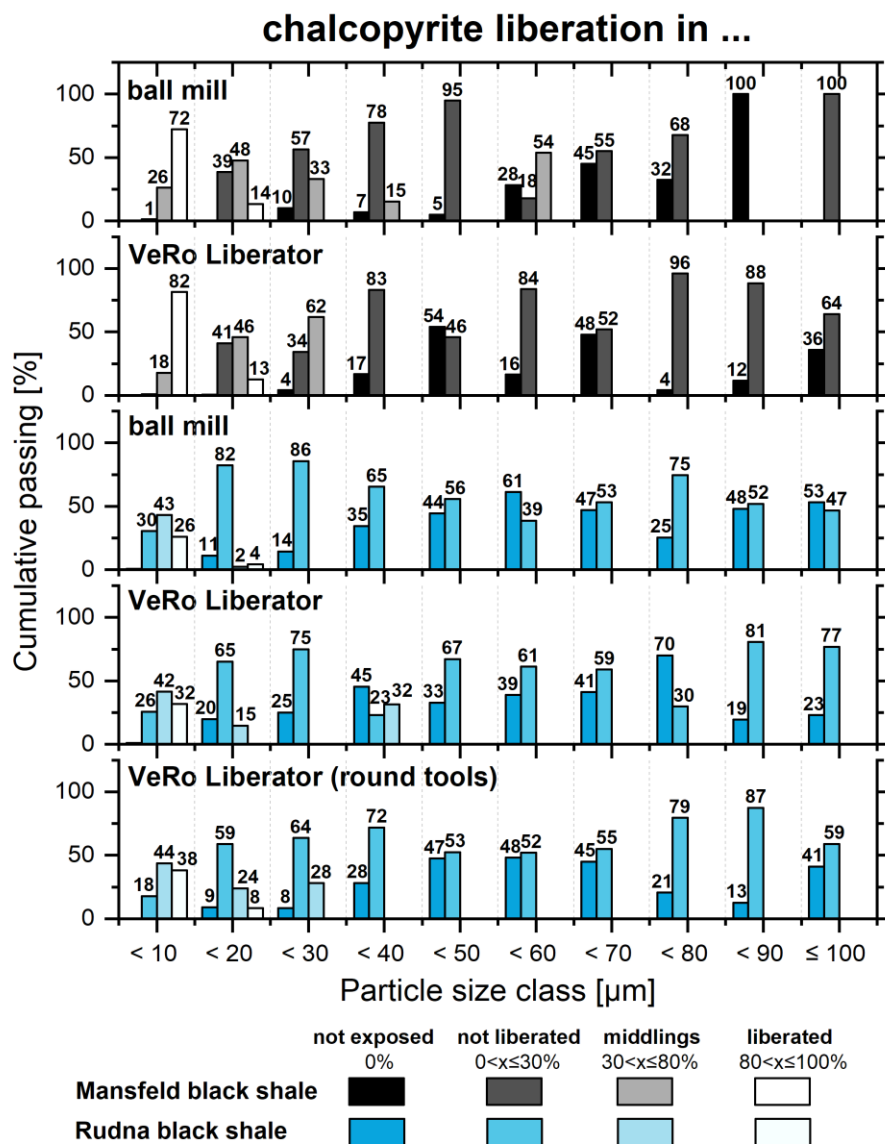


**Figure 3.1.32:** Column plots displaying proportions of liberation classes of chalcopyrite in particle size classes of VeRo Liberator® and ball mill products from Rudna and Mansfeld black shale. (Data: MLA-HIF)

Liberator® products was low and marked by varying proportions of not liberated or not exposed chalcopyrite. In comparison, the VeRo Liberator® test carried out with round hammer tools achieved slightly better liberation of chalcopyrite in the particle size range < 30 micron. In contrast to that, liberated chalcopyrite and chalcopyrite middlings occurred almost restricted in the < 10 micron particle size class of the ball mill product.

#### 3.1.3.6 Mineral locking of copper sulphides in VeRo Liberator® products of different black shale ores

Locking associations of value minerals in comminution products are a critical information for the subsequent beneficiation process. Therefore, the general locking association of VeRo Liberator® products and for comparability of ball mill products of Mansfeld and Rudna black shale ore were compiled according to particle size classes of these comminution products. The locking association of a mineral can be assigned to binary locked if another mineral phase occurs interlocked in a particle. More complex intergrowth associations are assigned to ternary+ locking, which describes the interlocking of a mineral grain of interest adjoining with at least two other mineral phases in one particle.

##### *Mansfeld black shale*

Figure 3.1.33 displays the locking association of bornite, chalcocite and chalcopyrite regarding the total particle size range and in particle size classes of VeRo Liberator® products and equivalent ball mill products of Mansfeld black shale. The locking association for both, the VeRo Liberator® product and ball mill product, revealed that copper sulphides in general were predominantly ternary locked. In the VeRo Liberator® product, the proportion of ternary locked bornite was high (82%), whereas binary locked (8%) and liberated (10%) bornite represented small portions. However, the ball mill product hosted significantly increased amounts of liberated (24%) and binary locked (20%) bornite. But generally, over the range of the particle size classes in both comminution products it is notable that ternary locked bornite occurred nearly exclusively in particles larger 30 µm.

In some exceptions partly increased amounts of binary locked bornite were detected, for example in the < 60 micron particle size class of the VeRo Liberator® product. In the particle size range below 30 microns, the content of binary locked bornite grains increased from 22% in the < 30 micron particle size class to 45% in the < 20 micron particle size class, whereas binary locking of bornite was low (14%) in the < 10 micron particle size class that was dominated by liberated bornite.

As for bornite, the locking association for chalcocite in the VeRo Liberator® product was dominated by ternary locking (77%) and low portions of bornite occurring binary locked as well as liberated. The locking association for chalcocite in the ball mill product was characterized by slightly lower amounts of binary and ternary locked chalcocite. While the < 10 micron particle size class of the VeRo Liberator® product was dominated by liberated chalcocite, the occurrence of binary locked chalcocite extended to the < 30 particle size class with an increased amount (31%) in the particle size class < 20 micron. However, ternary locked chalcocite was the dominant locking mode over the remaining particle size range of the VeRo Liberator® product. The distribution of the locking association in the ball mill product of the Mansfeld black shale is comparable but it contained significantly more binary locked chalcocite in the < 20 particle size class.

Chalcopyrite in the VeRo Liberator® product of Mansfeld black shale was generally marked by ternary locking (83%). Because of the fine-grained occurrence of chalcopyrite (see Chapter 3.1.3.4) in

the VeRo Liberator® product of Mansfeld black shale, ternary locked chalcopyrite was also detected to a wider extent (41%) in the < 10 micron particle size class. Besides that, the content of binary locked chalcopyrite was decreasing constantly up to the < 40 micron particle size class and disappeared in coarser particle size classes of the VeRo Liberator® product.

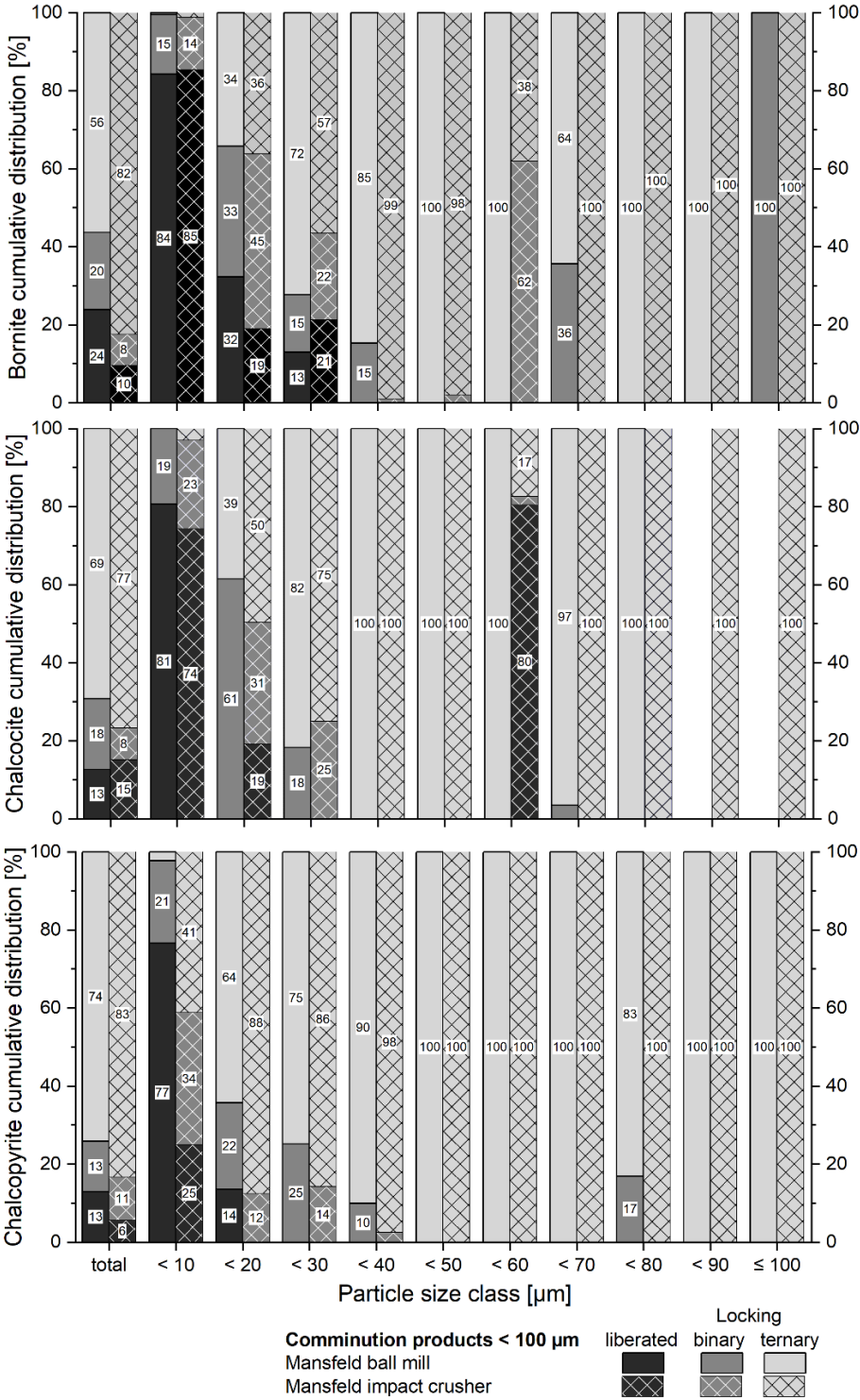


**Figure 3.1.33:** Stacked column plots of locking modes for bornite, chalcocite and chalcopyrite in the total VeRo Liberator® (< 100 µm fraction) as well as ball mill product from Mansfeld black shale and the distribution in the respective particle size classes of both comminution products. (Data: MLA-HIF)

The amount of liberated and binary locked chalcopyrite in the ball mill product was generally increased, but likewise to the VeRo Liberator® product liberated and binary locked chalcopyrite decreased constantly up to particle size class < 40 micron. Exceptionally, binary locked chalcopyrite was subordinately part of the locking mode in the < 80 micron particle size class, whereas ternary locked chalcopyrite was also dominant in the particle size range from 40 to 100 micron of the ball mill products.

#### *Rudna black shale*

VeRo Liberator® products of Rudna black shale ore showed commonly similar locking association for bornite and chalcocite, as shown in Figure 3.1.34. While for bornite in both impact crusher occurred an increased proportion of liberated grains, binary locking was comparable at moderate amounts. Ternary locking associations of bornite was detected slightly increased in regards to chalcocite. Slight differences of the locking mode of chalcopyrite were generally notable between the VeRo Liberator® product generated with regular hammer tools and the product achieved with round hammer tools. The latter contained more chalcopyrite in binary locking.

The distribution of binary locked bornite within particle size classes revealed that both VeRo Liberator® products from Rudna black shale ore hosted similar amounts up to the < 40 micron particle size class. Above that particle size class, proportions of binary locked bornite alternated between the VeRo Liberator® products up to the < 60 micron particle size class. In the particle size range 60-100 microns, binary locked bornite occurred erratic at low proportions, although the ≤ 100 micron particle size class of the VeRo Liberator® product achieved by regular hammer tools contained a significant portion of binary locked bornite (45%) as well as more increased (71%) in the < 90 micron particle size class of the VeRo Liberator® product generated with round hammer tools. Ternary locked bornite represented the main locking mode in particle size classes of the VeRo Liberator® product from Rudna black shale at nearly consistent amounts from the particle size range 10 to 60 microns (49-62%) and increased rapidly in the remaining particle size range.

The ball mill product in comparison had significantly higher amounts of ternary locked bornite in the total comminution product and also commonly in the individual particle size classes. Additionally, the proportion of binary locked bornite was generally lower in ball mill product of Rudna black shale ore.

The locking modes for chalcocite in the < 10 and < 20 micron particle size classes were similar for as well VeRo Liberator® products as ball mill product. From the < 30 micron particle size class the proportion of binary locked chalcocite increased partly in VeRo Liberator® products. While the ball mill product contained almost no binary locked chalcocite in the particle size range from 60 to 100 micron, VeRo Liberator® products showed differently increased proportions of binary locked chalcocite in the same particle size range. Generally, ternary+ locked chalcocite was the dominant locking mode in VeRo Liberator® products and reached up to 100% especially in the particle size range from 70 to 100 micron.

Figure 3.1.34 shows a general increase of liberated and binary locked chalcopyrite in VeRo Liberator® products regarding the total sample in comparison to the ball mill product. Amongst particle size classes, just the < 10 micron particle size class contained moderate amounts of binary locked chalcopyrite, whereas in the remaining particle size range binary locked chalcopyrite occurred occasionally with low amounts in both, VeRo Liberator® products and the ball mill product. Only the < 90 micron particle size class of the VeRo Liberator® product attained with round hammer tools showed exceptionally increased binary locked chalcopyrite (80%).

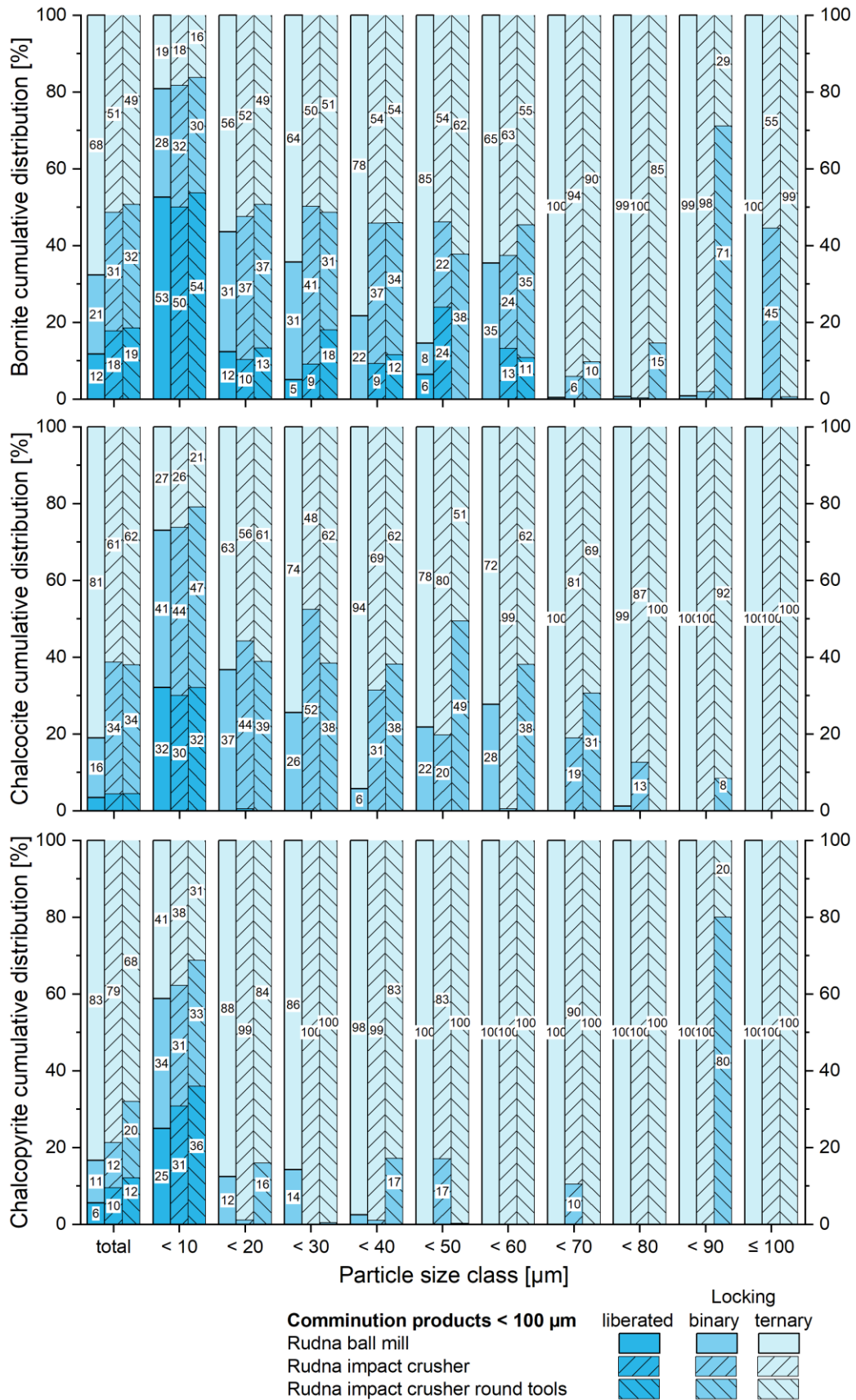


**Figure 3.1.34:** Stacked column plots of locking modes for bornite, chalcocite and chalcopyrite in the total VeRo Liberator® (< 100 μm fraction) as well as ball mill product from Rudna black shale and the distribution in the respective particle size classes of both comminution products. (Data: MLA-HIF)

### 3.1.3.7 Mineral distribution of locking associations for copper sulphides in VeRo Liberator® impact crusher products

A combined investigation of locking mode and the distribution of mineral species interlocked with copper sulphides was carried out on particle size classes  $\leq 100 \mu\text{m}$  of the VeRo Liberator® products. Copper sulphides, the main economic valuable minerals in Kupferschiefer-type black shale ores, were strongly intergrown with other minerals. To opens insights to the recoverability or even failed extraction yields, the mineral distribution analysis of binary or more complexly locked (ternary+) copper sulphides was carried for the total comminution products but also for individual particle size classes.

#### 3.1.3.7.1 Mansfeld black shale ore

##### *Bornite*

The distribution of minerals locked with bornite in binary and ternary+ mode in the VeRo Liberator® product of Mansfeld black shale is shown in Figure 3.1.35. Generally, the VeRo Liberator® product contained bornite complexly locked predominantly with gangue minerals as illite/clays, carbonates and quartz. It differed from the ball mill product by the lack of chalcocite, which was a notable constituent of ternary+ intergrowth of bornite and at increased proportion of binary locked bornite in the ball mill product. Binary locked bornite was distributed irregular over the particle size classes and also the mineral association changed significantly, which was generally also determined for the ball mill product. Similarities represented partly the coherent increase of the carbonates content and particle size in the VeRo Liberator®, but just up to particle size class  $< 50$  micron. While in lower particle size classes ternary locked bornite was moderately associated with chalcocite, the mineral association

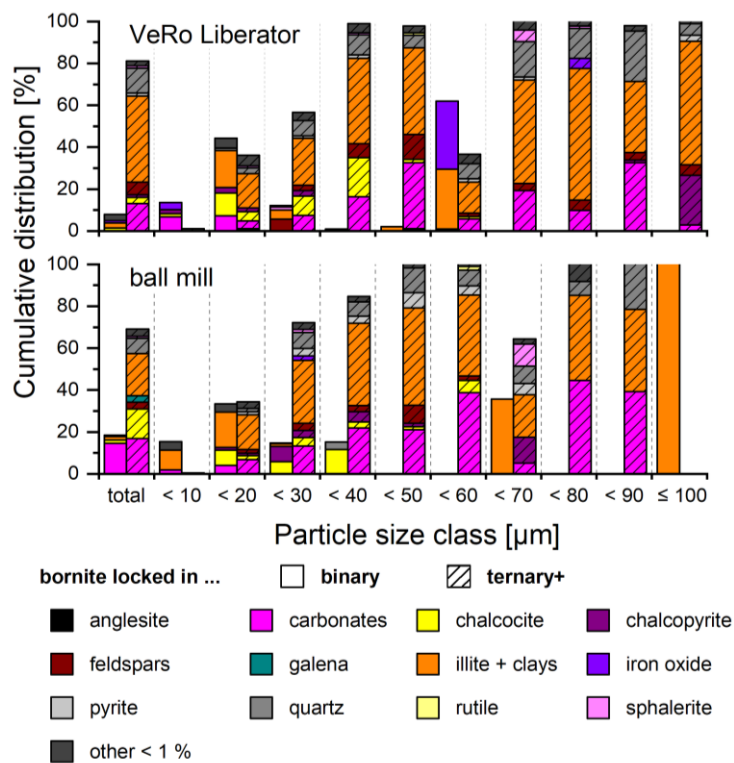


**Figure 3.1.35:** Stacked column plots illustrating the distribution of minerals associated with binary and ternary+ locked bornite in particle size classes and in the total VeRo Liberator® as well as ball mill product from Mansfeld black shale. (Data: MLA-HIF)

of complexly intergrown bornite comprised mainly illite/clays, carbonates, quartz as well as in some cases low proportion of feldspar, sphalerite, pyrite and iron oxide. Only in the  $\leq 100$  micron particle size class occurred significantly increased intergrowths of ternary locked bornite with chalcopyrite.

### Chalcocite

The distribution of minerals interlocked with chalcocite in the VeRo Liberator® product of Mansfeld black shale is shown in Figure 3.1.36. It contained generally low proportion of binary locked chalcocite, which occurred mainly in the lower particle size range ( $< 30 \mu\text{m}$ ) interlocked with bornite and illite/clays. Ternary+ locked chalcocite was also intergrown predominantly with illite/clays as well as bornite. The proportion of the latter decreased towards coarser particle size classes and intergrowths of carbonates were increasing in ternary locked chalcocite. Additionally, the proportion of illite/clays and to a minor extend interlockings with chalcopyrite, quartz and partly sphalerite and iron oxides were detected for ternary locked chalcocite.

Compared to the ball mill product of Mansfeld black shale, the VeRo Liberator® product contained a similar distribution of binary locked chalcocite. Otherwise, ternary+ locked chalcocite in the ball mill product was more related to carbonates, especially in the particle size fraction  $> 40 \mu\text{m}$ . Thus, the carbonate fraction interlocked with chalcocite was notable higher in the total ball mill product.

### Chalcopyrite

The distribution of minerals interlocked with chalcopyrite presents Figure 3.1.37. Most significant was the variability of mineral phases, what is expressed in particular in the mineral distribution associated with ternary locked chalcopyrite. While the proportion of binary locked chalcopyrite was generally low, except in the  $< 20$  micron particle size class, ternary+ locked chalcopyrite was dominating and multiple

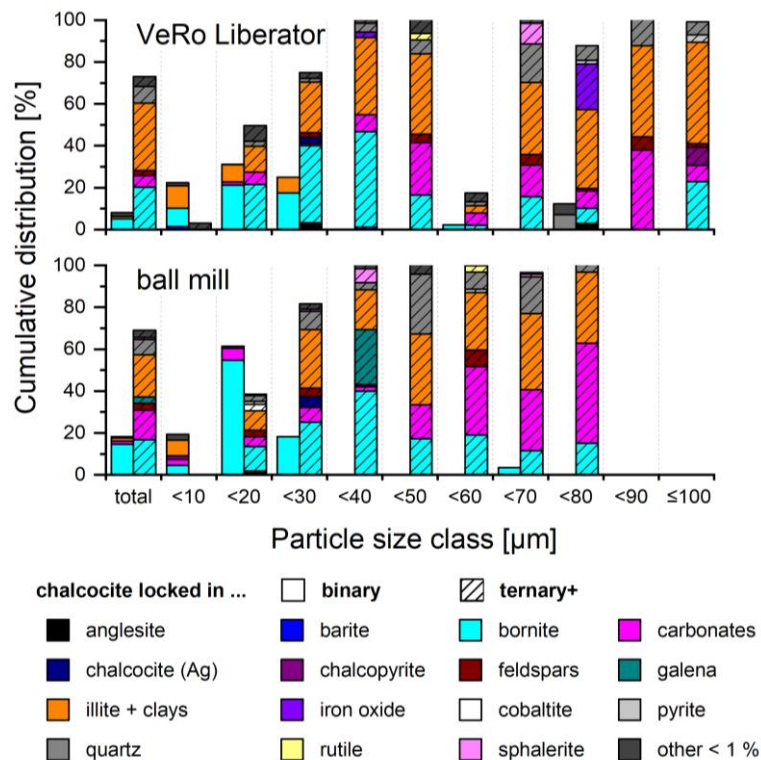


**Figure 3.1.36:** Stacked column plots illustrating the distribution of minerals associated with binary and ternary+ locked chalcocite in particle size classes and in the total VeRo Liberator® as well as ball mill product from Mansfeld black shale. (Data: MLA-HIF)

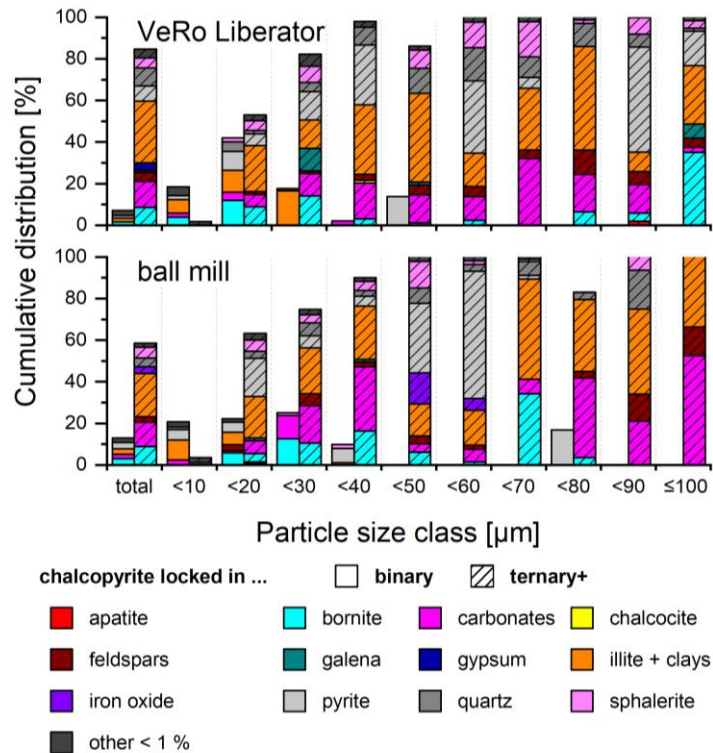


**Figure 3.1.37:** Stacked column plots illustrating the distribution of minerals associated with binary and ternary+ locked chalcopyrite in particle size classes and the total VeRo Liberator<sup>®</sup> as well as ball mill product from Mansfeld black shale. (Data: MLA-HIF)

interlocked with gangue minerals as well as other sulphides. The proportion of bornite in complex intergrowths with chalcopyrite was increased up to the < 40 micron particle size class, whereas illite/clays and partly pyrite were mainly interlocked ternary+ with chalcopyrite in the particle size range from 20 to 100 micron in the VeRo Liberator<sup>®</sup> product. Moderate to low proportions of quartz, sphalerite and feldspars interlocked complexly with chalcopyrite were detected in the particle size range +30  $\mu\text{m}$ . Galena was occasionally a constituent of complicated intergrowths of chalcopyrite. The VeRo Liberator<sup>®</sup> product differed from the ball mill product by increased ternary+ intergrowths of chalcopyrite with pyrite, especially in the upper particle size classes (> 60 micron), in which the ball mill products contained chalcopyrite ternary locked with predominantly carbonates and illite/clays. Additionally, sphalerite was subordinately part of complex intergrowths with chalcopyrite in nearly all particle size classes of the VeRo Liberator<sup>®</sup> product, but occurred primarily in the lower particle size fraction of the ball mill product. Furthermore, ternary locked chalcopyrite in the ball mill product was occasionally associated with iron oxides, while intergrowths with galena were not detected.

### 3.1.3.7.2 Rudna black shale ore

The sulphide association of the Rudna black shale ore samples comminuted by the VeRo Liberator<sup>®</sup> was dominated by bornite and chalcocite, whereas the Rudna black shale sample used for ball mill tests was additionally enriched in galena. The content of chalcopyrite was low in both comminution products. Equivalent to the Mansfeld black shale impact crusher product as well as all ball mill products, VeRo Liberator<sup>®</sup> products of batch tests with Rudna black shale ore carried out with regular (angular) as well as round hammer tools were investigated regarding the mineral distribution of binary and ternary+ locked copper sulphides. Both locking modes and their mineral locking association were

analysed for the total impact crusher products and particle size classes of 10 µm covering the particle size range up to 100 µm.

*Bornite*

Figure 3.1.38 contains the mineral distribution associated with binary and ternary locked bornite in VeRo Liberator® products and for comparison in the Rudna black shale ball mill product. Generally, it can be stated that the mineral association of binary and ternary+ locked bornite in both VeRo Liberator® products was quite similar. Binary locked bornite was mainly intergrown either with chalcocite or illite/clays. Regarding ternary interlockings, the proportion of carbonate minerals increased and additionally some quartz was detected. The only difference between both VeRo Liberator® products was the larger proportion of minor minerals (“other < 1%”-class) in the VeRo Liberator® product generated with angular hammer tools.

Within the particle size classes of VeRo Liberator® products, the mineral distribution associated with binary and ternary+ locked bornite was largely similar. It shows that chalcocite was the dominating mineral in fine-grained particle size classes (up to < 40 micron class) accompanied by illite/clays for

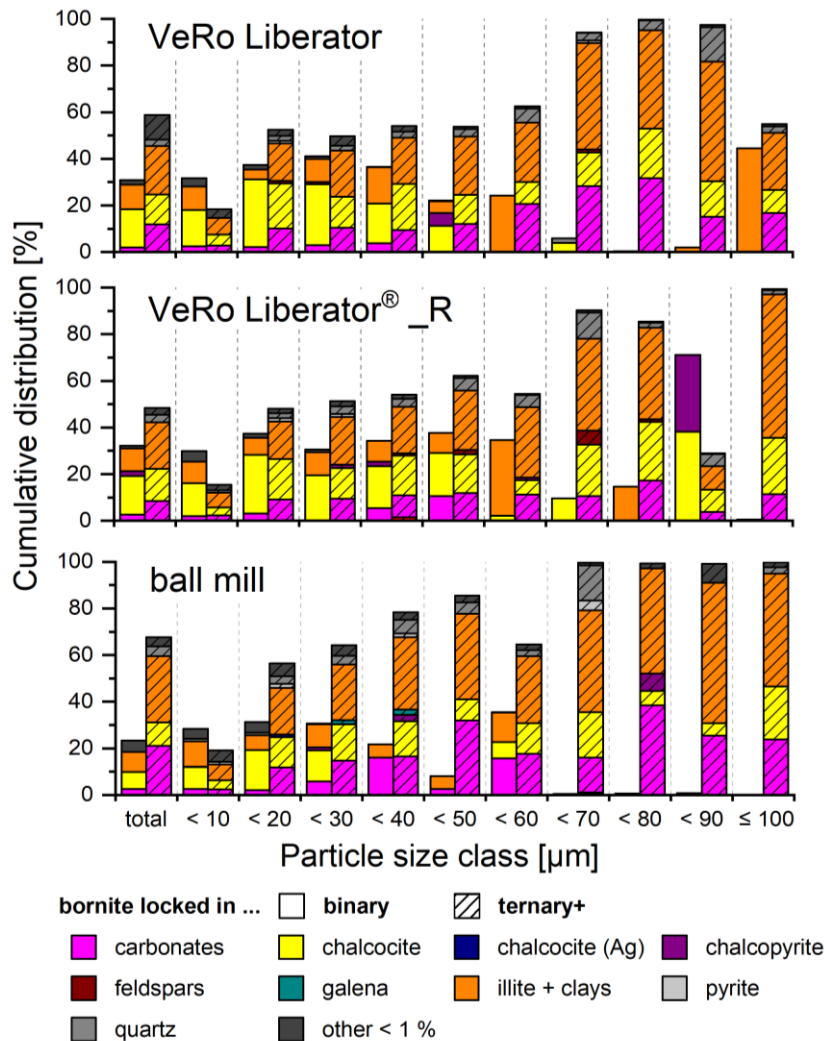


**Figure 3.1.38:** Stacked column plots illustrating the distribution of minerals associated with binary and ternary+ locked bornite in particle size classes and the total VeRo Liberator® products (angular/ round tools) as well as ball mill product from Mansfeld black shale. (VeRo Liberator®\_R=round tools, Data: MLA-HIF)

both, binary and ternary+ locked bornite. Towards larger particle sizes, the proportion of carbonates and illite/clays increased in intergrowths of ternary+ locked bornite. Few exceptions occurred for the VeRo Liberator® product generated with round hammer tools. It contains lower proportion of carbonates associated with ternary+ locked bornite in the upper particle size range. Further, it shows remarkable mineral associations for binary locked bornite in the particle size range 70-90 µm, especially in the < 90 micron particle size class, where increased proportion of chalcocite and chalcopyrite were intergrown binary with bornite, whereas exemplarily increased binary intergrowths of illite/clays with bornite existed in the ≤ 100 particle size class of the VeRo Liberator® product generated with angular hammer tools. The comparison with the ball mill product showed that the VeRo Liberator® product generated with angular hammer tools was similar in terms of mineral distribution associated with binary and ternary+ locked bornite, although the ball mill product contained slightly lower proportion of binary locked bornite.

#### *Chalcocite*

Proportions of minerals associated with binary and ternary locked chalcocite in VeRo Liberator® products is depicted in Figure 3.1.39. Regarding the total particle size range of both VeRo Liberator® products, the mineral association with binary as well as ternary+ locked chalcocite was nearly identical. Binary locked chalcocite was almost exclusively intergrown with bornite that was also the main constituent of complexly (ternary+) locked chalcocite. Additionally, mainly illite/clays and carbonates as well as low proportions of silver-rich chalcocite and quartz occurred in complexly intergrowths of chalcocite. Bornite binary locked with chalcocite was the significant associated mineral within the particle size classes, whereas the proportion was partly increased in the VeRo Liberator® product generated with round hammer tools. Bornite also dominated the mineral association of ternary+ locked chalcocite up to the < 50 micron particle size class of both impact crusher products. Besides that, carbonates, illite/clays and silver-rich chalcocite were subordinately associated in complex intergrowths with chalcocite. Their proportions increased markedly in the coarser-grained particle size range of VeRo Liberator® products, where low proportions of quartz were also associated with ternary+ locked chalcocite. The comparison to the ball mill product revealed that it contained generally higher proportions of ternary+ locked chalcocite, which was more intergrown with illite/clays, though bornite was largely also the dominating minerals in ternary locking with chalcocite. Bornite was additional exclusively binary locked with chalcocite, albeit with partially lower proportions.

#### *Chalcopyrite*

Compared to chalcocite and bornite, the mineral distribution related to binary and ternary+ locked chalcopyrite was more heterogeneous as Figure 3.1.40 shows. Generally, total VeRo Liberator® products showed similar mineral associations for binary locked as well as ternary locked chalcopyrite, but with higher proportion of binary locking in the VeRo Liberator® product generated with round hammer tools.

Binary locked chalcopyrite was mainly interlocked with bornite, pyrite and illite/clays and occurred sparsely and irregularly within particle size classes of VeRo Liberator® products. While binary locked chalcopyrite was associated with several minerals in the finest particle size fraction, mainly bornite, pyrite as well as illite/clays, intergrowths with binary locked chalcopyrite in coarser grain size classes were mostly monomineralic and dominated by bornite. The latter formed a conspicuous increased proportion with binary locked chalcopyrite in the < 90 micron particle size class of the VeRo Liberator® product generated with round hammer tools.

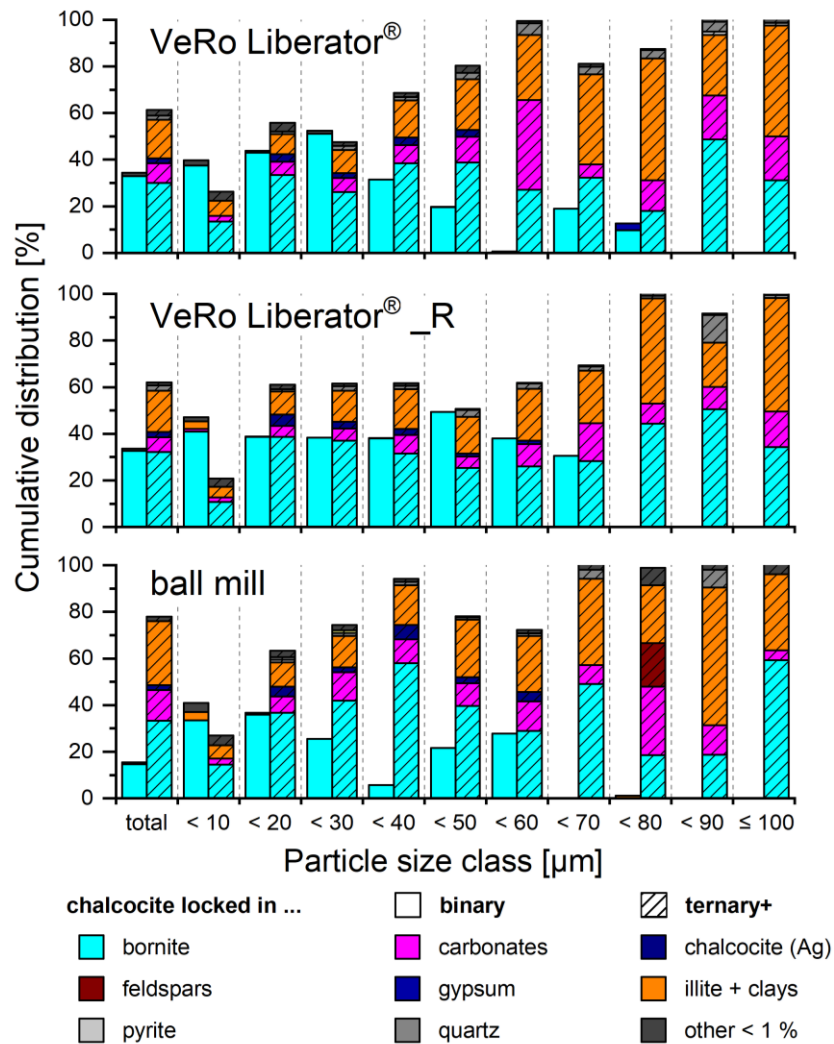


**Figure 3.1.39:** Stacked column plots illustrating the distribution of minerals associated with binary and ternary+ locked bornite in particle size classes and the total VeRo Liberator® products (angular/ round tools) as well as ball mill product from Mansfeld black shale. (VeRo Liberator®\_R=round tools, Data: MLA-HIF)

Ternary locked chalcopyrite was more complexly interlocked in terms of mineral variability. Generally, illite/clays represented main minerals of complex intergrowths with chalcopyrite. Additionally, bornite, carbonates and pyrite were common mineral phases intergrown with complexly locked chalcopyrite, whereas pyrite was constituent of complex intergrowths preferentially in fine-grained particles. The fine-grained fraction of the VeRo Liberator® product generated with round hammer tools showed also sphalerite, which was partly associated in complex intergrowths of chalcopyrite. The carbonate proportion in ternary+ locked chalcopyrite was slightly increasing in coarser-grained particle size classes of both VeRo Liberator® products, whereas proportions of bornite were decreasing. Small quantities of chalcocite, part of complex chalcopyrite intergrowths, were often detected. Generally, it was ascertained that the mineral distribution in regards to interlockings with chalcopyrite was largely quite similar to the ball mill product.

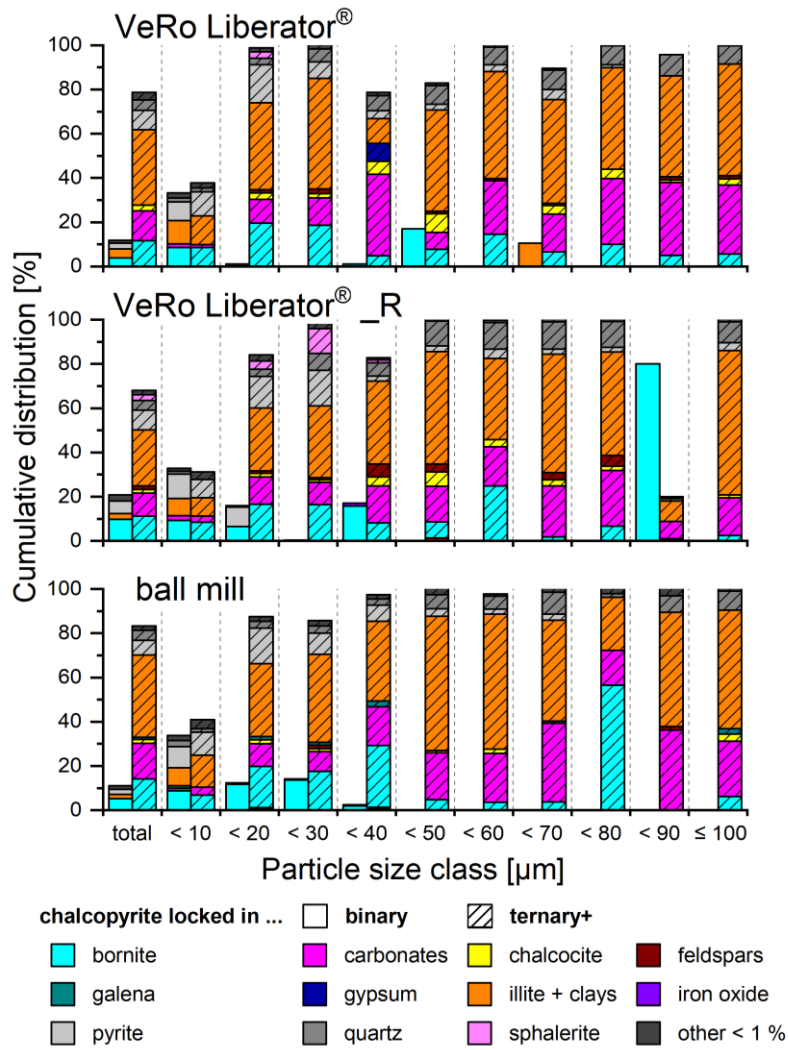


**Figure 3.1.40:** Stacked column plots illustrating the distribution of minerals associated with binary and ternary+ locked bornite in particle size classes and the total VeRo Liberator® products (angular/ round tools) as well as ball mill product from Mansfeld black shale. (VeRo Liberator®\_R=round tools, Data: MLA-HIF)

### 3.1.4 Summary

#### *Grain size distribution*

Ball mill products of black shale bulk samples were characterized by nearly identical particle size distribution for Rudna and Sangerhausen black shale ( $D_{50}=14.8\ \mu\text{m}$ ,  $D_{80}=15\ \mu\text{m}$ ). The particle size in the ball mill product of Mansfeld black shale was decisively finer ( $D_{50}=7.1\ \mu\text{m}$ ,  $D_{80}=20.4\ \mu\text{m}$ ).

PSD-analyses have shown that the VeRo Liberator<sup>®</sup> comminuted black shale ore very efficient in comparison to other crusher types. While for other crushers the proportion of the  $< 90\ \mu\text{m}$ -fraction was definitely below 10%, the VeRo Liberator<sup>®</sup> achieved comminution products, which contain commonly over 60% of particles in the grain size fraction  $< 90\ \mu\text{m}$ .  $D_{80}$  of VeRo Liberator<sup>®</sup>-products was 225 and 250  $\mu\text{m}$ . Generally, by the use of round hammer tools instead of angular tools, VeRo Liberator<sup>®</sup>-products were slightly more fine-grained. Comparison of the  $<100\ \mu\text{m}$ -fraction of VeRo Liberator<sup>®</sup>-products and ball mill products revealed that ball mill products were generally more fine-grained, but deviation to VeRo Liberator<sup>®</sup>-products were more significant for Mansfeld than for Rudna black shale

#### *Mineral distribution*

Mineral distribution analyses of comminution products showed that Rudna ore contains mainly bornite (3.2%) and chalcocite (1.5%). The sub sample of Rudna black shale comminuted by the VeRo Liberator<sup>®</sup> impact crusher hosted increased concentration of bornite (4.4%) and chalcocite (3.4%), whereas the ball mill product was additionally marked by increased contents of galena (3.5%) and pyrite (2.3%). Gangue minerals were dominated by carbonates (approx. 35%) and illite (ball mill: 19.5%; impact crusher: 11.7%) and quartz (avg. 17%).

Sangerhausen black shale contained bornite (2.8%) and chalcocite (1.3%), but was also slightly increased in galena (1.5%) and pyrite (2.6%) as well as rich in illite (26.4%), organic matter (14.4%) and quartz (21.4%).

Comminution products of Mansfeld black shale were low in copper sulphides (0.2-0.8% per mineral) but contained increased amounts of sphalerite (ball mill: 1.7%, VeRo Liberator<sup>®</sup>: 2.4%) and gangue minerals were mainly dolomite (24%) and quartz (avg. 26%).

Rudna black shale was marked by the most increased Cu values (ball mill: 3.6%, impact crusher: 5.5%), Sangerhausen black shale contained 2.5% Cu and hosted the most increased content of trace metals, except Ag, which was most increased in Rudna and Mansfeld, the latter was slightly increased in Zn, but low in copper (avg. 0.7% Cu).

#### *Grain size of copper sulphides*

The sulphide grain size in ball mill products was in particular varying for chalcocite, which was very fine-grained in Rudna black shale ( $D_{80}=6.9\ \mu\text{m}$ ), medium-grained in Mansfeld ( $D_{80}=22.0\ \mu\text{m}$ ) and coarser grained in Sangerhausen black shale ( $D_{80}=31.5\ \mu\text{m}$ ). The latter contained very fine-grained chalcocite ( $D_{80}=9.2\ \mu\text{m}$ ) compared to milled Rudna ( $D_{80}=26.6\ \mu\text{m}$ ) and Mansfeld ( $D_{80}=28.6\ \mu\text{m}$ ) ore, whereas the grain size of bornite was less deviating with  $D_{80}$ -values of 22.0  $\mu\text{m}$  for Mansfeld, 35.0  $\mu\text{m}$  for Rudna and 29.5  $\mu\text{m}$  for Sangerhausen black shale.

The grain size in VeRo Liberator<sup>®</sup>-products for bornite was generally lower for Rudna black shale feed, but larger in the impact crusher products of Mansfeld black shale, whereas grain sizes of

chalcocite and chalcopyrite were almost equal compared to ball mill products. Sulphide grain size were not affected by the use of round or angular hammer tools, it was no significant deviation noticeable.

#### *Liberation of copper sulphides*

The liberation of copper-bearing sulphides amongst ball mill products was most successful for bornite in Mansfeld ore (23.7%) and considerably lower in Rudna (11.8%) and Sangerhausen (15.0%) black shale at similar amounts of bornite middlings (approx. 30%) in all black shale samples. The liberation of bornite in VeRo Liberator®-products was low for Mansfeld black shale (11.4%), but significantly increased for Rudna black shale (up to 21.6%).

Liberated bornite grains existed mainly in the lower particle size classes, especially in the particle size range  $-10\ \mu\text{m}$ , in ball mill products of Mansfeld and Sangerhausen ore, liberated bornite was also found up to particle size range  $-40\ \mu\text{m}$ . In VeRo Liberator®-products of Rudna black shale, liberated bornite occurred in the particle size range up to the  $-50\ \mu\text{m}$  and up to the  $-60\ \mu\text{m}$ , respectively, whereas bornite middlings were present in the entire particle size range. Considerably smaller was the particle size range, in which liberated bornite and middlings occurred ( $< 40\ \mu\text{m}$ ), in the VeRo Liberator®-product of Mansfeld black shale, which was comparable to the ball mill product.

The amount of liberated chalcocite was low in Mansfeld and Sangerhausen ore (approx. 12 %) as well as extremely low in Rudna black shale (3.4%) and occurred almost exclusively in the  $-10\ \mu\text{m}$  particle size class in all comminution products. Chalcocite middlings were significantly increased in the Mansfeld ball mill product (30 %) compared to milled Sangerhausen (10.7%) and Rudna (12.1%) ore. VeRo Liberator®-products showed low liberation for chalcocite for Mansfeld (7.6%) and a very slight increase for Rudna black shale (4.7%).

The content of liberated chalcopyrite and chalcopyrite middlings was especially low in the ball mill product of Rudna black shale (6.4% liberated, 10.0% middlings), but the liberation of chalcopyrite was doubled in the ball mill product of Mansfeld black shale (liberated: 12.4%, middlings: 23.5%) as well as significantly increased in the ball mill product of Sangerhausen black shale (liberated: 19.3%, middlings: 36.8%). The VeRo Liberator®-product of Mansfeld black shale contained low proportions of liberated chalcopyrite (9.0%) and chalcopyrite middlings (10.5%), whereas chalcopyrite in Rudna black shale was slightly better liberated by VeRo Liberator® comminution (liberated: 9.8%, middlings: 18.4%). Significantly increased liberation of chalcopyrite was achieved by the VeRo Liberator®-using round hammer tools (liberated: 14.7%, middlings: 23.8%). Liberated chalcopyrite was substantially determined in the  $-10\ \mu\text{m}$  particle size of all comminution products.

#### *Locking of copper sulphides*

Mineral locking of bornite, chalcocite and chalcopyrite was predominantly marked by ternary+ locking association illustrating the complex intergrowths of sulphides in all comminution products of different black shale ores.

#### *Bornite*

Binary locked bornite occurred mainly in the lower particle size range ( $-30\ \mu\text{m}$ ) of the studied ball mill products and was primarily associated with illite as well as chalcocite. Intergrowths with illite dominated the particle size fractions  $-20\ \mu\text{m}$  of the Mansfeld and Sangerhausen ball mill products, chalcocite was the most common mineral interlocked with bornite in the Rudna ball mill product,

which also contained increasingly proportions of carbonates binary locked with bornite in coarser particle size classes.

Binary locked bornite in VeRo Liberator®-products was mainly associated with illite and chalcocite and occurred largely in the particle size range 10-30 µm in the product of Mansfeld black shale, but in the VeRo Liberator®-products of Rudna black shale binary locked bornite was considerably present in the particle size range 10-60 µm.

Complex (ternary+) locked bornite was generally intergrown with illite/clays accompanied by carbonates as well as chalcocite, subordinately quartz and chalcopyrite, whereas the proportion of illite/clay ternary+ locked with bornite in the Sangerhausen ball mill product was significantly increased over all particle size classes. Increasingly proportions of carbonates, chalcopyrite and sphalerite were part of complex intergrowths in the coarser particle size range +30 µm of Rudna and Mansfeld black shale ball mill products. Complexly locked bornite in VeRo Liberator®-products was mainly interlocked with chalcocite, illite and carbonates. The latter both with increasing proportions towards the coarser particle size range.

#### *Chalcocite*

Binary locked chalcocite was common in the 10-30 µm particle size range of the Mansfeld ball mill product and VeRo Liberator®-product, but occurred more pronounced in the 10-60 µm particle size range of Rudna and Sangerhausen ball mill products and Rudna VeRo Liberator®-products. Chalcocite binary locked was mainly associated with bornite over nearly all particle size classes in the Mansfeld and Sangerhausen ball mill product and also in VeRo Liberator®-products of Mansfeld and Rudna black shale.

Ternary+ locked chalcocite was intergrown chiefly with bornite in all comminution products. The +40 µm particle size range of the Mansfeld ball mill product and the VeRo Liberator®-product was additionally marked by increasing contents of illite, carbonates and quartz ternary locked with chalcocite. The Sangerhausen ball mill product showed an increasing amount of illite/clay, part of ternary locking with chalcocite, especially in the coarser particle size range. Ternary+ locked chalcocite in the Rudna ball mill product was, besides bornite, mainly associated with illite/clays and carbonate minerals at increasing proportions of illite/clay in the particle size range +40 µm similar to the VeRo Liberator®-products of Rudna black shale.

#### *Chalcopyrite*

Binary locked chalcopyrite was commonly contained in the particle size range -30 µm, but occurred extremely increased in the -80 particle size classes of the VeRo Liberator®-product generated with round hammer tools and the Sangerhausen ball mill products, in both associated with bornite. The latter was generally the main mineral binary locked with chalcopyrite. Additionally, pyrite was common in binary intergrowths with chalcopyrite in the Sangerhausen ball mill product as well as pyrite, illite and carbonates in the ball mill and VeRo Liberator®-products of Mansfeld and Rudna black shale.

Chalcopyrite was commonly ternary locked with illite, pyrite and bornite, in Mansfeld and Rudna ball mill products additionally with carbonates commonly with increasing proportion in the +30 µm particle size range similar to illite and pyrite. The latter represented the main mineral ternary locked in the 30-60 µm particle size range of the ball mill and VeRo Liberator® products of Mansfeld black shale, whereas pyrite occurred moderately in the particle size range -30 µm of ball mill and VeRo Liberator® products of Rudna black shale.

Key features of comminuted black shales:

- Similar grain size distribution of ball mill products from Sangerhausen and Rudna black shale, Mansfeld black shale ball mill product was decisively finer.
- VeRo Liberator®-products were by far more fine-grained than other crusher products ( $D_{80}=225$  and  $250\ \mu\text{m}$ ),
  - more than 60% of particles  $< 90\ \mu\text{m}$ . The  $-100\ \mu\text{m}$ -fraction of VeRo Liberator®-products was generally coarser-grained than ball mill products.
- Different sulphide content in the comminuted black shales,
  - Mansfeld black shale contains low amounts of copper sulphides, generally  $< 1\%$ ,
  - Rudna black shale showed increased amounts of bornite and chalcocite,
  - Sangerhausen black shale contained increased amounts of bornite and chalcopyrite.
- The grain size of sulphides in comminution products of different black shales was especially deviating for chalcopyrite, but also for chalcocite.
- Liberation of copper-bearing sulphides was generally low ( $< 10\%$ ) to moderate ( $< 25\%$ ),
  - most increased liberation for bornite (23.7%) in the ball mill product of Sangerhausen black shale,
  - liberation of bornite in VeRo Liberator®-products was lower (11.4%) compared to the ball mill product for Mansfeld black shale, but significantly increased for Rudna black shale (up to 21.6%),
  - liberated copper sulphide grains mainly in the  $-10\ \mu\text{m}$  particle size class up to  $-40$  in ball mill products, in particular wide distribution of liberated bornite and middlings in VeRo Liberator®-products of Rudna black shale,
  - partially liberated copper sulphide grains (middlings) generally in the lower particle size classes ( $-40\ \mu\text{m}$ ),
  - binary locked copper sulphides mostly intergrown with each other, pyrite and illite,
  - ternary+ locked sulphides commonly dominated in the particles size range  $+30\ \mu\text{m}$  and were predominantly associated with bornite, chalcocite, illite, carbonates and quartz.

## 3.2 Mineralogical and geochemical analysis of flotation products and tailings generated from black shale ores

### 3.2.1 Mass and copper recovery balance

Flotation tests carried out at UVR-FIA GmbH, Freiberg, Germany were aimed to improve the copper recovery of froth flotation of black shale ore by the application of new treatment approaches. Flotation tests were conducted with Sangerhausen and Rudna black shale ore, and revealed promising increased copper recovery in combination with markedly improved copper contents in products. Concentrates and related tailings from selected test series representing material from the most advanced and adapted stage of flotation tests were subjected to detailed mineralogical analyses. Thus, flotation concentrates and tailings from flotation tests using standard chemical agents, as shown in detail in Chapter 2.2.2, represented one sample set, whereas in two further sample sets this standard flotation set-up was extended by the usage of dextrin, an additional depressant, and a pre-treatment step of ethanol wetting of the feed.

As indicated in Table 3.1.12, the mass recovery achieved by standard flotation approach yielded in lower selectivity of gangue-type minerals so that nearly half mass of the feed was extracted in concentrates, whereas the mass portion in the concentrate generated from Sangerhausen ore was slightly lower (45.1 wt.%) compared to the concentrate from Rudna black shale (52.9 wt.%). Copper recovery achieved by flotation tests carried out with Rudna as well as Sangerhausen black shale feed were in general similar, whereas the copper recovery by standard flotation of Rudna feed (75.1%) was increased compared to the same flotation with Sangerhausen feed (67.8%)

**Table 3.1.12:** Compilation of recovery data for concentrates and tailings extracted by different froth flotation approaches from Rudna and Sangerhausen black shale feed.

Treatment	Black shale feed		Mass recovery $R_M$ [%]	Copper recovery $R_{Cu}$ [%]
Standard flotation	Rudna	concentrate	52.9	75.1
		tailing	47.1	24.9
	Sangerhausen	concentrate	45.1	67.8
		tailing	54.9	32.2
Flotation + dextrin	Rudna	concentrate	9.0	29.2
		tailing	91.0	70.8
	Sangerhausen	concentrate	5.7	26.2
		tailing	94.3	73.8
Ethanol pre-treatment_ Flotation + dextrin	Rudna	concentrate	26.7	72.1
		tailing	73.3	27.9
	Sangerhausen	concentrate	29.8	74.8
		tailing	70.2	25.2

A further flotation approach was conducted with added dextrin acting as depressant for organic matter. This test series yielded in enormous high selective mass/copper recovery and less than a percentile of the feed mass was extracted in the flotation products. Very low mass recovery rate was achieved by the dextrin-added flotation of Sangerhausen black shale, in which just 5.7% of the feed mass was extracted in the product accompanied by low copper recovery (26.2%), whereas the same flotation test setting on Rudna black shale yielded in 9.0 wt.% separated in the concentrate with a marginally increased copper recovery of 29.2%. Due to the low mass recovery further flotation tests were conducted with feed material subjected to an ethanol pre-treatment step combined with a dextrin added sulphide flotation. Mass recovery proportions of concentrates were improved along with copper recovery, so that the flotation product from Rudna black shale contained 26.7 wt.% of the feed mass at 72.1% copper recovery, whereas the flotation with pre-treated Sangerhausen black shale yielded in 29.8 wt.% mass and 74.8% copper recovery in the concentrate.

### 3.2.2 Particle size distribution

Flotation concentrates and tailings generated from Rudna and Sangerhausen black shale ore were investigated regarding their particle size distribution. The granulometric data for flotation products and tailings from Rudna black shale are displayed in Figure 3.2.1. Additionally, particle size data for  $D_{20}$ ,  $D_{50}$  and  $D_{80}$  were summarized for all concentrates and tailings in Table 3.2.1.

As Figure 3.2.1 shows, particle size curves for concentrate and tailings for single flotation tests vary. The flotation experiment using dextrin depressor led to most significant particle size separation between tailings and concentrate. The latter was decidedly more fine-grained with  $10.2 \mu\text{m}$  at  $D_{50}$

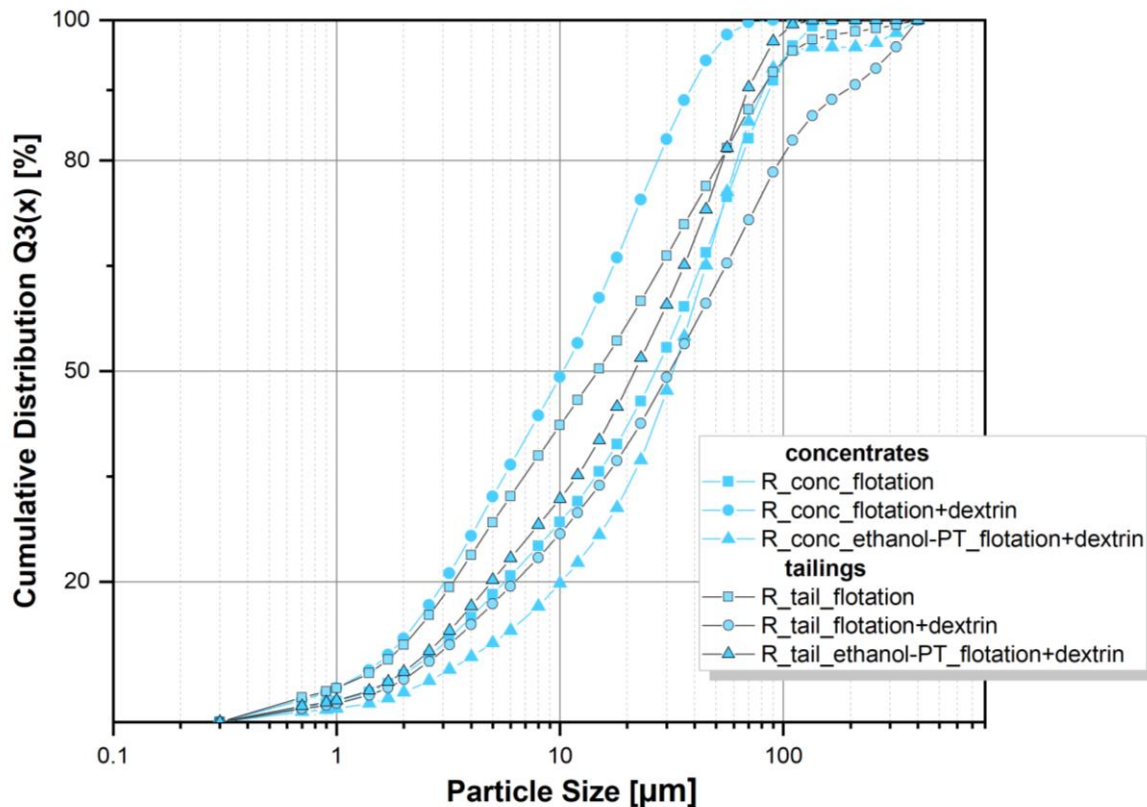


**Figure 3.2.1:** Particle size distribution curves of flotation concentrates and tailings generated from Rudna black shale feed. (Data: MLU)

compared to 31.0  $\mu\text{m}$  in the tailings. Even more marked was the deviation at  $D_{80}$ , where the particle size was 95.9  $\mu\text{m}$  in the tailings and 27.1  $\mu\text{m}$  in the concentrate.

Particle size curves of product and tailing of the flotation without usage of dextrin depressant showed lower general deviation, but, especially in the particle size range  $< 50 \mu\text{m}$ , particles were significantly finer in tailings with 14.9  $\mu\text{m}$  at  $D_{50}$  and 52.4  $\mu\text{m}$  at  $D_{80}$  in comparison to  $D_{50}$  at 26.6  $\mu\text{m}$  and  $D_{80}$  at 64.8  $\mu\text{m}$  in the concentrate, whereas the difference at the representative minimum grain size ( $D_{20}$ ) was markedly lower.

Similar to the particle size distribution in concentrate and tailing of the flotation without dextrin, the tailings from the flotation of ethanol pre-treated Rudna black shale were vastly finer compared to the particles in the concentrate. At  $D_{20}$  (10.0  $\mu\text{m}$ ) and  $D_{50}$  (32.1  $\mu\text{m}$ ), the concentrate showed the coarsest grain sizes amongst the other concentrates gained from Rudna black shale ore. Tailings of the flotation test using dextrin depressant and ethanol pre-treated feed showed a medium-grained particle size distribution in respect to the tailings of the other two flotation tests.

Particle size distribution curves of flotation products and tailings from Sangerhausen black shale ore covered generally a narrower grain size range (see Figure 3.2.2), so that differences in the particle size distribution between concentrates and tailings were far less pronounced. Clearly deviating particle size distribution curves were determined for the concentrate and tailings of the flotation test using dextrin and ethanol pre-treated Sangerhausen black shale. Here, the concentrate contained the finest particle sizes amongst all other samples derived from this ore ( $D_{20} \leq 5.0 \mu\text{m}$ ,  $D_{50} \leq 17.8 \mu\text{m}$ ,  $D_{80} \leq 39.3 \mu\text{m}$ ). Additionally, also corresponding tailings ( $D_{20} \leq 5.6 \mu\text{m}$ ,  $D_{50} \leq 20.8 \mu\text{m}$ ,  $D_{80} \leq 48.0 \mu\text{m}$ ) were more fine-grained in comparison to tailings of other flotation tests with Sangerhausen black shale ore.

**Table 3.2.1:** Comparison of particle sizes of various flotation products and tailings gained from Rudna as well as Sangerhausen black shale at defined passing fractions (20%, 50% and 80%). ( $R_M$  = mass recovery). (Data: MLU)

Treatment	Feed	Product	Passing fraction			
			$R_M$ [%]	D20 [ $\mu\text{m}$ ]	D50 [ $\mu\text{m}$ ]	D80 [ $\mu\text{m}$ ]
Standard flotation	Rudna	concentrate	52.9	5.7	26.6	64.8
		tailing	47.1	3.3	14.9	52.4
	Sangerhausen	concentrate	45.1	10.8	35.0	62.7
		tailing	54.9	8.4	32.2	68.7
Flotation + dextrin	Rudna	concentrate	9.0	3.0	10.2	27.1
		tailing	91.0	6.3	31.0	95.9
	Sangerhausen	concentrate	5.7	9.6	24.6	57.9
		tailing	94.3	7.1	24.3	52.7
Ethanol pre-treatment_ Flotation + dextrin	Rudna	concentrate	26.7	10.0	32.1	62.1
		tailing	73.3	5.0	21.4	53.2
	Sangerhausen	concentrate	29.8	5.0	17.8	39.3
		tailing	70.2	5.6	20.8	48.0

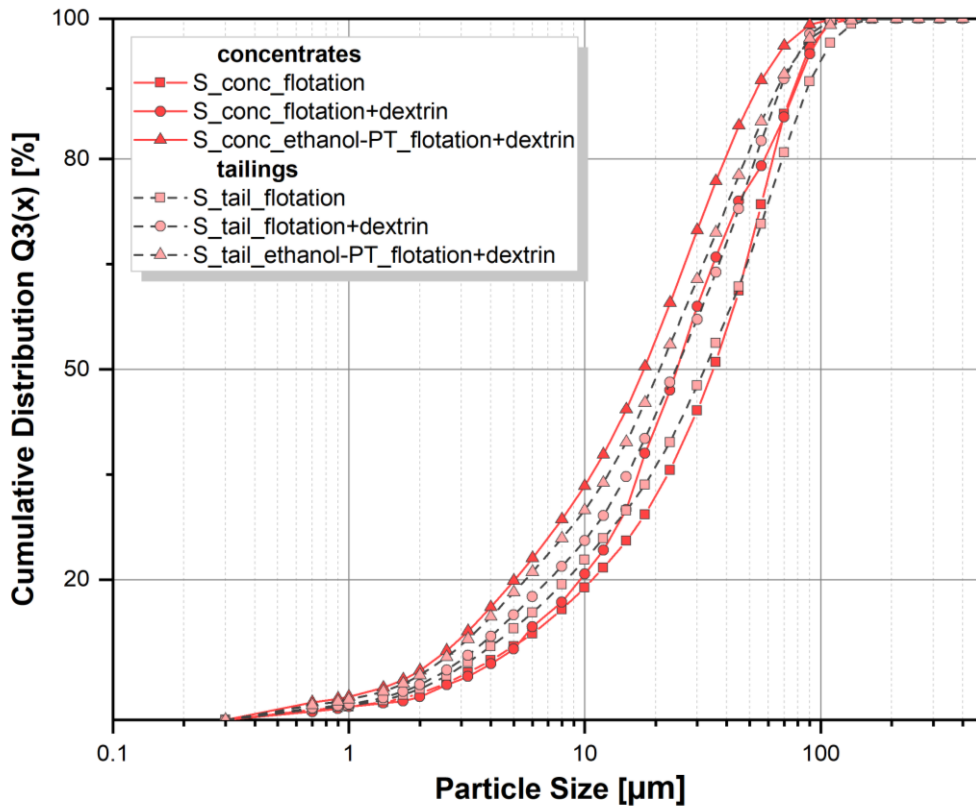


**Figure 3.2.2:** Particle size distribution curves of flotation concentrates and tailings generated from Sangerhausen black shale feed. (Data: MLU)

Concentrates and tailings gained from flotation tests with Sangerhausen black shale not subjected to an ethanol pre-treatment showed partly overlapping particle size curves in the coarser particle size range. Concentrate and tailings of the flotation test using dextrin contained a nearly equal particle size distribution in the particle size range from 18 to 53  $\mu\text{m}$ , which is also expressed in the mean particle size  $D_{50}$  (concentrate: 24.6  $\mu\text{m}$ , tailings: 24.3  $\mu\text{m}$ ) and thus, represented medium-grained particle size distributions amongst flotation concentrates and tailings generated from Sangerhausen black shale ore.

Coarser particle size distributions were determined for the concentrate and tailings produced by the standard flotation test without usage of dextrin and ethanol pre-treatment of the feed. The tailings was generally more fine-grained in the particle size range up to 45  $\mu\text{m}$ , which is indicated by lower particle sizes at  $D_{20}$  (concentrate  $\leq 10.8 \mu\text{m}$ , tailings  $\leq 8.4 \mu\text{m}$ ) and  $D_{50}$  (concentrate  $\leq 35.0 \mu\text{m}$ , tailings  $\leq 32.2 \mu\text{m}$ ). In the upper particle size range, particles in the concentrate were slightly finer, which is expressed in deviated particle size at  $D_{80}$  (concentrate  $\leq 62.7 \mu\text{m}$ , tailings  $\leq 58.7 \mu\text{m}$ ).

### 3.2.3 Sulphides in concentrates and tailings from black shale feed

The occurrence of sulphides in flotation products and tailings was mainly marked by the efficiency of the experimental flotation set-up, which promotes if a sulphides grain was recoverable or not. Additionally, liberation of sulphide surface areas represents the most important factor to realize particle-bubble attachments, which is generally a pre-requisite to separate sulphides grains into the froth product.

As microscopic investigations and liberation analyses have shown, sulphide grains were often interlocked, especially in the grain size range  $> 20 \mu\text{m}$ . Thus, interlocking or intergrowths with other sulphides or gangue minerals were generally observed in flotation products as well as tailings but intergrowth textures and mineral associations were similar to that in comminuted samples. Due to the selectivity of the flotation process, sulphide grains in tailings were almost exclusively intergrown with gangue minerals or occurred commonly liberated in a very low grain size range ( $< 5 \mu\text{m}$ ). As Figure 3.2.3 shows, the appearance and shape of sulphides in concentrates differ widely by containing grains and particles ranging from round to angular shapes. Sulphide intergrowth associations were commonly marked by anhedral to subeuhedral sulphides, often intimately intergrown as shown in Figure 3.2.5. According to that, particles in concentrates were partly strong marked by intergrowths of several sulphides with gangue minerals. Coarser sulphide grains or aggregates occurred predominantly in concentrates, whereas in tailings coarse-grained sulphides were found more sporadically. If they were present, they were mostly locked and commonly intergrown with gangue minerals (see Figure 3.2.6).

SEM-Imaging illustrates intergrowths of gangue and sulphides more impressive, because of sulphides containing elements with higher atomic number compared to gangue minerals such as quartz, illite and dolomite. While the micrograph of Figure 3.2.3 captured in reflected light showed sulphide grains and their shapes in a concentrate, Figure 3.2.7, a back-scattered electron image, shows particles in a concentrate generally marked by sulphide-gangue associations in varying extend. It is notable that a significantly part of particles was dominated by sulphides intergrown with gangue, but

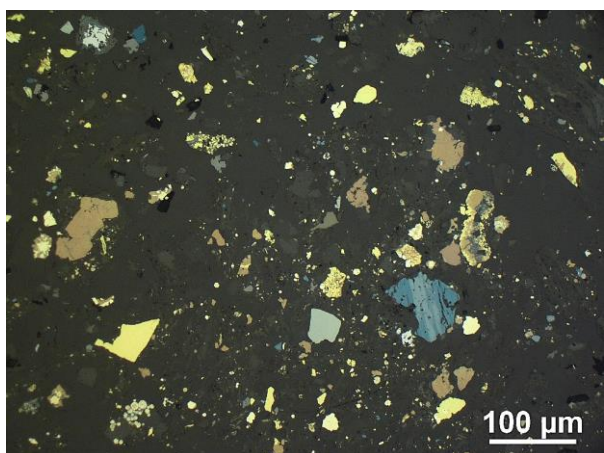


**Figure 3.2.3:** Microphotograph shows the increased occurrence of sulphides exhibiting numerous grain shapes in a flotation concentrate, which contained mainly bornite (brownish), chalcocite (bluish grey), chalcopyrite (yellow) and some covellite (brighter blue). (Lubin concentrate LC15a, reflected light)

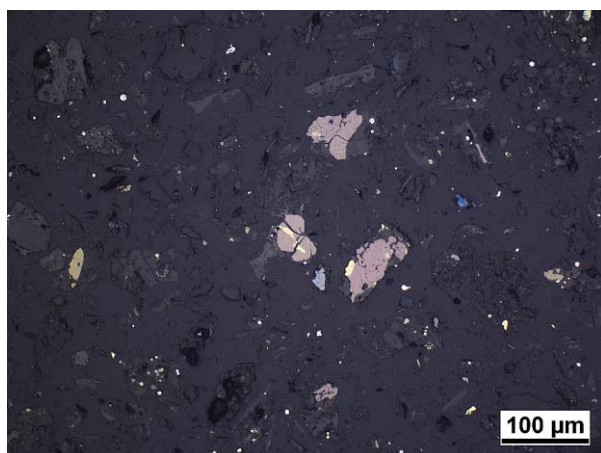


**Figure 3.2.4:** Overview image of tailings displaying the decreased content of sulphides. Besides some larger sulphide particles marked by intergrowths that consists of predominantly bornite (light purple) and minor chalcopyrite (yellow), tailings contained particularly fine-grained sulphides. (tailings from Sangerhausen black shale feed, reflected light)

equally sulphide grains nearly complete liberated hosted of partly very fine to minute gangue minerals sulphides (Figure 3.2.8). In flotation tailings, sulphides were often completely locked by gangue minerals or marked by low liberated grain surface. However, liberated sulphide grains were noticed regularly (see Figure 3.2.9 and Figure 3.2.10).

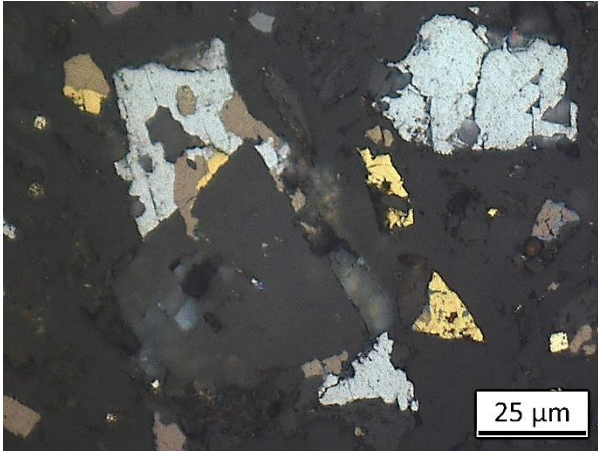


**Figure 3.2.5:** Complexly intergrowths in a particle exhibiting the intimately interlocking of as well sulphides as sulphides with a euhedral dolomite crystal. Bornite (brownish), chalcocite (grey) and chalcopyrite (yellow) form minute and irregular intergrowth associations. (product, dextrin-flotation using ethanol pre-treated Sangerhausen feed, reflected light)

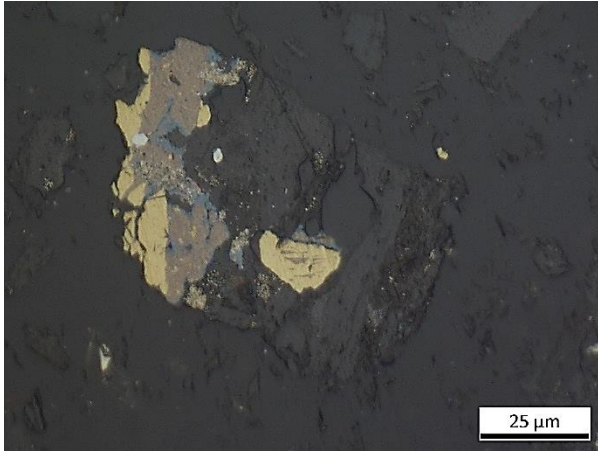


**Figure 3.2.6:** Larger particle in tailings marked by intergrowth of chalcopyrite (yellow), bornite (brownish), gangue (dark grey) and some small grains of chalcocite (light grey blobs). Chalcopyrite grain in the centre as well as bornite are largely to completely locked. Bornite shows slight alteration to covellite and tiny inclusions of chalcopyrite and chalcocite. (tailings, dextrin-flotation using ethanol pre-treated Sangerhausen feed, reflected light)

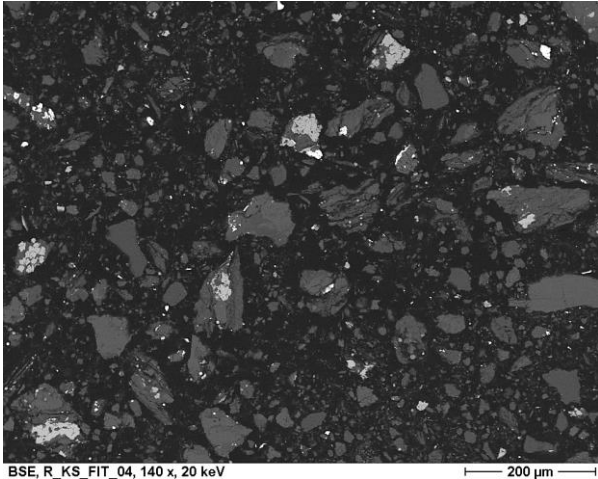


**Figure 3.2.7:** Overview SEM-image shows clearly the common interlocking of sulphides (bright phases) with gangue minerals (grey) in particles of concentrates. (product from flotation using dextrin and ethanol pre-treated Rudna feed, SEM-BSE image)

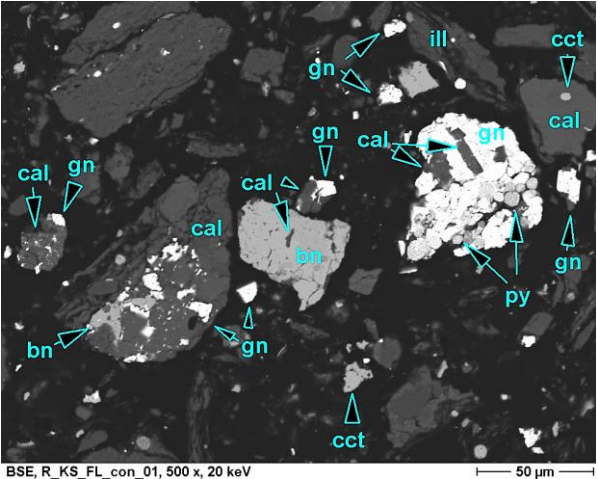


**Figure 3.2.8:** Examples of extremely fine-grained intergrowths of galena (gn) with bornite (bn) as well as galena with pyrite (py). In addition, sulphides, also some chalcocite (cct), are intergrown with mainly calcite (cal). (ill=illite; product from flotation using dextrin and ethanol pre-treated Rudna feed, SEM-BSE image)

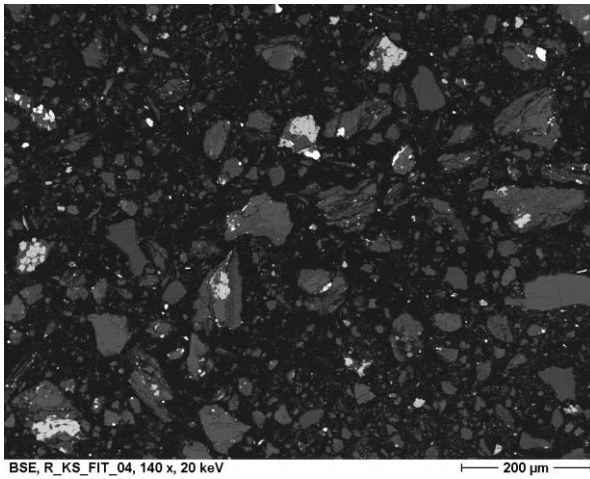


**Figure 3.2.9:** Overview SEM-image of tailings shows sulphides often completely locked by gangue minerals, but also sulphides considerably liberated. (tailings from the flotation of Rudna black shale feed, SEM-BSE image)

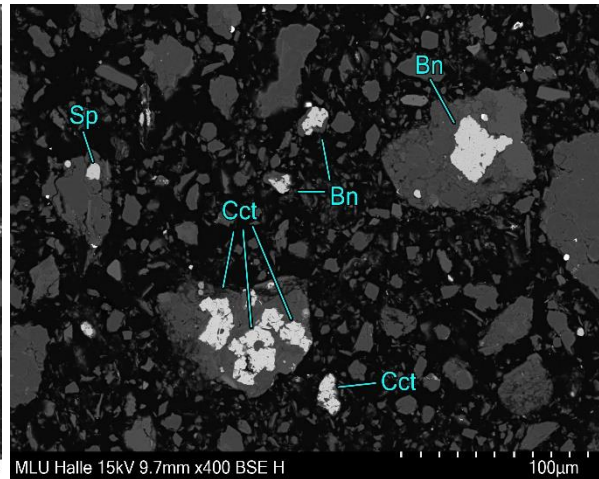


**Figure 3.2.10:** Large-sized particles in tailings marked by bornite (Bn), chalcocite (Cct) and sphalerite (Sp) (tailings mostly complete locked by gangue minerals. (tailings from the flotation of Rudna black shale feed, SEM-BSE image)

### 3.2.4 Concentrates and tailings from flotation tests with Rudna Mine black shale

#### 3.2.4.1 Mineral distribution of flotation products from Rudna black shale feed

The general distribution of sulphides and gangue minerals in flotation concentrates produced from Rudna black shale ore in Figure 3.2.11 shows generally an increased content of sulphides in concentrates gained from flotation tests using dextrin. The proportion of sulphides in Rudna black shale flotation products is partly lower compared to concentrates gained from Sangerhausen black shale ore, except for chalcocite. While the enrichment of sulphides was limited to 11.9% by the standard sulphide flotation, sulphides were noticeably more increased by the flotation using dextrin (22.3% sulphides). The pre-treatment of the comminuted ore with ethanol combined with dextrin added flotation led to the most increased sulphide fraction (29%) among the concentrates gained from Rudna black shale. The mineral distribution analysis of these concentrates revealed additionally substantial differences regarding the sulphide composition.

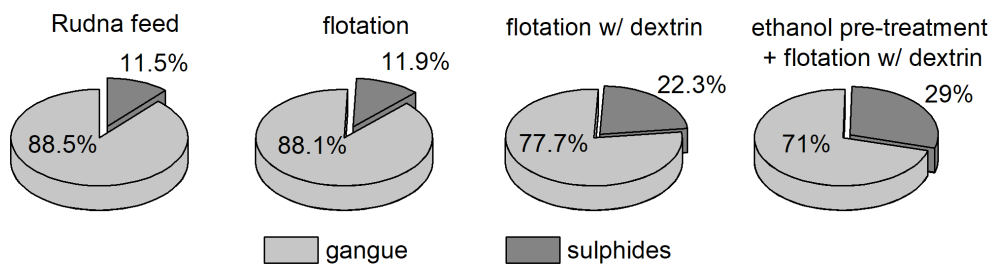


**Figure 3.2.11:** Pie charts representing the proportion of gangue and sulphide minerals in Rudna black shale feed and related copper flotation concentrates. (Data: MLU)

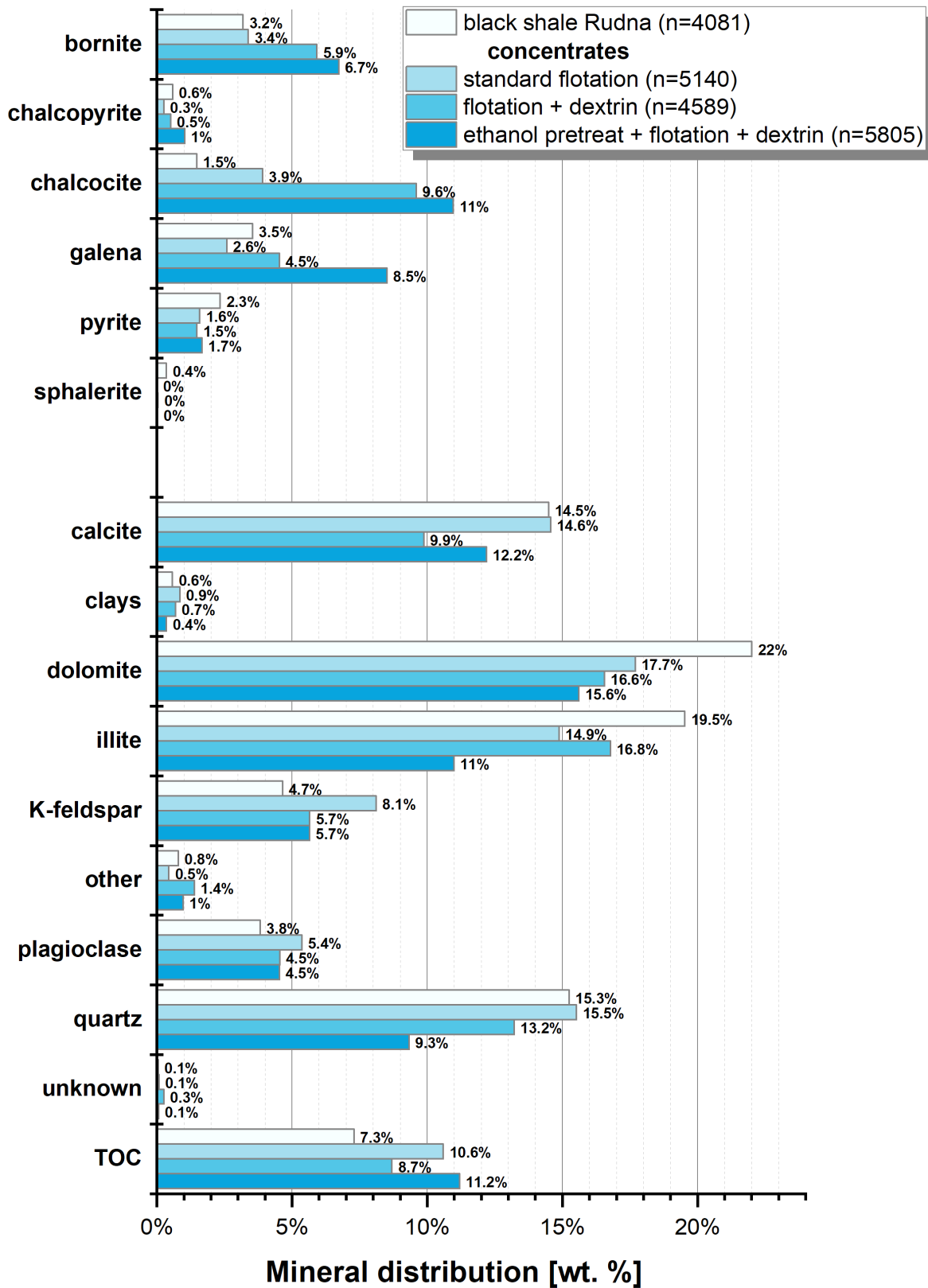


**Figure 3.2.12:** Compilation of mineral distribution analyses for Rudna black shale feed and related flotation concentrates showing proportion of sulphides (upper section) as well as gangue minerals (lower section). (Data: MLU)

Figure 3.2.12 presents mineral distribution analyses carried out on concentrates generated from Rudna black shale. The highest enrichments within the sulphide group was achieved for chalcocite that was enriched to 11.0% in the flotation concentrate from ethanol pre-treated feed and 9.6% by flotation using dextrin without feed pre-treatment. A substantial lower content of chalcocite (3.4%) was determined for the product of the standard flotation and represented virtually no enrichment in this case.

Generally, the sulphide content was clearly increased by the flotation considering an ethanol pre-treatment step and thus, the content of other sulphides such as bornite (6.7%), chalcopyrite (1.0%) and pyrite (1.7%) was generally slightly more increased compared to the other flotation products extracted from not pre-treated feed. According to that, the flotation without dextrin and pre-treatment of the feed achieved only a low enrichment of bornite (3.4%), but chalcopyrite (0.3%) and galena (2.6%) occurred not enriched and remained apparently in the tailings, respectively. However, a strong difference in the recovery of galena is obvious by almost twice the content in the concentrate extracted from ethanol pre-treated ore (8.5%) compared to the concentrate produced from feed not subjected to an ethanol pre-treatment (4.5%). The pyrite content in concentrates was generally lower than in the black shale feed, which indicated that it was mainly depressed into the tailings. Thus, a commonly decreased and almost equal content of pyrite was determined in all concentrates (standard flotation: 1.6%, dextrin-added flotation: 1.5%, flotation with ethanol pre-treatment step: 1.7%).

The distribution of gangue minerals in flotation products from Rudna black shale ore was dominated by increased amounts of carbonates. Concentrates contained mostly lower proportions of calcite and dolomite compared to the feed material. Reduced contents of dolomite were common in all concentrates but with noticeable differences of decreasing order from the concentrate of the standard flotation (17.7%) to the concentrates formed by flotation with the addition of dextrin (dextrin-added flotation: 16.6%, dextrin-added flotation with ethanol pre-treatment step: 15.6%).

The amount of calcite in the concentrates was more divergent. While the concentrate achieved by the dextrin-added flotation had the lowest calcite content of 9.9%, the concentrate generated from ethanol pre-treated ore showed 12.2% calcite. A nearly similar calcite proportion (14.6%) in regards to the feed (14.5%) was detected for the concentrates generated by standard flotation. It is important to note that products of dextrin-added flotation as well with (27.9%) as without (26.8%) ethanol pre-treatment contained a significantly lower fraction of total carbonates compared to the standard flotation product.

Other gangue-type mineral phases occurring in the concentrates were chiefly illite, quartz and minerals of the feldspar group. The lowest contents of these minerals were analysed in the concentrate derived by dextrin-added flotation of ethanol pre-treated Rudna black shale ore. The concentrate from dextrin-added flotation without feed pre-treatment showed similar low contents for feldspars, but it contained significant higher proportions of illite (16.8%) and quartz (13.2%). For comparison, the product of the flotation combined with an ethanol pre-treatment of the Rudna ore contained significantly lower proportions of quartz (9.3%) and illite (11.0%), which indicates a more advanced depression of illite and quartz, generally of gangue minerals, into the tailings. The standard flotation product showed a relative enrichment of quartz as well as more significantly of feldspars compared to the feed material. But feldspars were also slightly enriched in the concentrates formed by dextrin-added flotation.

The content of organic matter, separately analysed, was markedly increased in all flotation products indicating an enrichment. Consequently, the concentrate from flotation using dextrin but no ethanol pre-treatment of the feed contained 8.7%, whereas products of the standard flotation (10.6%) and dextrin-added flotation with ethanol pre-treated ore (11.2%) were marked by higher portions of organic matter.

### 3.2.4.2 Mineral distribution of tailings from flotation tests on Rudna black shale feed

The investigation of tailings from flotation tests on Rudna black shale ore revealed significant differences in the composition of sulphides, which were not extractable in terms of recovery in the concentrate. Mass recovery ratios of flotation tests investigated in this study were quite different. Table 3.1.12 shows that nearly 50% of the feed were depressed into tailing by standard flotation, the mass ratio shifted extremely by the flotation test using dextrin to a significantly increased mass proportion of 91% accumulated in tailings, whereas the flotation test using dextrin and ethanol pre-treated feed yielded an intermediate mass recovery, so that 73.3% of the feed material were depressed in the tailings.

The proportions of sulphides and gangue minerals in the Rudna black shale feed and related flotation tailings is displayed in Figure 3.2.13. Tailings of the standard flotation contained a significantly lower proportion of sulphides (4.0%) compared to tailings derived from flotation test using dextrin. Independently from far varying mass recoveries in tailings from dextrin-added flotation tests, the proportion of sulphides was nearly equal, 8.0% in tailings of flotation using dextrin and ethanol pre-treated feed and 8.2% in tailings of dextrin-added flotation without ethanol pre-treatment of the feed.

The mineral distribution analysis on flotation tailings of Rudna black shale feed in Figure 3.2.14 revealed partly widely varying contents of sulphides. The increased content of sulphides in the tailings of the dextrin-added flotation test executed on non-pre-treated Rudna black shale ore was largely caused by comparatively high amounts of chalcocite (1.6%) and galena (4.5%). But otherwise, the lowest proportion of bornite (1.4%) and pyrite (0.6%) were detected in the tailings of dextrin-added flotation.

The distribution of sulphides in the flotation product of the ethanol pre-treated Rudna black shale is characterized by comparably lower quantities of chalcocite (1.2%) and galena (2.8%), but also by an increased proportion of bornite (1.9%). The increased content of pyrite (1.9%) indicates that pyrite was enriched in the tailings by flotation using dextrin and ethanol pre-treated ore, whereas the tailings from the flotation only using dextrin had a remarkable lower content of pyrite (0.6%) similar to the tailings of the standard flotation (0.7%). The latter was characterized by a generally low sulphide

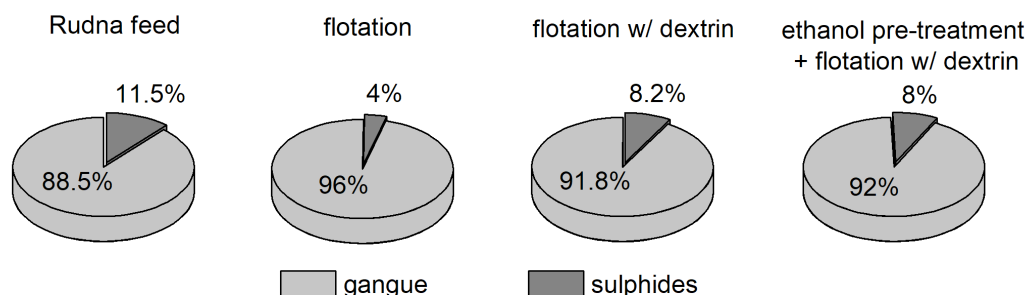


**Figure 3.2.13:** Pie charts displaying the proportion of sulphides and gangue minerals in Rudna black shale feed and tailings from different flotation tests. (Data: MLU)

proportion and contained furthermore chalcocite (0.3%), galena (0.9%) and also an increased amount of bornite (1.8%). Chalcopyrite and sphalerite were generally present in traces within the mineral distribution of the tailings.

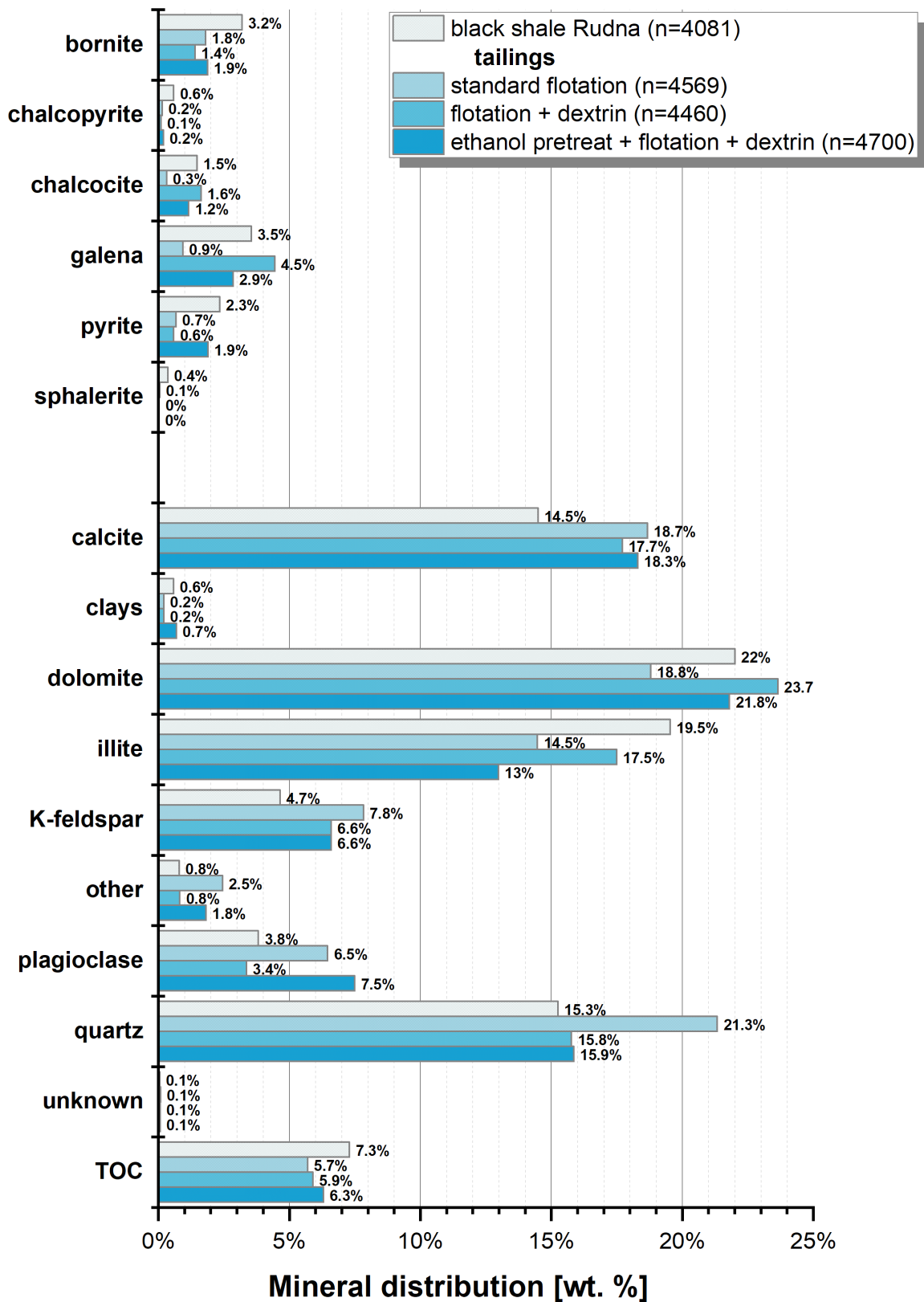


Figure 3.2.14: Mineral distribution of Rudna black shale feed and tailings from different flotation tests. (Data: MLU)

The proportion of gangue-type minerals in tailings of flotation tests carried out on Rudna black shale were dominated by carbonates. Additionally, quartz, illite and feldspars were main constituents of the tailings (see Figure 3.2.14). The total amount of carbonates in tailings of the flotation tests using dextrin was comparable (40.1% with and 41.4% without ethanol pre-treated feed), whereas it was lower in tailings of the standard flotation (37.5%). Commonly, the mineral distribution analysis showed that carbonate minerals were represented by calcite and dolomite, the latter occurred more increased in tailings of flotation tests using dextrin, whereas tailings from the standard flotation contained similar portions of calcite and dolomite.

Generally, calcite was enriched relatively in all tailings. The proportion of illite was varying in tailings of the flotation tests on Rudna black shale. The highest amount of illite (17.5%) was detected in tailings of the dextrin-added flotation. Markedly lower proportion were contained in tailings of the standard flotation (14.5%) and the flotation using ethanol pre-treated ore (13.0%). The contents of feldspar minerals were enriched relatively to the feed, most increased in tailings of the standard flotation (K-feldspar: 7.8%, plagioclase: 6.5%) and the flotation with ethanol pre-treated ore (K-feldspar: 6.6%, plagioclase: 7.5%). Tailings produced by dextrin-added flotation without pre-treatment of the ore showed the lowest portion of feldspars, especially plagioclase, as well as quartz (15.0%). The latter was more slightly enriched in the tailings of the flotation using ethanol pre-treated ore (quartz: 15.9%) and further more in the tailings of the standard flotation (quartz: 21.3%).

The total organic content (TOC) of tailings generated by flotation of Rudna black shale feed was very similar and ranges from 5.7% in the tailings of the standard flotation to 6.3% in the tailings of flotation with dextrin and ethanol pre-treated feed. Generally, TOC's were slightly decreased compared to the feed (7.3%).

#### 3.2.4.3 Content of base and trace metals in concentrates and tailings from the flotation of Rudna black shale

Geochemical analyses of as well concentrates as tailings derived from flotation tests with Rudna black shale revealed considerable variations regarding the content of base and trace metals. As results of the mineral distribution analyses have shown, in particular concentrates contained varying proportions of sulphide minerals especially for bornite, chalcocite and galena. Thus, concentrations of Cu, Fe and Pb were considerable different.

Table 3.2.2 summarizes geochemical data of base metals and trace metals for concentrates and tailings derived from Rudna black shale. According to the copper recovery shown in Chapter 3.2.1, the concentrate extracted by standard flotation tests showed the lowest Cu content (5.5%), whereas concentrates obtained by flotation using dextrin were substantially enriched in Cu, reaching 11.4% in the concentrate from untreated feed material and 10.0% in the concentrate from ethanol pre-treated feed. The Cu concentrations of tailings in turn deviated to a minor extent. The most increased Cu content was determined for tailings from the flotation using dextrin as well as untreated feed (2.7%), slightly lower was the Cu content in the tailings of the standard flotation (2.1%) and even lower in tailings of the flotation using pre-treated feed material (1.4%).

The content of Pb was nearly similar in concentrates of the standard flotation (5.4%) as well as the flotation using dextrin (5.0%), but it was considerably increased in the concentrate produced from pre-treated feed (7.1%). Tailings were marked by generally lower concentrations of Pb, which was nearly equal in tailings of the standard flotation (2.8%) and the flotation using ethanol pre-treated feed

**Table 3.2.2:** Content of base metals and trace metals in concentrates and tailings generated from Rudna black shale feed. (Data: ALS)

	concentrates			tailings		
	standard flotation	flotation with dextrin	flotation with dextrin + ethanol pre-treatment	standard flotation	flotation with dextrin	flotation with dextrin + ethanol pre-treatment
<b>Cu</b> %	5.50	11.40	10.00	2.05	2.73	1.41
<b>Pb</b> %	5.39	5.03	7.11	2.75	4.07	2.93
<b>Zn</b> %	0.06	0.09	0.07	0.03	0.04	0.03
<b>Fe</b> %	2.21	2.23	2.40	1.31	1.46	1.34
<b>Ag</b> ppm	344	746	611	144	196	104
<b>As</b> ppm	176	289	277	90	110	80
<b>Co</b> ppm	234	282	301	93	116	100
<b>Mo</b> ppm	395	382	439	251	273	258
<b>Ni</b> ppm	384	331	400	147	175	175
<b>V</b> ppm	1320	1240	1210	429	425	458

(2.9%), but the tailings of the flotation using dextrin and untreated feed were more increased in Pb (4.1%).

Concentrations of Zn were exclusively low, but very slightly increased in the concentrates. The content of Fe was also minor increased compared to the tailings (2.3% vs. 1.4% avg.) and the variance of the Fe content among concentrates as well as tailings was very low.

More pronounced differences between and amongst concentrates and tailings was notable for trace metals, which occurred generally more increased in concentrates. The flotation with dextrin and ethanol pre-treated ore achieved the most increased contents for Co (301 ppm), Mo (439 ppm) and Ni (400 ppm) in the product. The concentrate from the standard flotation contained partially the lowest concentrations of trace metals, especially for Ag, As, Co, but was most enriched in V (1320 ppm), whereas the product achieved by dextrin-added flotation with untreated feed showed mostly intermediate concentrations, except for Ag that was most enriched (746 ppm).

Tailings were characterized by considerably lower content of trace metal, often in a similar concentration range. However, more deviating concentrations existed for Ag, which was twice increased in the tailings of the flotation using dextrin and non-pre-treated feed (196 ppm) compared to tailings from the flotation of the pre-treated feed (104 ppm).

### 3.2.5 Concentrates and tailings from flotation tests with Sangerhausen black shale

#### 3.2.5.1 Mineral distribution of flotation products from Sangerhausen black shale feed

The concentrates derived from flotation tests with Sangerhausen black shale ore contained generally higher proportions of sulphides compared to concentrates from Rudna black shale. Figure 3.2.15 shows the ratio of sulphides and gangue minerals in the examined concentrates. A slightly increased sulphide proportion was determined in the flotation product of the standard flotation, whereas concentrates extracted by flotation using dextrin showed significantly higher sulphide proportions. The concentrate of the standard flotation was marked by the highest mass recovery (45.1%) and a sulphide proportion of 13.8%. Substantially more sulphides (42%) were extracted in the concentrate gained from flotation with addition of dextrin, but the mass recovery for this flotation test was very low ( $R_M=5.7\%$ ). However, the flotation with dextrin and ethanol pre-treated black shale yielded an improvement of the mass recovery ( $R_M=29.8\%$ ) at increased content of sulphides (50.1%) in the concentrate.

Mineral distribution analyses of flotation concentrates generated from Sangerhausen black shale feed are displayed in Figure 3.2.16. It shows generally an enrichment of bornite in concentrates for all tests carried out. Similar and especially elevated concentrations were noticed for the flotation products from the flotation using dextrin (bornite: 19.5%) and from the flotation using dextrin and ethanol pre-treated feed (bornite: 20.8%). Much lower enrichment of bornite has been achieved by the standard flotation test (6.2%). Generally, the enrichment of copper-bearing sulphides as well as galena and sphalerite proceeded more efficient by the flotation combined with an ethanol pre-treatment of the feed. That was particularly recognizable for the chalcopyrite content of 10.3%, opposing to 6.7% chalcopyrite in the concentrate gained from Sangerhausen black shale feed not subjected to an ethanol pre-treatment. A comparably lower content of chalcopyrite in the standard flotation product (1.5%) indicated no enrichment compared to the feed. The content of chalcocite was insignificant in the concentrate of the standard flotation (0.1%), slightly enriched by flotation using dextrin (0.6%), but extremely enriched in the concentrate extracted by dextrin-added flotation using ethanol pre-treated feed (1.7%).

The concentrates extracted by dextrin-added flotation contained further substantial amounts of galena, which was enriched to 8.6% in the concentrate produced by ethanol pre-treated feed and 8.0% in the concentrate from flotation using dextrin without feed pre-treatment. The galena content in the flotation product of the standard flotation was significant lower (2.4%) and showed slight enrichment regarding the feed.

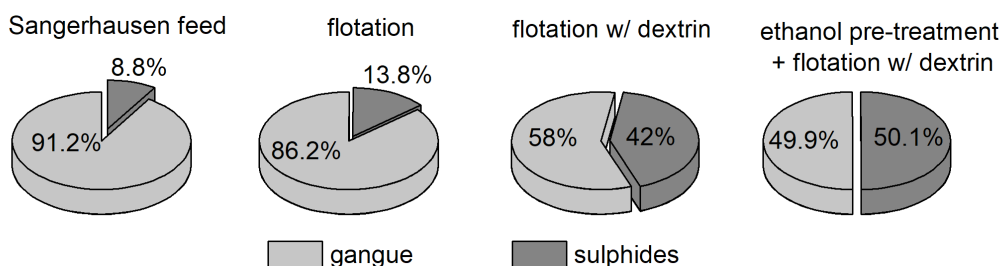


**Figure 3.2.15:** Proportions of sulphides and gangue minerals in different flotation concentrates and Sangerhausen black shale feed. (Data: MLU)

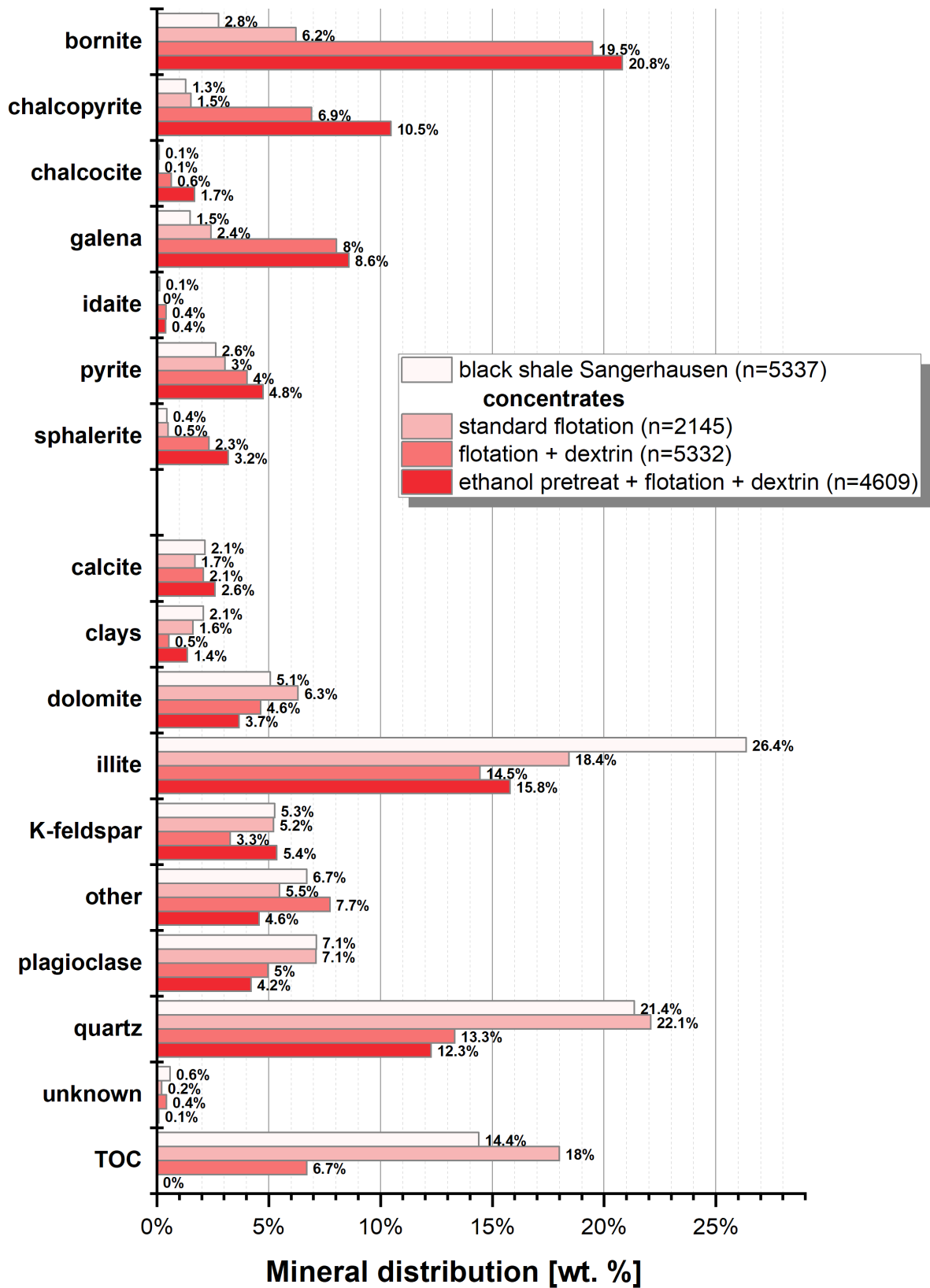


**Figure 3.2.16:** Mineral distribution for Sangerhausen black shale feed and related flotation concentrates showing the proportion of sulphides (upper section) as well as gangue minerals (lower section). (Data: MLU)

Additionally, concentrates gained by dextrin-added flotation were also enriched in sphalerite, which had a content of 3.2% in the flotation product achieved by ethanol pre-treated feed material as well as 2.3% in the concentrate generated without pre-treatment of the feed. Virtually no enrichment of sphalerite was determined in the concentrate of the standard flotation (0.5%). The content of pyrite in the concentrates was likewise most enriched by the flotation test using dextrin and ethanol pre-treated feed (4.8%) followed by 4.0% in the product of the flotation using dextrin, whereas low enrichment (3.0%) regarding the content in the feed was detected for the concentrate gained by standard flotation.

The distribution of gangue minerals was generally marked by increased contents of illite and quartz. The amount of carbonate minerals in concentrates gained by flotation of Sangerhausen black shale was decisively lower compared to concentrates produced from Rudna black shale ore. Calcite had similar concentration as determined in the feed (2.1%), slightly increased in concentrates from dextrin-added flotation with pre-treated ore as well as lower proportion in the product of the standard flotation. However, the content of dolomite in concentrates was contrary, most increased, relatively enriched to the amount in the feed, in the standard flotation concentrate (6.3%), whereas the products of the dextrin-added flotation contained significantly lower amounts of dolomite (4.6% for dextrin flotation, 3.7% for dextrin flotation plus ore pre-treatment).

The concentrate derived from the standard flotation test hosted additionally the most increased amount of illite (18.4%) and quartz (22.1%). For the latter, significantly lower content was detected in concentrates using dextrin-added flotation (13.3% without and 12.3% with ethanol pre-treated ore). These concentrates showed also lower amounts of illite, 15.8% in the flotation product using dextrin and ethanol pre-treatment of the feed and 14.5% in the concentrate generated by dextrin flotation. Feldspars occurred in moderate amounts in concentrates from Sangerhausen black shale. The total amount of feldspars was most increased in the concentrate of the standard flotation (5.2% K-feldspar + 7.1% plagioclase) and was slightly lower in the concentrate extracted by dextrin-added flotation (3.3% K-feldspar + 5.0% plagioclase), whereas the concentrate from ethanol pre-treated ore showed the lowest content of feldspars (5.4% K-feldspar + 4.2% plagioclase).

The most striking deviating feature of all concentrates investigated in this study was the content of organic matter (analysed by combustion analysis). Either the organic matter was completely removed as indicated for the flotation using dextrin and ethanol pre-treated feed or it had a medium content of 6.7% in the concentrate from the dextrin-added flotation without ethanol pre-treatment as well as was enriched to 18.0% in the standard flotation product.

### 3.2.5.2 Mineral distribution of tailings from flotation tests on Sangerhausen black shale feed

Tailings of flotation tests using Sangerhausen black shale feed contained, as displayed in Figure 3.2.17, partly comparable sulphide proportions especially in tailings derived from flotation tests using dextrin. The total content of 11.6% sulphides in tailings generated by flotation of not pre-treated feed was marginally lower as in tailings from the flotation of ethanol pre-treated feed (12.1%), whereas a nearly 50 % lower fraction of sulphides (6.1%, Figure 3.2.17) was determined in the tailings of the standard flotation.

Figure 3.2.18 indicates that tailings of the standard flotation accommodated 1.6% bornite and 1.8% chalcopyrite, whereas other sulphides, except pyrite (2.4%), can be neglected because of very low quantities that can be regarded as traces. In tailings of the flotation test using dextrin-depressant

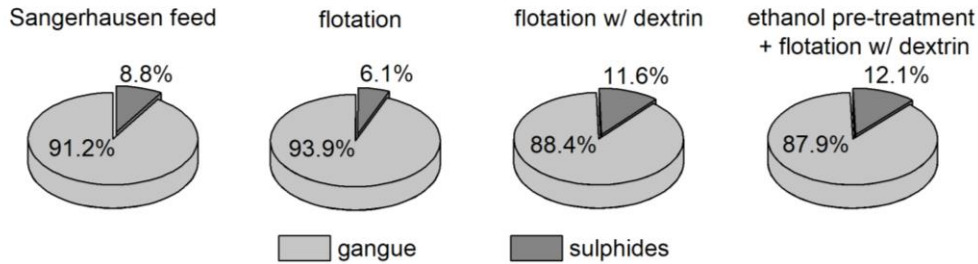


**Figure 3.2.17:** Pie charts indicating the proportion of sulphides and gangue minerals in flotation tailings from different flotation tests performed on Sangerhausen black shale feed. (Data: MLU)

occurred the highest proportions in respect the content of individual sulphides. In particular, bornite (3.3%) and chalcopyrite (1.5%) were slightly enriched regarding the content in the feed material. In comparison, tailings also possess the highest concentrations of other sulphides such as chalcocite and galena.

Main sulphides in flotation tailings derived from ethanol pre-treated feed were likewise bornite (2.2%) and chalcopyrite (1.2%). Other sulphides in tailings occurred subordinately, their concentration was clearly below 1% (0.5% galena, 0.1% chalcocite). A general exception applies to pyrite, which was obviously enriched in tailings of the pre-treated feed showing a content of 8.1%, whereas pyrite was depressed less efficient by the flotation test using non-ethanol pre-treated feed so the thus pyrite content was 4.9%. The lowest pyrite concentration (2.4%) was determined for tailings of the standard flotation, which contained slightly lesser pyrite than the feed material.

The distribution of gangue minerals in Figure 3.2.18 shows that the total content of carbonate minerals was similar in all tailings with slight increased amounts for dolomite as well as decreased calcite contents compared to the feed material. Illite occurred most increased in tailings of the dextrin-added flotation (24.0%) and showed a slightly lower content in tailings of the standard flotation (23.1%), whereas the content of illite in tailings of the flotation using ethanol pre-treated feed represented the minimal amount by 21.7% among the flotation tailings from Sangerhausen black shale feed.

A discernible enrichment of varying extend for feldspars was determined in tailings. Especially, tailings from the standard flotation test contained the most increased content of as well K-feldspar as plagioclase, whereas tailings derived from dextrin-added flotation tests contained similar amounts of total feldspars (approx. 14%). Quartz was slightly enriched in tailings of the standard flotation (22.3%) regarding the content in the feed. Progressively decreasing quartz contents were ascertained for tailings of the flotation using dextrin (17.7%) to the flotation tailings originated from ethanol pre-treated feed (15.5%).

Additionally, the proportion of organic matter in tailings differed remarkable. Tailings of the flotation using pre-treated feed were rich in organics (TOC: 22.0%), whereas organic matter in the flotation using dextrin and not ethanol pre-treated black shale feed (TOC: 15.1%) was depressed to lower extend into the tailings or was insufficiently depressed as clearly indicated for the tailings of the standard flotation (TOC: 11.0%).

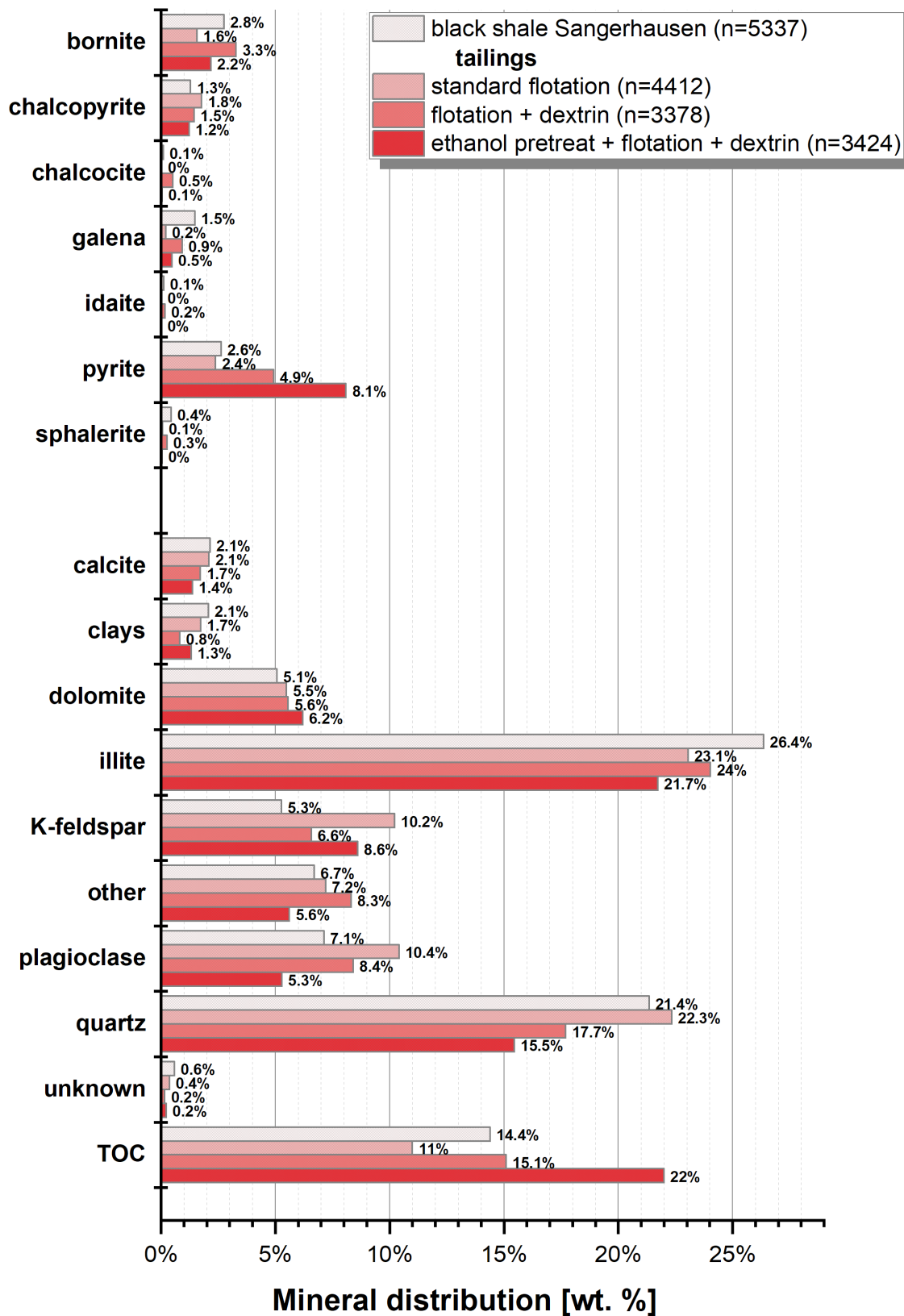


**Figure 3.2.18:** Mineral distribution showing the proportions of particular sulphide (upper part) and gangue minerals as well as total organic matter content (TOC) in Sangerhausen black shale feed and related tailings from different flotation tests. (Data: MLU)

### 3.2.5.3 Content of base and trace metals in concentrates and tailings from the flotation of Sangerhausen black shale

Geochemical data of base and associated trace metals in concentrates and tailings derived from Sangerhausen black shale are listed in Table 3.2.3. According to the composition of dominant sulphides detected by mineral distribution analyses, the content of metals was related to their abundance in the individual concentrates and tailings. Both were partly strong enriched in bornite, chalcopyrite, galena and pyrite. Because of strong variations of their proportions, metal concentrations deviated significantly.

The Cu content achieved by flotation using dextrin was considerably, so that the concentrate from not ethanol pre-treated feed contained 12.4% Cu and was more increased in the concentrate from pre-treated feed (14.4%). However, the concentrate gained by standard flotation showed an extremely lower Cu content with 3.9%. Related tailings in turn contained similar Cu concentrations, nearly equal for the tailings from the dextrin-added flotation (2.1%) and slightly lower for the tailing of the standard flotation (1.5%).

The proportion of Pb in the concentrates differed likewise and was most increased in the concentrate extracted from ethanol pre-treated feed material (7.43%), whereas the concentrate from the flotation with dextrin contained 6.2% Pb and the product of the standard flotation was marked by far the lowest Pb content (2.0%). Generally, Pb contents in tailings from the flotation of Sangerhausen black shale were decisively lower and nearly equal in the tailings derived from flotation tests using dextrin (approx. 1.0%) as well as slightly lower in the tailings from the standard flotation (0.7%). Zn occurred in traces in the tailings, but showed significant differences between concentrates extracted

**Table 3.2.3:** Content of base and associated trace metals in concentrates and tailings from different flotation tests using Sangerhausen black shale feed. (Data: ALS)

		concentrates			tailings		
		standard flotation	flotation with dextrin	flotation with dextrin + ethanol pre-treatment	standard flotation	flotation with dextrin	flotation with dextrin + ethanol pre-treatment
<b>Cu</b>	%	3.90	12.35	14.40	1.52	2.10	2.06
<b>Pb</b>	%	1.97	6.17	7.43	0.74	1.03	1.13
<b>Zn</b>	%	0.24	1.50	1.36	0.08	0.11	0.12
<b>Fe</b>	%	4.18	5.71	6.60	2.09	2.57	3.25
<b>Ag</b>	ppm	99	624	452	44	50	69
<b>As</b>	ppm	530	461	593	350	410	440
<b>Cd</b>	ppm	10.7	72.0	62	<5	5	7
<b>Co</b>	ppm	1150	905	1040	561	728	886
<b>Mo</b>	ppm	512	528	697	257	336	436
<b>Ni</b>	ppm	472	352	386	197	246	317
<b>Sb</b>	ppm	112	672	625	30	50	20
<b>V</b>	ppm	1980	1455	1620	618	633	717

by flotation with dextrin and the standard flotation, where it was comparably low (0.2%). An increasing content of Fe over the series of tests was obvious in both, the concentrates and tailings. The lowest Fe contents were analysed for the concentrate (4.2%) and tailings (2.1%) of the standard flotation, followed by the dextrin-added flotation of not pre-treated feed (conc.: 5.7%, tail.: 2.6%) and the flotation using ethanol pre-treated feed (conc.: 6.6%, tail.: 3.3%).

Trace metals showed generally increased contents in concentrates, whereas moderate to significantly lower concentrations occurred in tailings. The most increased contents of trace metals were partly determined in the product of the standard flotation, which contained 1980 ppm V, 1150 ppm Co and 472 ppm Ni, but also the lowest concentrations for Ag (99 ppm), Cd (10 ppm), Mo (512 ppm and Sb (112 ppm). The latter was most enriched (672 ppm) in the concentrate from the flotation using dextrin without ethanol pre-treatment of the feed accompanied by most increased contents of Ag (624 ppm) as well as Cd (72 ppm), whereas Ni (352 ppm), As (461 ppm) and V (1455 ppm) showed the lowest concentrations in comparison to the other concentrates. The concentrate gained from ethanol pre-treated feed contained most increased contents for As (593 ppm) and Mo (697 ppm), but other trace metals occurred comparatively with intermediate contents.

### 3.2.6 Liberation analysis of copper sulphides in flotation concentrates and tailings

The data presented in this chapter stem from a dataset of liberation analyses commissioned to Petrolab Ltd, Cornwall, UK. The samples analysed in the course of this order comprised the feed materials as well as selected pairs of concentrate and tailings of flotation tests. Thus, these data will be presented as a coherent study including grain size and liberation data of bulk black shale samples partly deviating from respective data presented in Chapter 3.1.3.

#### 3.2.6.1 Liberation of copper sulphides in flotation concentrates and tailings

The comparison of the liberation of sulphides in flotation concentrates and tailings is represented in Figure 3.2.19 and Figure 3.2.20. Liberation data were classified, according to the degree of liberation of the target mineral perimeter, in three groups: liberated sulphide grains with 80 to 100% liberated perimeter, middlings that represented intergrown particles showing 70 to 30% liberated proportion of the target mineral perimeter as well as particles that contain a target mineral predominantly enclosed/overgrown by other mineral phases showing < 30% free perimeter/surface.

Generally, the liberation data for concentrates showed an increased proportion of liberated and more partial liberated (middlings) copper sulphides from the standard flotation tests over the tests using dextrin to the dextrin-added flotation tests with ethanol pre-treatment of the ore. Apparently, increased proportion of liberated bornite and bornite middlings were recognized in flotation concentrates extracted from Sangerhausen black shale feed. Especially, the concentrate gained from ethanol-pre-treated feed contained a low portion of locked bornite particles (11%), contrastingly to the similar concentrate extracted from Rudna black shale that consists of 43% of locked bornite particles (see Figure 3.2.19).

Concentrates gained from Sangerhausen black shale feed contained around 80% cumulative chalcopyrite portion comprising of liberated chalcopyrite and middlings. In particular, the product of the standard flotation showed an increased proportion of liberated chalcopyrite particles (64%). However, concentrates extracted from Rudna black shale contained mostly locked chalcopyrite particles (73–81%), just a low amount of chalcopyrite occurred partially or completely liberated.

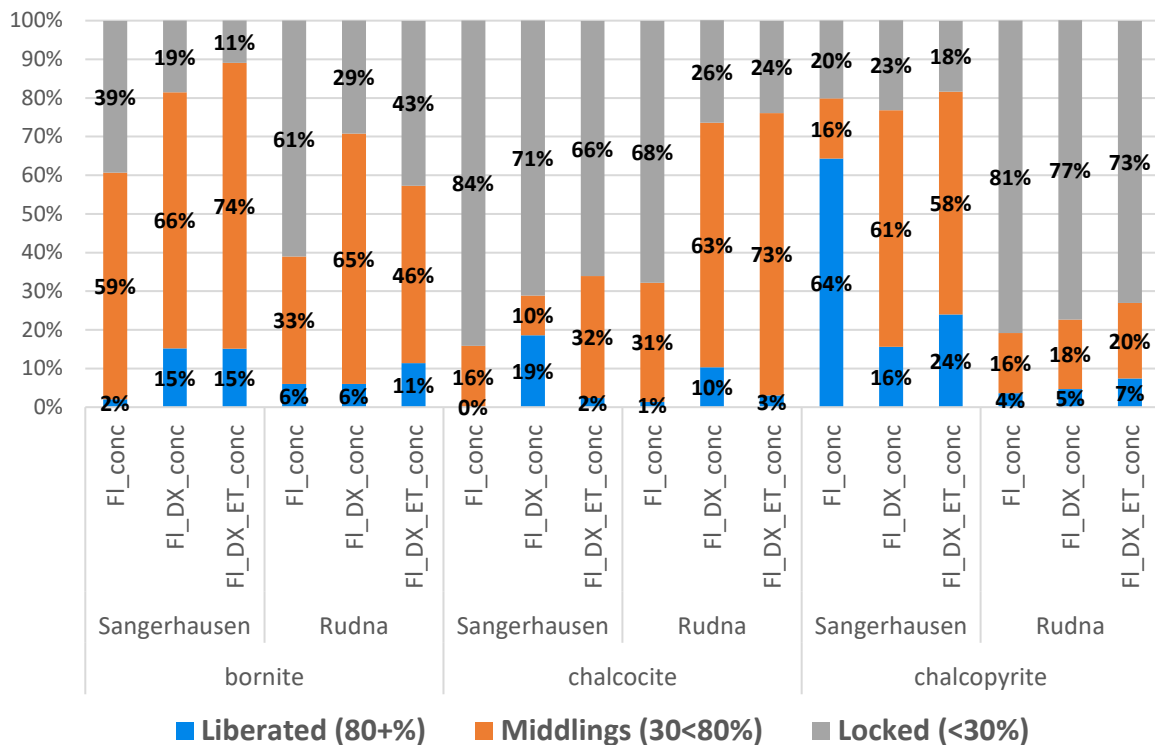


**Figure 3.2.19:** Distribution of liberation classes, according to free perimeter of the target mineral, for bornite, chalcocite and chalcopyrite in concentrates of different flotation test series with Sangerhausen as well as Rudna black shale feed. (FI\_conc=concentrate standard flotation, FI\_DX\_conc=concentrate flotation with dextrin, FI\_DX\_ET\_conc=concentrate flotation with dextrin and ethanol pre-treated feed; Data: Petrolab)

Chalcocite, which was very differentially contained in both black shale ores, showed significantly increased proportions of liberated chalcocite grains (> 80% free surface) and middlings in concentrates extracted from Rudna black shale feed. In particular an increased amount of chalcocite middlings was determined in the product generated by dextrin-added flotation with ethanol pre-treated feed, although the proportion of liberated chalcocite was generally low. Especially, the concentrate from the standard flotation test contained predominantly locked particles (68%).

Chalcocite in flotation concentrates from Sangerhausen ore occurred likewise mainly locked and the portion of liberated chalcocite was low. Only the flotation test with added dextrin was capable to enrich higher proportions of liberated particles (19%) into the concentrate regarding concentrates extracted from Sangerhausen black shale feed. Generally, liberation data revealed that concentrates contain higher proportions of liberated particles and middlings compared to the tailings.

Liberated chalcocite and chalcocite middlings were partly absent, for example in tailings of the standard flotation as well as the flotation using dextrin with Sangerhausen black shale feed, whereas the proportion of chalcocite middlings substantially decreased in tailings of the standard flotation tests and more extensive in tailings from the flotation test using dextrin and ethanol pre-treated Rudna black shale feed. A similar trend was obvious for bornite and chalcopyrite in flotation tailings from Rudna black shale feed. Tailings from the dextrin-added flotation using ethanol pre-treated Rudna black shale feed contained generally the lowest amount of liberated copper-bearing sulphides and middlings. Tailings from Sangerhausen black shale feed in turn showed an opposing trend that revealed the most increased portions of liberated copper sulphides and middlings was detected in tailings of the flotation using dextrin and ethanol pre-treated feed. For example, the proportion of locked bornite was 50% in tailings of the standard flotation, but in tailings from flotation tests with dextrin and ethanol

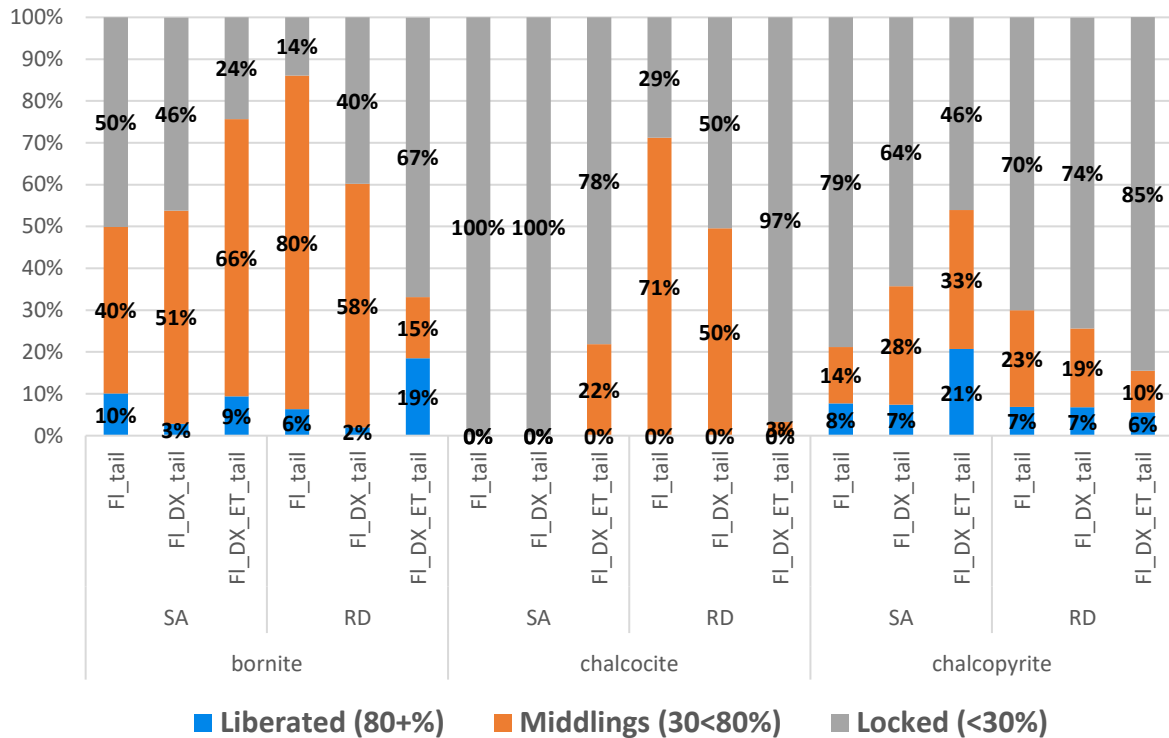


**Figure 3.2.20:** Stacked bar chart displaying the distribution of liberation classes, according to free perimeter of the target mineral, for bornite, chalcocite and chalcopyrite in concentrates of different flotation test series with Sangerhausen as well as Rudna black shale feed. (RD=Rudna, SA=Sangerhausen, FI\_tail=tailings standard flotation, FI\_DX\_tail=tailings flotation with dextrin, FI\_DX\_ET\_tail=tailings flotation with dextrin and ethanol pre-treated feed; Data: Petrolab)

pre-treatment it decreased to 24%. Correspondingly, the proportion of locked bornite and middlings increased, which also especially applied to chalcopyrite. The increasing content of liberated and partly liberated chalcopyrite in the tailings from Sangerhausen black shale feed is shown for the standard flotation (22%) over the flotation test using dextrin (35%) to the dextrin-added flotation with additional ethanol pre-treatment of the ore (54%).

### 3.2.6.2 Grain size distribution of copper sulphides in concentrates from Rudna and Sangerhausen black shale feed

The examination of grain sizes of copper-bearing sulphides in milled black shale feed and their respective flotation concentrates, depicted in Figure 3.2.21, shows strong variations in the cumulative mass intercepts at 20% ( $D_{20}$ ), 50% ( $D_{50}$ ) and 80% ( $D_{80}$ ). The lowest differences of the grain size were determined in the fraction  $D_{20}$ . Bornite grains had generally the same size (6  $\mu\text{m}$ ) in  $D_{20}$  of both comminuted black shale ores. The milled Rudna black shale contained generally coarser bornite grains, up to 6  $\mu\text{m}$  larger, in the fractions  $D_{50}$  and  $D_{80}$ . However, flotation concentrates derived from the Sangerhausen black shale contained coarser-grained bornite (up to 13  $\mu\text{m}$  larger) in all mass intercepts in comparison with bornite grains occurring in concentrates from Rudna ore. The grain size variance at  $D_{50}$  of the total bornite was striking different. Significant larger particles (23  $\mu\text{m}$  @  $D_{50}$ ) were extracted in the concentrate gained from the dextrin-added flotation using non-ethanol pre-treated Sangerhausen black shale feed. For comparison, 50% of bornite grains in the feed belonged to the grain size fraction  $\leq 12 \mu\text{m}$  as well as  $\leq 18 \mu\text{m}$  in the concentrate gained from ethanol pre-treated

Sangerhausen ore. This relationship was also notable for the  $D_{80}$ -fraction, in which bornite was coarser-grained in the concentrate extracted by flotation in addition of dextrin ( $D_{80}=46 \mu\text{m}$ ), whereas bornite grains were approximately one third smaller ( $D_{80}=32 \mu\text{m}$ ) in the concentrate generated from ethanol-pre-treated black shale feed ( $D_{80}=25 \mu\text{m}$ ). In comparison to the Sangerhausen ore, bornite in the milled Rudna black shale showed a similar grain size distribution, although the fractions  $D_{50}$  ( $16 \mu\text{m}$ ) and  $D_{80}$  ( $31 \mu\text{m}$ ) were slightly coarser-grained. Thus, bornite grains in the  $D_{50}$ - and  $D_{80}$ -fraction of the flotation product gained from feed not subjected an ethanol pre-treatment were slightly larger in average. A decline of the bornite grain size was recognized for the flotation product from ethanol-pre-treated Rudna feed ( $D_{50}=13 \mu\text{m}$ ;  $D_{80}=20 \mu\text{m}$ ).

The size of chalcocite grains in the milled Sangerhausen black shale was very fine-grained, even at  $D_{80}$  it was smaller than  $5 \mu\text{m}$ . Concentrates extracted from Sangerhausen black shale feed contained chalcocite with similar grain sizes in  $D_{20}$ - and  $D_{50}$ -mass intercepts but chalcocite was significant coarser-grained at  $D_{80}$  in both, the concentrate from pre-treated ( $15 \mu\text{m}$ ) and not pre-treated feed ( $12 \mu\text{m}$ ), respectively. Chalcocite represented the main copper ore mineral in the Rudna black shale. According to the grain size distribution, chalcocite grains were at least a magnitude coarser-grained ( $D_{80}= 66 \mu\text{m}$ ) than in the Sangerhausen feed. Interestingly, the  $D_{20}$ -fraction of both concentrates contained similar sized chalcocite grains as the milled ore, but decisively smaller chalcocite grains in the  $D_{50}$ - and  $D_{80}$ -fraction.

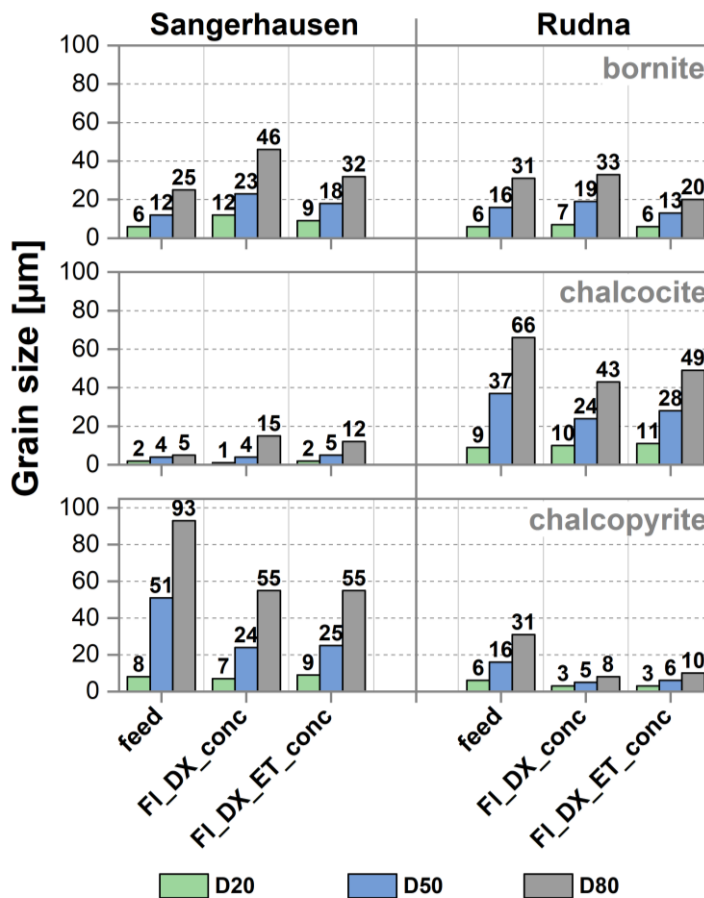


**Figure 3.2.21:** Grain size distribution of bornite, chalcocite and chalcopyrite in Sangerhausen as well as Rudna feed and related concentrates extracted by flotation using dextrin. (FI\_DX\_conc=concentrate flotation with dextrin, FI\_DX\_ET\_conc=concentrate flotation with dextrin and ethanol pre-treated feed; Data: Petrolab)

Chalcopyrite was a main copper sulphide in the Sangerhausen black shale but not in the Rudna black shale, in which it occurs accessorially. The ball mill product of Rudna black shale contained more fine-grained chalcopyrite, whereas chalcopyrite was definitely coarser-grained in the Sangerhausen black shale ore. Since the grain size was quite similar in the  $D_{20}$ -fractions of the feed and the concentrates, the milled Sangerhausen black shale contained roughly three times coarser chalcopyrite grains in fractions of  $D_{50}$  (51  $\mu\text{m}$ ) and  $D_{80}$  (93  $\mu\text{m}$ ). Chalcopyrite in the flotation products of the Sangerhausen black shale feed showed a similar grain size distribution, in which  $D_{80}$ -fractions contained chalcopyrite up to 55  $\mu\text{m}$  and  $D_{50}$ -fractions up to 25  $\mu\text{m}$  grain size. The flotation of Rudna black shale delivered generally significant smaller chalcopyrite particles in concentrates. Whilst the  $D_{80}$ -fraction of the milled Rudna black shale ore was marked by chalcopyrite grains up to 31  $\mu\text{m}$ , the corresponding mass fraction of the concentrate gained without ethanol feed pre-treatment step showed chalcopyrite grains with up to 8  $\mu\text{m}$  size as well as 10  $\mu\text{m}$  in the flotation product extracted from the feed subjected to an ethanol pre-treatment. Correspondingly lower chalcopyrite grain sizes showed the  $D_{50}$ -fraction and even more the  $D_{20}$ -fraction, in which very fine-grained chalcopyrite ( $\leq 3 \mu\text{m}$ ) occurred.

### 3.2.6.3 Liberation and locking association of copper sulphides in selected flotation concentrates from Rudna and Sangerhausen black shale feed

Detailed textural information about mineral association were available for selected flotation concentrates. These data comprise type of locking, proportions of mineral phases associated with a target mineral (copper sulphides), liberation mode of target minerals according to their occurrence in particle size classes as well as the cumulative mass of a target mineral in particle size classes. The latter is commonly displayed as theoretical mineral-recovery curve in combination with a bar chart containing mineral liberation modes in particle size classes.

Advanced locking information are in particular described in the following subchapters for the concentrates extracted by dextrin-added flotation as well as by dextrin-added flotation carried out with ethanol pre-treated black shale feed.

#### 3.2.6.3.1 Chalcocite in flotation concentrates from Rudna black shale ore

Important target minerals in terms of their abundance and economic significance in the concentrates gained from Rudna black shale represented bornite and chalcocite. Thus, the mode of liberation within individual particle size revealed the capability to extract copper sulphides in varying conditions by different flotation approaches.

##### *Chalcocite liberation - Flotation with dextrin*

Figure 3.2.22 shows the liberation mode of chalcocite in particle size classes and additionally the chalcocite recovery curve for the concentrate extracted by flotation using dextrin. The stacked column plot shows that the particle size range  $< 50 \mu\text{m}$  is dominated by chalcocite that was nearly complete or partially liberated, the latter representing chalcocite middlings, whereas in particles  $> 50 \mu\text{m}$  chalcocite was mainly locked. The proportion of liberated chalcocite as well as chalcocite middlings differed substantially in the particular particle size classes  $< 50 \mu\text{m}$ , except the particle size class  $+ 40 \mu\text{m}$ , which contained nearly exclusive liberated chalcocite (91%). This particle size class hosted apparently coarser-grained chalcocite according to the grain size distribution, in which  $D_{80}$  was 43  $\mu\text{m}$  (see Figure 3.2.21). Other particle size classes, in which liberated chalcocite was dominating, were classes  $+0 \mu\text{m}$  (50%) and  $+20 \mu\text{m}$  (82%), whereas chalcocite middlings occurred preferentially in classes

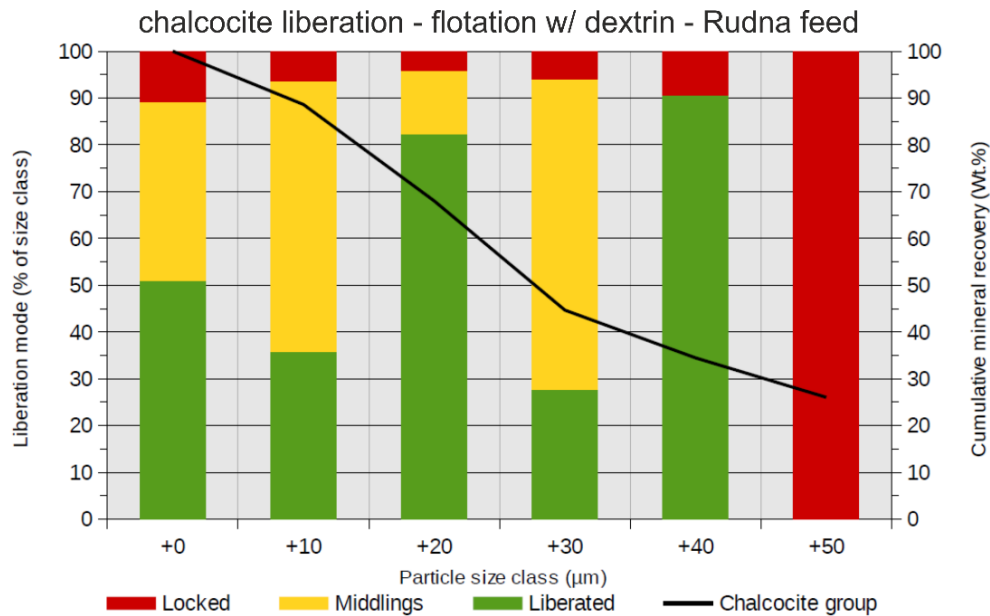


**Figure 3.2.22:** Distribution of liberation classes for chalcocite regarding to particle size classes in the concentrate extracted by flotation using dextrin from Rudna black shale feed. Black line graph shows the recovery curve of chalcocite. (Data: Petrolab)

+10 μm (48%) and +30 μm (66%). The portion of locked chalcocite in the particle size range < 50 μm was generally low (4-11%), however, in coarser particles chalcocite was generally complete locked.

The chalcocite recovery curve in Figure 3.2.22 indicates, according to the distribution, that chalcocite occurred substantially in the particles size class +50 μm (25%), which contained exclusively locked chalcocite, whereas the +20 μm particle size class showed a comparably increased proportion of chalcocite (25%) but predominantly liberated (82%). The proportion of total chalcocite in the particle size class +10 μm was 20%, but it contained a significant increased portion of partially locked chalcocite (middlings: 58%).

#### *Chalcocite liberation - Flotation with dextrin and ethanol pre-treated feed*

Figure 3.2.23 shows the liberation mode of chalcocite regarding its occurrence in particle size classes in the product gained by flotation with dextrin and ethanol pre-treated feed. Generally, locked chalcocite occurred subordinately over the entire particle size range of the concentrate. While the +50 μm particle size class of the concentrate extracted from feed without ethanol pre-treatment contained only locked chalcocite, the concentrate from pre-treated Rudna black shale feed was dominated by chalcocite middlings in this particle size range and likewise the +30 μm particle size class. Liberated chalcocite portion were partly lower in comparison to the concentrate gained from not pre-treated feed, in particular in the particle size range + 20 μm.

Fine-grained particles associated with chalcocite in the concentrate from pre-treated feed contained in turn an increased amount of liberated chalcocite compared to the concentrate extracted from feed not subjected an ethanol pre-treatment. Liberated chalcocite dominated the particle size classes +0 μm (50%), +10 μm (44%) and +40 μm (69%). The latter class represented an exception regarding increasing proportion of chalcocite middlings in coarser particle size classes and indicated that coarser-grained chalcocite was often liberated within the chalcocite grain size distribution ( $D_{80}=49$  μm, see Figure 3.2.21). As shown in Chapter 3.2.1, the mass recovery in the concentrate extracted from

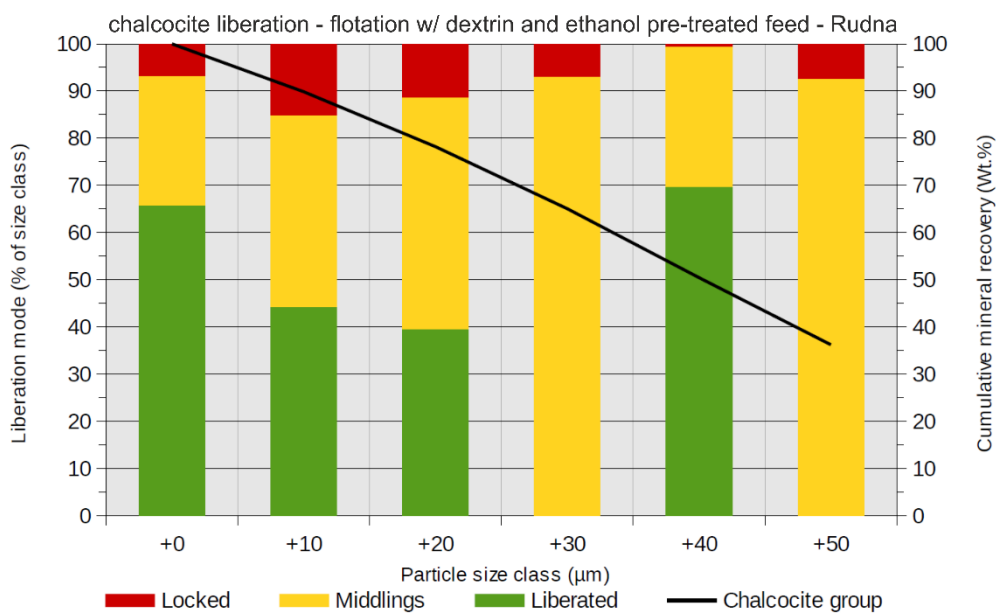


**Figure 3.2.23:** Liberation modes of chalcocite in particle size classes of the concentrate extracted by flotation using dextrin from ethanol pre-treated Rudna black shale feed. Black line graph indicates the chalcocite recovery curve. (Data: Petrolab)

ethanol pre-treated Rudna black shale feed was significantly increased, 26.7% vs. 9.0% for the concentrate from untreated feed. Thus, the increase of the mass recovery caused the extraction of more partially liberated chalcocite obviously in the finer particle size range, e.g. in the +20 µm particle size class.

The chalcocite recovery curve in Figure 3.2.1 indicates accordingly that 50% of the total chalcocite occurred in the particle size range > 40 µm, in which chalcocite middlings were the main locking mode. Towards finer particle size classes, the proportion of total chalcocite decreased, e.g. the +20 µm class hosted 15% and the +0 µm class contained 10% of the total chalcocite, respectively.

#### Locking and mineral association

Table 3.2.4 shows that the content of liberated chalcocite in both flotation products was different. Completely exposed chalcocite grains occurred increased in the concentrate from the flotation using dextrin but non-ethanol pre-treated feed (12.0% vs. 3.7% in the concentrate from ethanol pre-treated feed), whereas the proportion of binary locked chalcocite was low and nearly equivalent in both concentrates. According to the increased amount of liberated chalcocite, the concentrate from non-

**Table 3.2.4:** Lock types of chalcocite in flotation concentrates from Rudna black shale feed. (Data: Petrolab)

Lock type chalcocite	Flotation with dextrin	Flotation with dextrin + ethanol pre-treatment
<b>Liberated (&gt; 95 % free perimeter)</b>	12.0%	3.7%
<b>Binary locked</b>	3.0%	2.4%
<b>Complex (ternary+) locked</b>	85.1%	93.1%

**Table 3.2.5:** Mineral association of locked chalcocite in flotation concentrates extracted from Rudna black shale feed. (Data: Petrolab)

<b>Chalcocite locked with</b>	<b>Flotation with dextrin</b>	<b>Flotation with dextrin + ethanol pre-treatment</b>
<b>bornite</b>	75.0%	84.3%
<b>chalcopyrite</b>	37.0%	51.9%
<b>galena</b>	16.3%	30.5%
<b>pyrite</b>	8.0%	20.0%
<b>carbonates</b>	55.9%	72.1%
<b>feldspar</b>	58.3%	57.0%
<b>illite/clays</b>	66.3%	78.3%
<b>quartz</b>	57.3%	69.1%
<b>accessory minerals</b>	18.1%	18.1%

pre-treated feed contained a lower portion of complexly locked chalcocite particles (85.1% vs. 93.9% in the concentrate from ethanol pre-treated feed).

Locked chalcocite in concentrates extracted from Rudna black shale ore was associated with numerous mineral phases. On the one hand chalcocite was intimately intergrown with other sulphides of the sulphide assemblage, on the other hand chalcocite was also locked in particles by intergrowths with gangue-type minerals such as illite, quartz, carbonate and feldspars. According to the increased proportion of complex locked chalcocite in the flotation concentrate from ethanol pre-treated ore, locking associations, quantified by the overall proportion of chalcocite in mass % locked with sulphide and gangue minerals, were detected in higher percentages.

The mineral locking association of chalcocite in both concentrates were dominated by intergrowths with in particular bornite and illite/clays, as Table 3.2.5 displays. Additionally, chalcocite was moderately interlocked with chalcopyrite and to lower extent with galena and pyrite, which illustrates the intimately and fine-grained intergrowth of the sulphide association. Besides the locking by other sulphides, chalcocite in complexly intergrown particles was associated, in decreasing abundance, with illite/clays, quartz, feldspars and carbonate minerals (mainly dolomite).

#### 3.2.6.3.2 Bornite in flotation concentrates from Rudna black shale ore

Bornite extracted by the flotation of Rudna black shale feed was more fine-grained compared to the grain size of chalcocite. Thus, the  $D_{80}$  grain size for chalcocite was 43  $\mu\text{m}$  and 33  $\mu\text{m}$  for bornite, respectively, in the product gained by flotation using dextrin without ethanol pre-treatment of the feed (see Figure 3.2.21). The concentrate achieved from ethanol pre-treated feed contained chalcocite with  $D_{80}$  grain size at 49  $\mu\text{m}$ , whereas bornite grains were decisively more fine-grained ( $D_{80}=20 \mu\text{m}$ ), also in comparison to the flotation product from non-ethanol pre-treated feed.

#### *Bornite liberation - Flotation with dextrin*

Furthermore, the mass recovery influenced the occurrence of sulphides in concentrates regarding their grain size and liberation mode. Figure 3.2.24 shows the distribution of liberation modes of bornite in particle size classes of the concentrate extracted by dextrin-added flotation. It displays that particles,

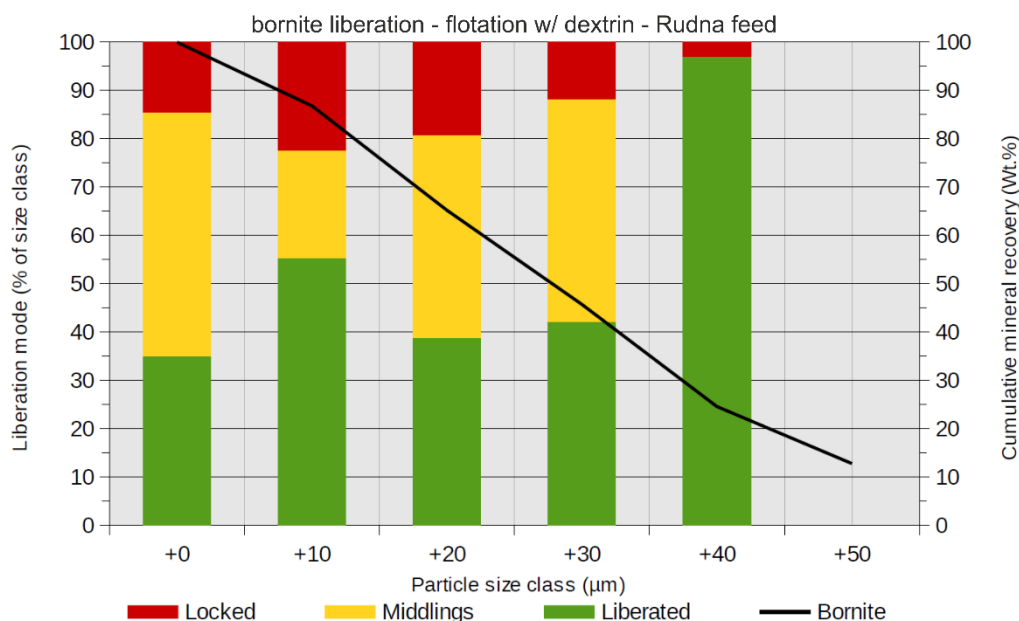


**Figure 3.2.24:** Distribution of liberation modes of bornite in particle size classes of the concentrate extracted by flotation using dextrin from Rudna black shale feed. Black line graph represents the recovery curve for bornite. (Data: Petrolab)

in which bornite was completely locked, occurred more increased (up to 23% in class +10 μm) in comparison to chalcocite (max. 11%) in the same concentrate.

Generally, the proportions of liberated bornite and bornite middlings varied within the particle size classes. Apart from the +50 μm class, which contained no bornite, liberated bornite was dominating in particle size class +10 μm (55%) and more striking in class +40 μm (97%). The latter class was also marked by an extremely low proportion of locked bornite and showed an accumulation of more coarse-grained and liberated bornite. Furthermore, the increased portion of liberated bornite (55%) and the lowest content of bornite middlings (33%) in the +10 μm particle size class indicates that a significant proportion of fine-grained and liberated bornite occurred at the 50%-fraction of total bornite ( $D_{50}=19 \mu\text{m}$ ). Bornite middlings were predominant in the +0 μm particle size class (50%), whereas the +20 and +30 particle size classes contained equivalent proportions (approx. 40% each) of liberated bornite and bornite middlings. The bornite recovery curve in Figure 3.2.24 reveals that the main proportion of bornite by mass percent was accumulated in particle size range 10-40 μm (64% of total bornite) and subordinate equivalent portions (13%) occurred in the particle size ranges below and above.

#### *Bornite liberation - Flotation with dextrin and ethanol pre-treated feed*

The comparison to the liberation mode of bornite according to particle size classes in the flotation concentrate produced from ethanol pre-treated Rudna black shale in Figure 3.2.25 showed that bornite extracted in the concentrate was marked by intergrowths and locking with other minerals, especially in the particle size range < 30 μm, which can be attributed to the fineness of bornite grains. Bornite associated in particles in the size range > 40 μm was completely locked, but particles < 40 μm contained progressively more liberated bornite with decreasing particle size, so that the particle size classes +0 μm (53%) and +10 μm (58%) were dominated by liberated bornite grains. The particle size class +20 μm represented a transition range, in which predominantly bornite middlings (51%) and similar proportions of liberated as well as locked bornite occurred. The proportion of locked bornite

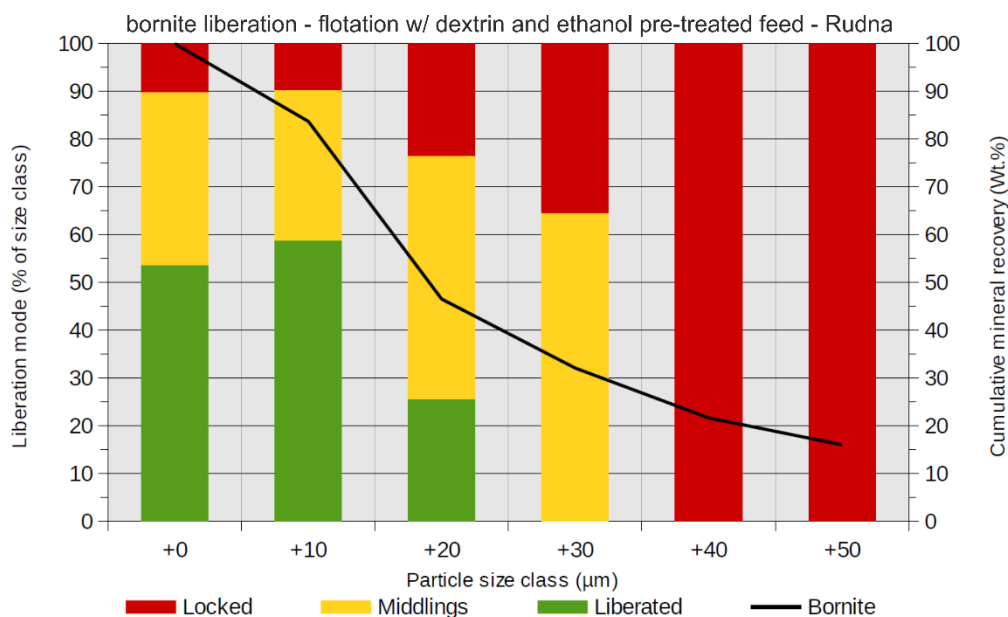


**Figure 3.2.25:** Stacked column plot for liberation modes of bornite in particle size classes of the concentrate generated by flotation using dextrin and ethanol pre-treated Rudna black shale feed. (Data: Petrolab)

decreased constantly to 10% in fine-grained particle size range < 20 µm, which also contained a substantial portion of bornite middlings (+0 µm: 37%; +10 µm: 32%).

The bornite recovery curve in Figure 3.2.25 for the concentrate extracted from ethanol pre-treated Rudna black shale feed revealed that most increased proportion of bornite was accumulated in the +10 µm particle size class (38%). A constantly decreasing proportion of the total bornite was determined in coarser particle size classes and was accompanied by decreasing liberation of bornite.

#### *Locking and mineral association*

The proportions of the lock type for bornite in the concentrates extracted by flotation using dextrin as well with ethanol pre-treatment of the feed as without are compared in Table 3.2.6. It shows that the portion of free, completely liberated bornite was significantly increased in the flotation concentrate from ethanol pre-treated feed (18.9%) compared to the concentrate extracted from not pre-treated feed (3.8%), which was the opposite relation as observed for chalcocite. Binary locked bornite occurred rarely in both concentrates. However, according to the proportion of free bornite, complexly locked bornite was more prominent in the concentrate derived from non-ethanol pre-treated feed (93.5% vs. 79.7% in the concentrate from pre-treated ore).

**Table 3.2.6:** Lock types of chalcocite in flotation concentrates from Rudna black shale feed. (Data: Petrolab)

Lock type bornite	Flotation with dextrin	Flotation with dextrin + ethanol pre-treatment
<b>Liberated (&gt; 95 % free perimeter)</b>	3.8%	18.9%
<b>Binary locked</b>	2.7%	1.3%
<b>Complex (ternary+) locked</b>	93.5%	79.7%

The mineral association of nearly exclusively complex locked bornite in the concentrates gained from Rudna black shale is listed in Table 3.2.7. Due to the lower proportion of complex locked bornite in the concentrate extracted from ethanol pre-treated Rudna black shale feed, the shares of minerals associated with bornite were commonly lower compared to the concentrate extracted from non-ethanol pre-treated feed. Bornite was mainly locked with chalcocite in both concentrates, but also chalcopyrite and galena were substantial constituents of intergrowths with bornite in the concentrate from non-ethanol pre-treated feed, whereas galena in the concentrate from ethanol pre-treated feed and generally also pyrite were subordinately intergrown with bornite. Besides intense intergrowths with other sulphides, gangue minerals were slightly more subordinated part of intergrowths with bornite, in which illite / clays were most prominent, followed by carbonates, quartz and feldspars. It was noticeable that intergrowths with carbonate minerals were more common than with quartz, which was the opposite for intergrowths of chalcocite.

**Table 3.2.7:** Distribution of minerals associated with locked bornite in flotation concentrates extracted from Rudna black shale feed. (Data: Petrolab)

<b>Bornite locked with</b>	<b>Flotation with dextrin</b>	<b>Flotation with dextrin + ethanol pre-treatment</b>
<b>chalcocite</b>	83.0%	62.0%
<b>chalcopyrite</b>	48.3%	49.2%
<b>galena</b>	41.1%	21.0%
<b>pyrite</b>	11.8%	17.8%
<b>carbonates</b>	58.7%	45.6%
<b>feldspar</b>	40.1%	37.6%
<b>illite/clays</b>	61.4%	51.5%
<b>quartz</b>	47.6%	39.7%
<b>accessory minerals</b>	12.6%	23.8%

### 3.2.6.3.3 Bornite in flotation concentrates from Sangerhausen black shale ore

Bornite in the ball mill product of Sangerhausen black shale was slightly more fine-grained ( $D_{80}=25\ \mu\text{m}$ ) than bornite in the ball milled Rudna black shale ( $D_{80}=31\ \mu\text{m}$ ), as shown in Figure 3.2.21. However, bornite in the concentrates from Sangerhausen black shale was commonly more coarse-grained, especially in the concentrate from non-ethanol pre-treated feed ( $D_{80}=46\ \mu\text{m}$ ), but showed slightly lower grain size up to  $32\ \mu\text{m}$  at  $D_{80}$  in the concentrate from ethanol pre-treated ore (see Figure 3.2.21). Additionally, the flotation test using dextrin and non-ethanol pre-treated feed was highly selective, so that the mass recovery was quite low (5.7 wt.%), while the mass recovery in the flotation tests using ethanol pre-treated ore was decisively increased (29.8 wt.%).

#### *Bornite liberation - Flotation with dextrin*

Figure 3.2.26 shows the distribution of liberation modes of bornite in particle size classes of the concentrate extracted by dextrin-added flotation. It is obvious that commonly 50% and more of the total bornite in each particle size class occurred liberated and bornite middlings dominated only in the  $+30\ \mu\text{m}$  particle size class (65%). Equal proportions of liberated bornite and bornite middlings shared

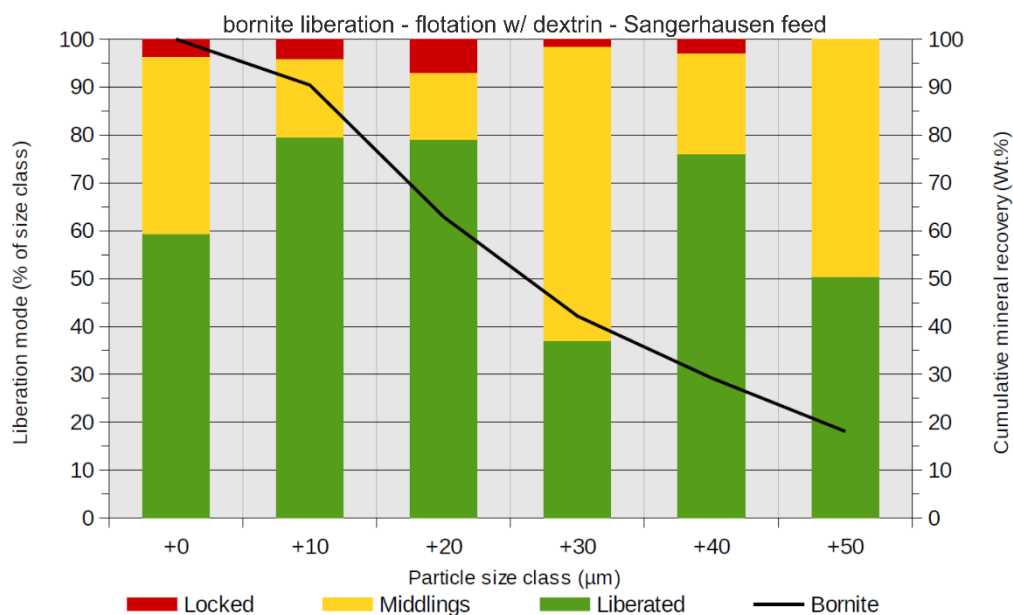


**Figure 3.2.26:** Stacked column diagram representing proportions for liberation modes of bornite in the concentrate gained by flotation using dextrin from Sangerhausen black shale feed. Black line graph indicates the theoretical recovery curve for bornite. (Data: Petrolab)

the +50 µm particle size class. The content of liberated bornite over the entire particle size range was exemplarily high and locked bornite showed minimum proportion in the product of the flotation from non-ethanol pre-treated feed.

The bornite recovery curve in Figure 3.2.26 shows that nearly 50% of the total bornite was detected in the particle size range 10-30 µm, which corresponded to the average grain size of bornite ( $D_{50}=23$  µm, in Figure 3.2.21). Another main part of the total bornite mass was distributed with similar proportion over the particle size classes > 30 µm.

#### *Bornite liberation - Flotation with dextrin and ethanol pre-treated feed*

The distribution of locking modes of bornite in the concentrate from ethanol pre-treated feed is shown in Figure 3.2.27 and was in comparison marked by increased amounts of bornite middlings. Liberated bornite occurred exclusively in the particle size range up to 40 µm, but dominated the distribution of liberation modes with proportions from 55% up to 75% in the < 40 µm particle size range. The proportion of locked bornite was commonly low (< 10%), but exceeded significantly in particle size class +40 µm. The coarse-grained particle size classes > 40 µm were dominated by the occurrence of bornite middlings that represented almost entirely the bornite locking mode, besides some locked bornite in particle size class + 50.

According to the bornite recovery curve in Figure 3.2.27, the main part of bornite (58%) was accumulated in the particle size range 10-30 µm similar to the main portion of bornite in the concentrate from non-ethanol pre-treated feed, but with a slightly increased proportion on the total bornite mass. This stands in agreement with the grain size distribution of bornite in the concentrate from ethanol pre-treated feed ( $D_{50}=18$  µm). In comparison to the mass distribution of bornite in the concentrate from non-ethanol pre-treated feed, the particle size classes > 30 µm contained partly lower proportions of the total bornite mass, whereas the +0 µm particle size contained some more bornite (16% vs 9%).

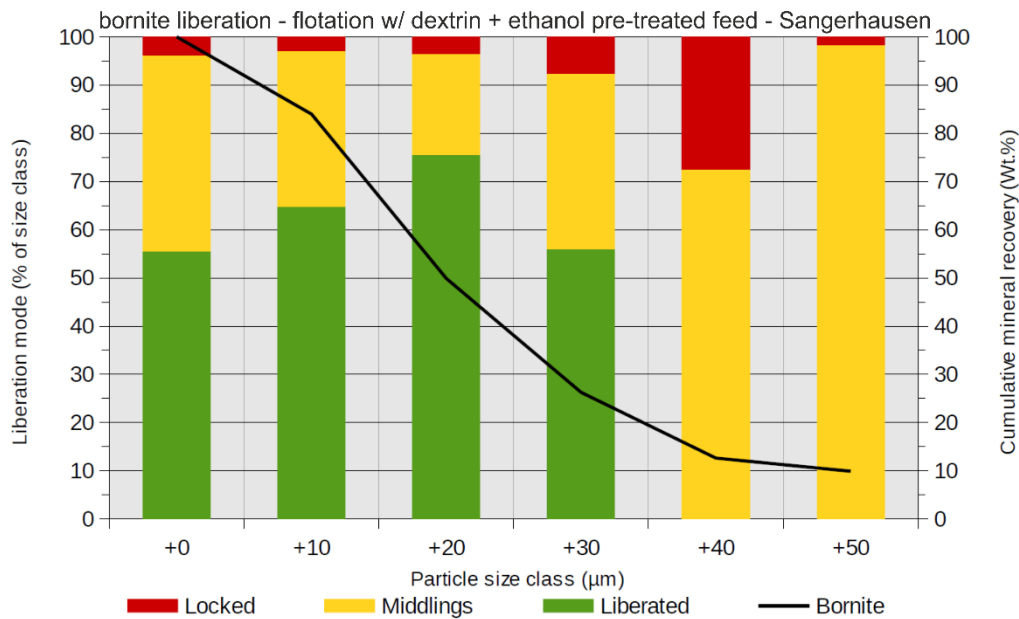


**Figure 3.2.27:** Stacked column diagram representing proportions for liberation modes of bornite in the concentrate gained by flotation using dextrin and ethanol pretreated Sangerhausen black shale feed. Black line graph indicates the theoretical recovery curve for bornite. (Data: Petrolab)

#### Locking and mineral association

Table 3.2.8 shows the proportion of locking modes associated with bornite in the flotation concentrates. Generally, the content of free bornite, completely liberated, was increased compared to bornite in the concentrates from Rudna black shale. However, the flotation product from non-ethanol pre-treated Sangerhausen black shale feed was more enriched with liberated bornite (21.4%) contrary to the product of non-ethanol pre-treated Rudna black shale feed (3.8% free bornite). The flotation product of ethanol pre-treated Sangerhausen feed hosted markedly lower liberated bornite (14.8%) compared to the concentrate from non-ethanol pre-treated feed. The proportion of binary locked bornite was low in both concentrates extracted from Sangerhausen black shale, but slightly increased in the concentrate from ethanol pre-treated feed. Similarly, the content of complex locked bornite was insignificantly increased in the concentrate from pre-treated feed (80.9% vs. 76.1%).

The proportion of minerals associated with bornite in intergrowths was partly similar as Table 3.2.9 shows. Bornite in both concentrates was mainly intergrown with chalcocite and chalcopyrite, whereas locking associations with galena and pyrite were found subordinately. Intergrowths of bornite with gangue minerals were marked dominantly by illite/clays and to minor extent by quartz, carbonate

**Table 3.2.8:** Lock types of bornite in concentrates from Sangerhausen black shale feed. (Data: Petrolab)

Lock type bornite	Flotation with dextrin	Flotation with dextrin + ethanol pre-treatment
Liberated (> 95 % free perimeter)	21.4%	14.6%
Binary locked	2.4%	4.1%
Complex (ternary+) locked	76.1%	80.9%

minerals and feldspars. The latter occurred significantly increased (29.7%) in complex intergrowths of bornite in the concentrate from non-ethanol pre-treated feed, contrary to 14.7% in the concentrate from pre-treated feed. Locking properties of chalcopyrite in flotation concentrates from Sangerhausen black shale ore. Chalcopyrite represented, besides bornite, a main copper sulphide in the concentrates gained from Sangerhausen black shale ore unlike to the concentrates from Rudna black shale, in which it occurred more accessorially. The grain size of chalcopyrite in the feed was comparatively coarse-grained ( $D_{80}=93 \mu\text{m}$ ), so that the concentrates extracted from the feed were also marked by the occurrence of more coarse-grained chalcopyrite ( $D_{80}=55 \mu\text{m}$ ,  $D_{50}=25 \mu\text{m}$ ; see Figure 3.1.15) most likely to chalcocite in the concentrates from Rudna black shale. Generally, the grain size distribution of chalcopyrite in both concentrates extracted from Sangerhausen black shale was nearly equivalent. However, both concentrates showed considerable variance in terms of mass recovery, which was 9.0% for the concentrate from untreated feed and 29.8% for the concentrate from pre-treated black shale ore.

**Table 3.2.9:** Proportions of minerals associated in locking association with bornite in concentrates from Sangerhausen black shale feed. (Data: Petrolab)

<b>Bornite locked with</b>	<b>Flotation with dextrin</b>	<b>Flotation with dextrin + ethanol pre-treatment</b>
<b>chalcocite</b>	62.8%	67.1%
<b>chalcopyrite</b>	57.6%	60.0%
<b>galena</b>	18.8%	11.6%
<b>pyrite</b>	18.4%	12.1%
<b>carbonates</b>	16.5%	14.7%
<b>feldspar</b>	29.7%	14.6%
<b>illite/clays</b>	55.8%	58.2%
<b>quartz</b>	25.5%	36.6%
<b>accessory minerals</b>	12.1%	18.1%

#### 3.2.6.3.4 Chalcopyrite in flotation concentrates from Sangerhausen black shale ore

##### *Chalcopyrite liberation - Flotation with dextrin*

The locking modes of chalcopyrite according to particle size classes in the concentrate from non-ethanol pre-treated Sangerhausen black shale feed is displayed in Figure 3.2.28. The stacked column diagram indicates that the proportion of liberated chalcopyrite increased corresponding with the increase of the particle size up to the +40  $\mu\text{m}$  particle size class. While in the +0  $\mu\text{m}$  particle size class just 34% liberated chalcopyrite occurred, the proportion was significantly higher in the particle size range from 10 to 50  $\mu\text{m}$ , in which liberated chalcopyrite represented the main liberation mode (53-78%).

The most increased portion of chalcopyrite middlings was determined in the +0 particle size class (42%), whereas chalcopyrite middlings in the particle size range 10-40  $\mu\text{m}$  occurred with lower proportions (13-28%). Generally, the concentrate from non-ethanol pre-treated Sangerhausen feed contained significantly increased portions, in comparison to bornite, of locked chalcopyrite, especially in the +50 particle size class that consisted solely of locked chalcopyrite.

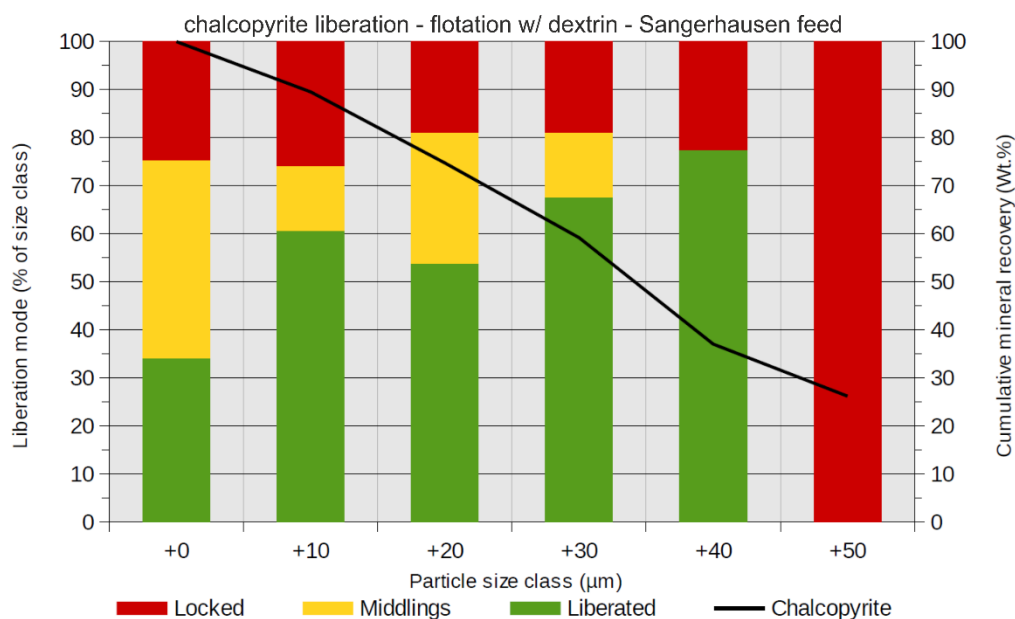


**Figure 3.2.28:** Liberation modes of chalcopyrite in particle size classes of the concentrate extracted by flotation using dextrin from Sangerhausen black shale feed. Black line graph indicates the chalcocite recovery curve. (Data: Petrolab)

The recovery curve for chalcopyrite in the concentrate from non-ethanol pre-treated feed shows that 60% of the total chalcopyrite was contained in the particle size range  $> 30 \mu\text{m}$ , in which 28% were hosted in the +50 particle size class. The remaining proportions of chalcopyrite in the more fine-grained particle size classes ( $< 30 \mu\text{m}$ ) were limited up to 15% in maximum in each class.

#### *Chalcopyrite liberation - Flotation with dextrin and ethanol pre-treated feed*

The distribution of locking modes of chalcopyrite in the concentrate extracted from ethanol pre-treated Sangerhausen feed in Figure 3.2.29 shows similarities to the locking modes of chalcopyrite ascertained in respect to the concentrate from non-ethanol pre-treated feed. It contained likewise increased proportions of locked chalcopyrite, especially in the +50 particle size class that was marked exclusively by locked chalcopyrite. Chalcopyrite middlings occurred up to the particle size range  $< 50 \mu\text{m}$  likewise as liberated chalcopyrite, which was mostly dominating (51-62%), except in the +40 particle size class (36%). A slight increase of chalcopyrite middlings was discernible from the finer to the coarser particle size classes (21-36%). The chalcopyrite recovery curve indicates nearly equally distributed proportions of chalcopyrite with a slight increased portion of the total chalcopyrite in the +50 particle size class (22%).

#### *Locking and mineral association*

Locking types for chalcopyrite are summarized Table 3.2.10. The proportion of liberated chalcopyrite was contrary to the proportion of liberated bornite in concentrates from Sangerhausen black shale. The concentrate extracted from ethanol pre-treated feed contained a significantly increased proportion of completely liberated chalcopyrite (27.9%), whereas the portion in the concentrate from non-ethanol pre-treated feed was 16.3%. Binary locked chalcopyrite occurred quite subordinate and the proportion was generally low. However, complex locked chalcopyrite was more common in the concentrate extracted from non-ethanol pre-treated feed (81.9%) compared to the concentrate gained from pre-treated feed (69.5%).

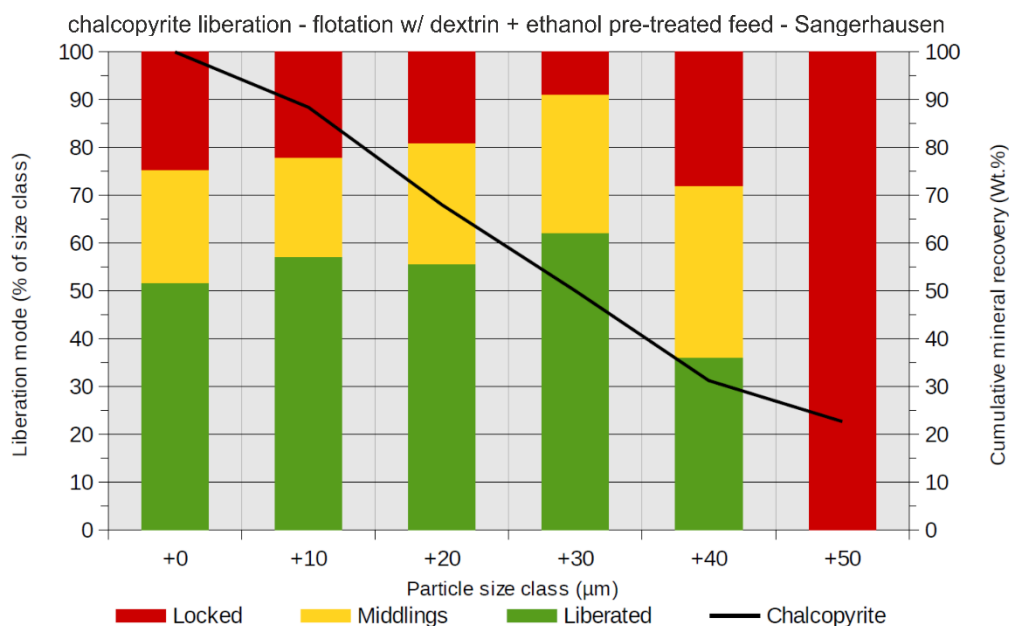


**Figure 3.2.29:** Stacked column plot showing liberation modes of chalcopyrite in particle size classes of the concentrate generated by flotation using dextrin and ethanol pre-treated Sangerhausen black shale feed. Black line graph shows the recovery curve of chalcopyrite (Data: Petrolab)

Table 3.2.11 shows that the mineral associations of predominantly complexly locked chalcopyrite were dominated by illite/clays with similar proportions as for bornite. The proportions of other sulphides interlocked with chalcopyrite were significantly lower, also in comparison to sulphide associations locked with bornite.

**Table 3.2.10:** Lock types of chalcopyrite in flotation concentrates from Sangerhausen black shale feed. (Data: Petrolab)

Lock type chalcopyrite	Flotation with dextrin	Flotation with dextrin + ethanol pre-treatment
<b>Liberated (&gt; 95 % free perimeter)</b>	16.3%	27.9%
<b>Binary locked</b>	1.8%	2.5%
<b>Complex (ternary+) locked</b>	81.9%	69.5%

Mineral associations of locked chalcopyrite in the concentrate extracted from non-ethanol pre-treated feed were commonly marked by higher proportions compared to the intergrowth associations of chalcopyrite in the concentrate extracted from ethanol pre-treated feed. Exceptions were determined for galena and feldspars, both increased associated in intergrowths with chalcopyrite in the concentrate from pre-treated feed. Besides illite/clays, chalcopyrite was considerably intergrown with quartz, but generally to a lower extent with carbonate minerals and feldspars.

**Table 3.2.11:** Mineral association of locked chalcopyrite in flotation concentrates extracted from Sangerhausen black shale feed. (Data: Petrolab)

<b>Chalcopyrite locked with</b>	<b>Flotation with dextrin</b>	<b>Flotation with dextrin + ethanol pre-treatment</b>
<b>bornite</b>	41.6%	34.8%
<b>chalcocite</b>	23.2%	7.5%
<b>galena</b>	19.2%	32.0%
<b>pyrite</b>	55.4%	46.3%
<b>carbonates</b>	32.1%	28.2%
<b>feldspar</b>	20.4%	26.9%
<b>illite/clays</b>	66.5%	55.9%
<b>quartz</b>	50.5%	47.8%
<b>accessory minerals</b>	24.0%	25.6%

### 3.2.7 Copper deportment in concentrates and tailings from black shale feed

According to the distribution of copper-bearing phases, the proportion of Cu associated with a specific mineral phase can be calculated. Due to sulphides were almost exclusively copper carrier and bornite, chalcocite and chalcopyrite represented main copper sulphide minerals in concentrates and tailings generated from black shale ore, the copper deportment is shared by these three sulphides.

Figure 3.2.30 shows the proportion of copper-bearing sulphides regarding the copper deportment for concentrates and tailings generated from Rudna black shale feed. The main copper carrier in flotation concentrates was chalcocite, which contained up to two third of total Cu. In particular concentrates gained by addition of dextrin showed identical proportions of copper deportment. While chalcocite was clearly dominating (66%), bornite contained virtually a third of the total Cu, whereas the Cu amount associated with chalcopyrite was negligible (2-3%). Only the concentrate extracted by standard flotation was characterized by a slightly different copper deportment ratio, in which also chalcocite (58%) was the prevalent copper carrier and the proportion of bornite (40%) was slightly increased compared to the concentrates extracted by dextrin-added flotation.

Tailings from the flotation of Rudna black shale ore showed a more varying distribution of the copper deportment. As shown in Figure 3.2.30, bornite (79%) was the dominant copper sulphide regarding the total Cu content in tailings from the standard flotation and Cu was subordinately associated with chalcocite (17%) and chalcopyrite (5%). A significantly increased proportion of chalcocite (58%) was determined in tailings of the flotation using dextrin, in which bornite was the second most copper carrier containing 40% of the total Cu. Bornite was again the dominant copper carrier in tailings from flotation using dextrin and ethanol pre-treated feed and contained 54% of the total Cu, whereas a further significant portion of Cu was associated with chalcocite (43%). Chalcopyrite, likewise to the concentrates, was generally insignificant regarding the copper deportment in tailings from flotation tests with Rudna black shale feed.

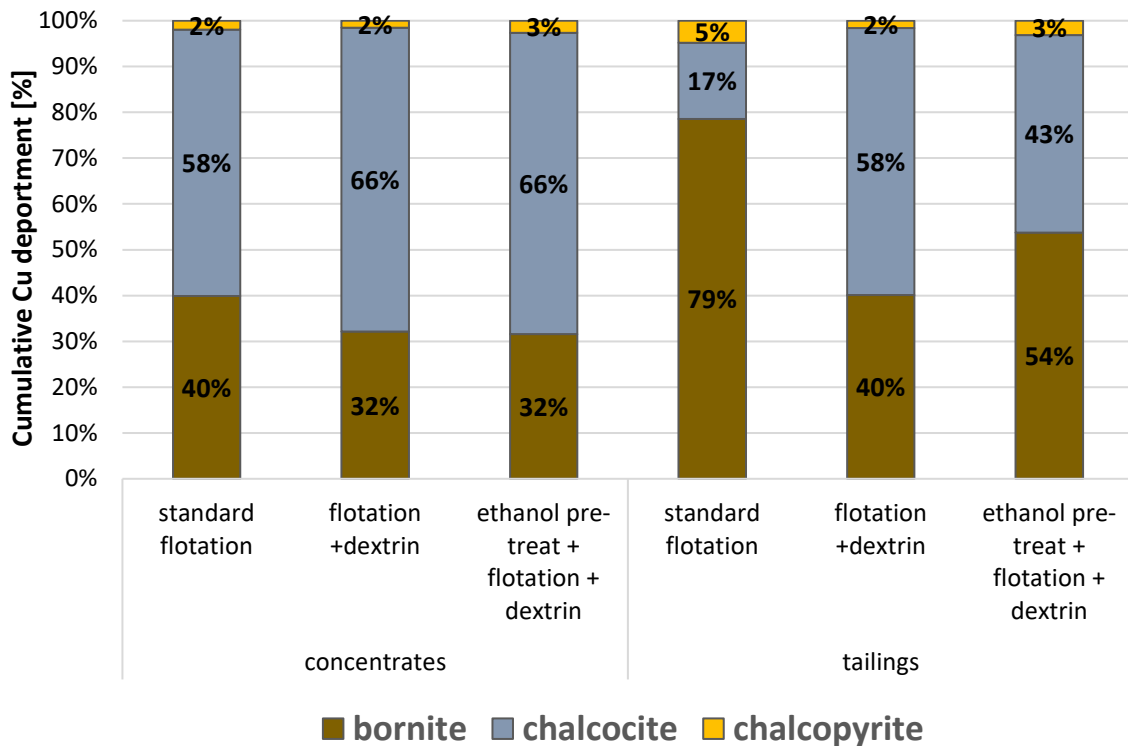


**Figure 3.2.30:** Stacked column plot indicating the department of Cu in concentrates and tailings from different flotation tests carried out with Rudna black shale feed. (Data: MLU)

Figure 3.2.31 shows that bornite was exclusively the main copper carrier in concentrates and tailings produced from Sangerhausen black shale feed. The most increased Cu department in bornite was determined in the concentrate of the standard flotation (87%) and the remaining Cu amount was clearly associated with chalcopyrite (12%) as well as insignificantly with chalcocite (2%). The proportion of Cu related to chalcopyrite and to a lower extent to chalcocite was increasing in the concentrates extracted by flotation using dextrin so that chalcopyrite contained 16 % of total Cu in the concentrate produced by dextrin-added flotation, but the proportion of chalcocite was low (3%). The proportion of Cu department increased for the latter to 7% and also for chalcopyrite (20%) in the concentrate from the flotation using dextrin and ethanol pre-treated feed.

A very similar ratio of the Cu department as determined in concentrate from the flotation using dextrin and ethanol pre-treated feed shows Figure 3.2.31 for the related tailings, in which 73% of total copper was associated with bornite, 4% with chalcocite and 22% with chalcopyrite. While the Cu department in the tailings of the standard flotation was shared by dominating bornite (62%) and chalcopyrite (38%), the proportion of copper associated with chalcocite (13%) was most increased in the tailings of the dextrin-added flotation, in which also bornite (69%) hosted the main part of copper and the proportion of chalcopyrite (17%) contained a subordinate amount of the total Cu.

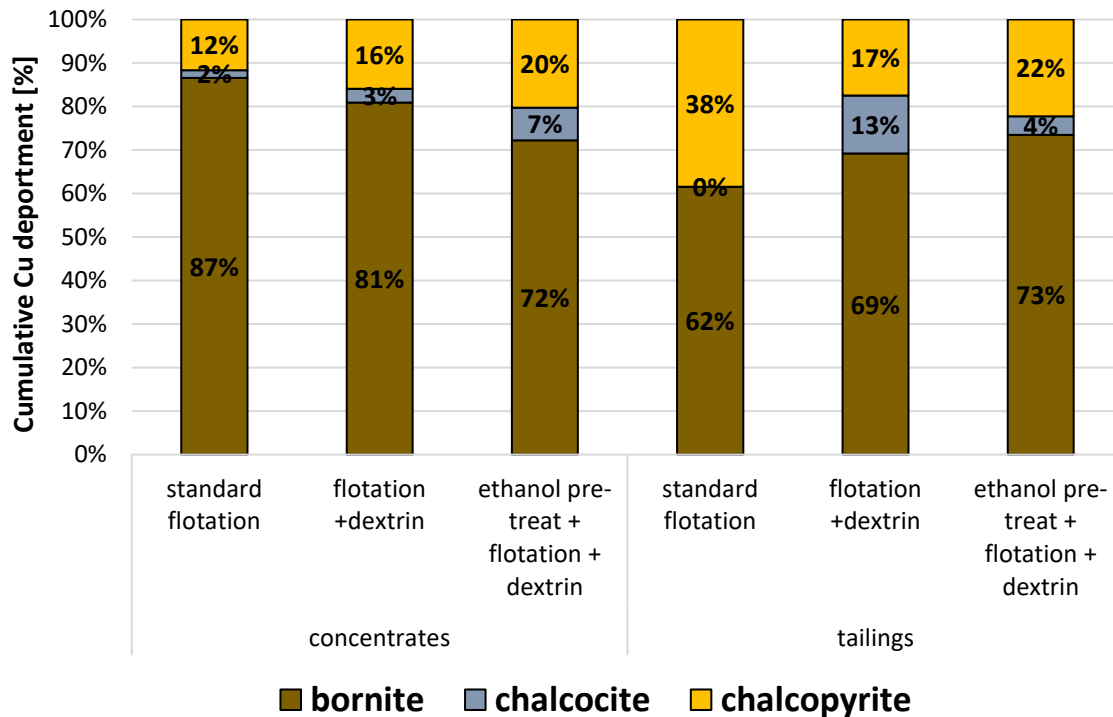


**Figure 3.2.31:** Stacked column plot indicating the department of Cu in the main three copper-bearing sulphides in concentrates and tailings from different flotation tests carried out with Sangerhausen black shale feed. (Data: MLU)

### 3.2.8 Mineralogy and metal content of copper concentrates from Lubin, Poland

Three different copper concentrates from the KGHM processing facilities in Lubin were used for feed materials of bioleaching tests, which residues were investigated in this study (see Chapter 2.1). The copper concentrate LCA06 represented a material extensively used for experiments in the frame of the “Bioshale” European project in collaboration with CUPRUM (Poland), whereas two other concentrate samples, LC15a and LC15b, originated from a bulk sample provided by KGHM for the French-German project “Ecometals” in 2015. This bulk sample (sample size: 3.8 t) was split and delivered to BRGM (LC15a) and UVR-FIA (LC15b), the latter representing a significantly smaller subsamples of the bulk sample (10 kg).

#### 3.2.8.1 Mineral distribution of Lubin concentrates

Copper concentrates from the Lubin processing plant represent flotation products extracted from several feed lines designated to the different ore-bearing host rock types of the deposit. Thus, concentrates were gained from a blended feed consisting of sandstone, black shale and dolomite, which affected the general composition of flotation products.

The proportion of sulphides and gangue minerals of the examined Lubin concentrates was generally in the same range, as Figure 3.2.32 shows. However, LCA06 contained the lowest portion of sulphides (33.9%), whereas the sulphide content in both LC15 concentrates was increased (LC15a: 42.1%; LC15b: 36.9%). Detailed results of mineral distribution analyses carried out on Lubin copper concentrates in the frame of this study are displayed in Figure 3.2.33.

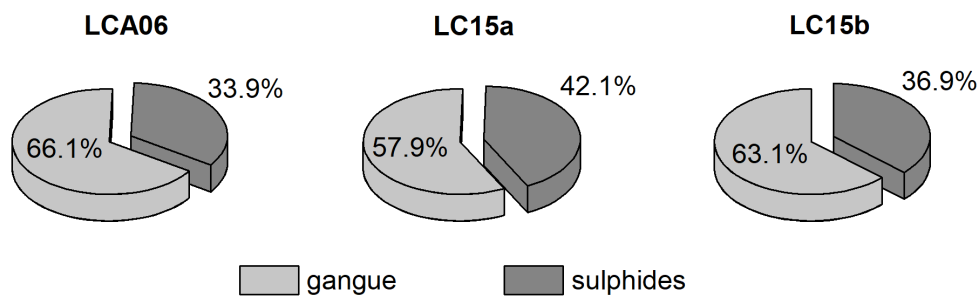


**Figure 3.2.32:** Proportions of sulphides and gangue minerals in concentrates produced by the Lubin concentrator, Poland. (Data: MLU)

Prefaced must be mentioned that the concentrate sample LCA06 was acidified with sulfuric acid in order to remove the carbonate fraction prior to feed the concentrate to bioleaching experiments. Thus, this concentrate contained a marginally remaining content of carbonate minerals (0.7% dolomite; 0.3% calcite), which was considerably lower compared to the concentrate LC15.

The sulphide assemblage of LCA06 was dominated by mainly three copper-bearing sulphides (bornite: 8.0%, chalcopyrite: 3.1%, chalcocite: 5.9%) and pyrite (7.2%). Additional sulphides with lower proportions were covellite (1.5%), galena (2.2%) and idaite (1.3%), whereas sphalerite, cobaltite and tennantite occurred in traces.

The predominating gangue mineral in the concentrate LCA06 was illite (28.5%). Far lower proportions were detected for quartz (10.2%) and feldspar (6.7%). A remarkable content of sulphates (6.5%) was observed as main part of the accessory mineral phases and their occurrence can be regarded as alteration products caused by the acid treatment of the initial concentrate. These secondary formed compounds comprised mainly Cu-Fe-Zn-containing sulphates, but also Pb-sulphate (anglesite) and Ca-sulphate (gypsum), respectively. In comparison to LCA 06, the proportion of sulphides was slightly increased in the concentrate LC15. While the main copper sulphides in LCA06 occurred in a comparable concentration range, the concentrate LC15 was significantly enriched in chalcopyrite (LC15a: 15.6%, LC15b: 15.3%) and contained lower proportions of chalcocite (LC15a: 3.3%, LC15b: 3.2%). The content of bornite (LC15a: 7.5%, LC15b: 5.2%) was varying and partly similar to LCA06. Besides copper sulphides, the concentrate LC15 was also increased regarding the content of pyrite (LC15a: 9.2%, LC15b: 7.6%) and was generally marked by subordinate proportions of galena (LC15a: 2.3%, LC15b: 1.7%) and sphalerite (LC15a: 1.6%, LC15b: 1.8%). Other sulphides occurred accessorially ( $\leq 1\%$ ) and comprised cobaltite, covellite, idaite and tennantite.

The association of gangue minerals was dominated by dolomite, illite and quartz, whereas feldspars and calcite represented minor mineral phases in both sample splits of concentrate LC15. Metal and Ca-bearing sulphate and Pb-oxide compounds (LC15a: 4.2%, LC15b: 4.0%) were predominant within the fraction of accessory minerals, in which lead oxides, more cerussite, showed increased proportions compared to LCA06. Their formation can be considered to be a product of sulphide oxidation caused by long-termed storage at wet condition of the concentrate (10 wt.% water content) prior shipping.

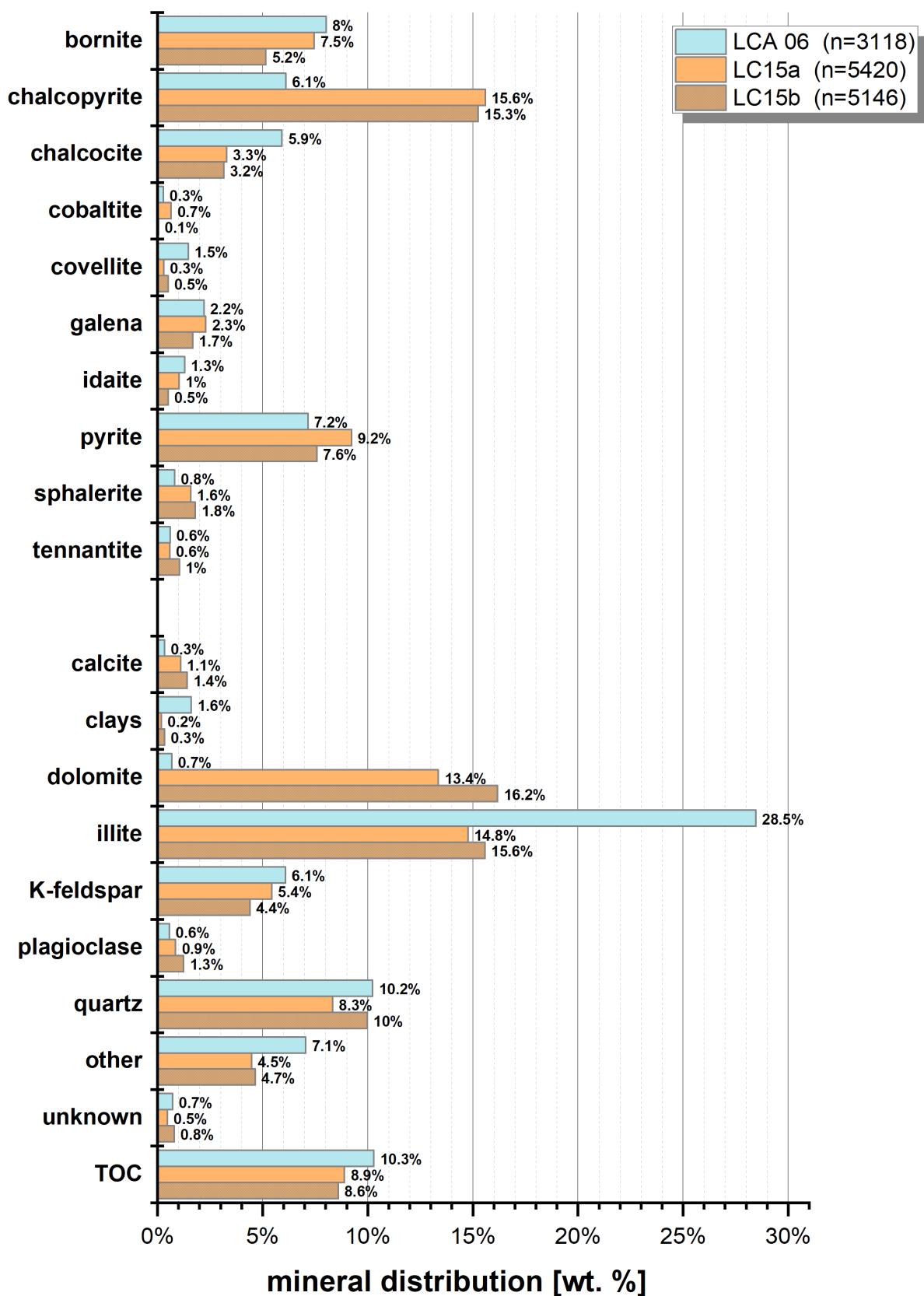


Figure 3.2.33: Mineral distribution showing the proportions of particular sulphide (upper part) and gangue minerals as well as total organic matter content (TOC) in Lubin concentrates LCA06, LC15a, LC15b. (Data: MLU)

### 3.2.8.2 Metal content in Lubin copper concentrates

The concentrates LCA06 and LC15 were produced at different times in the Lubin concentrator facilities (see Chapter 2.1). Table 3.2.12 lists contents of base metals and selected trace metals for Lubin concentrates LC06, LC15a and LC15b and shows that the Cu content among the concentrates was similar, but slightly enriched in LCA 06 that contained 14.7% in comparison to LC 15 (LC 15a: 14.4%, LC 15b: 13.7%). Other base metals were more enriched in LC15, which was marked by moderately increased content of Pb (avg. 4.55% vs. 2.86% in LCA06) and Zn (avg. 1.23% vs. 0.44% in LCA06). The most varying contents among the main metals were determined for Fe, which was a third lower in LCA06 (6.47%) than analysed for LC15 (avg. 9.83%), mainly attributed to the significant lower amount of chalcopyrite in LCA06.

Trace metals were commonly increased in concentrate LC15, except Ag, which was perceptible enriched in LCA06 (782 ppm). Contents of As and Co were in particular increased in both splits of the LC15 in comparison to LCA06 and all other concentrates investigated in this study. As and Co are mainly linked to the occurrence of cobaltite and pyrite, whereas trace amounts of Cd, slightly increased in LC15, are clearly related to sphalerite. Contrary to the increased amount of Ag, As, Co and Ni, the concentrations of Sb and Mo in LCA06 and LC15 was comparably low and similar as to that detected in concentrates extracted from the Rudna ball mill product (see Chapter 3.2.4.3).

**Table 3.2.12:** Base metal concentrations and content of selected trace metals in different copper flotation concentrates from the Lubin processing plant, Poland. (Data: ALS)

Element	Unit	Lubin concentrate		
		LCA 06	LC 15a	LC 15b
<b>Cu</b>	%	14.70	14.35	13.65
<b>Pb</b>	%	2.86	4.59	4.51
<b>Zn</b>	%	0.44	1.255	1.210
<b>Fe</b>	%	6.47	9.92	9.76
<b>Ag</b>	ppm	782	707	636
<b>As</b>	ppm	2596	4340	4230
<b>Cd</b>	ppm	34	68.6	63.8
<b>Co</b>	ppm	1059	1480	1480
<b>Mo</b>	ppm	279	375	361
<b>Ni</b>	ppm	455	610	606
<b>Sb</b>	ppm	87	116	112
<b>V</b>	ppm	550	792	766

### 3.2.9 Summary

Flotation tests with ball mill products of Rudna and Sangerhausen black shale resulted in concentrates with different copper and mass recovery as well as copper content.

#### *Cu content and recovery*

Low copper contents in concentrates were achieved by standard sulphide flotation. The concentrate gained by standard flotation from Rudna black shale was marked by 5.5% Cu, 75.1% Cu recovery and 52.9% mass recovery. Increasing copper contents were obtained by flotation using dextrin, which produced a concentrate with 11.4% Cu, but low copper recovery (29.2%) and extremely low mass recovery (9.0%). The concentrate produced by dextrin-added flotation with ethanol pre-treated feed was marked by an improve copper (72.1%) and mass (26.7%) recovery and contained 10.0% Cu.

The concentrate produced by standard flotation of Sangerhausen black shale showed a considerably low copper content of 3.9% with 67.8% Cu recovery and 45.1% mass recovery. In the concentrate gained from dextrin-added flotation, copper recovery was low (26.2%) at the lowest mass recovery (5.7%). The most increased copper content was achieved by flotation using dextrin and ethanol pre-treated Sangerhausen black shale feed, which yielded in 14.4% Cu with 74.8% copper and 29.8% mass recovery.

#### *Grain size distribution*

The concentrate from the flotation test using dextrin and Rudna black shale feed was more fine-grained compared to the corresponding tailings. Concentrates gained by standard flotation and dextrin-added flotation using ethanol pre-treated feed were significantly coarser-grained than their tailings. Flotation tests with Sangerhausen black shale feed result in a more fine-grained concentrate produced by dextrin-added flotation with ethanol pre-treated feed in comparison with tailings. Similar to slightly more coarse-grained compared to the tailings were the concentrates extracted by standard flotation and dextrin-added flotation of Sangerhausen black shale.

#### *Mineral distribution*

The mineral distribution of concentrates gained from Rudna black shale revealed that the sulphide portion was generally dominated by chalcocite, bornite and galena. Most increased proportions were achieved by the flotation test using dextrin and ethanol pre-treated feed (bornite: 6.7%, chalcocite: 11.0%, galena: 8.5%), which also contained the lowest proportion of gangue minerals, in particular for illite and quartz. Tailings from the flotation of Rudna black shale contained moderate to increased contents of bornite (1.4-1.9%), chalcocite (0.3-1.6%) and galena (0.9-4.5%) and were generally enriched in carbonates and quartz.

Flotation of Sangerhausen black shale yielded likewise in most increased sulphide content by the usage of dextrin and ethanol pre-treated feed. The concentrate was rich in bornite (20.8%), chalcopyrite (10.5%) and galena (8.6%) as well as moderately enriched in sphalerite (3.2%). Gangue-type minerals in concentrates generated from Sangerhausen black shale feed were dominated by illite and quartz. Tailings contained significant amounts of pyrite (up to 8.1%), bornite (1.6-3.3%) and chalcopyrite (1.2-1.8%) as well as partly substantially increased content of illite and quartz.

### *Liberation*

The content of liberated sulphides in concentrates and also in tailings was low and generally below 20%. Only concentrates gained from Sangerhausen black shale showed party considerable proportions of liberated chalcopyrite above 20%. Middlings (30-80% free surface) were common for bornite in both Sangerhausen and Rudna concentrates (33-74%) and tailings (15-80%), whereas the proportion of chalcocite middlings were partly increased in the Rudna flotation concentrates (31-73%) and tailings (3-71%). Chalcocite middlings occurred mainly in concentrates from Sangerhausen black shale (16-61%), but the corresponding tailings contained significantly lower proportions (14-33%) similar to the chalcopyrite middlings in concentrates (16-20%) and tailings (10-23%) from Rudna black shale.

The grain size of copper sulphides in concentrates was partially very different. While bornite was in a similar grain size range in concentrate of both, Sangerhausen (25-46  $\mu\text{m}$ ) and Rudna (20-33  $\mu\text{m}$ ) black shale, the grain size distribution for chalcocite and chalcopyrite was strongly divergent. Chalcocite was decisively coarser-grained in concentrates of Rudna black shale feed (43-66  $\mu\text{m}$ ) compared to concentrates from Sangerhausen feed (5-15  $\mu\text{m}$ ). Contrarily, chalcopyrite in the latter was far more coarse-grained (55-93  $\mu\text{m}$ ) compared to concentrates extracted from Rudna black shale (8-31  $\mu\text{m}$ ).

#### *a) Rudna*

Chalcocite and bornite were the main copper sulphides in concentrates from the Rudna ball mill product. Liberated chalcocite occurred generally in the particle size class – 50  $\mu\text{m}$ , where it was mainly liberated or occurred as middlings. The proportion of liberated chalcocite was increased in the concentrate produced by dextrin-added flotation. Chalcocite was almost exclusively ternary+ locked in concentrates from Rudna black shale and was associated mainly with bornite, illite, carbonates and quartz, especially in the concentrate generated by flotation with dextrin and ethanol pre-treated feed.

Liberated bornite was more present in the concentrate from dextrin-added flotation, whereas notable amounts (20% of total bornite) of locked bornite were hosted in the +40 particle size range of the concentrate produced by flotation with dextrin and ethanol pre-treated Rudna feed. Bornite was mainly complexly locked, 93% in the concentrate of dextrin-added flotation, in which bornite was considerably associated with chalcocite, illite and carbonates. 80% represented ternary+ locked bornite in the concentrate from ethanol pre-treated feed mainly intergrown with chalcocite, illite and chalcopyrite.

#### *b) Sangerhausen*

Bornite in concentrates from Sangerhausen black shale feed occurred liberated in particular in the particle size range -30  $\mu\text{m}$ , although the concentrate extracted by flotation using dextrin and ethanol pre-treated feed contained more bornite middlings, especially in the particle size range +40  $\mu\text{m}$ . The liberation of bornite in concentrates from Sangerhausen ore was generally increased, but binary locked bornite was generally low, whereas similar amounts (approx. 80%) of ternary+ locked bornite occurred in both concentrates gained by flotation with dextrin. Bornite was mainly locked with chalcocite, chalcopyrite and illite.

Liberated chalcopyrite and chalcopyrite middlings were exclusively determined in the particle size range -50  $\mu\text{m}$ , which contained 65-70% of total chalcopyrite mainly liberated, although the proportion of chalcopyrite middlings in the concentrate extracted by flotation with dextrin and ethanol pre-treated Sangerhausen feed was generally increased. Also chalcopyrite occurred mostly ternary+ locked in both concentrates and was chiefly associated with illite, quartz and pyrite.

### *Copper deportment*

According to mineral distribution data, the copper deportment of total copper in concentrates from Rudna black shale was mainly contained in chalcocite and moderate amounts of bornite, whereas in tailings the copper distribution was changing from bornite- to chalcocite-associated. Copper deportment in concentrates and tailings from the flotation of Sangerhausen black shale can be clearly attributed to bornite, which was by far the main copper-bearing mineral.

### *Lubin concentrates*

Mineral distribution analyses of Lubin concentrates have shown that LCA06 contained similar amounts of bornite (8.0%), chalcopyrite (6.1%) and chalcocite (5.9%) at 14.7% Cu. Due to an acid pre-treatment the concentrate contained largely illite in the gangue mineral fraction. Lubin concentrate LC15 was generally enriched in chalcopyrite (15.4%), but the content of chalcocite lower (3.3%) and bornite was different in two sample splits (5.2% and 7.5%), which is also indicated by slightly deviating copper content (13.7% and 14.4%).

### *Key features of concentrates and tailings:*

- Most increased copper content with increased copper recovery for concentrates extracted by flotation using dextrin and ethanol pre-treated feed.
- Concentrates extracted by flotation using dextrin and ethanol pre-treated were significantly enriched in sulphides,
- Rudna feed: chalcocite (11.0%), bornite (6.7%) and galena (8.5%),
- Sangerhausen feed: bornite (20.8%), chalcopyrite (10.5%) and galena (8.6%).
- The content of liberated sulphides in concentrates and tailings was low and generally below 20%.
- Partially strong deviating grain size of copper sulphide in concentrates, especially for chalcocite (Sangerhausen: fine, Rudna: coarse) and chalcopyrite (Sangerhausen: coarse, Rudna: fine).
- Proportion of liberated copper sulphides and middlings was generally increased in concentrates extracted by flotation using dextrin and ethanol pre-treated feed.
- Intergrown copper sulphides were mainly complexly (ternary+) locked predominantly among themselves as well as illite, carbonates and quartz.
- Lubin concentrate LCA06 was marked by similar amounts of bornite (8.0%), chalcopyrite (6.1%) and chalcocite (5.9%) at 14.7% Cu.
- Lubin concentrate LC15 was rich in chalcopyrite (15.4%) but lower in chalcocite (3.3%) and bornite (avg. 6.3%).

## 3.3 Mineralogy and geochemistry of bioleaching residues

### 3.3.1 Introduction

Bioleaching test series were mainly carried out in the frame of the joint research project “Ecometals” by the Geomicrobiology department of at the Federal Institute for Geosciences and Natural Resources (BGR) in Hanover (see chapter 2.2.3). Additional bioleaching residue samples originated from the Department “Direction Eau, Environnement, et Ecotechnologies of the French Bureau Recherche de Géologique et Minières” (BRGM, France). The bioleaching experiments on milled black shale ores and copper flotation concentrates were conducted using a consortium of acidophilic, autotrophic mineral-oxidizing bacteria (for details see Chapter 2.2.3). Bioleaching test series comprised several experimental stages, in which the bacteria community was adapted to refined adjusted leaching parameters stepwise in order to increase and optimize the leaching efficiency in respect to copper and associated metals. Investigations of the mineral distribution in bioleaching residues in this study considered exclusively residues from the last experimental step with the most adapted leaching set up. Feed materials for bioleaching tests were milled black shale ores from central German “Kupferschiefer”-deposits, flotation concentrates extracted from two different black shales (Rudna, Sangerhausen) as well as copper flotation concentrates produced by KGHM Miedz Polska in the processing facilities in Lubin, Poland. Mineralogical and geochemical analyses were mainly undertaken on bioleaching residues, but also in comparison on residues of sterile control leaching conducted under equal test conditions.

### 3.3.2 General mineralogical composition of bioleaching residues from black shale ores and related flotation concentrates

Bioleaching residues consisted of a fine-grained mineral mixture that contained on the one hand initial mineral components remaining from the feed material and on the other hand mineral phases formed as a product of the bioleaching process. The latter can be mainly considered as precipitation products crystallized from the leaching solution either during the progressively active leaching process or during the fade out of the experiment depending on the supply of ion species in the solution and mineral stability condition. Due to the interaction of mineral particles of the feed and the inoculated leaching solution, primary mineral phases were solved partly or completely during their retention time. Only few minerals showed little to no indications of alteration by the acidic treatment and can be thus regarded as inert mineral phases that had not experienced interaction within the bioleaching process.

Main mineral phases present in bioleaching residues were chiefly initial gangue minerals of the feed. Thus, quartz, feldspars and clay minerals constituted commonly over 60% of the residues. Mineral particles of this mineral groups showed very slight traces of alteration by the acidic conditions during bioleaching. One particular feature that was recognized is a surface roughening of particles, which can be regarded as very weak dissolving texture (see Chapter 3.3.3). Gangue mineral groups found in bioleaching residues were feldspars comprising several members: albite, anorthite, potassium feldspar and plagioclases. Clay minerals or sheet silicates were predominantly represented by illite, seldom as iron-rich variety Fe-illite, and accessorially by biotite, kaolinite and muscovite.

Carbonate minerals of the feed materials, mainly dolomite and subordinately calcite, were commonly dissolved almost completely or to a large extend, because of the acidic leaching conditions using sulfuric acid. If carbonate particles remained in the residue, a coating of calcium sulphate was

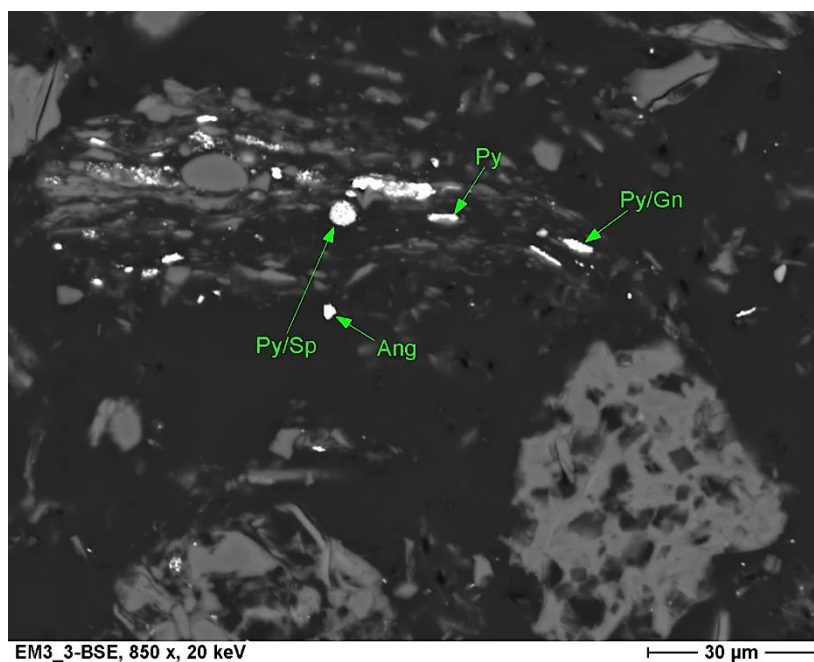


**Figure 3.3.1:** SEM-image of highly altered silicate particles in the lower part exhibiting dissolution features such as embayment and boxwork-like textures of dissolved mineral phases (carbonates and sulphides). The large elongated particle in the upper part consisted substantially of organic matter-clay intergrowths that hindered the dissolution of enclosed soluble mineral grains such as pyrite (Py) and sphalerite (Sp). (bioleaching residue of Mansfeld black shale, SEM-BSE)

notable that obviously hindered the complete dissolution. Dissolution textures on remaining silicate particles were quite common, whereas particles consisting of organic matter-clay intercalation seem to preserve the enclosed mineral association from dissolution (Figure 3.3.1). Additionally, bioleaching residues related to Sangerhausen black shale ore contained some wt.% of barite that was completely absent in the residues of Rudna black shale-derived feed materials. Other minerals contained in traces were rutile and zircon.

A further group of minerals with subordinate abundance that represented initial constituents of the feed material were sulphides. Generally, the proportions of sulphides in the feed were considerable minimized in residues of bioleaching. However, some of them, readily leachable sulphides as chalcocite or bornite, were mostly complete dissolved, occasionally remained traces in the residues. Other sulphides as pyrite, galena, sphalerite or chalcopyrite displayed remnants that occurred regularly, the latter partly pervading replaced by covellite (Figure 3.3.2).

Secondary, process-related formed mineral phases were constituents of the bioleaching residues and occurred besides the minerals of the initial mineral assemblage. These secondary, leaching-induced mineral formations comprised mainly sulphates that represent mineral precipitations from the leaching solution. In particular gypsum and fine precipitates of lead sulphate with anglesite composition were detected commonly and obtained amounts of up to several wt.% in some bioleaching residues. They often enclose, envelope or overgrow other mineral phases. Subordinate it also occurred iron sulphates, partly with jarosite composition, and iron oxihydroxides, rather rare zinc (hydroxi)-carbonates or lead carbonates. Additionally, secondary formed covellite, especially as coating on galena grains, was observed sporadically (Figure 3.3.3).



**Figure 3.3.2:** Large particle showing small remnants of chalcopyrite (bright yellow) almost completely replaced by covellite (bluish to deep purple). A further smaller chalcopyrite particle (below left) shows nearly no indication of alteration. (bioleaching residue of LCA06, reflected light)

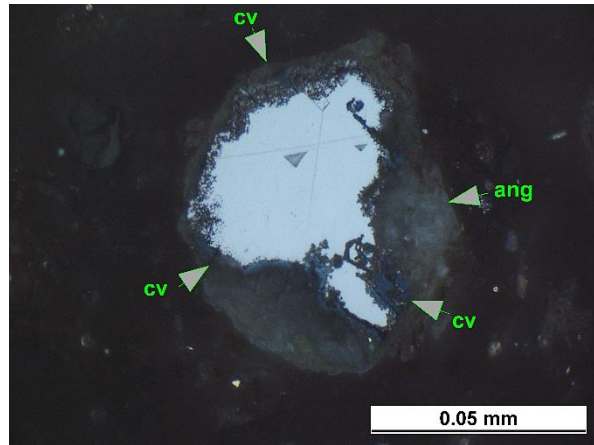


**Figure 3.3.3:** Galena showing dissolution features at the grain edge and thin coatings of covellite that is overgrown by anglesite. (bioleaching residue of LCA06, reflected light)

Chemical control leaching residues comprised generally the same mineral association described above, but contained higher proportions of sulfide minerals and partly sulphates.

### 3.3.3 Particle properties in (bio)-leaching residues

Bioleaching residues represent fine-grained mineral mixtures, in which diverse particle shapes of either initial feed-related minerals or secondary, during the bioleaching process, formed mineral phases occur. Feed minerals were often marked by dissolution features, whereas process-related mineral precipitation showed idiomorphic crystal habitus up to amorphous aggregates. Both, formation of new mineral phases and dissolution of initial sulphide but also gangue mineral particles affected the grain size distribution of bioleaching residues in respect to the feed material.

Figure 3.3.4 shows the comparison of the grain size distribution for copper concentrate feeds extracted from Rudna as well as Sangerhausen black shale ore and their respective bioleaching residues. Grain size distribution curves show that the Sangerhausen concentrate was decisively more fine-grained in comparison to the Rudna concentrate, whereas the grain size distribution of both bioleaching residues was less deviating. However, bioleaching residues from Rudna concentrate were markedly more fine-grained than the feed, although in turn bioleaching residues of the Sangerhausen concentrate were more coarse-grained than the feed. This opposing trend was apparently coupled with the content of soluble mineral species in the feed material. Minerals decisively dissolved by bioleaching using strong acidic leaching solution comprise carbonates and sulphides. Due to the increased content of carbonate minerals (27.8%) and their occurrence over the entire grain size spectrum, a significant proportion, besides sulphides, represented the soluble mineral fraction in the Rudna concentrate. Thus, the dissolution of mainly carbonates led to the general decrease of the grain size in bioleaching residues. The opposite effect was caused by the bioleaching of the Sangerhausen concentrate, in which large amounts of sulphides were dissolved. The common grain size range of sulphides in the Sangerhausen concentrate was < 50 μm and the carbonate content in the Sangerhausen concentrate was comparatively low (6.3%). Thus, the predominantly leaching of fine-

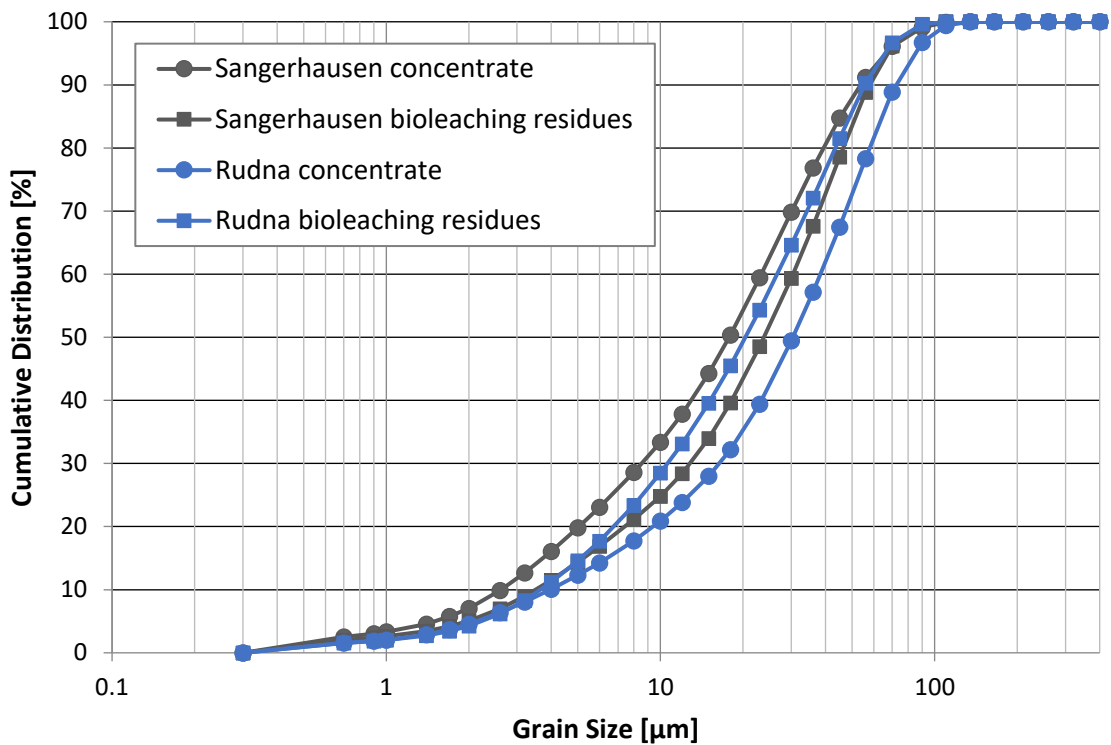


**Figure 3.3.4:** Grain size distribution curves for Sangerhausen and Rudna concentrate and related bioleaching residues. (Data: MLU)

grained sulphides resulted in a coarsening of the grain size distribution of remaining mineral grains in bioleaching residues from the Sangerhausen concentrate.

The most widespread and economic important feature of bioleaching residues represented mainly undissolved chalcopyrite as well as more subordinate idaite particles often showing a pattern-like disintegration texture, in which dissolved domains were visible as intraparticle transects. Obviously, idaite particles showed a higher level of decomposition compared to chalcopyrite remnants and decomposition patterns seemed to follow crystallographic preferred axes. Remaining chalcopyrite was partly intergrown with other minerals, mainly with gangue phases such as illite (Figure 3.3.5). Strong dissolution textures on chalcopyrite particles were observed often, but otherwise bioleaching and sterile control leaching residues also contained throughout commonly chalcopyrite that showed little to no indications of dissolution.

Traces of bacterial attachment were hard to find, but isolated corrosion pits on chalcopyrite were detected as shown in Figure 3.3.6. Chalcopyrite particles found in the bioleaching residue showed both, smooth unaltered and highly corroded surfaces that showed pits and holes of few micrometres diameter and represented highly roughened particle surfaces (Figure 3.3.7). Partially disintegrated chalcopyrite particles were incidental marked by sponge-like replacement textures of copper sulphate and iron hydroxides forming coatings onto chalcopyrite grains (Figure 3.3.8) or occupying interstices and internal cracks created by dissolution of initial minerals. Additionally, chalcopyrite grains completely encapsulated by sulphur or lead sulphate were occurred widespread as well as also galena coated by anglesite. Jarosite-like precipitates were often associated with anglesite enveloping chalcopyrite and other residual sulfide grains. Remaining portions of accessory sulfides such as

tennantite ( $\text{Cu}_6[\text{Cu}_4(\text{Fe,Zn})_2]\text{As}_4\text{S}_{13}$ ) showed irregular distributed pits but also layer-like delamination on the particle surface. Bioleaching as well as sterile control leaching residues contained generally low portions of jarosite, but secondary formed gypsum was abundant. The latter was crystallized as laths that often overgrew minute anglesite particles apparently providing growth nuclei. Other remaining sulfides such as chalcocite or sphalerite also exhibited strong indications of dissolution by holes and cellular-pitted surface structures.

As Figure 3.3.9 depicts, bioleaching residues contained large (up to 100  $\mu\text{m}$  in length), irregular formed chalcopyrite particles partially less affected by acid attack and microbial activity. Intergrown particles of chalcopyrite and galena showed apparently that galena had suffered by leaching resulting in a several micrometre-thick anglesite rim that often envelopes galena grains. Lead sulfate precipitation took also place onto minute particles ( $< 5 \mu\text{m}$ ) that offer suitable growth nuclei for the accretion of lead sulfate as indicated by the anglesite formation around tiny barite cores in Figure

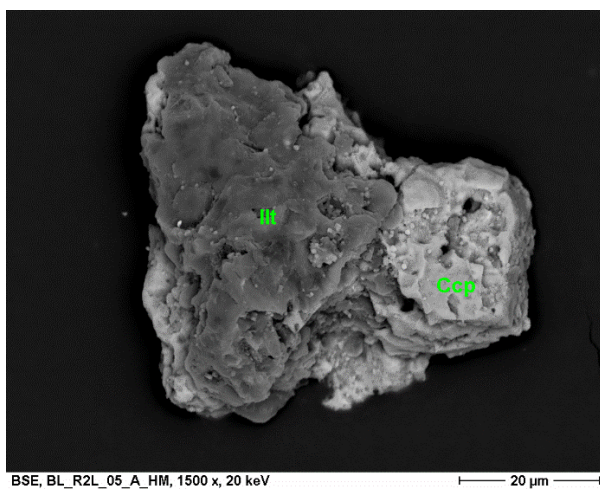


**Figure 3.3.5:** SEM-image of a particle illustrating common intergrowths consisting of illite (Ill) and chalcopyrite (Ccp) as found in bioleaching residues of Lubin concentrate LCA06. (SEM-BSE)

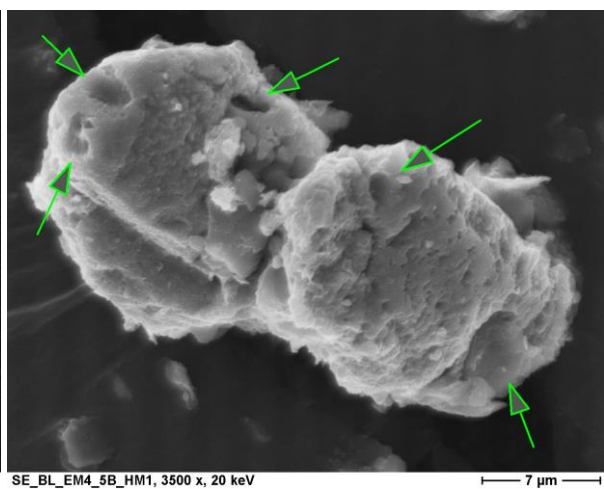


**Figure 3.3.6:** Chalcopyrite particle exhibiting isolated bacterial corrosion pits (arrows) as categorized by Bennett and Tributsch (1978) detected in the bioleaching residues of Sangerhausen black shale feed. (SEM-SE)

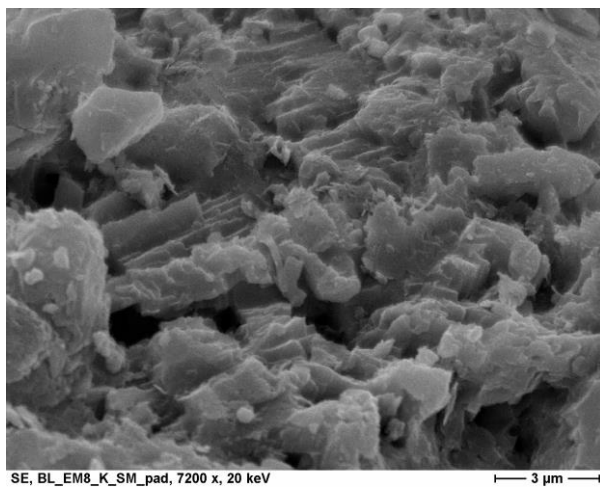


**Figure 3.3.7:** Surface of a chalcopyrite particle in the chemical control exhibiting areas marked by crystal plane cleavage (etching structure) and irregular forms of altered mineral surface. (SEM-SE)

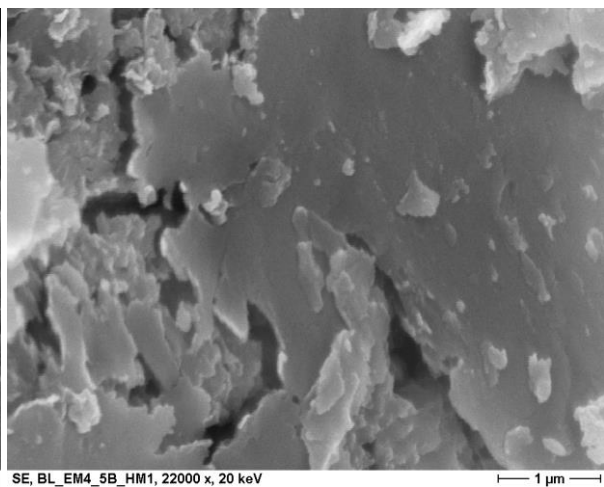


**Figure 3.3.8:** Detail image of secondary formed coatings of copper sulphate occupying a previously corroded chalcopyrite particle. (SEM-SE)

3.3.10. Thus, lead sulfate represented a widespread secondary formed microcrystalline phase in bioleaching residues. It occurred either as *in situ* formed coating onto galena particles (Figure 3.3.11) or was precipitated as framework-like formations from the leaching solution.

The microcrystalline, porous accretions of lead sulfate around galena particles was a common feature as well in bioleaching as in the sterile control leaching residues (Figure 3.3.12). Additionally, small particles of lead sulfate, often few micrometres in size, occurred abundant. They were either formed as crystals or irregular mineral aggregates precipitated from the leaching solution.

Chalcopyrite particles remaining in bioleaching residues showed on the one hand very little indications of alteration, they were partially sharp edged and exhibited smooth surfaces, on the other hand chalcopyrite particles were marked by strong dissolution textures and showed intensely

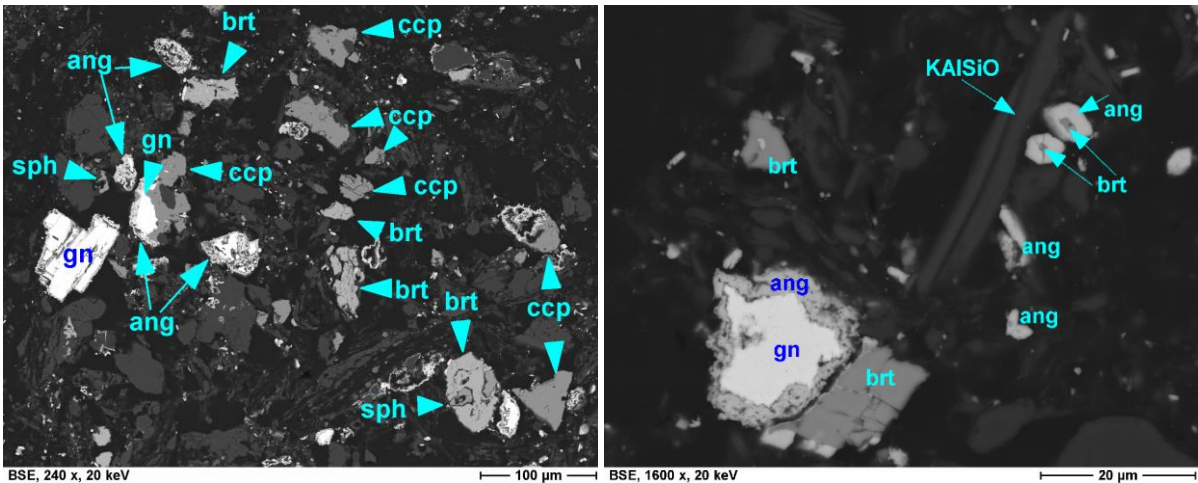


**Figure 3.3.9:** Overview image of particles in bioleaching residues of the Sangerhausen black shale feed lead sulphate developed as microcrystalline anglesite demonstrates the abundant occurrence of undissolved (ang) envelopes of galena (gn) or barite (brt) particles sulfides (ccp–chalcopyrite, gn–galena, sph–sphalerite), often represents an common in-situ replacement in barite (brt) and anglesite (ang). (SEM-BSE)

**Figure 3.3.10:** The widespread formation of secondary residues of the Sangerhausen black shale feed lead sulphate developed as microcrystalline anglesite demonstrates the abundant occurrence of undissolved (ang) envelopes of galena (gn) or barite (brt) particles sulfides (ccp–chalcopyrite, gn–galena, sph–sphalerite), often represents an common in-situ replacement in barite (brt) and anglesite (ang). (SEM-BSE)

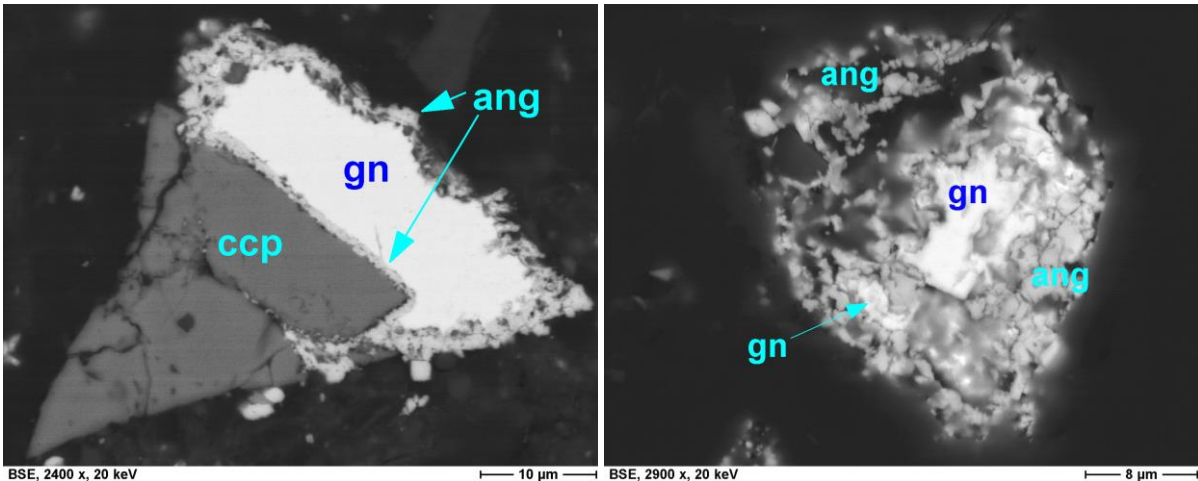


**Figure 3.3.11:** Particle consisting of galena (gn) and chalcopyrite (ccp) shows lead sulphate formation at the galena (gn) grain replaced extensive by massive to cellular anglesite (ang), which was an common replacement texture detected in bioleaching as well as sterile control residue. (SEM-BSE)

**Figure 3.3.12:** Image of nearly completely dissolved chalcopyrite (ccp) shows lead sulphate formation at the galena (gn) grain replaced extensive by massive to cellular anglesite (ang), which was an common replacement texture detected in bioleaching as well as sterile control residue. (SEM-BSE)

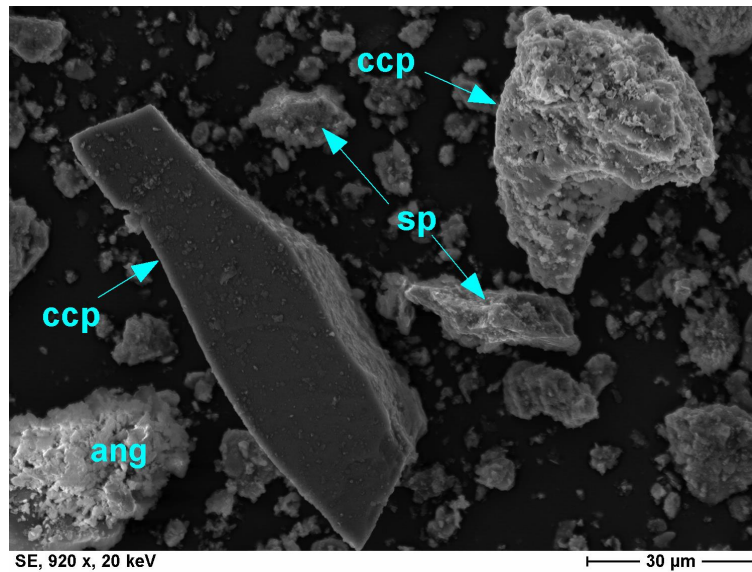


**Figure 3.3.13:** Chalcopyrite (ccp) grains exhibited very different shapes in bioleaching residues. They were either smooth and angular showing hardly any indications of alteration or strongly corroded particle marked by roughened and pitted surfaces. Image shows also partial dissolved sphalerite (sp) and precipitates of anglesite (ang). (SEM-SE)

corroded, highly roughened particle surfaces (Figure 3.3.13). SEM-observations showed that both textures of grain surfaces occurred independently from the grain size. The ore accommodated apparently three types of chalcopyrite particles: type one was completely dissolvable, a second type was partly not dissolved showing strong dissolution features and the third type remained scarcely altered by showing smooth particle surfaces comparable to chalcopyrite grains from the ore/ flotation concentrate. A chalcopyrite grain on a state of an advanced disintegration is displayed in Figure 3.3.14. Texturally, such particles exhibited an irregular pattern of undissolved domains disrupted by dissolution channels tracing intraparticle fissures and cracks that can be partially subsequently replaced by copper and iron-bearing sulphate. Cu-Fe sulphate was also found as outer particle coating covering individual chalcopyrite particles (Figure 3.3.15).

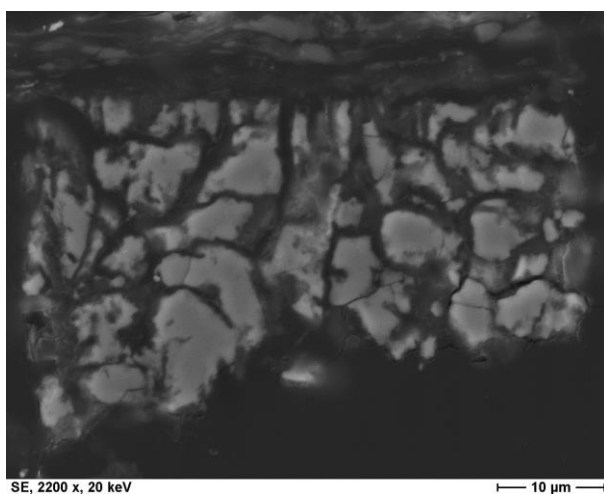


**Figure 3.3.14:** Dissolution pattern transecting a chalcopyrite particle documents the advanced but not complete disintegration common in bioleaching residues. (SEM-SE)

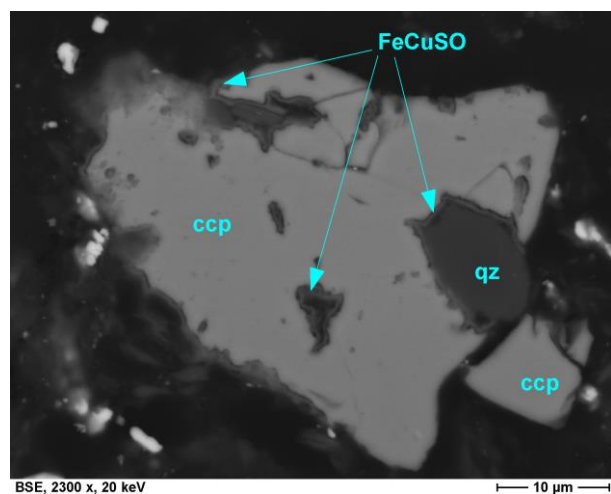


**Figure 3.3.15:** Example of chalcopyrite (ccp) particles in bioleaching residues displays iron and copper-bearing sulphate (FeCuSO) on the grain surface as well as within interstices (BSE-SEM-image).

### 3.3.4 Results

#### 3.3.4.1 Bioleaching residues derived from black shale ores

##### 3.3.4.1.1 Bioleaching residues of black shale- as well as limestone-hosted low-grade ore, Mansfeld district, central Germany

###### 3.3.4.1.1.1 Metal content and recovery

Bioleaching tests series conducted with low-grade copper ore showed no conspicuous differences between bioleaching and chemical control residues. The low content of especially remaining copper sulphides allowed no clear conclusions about the leaching performance achieved by bioleaching and chemical leaching.

Chemical analyses of feed material and leaching residues in Table 3.3.1 show very low differences regarding the content of metals in both, sterile control and bioleaching residues. Most notable deviating metal contents were analysed for Pb, Zn and Fe, whereas Pb occurred relatively enriched in both leaching residues showing similar concentrations (approx. 1.1%). The difference regarding the Zn content revealed that the leaching of Zn was improved by bioleaching, in which Zn minerals, decisively represented by sphalerite, were dissolved largely (77%) in contrast to the sterile control leaching tests (38%) as indicated in Table 3.3.1. For some other metals, the content in bioleaching and sterile control residues is quite similar, although small differences existed. However, the lower content of Cu and Fe in the sterile control residues point to elevated dissolution of Cu- and Fe-bearing minerals. Trace metals showed also partially lower contents in the sterile control residues, in particular Mo, V and As, whereas a slightly lower concentration of Co was analysed in bioleaching residues. Generally, the recovery for several metals was similar, as Table 3.3.1 shows. Significant improved recovery by bioleaching was observed for Zn (77% vs 38%) and more slightly for Co (55% vs. 47%). Other metals were leached equivalent or better (Mo, Fe) by the sterile control leaching experiment, but commonly the metal recovery was comparable to bioleaching.

The metal recovery rates in Table 3.3.2 of the bioleaching experiments were hardly distinguishable from recovery rates of sterile control leaching. Geochemical analyses of the residues revealed no significant differences in terms of metal mobilization in both leaching approaches. It must be assumed that the main part of the sulphides, in particular copper-bearing sulphides, but also pyrite and sphalerite were leached chemically by the usage of sulfuric acid, which represented a substantial part of the leaching solution to depress and adjust pH conditions. Thus, in both, the residues of bioleaching and sterile leaching control, boxwork-like textures assumedly of dissolved carbonate as well as sulphide mineral particles were detected in formerly intergrowths with silicate minerals that remained in the residues. The inventory on remained sulphides mainly comprised of irregular remnants of sphalerite, pyrite and galena. The latter often enveloped with a thin layer of lead sulfate (anglesite),

**Table 3.3.1:** Contents of base metals and trace metal in the Mansfeld black shale low-grade ore as well as bioleaching and sterile leaching residues. (Data: BGR)

Element	Cu	Pb	Zn	Fe	Ag	As	Co	Mo	Ni	V
	ppm	ppm	ppm	ppm	ppm	ppm	ppm	ppm	ppm	ppm
<b>Mansfeld black shale</b>	5550	8092	9706	20773	58	55	54	129	141	413
<b>Sterile control residues</b>	184	10974	6033	7354	166*	25*	29	72	97	157
<b>Bioleaching residues</b>	260	11700	2211	9613	190*	27*	24	87	96	169

**Table 3.3.2:** Comparison of the recovery performance for selected metals by bioleaching and sterile chemical leaching of black shale low-grade ore from Mansfeld, Germany. (Note: negative values represented relative enrichment in the leaching residues)

Metal recovery	Cu	Pb	Zn	Fe	Ag	As	Co	Mo	Ni	V
sterile control residues	97%	-36%	38%	65%	-185%	55%	47%	44%	31%	62%
bioleaching residues	95%	-45%	77%	54%	-227%	51%	55%	33%	32%	59%

while sphalerite particles showed generally rounded, irregular solution embayments. Copper-bearing sulphides were rare, but if present they had similar solution features. Apparently, unaltered sulphides were exemplarily found in larger particles (> 30 µm), in which they occurred armoured and overgrown by silicate minerals.

Bioleaching tests carried out on milled limestone-dominated low-grade ore were not continued. Exemplary investigations of (bio)-leaching residues had shown that the before-mentioned solution features were evolved more intensive even in the sterile control leaching residues, which had demonstrated a dominant chemical leaching performance. Furthermore, the proportion of the carbonate fraction was significantly higher compared to the black shale low grade ore, and thus bioleaching experiments required a strong increased addition of sulfuric acid in order to stabilize the optimum leaching condition for the bacterial community.

### 3.3.4.1.2 Bioleaching residues of Sangerhausen black shale-hosted ore

#### 3.3.4.1.2.1 Mineral distribution

Further bioleaching tests with black shale feed were carried out on a black shale ball mill product from the former Sangerhausen mining district. Generally, the Sangerhausen black shale ore contains significantly more copper (2.6% Cu) compared to the low-grade black shale ore from Mansfeld (0.6% Cu). Similar to the bioleaching tests conducted with low-grade copper ore, the bacterial community used for the experiments was stepwise adapted and conditioned for the bioleaching approaches. Chemical analyses of the residues of bioleaching and sterile control leaching approach revealed that the leaching efficiency was commonly better for the bacterial-supported leaching tests. However, the copper extraction in respect to the dissolution of copper-bearing sulphides by bioleaching was slightly lower in comparison to the corresponding sterile control tests.

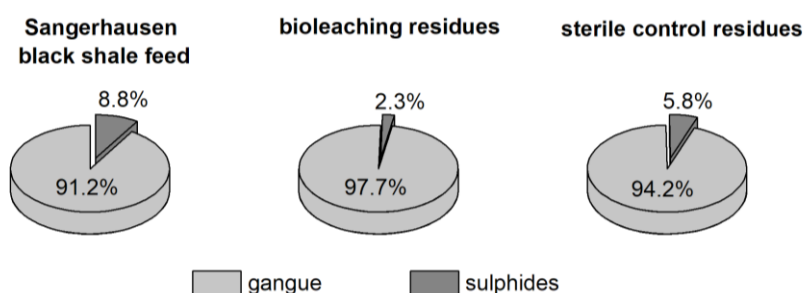


**Figure 3.3.16:** General proportions of gangue and minerals indication the more advanced dissolution of sulphides in the bioleaching residues of the Sangerhausen black shale feed. (Data: MLU)

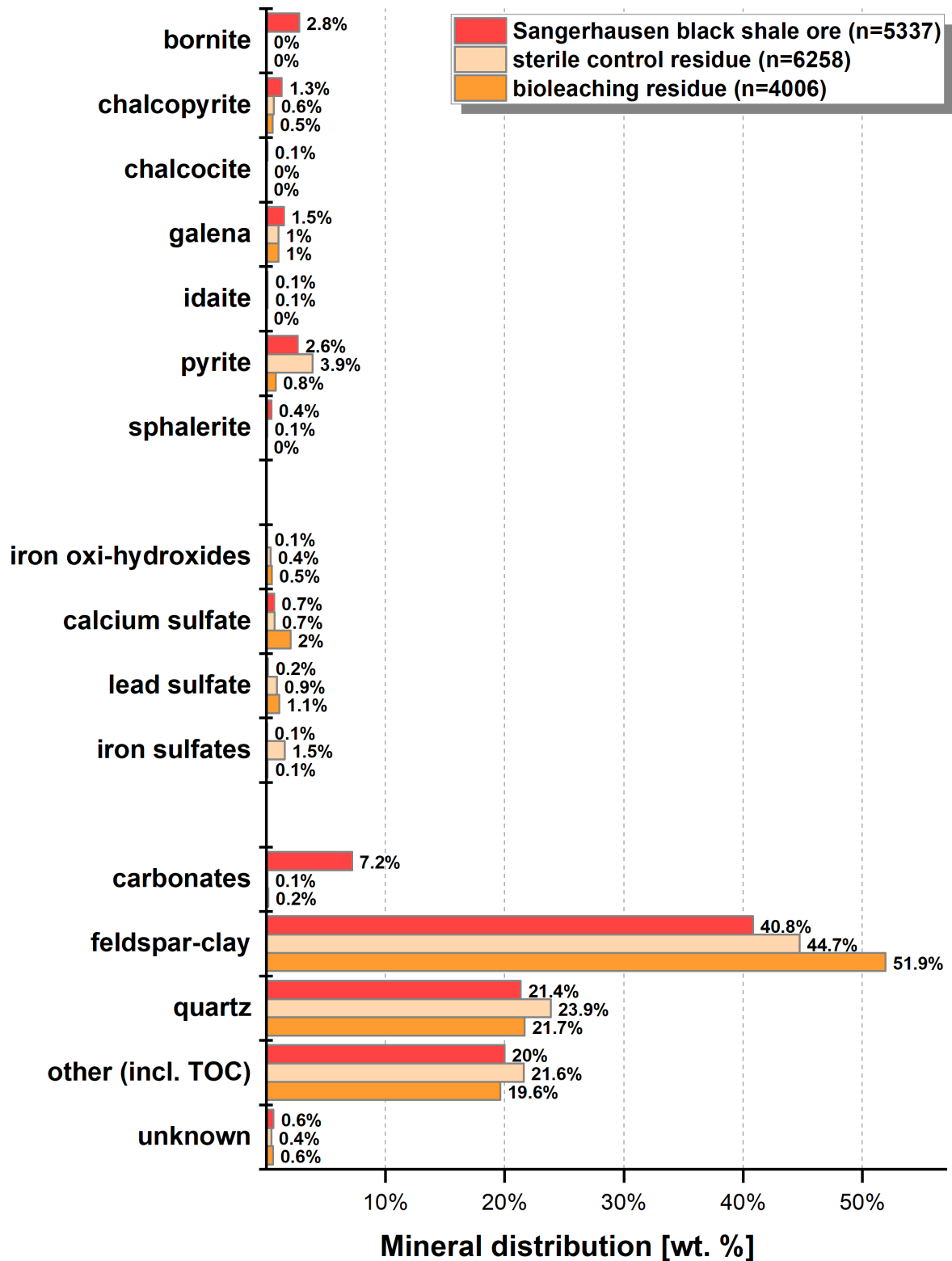


Figure 3.3.17: Mineral distribution of Sangerhausen black shale feed, bioleaching as well as sterile control leaching residues. (Data: MLU)

The mineral distribution analysis of the milled black shale ore (< 100 µm) was shown in Chapter 3.1.2.1. Generally, as shown in Figure 3.3.16, a noticeable difference of the sulfide content in bioleaching residues (2.3%) and chemically leached residues (5.8%). Figure 3.3.17 shows the refractory portion of sulfides in both, bioleaching and chemical control residues. Sulfide particles of the sterile control residue were clearly dominated by pyrite (4.5%) that was substantially removed by bioleaching (0.9%).

The mineral distribution analysis also revealed that similar contents of chalcopyrite remnants occurred in both residues, whereas bornite and chalcocite were completely dissolved, but idaite and sphalerite occurred in low traces (0.1%) only in the chemically leached sample. The amount of galena in both residues was similar (1.2%). While bioleaching residues were completely free of other sulphides, sterile control residues hosted subordinate constituents of idaite (Cu<sub>5</sub>FeS<sub>6</sub>, 0.1%) and sphalerite (ZnS, 0.0%).

Gangue minerals in both leaching residues comprised predominantly minerals of the feldspar-clay group, whereas illite represented the majority within this mineral class (28% sterile control residues, 41% bioleaching residues). The feldspar portion was dominated by potassium feldspar. An additional main mineral constituent was quartz (28% in sterile control residues, 25% in the bioleaching residues). Calcium sulphate, gypsum, was significantly detected in bioleaching residues, in which it attained 2.4% in comparison to 0.8% in the sterile control residues. Generally, bioleaching residues contained increased amounts of secondary formed phases such as lead sulphate (anglesite) and iron sulphate (jarosite) as shown in Figure 3.3.17. Further minerals determined in both, bioleaching and chemical control leaching residues, and resumed under the “other”-class were mainly barite (> 80 % in this class) and traces of rutile and zircon.

#### 3.3.4.1.2.2 Metal content and recovery

The feed material for this bioleaching approach represented an organic-rich black shale ore from the Sangerhausen mining district, which contained elevated base metal concentrations for Cu (2.62%) and Pb (1.22%). Geochemical data for selected metals of black shale ore, bioleaching as well as sterile control leaching residues are listed in Table 3.3.3. The content of Cu, Pb and Zn in both, bioleaching and sterile control residues was quite similar, but the Fe content was decidedly lower in the bioleaching residues (0.65 %) in comparison to the sterile control residues (2.19%). Larger differences in terms of the metal content in both residues was analysed for Co, As, Mo and U, that were likewise notably lower in the bioleaching residues, whereas differences in Ni, V, Ag and Sb were barely noticeable.

The compilation of recovery yields for selected metals in Table 3.3.4 clarifies that bioleaching was generally more efficient, especially in the recovery of Zn and Fe. Other accompanying trace metals,

**Table 3.3.3:** Geochemical data of selected base and trace metals contained in the Sangerhausen black shale ore feed and its bioleaching and sterile control leaching residues. (Data: BGR)

Element	Cu	Pb	Zn	Fe	Ag	As	Co	Mo	Ni	Sb	U	V
	%	%	%	%	ppm							
<b>Sangerhausen black shale ore</b>	2.62	1.22	0.17	3.25	61	453	856	362	266	41	124	171
<b>Sterile control residues</b>	0.16	1.48	0.04	2.19	64	348	493	307	245	17	77	99
<b>Bioleaching residues</b>	0.21	1.44	0.01	0.65	66	101	392	155	253	15	47	100

**Table 3.3.4:** Leaching yields for base and trace metals achieved by bioleaching and chemical control leaching of Sangerhausen black shale ore. (Note: negative values for Pb and Ag indicate a relative enrichment in the residues)

Metal recovery	Cu	Pb	Zn	Fe	Ag	As	Co	Mo	Ni	Sb	U	V
<b>Sterile control residues</b>	94%	-21%	79%	33%	-6%	23%	42%	15%	8%	58%	38%	42%
<b>Bioleaching residues</b>	92%	-18%	93%	80%	-9%	71%	54%	57%	5%	63%	62%	42%

such as As, Co, Mo, and U, showed adequate leaching behaviours, whereas Ag, Sb and V indicated leaching recovery portions very similar to sterile control leaching tests. In particular Pb was marked by relative enrichment in both leaching residues, which illustrated the limited solubility of predominantly galena as well as the missing capability of dissolved lead ions to remain in the process solution by the onset formation of lead sulphate compounds at low pH conditions. Because Ag showed also slight increased concentrations in leaching residues, it seemed to be either associated with undissolved galena that acted as Ag-carrier or represented a trace element incorporated into secondary formed precipitations.

The investigation of the mineral distribution, particularly of sulphides, in bioleaching and sterile control residues permitted conclusion to the mineral recovery of the leaching tests. As Table 3.3.5 displays, copper-bearing sulphides were completely dissolved with an exception for chalcopyrite that was detected with similar proportion in bioleaching as well as in sterile control residues. Both leaching approaches yielded leaching rates for chalcopyrite just over 50%. Improved mineral recovery by bioleaching was determined for sphalerite and pyrite, the latter with comparatively lower solubility in the sterile control leaching test, which led to a relative enrichment in the residues (-48%).

**Table 3.3.5:** Mineral leaching recovery for base metal sulphides as determined by mineral distribution analyses. (Negative percentages represent relative enrichment. (Data: MLU)

	bornite	chalcopyrite	chalcocite	covellite	idaite	pyrite	sphalerite	galena
<b>sterile control residues</b>	100%	52%	100%	100%	0%	-48%	85%	30%
<b>bioleaching residues</b>	100%	60%	100%	100%	100%	70%	100%	31%

### 3.3.4.2 Bioleaching residues from copper flotation concentrates

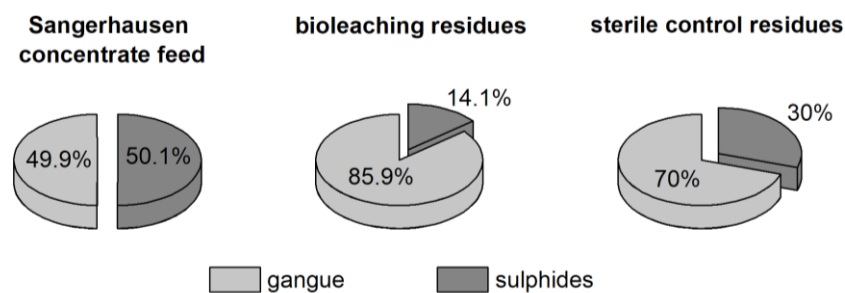
#### 3.3.4.2.1 Bioleaching residues of flotation concentrate extracted from Sangerhausen black shale ore

##### 3.3.4.2.1.1 Mineral distribution

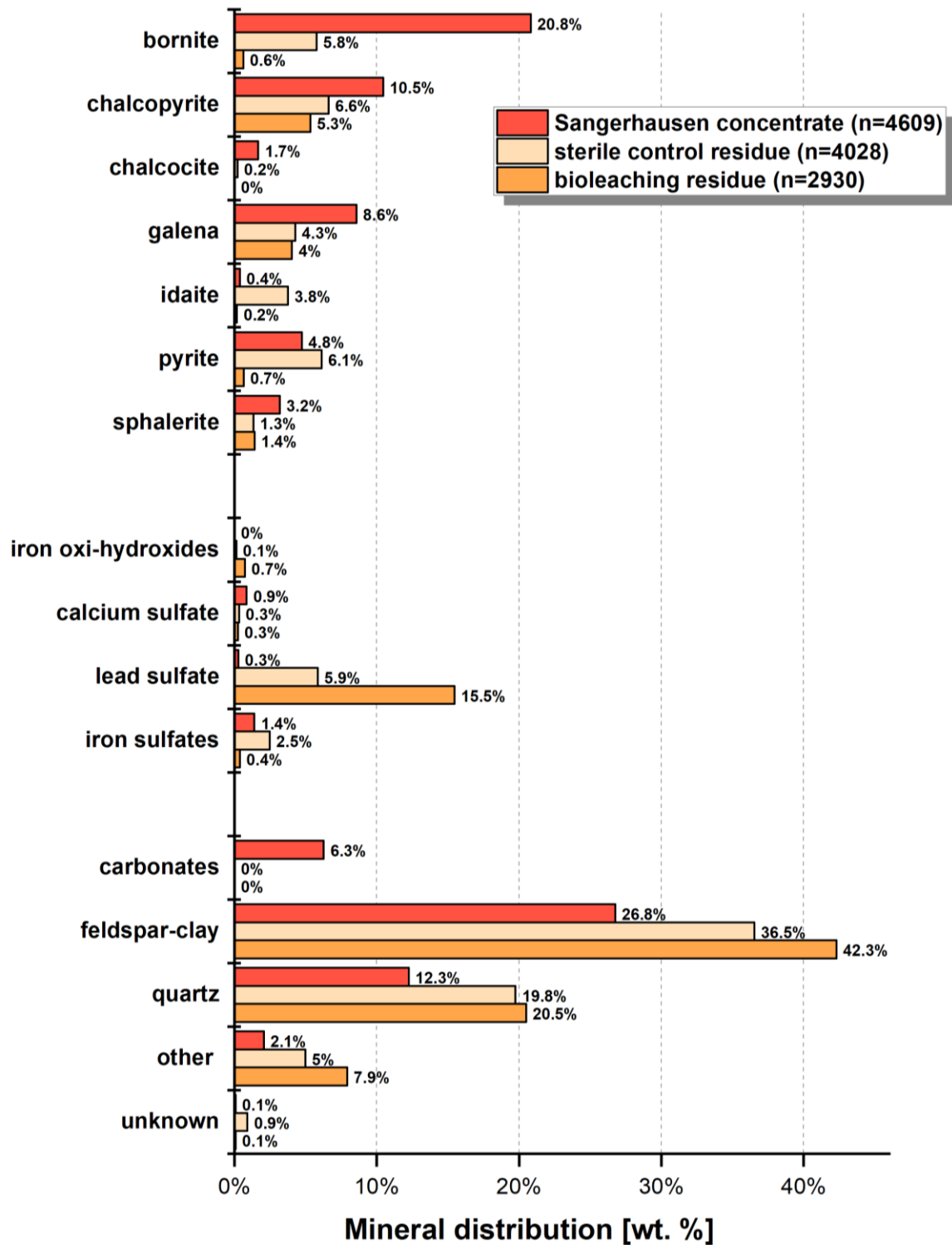
More advanced bioleaching tests with black shale-related feed material were carried out on a flotation concentrate gained from Sangerhausen black shale ore, which was produced by the usage of dextrin and ethanol pre-treated feed (see Chapter 2.2.2 & 3.2.5.1). Due to generally increased proportions of sulphides in the concentrate (50.1%, Figure 3.3.18), in particular of copper-bearing sulphides, the differences in their distribution between bioleaching and sterile control leaching residues were more notable compared to the experiments conducted with black shale ore (see above, Chapter 3.3.4.1.2).

Figure 3.3.18 displays that bioleaching residues contained a significantly lower portion of sulphides (14.1%) compared with residues of the sterile control leaching tests (30%). Figure 3.3.19 revealed that the latter hosted considerable amounts of bornite (5.8%), chalcopyrite (6.6%), idaite (3.8%), pyrite (6.1%) and sphalerite (1.4%). Opposing to that, the bioleaching residues contained either partly much lower concentrations of some sulphides or other sulphides were dissolved completely. Thus, remaining sulphides comprised bornite (0.6%), chalcopyrite (5.3%), pyrite (0.7%), sphalerite (1.4%) and some idaite (0.2%). Interestingly, in comparison with the flotation concentrate feed, in sterile control residues occurred a slightly enriched amount of covellite, which was considered to be formed secondary within the leaching experiments. The only sulphide that presented similar contents was galena with 4.1% in bioleaching residues and 3.9% in sterile control residues.

Main constituents of both leaching residues were gangue minerals and mineral groups. According to the considerable varying proportions of sulphides between bioleaching and sterile control leaching residues, the latter hosted 70% of total gangue minerals, whereas in bioleaching residues their proportion was significantly increased (86%). Major portions were quartz and minerals belonging to the feldspar and clay mineral class, whereas generally potassium feldspar and illite represented the main minerals in this grouping. Attributed to the significant lower proportion of sulphides in the bioleaching residues, the portion of quartz and feldspar-clay-minerals was markedly increased (42.3%) compared to the sterile control residues (36.5%). Additionally, lead sulphate formed during the leaching process was particular enriched in the bioleaching residues (15.5%) compared to the residues of the sterile control leaching (5.9%).



**Figure 3.3.18:** Proportion of gangue minerals and sulphides in the Sangerhausen concentrate feed and related bioleaching and sterile control leaching residues. (Data: MLU)



**Figure 3.3.19:** Mineral distribution diagram for Sangerhausen copper concentrate feed as well as bioleaching and sterile leaching residues. (Data: MLU)

### 3.3.4.2.1.2 Metal content, metal and mineral recovery

The source material used for these leaching experiments represented a flotation concentrate extracted from Sangerhausen black shale ore and was especially enriched in Cu (14.40%) and Pb (7.43%). Moreover, it contained moderately to strong increased proportion of trace metals as for Ag, Mo, Ni, Sb and V (for details see Chapter 3.2.5.3). Table 3.3.6 shows the base metal and trace metal content in the flotation concentrate as well as related bioleaching and sterile control leaching residues.

Generally, bioleaching residues hosted in comparison to sterile control residues lower quantities of metals with the exception of Pb, Ni and V. Most striking was the difference of Cu and Fe, whereas the significant lower Cu-content in bioleaching residues (2.14%) pointed to the far improved dissolution of copper-bearing minerals, in contrast to sterile control residues that contained still 7.10% Cu. The advanced dissolution of iron-bearing copper sulphides was also indicated by a considerably lower Fe-content in the bioleaching residues (2.92%), which was nearly the half of that in the sterile control leaching residues (4.67%). This was accompanied by an almost consistent Pb-content (7.45%) in respect to the feed (7.43%), whereas an increased concentration of Pb (8.84%) was analysed in the bioleaching residues.

Amongst the leaching residues, the content of selected trace metals was mostly lowest in bioleaching residues, exceptions represented Ni, Sb and V, which showed the lowest concentrations in the sterile leaching residues. Additionally, markedly lower concentrations of trace metals concerning As, Co Mo, Sb and U were detected in the bioleaching residues compared to the feed. While the content of V and Ni in the sterile control leaching residues was the lowest, both elements showed likewise the lowest solubility due to the slight decrease in comparison to the feed. A general exception was observed for Ag, which occurred commonly enriched in both leaching residues regarding to the content in the feed, notably in the sterile control residues, which illustrated the missing capability of Ag-recovery by sulfuric acid leaching.

According to the chemical composition, the metal recovery by bioleaching was chiefly more advanced and recovery rates were largely higher in comparison to the sterile control leaching as listed in Table 3.3.7. In particular Cu was significantly more recoverable by bioleaching tests (85%), while by sterile chemical leaching only 51% of the Cu-content was extracted. Moreover, Fe was recovered to a larger extent by bioleaching (51%) and exceeded the Fe-recovery by sterile control leaching with 29%. The recovery rates for trace metals by sterile leaching, particularly for As, Co, Mo and U, were generally lower in comparison to bioleaching. However, individual trace metals were seldom more than 50%

**Table 3.3.6:** Geochemical data of some selected elements comprising base and trace metal contents in the Sangerhausen floatation concentrate, bioleaching and sterile control leaching residues.(Data: ALS)

Element	Cu	Pb	Zn	Fe	Ag	As	Co	Mo	Ni	Sb	U	V
	%	%	%	%	ppm							
<b>Sangerhausen concentrate</b>	14.40	7.43	1.36	5.99	132	371	912	697	468	625	120	881
<b>Sterile leaching residues</b>	7.10	7.45	0.70	4.67	473	328	655	667	412	445	74	646
<b>Bioleaching residues</b>	2.14	8.84	0.68	2.92	384	227	523	548	424	456	56	731

**Table 3.3.7:** Recovery rates of selected metals for bioleaching as well as sterile control leaching tests of Sangerhausen black shale ore flotation concentrate.

<b>Metal recovery</b>	<b>Cu</b>	<b>Pb</b>	<b>Zn</b>	<b>Fe</b>	<b>Ag</b>	<b>As</b>	<b>Co</b>	<b>Mo</b>	<b>Ni</b>	<b>Sb</b>	<b>U</b>	<b>V</b>
<b>Sterile leaching residues</b>	51%	0%	48%	22%	-258%	12%	28%	4%	12%	29%	38%	27%
<b>Bioleaching residues</b>	85%	-19%	50%	51%	-191%	39%	43%	21%	9%	27%	53%	17%

recovered, neither by bioleaching nor by sterile chemical leaching. Explicitly low recovery rates were determined in general for Ni and Mo, whereas no recovery was achieved for Pb and Ag.

The recovery of sulphides listed in Table 3.3.8 shows nearly to complete dissolution by bioleaching, especially for copper-bearing sulphides such as bornite, chalcocite and covellite. Additionally, covellite was leached partly by bioleaching, while it was relatively enriched along with pyrite in sterile control residues. Galena and sphalerite showed similar recovery percentages of about 50%. According to the mineral distribution analysis, pyrite was relatively enriched in the sterile control residues, while pyrite was extensively leached by bioleaching. Some of the trace metals showed improved recovery rates by bioleaching such as As, Co and Mo. These trace metals are generally considered to be associated with pyrite often incorporated as trace elements in the pyrite crystal lattice so that their advanced recovery was presumably caused by the increased dissolution of pyrite in the bioleaching experiments. The sterile control residues are characterized additionally by enrichment of copper sulphides as idaite and covellite. Both regarded to be formed secondary, idaite from incomplete leached and altered bornite particles, whereas covellite is considered to be formed secondary from the process solution often associated with lead sulphate precipitations.

**Table 3.3.8:** Recovery rates for sulphides according the mineral distribution analyses of Sangerhausen copper concentrate feed, bioleaching and sterile control leaching residues. (Data: MLU)

<b>Mineral recovery</b>	<b>bornite</b>	<b>chalcopyrite</b>	<b>chalcocite</b>	<b>covellite</b>	<b>idaite</b>	<b>pyrite</b>	<b>sphalerite</b>	<b>galena</b>
<b>Sterile control leaching</b>	72%	37%	87%	-732%	-852%	-26%	58%	50%
<b>Bioleaching</b>	97%	49%	100%	100%	54%	87%	56%	53%

### 3.3.4.2.2 Bioleaching residues of the flotation concentrate from Rudna black shale ore

#### 3.3.4.2.2.1 Mineral distribution

Further investigations regarding residue analyses concerned leaching experiments on a flotation concentrate gained from Rudna black shale ore (see Chapter 3.2.4.1). The sulphide assemblage of the Rudna black shale copper concentrate formed a fraction of 29%, which was significantly lower as analysed in the Sangerhausen concentrate and was dominated by chalcocite (11.0%), bornite (6.7%) and galena (8.5%). Figure 3.3.20 shows that the proportion of sulphides (7.4%) in the bioleaching residues was more than the half of that in the sterile control leaching residues (15.9%).

Mineral distribution analyses for copper concentrate, bioleaching residues and sterile control residues are shown in Figure 3.3.21. Generally, the bioleaching residues contained low quantities of copper-bearing sulphide, namely 0.6% chalcocite and 0.3% chalcopyrite. Bornite was dissolved completely.

Despite of the high recovery of copper sulphides by bioleaching, the sterile control residues contained essentially larger portions of remained copper-bearing sulphides. Accordingly, the sterile control residue contained 2.6% bornite, 2.6% chalcocite and 1.7% chalcopyrite. The latter indicated a relative enrichment in comparison to the feed. In addition, covellite (1.9%) was determined significantly in the sterile control residues and indicated to be formed secondary in the sterile control assays. Furthermore, the sterile control residues contained 1.1% idaite that had a comparably lower amount in the feed material, whereas it was absent in the bioleaching residues. Idaite might represents a modification of bornite. Galena, which was one of the major sulphides in the feed material, was more intense dissolved by the sterile control leaching (4.8%; bioleaching: 5.4%) and was supposed to be the prerequisite for the leaching-induced formation of lead sulphate.

The mineral distribution revealed that anglesite-like lead sulfate precipitations occurred enriched in both, in the sterile control residues to a lower amount (3.0%) and increased in the bioleaching residues (4.6%). However, due to the partly extremely fine-grained nature of these precipitations, a portion of lead sulphate particles might not been detected because of the grain size detection limit (5  $\mu\text{m}$ ). According to the global mineral mass balance, gangue minerals such as quartz and minerals of the feldspar-clay group were especially enriched in the bioleaching residues. Thus, bioleaching residues consisted of 52.0% of clay and feldspar minerals and 13.8% quartz. Opposite to that, the sterile control residues consisted of 42.1% minerals belonging to feldspar-clay group and 12.6% quartz and was enriched in calcium sulphate (gypsum, 13.2%) and iron sulphate (mainly jarosite, 1.0%). The

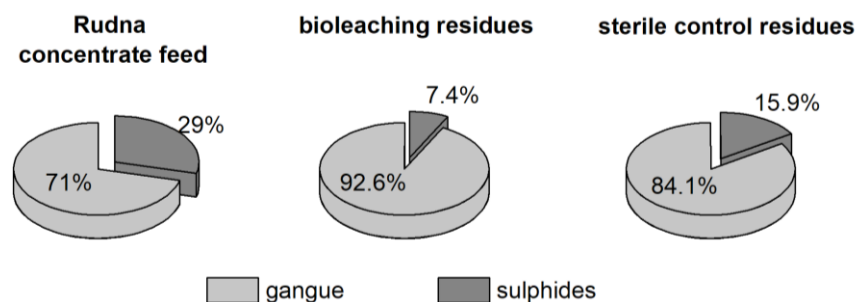


**Figure 3.3.20:** Pie charts for Rudna concentrate feed and related bioleaching as well as sterile control leaching residues showing the proportion of sulphides and gangue minerals. (Data: MLU)

bioleaching residues accommodated similar quantities of gypsum (9.9%), but only traces of iron sulphate minerals (0.1%).

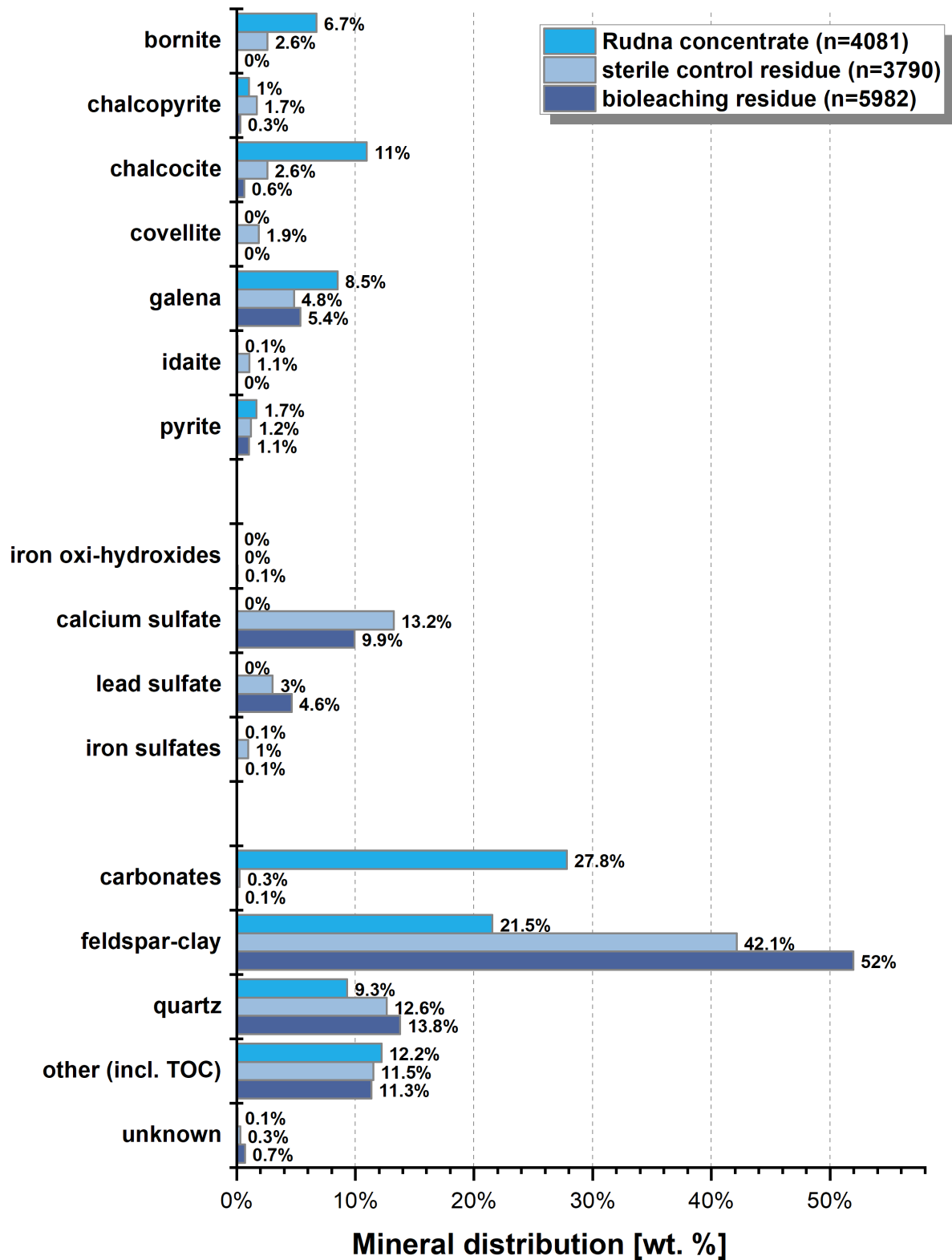


**Figure 3.3.21:** Bar chart displaying the distribution of sulphides as well as gangue-type minerals and mineral groups in the Rudna copper concentrate and its bioleaching and sterile control leaching residues. (Data: MLU)

### 3.3.4.2.2.2 Geochemical composition, mineral and metal recovery

The compilation of geochemical data in Table 3.3.9 displays the content of selected metals in the flotation concentrate extracted from Rudna black shale as well as the corresponding sterile control and bioleaching residues. The concentrate was enriched in Cu (10.10%) and Pb (7.11%), but the content of trace metals was significantly lower in comparison to the concentrate gained from Sangerhausen black shale feed.

In general, among the leaching residues, sterile control residues contained significant amounts of Cu (6.12%) and Pb (7.33%) as well as trace metal contents for As, Co and Mo were increased compared to the bioleaching residues, whereas in turn Ag, Ni and V showed lower concentrations in the sterile control residues. Ag had the almost identical concentration as analysed in the feed.

The bioleaching residues were characterized by low contents of Cu (0.28%), Fe (0.38%), but was also marked by Pb enrichment (8.26%) regarding the feed material. The concentration of individual trace metals was commonly deciding lower as ascertained for the sterile control leaching residues, except for V (554 ppm) and Ag (631 ppm), the latter was slightly enriched in the bioleaching residues in relation to the feed.

**Table 3.3.9:** Base metal and trace metal content in the Rudna copper concentrate as well as in the residues of the bioleaching and sterile control leaching experiments. (Data: ALS)

Element	Cu	Pb	Zn	Fe	Ag	As	Co	Mo	Ni	V
	%	%	%	%	ppm	ppm	ppm	ppm	ppm	ppm
<b>Rudna concentrate</b>	10.10	7.11	0.07	2.40	611	391	301	439	400	852
<b>Sterile control residues</b>	6.12	7.33	0.05	1.31	595	171	183	346	105	480
<b>Bioleaching residues</b>	0.28	8.26	0.05	0.38	631	59	24	218	127	554

According to the varying contents of single metals in sterile control and bioleaching residues, the recovery from the feed material was differently. Table 3.3.10 indicates that the recovery of Cu and Fe was nearly complete by bioleaching, Pb was enriched in both leaching approaches, whereas the initial low content of Zn in the concentrate was leached completely. Almost complete leaching rates by bioleaching were also ascertained for As and Co, but the leaching efficiency of the sterile control leaching tests stood far behind and reached just 30-50% of the metal recovery achieved by bioleaching. Exceptions were noticed for Ni and V; both showed in comparison to bioleaching a slight increased recovery by sterile control leaching.

The leaching yields for sulphides are displayed in Table 3.3.11. Bioleaching achieved generally increased recovery rates, except for galena. Bioleaching of Rudna concentrate dissolved bornite completely as well as chalcocite largely (94%), whereas the leachability of sulphides by sterile control leaching was limited, so that 45% of bornite remained in the residue. Additionally, the content of chalcopyrite in the sterile control leaching residues was slightly increased in respect to the concentrate. Hereof, two-third of the total chalcopyrite content were recovered by bioleaching. Sterile control residues contained furthermore increased amounts of idaite and secondary covellite, which was not present in the feed material.

**Table 3.3.10:** Recovery rates of selected metals by sterile control leaching and bioleaching tests.

Metal recovery	Cu	Pb	Fe	Ag	As	Co	Mo	Ni	V
<b>Sterile control leaching</b>	39%	-3%	45%	3%	56%	39%	21%	74%	44%
<b>Bioleaching</b>	97%	-16%	84%	-3%	85%	92%	50%	68%	35%

The leaching efficiency for pyrite was low in both leaching experiments, but nearly one-third was extracted by bioleaching opposing to just over 10% achieved by sterile control leaching tests. Galena was slightly better dissolved by sterile control leaching (43%) than by bioleaching (30%), but dissolved lead ions were transferred into lead sulphate precipitates, a common constituent in both, the bioleaching and sterile control residues.

**Table 3.3.11:** Leaching recovery proportion of base metal sulfides dissolved by bioleaching as well as sterile control leaching tests. (Data: MLU)

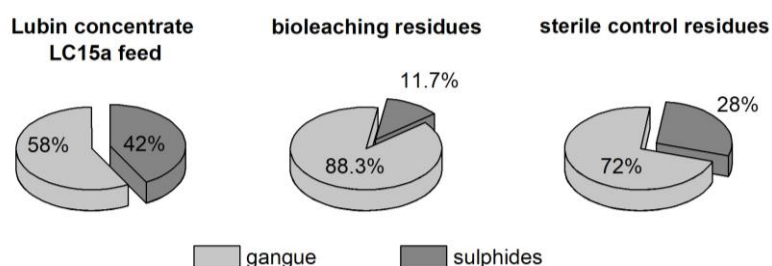
Mineral recovery	bornite	chalcopyrite	chalcocite	covellite	idaite	pyrite	galena
<b>Sterile control leaching</b>	61%	-64%	77%	-190%	-124%	28%	43%
<b>Bioleaching</b>	100%	69%	94%	0%	100%	37%	37%

### 3.3.4.2.3 Bioleaching residues of Lubin concentrate LC15a

#### 3.3.4.2.3.1 Mineral distribution

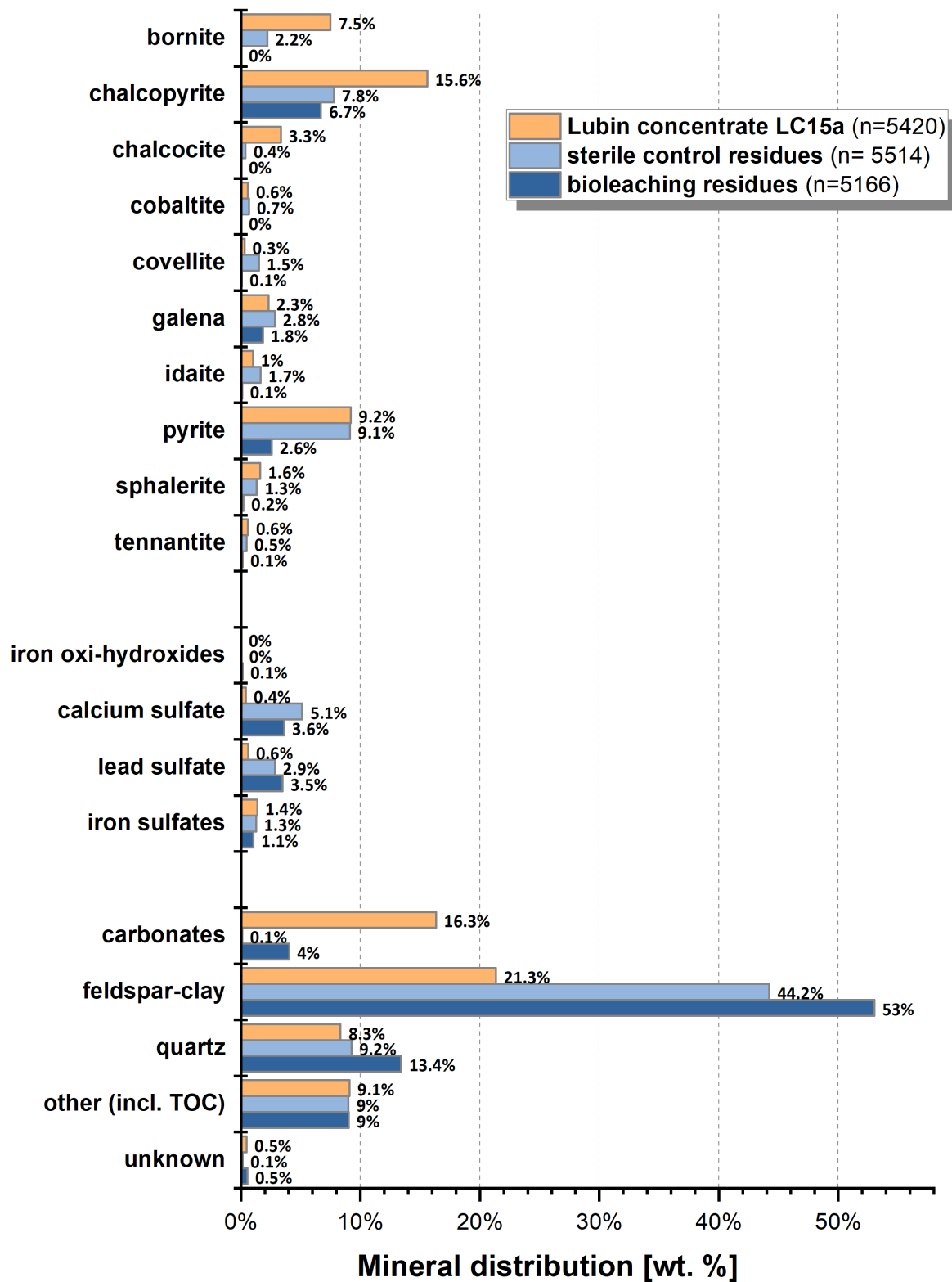
As shown in the previous chapters, bioleaching of flotation copper concentrates extracted from black shale ore was more efficient compared to sterile control leaching. Flotation concentrates generated in the mineral processing plant in Lubin, Poland, are produced by a mixture of several ore-bearing rock types (see Chapter 2.1) The mineralogical composition of the Lubin flotation concentrate LC15a in Chapter 3.2.8.1 revealed that the sulphide assemblage extracted in LC15a was enriched by almost all sulphides commonly associated with Kupferschiefer-type deposits, whereas concentrates extracted from Rudna and Sangerhausen black shale contained sulphide associations more pronounced to individual sulphide minerals.

Figure 3.3.22 shows that the proportion of sulphides differed substantially between bioleaching residues and sterile control residues. While in the bioleaching residues a total sulphide portion of 11.7% remained, the proportion in the sterile control residues was significantly, almost three times, increased (28.0%), which indicated that only a quarter of sulphides originally contained in the concentrate was dissolved.



**Figure 3.3.22:** Pie charts indicating the proportion of sulphides and gangue minerals in Lubin concentrate LC15a and related leaching residues. (Data: MLU)

Figure 3.3.23 indicates that Lubin concentrate LC15a was enriched in chalcopyrite (15.6%), pyrite (9.2%) and bornite (7.5%). The proportion of sulfides in the bioleaching residue of LC15a was dominated by chalcopyrite (6.7%), pyrite (2.6%) and galena (1.8%). Other copper sulphides such as



**Figure 3.3.23:** Distribution of sulphides, sulphates and gangue minerals in the Lubin concentrate LC15a in comparison with the bioleaching as well as sterile control leaching residues.

bornite and chalcocite were completely dissolved, but very low quantities of covellite and idaite (each 0.1%) were detected in the bioleaching residue. Sphalerite and tennantite were dissolved to a large extent and remained likewise as traces in the bioleaching residues, whereas the low content of copper and nickel containing cobaltite in the concentrate was completely leached.

In comparison, the residues of sterile control leaching hosted higher quantities of chalcopyrite (7.8%) and also incomplete leached bornite (2.2%). A relative enrichment of idaite (1.7%) and covellite (1.5%) regarding the concentrate feed was apparent and was supposed to be caused by secondary formation during the leaching. Galena (2.8%) was also relatively enriched to more than 50%, which was attributed to the changing overall mass balance from the initial mineral content in the feed to the remaining mineral phases in the leaching residues. The residues of sterile control leaching contained additionally comparably increased portions of sphalerite (1.3%) and tennantite (0.5%). Also, the increased content of pyrite (9.7%) corresponded to the low dissolution in the sterile control leaching tests and pertained as well cobaltite (0.7%) that was determined equally in the feed. Thus, some of the sulphides were resistant in terms of abiotic leaching with sulfuric acid.

Considering the distribution of gangue-type minerals and mineral groups, it is obvious that the bioleaching residues contained generally higher proportions of these minerals. They represented nearly 90% of the bioleaching residues, in which some mineral phases are considered as undissolved constituents of the original feed concentrate. Other mineral groups were formed exclusively secondary within the leaching process. Leaching resistant minerals had comprised mainly quartz and minerals of the feldspar-clay group. For these minerals, the bioleaching residues showed an intense relative enrichment, which is due to the higher proportion of dissolved sulphides in regards to the total mineral mass balance. The bioleaching residues were dominated by 53.0% of minerals of the feldspar-clay group, in which feldspars (8.4%) and illite (34.8%) prevailed next to some other clay minerals (biotite, muscovite, and kaolinite). Furthermore, it contained 13.4% quartz and 4.0% carbonate minerals (calcite). The proportion of primary gangue minerals in the sterile control residues was generally lower and included 44.2% minerals of the feldspar-clay group (31.3% illite; 10.9% feldspars), 9.2% quartz as well as traces of calcite (0.1%).

Secondary mineral phases formed in both leaching residues were mainly calcium (gypsum) and lead (anglesite) sulphate. Generally, the bioleaching residues hosted a slightly higher amount of lead sulphates (5.1%) and some lower content gypsum of (4.0%) in comparison to the sterile control leaching residues (5.1% calcium sulfate; 2.9% lead sulfate). Iron oxi-hydroxides were found in traces, whereas the occurrence of low quantities (avg. 1.3%) of iron sulphates containing partly increased concentrations of Cu, Zn, Pb was detected coequal in the feed and both leaching residues.

Additionally, substantial amounts of covellite were formed during sterile leaching and thus the residues were accordingly enriched.

#### 3.3.4.2.3.2 Metal content, metal and mineral recovery

The source material for the leaching tests represents a flotation concentrate gained in the production line of the mineral processing plant in Lubin, Poland. The concentrate was generally enriched in base metals, Cu (13.70%), Fe (9.84%), Pb (4.49%) and Zn (1.20%), but also contained significantly amounts of Co (1480 ppm), As (4230 ppm) and Ag (707 ppm), which were generally increased in Lubin concentrates examined in this study.

**Table 3.3.12:** Element concentration of base metals and selected trace metals in the copper concentrate LC15a as well as the residues of bioleaching and sterile control leaching tests. (Data: ALS)

Element	Cu	Pb	Zn	Fe	Ag	As	Co	Mo	Ni	V
	%	%	%	%	ppm	ppm	ppm	ppm	ppm	ppm
<b>Concentrate LC15a</b>	13.70	4.49	1.26	9.84	707	4230	1480	361	606	766
<b>Sterile control residues</b>	6.39	5.75	0.87	7.03	695	3820	1060	330	291	119
<b>Bioleaching residues</b>	2.06	6.80	0.39	2.80	902	961	79	258	105	142

Table 3.3.12 displays the metal content of copper concentrate LC15a as well as sterile control and bioleaching residues. Both residues showed strong differences regarding their metal content. Generally, the bioleaching residues was marked by a decreased content in nearly all listed metals, except Pb, Ag and V that were analysed with lower concentrations in the sterile control leaching residues. Cu- and Fe-content in the bioleaching residues (Cu: 2.06%, Fe: 2.80%) were decisively lower compared to the sterile control residues (Cu: 6.39%, Fe: 7.03%). Moreover, bioleaching residues were also characterized by lower concentrations of other metals (Zn, As, Co, Ni), especially in respect to Co (79 ppm vs. 1480 ppm in the feed concentrate). Pb and Ag were enriched in both residues, but occurred more increased in the bioleaching residues.

According to the metal contents in bioleaching and sterile control leaching residues, recovery rates for base metals and associated metals are summarized in Table 3.3.13. In regards to the overall balance, bioleaching achieved the highest recovery rates compared to sterile chemical leaching. Strong differences regarding the leaching efficiency were observed for Cu, Zn and Fe amongst the base metals and in addition for As, Co and Ni for trace metals. While at least two-third of the respective metal were recovered by bioleaching, the leaching rates in the sterile control leaching tests were very limited and exceeded just for few metals the one-third level. Cu, for instance, was leached to more than 50% (85% by bioleaching) and also V showed high recovery rates, which were very similar for both leaching experiments. In particular, Fe and Mo were marked by low recovery rates by sterile leaching, which was apparently attributed to very low dissolution of pyrite (see Table 3.3.14). The increased recovery of As, Ni and Co by bioleaching could be achieved by the advanced dissolution of pyrite and additionally of cobaltite that was contained accessorially in the concentrate feed. The recovery of Mo was generally low, but moderately increased by bioleaching (29% vs. 9% by sterile control leaching). Best recovery rates among the leaching tests of copper concentrates were achieved for V by as well bioleaching as sterile control leaching, which was also observed for the bioleaching tests performed on LC15b (see Chapter 3.3.4.2.5.2).

**Table 3.3.13:** Comparison of metal recovery rates generated by sterile control leaching and bioleaching of LC15a..

Metal recovery	Cu	Pb	Zn	Fe	Ag	As	Co	Mo	Ni	V
<b>Sterile control leaching</b>	53%	-28%	31%	29%	2%	10%	28%	9%	52%	84%
<b>Bioleaching</b>	85%	-51%	69%	72%	-28%	77%	95%	29%	83%	81%

**Table 3.3.14:** Percentual recovery of common metal sulphides by sterile chemical leaching and bioleaching of Lubin copper concentrate LC15a. (Data: MLU)

Mineral recovery	bornite	chalcopyrite	chalcocite	pyrite	galena
Sterile control leaching	61%	-64%	77%	28%	43%
Bioleaching	100%	69%	94%	37%	37%

Table 3.3.14 shows the leaching rates for sulphides in sterile control leaching and bioleaching tests with Lubin concentrate LC15a. Chalcocite and bornite were partially dissolved reaching a two-third recovery yield by sterile control leaching, which also caused the lower dissolution of pyrite. The recovery of galena was relatively equal in both leaching experiments. Bioleaching caused a complete recovery of bornite as well as an almost complete dissolution of chalcocite. Pyrite was dissolved in a equal extend by both leaching tests reaching recovery rates of 37% by bioleaching and 28% by sterile control leaching. However, the dissolution yield of chalcopyrite was quite different. While chalcopyrite was relatively enriched by sterile control leaching, the leaching yield was significantly improved by bioleaching (69%).

#### 3.3.4.2.4 Bioleaching residues of flotation concentrate LCA06, Lubin, Poland

##### 3.3.4.2.4.1 Mineral distribution

Bioleaching batch tests were carried out on a second sulfide concentrate sample (LCA06) originating from the Lubin concentrator, Poland. Prior to bioleaching, the copper concentrate was treated with sulfuric acid in order to reduce the carbonate fraction significantly. Microscopic investigations had shown that the concentrate hosted alteration products mainly manifested by occurring sulphates that were formed as a consequence of sulphide oxidation favoured by acid pre-treatment.

The mineral distribution of the acidified concentrate LCA06 and the corresponding bioleaching residues in Figure 3.3.25 shows that 33.9% of concentrate LCA06 consists of sulphides (Figure 3.3.24). Generally, the sulphide mineral assemblage of the copper concentrate LCA06 consisted mainly of bornite (8.0%), chalcopyrite (6.1%), and chalcocite (5.9%). Lower contents for copper-bearing sulphides were determined for idaite (1.3%) and covellite (1.5%). Pyrite (7.2%) and moderate contents of galena (1.6%) as well as accessorially sphalerite (0.6%) and tennantite (0.9%) represented other sulphides in the LCA06 concentrate. For a detailed mineral distribution analysis is referred to Chapter 3.2.8.1.

Generally, bioleaching residues of LCA06 consisted of 11.8% sulphides (see Figure 3.3.24) and contained mainly pyrite (4.9%), galena (3.3%) and chalcopyrite (1.3%), whereas galena has relatively

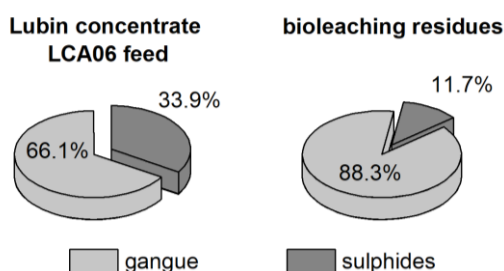


**Figure 3.3.24:** Proportion of sulphides and gangue minerals in Lubin concentrate LCA06 and related bioleaching residues. (Data: MLU)

enriched due to changes of mineral mass balance by selective leaching of mineral phases of the bioleaching process. Traces of bornite (0.6%), covellite (0.3%) and tennantite (0.1%) represented a subordinate part of the sulphide assemblage of the bioleaching residues.

The fraction of gangue minerals was dominated by feldspar-clay group minerals (total: 53.5%; illite: 28.7%; feldspars: 18.9%) and quartz (13.1%), whereas the low portion of carbonate minerals in the feed concentrate was dissolved almost completely. Sulphate phases, in particular calcium as well as base metal sulphate, occurred in the copper concentrate and its bioleaching residues, respectively. While iron-dominated sulphates were present in nearly equal concentration in the concentrate LCA06 (3.1%) and bioleaching residues (2.5%), lead sulphate (4.2% vs. 1.2%) was particularly enriched in the latter, which contained calcium sulphate with slightly lower proportion (1.1%) compared to concentrate LCA06 (Ca-sulphate: 2.2%).

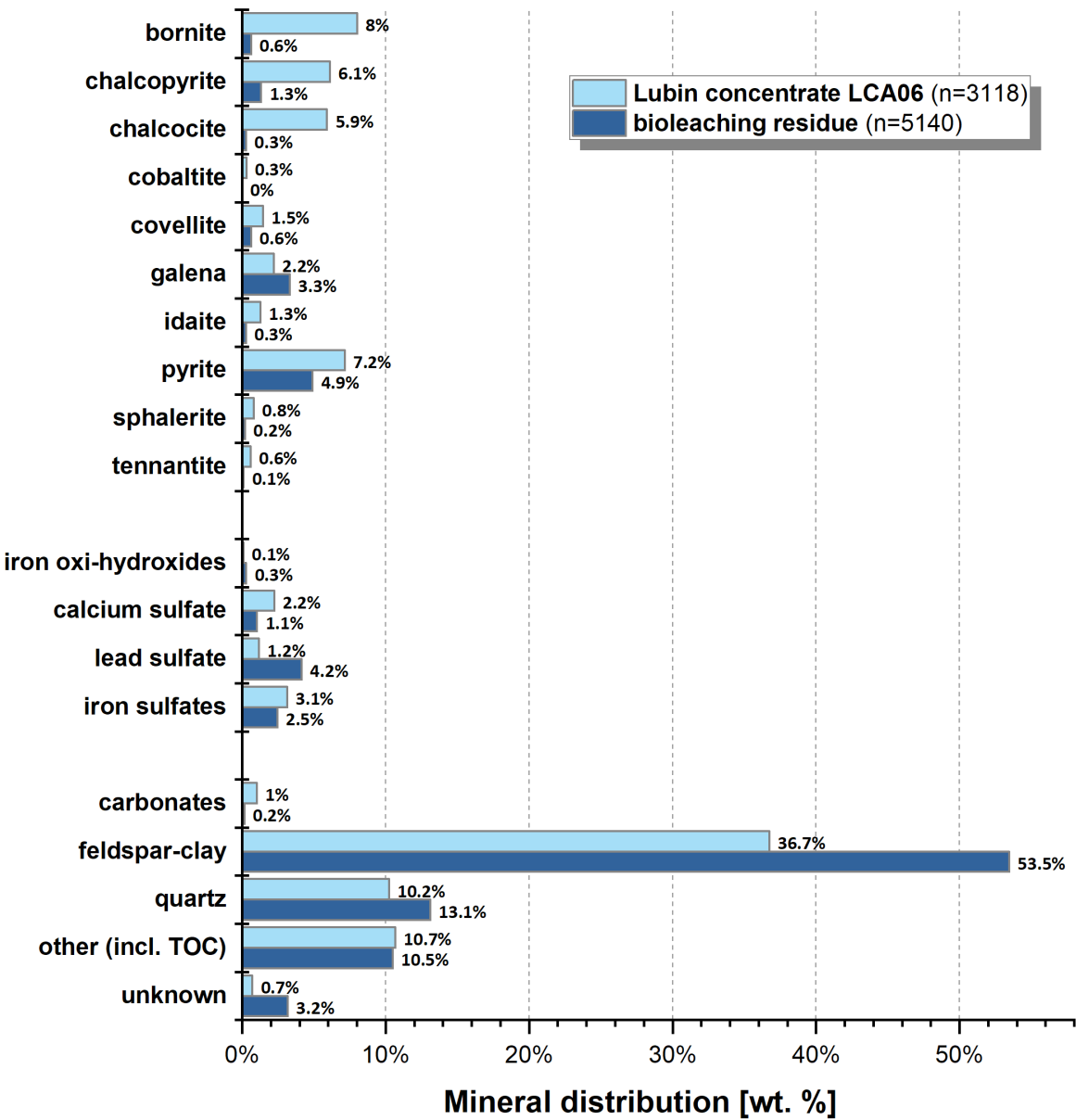


**Figure 3.3.25:** Mineral distribution of Lubin concentrate LCA06 in comparison to the bioleaching residue. (Data: MLU)

### 3.3.4.2.4.2 Geochemical composition, mineral/elemental recovery

The copper concentrate LCA06 originating from the Lubin mineral processing plant was characterized by a slightly increased Cu-content (14.70%) in comparison with the copper concentrate LC15a (13.70%), but had considerably lower amounts of Pb, Zn and Fe (see Chapter 3.2.8.2). Also trace metal amounts were slightly lower as in concentrate LC15a. Table 3.3.15 shows that the bioleaching residues were marked by a strong reduced Cu-content (1.23%), although the Fe-content was decreased moderately, Pb occurred notably enriched in the bioleaching residues. Among the trace metals, Ag, Mo and V showed increased contents in comparison to the source concentrate indicating a low recoverability by bioleaching. The content of other trace metals were moderately lower (As, Mo, Ni, Sb), whereas the content of Co was strong reduced regarding the feed.

**Table 3.3.15:** Selected metal elements in the Lubin concentrate LCA06 and the corresponding bioleaching residues. (Data: ALS)

Element	Cu	Pb	Zn	Fe	Ag	As	Co	Mo	Ni	Sb	V
	%	%	%	%	ppm	ppm	ppm	ppm	ppm	ppm	ppm
<b>Lubin concentrate LCA06</b>	14.70	2.86	0.44	6.47	782	2596	1059	279	455	87	550
<b>Bioleaching residues</b>	1.23	4.20	0.26	4.49	1072	1452	168	382	355	79	760

Table 3.3.17 displays the metal recovery achieved by the bioleaching experiments carried out on copper concentrate LCA06. While Cu was nearly complete extracted, the recovery rates for Zn (41%) and Fe (31%) indicated to a limit dissolution yield of respective minerals. Other metals as Pb, Ag, Mo and V showed enrichments in the bioleaching residues and could not be extracted successfully. However, the leaching efficiency for Co (84%) was high, while As, Ni and Sb were leached from moderately to low, in that order. The high recovery yield for Co correlated with the complete dissolution of cobaltite, which was contained accessorially in concentrate LCA06.

**Table 3.3.16:** Recovery rates for sulphides attained by bioleaching experiments on copper concentrate LCA06. (Data: MLU)

Mineral recovery	bornite	chalcopyrite	chalcocite	covellite	idaite	pyrite	sphalerite	galena
<b>Bioleaching</b>	92%	78%	95%	56%	79%	31%	74%	-51%

According to the mineral distribution analysis of concentrate LCA06 and its bioleaching residues, the recovery of sulphides is given in Table 3.3.16. The recovery rates for copper sulphides were generally high, in particular bornite and chalcocite were nearly completely extracted. The proportion of recovered chalcopyrite and idaite ranges to 80%, while covellite had a markedly lower recovery rate (59%) possibly by secondary process-related formation. The low content of sphalerite in the concentrate was dissolved considerably (74%) by bioleaching, while the recovery of pyrite (38%) was significantly lower (31%). Galena occurred relatively enriched in the bioleaching residues, thus, a recovery could not be detected.

**Table 3.3.17:** Metal recovery by bioleaching of Lubin concentrate LCA06.

Metal recovery	Cu	Pb	Zn	Fe	Ag	As	Co	Mo	Ni	Sb	V
<b>Bioleaching</b>	92%	-47%	41%	31%	-37%	44%	84%	-37%	22%	9%	-38%

#### 3.3.4.2.5 Analysis of residues from bioleaching tests with increasing retention times on flotation concentrate LC15b

In order to quantify leaching efficiency and recovery rates of bioleaching experiments and their implementation to technical use it is important to know the process flow of value minerals as accurately as possible. This study comprised an advanced mineral characterization in order to trace mineralogical mass balances within the bioleaching process and further to assess the efficiency for the treatment of the complex ores. Therefore, five bioleaching residues sampled after defined process retention time (1, 2, 4, 7, 10 days) and the source copper concentrate (LC15b, 2015) from the Lubin mineral processing plant in Poland were investigated regarding their mineral distribution. For detailed information of the experimental set-up is referred to Chapter 2.2.3.

##### 3.3.4.2.5.1 Mineral distribution

The copper concentrate LC15b represented a subsample of a bulk sample (3.8 t) of the copper concentrate LC15 delivered 2015 from the processing facilities of KGHM Polska Miedź S.A. to the mineral processing laboratories of BRGM (for details see Chapter 2.1).

Generally, concentrate LC15b consisted of a similar mineral composition as determined in LC15a. It was particularly enriched in chalcopyrite (15.3%) and contained moderate amounts of bornite (5.2%) and chalcocite (3.2%). In comparison to the mineral composition determined for Lubin concentrate LC15a, slightly lower amounts of bornite, pyrite and idaite were detected and gangue minerals such as carbonates and quartz showed increased proportions (see Chapter 3.2.8.1).

The investigation of bioleaching residues revealed information of the chronological leaching performance of specific sulphides. The mineral distribution analyses, depicted in Figure 3.3.26, showed that after two days of the experiment the content of bornite and chalcocite was decreased significantly, while a decidedly smaller proportion of chalcopyrite was dissolved. Moreover, the main decrease of bornite and chalcocite, the latter more intense, took place during the first day of leaching. Opposite to that, the low content of covellite (0.3%) in concentrate was rapidly increased by secondary formation to 1.3% during the first day of leaching. But thereafter, the amount of covellite decreased constantly in the further course of the experiment and was leached completely after ten days. A similar initial and rapid enrichment was detected for idaite that showed a low content (0.5%) in the concentrate feed, but was enriched continuously up to the fourth day (1.6%) and was then dissolved nearly completely (0.2%) to the end of the bioleaching test. A uniform decrease was determined for pyrite, which was largely dissolved to a remaining amount of 0.7% in the final bioleaching residues (day 10). A rapid decrease after the first day of the bioleaching test was also determined for sphalerite, for which the content was 50% reduced from 1.8% to 0.9%. In the further course of the experiment the content of sphalerite was continuously decrease up to 0.5% at the end of the bioleaching test. Galena in turn, showed a strong decrease in the beginning of the experiment, but was enriched steadily up to the end of the bioleaching test. Tennantite, which occurs often in concentrates gained from Kupferschiefer"-type black shale ores as associated sulphide, was slightly enriched in the feed material (1.0%) and dissolved rapidly during the first day and completely after the total leaching test time.

The feed concentrate consists of 63% of gangue minerals, usually assigned to. This portion of the sample was dominated by feldspar and clay minerals (21.8%), carbonates (17.6%) and quartz (10.0%). Further details of the mineral distribution regarding gangue minerals in concentrate LC15b is given in chapter 3.2.8.1. The portion of gangue minerals changed significantly during the bioleaching test especially for carbonates and minerals in the feldspar-clay group. While carbonates, mainly dolomite

and calcite, were dissolved immediately after the beginning of the experiment by the addition of sulfuric acid, clays and feldspars were enriched progressively during the test run. The main phases compiled under the feldspar-clay-group were illite-type clays, their proportion was steadily growing from 15.6% in the concentrate to 48.0% in the final bioleaching residues. The second most common mineral assigned to this group was potassium feldspar, which was enriched from 4.4% to 10.6% during the entire bioleaching test run. Strong increase of secondary, process-induced mineral formations was remarkably observed for calcium sulphate, which was formed substantially short after the beginning of the bioleaching test. After the first day, 17.4% of the residues consisted of calcium sulphates, increased to 19.4% after the second day and decreased rapidly to 10.2% after the fourth day, whereas the content increases again towards the end of the bioleaching test (15.2%). Mineral phases formed secondary by bioleaching were mainly sulphates. Besides calcium sulphate, lead sulphates, iron sulphates and sulphates with varying metal content, mainly Cu, Fe and Zn-dominated, were detected in the bioleaching residues. While the content of lead sulphates increased continuously from 1.2% in the initial concentrate feed to 3.5% in the bioleaching residues after the entire test run, the metal-bearing sulphates were formed to a lower extent and were dissolved decisively towards the end of the experiment. The various bioleaching residues contained also traces of rutile and some barite.

### 3.3.4.2.5.2 Geochemical composition, metal and sulphide recovery

The copper concentrate LC15b was characterized by an increased content of Cu (13.45%) as well as moderate contents of Pb (4.05%) and Zn (1.26%). Generally, the amount of base and trace metals was comparable to concentrate LC15a. Figure 3.3.27 and Table 3.3.18 display the change of the metal content in the bioleaching residues after defined dwell times in the bioreactor. A progressive decrease of the amount of the most metals was noticed, except for Pb and Ag, which were enriched relatively during the bioleaching experiment. The geochemical data showed that the decrease of the Cu-content

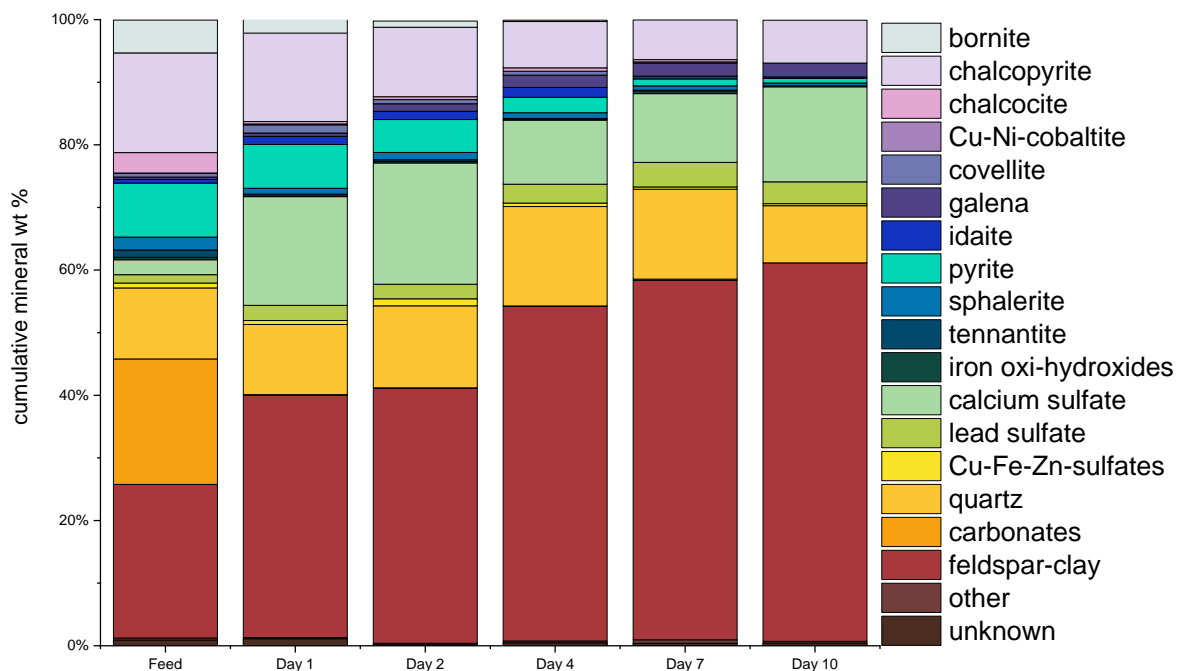


**Figure 3.3.26:** Stacked column plot illustrating the shift of the mass balance of mineral from the LC15b concentrate feed over bioleaching residues taken on distinct retention times during and after the bioleaching test. In particular, proportional changes for chalcocite, chalcopyrite, pyrite, carbonates and minerals of the feldspar-clay group are very obvious. For detailed explanation see text. (Data: MLU)

took place especially during the first two test days, after that 5.67% Cu from the initial Cu-content (13.45%) remained in the bioleaching residues. In the following course of the bioleaching test, which continued over eight more days, only about 3% Cu were leached additionally. At the end of the experiment 2.84% remained in the bioleaching residues. A similar reduction was observed for the Fe-content, which was reduced after two days from 9.76% to 6.46%, but the decrease slowed down towards the end of the experiment and 2.45% Fe remained in the final residues. The significantly decrease of the content during the first two days was also conspicuous for the trace metals, from which Co, Ni, Sb and V showed the strongest decline. The greatest decrease over the total time of the bioleaching test was noticed for Co.

According to the geochemical data, the recovery of selected metals was calculated. The recovery rates for the individual metals are listed in Table 3.3.19. It revealed that after two days of bioleaching nearly 60% of Cu was dissolved. The recovery yield was improved significantly up to the seventh day (77%), but in the remaining test period slightly more Cu could be extracted (79%). In the case of Fe, the main part was extracted up to the fourth day (63%) and similar as Cu, the recovery was further noticeable improved up to the seventh day, whereas during the last three days of the experiment only a marginally increase of the Fe-recovery took place. The greatest proportion of the recovery of Zn was also achieved until the fourth day of the experiment, up to that time 50% of Zn was extracted. A moderate increase of the recovery followed up to the seventh day (64%), but in the remaining course of the experiment just 3% of Zn were recovered additionally. Also in respect to trace metals, a significant increase of the recovery could not detected after the fourth day of the experiment. However, the entire portion of recoverable V was extracted at the beginning of the bioleaching test. Co, which showed the highest final recovery rate generally, was recovered to 53% after two days and reached a nearly complete recovery (93%) after four days. Just 3% Co were additionally extracted in the six following days of the experiment. Mo, which showed the overall recovery rate of 60%, was

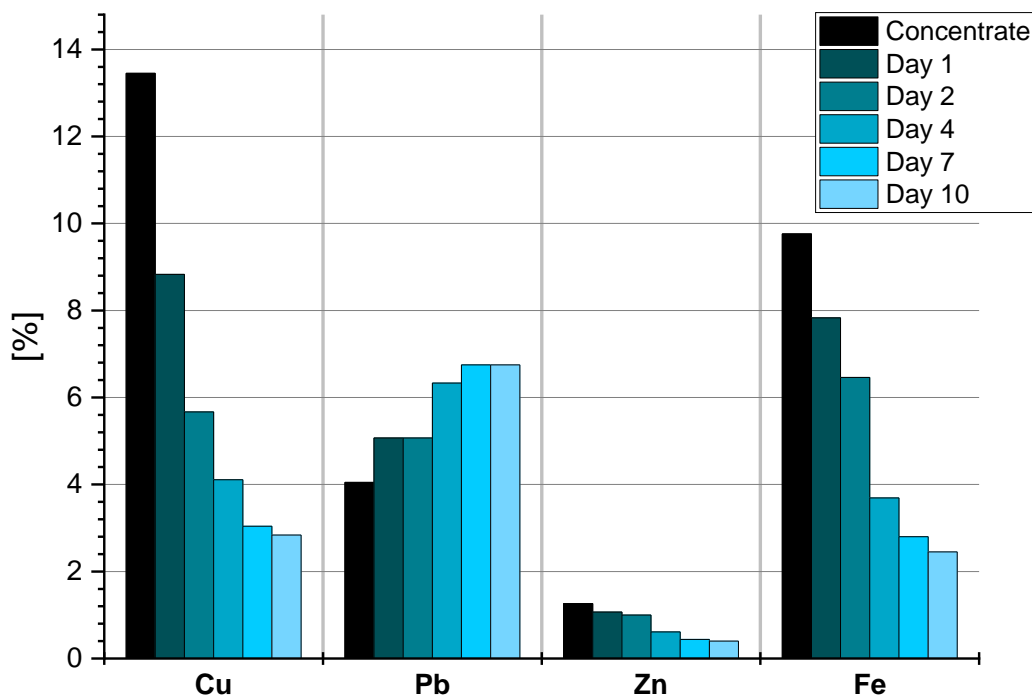


**Figure 3.3.27:** Gradual change of base metal content in bioleaching residues after progressively increasing retention times in the process solution. (Data: ALS)

**Table 3.3.18:** Base and trace metal contents in the feed concentrate LC15b and bioleaching residues sampled after increasing retention times. (Data: ALS)

Element	Cu	Pb	Zn	Fe	Ag	As	Co	Mo	Ni	Sb	V
	%	%	%	%	ppm	ppm	ppm	ppm	ppm	ppm	ppm
<b>Concentrate LC15b</b>	13.45	4.05	1.26	9.76	636	4230	1480	361	606	112	766
<b>Day1 residues</b>	8.83	3.85	1.07	7.83	721	3820	1025	239	269	73	116
<b>Day2 residues</b>	5.67	5.07	1.00	6.46	799	2470	689	227	211	65	125
<b>Day4 residues</b>	4.11	6.33	0.61	3.69	876	820	105	159	104	67	127
<b>Day7 residues</b>	3.04	6.65	0.44	2.80	914	628	72	159	102	69	137
<b>Day10 residues</b>	2.84	6.75	0.40	2.45	922	586	61	143	104	70	133

mainly extracted over the first four days similar to Ni that had a total recovery yield of 83%, which was extracted after four days bioleaching. Further, a quiet analogous recovery rate was achieved for As, which was steadily increased dissolved up to day four (81%). Subsequently in the remaining six days of the bioleaching experiment just 5% of As were leached additionally.

The mineral distribution analysis of the temporary and final residues of the bioleaching experiment with Lubin concentrate LC15b in Table 3.3.20 shows that several sulphides were dissolved completely or nearly completely. Amongst the copper-bearing sulphides, bornite, chalcocite and covellite were leached fully during the experiment, while a significant portion of chalcopyrite (56%) remained in the final bioleaching residues. Chalcopyrite was recovered increasingly up to the sixth day of the experiment, whereas nearly 90% of chalcocite was dissolved on the first day. Similar fast incipient dissolution was detected for bornite, which was mainly dissolved during the first two days (81%) and nearly completely recovered after day four (96%) of the experiment. Covellite and idaite showed similarities regarding their recoverability during the bioleaching test, both were enriched during the first day of the experiment to be dissolved in turn increasingly in the further course of the experiment. Pyrite, which was one of the main sulphides in concentrate LC15b, was steadily increasing dissolved during the course of the experiment and was finally extracted with 91% recovery. A moderate final

**Table 3.3.19:** Leaching recovery rates for bioleaching residues after defined retention times achieved of the concentrate LA15b.

Metal recovery	Cu	Pb	Zn	Fe	Ag	As	Co	Mo	Ni	Sb	V
<b>Day1 bioleaching</b>	34%	5%	12%	21%	-13%	10%	31%	34%	56%	35%	85%
<b>Day2 bioleaching</b>	58%	-25%	17%	35%	-26%	42%	53%	37%	65%	42%	84%
<b>Day4 bioleaching</b>	69%	-56%	50%	63%	-38%	81%	93%	56%	83%	40%	83%
<b>Day7 bioleaching</b>	77%	-64%	64%	72%	-44%	85%	95%	56%	83%	39%	82%
<b>Day10 bioleaching</b>	79%	-67%	67%	75%	-45%	86%	96%	60%	83%	37%	83%

**Table 3.3.20:** Recovery rates of copper-bearing and associated sulphides by bioleaching of copper concentrate LC15b, determined according to the mineral distribution analyses. (Data: MLU)

Mineral recovery	bornite	chalcopyrite	chalcocite	covellite	idaite	pyrite	sphalerite	galena
Day1	57%	10%	88%	-126%	-222%	18%	53%	72%
Day2	81%	27%	86%	-17%	-123%	38%	42%	44%
Day4	96%	53%	83%	-11%	-169%	71%	55%	-3%
Day7	100%	60%	89%	63%	22%	87%	66%	-8%
Day10	100%	56%	100%	100%	60%	91%	77%	-17%

recovery was detected for sphalerite, which was dissolved mainly during the first 24 hours, whereas a subsequent phase of slightly advanced dissolution followed up to the end of the experiment and a total recovery yield of 77% was attained. While bioleaching caused the disintegration and dissolution of the aforementioned sulphides, galena showed recovery rates at the beginning of the experiment, but after 48 hours a relative enrichment in the bioleaching residues took place and galena remained incomplete dissolved in the final residues.

### 3.3.5 Summary

Bioleaching tests with low-grade copper Mansfeld black shale showed that minor differences in the recovery of metals compared to sterile control leaching existed. Copper sulphides were nearly completely dissolved by both leaching approaches but the recovery of sphalerite was substantially increased by more advanced dissolution of sphalerite by bioleaching.

Also bioleaching tests on copper-rich Sangerhausen black shale confirmed that copper sulphides were dissolved nearly completely, but it was notable that chalcopyrite remained in both, the bioleaching and chemical control experiments. Mineral distribution showed that nearly 50% of chalcopyrite was not dissolved, but sphalerite was completely recovered by bioleaching, but remained to a low amount in the chemical control residues.

The copper-rich concentrate generated by flotation with dextrin and ethanol pre-treated Sangerhausen black shale feed was used for bioleaching tests, which showed clearly more advanced recovery of copper sulphides and pyrite. While the bioleaching residues contained 2.1% Cu, the chemical control leaching residues were marked by significant increased copper content (7.1%). Thus, complete dissolution of bornite and chalcocite was achieved by bioleaching and the dissolution of chalcopyrite was moderately increased (49%) compared to the sterile control leaching (37%).

Similar recovery yields were obtained by the bioleaching of the concentrate extracted by flotation with dextrin and ethanol pre-treated Rudna black shale feed. Bornite and chalcocite were completely dissolved in notable difference to the sterile control leaching. The generally low amount of chalcopyrite in the concentrate (1.0%) was relatively enriched by sterile control leaching, but more advanced dissolved (69%) by bioleaching. Lubin concentrate LC15a comparatively richer in chalcopyrite was used for bioleaching tests and showed similar recovery yields, which were also obtained by bioleaching of Lubin concentrate LCA06.

Mineral distribution analyses on residues sampled after defined process retention time (1, 2, 4, 7, 10 days) in a bioleaching experiment carried out on Lubin concentrate LC15b revealed that the copper recovery was mainly achieved after 4 days leaching time (69%) and that in the following 6 days the copper recovery slowed down to additional 10% till the end of the bioleaching test (79% total copper recovery). After four days bornite was almost completely dissolved, whereas the complete recovery of chalcocite was achieved continuously to the end of the bioleaching test. Chalcopyrite was recovered to slightly more than 50% after four days retention time and a further dissolution was insignificant until the end of the bioleaching experiment (56%). Besides bornite and chalcocite, pyrite was nearly complete dissolved and sphalerite, likewise to pyrite, was continuously recovered to 77% during the course of the bioleaching test.

Key features of bioleaching residues:

- Bioleaching of black shale ore revealed an increased recovery of sphalerite but not for chalcopyrite in comparison to sterile control leaching.
- Almost complete recovery of bornite and chalcocite by bioleaching of copper concentrates.
  - Moderate recovery for chalcopyrite (49%) by bioleaching of the concentrate extracted by flotation with dextrin and ethanol pre-treated Sangerhausen black shale feed.
  - Increased recovery for chalcopyrite (69%) by bioleaching of the concentrate extracted by flotation with dextrin and ethanol pre-treated Rudna black shale feed.
  - Chalcopyrite recovery by bioleaching of Lubin concentrate LC15 was 69% and most increased by bioleaching of Lubin concentrate LCA06 (78%).
- Analyses of bioleaching residues sampled after defined process retention time showed that the main part of soluble copper was dissolved after 4 days leaching time, just 10% were leached in the following 6 days of the experiment.

## Chapter 4 Discussion

The discussion is subdivided into the three main topics comminution, flotation and bioleaching covered in this study and accordingly to the result chapters. Combining granulometry and SEM-based automated mineralogy of processing products, tailings and residues derived from different black shale ores has proven to be powerful means for the characterization of mineralogical and textural physico-chemical information relevant to the mineral processing of Kupferschiefer-type black shale ores. Data from particle size and mineral distribution analyses as well as liberation analyses have been summarized and used to outline the efficiency of mineral recovery by detailed considerations. Advances regarding process optimization and recoverability were demonstrated and physico-chemical mechanism were quoted to explain factors related to improvements but also diminishments caused by a certain mineral dressing method.

### 4.1 Comminution

Black shale ores are generally difficult to treat. In order to introduce these ores to an improved mineral processing route, it is important to use effective processing methods. Comminution, comprising crushing and grinding, is the most cost and energy consuming treatment step in mineral processing. It has been shown that nearly 50% of the overall operating costs in mineral processing plants are caused by comminution to prepare ore feed for subsequent extraction techniques such as flotation (Curry et al., 2014; Herbst et al., 2003; Wills and Napier-Munn, 2005). Consequently, a significant reduction of energy used for particle size reduction is desired to improve the overall balance of mineral processing routes. The following subchapters discuss outcomes of this study in respect to comminution efficiency of black shale ores and mineralogical features as well as liberation of copper sulphides in ball mill and VeRo Liberator® impact crusher products.

#### 4.1.1 Ball milling

##### 4.1.1.1 Mineral specific parameters affecting the grain size distribution and energy consumption of ball mill products from black shale ores

The final stage of the comminution of three different black shale bulk samples was ball milling at a defined product particle size of  $-100\ \mu\text{m}$ . These final comminution products were marked by particle properties obtained by ball milling, which were a crucial prerequisite for subsequent extraction techniques such as flotation and were investigated in detail in the frame of this study.

Key factors in the comminution of mineral mixtures such as rocks or concrete are the tenacity of a certain mineral and its abundance in the feed. Generally, tenacity, in a mineralogical sense, is mainly controlled by hardness, specific density and crystallographic properties. While rock-forming minerals in black shales, namely calcite, dolomite, illite, feldspar and quartz, can be considered to have a similar density (approx.  $2.7\ \text{g/cm}^3$ ), their hardness varies significantly. In particular, quartz (H 7) and illite (H 1-2) represent extreme opponents, which constitute considerable but by varying amounts in black shales. Quartz, feldspar as well as dolomite and calcite can be regarded to act brittle encountered by deformation, whereas illite concerning its crystallographic structure (monoclinic sheet silicate) and its low hardness tend to be flexible and elastic affected by impact or compression forces resulting in elastic rebound or shearing along (001)-oriented basal planes of illite crystals. Thus, an increased content of illite that is mostly intergrown with other gangue minerals as well as sulphides in black shale

ores represents a portion of the feed, which is potentially harder to treat by ball milling. Additionally, organic matter of mainly kerogen II-type and intimately intergrowths of organic matter with illite associated in layered zones that occur intercalated between quartz and carbonate-rich layers commonly present in black shales investigated in this study. The partly considerable amount of organic matter (up to 14.4%) in the ball mill feed supports additionally the elastic behaviour of particles when hit by impacts as well as prevents and increase the resistance of particle breakage, respectively. Carbonates, quartz and to a lesser extend feldspar and sulphides, due to their lower abundance, are common constituents, which contribute by their brittle tenacity to progressive comminution of particles treated by ball milling, whereas illite and organic matters impede the particle size reduction.

Another important feature of the mineralogy in black shale feed intended for comminution represents the prevalent crystal size of minerals. Due to crystal/grain boundaries provide pre-defined breakage zones of intergrown mineral grains, the size of individual crystals and their mono- or polymineralic locking mode influences the breakage behaviour. Multiple intergrowths of various mineral phases result in different states of stress affected by impact forces that cause as well breakage at a distinct area of a particle as that the bonding energy at grain boundaries of mineral crystals cannot be overcome and breakage formation fail. Thus, the grain size of a certain mineral within the rock fabric but also the size of intergrown adjacent mineral grains can affect the process of particle size reduction. Microscopic observations have shown that main mineral constituents that form the rock fabric of black shales consisted of different grain size.

Table 4.1.1 contains compositional, chemical and technical parameters of ball mill products investigated in this study. It shows that the representative maximum particle size ( $D_{80}$ ) of ball mill products from Rudna and Sangerhausen black shale are quite similar (45  $\mu\text{m}$ ) but it is substantially finer-grained (20.4  $\mu\text{m}$ ) in the ball mill product of Mansfeld black shale. Interestingly, this strong deviation was far less pronounced for the lower particle size fraction, especially at  $D_{20}$  as shown in Chapter 3.1.3.1.

Organic matter is an immanent feature of black shales and its content was one of the most striking but also deviated features in black shale ball mill products. Mansfeld black shale feed, a bulk sample

**Table 4.1.1:** Comparison of compositional features and grain size as well as energy consumption of ball mill product from different black shale deposits.

Parameter	Unit	black shale ball mill product		
		Mansfeld	Rudna	Sangerhausen
<b><math>D_{80}</math></b>	[ $\mu\text{m}$ ]	20.4	44.6	45.2
<b>Bond-Index</b>	[kWh/t]	12.8	16.2	18.5
<b>CaO</b>	[%]	12.9	15.7	3.8
<b>SiO<sub>2</sub></b>	[%]	36.2	28.1	38.4
<b>carbonates</b>	[%]	26.1	36.5	6.9
<b>illite/clay</b>	[%]	19.4	20.1	28.5
<b>feldspar</b>	[%]	20.5	8.5	12.4
<b>quartz</b>	[%]	23.3	15.3	21.4
<b>sulphides total</b>	[%]	3.9	11.5	8.7
<b>organic matter</b>	[%]	2.4	7.3	14.4

from a dump, represent a low-grade ore deposited on dump nearly 80 years ago and consisted of lumps extracted underground directly adjacent hanging wall to the main mineralized zone, which is commonly both, richer in sulphides and organic matter. This is the main reason why the organic carbon content in the Mansfeld black shale was comparatively low (2.4%). Increased silica contents in ball mill products, predominantly evoked by quartz and feldspar portions, corresponded clearly to Sangerhausen and Mansfeld black shales, which were though characterized by substantial deviating grain size distributions in the respective ball mill products. Thus, proportions of harder minerals hosted in black shales was not the decisive criterion for the grain size differences in ball mill products, which is also illustrate by the significantly lower proportion of quartz in the Rudna black shale and its coarser grain size distribution in the ball mill product. The content of carbonates can be excluded as well, because Sangerhausen was extremely low in carbonates compared to Rudna black shale, although both ball mill products showed nearly identical particle size distributions by far coarser as in the Mansfeld ball mill product.

While carbonates, quartz, feldspar and sulphides represented the brittle part of constituents in black shales, illite and organic matter can be regarded as elastic counterparts. As Table 4.1.1 indicates, differences in the content of illite/clays among ball mill products were notable but in particular low between Mansfeld and Rudna black shale, whereas the ball mill product of Sangerhausen black shale contained significantly more illite/clay. Thus, the proportion of illite/clay seems not affect solely the grindability of black shale feeds.

A varying main feature of the composition of black shales represented the organic carbon content, which was low in the Mansfeld black shale (2.4%), moderate in the Rudna black shale (7.3%) and extremely increased in the Sangerhausen black shale (14.4%). Microscopic examination of black shale samples revealed that organic matter was often tightly intergrown with illite resulting in finely band-



**Figure 4.1.1:** Common rock fabric of black shales featuring elongated mineral aggregates that consist mainly of anhedral carbonates, quartz and feldspar grains, which are enclosed by differently thick, schlieren-like association of intimately intergrown illite-organic matter bands. (Mansfeld black shale, thin section, plane planar polarisation)

**Table 4.1.2:** Bond Indices for different standard materials widely occur in black shales (from Wills and Napier-Munn, 2007).

<b>Material</b>	<b>Work index [kWh/t]</b>
<b>barite</b>	4.73
<b>dolomite</b>	11.27
<b>graphite</b>	43.56
<b>limestone</b>	12.74
<b>quartz</b>	13.57

like organic-rich layers, which envelop schlieren-like elongated mineral aggregates of different size that consist primarily of carbonate-feldspar-quartz associations (see Figure 4.1.1). These mineral aggregates contained preferentially brittle constituents and can be separated consequently by compression and shear forces easily, whereas areas at the margin of mineral aggregates are marked by intergrowths of brittle constituents with the elastic-acting illite-organic matter association, in which the separation of individual mineral grains cannot be achieved easily due to resilient properties. Thus, primarily the increased content of organic matter associated with increased amounts of illite seem to hinder the grain size reduction by compression and shear forces exerted by ball milling.

Table 4.1.1 lists additionally the Bond Work Indices for ball mill products examined in this study. The determination of the work index after Bond (1952) is a standardized grindability test to characterize the comminution behaviour of mineral feeds and is stated in specific energy consumption used for the comminution of a feed. As Table 4.1.2 indicates, standard work indices for dolomite, limestone and quartz are in a similar range, whereas barite with the same hardness as dolomite or calcite shows the lowest work index, which indicates its strongly developed brittleness. More striking is the extremely high work index for graphite, which is genetically the endmember in the maturity process of hydrocarbons and closely related to black shale-hosted kerogen.

Bond tests of ball mill products of black shale samples from different deposits show that for the comminution of Mansfeld black shale significantly lower energy was consumed (12.8 kWh/t) than for Rudna (16.2 kWh/t) or Sangerhausen (18.5 kWh/t) black shale. Thus, it can be assumed that a considerable amount of kerogen hosted in the rock matrix of black shales mainly influences increased Bond work indices of black shale ball mill products.

Very few data, concerning the relationship between Bond work index and mineralogical properties of black shale feed material can be found in the literature. However, Menard (2011) reported in the frame of the European "ProMine" research project that untreated Lubin black shale used for a microwave-induced comminution study was marked by a Bond work index of 13.8 kWh/t at an organic matter content of 9%. A further comparable Bond work index was reported by Refahi et al. (2009) for grindability tests of a black shale from an Iranian deposit, which yielded in 14.4 kWh/t.

Bond test data of black shale from Polish mineral processing operations were only accessible for run-of-mine mixtures containing predominantly the lithotypes sandstone and dolomite as well as subordinately black shale feed. Saramak et al. (2016) indicated changing Bond work indices at varying

proportion of lithotypes in the feed. While the standard Bond tests for Rudna ore consisting of 47% sandstone, 11% black shale and 42% dolomite yielded in 14.1 kWh/t, the same test protocol applied to Polkowice run-of-mine ore resulted in 11.2 kWh/t at significantly increased dolomite fraction (62%), lowered sandstone portion (26%) and equal portion of black shale. This shows clearly that an increasing carbonate content facilitates the crushability and reduce the energy consumption.

Finally, the kerogen portion of black shales represents an important if not the most crucial feature that decides about to the grindability and thus, to the energy demand necessary to unlock value minerals. This relationship is manifested by Bond indices given for the studied black shale ball mill products, in which the lowest bond index determined for Mansfeld black shale (12.8 kWh/t) correlating with the lowest organic matter content (2.4%) and vice versa the highest bond index (18.5 kWh/t) with the highest organic carbon content (14.4%) in the Sangerhausen black shale. The most increase carbonate and the moderate organic matter content in the Rudna black shale causes lower energy consumption (16.2 kWh/t) as already shown by Saramak et al. (2016).

In addition, the ratio of brittle to elastic constituents in the studied ball mill products determined by mineral distribution analyses can give indications of the grindability of black shale ore feed. While Mansfeld black shale containing the most increased brittle fraction of 77.2% (22.8% elastic) showed the lowest Bond work index (12.8 kWh/t), Rudna black shale was marked by a slightly lower portion of brittle minerals (72.4%), which resulted in an increased Bond work index (16.2 kWh/t). By far the least portion of brittle minerals (53.5%) was determined for the Sangerhausen black shale, which was marked by the most increased Bond work index of 18.5 kWh/t. Thus, the total amount of brittle components represents an additional key factor in regards to the grindability of black shales.

A further parameter regarded to be immanent for comminution represents hardness of constituents in relation to their distribution in the feed. The rock-forming mineral components in black shale ores can be basically subdivided regarding their Mohs hardness into three groups. Common minerals in black shales that possess a high hardness are quartz (H 7) and feldspar (H 6.5), whereas carbonates show a significantly lower hardness (H 3.5-4) and illite together with kerogen can be considered to be soft (H 1-2).

Figure 4.1.2 illustrates the distribution of rock constituents according their hardness. It is well noticeable that Mansfeld black shale contained by far the most increased proportion of minerals with high hardness (> 6) simultaneous with the lowest portion of soft components. The content of the latter was slightly increased in Rudna black shale, which is, however, dominated by components with moderately hardness, mainly carbonates, and mechanically more resistive constituents occurred subordinate. As shown above, the Sangerhausen black shale is rich in illite and organic matter, thus, it is dominated by soft constituents (H < 2) but hosts simultaneous a considerable proportion of components with high hardness. Sangerhausen black shale is accordingly marked by elastic-acting constituents and additionally by a considerable part of mechanically resistive components, which is expressed by a relatively coarse-grained ball mill product and the most increased Bond work index among the examined black shales.

Rudna black shale contains significantly higher portion of moderately hard components accompanied by an increased content of organic matter, so that particle size reduction was mainly controlled by the mechanical properties of carbonates, which are comparatively significantly softer than quartz and feldspar. The elevated content of organic matter, hindering particle breakage, result

obviously in a similar grain size distribution of the ball mill product in comparison to Sangerhausen black shale but at lower energy consumption.

The lowest content of organic carbon determined in Mansfeld black shale seems to justify the lowest energy consumption expended by ball milling. However, a large part of the constituents represents minerals (quartz, feldspar) with hardness > 6, which usually result in an increase of the energy consumption of feed material being comminuted. As Gent et al. (2012) have shown, the hardness of minerals affect the Bond work indices proportionally, which result in increase of the energy consumption by increased proportion of harder minerals.

The grain size distribution of comminution products is also a function of properties of the incipient feed in terms of rock fabric and grain size of mineral constituents. Apparently, the mineral size in feed influences both, the energy used to reduce particles size and also the grain size distribution in the comminution product. Due to its origin, Mansfeld black shale represents a low-grade ore extracted from a waste dump, which commonly contained the leavings of mining. In particular, leavings of black shale in the Mansfeld-Sangerhausen mining district represented usually the upper part of the black shale layer considered to be low in mineralization and thus deposited on dump. It is known that sedimentological black shale in the upper part of the Mansfeld basin contains low portion of organic matter (< 5%) and that the carbonate content increases towards hanging wall Werra limestone significantly. Generally, grain size distribution data of rock samples of the basal Zechstein unit are not available and thus, a reliable evidence cannot be executed but the assumption that the grain size of mineral constituents in Mansfeld black shale was generally lower than in the other black shale investigated in this study could interpret the significantly lower grain size of the Mansfeld black shale ball mill product and its low energy consumption.

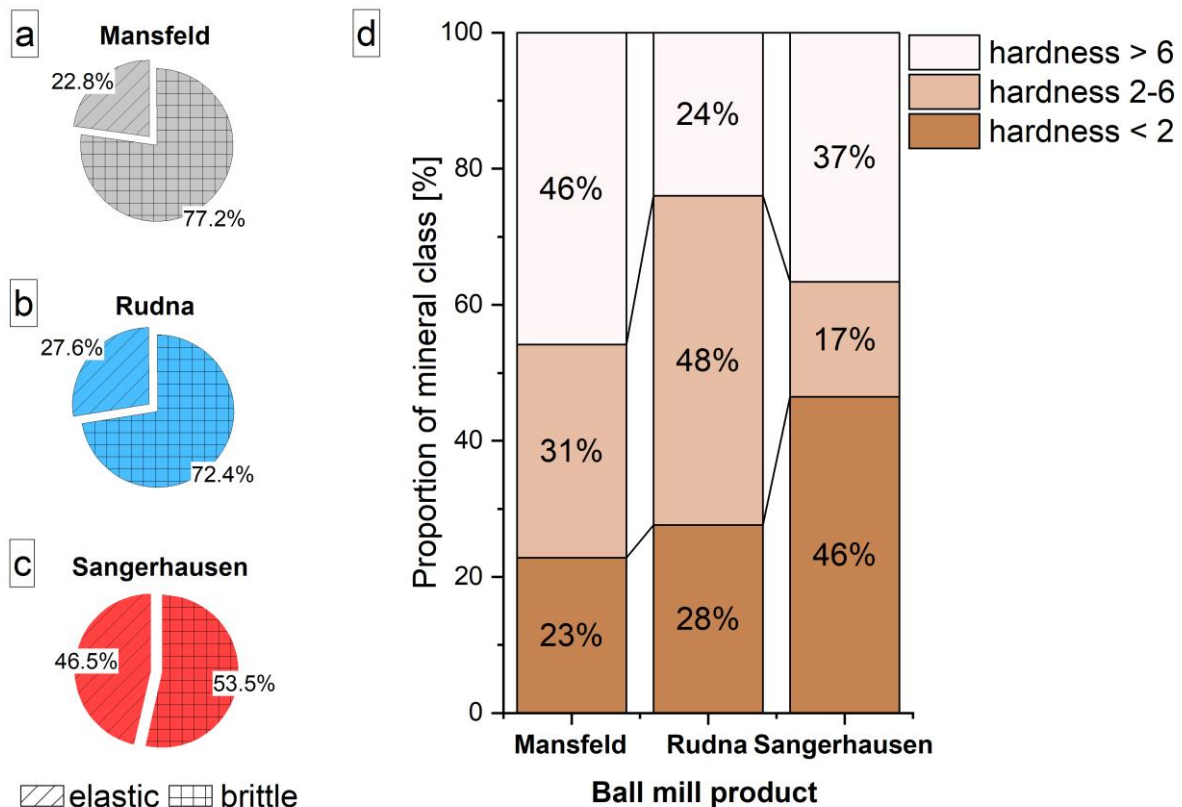


**Figure 4.1.2:** Distribution of brittle and elastic minerals (a-c) as well as distribution of hardness classes according to mineral hardness (d) in ball mill products of different black shale ores.

#### 4.1.1.2 Textural properties and mineralogical associations of copper sulphides in ball mill products of black shale ores

Incomplete particle liberation of value minerals is a major challenge affecting many subsequent extraction techniques, e.g. direct heap/ tank leach, or classic separation methods such as froth flotation. Currently, incomplete particle liberation of complexly intergrown and extremely finely intergrown raw materials is dealt with by ultra-fine grinding, which increases the energy consumption drastically and, in many cases, leads also to overgrinding. Especially liberated and partially liberated (middlings) value minerals are of economic interest due to the recoverability in downstream extraction processes. Thus, mineral liberation data of value minerals represent fundamental parameters taken into account for the optimization in modern mineral processing plants.

##### 4.1.1.2.1 Liberation of copper sulphides

Liberation analyses of copper sulphides (bornite, chalcocite and chalcopyrite) in ball mill products of different black shale ores have shown that the performance to unlock of these value minerals was different and ranged generally from moderate to almost no liberation.

Figure 4.1.3 shows that more advanced liberation of copper sulphides occurred in ball mill products of Mansfeld and Sangerhausen black shale indicated by partly increased proportions of liberated copper sulphides, exclusively over 10%, as well as additionally moderate amounts of middlings. In particular, bornite in the ball mill product of Mansfeld black shale was more liberated (24%, 32% middlings) but also chalcopyrite in the ball mill product of Sangerhausen black shale was marked by increased liberation (19.3%, 36.8% middlings).

Moderate liberation was achieved for chalcocite (11.7%, 30% middlings) and chalcopyrite (12.4%, 23.5% middlings) in the Mansfeld black shale ball mill product. Milled Rudna black shale hosted generally low to moderate liberated copper sulphides (bornite: 11.8% liberated, 31.7% middlings; chalcocite: 3.4% liberated, 12.1% middlings; chalcopyrite (6.4% liberated, 10.0% middlings), whereas

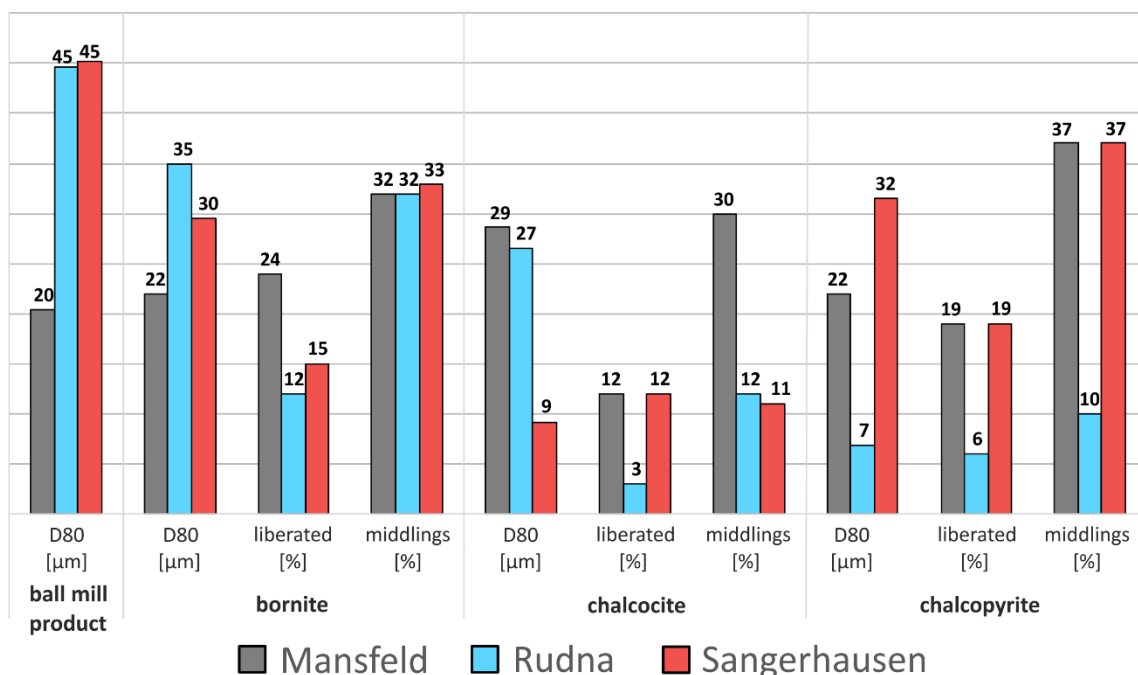


**Figure 4.1.3:** Column chart illustrating the proportions of liberated bornite, chalcocite and chalcopyrite and their middlings in ball mill products of different black shale ores.

the degree of liberation in the ball mill product of Sangerhausen black shale was considerably increased (bornite: 15.0% liberated, 33.0% middlings; chalcocite: 12.1% liberated, 10.7% middlings).

Generally, can be stated, liberation data of the examined ball mill products reveal that the degree of particle size reduction by ball milling was not sufficient to unlock the main part of target minerals successfully, which remained deficient liberated (<30% free surface) or even not exposed (0% free surface). Moreover can be declared that the proportion of copper sulphides potentially recoverable by mineral extraction methods was mostly below 50% and even lower at 25% (addition of liberated and middlings portions in Figure 4.1.3), which indicates that at least 50% of the value minerals are potentially lost in subsequent processing steps due to low liberation. Additionally has to be considered that even the proportion of middlings is not fully recoverable so that it is a common approach to separate the fraction of middlings and recharge it to a further comminution step in order to achieve improved liberation of target minerals (Wills and Napier-Munn, 2005).

Granulometric data of copper sulphides and total ball mill products in Figure 4.1.3 show that the general  $D_{80}$  grain size of ball mill products often not lasts to meet grain sizes of copper sulphides. However, it shows further that the explicit finer ball mill products of Mansfeld black shale correlates with generally enhanced liberation indicated by increased portions of liberated copper sulphides and/or middlings. The fineness of copper sulphides in comparison to a coarser ball mill product causes in particular a lower liberation in the ball mill product of Rudna black shale. It is obvious that the lower the difference of the grain size of copper sulphides to the grain size of the ball mill product the more increased is the liberation.

Detailed investigations of the distribution of liberated copper sulphides within particle size classes have additionally shown that liberated copper sulphides predominantly occurred in the particle size class  $-10\ \mu\text{m}$  and that their portion fades out rapidly up to the particle size class  $-30\ \mu\text{m}$ . This shows clearly that ball milling produces liberated copper sulphides partly decidedly more fine-grained than their initial grain size as shown in Chapter 3.1.3.1. The prevalent fineness of liberated copper sulphides in ball mill products in comparison to their general grain size point to preferential intragranular breakage of particles by two point loading usually caused by ball milling, which forms very fine-grained liberated fragments of copper sulphides but grain boundaries of sulphides to gangue minerals can obviously not activated for fracture formation and propagation.

This conclusion is in particular applicable for bornite to all ball mill products. However, liberated chalcocite occurred exclusively in  $-10\ \mu\text{m}$  particle size classes, although its representative grain size in Rudna and Mansfeld ball mill products was considerably more coarse-grained. Liberated chalcopyrite in the Mansfeld ball mill product was similar distributed exclusively in the  $-10\ \mu\text{m}$  particle size class, which indicates that liberation is accompanied by grain size reduction of chalcopyrite. The distribution of liberated chalcopyrite in the ball mill product of Sangerhausen black shale was more extensive within the  $-30\ \mu\text{m}$  particle size fraction and even significantly increased exemplarily within the  $-80\ \mu\text{m}$  particle size class, whereby it is obvious that chalcopyrite was partly active comminuted to be liberated.

The commonly very fine-grained occurrence ( $< 10\ \mu\text{m}$ ) of liberated copper sulphides indicates that breakage occurred preferentially along intramineral fissures within the copper sulphide grains and thus, internally areas result in liberated fragments definitely more-fine grained than the initial grain, whereas outer areas of copper sulphide grains remained intergrown with other mineral constitutes forming copper sulphide middlings. Apparently, the crack propagation and finally the breakage was

preferred triggered along either grain boundaries of the same sulphide phase, which is more implausible by highly selective crack formation, or on fissures transecting copper sulphide grains and intergrown gangue minerals.

Sulphide middlings, per se particles, in which a target mineral is partly locked by either other sulphides and/or gangue minerals were generally very different distributed within the particle size range of the studied ball mill products. According to mineral liberation data, copper sulphide middlings in the ball mill product of Mansfeld black shale were predominantly detected in the -40 µm particle size range, just few exceptions in coarser particle size classes were noticed. However, the Sangerhausen black shale ball mill product showed moderate to most increased proportion of bornite and chalcopyrite middlings occurring over the entire particle size spectrum. Comparatively lower proportions of copper sulphide middlings were determined in the ball mill product of Rudna black shale, in which the portion of bornite middlings continuously decreased up to -60 µm particle size class, whereas commonly significantly lower fractions of chalcocite middlings constantly decreased up to -50 particle size class. Chalcopyrite middlings were just found in the -10 µm particle size class. These observations show that copper sulphide middlings are generally more coarse-grained than liberated copper sulphides.

Based on the distribution of liberated copper sulphides and middlings can be deduced that the initial grain size of copper sulphides in the feed was coarser-grained in Sangerhausen black shale in particular for bornite and chalcopyrite. Rudna black shale feed contained obviously coarser-grained bornite and rather fine-grained chalcocite, which is indicated for the latter by low liberation and comparatively low amounts of middlings restricted to the particle size range -40 µm. The copper sulphide association in the Mansfeld black shale was apparently characterized by coarser-grained bornite, whereas chalcocite and chalcopyrite were generally more fined-grained than bornite. Thus, the initial grain size of copper sulphides in the feed define the grain sizes of liberated fragments and middlings, the latter are commonly more coarse-grained.

#### 4.1.1.2.2 Relationship of locking mode and the degree of liberation

Sulphide middlings represent generally intergrowths among sulphides and with gangue minerals. It was shown in Chapter 3.1.3.3, that locking associations of copper sulphides were mineralogically complex, especially in the ternary+ locked mode. It was apparent that only a very limited part (20%) of bornite and chalcocite was locked in particles solely with a second mineral (binary) in ball mill products of black shale ore in general. This proportion was again significantly lower, just over 10%, for chalcopyrite in ball mill products of Rudna and Mansfeld black shale, whereas a considerably increased amount of binary locked chalcopyrite (31%) was determined in the ball mill product of Sangerhausen black shale.

The low portion of binary locking of copper sulphides shows evidently that the main part of particles containing copper sulphide were marked by complex mineralogy. However, the distribution of binary locked copper sulphides within the particle size range corresponded to the distribution of copper sulphide middlings, as Figure 4.1.4 and Figure 4.1.5 show, and indicates that middlings were predominantly marked by less complex intergrowths. According to that, the ball mill product of Sangerhausen black shale host copper sulphide middlings (30-80% liberated surface) over the whole particle size range that are additionally marked by partly increased binary locking, especially for chalcopyrite and chalcocite. For ball mill products of Rudna and Mansfeld black shale, proportions of

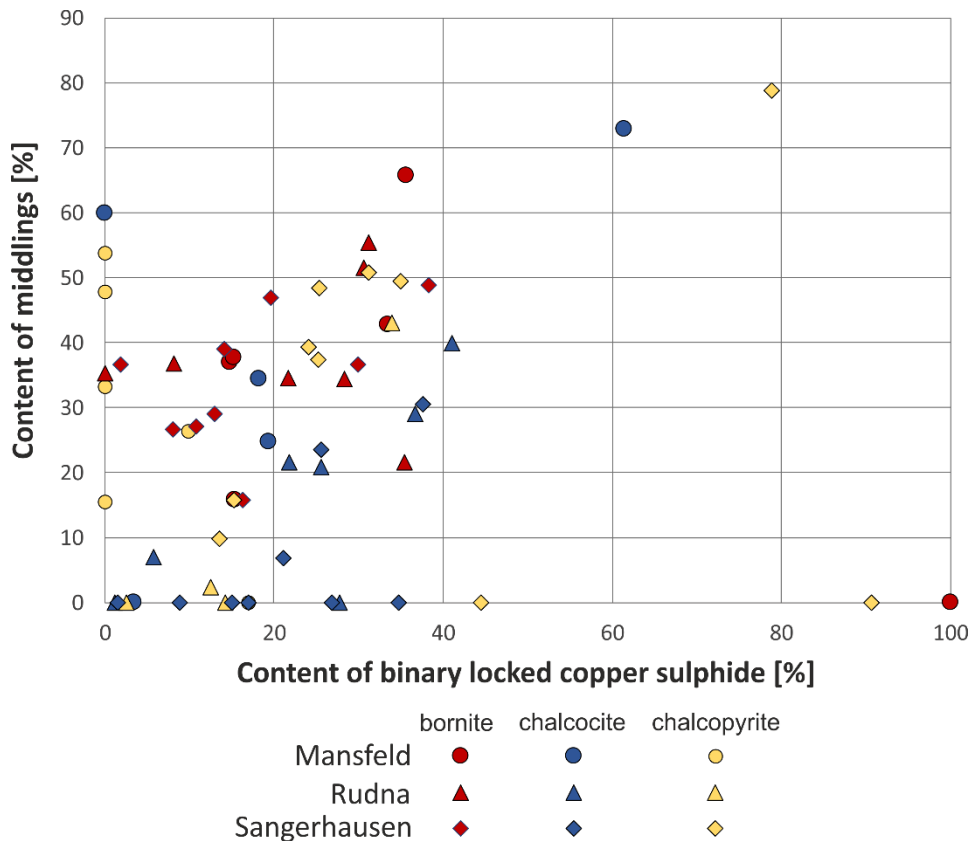


**Figure 4.1.4:** Scattered plot showing the content of middlings in relation to the content of binary locking for copper sulphides. The distribution indicating that copper sulphide middlings are often binary locked.

binary locked copper sulphides were generally coequal but the distribution was rather limited to fine-grained particle size classes.

The mineral association determined for binary locked copper sulphides, listed in Table 4.1.3 was mainly dominated by intergrowths of copper sulphides with each other as well as pyrite and illite.

Bornite was binary locked mainly with illite and chalcocite at slight changing proportion in the individual ball mill product. Binary locked chalcocite was exclusively associated with bornite in all studied ball mill products. However, the mineral association of binary locked chalcopyrite was more complex in ball mill products of Mansfeld and Sangerhausen black shale, in which, besides bornite, pyrite, carbonates and illite were associated with binary locked chalcopyrite. In particular the proportion of pyrite and bornite was considerably increased in the ball mill product of Sangerhausen black shale, especially in the coarser particles size range. Thus, it can be assumed that copper sulphide middlings consist of predominantly binary intergrowths mostly marked by mineral associations with a second copper sulphide or pyrite as well as with illite or carbonates.

Ternary+ locked copper sulphides were the common locking mode of copper sulphides in all examined ball mill products. Figure 4.1.5 shows the portion of binary and ternary+ locking of copper sulphides as well as the portion of middlings. While ternary+ locked copper sulphides generally represents the most common lock type, the proportions deviate considerably and indicate that in particular chalcopyrite in ball mill products of Mansfeld and Rudna black shale is primarily complexly intergrown. Both ball mill products show additionally that bornite is at least ternary+ locked. The

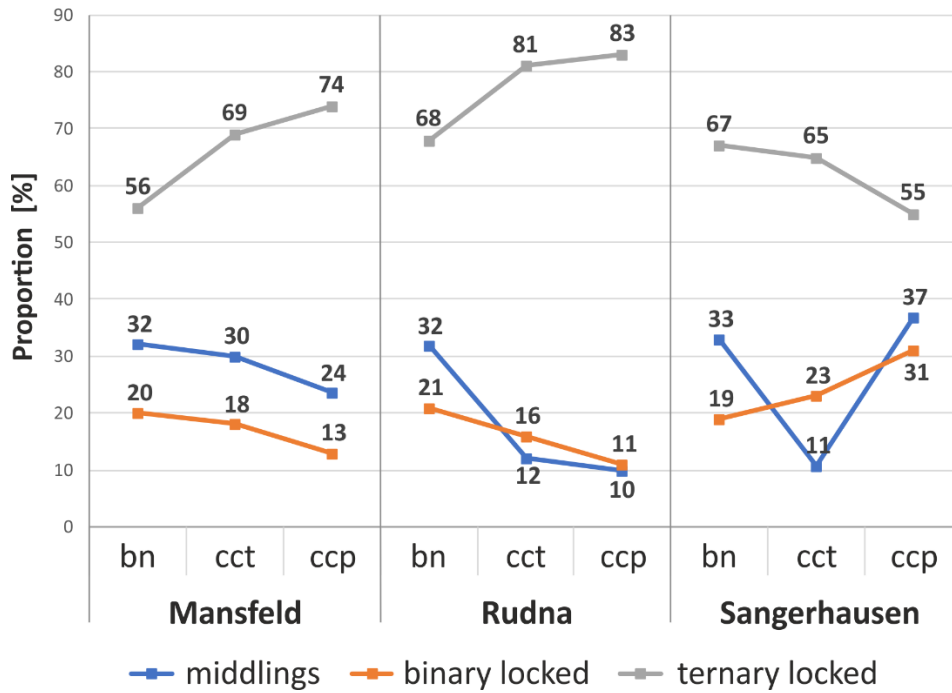


**Figure 4.1.5:** Relationship between copper sulphide middlings (30-80% liberated) and binary and ternary+ locked copper sulphides. It shows that copper sulphides are mainly ternary+ locked but in particular for ball mill products of Mansfeld and Rudna black shale it is apparent that the occurrence of copper sulphide middling coincide with binary locking.

portions of ternary+ locked chalcocite are generally below ternary+ locked chalcopyrite, although ternary+ locked chalcocite and chalcopyrite in the Rudna ball mill products occur nearly coequal.

Generally, can be stated that ball mill products of Mansfeld and Rudna black shale contain relatively lower proportions of complexly locked bornite, whereas chalcocite and chalcopyrite are considerably more ternary+ locked. Opposite to that, chalcopyrite is at least ternary+ locked in the ball mill product of Sangerhausen black shale and complexly locked chalcocite and bornite occurred more often.

Chapter 3.1.3.3 shows that constantly increasing proportions of ternary+ locked copper sulphides occur generally towards coarser particle size classes. Illite was the main gangue minerals associated with complex locked copper sulphides, as indicated in Table 4.1.3. Ball mill products of Mansfeld and Rudna black shale contain additionally illite and carbonates and their proportion in complex intergrowth with copper sulphides increases proportionally with the particle size.

**Table 4.1.3:** Predominant mineral phases associated with binary and ternary+ locked copper sulphides in ball mill products of different black shale feeds in order of abundance.(bn=bornite, carb=carbonates, cct=chalcocite, ill=illite, py=pyrite; dominant minerals are underlined)

	binary locked			ternary+ locked		
	bornite	chalcocite	chalcopyrite	bornite	chalcocite	chalcopyrite
<b>Mansfeld</b>	<u>ill</u> , cct	<u>bn</u>	<u>py</u> , ill, bn	<u>ill</u> , carb	<u>ill</u> , <u>bn</u> , carb	ill, py, carb, bn
<b>Rudna</b>	<u>ill</u> , <u>cct</u>	<u>bn</u>	<u>bn</u>	<u>ill</u> , <u>carb</u> , cct	<u>bn</u> , <u>ill</u> , carb	ill, carb, bn, py
<b>Sangerhausen</b>	<u>ill</u> , <u>cct</u>	<u>bn</u>	<u>py</u> , <u>bn</u>	<u>ill</u> , cct	<u>bn</u> , ill	ill, py, bn

The mineralogy of ternary+ locked copper sulphides was generally more complex in ball mill products of Mansfeld and Sangerhausen black shale but with dominance of illite. Quite varying proportions of numerous mineral species (feldspars, iron oxides, pyrite, quartz, and sphalerite) were complexly intergrown in particular with chalcopyrite. Proportions of minerals ternary+ locked with chalcopyrite were changing strongly within the particle size range of the ball mill product of Mansfeld black shale, whereas the content of multiple minerals ternary+ locked with chalcopyrite was more constant in the ball mill product of Sangerhausen black shale. Complex intergrowths among copper sulphides were generally decreasing toward coarser particle size but the ball mill product of Rudna black shale contained otherwise considerable portions of bornite and chalcocite ternary+ locked with each other in the particle size range > 80 microns.

The enhanced association of copper sulphides with gangue minerals in the coarser-grained particle size range points, at least partly, to an origin from disseminated ore particles of the feed.

Under the assumption, that partly liberated copper sulphides (middlings: 30-80% liberated) correspond to binary locked copper sulphides, ternary+ locked sulphides can be considered to represent primarily locked and not exposed particles containing target minerals. Due to the commonly increased content of gangue minerals such as illite and carbonates, ternary+ locked copper sulphides may originate in large parts from disseminated copper sulphides in the feed. However, in particular bornite was notably part of complexly locked chalcocite within the entire particle spectrum in the ball mill products of Rudna and Sangerhausen feed as well as to a lesser extend in the ball mill product of Mansfeld black shale, which may indicate that ternary+ locked bornite and chalcocite stem from larger sulphide aggregates or veins.

The prevalent occurrence of complexly intergrown copper sulphide grains in the studied ball mill products documents the inability to unlock copper sulphides satisfactorily by ball milling. The mineral distribution of locking associations reveal further that preferential breakage or shearing to separate feed particles occurred mainly at mineral interfaces that consists of primary illite, at which attrition (shear failure) is the main separation process, and more brittle mineral constituents such as carbonates, quartz and likewise sulphides that indicate compression related particle separation by transmineral fractures. Commonly, the fracture propagation did apparently not place along grain boundaries of minerals with different hardness, which is shown by the variety of minerals interlocked complexly with copper sulphides. However, breakage at interfaces of minerals with strong deviating hardness occurred probably, because binary locking of similar hard minerals in particular of bornite and chalcocite as well as of carbonates implies separation by fracture propagation between minerals of different hardness, but cannot be assessed finally within the frame of this study, since also pyrite with decisively higher hardness was partly associated with binary locked copper sulphides.

#### 4.1.1.3 Influence of the mineralization style to grain size and liberation of sulphides in ball mill products of black shale ores

As mentioned previously, copper sulphides in black shale ores can be associated to different ore textures. The style of ore mineralization in the feed, which was varying from fine-grained disseminated sulphide particles to coarser-grained mostly elongated sulphides aggregates up to bedding parallel and cross-cutting veins reaching up to several millimetres thickness might represent a further criterion for the liberation of copper sulphides in the examined black shales. Sulphide veins, recognizable in meso- and micro-scale, were common in Rudna and Sangerhausen black shale accompanied by finely disseminated sulphide particles, whereas the latter nearly exclusively occurred within the rock fabric

of the Mansfeld black shale. Commonly, textural relationships of sulphides hosted in black shale ore are of microscopic scale, especially the disseminated portion, so that their features can be observed by optical and scanning electron microscopy and quantified by BSE-based automated mineralogy techniques. Recently, textural-based information of ores are regarded to be important to influence plant efficiency, grade and recovery, and operational economics (Cropp and Goodall, 2013; Cropp et al., 2013). Bonnici (2012) gives a global overview of textural-based features of minerals extractable by modern automated mineralogy techniques. Crucial features defining textural properties of a mineral represent size, the mineral's distribution as well as association to other minerals.

As shown in Chapter 3.1.3.1, the grain sizes for bornite, chalcocite and chalcopyrite in the ball mill product of Mansfeld black shale were similar ranging between 22.0 and 28.6  $\mu\text{m}$ . As already reported in Kamradt et al. (2012) grain size of copper sulphides in Mansfeld low-grade black shale ore range commonly between 10 and 40  $\mu\text{m}$ , which means that the main part of copper sulphides had not to be comminuted but liberated. Macroscopically well recognizable is the vein-type copper mineralization in Rudna and Sangerhausen ore, which consisted of commonly very long lasting, over tens of cm, bedding parallel veins up to several mm in thickness and additionally mostly thinner crosscutting veins. Here, the grain size of copper sulphides exceeds the size of disseminated ore particles by one or two magnitudes. The vein-type sulphide association consisting mainly of bornite and chalcopyrite in the Sangerhausen ore as well as bornite and chalcocite in the Rudna ore had to be actively comminuted to meet the requirements of the desired ball mill product. Thus, the more coarse-grained size of vein-type copper sulphides that also considerable contribute to the copper mineralization as shown in Chapter 3.1.2.1, causes increased grain sizes of copper sulphides as determined in ball mill products of Rudna and Sangerhausen black shale ore.

Figure 4.1.6 illustrate the  $D_{80}$  grain size of copper sulphides and related ball mill products compared to the proportion of liberated copper sulphides and their middlings. It is well recognizable that liberation is promoted if the grain size of the ball mill product correlates with the grain size of copper sulphides, which is especially apparent in the ball mill product of Mansfeld black shale. Strongly deviating grain sizes of copper sulphides and the ball mill product result in particularly hamper liberation significantly as shown for chalcopyrite in the ball mill product of Rudna black shale. However, it depends also on the association to other copper sulphides as it is shown for chalcocite in the Sangerhausen ball mill product that predominantly intergrown with bornite.

However, apart from the initial grain sizes in the feed, the lack of liberation especially in terms of chalcocite in the ball mill product of Rudna ore feed seeks for interpretations. In the case that the vein-type copper mineralization would be monomineralic, a significant higher liberation would be expected. However, as shown in Chapter 3.1.3.3, chalcocite occurred binary locked exclusively with bornite, as commonly ascertained in all studied ball mill products, whereas ternary locked chalcocite was in addition associated with dominant gangue minerals (illite, carbonates, quartz). It can be assumed that liberated and binary locked chalcocite originate potentially from the vein-type mineralization, whereas ternary+ locked chalcocite derived from edge areas of veins, where it was interlocked with gangue minerals, as well as from fine-grained, disseminated sulphide particles, which are completely embedded in the gangue matrix. In particular binary locked copper sulfides in coarser particle size classes should be representative for the vein-type copper sulphide association in the ore.

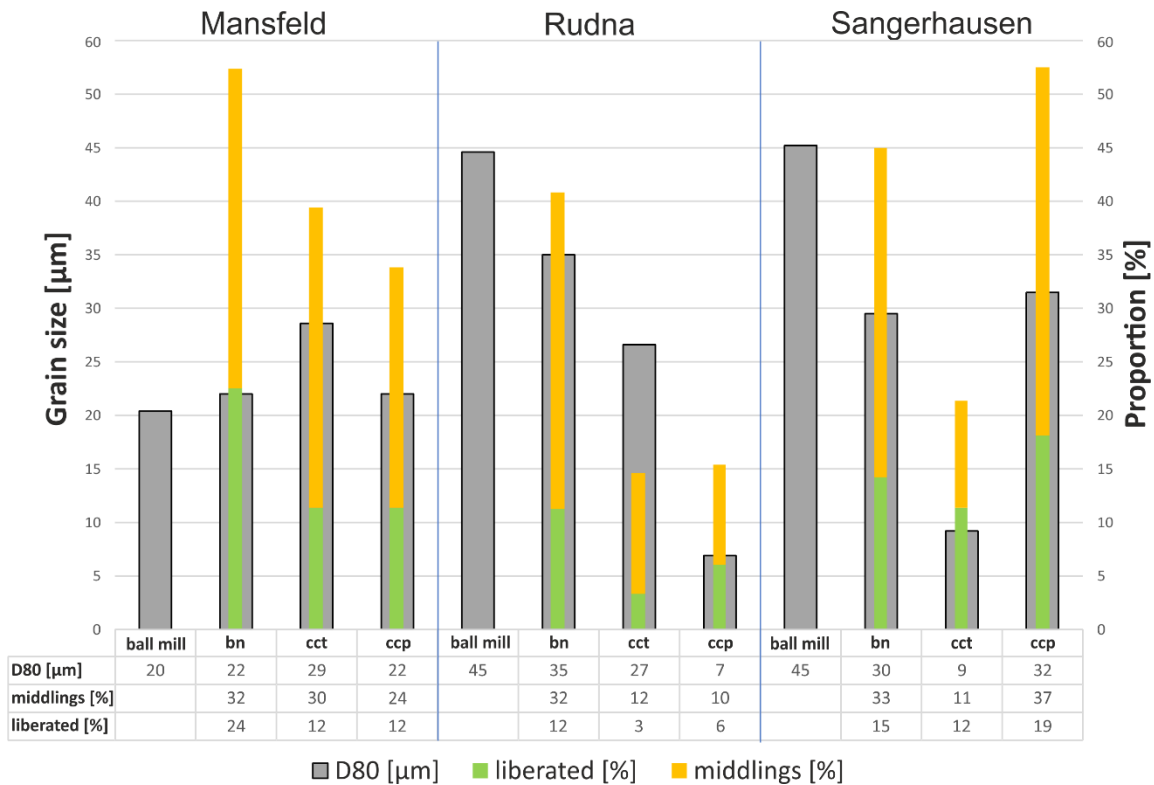


**Figure 4.1.6:** Diagram illustrates the dependency of the  $D_{80}$  grain size of the total ball mill products and of copper sulphides in regards to the distribution of liberated copper sulphides and partly liberated middlings (30-80% free surface)

Accordingly, it can be concluded that the copper mineralization in the Mansfeld black shale was dominated by disseminated sulphides and contained an insignificantly amount of vein-type ore or large-sized sulphide aggregates indicated by a coarser-grained chalcopyrite-pyrite association detected in coarser particle size classes of the ball mill product.

Rudna black shale hosted apparently vein-type ore containing a bornite-chalcocite association, possibly in a spatially smaller-scaled extent, because binary locking of bornite and chalcocite was restricted up to 60 μm particle size.

Binary locked copper sulphides occurred over the entire particle size range in the ball mill product of Sangerhausen black shale indicating that vein-type ore hosted a more complex copper sulphide association containing bornite, chalcocite, chalcopyrite and pyrite as well as gangue-type minerals such as barite and apatite.

A main concluding outcome of the investigation of ball mill comminuted black shale ores is that the ball mill product of Mansfeld black shale and its most advanced particle size reduction provided comparatively good liberation of copper sulphides originating mainly from disseminated sulphide particles in the ore. The ball mill products of Rudna and Sangerhausen black shale were significantly more coarse-grained, twice the size, so that they contained assumedly liberated copper sulphides originating substantially from vein-type ore, whereas the particle size reduction by ball milling was not sufficient to liberate in particular the disseminated but also in parts the vein-type associated portion of copper sulphides in the ore as shown for the extremely low liberation of chalcocite in the ball mill product of Rudna black shale.

Finally, larger-scale ore textures in the feed such as veins or irregular sulphide aggregates are not necessarily contribute essentially to the liberation of copper sulphides by ball milling, which is demonstrate by the most advance liberation of bornite in the ball mill product of Mansfeld black shale. However, vein-type associated copper sulphides influences enhanced liberation as indicated for the increased portions of liberated bornite and chalcopyrite in the ball mill product of Sangerhausen black shale.

#### 4.1.2 Black shale comminution using the VeRo Liberator® impact crusher

Batch comminution tests on Rudna and Mansfeld black shale ore were carried out using the VeRo Liberator® impact crusher platform in order to investigate its efficiency in particle size reduction and liberation of minerals of interest in comparison to ball mill products.

Crushers are used mainly in the first and second step of comminution routes in order to pre-crush the ore to a suitable feed size required for grinding mills. Impact crusher are mostly used in secondary comminution stages, although large impact crusher also contrive primary crushing of feed material up to 1.5 m in size (Wills and Napier-Munn, 2005). Most of the impact crushers are chiefly employed in the quarry industry producing aggregate material for concrete (Bengtsson and Evertsson, 2006), although impact crusher are occasionally preceded to grinding stages in metal extracting mining operations .

While the particle size reduction in grinding processes such as ball or rod mills generally based on fracturing caused by compression and shear forces (Wills and Atkinson, 1993), the fragmentation of particles provoked by impact crushing result in interparticle breakage by attrition and cleavage (Bengtsson and Evertsson, 2008; Evertsson, 2000).

The VeRo Liberator® impact crusher works with an axle-in-axle high speed rotation shaft equipped with three separate levels of hammer tools rotating variable adjustable clockwise and counter clockwise against each other, which cause high velocity impacts to feed particles and result in preferential inter-particle breakage (Borg et al., 2015b). Due to the partly different deformation behaviour of various minerals affected by impact energy, fracture nucleation and propagation takes place mainly on mineral/grain boundaries. It is assumed that this breakage principle, shown in Figure

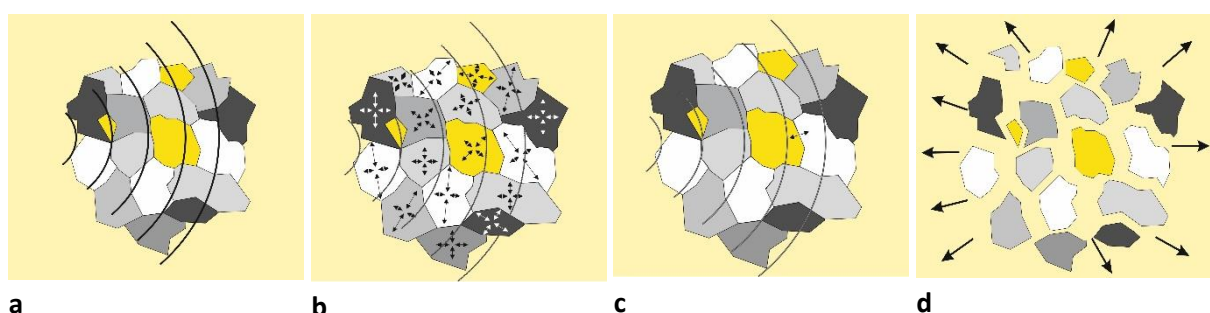


**Figure 4.1.7:** Schematic illustration of the proposed working principle of VeRo Liberator® impact crushing technology from Borg et al. (2015b). a) impacting energy inflicted on inhomogeneous material by hammer tools send through the material. b) The various particles react differently to shock waves according to their specific compressibility and elasticity moduli under high-frequency stimulation. c) tensional and/or shear stress is accumulated at grain boundaries between different minerals or along weak intra-mineral crystal zones (cleavage) and eventually causing breakage by shearing. d) Predominance of inter-granular, rather than intra- or cross-granular fracturing.

4.1.7, leads to reduced energy consumption and increased liberation of target minerals (Borg et al., 2019, 2015a).

While particle size reduction in horizontal tumbling mills is considered to be caused by compression loading of particles resulting in cracks between the nearest points of the two-surface loading, impact crushing generally comminute particles by one-surface fast compression loading due to the high velocity in impact crushers. Impact times of decisively slower rotating ball mills, up to 20 m/s, are comparatively 10 times longer and due to the increased contact time of the force termed as slow compression loading (Herbst et al., 2003).

Particle size distribution analyses in Chapter 3.1.1.2.1 have shown that a significantly more-fine-grained crushing product can be achieved by VeRo Liberator® impact crushing of black shale ore, contrastingly to common-in-use and established crusher types. While the particle size reduction ratio for these crusher types was generally  $< 3$ , the VeRo Liberator® impact crusher provide comminution products marked by considerable increased particle size reduction. According to grain size distribution in VeRo Liberator® products, the particle size reduction ratio (PSRR) for the operation with angular tools was 480 and slightly decreased by the usage of round hammer tools achieving a PSRR of 450. The product grain size was generally independent from the grain size of the feed, as shown in Chapter 3.1.1.2.2.

The comminution of black shale ores by VeRo Liberator® impact crushing delivered products, in which 60-65% of the product cover the particle size range  $< 100 \mu\text{m}$ . A remarkable portion when it is considered that the comminution products were generated by a single-pass comminution step, whereas comparable ball mill products with the same final product size run through a multistage comminution line consisting of primary and secondary crusher stages. Indeed, ball mill products were more-fine grained ( $10\text{-}15 \mu\text{m} @D_{80}$ ) but depending on the prevalent style of mineralization (vein-type or disseminated ore), coarser-grained sulphides could occur in particular potentially more liberated in the  $\text{-}100 \mu\text{m}$ -fraction of VeRo Liberator-products.

Granulometric data of the  $\text{-}100 \mu\text{m}$  particle size range of VeRo Liberator® products revealed that the grain size distribution was generally coarser than in ball mill products. Additionally, was shown that the VeRo Liberator® product of Mansfeld black shale was significantly finer-grained ( $D_{80}=34.5 \mu\text{m}$ ) in comparison to VeRo Liberator® products of Rudna black shale ( $D_{80}=56.0 \mu\text{m}$ ). A relationship also determined in respect to ball mill products of Mansfeld and Rudna black shale. As it was stated regarding ball mill products, the main argument for the large difference in the grain size distribution of the VeRo Liberator® products is given by rock fabric properties and related grain sizes of main mineral constituent. It was concluded that rock-forming minerals in the Mansfeld black shale feed are generally more fine-grained than in Rudna black shale. Additionally, Rudna black shale was enriched in organic matter that by itself and especially in association with illite act as elastic component. Due to the low portion of shear forces encountering impacted particles, particle separation by shearing plays a minor role in the comminution by impact crushing. However, compression forces affected by impact energy result in tensile strain that causes the particle to split and to shatter along pre-defined mineral interfaces such as grain boundaries (Borg et al., 2015b; Djordjevic et al., 2003).

Power consumption data recorded in the frame of comminution tests carried out with the VeRo Liberator® impact crusher showed great accordance to Bond work indices determined for ball mill products examined in this study. Thus, the power consumption effectively used in VeRo Liberator® comminution tests was significantly lower for Mansfeld black shale compared to Rudna black shale

and therefore Bond work indices are relatively transferable. However, due to confidentially use of energy consumption data encouraged by the company producing and marketing the VeRo Liberator® impact crusher, absolute energy consumption values cannot state here.

#### 4.1.2.1 Comparison of textural properties of copper sulphides in VeRo Liberator® impact crusher products

The comparison of the -100 µm-fraction of VeRo Liberator® products with ball mill products in Chapter 3.1.1.2.3 revealed partly deviating results in terms of grain size of copper sulphides, their liberation, locking mode as well as mineral association of locked copper sulphides. Thus, this subchapter delineates differences but shows also common features concerning the mineralogical and textural properties of copper sulphide in VeRo Liberator® products.

##### 4.1.2.1.1 Grain size of copper sulphides

The grain size of target minerals in comminution products represents an important feature considered in downstream processes such as froth flotation. MLA-data have shown that the grain size distribution of copper sulphides in VeRo Liberator® products (-100 µm) was comparable to ball mill products. In particular grain sizes of chalcocite and chalcopyrite showed close accordance in the  $D_{20}$ - and  $D_{50}$ -fraction, whereas in  $D_{80}$  just insignificant deviations existed. Here, the VeRo Liberator® product (-100 µm) generated with round hammer tools contained chalcocite and chalcopyrite slightly more coarse-grained than in the ball mill product (see Figure 4.1.8). However, the grain size of bornite was more differently. While bornite in the VeRo Liberator® product of Mansfeld black shale was significantly more coarse-grained ( $D_{80}=47.2$  µm) compared to the respective ball mill product ( $D_{80}=22.0$  µm), grain sizes of bornite in VeRo Liberator® products of Rudna black shale were considerably more fine-grained (avg.  $D_{80}=26$  µm) than in the ball mill product ( $D_{80}=34.6$  µm). This discrepancy though was not ascertained for the  $D_{20}$ - and  $D_{50}$ -fractions that were more consistent in ball mill and VeRo Liberator® products. However, regarding the general grain size of VeRo Liberator® products can be concluded that the grain size of copper sulphides is considerably finer especially for Rudna black shale. An exception represents bornite, which exceeds the grain size of the VeRo Liberator® product from Mansfeld black shale vastly ( $D_{80}$ product=34.5 µm vs.  $D_{80}$ bornite=47.2 µm).

##### 4.1.2.1.2 Liberation of copper sulphides

Mineral liberation as main feature in the recovery of a certain commodity is of great importance. Grain size analyses of the -100 µm-fraction of VeRo Liberator® products have shown, the granulometric distribution was comparable to ball mill products. However, liberation analyses of the main sulphides defining the copper mineralisation in the studied black shale ores revealed substantial differences, as Figure 4.1.9 depicts.

Generally, can be stated that VeRo Liberator® impact crushing delivers in general neither lower nor increased liberation of copper sulphides in comparison to ball mill products. Commonly improved liberation results were achieved in VeRo Liberator® products of Rudna black shale ore. Especially bornite was vastly more liberated (avg. 20.6% liberated), almost twice as much as in the respective ball mill product (11.8%), and the content of bornite middlings was additionally significant increased (40.3% vs. 31.7% by ball mill). However, contrary to that, the liberation of bornite in the VeRo Liberator® product of Mansfeld black shale was 50% lower (11.4%) than in the ball mill product (23.7%) and more substantially decreased in terms of the content of bornite middlings that was 75% lower (8.5%) opposing to 32% in the ball mill product.

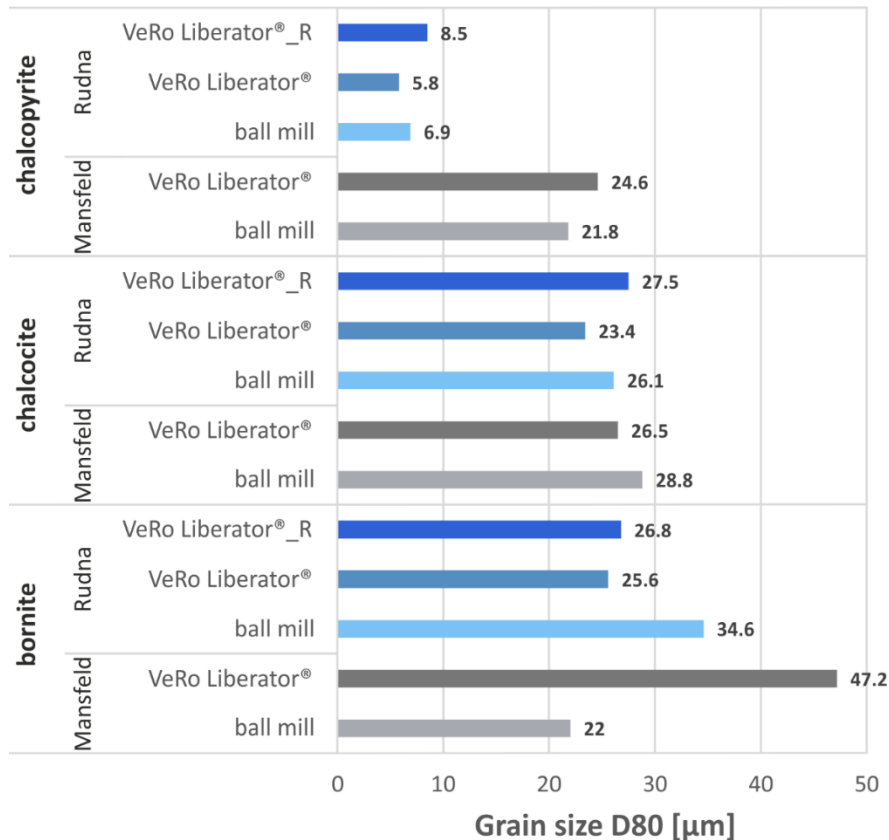


**Figure 4.1.8:** Comparison of the representative maximum grain size of copper sulphides in VeRo Liberator® and ball mill products indicating largely coincident grain sizes for chalcopyrite and chalcocite. Bornite is finer-grained in Rudna VeRo Liberator® products and coarser-grained the ball mill product of Mansfeld black shale. (VeRo Liberator®\_R= round hammer tools)

The liberation of chalcocite was generally low and showed minor differences concerning the origin of the feed. In comparison to ball milling, the VeRo Liberator® product of Mansfeld black shale was marked by slightly lower chalcocite liberation (liberated: 7.6% vs. 11.7% ball mill; middlings: 25.5% vs. 30.0% ball mill).

The portion of liberated chalcocite was extremely low in both, VeRo Liberator® products (4.7 and 4.5%) and ball mill product (3.4%) of Rudna black shale. However, the chalcocite middlings were considerably increased in the VeRo Liberator® products of Rudna black shale, of which especially the product generated with angular hammer tools showed a more increased content of chalcocite middlings (31.0% vs. 12.1% by ball milling). Thus, overall, the liberation of chalcocite was more advanced in the VeRo Liberator® products of Rudna black shale, where especially the amount of chalcocite middlings was significantly increased compared to the ball mill product. Chalcocite in the VeRo Liberator® product of Mansfeld black shale was marked by slightly lower liberation compared to the ball mill product.

Similar to the comparable lower liberation of bornite and chalcocite by VeRo Liberator® comminution of Mansfeld black shale, chalcopyrite was liberated more deficient (9.0%) compared to the ball mill product (12.4%), which also contained significantly more chalcopyrite middlings (23.5% vs. 10.5% VeRo Liberator®). VeRo Liberator® products of Rudna black shale showed in turn considerably improved liberation of chalcopyrite, in particular by the usage of round hammer tools

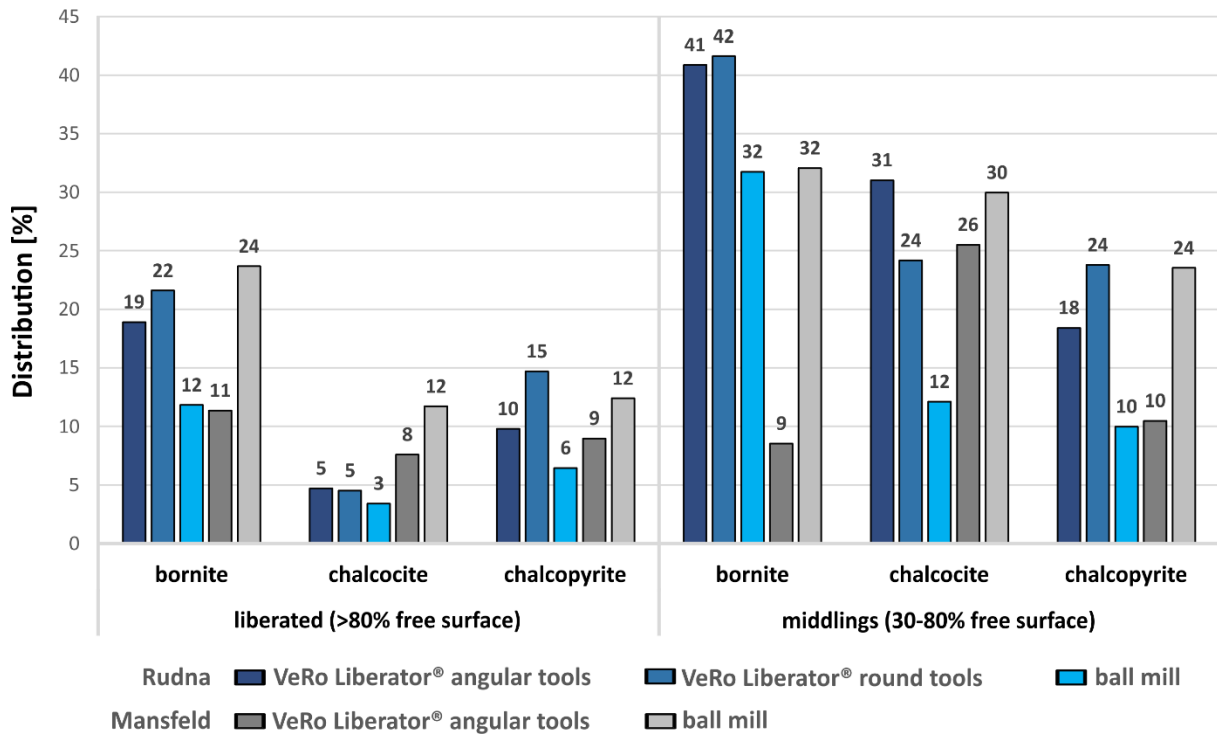


**Figure 4.1.9:** Comparison of the proportions of liberated copper sulphides and middlings in VeRo Liberator® products from Mansfeld and Rudna black shale in respect to ball mill products.

(14.7% vs. 6.4% by ball milling). Noteworthy is also twice the content of chalcopyrite middlings compared to the ball mill product (avg. 21.1% vs 10.0% by ball milling). Consequently, compared to the ball mill products, the liberation of chalcopyrite was considerably lower in the VeRo Liberator® product of Mansfeld black shale but strongly increased in VeRo Liberator® products of Rudna black shale.

It has been shown that significant differences exist in the liberation of copper sulphide by VeRo Liberator® comminution, which mainly based on the different properties of black shale feeds. The comminution of Mansfeld black shale by the VeRo Liberator® impact crusher yield generally in lower liberation of copper sulphides, in particular in respect to bornite, for which the deviation to the ball mill product is especially pronounced. By far more advanced liberation, almost twice increased in comparison to ball milling, was achieved for bornite and chalcopyrite in VeRo Liberator® products of Rudna black shale, whereas liberation of chalcocite is low but coequal to the ball mill product.

#### 4.1.2.1.3 Locking modes of copper sulphides

Textural properties of particles in comminution products such as locking modes of target minerals and their mineralogical association are useful information to trace the breakage behaviour of feed. Due to the different working principle of impact crushers and tumbling mills, the following paragraphs are used to delineate textural features of copper sulphides caused by differently breakage behaviour of mineral constituents.

A common observation was that locked copper sulphides in VeRo Liberator® products occurred chiefly in complex (ternary+) mineral associations, which stands in accordance to ball mill products. However, it was obvious that the proportions of binary locked copper sulphides are considerably lower, commonly about 10% and slightly below, in the VeRo Liberator® product of Mansfeld black shale

but comparatively increased in VeRo Liberator® products of Rudna black shale in particular for bornite (32%) and chalcocite (34%).

*VeRo Liberator® product of Mansfeld black shale*

Detailed investigations of the distribution of copper sulphides in regards to liberation in VeRo Liberator® products of Mansfeld black shale have shown that the majority of liberated copper sulphide grains occurred in the particle size fraction <math>-10 \mu\text{m}</math>. Beyond this particle size, significantly increased portion of liberated were basically not detected. More widespread and generally comparable to ball mill products was the occurrence of copper sulphide middlings in the <math>-40 \mu\text{m}</math> particle size range, although few exceptions were ascertained in some coarser-grained classes.

Figure 4.1.10 shows the proportions of locking modes of copper sulphides in the VeRo Liberator® product and ball mill product of Mansfeld black shale. The VeRo Liberator® product contains generally lower proportions of binary locked copper sulphides, particularly in respect to bornite and chalcopyrite, of which the proportion of binary locking was about 50% lower than in the ball mill product and thus, ternary+ locked copper sulphides were consequently substantial increased. However, the distribution of binary locked bornite and chalcocite was similar to the respective ball mill product, mainly in the particle size range <math>10\text{-}30 \mu\text{m}</math> as well as in the <math>-60 \mu\text{m}</math> particle size class, in which extraordinary high proportions of binary locked bornite and liberated chalcocite occurred. This may indicate that larger sulphides aggregates existed subordinately in the feed. Binary locked chalcopyrite in the VeRo Liberator® product was present up to the <math>-40 \mu\text{m}</math> particle size class but with decisively lower proportions than bornite or chalcocite and also in regards to chalcopyrite in the ball mill product. This shows clearly that VeRo Liberator® comminution of Mansfeld black shale delivers admittedly

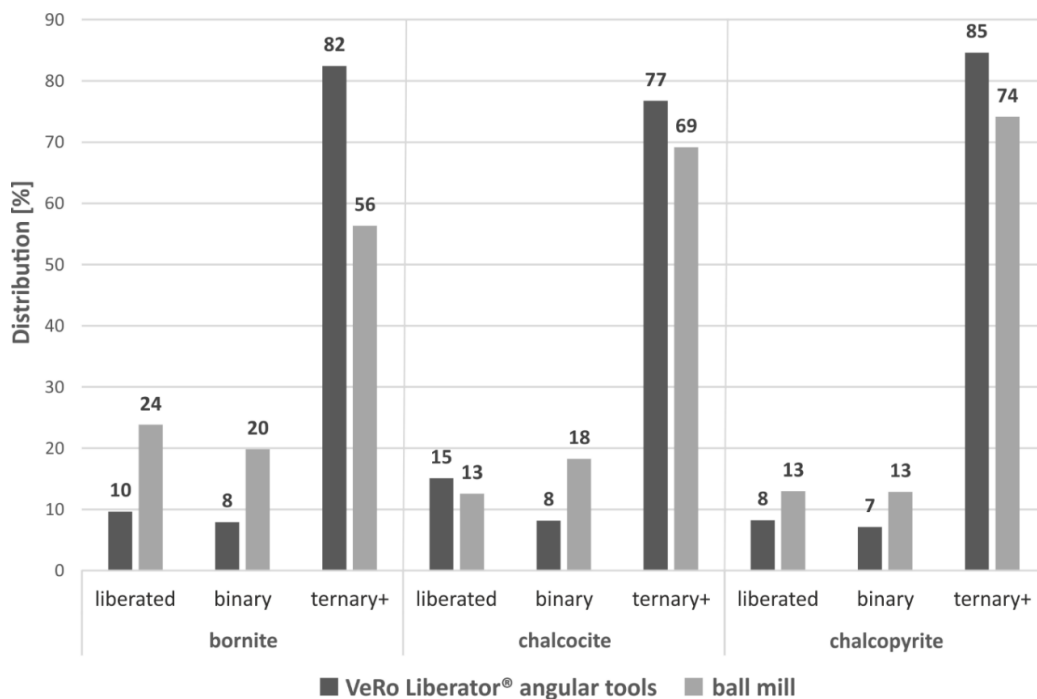


**Figure 4.1.10:** Column chart illustrating the locking mode of copper sulphides in the VeRo Liberator® product compared to the ball mill product of Mansfeld black shale. The proportion of liberated copper sulphides and also binary locked copper sulphides is commonly increased in the ball mill product.

**Table 4.1.4:** Predominant mineral phases associated with binary and ternary+ locked copper sulphides in the VeRo Liberator® product and related ball mill product from Mansfeld black shale feed.(bn=bornite, carb=carbonates, cct=chalcocite, ill=illite, py=pyrite, qtz=quartz; dominant minerals are underlined)

Locking mode	binary locked			ternary+ locked		
	bornite	chalcocite	chalcopyrite	bornite	chalcocite	chalcopyrite
<b>Mansfeld VeRo Liberator®</b>	ill	<u>bn</u>	ill, bn, py	<u>ill</u> , carb, qtz	<u>ill</u> , bn	ill, carb
<b>Mansfeld ball mill</b>	<u>ill</u> , cct	<u>bn</u>	<u>py</u> , ill, bn	<u>ill</u> , carb	<u>ill</u> , <u>bn</u> , carb	ill, py, carb, bn

lower proportions of binary locked copper sulphides, which could be more easily recovered, but with a distribution mainly in the particle size range < 30 µm comparatively to the ball mill product.

Mineral associations of binary locked copper sulphides in the VeRo Liberator® product of Mansfeld black shale were marked by slightly different mineral associations but generally comply with locking association in the respective ball mill product (see Table 4.1.4). Intergrowths, generally marked by mineral association of copper sulphides among each other, pyrite and illite, contain almost no carbonates, which are an essential component locked binary with copper sulphides in the ball mill product. It is apparent that complexly (ternary+) locked copper sulphides, associated mostly with illite, are rather more intergrown with carbonates in the ball mill product, which was also recognized in the VeRo Liberator® product for binary locking associations of chalcocite and chalcopyrite.

#### *VeRo Liberator® products of Rudna black shale*

VeRo Liberator® products of Rudna black shale were marked by generally increased content of liberated copper sulphides, though only to a lesser extent as in the case of chalcocite as Figure 4.1.11 shows. Liberated copper sulphides occur nearly exclusively in the -10 µm particle size class. VeRo Liberator® products hosted also increased amounts of middlings compared to the ball mill product, especially of chalcocite and chalcopyrite, which can be attributed to their comparatively increased amounts in the particle size range -50 µm. That apparently does not apply to bornite middlings that occurred rather in particle size range -30 µm but comparably increased.

Basically, liberated copper sulphides are very fine-grained (< 10 µm), whereas middlings occur in different particle size ranges. Bornite middlings are more fine-grained with lower proportions compared to the ball mill product. The distribution of chalcocite middlings is consistent but their proportions are comparatively increased likewise to chalcopyrite middlings that occur in a coarser particle size range in VeRo Liberator® products of Rudna black shale.

Locked bornite is generally intergrown with chalcocite and illite in the binary mode as well as with carbonates in the ternary+ mode. Due to the increased liberation of bornite in the VeRo Liberator® product generated with round hammer tools, proportions of binary and ternary locked bornite are lower. Additionally, bornite is mainly binary associated with chalcocite and less intergrown in both, binary and ternary locking, with carbonates in comparison to the ball mill product. Carbonate proportions of locked bornite are more pronounced in the VeRo Liberator® product generated with angular hammer tools.

VeRo Liberator® products of Rudna black shale contain binary locked chalcocite exclusively intergrown with bornite, which was consistent to the ball mill product, as Table 4.1.5 shows. But VeRo

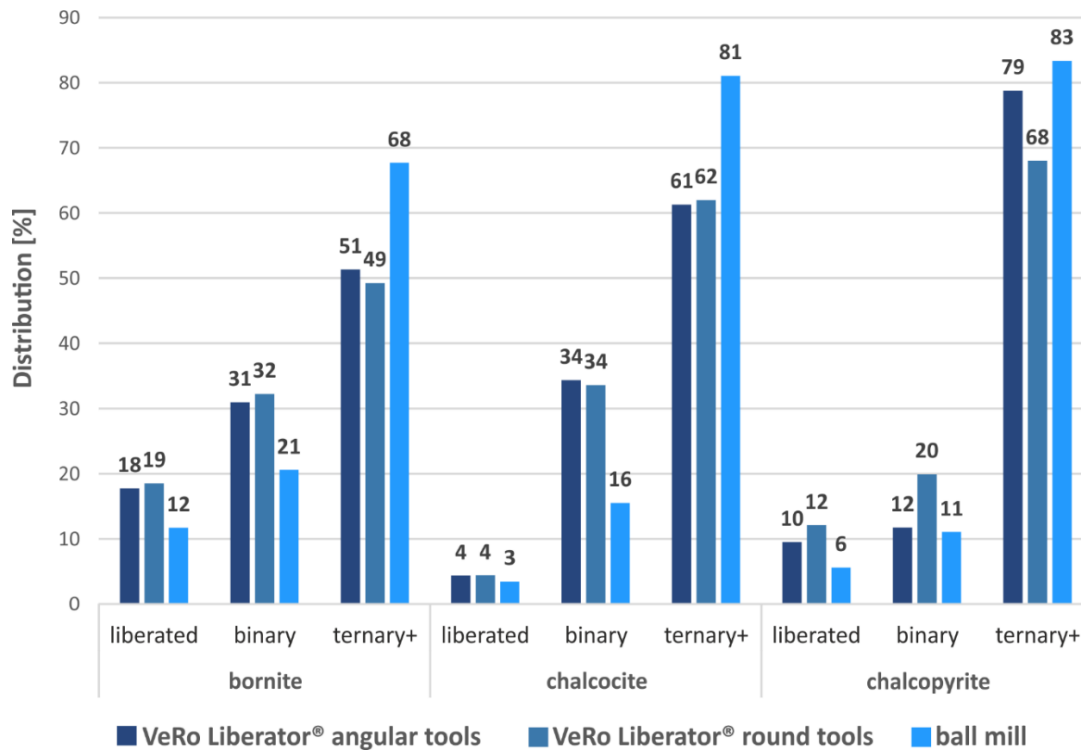


**Figure 4.1.11:** Compilation of locking associations of copper sulphides in VeRo Liberator® products of Rudna black shale in comparison to the respective ball mill product. Copper sulphides in VeRo Liberator® products are more liberated and binary locked than in the ball mill product, in particular in the VeRo Liberator® product generated by round hammer tools.

Liberator® products have notable increased amounts of binary locked chalcocite compared to the ball mill product and consequently lower portion of ternary+ locked chalcocite. Mineral association are generally identical to the ball mill product. However, complexly intergrowths of chalcocite are dominated by bornite, besides moderate amounts of illite. The usage of angular tools causes increased carbonate and illite fractions in particular in the coarser particle size range.

The content of chalcopyrite in comminution products of Rudna black shale is neglectable low. Additionally, chalcopyrite is marked by the lowest grain size (7 µm) among copper sulphides (25-35 µm) in the studied comminution products of Rudna black shale. However, the liberation of chalcopyrite in VeRo Liberator® products of Rudna black shale was much more enhanced, especially by the usage of round hammer tools, simultaneous with more increased production of chalcopyrite middlings, which not only occurred in the finest fraction as ascertained for the ball mill product. In comparison to

**Table 4.1.5:** Predominant mineral phases associated with binary and ternary+ locked copper sulphides in VeRo Liberator® products and ball mill product of Rudna black shale. (bn=bornite, carb=carbonates, cct=chalcocite, ill=illite, py=pyrite; dominant minerals are underlined)

	binary locked			ternary+ locked		
	bornite	chalcocite	chalcopyrite	bornite	chalcocite	chalcopyrite
<b>Rudna VeRo Liberator®</b>	<u>cct</u> , ill	bn	bn, ill, py	<u>ill</u> , cct, carb	<u>bn</u> , ill	<u>ill</u> , bn, carb, py
<b>Rudna ball mill</b>	<u>ill</u> , <u>cct</u>	<u>bn</u>	<u>bn</u>	<u>ill</u> , <u>carb</u> , cct	<u>bn</u> , <u>ill</u> , carb	ill, carb, bn

the latter, binary chalcopyrite was more widespread within the product particle size range partly with moderate to considerably increased proportions.

Generally, the mineral association of locked chalcopyrite was largely consistent to the ball mill product and contained for binary locked chalcopyrite mainly bornite, illite and pyrite. The VeRo Liberator® product generated by round hammer tools was marked by increased proportions of binary locked chalcopyrite and contained an enormous portion of bornite binary locked with chalcopyrite in the -80 µm particle size class.

The proportion of ternary locked chalcopyrite was significantly lower in the VeRo Liberator® product generated by round hammer tools compared to the VeRo Liberator® product crushed with angular hammer tools and ball mill product. The distribution of minerals complexly intergrown with chalcopyrite in VeRo Liberator® products of Rudna black shale was generally dominated by illite, whereas bornite, pyrite and carbonates occurred subordinately. However, the proportion of bornite and pyrite fade out and carbonate proportions increase toward coarser-grained particle size classes, which indicates, in addition to the small grain size, that chalcopyrite was mainly part of the disseminated sulphide fraction in the Rudna black shale feed. It was obvious that the VeRo Liberator® product generated by round hammer tools contained lower proportions of carbonates associated with ternary+ locked chalcopyrite.

#### *General conclusion*

It was shown that the -100 µm-fraction of VeRo Liberator® products can be comparable to classic comminution products such as final stage ball mill products. However, the main challenges to liberate the complex sulphide association of black shale-hosted Kupferschiefer-type mineralization also exist in the comminution using the VeRo Liberator® impact crusher. Due to considerable differences regarding the mineralogical composition and ore textures of the two tested black shale ores, VeRo Liberator® comminution products are quite different. While in Rudna black shale copper sulphides were significantly more advanced liberated by VeRo Liberator® impact crushing, liberation of copper sulphides in Mansfeld black shale feed failed largely and is reduced significantly in comparison to the ball mill product. Thus, comminution tests with VeRo Liberator® yield in very contrary results regarding the properties of the impact crusher products.

The particle size distribution of the -100 µm-fraction of VeRo Liberator® products is generally more coarse-grained compared to ball mill products but in respect to VeRo Liberator® products of Rudna black shale the deviation to the ball mill product is lower than among comminution products of Mansfeld black shale. As the examination of ball mill products reveals, the product fineness to liberate predominantly disseminated copper sulphides in the Mansfeld black shale was partly sufficient, but could be improved by finer grinding. Due to general increased particle size in the VeRo Liberator® product, the achieved particle size reduction was even less able to unlock copper sulphide from the gangue matrix.

Comminution tests with Rudna black shale indicate that improvements in the liberation of copper sulphide can be obtained by the use of the VeRo Liberator®. Two factors are noticeable controlling the successful comminution of black shale-hosted Kupferschiefer-type ore. It is on the one hand the style of mineralization and related ore textures in the feed and on the other hand the rock matrix, in which copper sulphides are embedded. In Chapter 4.1.1.1, mineral distribution and mineral specific properties such as hardness and tenacity has been used to delineate differences in work bond indices

and particle size distribution of the examined ball mill products, which can be also cited to explain differences in VeRo Liberator® products.

Because impact crushing represents a one-sided loading of particles afflicted by hammer tools, the breakage is mainly caused by compression forces that form tensile strain resulting in ruptures. Elastic components such as widespread illite and organic matter can enhanced absorb tensile forces, thus, mineral interfaces consists of intergrowth with these flexible minerals are comparatively harder to separate than interfaces between brittle minerals. Mineral associations of locked copper sulphides in the VeRo Liberator® product of Mansfeld black shale indicate that as well binary as ternary locked copper sulphides were generally more linked to illite in comparison to the ball mill product, whereas the portion of carbonates was generally lower. Thus, copper sulphides in VeRo Liberator® product of Mansfeld black shale were more intergrown with flexible illite that prevented the further separation of particles and the increase of the liberation of copper sulphides. Carbonates, generally having the lowest hardness among brittle rock-forming minerals in black shales, seem to provide suitable interfaces by sharing grain boundaries with differently hard mineral components. Fracture release and propagation up to breakage are favoured at these mineral grain boundaries with increased hardness potential. Thus, breakage occurred preferentially along grain boundaries of differently hard minerals (dolomite <>quartz, feldspar, pyrite).

It was determined that the proportion of carbonates in binary as well as ternary+ locked copper sulphides in VeRo Liberator® products was generally lower than in ball mill products, which indicate that intergrowths of copper sulphides are more dominated, besides illite, by other, mostly harder, mineral phases. The hardness of individual minerals and their distribution in VeRo Liberator® products

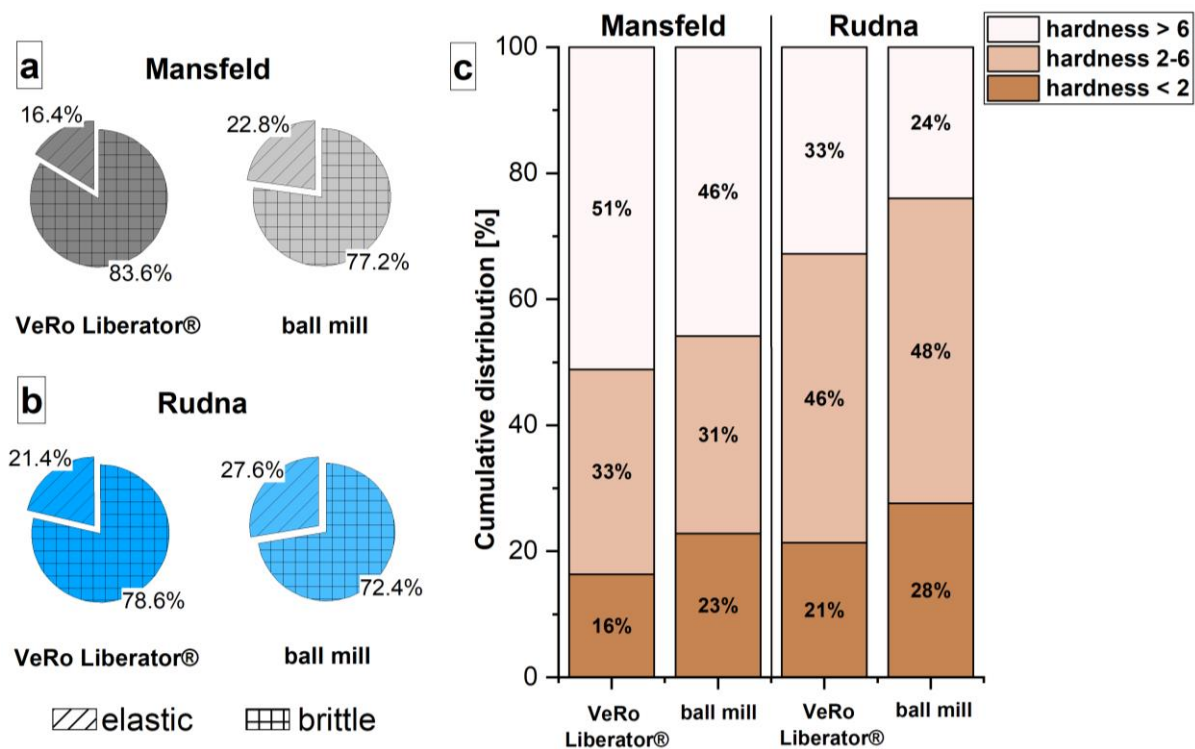


**Figure 4.1.12:** Comparison of the proportion of brittle and elastic-acting mineral constituents in VeRo Liberator® and ball mill products of Mansfeld (a) and Rudna black shale (b). The distribution of rock-forming minerals according to their affinity to different hardness classes (c) shows that Mansfeld black shale contains a generally increased amount of minerals with hardness > 6 that are obviously most increased in the VeRo Liberator® product.

of Mansfeld and Rudna black shale outlined in hardness classes indicating the abundance of minerals with similar hardness. As Figure 4.1.12 shows, the VeRo Liberator<sup>®</sup> product of Mansfeld black shale is dominated by mineral constituent with hardness > 6 that are represented by quartz and feldspar. The VeRo Liberator<sup>®</sup> product of Rudna black shale contains predominantly minerals with hardness 2-4, mainly carbonates and subordinate sulphides. Additionally, Rudna black shale is considerable enriched in copper sulphides that are substantially vein-type associated and coarser-grained. Thereby copper sulphides in Rudna black shale are more easily to liberate than disseminated ore, which was prevalent in the Mansfeld black shale. These observations indicate clearly, why the liberation of copper sulphides by VeRo Liberator<sup>®</sup> comminution of Rudna black shale was more successful, in particular because particles afflicted by impact energy break preferentially at mineral interfaces such as grain boundaries of differently hard minerals. Thus, breakage takes place at interfaces, on which the lowest bonding energy must be overcome.

Although illite and organic matter are potentially softer than all other mineral constituents in black shales, they react elastic to ductile when affected by compression. However, breakage take place principally at grain boundaries where brittle components with low hardness occur, namely the partly abundant carbonates in black shales. It can be assumed that small differences in hardness are sufficient to cause breakage so that the slightly softer copper sulphides were potentially more separated from carbonate gangue, which is also indicated by generally lower proportions of carbonates associated with binary and ternary+ locked copper sulphides as Figure 4.1.13 indicates. This was also observed in the VeRo Liberator<sup>®</sup> product of Mansfeld black shale, but here copper sulphides were more associated with elastic-acting illite and harder components, such as quartz and feldspars, and the impact energy was obviously insufficient to release cracks at such mineral interfaces.

The influence of the grain size of sulphides in the feed regarding their liberation by ball milling was discussed in Chapter 4.1.1.2.1. The occurrence of copper sulphide middlings that are also regarded to be potentially represent copper sulphides binary locked with each other stands in relation to their initial grain size defined by the style of mineralization, which is generally more fine-grained for the disseminated portion of the ore and more coarse-grained for sulphides associated with vein-type

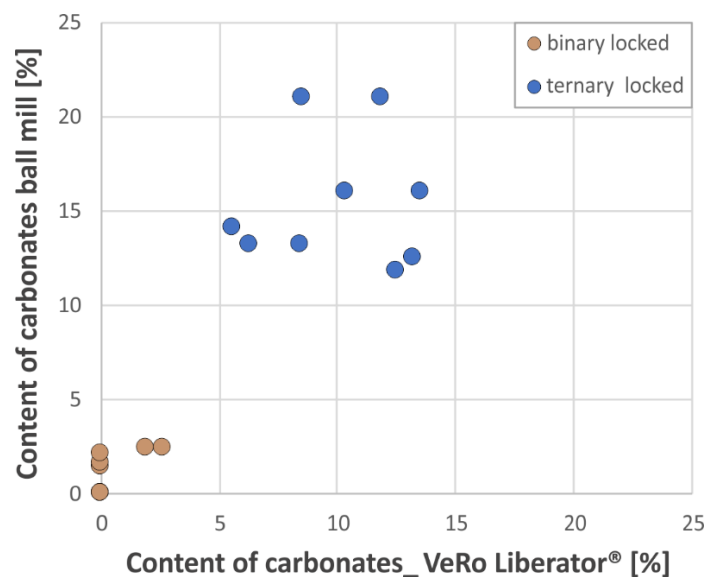


**Figure 4.1.13:** Proportion of carbonates in binary and ternary+ locked copper sulphides in VeRo Liberator<sup>®</sup> products compared to ball mill products. Ball mill products contain generally increased proportions of carbonates interlocked with copper sulphides.

mineralization. It was proposed that binary locked sulphides in particle size classes  $> 50 \mu\text{m}$  indicate sulphide particles originating from vein-type mineralization, which applies rarely for the VeRo Liberator<sup>®</sup> product of Mansfeld black shale, because binary locked bornite and chalcocite occurred only exemplarily in coarser particle size classes. The increased occurrence of binary locked bornite and chalcocite across nearly the complete particle size spectrum in the VeRo Liberator<sup>®</sup> products of Rudna black shale indicates clearly that a portion of copper sulphide was associated with vein-type ore in the feed. However, liberated copper sulphides occurred nearly exclusively in the particle size range  $< 10 \mu\text{m}$  what implies that copper sulphide grains in feed particles were affected by intragranular formation of fissures, of which breakage caused the separation to very fine-grained copper sulphide fragments.

Additionally, was determined that liberation of copper sulphides was partly more increase in the VeRo Liberator<sup>®</sup> product of Rudna black shale generated with round hammer tools. Due to their geometry, direct input of the maximum impact energy is more probable when particles are hit by round rod tools, whereas by angular tools the impact energy is more reduced depending the angle of incidence to the planar surface of the tools by a hit particle. While maximum impact energy affecting particles if they encounter perpendicular to the plane facing to the rotation direction, the impact energy will be reduced at deviation from that ideal impact geometry. Thus, the probability that increased impact energy is imparted to hit particles could be rather provided by round hammer tools causing enhanced particle breakage and thus facilitate increased liberation of target minerals, which was in particular noticed for bornite and chalcopyrite. In the case of the latter, enhanced breakage behaviour triggered by round hammer tools could explain the significantly increased liberation of small-grained chalcopyrite in VeRo Liberator<sup>®</sup> product of Rudna black shale. However, these observations and interpretations need to investigate more detailed to draw far-reaching conclusions.

## 4.2 Flotation

The physico-chemical separation process of flotation is the most important and applied mineral processing technique used for the beneficiation of copper ores. In the frame of this study, flotation concentrates and tailing have been investigated to reveal the flotability of particularly copper sulphides by the use of different flotation agents. Geochemical assays and mineral distribution analyses were used to characterize the recovery of metals in general and of sulphide and gangue minerals in particular. In order to delineate the flotability of copper sulphides in the different flotation tests, liberation data and textural relationships of target minerals in feed and concentrates were used to demonstrate that mineralogical properties affect the capability to recoverability of individual copper sulphides significantly.

### 4.2.1 Recovery of copper sulphides by flotation of Rudna and Sangerhausen black shale ore

Flotation tests carried out on ball mill products of Rudna and Sangerhausen black shale ores have shown that the usage of dextrin, mainly employed to depress the organic carbon content, combined with ethanol pre-treatment of feeds resulted in high copper recovery at simultaneous increased mass recovery compared to dextrin-added flotation with untreated feed. Standard sulphide flotation tests were characterized by high mass and copper recovery in flotation products, the dextrin-added flotation using ethanol pre-treated feeds showed similar copper recovery rates at lower mass recovery, which indicates a higher selectivity to recover copper sulphides in concentrates by considerably reduction of the gangue portion.

The flotation of Rudna black shale with dextrin and ethanol pre-treatment yield in more than 50% mass reduction in the product (26.7% vs. 52.9% standard flotation) at nearly equal copper recovery (72.1% vs. 75.1% standard flotation). However, the mass reduction by the dextrin-added flotation of ethanol pre-treated Sangerhausen black shale was lower (30%) but related to notable increase of the copper recovery (74.8% vs. 67.8% standard flotation). Concluding can be stated that the usage of dextrin in combination with ethanol pre-treatment of the feed yielded in consistently improved selectivity regarding the recovery of copper sulphides indicated by high copper and reduced mass recovery, which was not obtained by flotation tests performed with dextrin but without ethanol pre-treatment of the feed. Thus, the ethanol pre-treatment step seems to be crucial to gain copper-rich concentrates by enhanced selective flotability of copper sulphides.

Generally, copper concentrates extracted by flotation using dextrin and ethanol pre-treated Rudna and Sangerhausen black shale feed were marked by significantly increased copper contents (Rudna: 10.0%, Sangerhausen: 14.4%), whereas the corresponding tailings showed the lowest copper values in comparison to tailings of both, standard flotation and dextrin-added flotation without ethanol pre-treated feed. The low content of copper sulphides in tailings substantiates additionally the increased flotability of copper sulphides caused by the ethanol pre-treatment of the feed.

Mineral distribution analyses revealed that copper sulphides were enriched differently in concentrates extracted by various flotation tests. Figure 4.2.1 illustrates the recovery rates of copper sulphides, mainly accountable for the copper mineralization in the studied black shales, achieved in concentrates and tailings. According to mineral distribution data and mass recovery, copper sulphides showed generally differences in recovery rates within individual flotation tests but also in respect to

the black shale feed used. Basically, the recovery of copper sulphides was partly moderate but mostly increased in concentrates generated by standard sulphide flotation and dextrin-added flotation with ethanol pre-treated feed, whereas copper sulphides in the flotation using solely dextrin were generally depressed in the tailings showing high, partly extremely proportions, e.g. 93% for chalcocite in tailings from Sangerhausen ore.

Among the recovery rates of copper sulphides by dextrin-added flotation, chalcocite showed the most deviating proportion regarding Rudna and Sangerhausen feed. Although the latter contained more liberated chalcocite and middlings, the recovery in the concentrate was very low (7%) compared to 37% in the concentrate from Rudna black shale feed. However, liberated chalcocite and middlings in the ball mill product of Sangerhausen black shale occurred only in the particle size range < 20 µm with low proportions and additionally the grain size of chalcocite was considerably low ( $D_{80}=9.2 \mu\text{m}$ ), whereas chalcocite was three times coarser-grained ( $D_{80}=26.6 \mu\text{m}$ ) in the ball mill product of Rudna black shale and chalcocite middlings occurred in a wider particle size range up to 50 µm, which apparently favoured the recovery in the flotation product. Further, the grain size distribution of chalcocite in the concentrate was consistent with that in the feed material, as shown in Chapter 3.2.6.2. Additionally, the content of liberated chalcocite and middlings in the concentrate from Rudna black shale was about 90% and more within the particle size range < 50 µm, in which liberated chalcocite or middlings were alternating predominant. Liberation data of chalcocite in the related concentrate from Sangerhausen black shale were not available, mainly due to the low chalcocite concentration (0.6%) considered to have lower importance. Nevertheless, the recovery of copper sulphides was low by the flotation with dextrin, which was indicated in addition by low but similar recovery rates of bornite and chalcopyrite in concentrates from Rudna and Sangerhausen black shale.

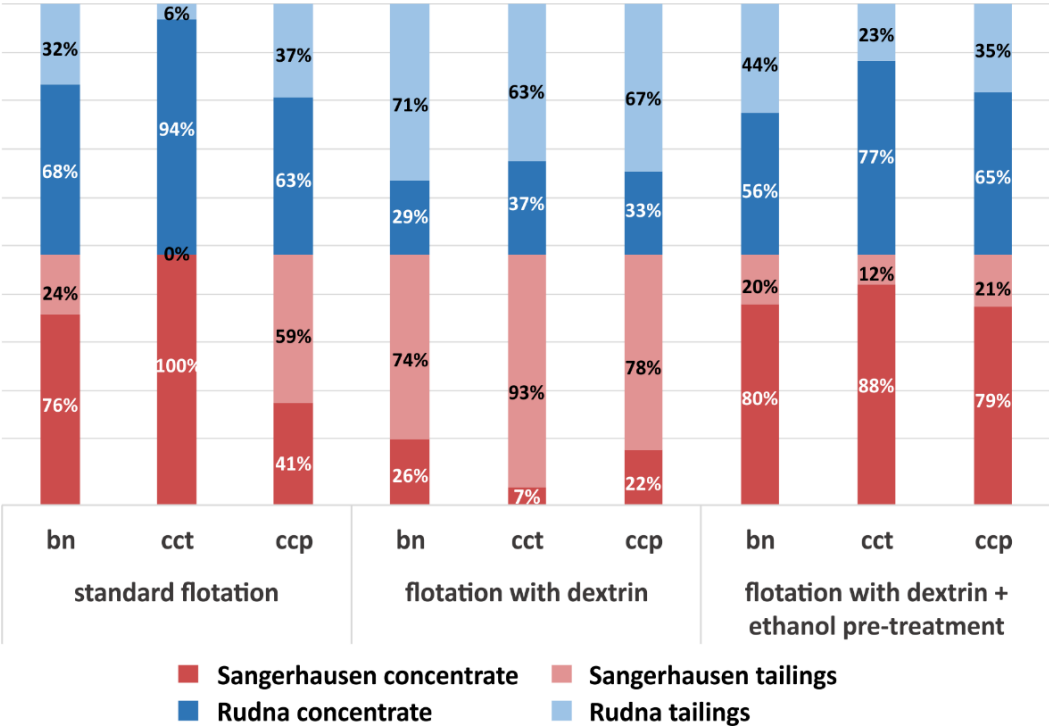


**Figure 4.2.1:** Recovery rates of copper sulphides by different flotation tests indicating that the flotation with dextrin without ethanol pre-treatment of the feed achieves generally low recovery, flotation with dextrin and ethanol pre-treated feed generates flotation products marked by recovery rates similar to the standard flotation at reduced mass recovery.

Differences in the recovery of copper sulphides by standard flotation and flotation using dextrin and ethanol pre-treated feed were less substantial. However, most increased recovery rates for chalcocite were detected in concentrates extracted by standard flotation (94% Rudna, 100% Sangerhausen). Commonly, an increased copper sulphide recovery was achieved by flotation with dextrin and ethanol pre-treated Sangerhausen black shale in comparison on the one hand to standard flotation and on the other hand to recovery rates achieved by the same applied flotation protocol on Rudna black shale. In the case of the latter, the recovery of bornite and chalcocite, both representing the main copper sulphides in the feed, was notably lower by dextrin-added flotation with ethanol pre-treated feed compared to standard flotation.

A significantly improved recovery of chalcopyrite and bornite was ascertained in the concentrate extracted by flotation with dextrin and ethanol pre-treated Sangerhausen black shale feed. While just 41% chalcopyrite were recovered in the concentrate produced by standard flotation, the flotation with ethanol pre-treated feed yield in nearly doubled recovery (79%) of chalcopyrite and slightly increased recovery of bornite.

As mentioned previously, flotation with dextrin and ethanol pre-treated feed yielded in increased recovery of copper sulphides in concentrates from Sangerhausen black shale. The lower recovery of copper sulphides in the concentrate extracted from Rudna black shale feed caused their significantly accumulation in tailings, which host partly up to nearly 50% of the value mineral. Especially pronounced was the diverging recovery of bornite, which was in general a main copper sulphide in both black shale feed. While 80% of bornite were extracted in the concentrate from Sangerhausen feed, the recovery rate in the concentrate from Rudna black shale was considerably lower with 56%.

#### 4.2.1.1 Textural properties of copper sulphides affecting recoverability

As shown in Chapter 3.1.3.1, the grain size distribution of bornite in ball mill products of Rudna ( $D_{80}=35.0\ \mu\text{m}$ ,  $D_{50}=10.1\ \mu\text{m}$ ) and Sangerhausen ( $D_{80}=29.5\ \mu\text{m}$ ,  $D_{50}=14.2\ \mu\text{m}$ ) black shale revealed notable but no strong deviations. The liberation of bornite was slightly increased in the ball mill product of Sangerhausen black shale. Liberated bornite (Rudna: 11.8%, Sangerhausen: 15.0%) and middlings (Rudna: 31.7%, Sangerhausen: 33.0%) occurred generally in the particle size range 0-30  $\mu\text{m}$ , whereas considerable increased amounts, especially in the -10  $\mu\text{m}$  particle size class (Sangerhausen: 82%, Rudna: 54%), were detected in the ball mill product of Sangerhausen black shale. Additionally, bornite middlings in the latter were distributed constantly over the entire particle size range with moderately increased proportions between 30 and 50%, while bornite middlings in Rudna black shale had a more restricted distribution (0-60  $\mu\text{m}$  particle size range) but with similar proportions. Locking modes of bornite were generally coequal and dominated by ternary+ locked bornite (20% binary, 66% ternary+), which was mainly associated with illite and chalcocite in both black shale feeds, but additionally with a moderate amount of carbonates in the ball mill product of Rudna black shale.

As Figure 4.2.2 shows, liberation analyses of concentrates generated by flotation with dextrin and pre-treated feed indicate similar amounts of liberated bornite (Rudna: 11%, Sangerhausen: 15%) but concerning bornite middlings, the concentrate extracted from Sangerhausen black shale was marked by a considerable increased proportion (74%) compared to the content of bornite middlings (46%) in the concentrate from Rudna black shale. Additionally, a comparatively more increased proportion of liberated bornite of 19% and low content of middlings (15%) was hosted in the related tailings (see Chapter 3.2.6.1. Contrary to that, a far more increased portion of bornite middlings (66%) but a

significantly lower portion of liberated bornite (9%) were detected in tailings from the flotation with dextrin and pre-treated Sangerhausen feed.

The main reason why the recovery of bornite and also to a lower extent of chalcocite was relatively lower by flotation with dextrin and ethanol pre-treated Rudna black shale is obviously the degree of liberation in the feed but also the recoverability by flotation, as Figure 4.2.2 indicates. The liberation of bornite in ball mill products of Rudna and Sangerhausen was coequal, only slightly increased in milled Sangerhausen ore. Thus, the flotability of bornite in Rudna black shale seems to be hindered. The lower recovery of chalcocite in the product from the flotation with dextrin and pre-treated Rudna feed is apparently due to the lower liberation of chalcocite in the ball mill product. However, an additional effect caused by the presence of carbonates, which are considerably intergrown with complexly locked bornite, could restrict the flotability of bornite in Rudna black shale feed due to the depression of carbonate phases into tailings.

Concentrates from various flotation tests were generally marked by low to extremely low contents of liberated copper sulphides, few exceptions were noticed in particular for chalcopyrite in concentrates extracted from Sangerhausen feed (64% liberated by standard flotation), which stands in

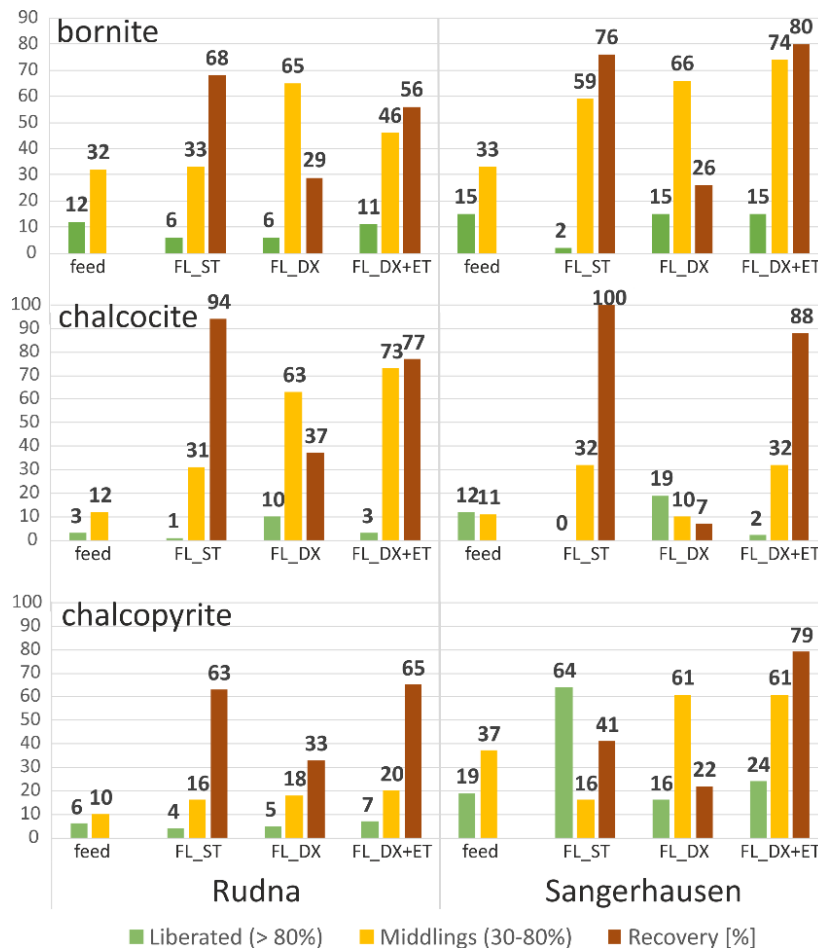


**Figure 4.2.2:** Compilation of the proportion of liberated copper sulphides and middlings in feed and different concentrates. The comparatively increased recovery in general for copper sulphides by flotation using dextrin and ethanol pre-treated feed is caused by commonly increased portions of liberated and partly liberated copper sulphide grains that have been intensified entrained in the flotation product affecting recovery rates. (FL\_ST=standard flotation, FL\_DX=Flotation with dextrin, FL\_DX+ET=flotation with dextrin and ethanol pre-treated feed)

agreement with the more advance liberation of chalcopyrite in the ball mill product of Sangerhausen black shale. A generally more advanced recovery of copper sulphides into concentrates was prevented by the accumulation of partly enormous portions of middlings in tailings. In particular bornite middlings were present with increased portions in flotation tailings of both black shale ores. Additionally, partially moderate portions of chalcopyrite middlings remained in tailings.

Figure 4.2.3 shows the D<sub>80</sub> grain size of copper sulphides in feed and concentrates as well as their recovery in the respective concentrate. As shown previously, the copper sulphide recovery was moderately to extremely increased by flotation using dextrin and ethanol pre-treated feed. Generally, the grain size of chalcocite and chalcopyrite was coarser-grained in flotation concentrates compared to feed. The D<sub>80</sub> grain size of recovered bornite in concentrates gained by flotation with ethanol pre-treated feed was significantly lower to bornite in concentrates from flotation without pre-treatment of the feed, whereas grain sizes for chalcocite and chalcopyrite are coequal with slight deviations. However, it is indicated that in general the recovery of copper sulphides is vastly improved by flotation using ethanol pre-treated feed independently from the grain size.

It was shown that the recovery of copper sulphides was generally improved by flotation using ethanol pre-treated feed. Detailed investigations of liberation data from copper sulphides in

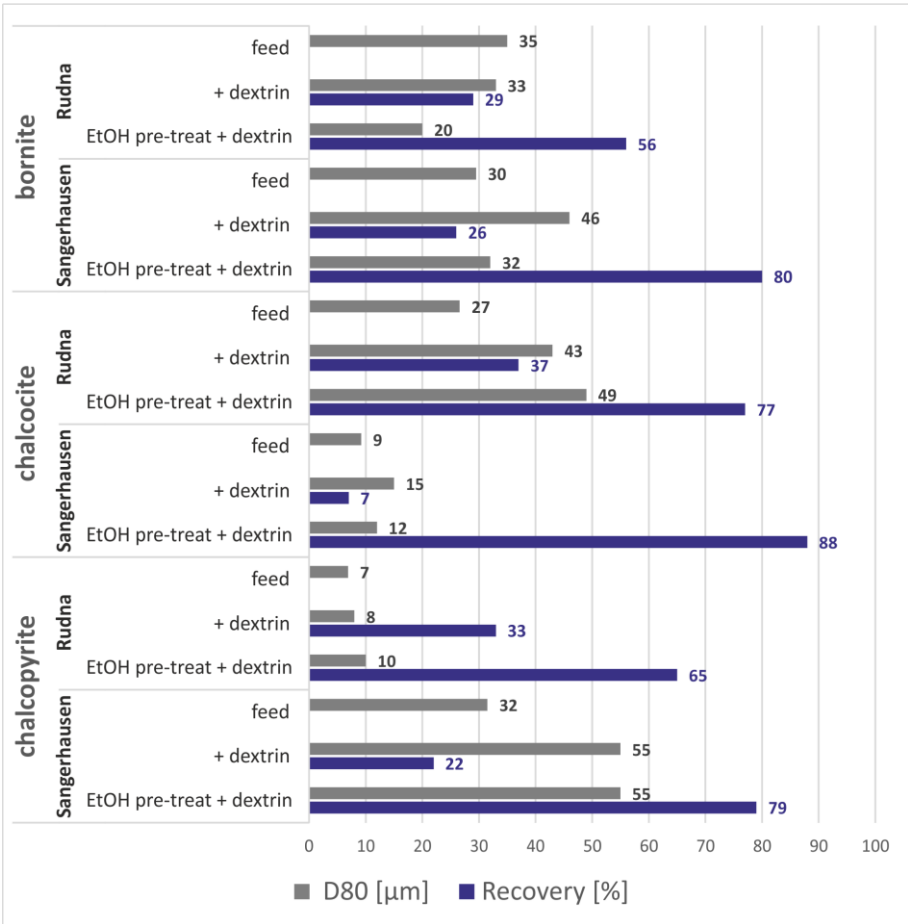


**Figure 4.2.3:** Comparison of the D<sub>80</sub>-grain size of copper sulphides in Rudna and Sangerhausen feed as well as related concentrates gained by flotation using dextrin (+ dextrin) and concentrates from flotation with dextrin and ethanol -pre-treatment (EtOH pre-treat + dextrin) of the feed. The grain size of extracted copper sulphides is partly finer-in the concentrates from flotation using ethanol pre-treated feed or coinciding with concentrated from flotation using only dextrin.

concentrates extracted by flotation with dextrin as well as flotation with dextrin and ethanol pre-treated feed in Chapter 3.2.6.3 revealed that generally increased portions of middlings and partly locked copper sulphides were extracted by flotation using ethanol pre-treated feed. This was especially apparent for bornite in the concentrate from Rudna as well as Sangerhausen black shale feed. Additionally, bornite occurred comparatively increased in the fine-grained particle size range in concentrates from ethanol pre-treated feed. For example, 55% of total bornite occurred in the particle size range -30  $\mu\text{m}$  of the concentrate from the flotation using only dextrin and untreated Rudna black shale feed, whereas 55% of total bornite in the flotation concentrate from ethanol pre-treated Rudna feed were hosted in the -20  $\mu\text{m}$  particle size range. Similar relationships were observed for chalcocite but an increased recovery of more fine-grained chalcopyrite was not observed in the concentrate extracted from ethanol pre-treated Sangerhausen feed, in which however the content of chalcopyrite middlings was also significantly increased.

The proportion of liberated copper sulphides in concentrates was generally increased by flotation using dextrin and untreated feed, but considerably lower amounts of copper sulphide middlings point to a lower recoverability of middlings. However, as was shown, the recovery of copper sulphide middlings was enhanced by flotation using ethanol pre-treated feed.

Sulphides middlings due to their limited liberation consisting of intergrowths of sulphides with each other and/or with gangue mineral phases. Generally, mineral associations of primary occurring complexly (ternary+) locked sulphides in flotation concentrates from as well Rudna as Sangerhausen black shale were dominated by sulphide to sulphide and illite intergrowths, whereas quartz was interlocked subordinately but carbonates were additional moderately associated with copper sulphides in flotation concentrates from Rudna black shale.

Partially considerable differences in the distribution of minerals intergrown with copper sulphides were noticed in the comparison of the concentrate extracted by flotation using dextrin and the concentrate using additionally ethanol pre-treated feed. In the flotation products of Rudna black shale feed, chalcocite was in particular intergrown with bornite and illite. The proportions of mineral phases locked with chalcocite in the concentrate from ethanol pre-treated feed was significantly increased, especially for interlocked sulphides in general and also illite, quartz and carbonates.

Interestingly, for locked bornite it was the opposite in the concentrate from ethanol pre-treated feed, in which generally lower proportions of minerals interlocked with bornite occurred. However, the change of locking proportions was dependent from the content of fully liberated bornite or chalcocite (>95% free perimeter), which was comparatively high for bornite (18.9%) and low for chalcocite (3.7%) in the concentrate extracted from ethanol pre-treated Rudna feed.

In concentrates from Sangerhausen feed the proportion of completely liberated bornite was more increased by dextrin-added flotation but also the concentrate from ethanol pre-treated feed contained a notable amount of liberated bornite. A comparatively high proportion of fully liberated chalcopyrite (28%) was detected in the concentrate from ethanol pre-treated feed, whereas flotation with dextrin and untreated feed extracted comparably less complete liberated chalcopyrite, which was also indicated by the improved recovery of chalcopyrite in the flotation product extracted from ethanol pre-treated feed.

The increased recovery of copper sulphide middlings by ethanol pre-treatment of black shale feed is also expressed by increased proportions of minerals involved in predominantly occurring complex (ternary+) intergrowths of copper sulphides.

#### 4.2.1.2 Influence of dextrin and ethanol pre-treatment regarding the flotability and recovery of sulphides

The main aim in the flotation of sulphides is to bring their exposed particle surfaces in a hydrophobic state in order to be entrained by bubble interaction into the froth product, whereas rock-forming gangue mineral surfaces are being held in a hydrophilic state in order to depress them into tailings. The usage of polysaccharides in mineral flotation is widely known and established for almost 90 years. Starch and its derivate dextrin are natural organic polymers that are non-toxic and biodegradable. Thus, dextrin used in flotation as a selective depressant was used to target the selective separation of different mineral species. Commonly, dextrin is used as selective depressant due to the different adsorption on various minerals. Applications of dextrin for selective flotation were conducted to achieve the depression of galena or pyrite but also graphite (Drzymala et al., 2003; López Valdivieso et al., 2004; Subramanian and Laskowski, 1993). Generally, dextrin adsorbs by interaction of acidic hydroxyl groups with metal hydroxide species formed by oxidation onto sulphide surface. This takes place on various sulphides at different pH values as it was shown, for instance, for copper (pH 4-9) and lead hydroxides (pH 10-11) (Liu and Laskowski, 1989a). Thus, an oxidation layer onto sulphide mineral surfaces is a prerequisite to their flotability. It was determined that increased surface hydrophobicity enhances to the adsorption of dextrin, which result in preferred flotability of copper sulphides (Liu and Laskowski, 1989b). The flotation tests using dextrin carried out on not ethanol pre-treated Rudna and Sangerhausen black shale showed clearly that the selectivity to flotate copper sulphides was attained to a high degree, which is expressed by the extremely low mass recovery in flotation products.

Flotation experiments with Rudna and Sangerhausen black shale were conducted generally at pH 10 and the usage of dextrin commonly yield in an increased content of galena in tailings, more enhanced by flotation of Rudna feed and rather less for Sangerhausen feed in comparison to standard flotation and flotation with ethanol pre-treated feed. Similar observations regarding the separation and depression of galena were reported by several authors (Drzymala et al., 2003; Liu and Laskowski, 1989b; Rath and Subramanian, 1999). Stronger depression into tailings was noticed for pyrite in particular by flotation of Sangerhausen feed with dextrin. This stands in agreement to earlier works, which emphasized that dextrin is considered to be a good depressant for pyrite in the pH range above pH 4 so that the usage of dextrin in sulphide flotation favour the depression of pyrite into tailings (Kydos et al., 1994; López Valdivieso et al., 2004). The depression of pyrite into tailings was though only ascertained in respect to the flotation with dextrin of Sangerhausen black shale, although Rudna and Sangerhausen feed contained similar proportions of pyrite. Flotation with dextrin and ethanol pre-treated Sangerhausen feed yielded in even more enhanced accumulation of pyrite in the respective tailings.

Additionally, the organic carbon content was substantially decreased in concentrates extracted by flotation using dextrin. Approaches to diminish the organic carbon content in flotation products were followed by several studies (Drzymala et al., 2003; Liu et al., 2000; Liu and Laskowski, 1989a; Qin et al., 2013).

Although copper sulphides were considerable enriched in concentrates by flotation using dextrin, the selectivity concerning their flotability was extremely pronounced and liberated copper sulphide grains were primarily entrained into the froth product as shown in Chapter 3.2.6.3. The recovery of middlings and even more locked copper sulphide was significantly lower by application of dextrin without ethanol pre-treatment of the feed, which is clearly documented by liberation analyses and

contributes vitally to the low mass and copper recovery in the products of dextrin-added flotation without ethanol pre-treated feed.

By far improved copper and mass recovery rates were achieved by flotation combining the application of dextrin and ethanol pre-treated feed. Liberation analyses of dominant copper sulphides in concentrates extracted by flotation with dextrin as well as with dextrin and ethanol pre-treated Rudna and Sangerhausen black shale feed have shown that a significantly increased recovery of copper sulphide middlings was caused by ethanol pre-treatment of the feed. The use of dextrin lead to higher selectivity in the flotation of base metal sulphides, whereas the ethanol pre-treatment obviously achieves that increased portions of copper sulphides marked by intergrowths with gangue were entrained in the froth product.

Generally, entrainment is mainly controlled by the interaction of hydrophobic mineral particle surfaces with the air bubble flow. Key factors of particle attachment onto air bubbles are contact angle and attachment area.

It is known that ethanol is better solved by gases (air) than in water (flotation solution) by its higher gas solubility. Due to that, molecules of gas (air) diffuse out the ethanol attached onto mineral surfaces and nanobubbles are formed on the hydrophobic mineral surfaces. The formation of nanobubbles, which widens generally the potential attachment area from tenth to more than hundred nanometres. Nanobubbles represent interfaces on which larger air bubbles can potentially attach and consequently particles occupied by nanobubbles are entrain into the froth product (Hampton and Nguyen, 2010; Holuszko et al., 2008).

It was found that the presence of nanobubbles mediate hydrophobic forces, which result in an increasing strength of attachment on larger gas bubbles (Zhang et al., 2006). Although the hydrophobic force is rather considered to be a nanobubble bridging capillary force, which is thought to be a combination of two mechanism: the force resulting from the rupture between two nanobubbles or a nanobubble and a hydrophobic mineral surface as well as the capillary force of the resulting gas bridge between the ethanol film onto mineral surface and gas (Hampton and Nguyen, 2010). Consequently, ethanol wetted hydrophobic mineral surfaces have stronger attraction forces by attached nanobubbles and also larger potential areas, where the interaction of bubble attachments result in larger capillary bridges (Holuszko et al., 2008).

Thus, the relationship that ethanol wetted particles favouring the formation of nanobubbles onto hydrophobic mineral (sulphide) and enhancing the attractive force to the attachment onto gas bubbles by increasing attachment areas can be regarded to be the main process, by which concentrates generated by flotation of ethanol pre-treated Sangerhausen and Rudna black shale feed contained generally increased proportions of copper sulphide middlings. It is obvious that particles containing partially liberated copper sulphide can be successfully flotated if their surface is wetted by ethanol. Up to date, improved flotability of copper sulphides achieved by an ethanol pre-treatment step of the feed are not documented neither for similar complex ores nor in relation to black shales.

The use of dextrin plays apparently a decisive role in the selectivity to recover copper sulphides and the combination with ethanol pre-treatment of the feed increases the capability to form suitable attachment areas for the interaction of gas and particle surfaces providing stronger capillary bridges to entrain increasingly also less liberated copper sulphides into the froth product.

#### 4.2.2 Content of copper and associated metals in concentrates from Kupferschiefer-type ore

Concentrates gained from ethanol pre-treated black shale feed were marked by an increased copper content (Rudna: 10.0%, Sangerhausen: 14.4%) but generally the copper enrichment was too low to be exploitable concentrates and thus they would not be saleable to smelters, even by the issues arise by their processability in particular in flash smelters, mainly caused by increased organic carbon and galena content. Constantly decreasing copper contents in concentrates produced in the three mineral processing plants of the Lubin-Sieroszowice mining district is recently an economically important issue, of which KGHM is generally faced with and influences the company's copper production notably. Due to the decreasing thickness of ore zones and fading copper content in the mineable sandstone layer, increased proportions of highly mineralized black shale were used to balance the copper content in the mixed ore fed to flotation plants. Since the last 30 years, a partly doubled black shale fraction in the mixed ore was processed especially in Rudna and Polkowice concentrators. However, it was reported that finely disseminated copper sulphides hosted in the black shale feed are considerably enriched in tailings of the 1<sup>st</sup> stage cleaning flotation, which result in serious problems in the recovery of copper (Chmielewski et al., 2014; Konieczny et al., 2013). Drzymala et al. (2013) showed by modelling of grade-recovery curves that the maximal theoretical copper content in concentrates from black shale ore was generally significantly below of that from sandstone feed. Due to that organic carbon is regarded to interfere the recovery of fine-grained copper sulphide particles principally, lab-to industrial scale approaches to diminish organic carbon content prior to flotation were undertaken by KGHM and ended up finally in the segregation in pre-concentrates, one poor and a second rich in organic matter (Konieczny et al., 2013). Previous studies to depress organic matter by refloatation (segregation flotation) of final flotation concentrates into two copper concentrates marked either by increased copper or increased organic carbon content were successfully carried out by using

**Table 4.2.1:** Concentrations of base metals and associated trace metals in different copper concentrates produced from different feeds. (<sup>A</sup> black shale feed, KGHM; <sup>B</sup> mixed ore feed, KGHM, data from Chmielewski (2015) and Chmielewski et al. (2014a); <sup>C</sup> mixed ore feed, KGHM; <sup>D</sup> black shale feed, UVR-FIA, flotation with dextrin and ethanol pre-treatment of the feed. (grey background=this thesis))

Feed	Year	Cu	Pb	Zn	Ag	Co	Ni	Mo	V
		[%]	[%]	[%]	[ppm]	[ppm]	[ppm]	[ppm]	[ppm]
Lubin <sup>A</sup>	2006	14.7	2.9	0.4	782	1059	455	279	455
Lubin <sup>B</sup>	2009	15.9	2.7	0.9	877	1040	415	344	708
Lubin <sup>B</sup>	2010	15.3	4.0	0.9	938	1206	488	265	569
Lubin <sup>B</sup>	2011	14.6	3.9	0.6	755	1250	483	221	672
Lubin <sup>B</sup>	2012	14.0	4.8	0.7	736	1325	461	257	670
Lubin <sup>B</sup>	2013	12.9	5.4	0.7	455	1482	494	272	657
Lubin <sup>C</sup>	2015	14.0	4.6	1.2	672	1480	608	368	779
Rudna <sup>D</sup>	2017	10.0	7.1	0.1	611	301	400	439	1210
Sangerhausen <sup>D</sup>	2017	14.4	7.4	1.3	452	1040	386	697	1620

maltodextrin as frother (Foszcz and Drzymala, 2011). The depressing feature of dextrin in the flotation of black shale feed can be supported by investigations within this study.

Copper contents achieved for concentrates generated in the flotation plants of KGHM-owned processing facilities are similar to that of the concentrate from ethanol pre-treated Sangerhausen feed (14.4% Cu), as copper contents of different Lubin concentrates investigated additionally in this study indicated likewise. However, recently copper contents of Polish concentrates are decreasing as reported exemplarily for Lubin flotation concentrates, which had 15.9% Cu in 2009 and decreased to 12.9% Cu in 2013, as Table 4.2.1 indicates. This was accompanied by a significant increase of the lead content (2009: 2.7%, 2013: 5.4%), which is unwanted regarding the processing in the smelter. Similar reductions of the copper content were reported for concentrates originate from the concentrator facilities in Rudna and Polkowice and were substantially caused by increasing black shale fractions in flotation feeds (Chmielewski et al., 2014).

Copper concentrates derived from Kupferschiefer-type ore contain, besides copper, numerous value trace metals such as Ag, Co, Ni, Mo and V. While the content of Ag was significantly increased in the Rudna black shale feed (226 ppm), Sangerhausen black shale contained only a third (73 ppm). However, in particular the content of V (737 vs. 462 ppm) and Co (743 vs. 120 ppm) were more

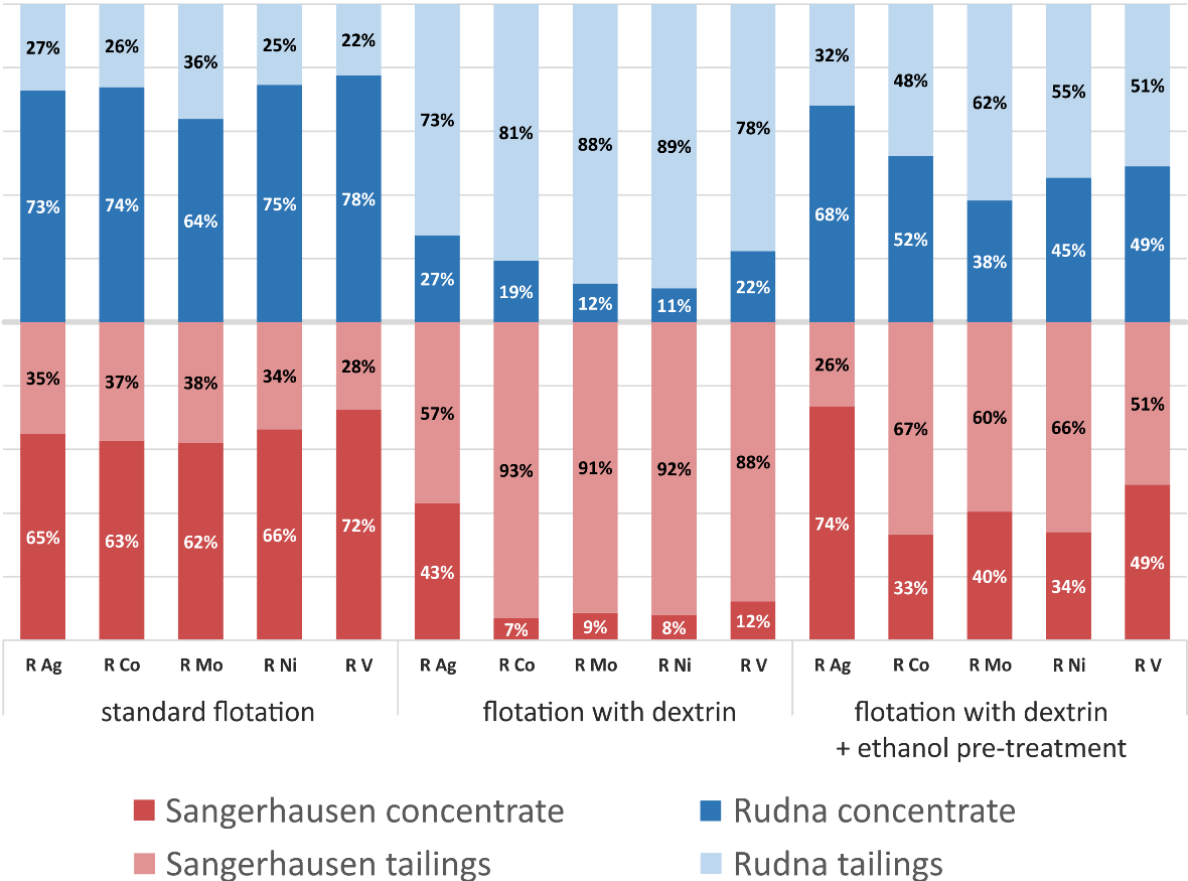


**Figure 4.2.4:** Recovery proportions of selected trace metals associated with Kupferschiefer-type mineralization. According to the low and selective recovery of copper sulphides as well as other sulphides (e.g. pyrite) by flotation using dextrin, trace metal recovery is extremely low. Similar increased recovery rates for Ag are displayed for standard flotation and flotation with dextrin and ethanol pre-treated feed. Low recovery of Co, Mo, Ni, V are mainly caused by depression of pyrite and organic matter by flotation using dextrin. Moderate recovery rates were achieved by flotation using dextrin and ethanol pre-treated feed.

increased in Sangerhausen feed, whereas concentrations of Mo and Ni were generally lower and a coequal range in both black shale feed.

As shown in Chapters 3.2.4.1 and 3.2.5.1, flotation with dextrin yield in considerable increase of the content of the most trace metals in concentrates from as well Rudna as Sangerhausen feed. However, the recovery of trace metals was generally most increased by the standard sulphide flotation tests of both, Rudna and Sangerhausen black shale feed, which can be attributed to the high mass recovery in the concentrates of about 50%. Recovery proportions of selected trace metals are depicted in Figure 4.2.4, which indicates that their recovery was slightly increased in the concentrate gained by standard flotation of Rudna black shale (64-78%), whereas in the concentrate from Sangerhausen feed recovery rates were slightly lower (60-72%). Flotation with dextrin was generally marked by low mass recovery in the product, which is also accompanied by commonly low recovery rates (< 20%) for trace metals, just Ag was enriched moderately, especially in the product from Sangerhausen feed (Rudna: 27%, Sangerhausen: 43%). Flotation with dextrin and ethanol pre-treated feed extracted generally mass proportions of about 30% and showed exemplarily a similar recovery rate for Ag (Rudna:68%, Sangerhausen: 74%) as achieved by standard flotation. Recovery rates for Co, Mo, Ni and V are in comparison considerably lower, commonly below 50%, which indicates that the main portion of trace metals occurred in tailings and thus difficult to recover.

Lubin concentrates investigated in this study showed comparable increased amounts of in particular Ag (between 636 and 782 ppm) as well as Co (1059-1480 ppm) that correspond to reported contents of concentrates from the Lubin Concentrator (Chmielewski, 2015). Concentrates from flotation tests using dextrin and ethanol pre-treated feed show comparable increased Ag-contents (Rudna conc.: 611 ppm, Sangerhausen conc.: 452 ppm) but the Co content is very different, low in the concentrate from Rudna black shale(301 ppm) and similar increased as for Lubin concentrates in the concentrate from Sangerhausen black shale feed (1040 ppm).

Geochemical data of concentrates and tailings from the flotation tests conducted with Rudna and Sangerhausen black shale revealed metal-to-metal correlations. In particular Cu- and Ag-values of flotation products and tailings from Rudna black shale feed correlate as Figure 4.2.5 shows indicating that Ag is mainly hosted in chalcocite, which is known to be a decisive Ag-carrier among the sulphide assemblage in the Rudna ore. Additionally, Figure 4.2.6 depicts the correlation of Fe with Co and As,

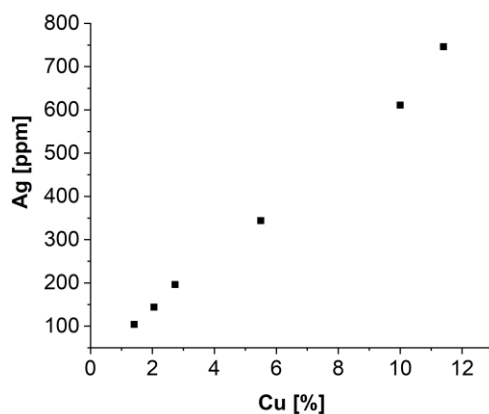


**Figure 4.2.5:** Extremely good correlation of Cu and Ag in Rudna concentrates and tailings indicating that chalcocite hosts significant amounts of Ag.

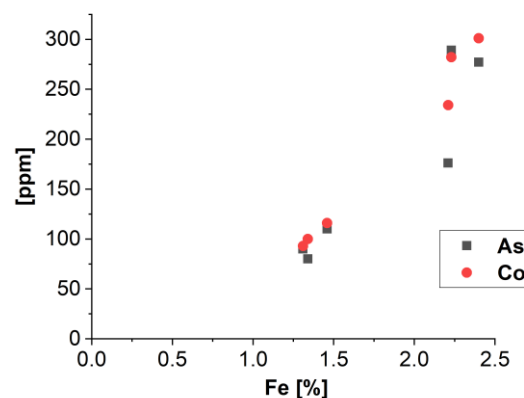


**Figure 4.2.6:** The correlation of As and Co with Fe in Rudna concentrates and tailings reveal the association with pyrite.

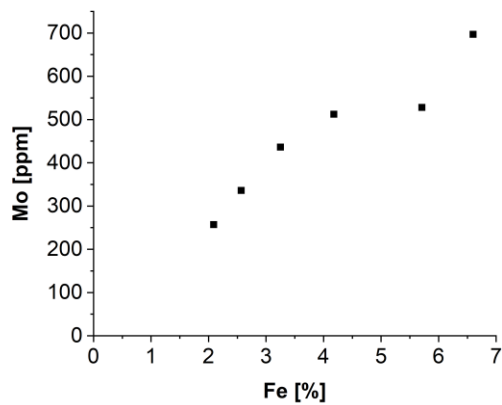


**Figure 4.2.7:** Correlation of Mo and Fe in Sangerhausen concentrates and tailings indicate that occurrence of Mo is related to pyrite.

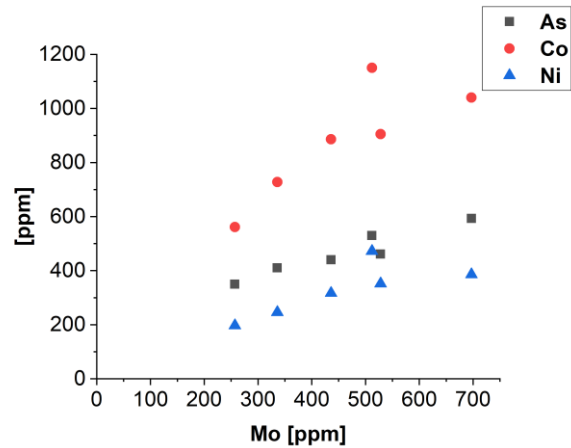


**Figure 4.2.8:** Additional correlation of Mo with As, Co and Ni implies that Mo could also associated to cobaltite or gersdorffite.

by what clearly points to cobaltite (CoAsS) occurrence as well as that Co and As are associated with pyrite, which can substitute several percent of Co into the crystal lattice. Furthermore, the correlation of Fe- and Mo-contents reveals that Mo was obviously also incorporated in pyrite.

In concentrates and tailings of Sangerhausen black shale, a correlation of trace metals was mainly found for Co, which was related to Ni, As and Fe, indicating the presence of cobaltite but also that Co was partly associated with pyrite. The latter hosted apparently also Mo by the correlation with Fe, shown in Figure 4.2.7, whereas Mo correlated furthermore with Ni, Co and As, as Figure 4.2.8, whereby a substitution into cobaltite or even gersdorffite seems to be obvious.

## 4.3 Bioleaching

Results of mineral distribution analyses of bioleaching residues were mainly used to draw relationships of mineral constituents soluble by bioleaching and residual minerals phases. Additionally, mineral distribution was used to quantify mineral dissolution both in final bioleaching residues and consecutive residues of a slightly different bioleaching approach. Recovery rates of copper and base metal sulphides determined by a methodology based on advanced mineral characterization as well as process-related features of minerals of interest were used to determine the leaching performance of sulphides, especially copper sulphides but with special attention to chalcopyrite. Mineralogical mass balances instead of simple metals mass balances were used to draw conclusions in respect to leaching efficiency and of the bioleaching process prior to upscaling.

### 4.3.1 Leaching performance of copper sulphides and copper recovery by bioleaching of different black shale related feed

The performance to dissolve copper mineral species represents the most crucial factor for the economic feasibility in bioleaching operations extracting copper. Therefore, the mineralogical composition of the feed regarding both, copper sulphides and gangue minerals, is the driving key factor, besides technological parameters, to recover copper and associated by-products. Gangue minerals in feeds of bioleaching operations using acidophilic bacteria communities are generally considered to be a cost factor in the overall economic balance. Especially, rock-forming minerals readily soluble under acid condition such as carbonate minerals cause increasing consumption of acid due to their dissolution in the leaching process by keeping pH condition stable for suitable ambient conditions that promote the optimal activity for the bacteria community. Because the pH optimum for acidophilic, autotrophic, mineral oxidising bacteria is at pH 1.7, feed material rich in carbonates consume accordingly higher amounts of acid.

Investigation of the mineral distribution in feed material and bioleaching residues have shown on the one hand that sulphide assemblages were differently in feeds and on the other hand that in particular the dissolution of individual copper sulphide minerals by bioleaching was strong varying. Additionally, the grade of target minerals in the feed was a crucial prerequisite if bioleaching promotes advanced dissolution rates as shown for bioleaching experiments on black shale ball mill products, in which generally the metal recovery by bioleaching insignificantly differed, especially for Cu, from sterile acid leaching tests. But it has to be conceded that bioleaching of Sangerhausen black shale achieved a far advanced Cu-recovery (92%), which represents a comparatively improved recovery yield considering that long-time bioleaching bath tests (26 days) of Cu-rich Rudna black shale (7.0% Cu) achieved a considerable lower Cu-recovery (60%) and even lower by bioleaching in columns over a period of 95 days (33.4%) (Szubert et al., 2017).

It was shown that increased contents of base metal sulphides provided by flotation concentrates of black shale feed revealed substantial deviations in the leaching performance of bioleaching in comparison to sterile control leaching. While improved recovery rates were conspicuous for Zn by bioleaching of black shale ores, a more advanced dissolution commonly of base metal sulphides is clearly apparent by bioleaching of flotation concentrates, in which the leaching performance exceeds that of sterile control leaching substantially. However, it has to be mentioned that the bioleaching of Sangerhausen black shale yield also in partly improved recovery of particularly trace metals, especially

for As, Mo and U, which has also been mentioned in the course of bioleaching experiments using *Acidithiobacillus ferrooxidans* on black shale feed from a Pakistan occurrence (Anjum et al., 2009).

Figure 4.3.1 summarizes recovery yields achieved by bioleaching and sterile control leaching of three concentrates originating from feed of different black shale deposits. Substantially increased copper recovery in comparison to sterile control leaching was achieved by bioleaching of flotation concentrates. Here, exceptionally elevated Cu-recovery (87%) was obtained by bioleaching of the concentrate extracted by flotation using dextrin and ethanol pre-treated Rudna black shale feed, by which 58% more Cu was extracted compared to sterile control leaching. Significant lower but improved recovery rates in comparison to sterile leaching were achieved by bioleaching of flotation concentrate from Sangerhausen (+34%) black shale as well as Lubin concentrate LC15a (+32%), although the general high copper recovery of 85% was coequal to bioleaching of the Rudna concentrate. Furthermore, bioleaching of Lubin concentrate LC15b yield in 79% Cu-recovery, whereas the recovery of Cu from Lubin concentrate LCA06 was more efficient (92%), as indicated in Figure 4.3.2. Comparative data from sterile leaching tests were not available so that an improvement for these bioleaching tests cannot be quoted. However, slightly increased Cu-recovery rates (95-97%) were reported for similar bioleaching batch tests on a acidified Lubin concentrate, slightly different in terms of chemical and mineralogical composition to Lubin concentrates addressed in this thesis, were reported by several authors involved to the “Bioshale” research project (Gouin, 2008; Spolaore et al., 2011, 2009). Spolaore et al. (2011, 2009). argued that a complete copper recovery was limited due to the incomplete dissolution of chalcopyrite and that an improved copper recovery could be achieved by finer milling of the feed (< 20 µm), which is however, economically disadvantageous by increasing operational costs as previously already noted by Watling (2006). Although it was also conceded that chalcopyrite is passivated during the bioleaching process (Spolaore et al., 2011).

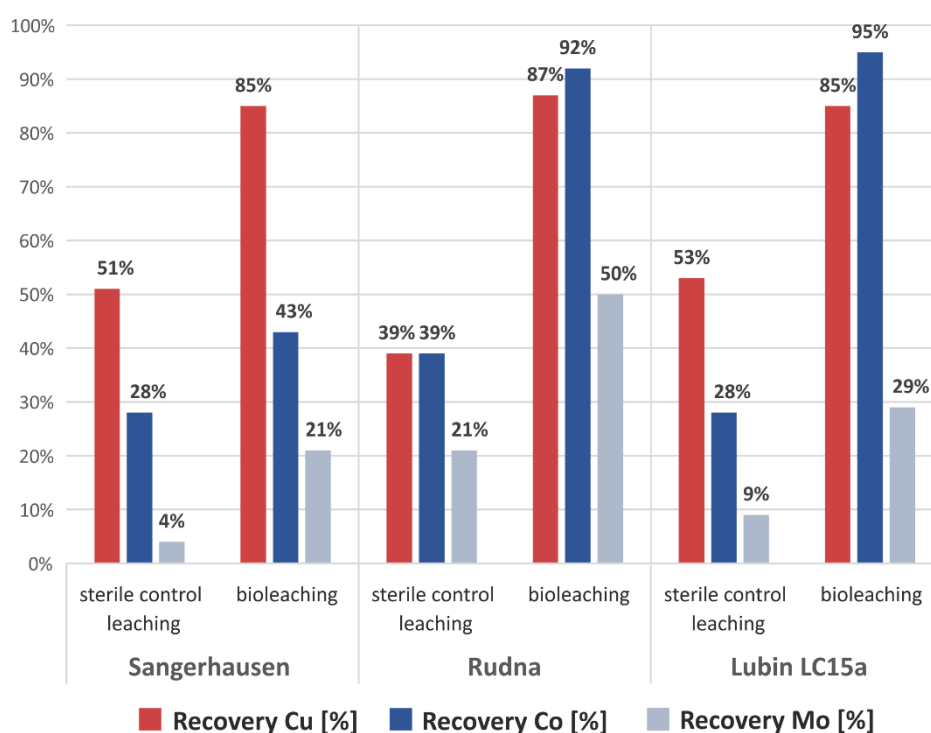


**Figure 4.3.1:** Comparison of the recovery of Cu, Co and Mo by bioleaching tests of different copper flotation concentrates. Bioleaching yielded generally in considerably increase recovery, recovery rates for bioleaching of Rudna and Lubin concentrate LC15a were especially increased.

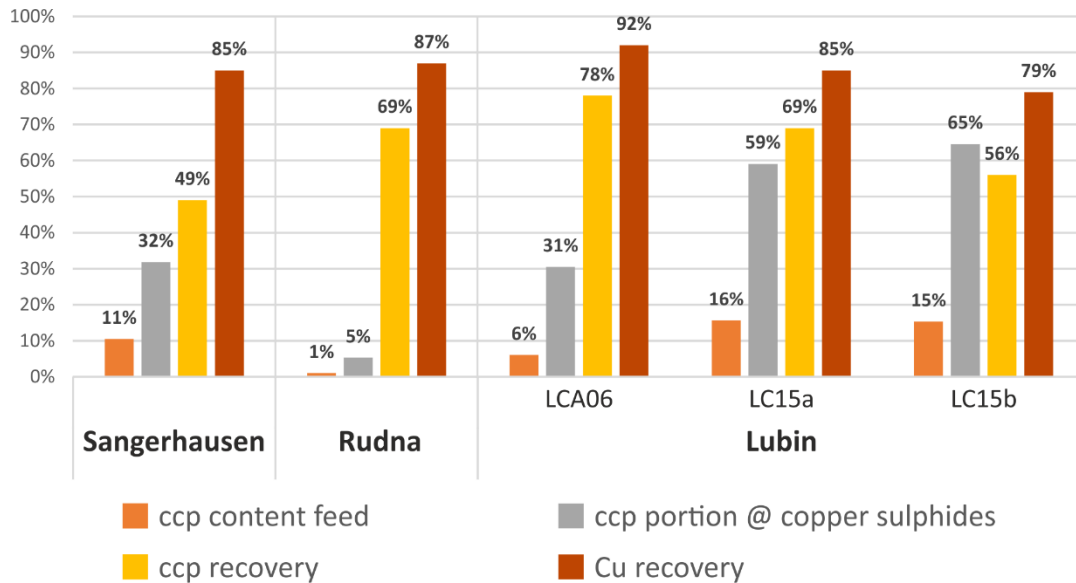


**Figure 4.3.2:** Relationship of chalcopyrite (ccp) content in feed and the portion among copper sulphides in regards to the dissolution capacity (recovery) of chalcopyrite and to the total Cu-recovery. The amount of chalcopyrite in the feed is not decisive for dissolution capacity by bioleaching but its portion of copper sulphides and the rate of dissolution affect obviously the Cu-recovery

Mineral distribution analyses on feed concentrates and related bioleaching residues revealed nearly complete to complete dissolution of bornite (92-100%) and chalcocite (94-100%). In contrast to that, the dissolution of chalcopyrite was considerably lower and different in the various bioleaching tests. Depending on the content of chalcopyrite and its proportion among the three main copper sulphides in the feed, the limited dissolution of chalcopyrite influences the Cu-recovery crucially. As Figure 4.3.2 illustrates, the copper sulphide assemblage of Lubin concentrates LC15a and LC15b is dominated by chalcopyrite by a portion of around 60%. The increased dissolution of chalcopyrite by bioleaching of LC15a (69%) has a notable contribution to the more advanced Cu-recovery (85%), whereas the lower recovery rate of chalcopyrite in LC15b (56%) affected the Cu recovery negatively so that it is notably lower (79%).

Moderate proportion of chalcopyrite of around 30% among the copper sulphides occurred in the flotation concentrate of ethanol pre-treated Sangerhausen black shale and in the Lubin concentrate LCA06. Despite the similar proportion of chalcopyrite, the Sangerhausen concentrates was marked by more increased chalcopyrite content (10.5% vs. 6.1% in LCA06) but the recovery of chalcopyrite was significantly lower (49% vs. 78% in LCA06) and thus, accordingly the total Cu-recovery in LCA06 was increased and with 92% the most advanced among the bioleaching tests, whereas bioleaching of Sangerhausen concentrate yield in 85% Cu-recovery. Apparently, the dissolution of chalcopyrite by bioleaching of Lubin concentrate LCA06 was more advanced, which was possibly promoted by the acidification step with sulphuric acid prior to bioleaching. Acidification was mainly aimed to remove the carbonate fraction and caused additionally increased liberation of chalcopyrite in front of the bioleaching test. However, due to the usage of sulfuric acid in bioleaching tests to lower and stabilize the required pH conditions, carbonates are readily dissolved during the first day in the course of bioleaching using acidophilic bacteria. Thus, an increased liberation of generally sulphides/copper sulphides and in particular chalcopyrite is achieved likewise at the beginning of bioleaching. However, it was observed that due to the treatment by sulfuric acid, Lubin concentrate LCA06 contained

considerable amounts of Pb-, Cu-, Fe-sulphates commonly enclosing sulphides caused by oxidation. Thus, the treatment with sulphuric acid creates on the one hand enhanced liberation of copper sulphides but on the other hand it forms secondary sulphate coatings on sulphide surfaces, which though are partly readily soluble when introduced into the bioleaching liquor, whereas in not pre-treated feeds the dissolution of carbonates and oxidation of sulphides starts from the insertion into the bioleaching liquor. Thus, acidification of the feed prior to bioleaching could affect the dissolution of chalcopyrite and support improved Cu-recovery rates.

Due to the low content of chalcopyrite (1%) in the Rudna concentrate, the moderately increased recovery of chalcopyrite (69%) had a slight influence to the Cu-recovery and therefore can be neglected.

#### 4.3.2 Recoverability of trace metals concerning dissolution of sulphides in bioleaching processes

The compilation of recovery yields for selected metals in Figure 4.3.1 clarifies that bioleaching was more efficient not only for Cu, as increased recovery rates of Zn and Fe indicate. Other accompanying trace metals, such as As, Co, Mo, and U, showed adequate leaching behaviours, whereas Ag, Sb and V indicate lower recoverability very similar to sterile control leaching tests. In particular Pb was marked by relative enrichment in both types of leaching residues, which is illustrated by the limited solubility of predominantly galena as well as the missing capability of dissolved lead ions to remain in the process solution by the onset formation of lead sulfate compounds at low pH conditions.

Copper flotation concentrates extracted from Kupferschiefer-type ores were partly enriched in Ag. However, bioleaching and even sterile control leaching was not capable to extract Ag, which was indicated especially by the relative enrichment in the residues. SEM-observations and mineral distribution analysis revealed that Ag was mainly associated with secondary formed precipitates such as Fe-Cu-sulphate and widespread anglesite-like Pb-sulphate but was also found in bioleaching residues as argentite or incorporated into galena. It is known that besides galena, chalcocite hosts partly significantly amounts of Ag. Due to the complete dissolution of chalcocite by bioleaching, Ag-ions are released to the leaching solution, where they obviously attached onto metal-sulphate complexes and remain as amorphous or microcrystalline coatings onto other remaining mineral particles or as irregular porous precipitate aggregates. Increasing Ag concentrations in the leaching residues indicate that Ag is not recoverable, even though it is partly dissolved from the dissolution of mainly chalcocite and subordinate galena. However, Ag-ions cannot keep in the bioleaching liquor due to preferred chemical affinity to sulphate and chlorine-complexes, abundant in the leaching solution, at low pH- conditions.

Bioleaching of copper concentrates generated from lithotypes hosting Kupferschiefer-type mineralization yield in partly improved recovery of trace metals in comparison to sterile acid leaching. In particular Co and Mo showed significantly increased recovery rates by bioleaching of Rudna and Lubin concentrates. While the latter contained trace amounts of cobaltite (0.1-0.7%), cobaltite in Rudna concentrate was not detected by mineral distribution analysis, which is also expressed by considerable deviating amounts of Co in geochemical data (Rudna: 301 ppm; Lubin: 1040-1480 ppm). Generally, the Co-recovery by bioleaching was improved by more than 50% compared to sterile leaching and rose to 84-96%, as Figure 4.3.3 shows. This can be mainly attributed to the dissolution of cobaltite in the case of Lubin concentrates, whereas the lower but increased Co-recovery by

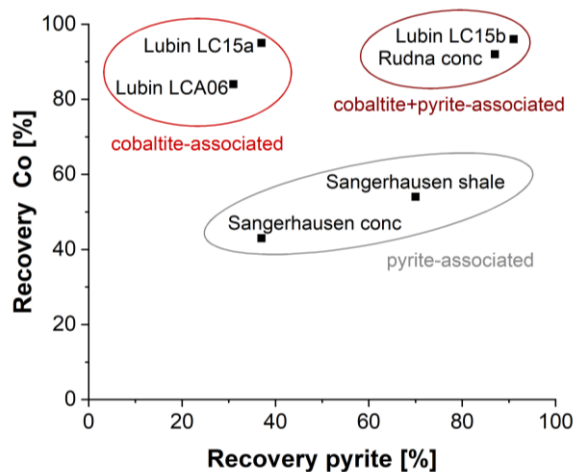


**Figure 4.3.3:** Binary plot illustrating the relationship of recovered Co in respect to dissolution of pyrite. It seems that cobalt in Lubin concentrates is more associated with cobaltite. In Sangerhausen feed Co is more related to pyrite.

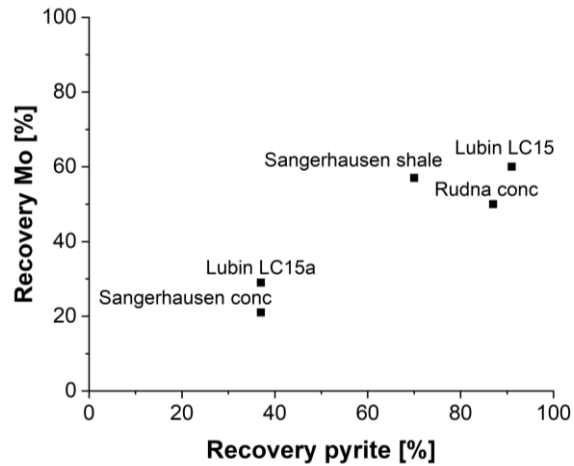


**Figure 4.3.4:** Correlation of the dissolution capacity of pyrite with recovery rates of Mo, which applies for most of the bioleaching tests. Only bioleaching of Lubin concentrate LCA06 showed no association with pyrite at all.

bioleaching of Rudna and Sangerhausen concentrate is apparently coupled with the elevated dissolution of pyrite resulting in 40% more recovery compared to sterile leaching, which was in accordance to bioleaching of Lubin concentrates. Thus, the increased recovery of pyrite favours significantly the improvement of Co-recovery rates. Comparable recovery rates of Co by bioleaching of black shale-related feed were differently reported. While Gouin (2008) stated 85% Co-recovery, bioleaching of two Lubin concentrates (12.3% Cu) with pure *acidithiobacillus ferrooxidans* yield in 91.1% and 79.2% Co-recovery at similar Co-contents of 1260 and 1350 ppm in the feed (Uryga et al., 2004)

A moderately improved recovery of Mo by bioleaching is generally feasible, which is documented by 20-30% higher recovery compared to sterile leaching. Mo minerals were not detected neither by mineral distribution analyses nor by microscopic investigations but fine and rarely occurring molybdenite is known to be associated with black shale (Alderton et al., 2016). Although molybdenite is rather depressed by flotation with dextrin into tailings (Drzymala et al., 2003), fine-grained molybdenite could be entrained in particles containing organic matter or copper sulphides, with which finely intergrown molybdenite is mainly associated. However, Mo in concentrates is also considered to be entrapped in the pyrite crystal lattice, although increased substitution into cobaltite minerals is also eligible. The increasing recovery rates of pyrite correlate mostly with the increasing recovery of Mo, as shown in Figure 4.3.4, which was in particular ascertained for bioleaching of Rudna and Lubin concentrates, whereas the considerably lower recovery of pyrite by bioleaching of the Sangerhausen concentrate yield in the noticeable lower recovery of Mo.

A well-recognizable common trend of the recovery of pyrite as well as Co, Mo and Ni shows Figure 4.3.5, which present recovery rates from bioleaching tests with increasing leaching time of Lubin concentrate LC15b. However, the recovery curves of the trace metals demonstrate especially that the main part is recovered during the first four days of total leaching time, which stands in agreement with correlating recovery rates of sulphides in general. After day 4, the increase of the recovery for Co, Mo and Ni slows down and also the pyrite recovery rate is lowered, besides that the main portion of total

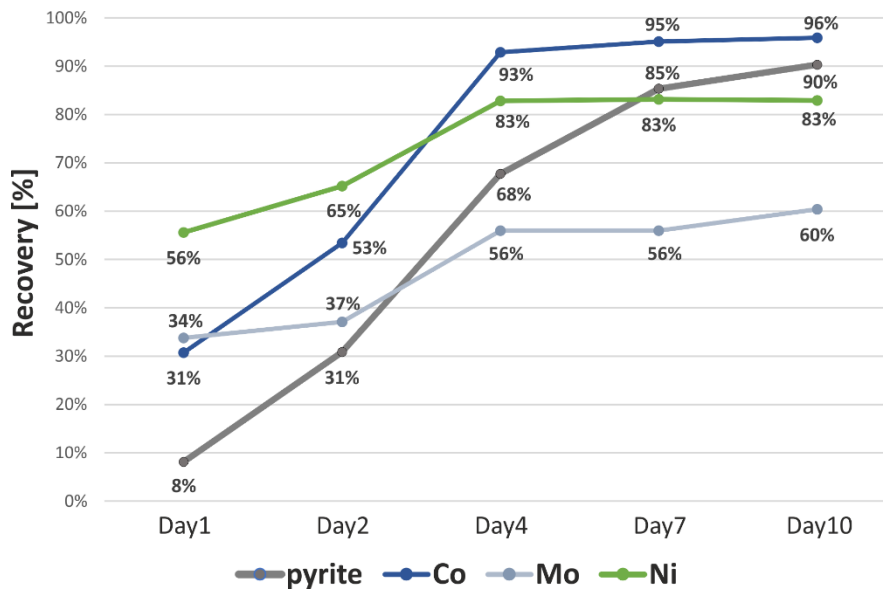


**Figure 4.3.5:** Dissolution rates of Co, Mo and Ni in relation to pyrite showing continuously increasing recovery up to Day 4 in the bioleaching experiment with Lubin concentrate LC15b, which is partly congruent with the dissolution of pyrite. But the considerable recovery of pyrite from Day 4 to Day 10 seems to affect recovery rates of Co, Mo and Ni insignificantly.

recovered pyrite (75%) was dissolved beforehand. Thus, the pyrite dissolution promotes obviously the recovery of trace metals such as Co, Mo and Ni.

#### 4.3.3 Mineralogical factors controlling the restricted dissolution of chalcopyrite

The main challenge to improve copper recovery by bioleaching of polymetallic complex feeds containing several copper sulphides represents the enhanced dissolution of the chalcopyrite, because obviously a complete recovery is commonly hindered. Mineral distribution analyses of bioleaching residues originating from different copper flotation concentrates have shown that the chalcopyrite recovery in bioleaching experiments was partly considerably deviating. Regarding comparable bioleaching tests, the recovery rate of chalcopyrite was substantially lower at nearly 50% by bioleaching of the Sangerhausen concentrate, whereas more advanced recovery of chalcopyrite was achieved by bioleaching of the concentrate extracted from Rudna black shale (69%) as well as Lubin concentrates LCA06 (78%) and LC15a (69%). In a different experimental approach of bioleaching of Lubin concentrate LC15b, the Cu-recovery was in turn significant lower (56%).

Generally, the comparison of mineralogical properties of chalcopyrite in different feed materials shows that the degree of liberation, chalcopyrite grain size as well as locking association of locked chalcopyrite indicate no favourable trend, why chalcopyrite was more advanced dissolved by bioleaching from distinct feed concentrates. Low liberation of chalcopyrite as ascertained in the concentrate generated from ethanol pre-treated Rudna black shale was not decisively as shown by far increased liberation in concentrate gained from ethanol pre-treated Sangerhausen black shale, by which the recovery of chalcopyrite by bioleaching was substantially lower (49% vs. 69%). However, chalcopyrite is generally more intergrown with carbonates in Rudna black shale, while in Sangerhausen black shale chalcopyrite is mainly associated, besides other sulphides, with gangue minerals such as illite, quartz, feldspar or barite and apatite, which in sum all represent hardly leachable minerals mostly

considered to be refractory by leaching. It can be assumed that the excess of sulfuric acid in the bioleaching liquor during the whole course of the tests caused the extensively dissolution of carbonate minerals but not the silicate phases, which leads to highly enhanced liberation of the sulphide assemblage in the feed related to Rudna black shale ore, whereas sulphides remain locked by gangue minerals in Sangerhausen black shale related feed. Thus, the strongly divergent recovery of chalcopyrite from feed related to Rudna and Sangerhausen black shale seem to be reasonable.

Additionally, was found that the amount of chalcopyrite in the feed is not critical, which is indicated by increased chalcopyrite portions in the Sangerhausen concentrate (10.5%) and Lubin concentrates LCA06 (6.1%) and LC15a (15.6%) but significantly increased chalcopyrite recovery was just achieved by bioleaching of LCA06 (78%) and LC15a (69%). Moreover, the grain size of chalcopyrite was almost identical in Sangerhausen as well as Lubin concentrates ( $D_{80} = 55 \mu\text{m}$ ). Locking associations of chalcopyrite with gangue minerals, determined in Sangerhausen and Rudna concentrate as well as Lubin concentrate LCA06 (not shown in the results chapter), were generally dominated by illite that represents a refractory mineral in terms of sulfuric acid leaching. However, in LCA06 illite was less predominating, which could explain the most increased recovery of chalcopyrite by bioleaching of LCA06 amongst the investigated bioleaching tests.

The comparison of bioleaching residues concerning secondary formed sulphates induced by the bioleaching process shows a remarkable portion of lead sulphate contained in the bioleaching residue of the Sangerhausen concentrate (15.5%), whereas in other bioleaching residues the content of Pb-sulphates was generally below 5%. Geochemical data of the bioleaching residue of Sangerhausen concentrate point to an overestimation of Pb-phases determined by mineral distribution analysis. However, a correction regarding the content of Pb-sulphates according to the chemical assay indicates that the residue contained at least 10% of Pb-sulphates, which was more than twice the content compared to bioleaching residues of other concentrates. Mineral distribution analyses of bioleaching residues sampled after increasing retention times from the bioleaching solution within bioleaching tests using Lubin concentrate LC15b in Chapter 3.3.4.2.5 showed that the soluble portion of galena was mainly dissolved during the first day. Thus, this indicates that dissolved Pb ions are available early in the leaching solution of bioleaching experiments using galena containing feed material. Additionally, the Sangerhausen concentrate was enriched in galena (8.6%) likewise the Rudna concentrate (8.5%) but the carbonate content was striking different (Sangerhausen: 6.3%, Rudna: 27.8%). It can be assumed that at the beginning of the bioleaching tests carbonates were preferred dissolved. Because the Sangerhausen concentrate was poor in carbonates, the initial dissolution of galena and also other sulphides was probably more advanced, which result in the increased release of Pb ions and other metal ions potentially available for the formation of sulphate compounds in the further course of the bioleaching experiment. Thus, the increased content of galena and low portions of carbonate minerals in the feed cause apparently the enhanced formation of Pb-sulphate.

SEM-observations of bioleaching residues revealed that Pb-sulphate coatings and aggregates occur predominantly in association with galena but also chalcopyrite. These precipitates often enclose remaining, apparently not completely dissolved sulphide particles. In terms of chalcopyrite, zoned overgrowths of first Fe-Cu-sulphate followed by a thin layer of covellite that is again overgrown by lead sulphate were detected often. Thus, an increased content of lead sulphate in bioleaching residues could point to a more advanced chalcopyrite passivation. According to the pH-stability, lead sulphate is insoluble at conditions of the leaching solution and thereby the passivation of chalcopyrite by

predominantly Pb-sulphate could be accounted generally for the hindered complete dissolution of chalcopyrite and in particular in the bioleaching test with Sangerhausen concentrate.

The microcrystalline, porous accretions of lead sulphate around galena particles was a common feature as well in bioleaching as in the sterile control leaching residues. Additionally, small particles of lead sulphate, often few micrometres in size, occurred abundant. They were either formed as crystals or irregular mineral aggregates precipitated from the leaching solution. Such passivation effects of galena particles in bioleaching experiments were observed previously and documented in detail (Mejia et al., 2012; Pacholewska, 2004). According to Mejía et al. (2012) investigating bioleaching tests on a galena ore with *A. ferrooxidans*- and *Acidithiobacillus thiooxidans*-like strains, the formation of needle-like precipitations of anglesite/lead sulphate was observed in an incipient oxidation state (at day 5), while passivation of galena particles by porous anglesite coatings and advanced oxidation of galena along intramineral fractures were identified to be formed at a later stage (day 15) of the bioleaching experiment. A similar period (16 days) for the passivation of galena was demonstrated by Pacholewska (2004). Furthermore, Mejía et al. (2012) had pointed out that the passivation by anglesite had also affected other associated sulfides such as pyrite and sphalerite. This was likewise observed sporadically on chalcopyrite particles in the bioleaching residues examined in this study.

Bioleaching of Lubin concentrate LC15b and the sampling of residues after defined process retention times revealed that the dissolution of copper sulphides in the feed material mainly takes place within the first four days of the experiment, whereas the recovery in the following six days only marginally increased, as Figure 4.3.6 shows. Based on mineral distribution analyses of residues from various bioleaching experiments was shown that the leaching performance of chalcopyrite was partly considerable different. Residues of the bioleaching of Lubin concentrate LC15b revealed a progressive dissolution of chalcopyrite up to day 4 that slowed down up to day 7, whereas no further dissolution was detected from day 7 to the end of the bioleaching experiment (day 10). Bioleaching experiments, of which residues were investigated in this study, were generally conducted at pH < 2 and under oxygenated condition (aerated). Under such conditions copper sulfides are commonly not stable. However, the content of chalcopyrite and pyrite in bioleaching residues as well as of base metal sulphides generally in sterile control leaching residues demonstrate that the dissolution was hindered. Investigations on the stability of selected sulphides in sulfuric acid solution at comparable low pH (pH 2) have shown that pyrite and chalcopyrite being the least reactive and chalcocite and bornite being the most reactive of the examined sulfides (Safarzadeh et al., 2012).

A generally different leaching performance was determined for pyrite and sphalerite, both were dissolved continuously through the entire course of the bioleaching experiment (10 days) as Figure 4.3.6 indicates. It was also shown that galena is mainly dissolved during the first day. Intermediate copper sulphides such as covellite and idaite were detected additionally. While covellite is considered to be formed secondary out of the solution by available Cu ions released from the oxidation of copper sulphides generally, idaite can be regarded to be a decomposition product of bornite. The intense production of dissolved Cu ions by the breakdown of in particular chalcocite and bornite at the inception of the bioleaching tests causes an excess of Cu in the solution that is consumed by bonding with sulphur provided by the decomposition of sulfuric acid during decarbonatization and sulphide oxidation. Due to the instability under acid condition, covellite is completely dissolved at the end of the experiment. In other bioleaching tests, of which residues have been investigated in this study, however, covellite was not completely dissolved finally so that traces occurred in the bioleaching residues. The mainly temporal formation of covellite by oxidation / dissolution of copper sulphides was

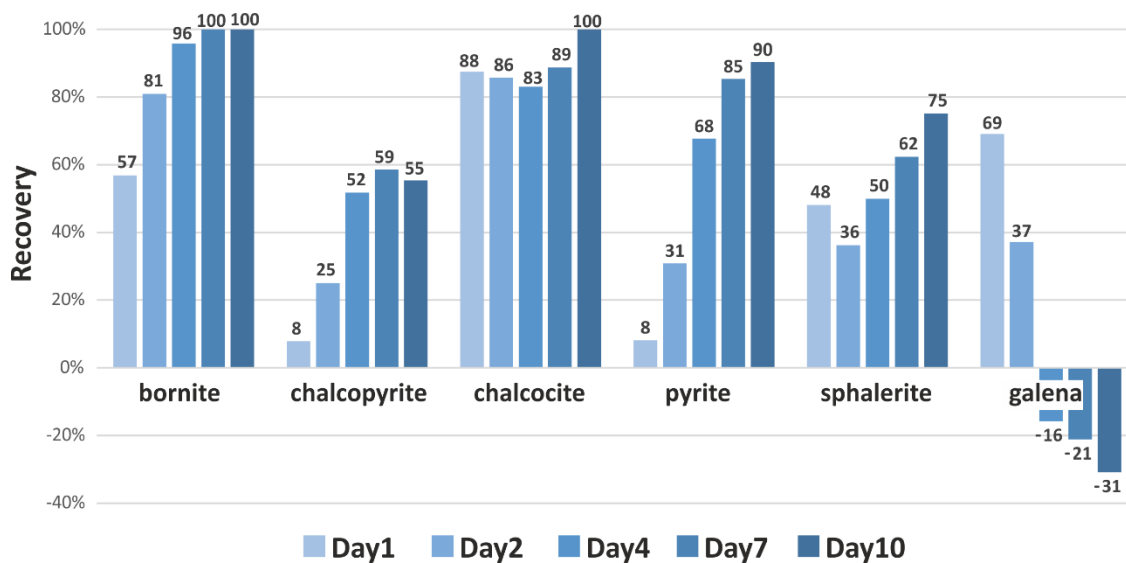


**Figure 4.3.6:** Recovery rates of copper sulphides as well as pyrite, sphalerite and galena within the bioleaching tests of Lubin concentrate LC15b. Chalcocite is largely dissolved and bornite is moderately dissolved at the beginning of the experiment but both are completely dissolved at the end. Chalcopyrite and pyrite show low dissolution at the beginning, which is constantly increasing to the end for pyrite. Chalcopyrite dissolution is consistent to pyrite up to day 4, where it stops and a further dissolution at progressive leaching time is obviously hindered. Sphalerite and galena dissolve moderately at the beginning, whereas sphalerite is continuously dissolved to the end, galena is not dissolved in the following course of the bioleaching tests and remains relatively enriched in the residues.

also ascertained in bioleaching tests conducted on Lubin concentrates in the frame of the Bioshale project and was repeatedly reported (Gouin et al., 2007; Spolaore et al., 2011, 2009).

Idaite contains more Fe incorporated in the crystal lattice compared to bornite. It represents obviously a chemical alteration product of either chalcopyrite or bornite, which has been described both in relation to supergene oxidation of copper sulphides in ore deposits as well as chemical alteration in leaching experiments by several authors (Dutrizaç et al., 1985; Pesic and Olson, 1984; Rice et al., 1979). Because of concomitant increasing idaite portions at decreasing chalcopyrite portions during the course of the bioleaching experiment with Lubin concentrate LC15b, the origin of idaite is rather thought to be related to chalcopyrite. But there is no clear evidence and detailed investigations are needed to raise the level of knowledge regarding the formation of idaite by bioleaching of bornite and chalcopyrite-rich feed materials. However, likewise to covellite several bioleaching residues examined in this study contained traces of idaite, which was apparently not completely dissolved but the dissolution was more advanced by bioleaching, which was indicated by significantly increased contents of idaite in sterile control leaching residues. Thus, the formation of idaite is induced chemically by leaching of chalcopyrite with sulfuric acid but idaite can be largely dissolved by bioleaching.

The most widespread and economic important feature of bioleaching residues represented mainly undissolved chalcopyrite as well as more subordinate idaite particles often showing a pattern-like disintegration texture, in which dissolved domains were visible as intraparticle transects. Obviously, idaite particles showed a higher level of decomposition compared to chalcopyrite remnants and decomposition patterns seemed to follow crystallographic preferred axes. Remaining chalcopyrite was partly intergrown with other minerals, mainly with gangue phases such as illite. Strong dissolution

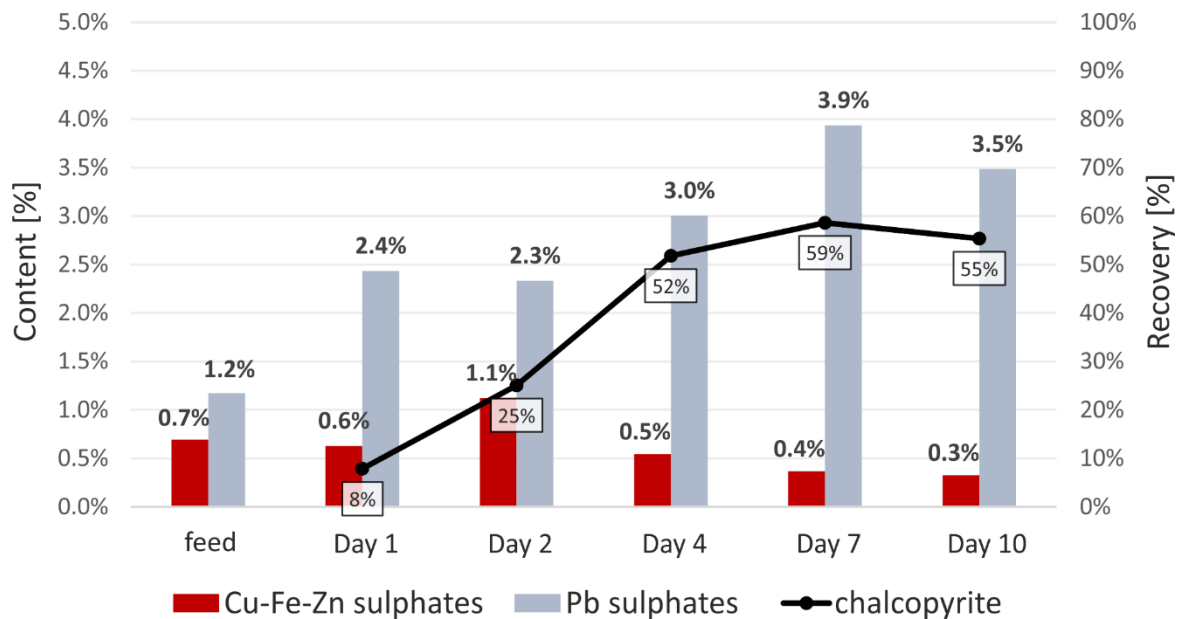


**Figure 4.3.7:** Content of secondary formed sulphate species in bioleaching residues sampled after consecutive retention times within the bioleaching of Lubin concentrate LC15b in relation to chalcopyrite recovery. Pb sulphate is formed mainly at the beginning of the bioleaching test but additionally in the period from day 2 to day 7. Increased amounts of sulphates from day 4 to day 10 seem to affect the dissolution of chalcopyrite by flattening the slope of the chalcopyrite recovery curve.

textures on chalcopyrite particles had also been observed by Zhao et al. (2013) in long-term bioleaching experiments.

The investigation of bioleaching residues sampled after increasing retention times in the bioleaching solution revealed furthermore that secondary sulphates such as Pb sulphates and Cu-Fe-Zn sulphates as well as gypsum were formed shortly after the inception of the bioleaching test. Figure 4.3.7 indicates that the enrichment of Pb sulphate in subsequently sampled residues takes place mainly at the beginning of the bioleaching experiment. Because dissolution of galena is highly limited during the further course of the bioleaching tests, the renewed increase of the content of Pb-sulphates between day 2 and day 7 may attributed to both, the further formation of Pb-sulphate and the changing mass balance of remained and dissolved portions of mineral phases. However, it indicates that the increased occurrence of amorphous to microcrystalline Pb-sulphate from day 4 up to the end of the entire bioleaching test period (10 days) is consistent with the decrease of chalcopyrite recovery from day 4. Thus, the lowered chalcopyrite dissolution from day 4 is obviously related to the substantial presence of Pb-sulphate that potentially hinders the further dissolution of chalcopyrite by the formation of coatings generally present from the early stage of the bioleaching test as microscopic studies have shown.

Chalcopyrite particles remaining in the bioleaching residues showed on the one hand very little indications of alteration, they were partially sharp edged and exhibited smooth surfaces, on the other hand chalcopyrite particles were marked by strong dissolution textures and showed intensely corroded, highly roughened particle surfaces (see Figure 4.3.8). SEM-observations showed that both textures of grain surfaces occurred independently from the grain size. The ore accommodated apparently three types of chalcopyrite particles: type one was completely dissolvable, a second type was partly not dissolved showing strong dissolution features and the third type remained scarcely

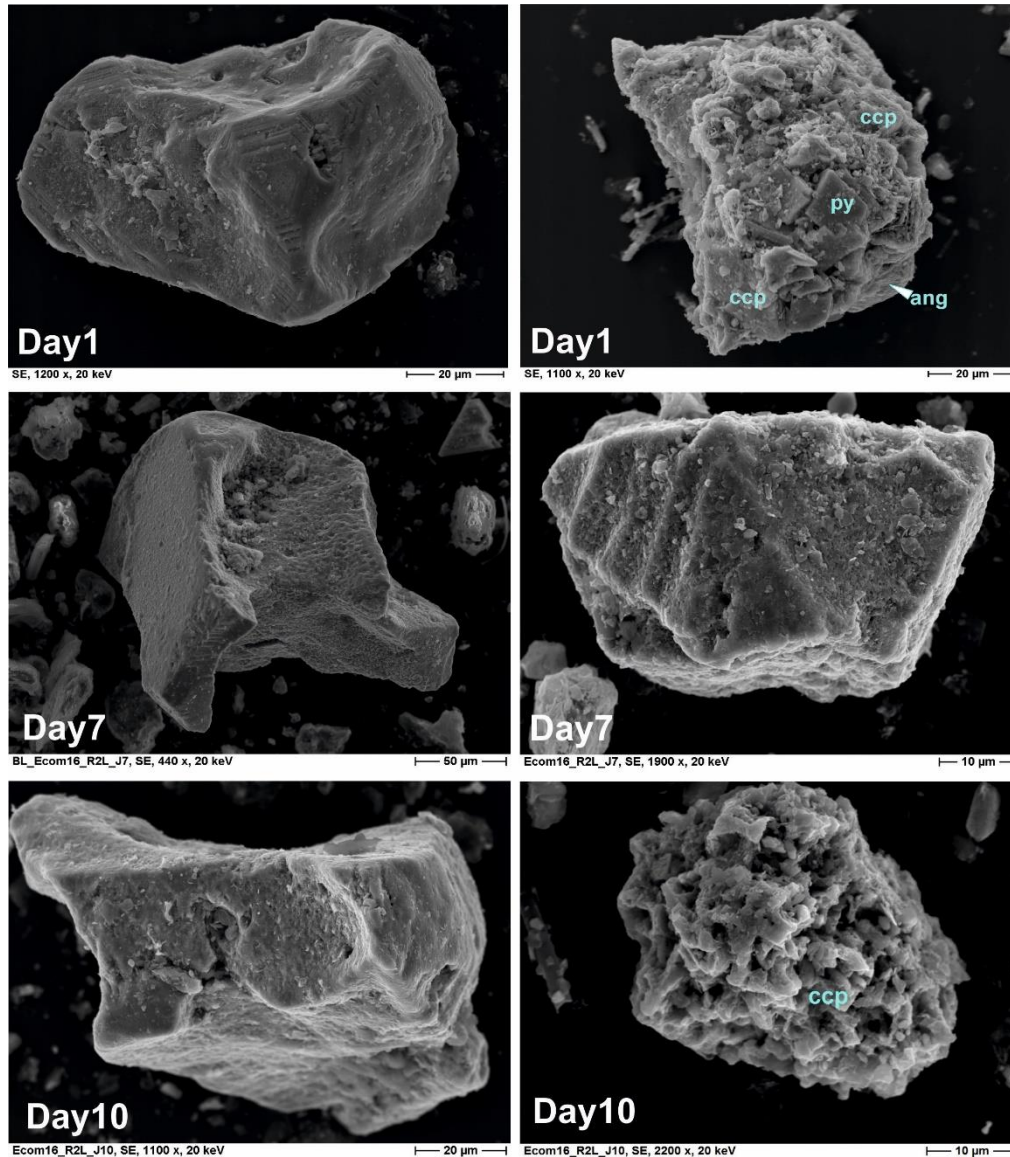


**Figure 4.3.8:** Comparison of chalcopyrite particles at different stages of the leaching test. Little affected by bioleaching (left column) and exhibiting dissolution features with varying extend (right column). (SE-SEM-images; ang=anglesite, ccp=chalcopyrite, py=pyrite)

altered by showing smooth particle surfaces comparable to chalcopyrite grains from the ore/ flotation concentrate. Chalcopyrite grains on a state of an advanced disintegration are displayed in Figure 4.3.8.

Texturally, such particles exhibited an irregular pattern of undissolved domains disrupted by dissolution channels tracing intraparticle fissures and cracks that can be partially subsequently replaced by copper and iron-bearing sulphate. Cu-Fe-sulphate was also found as outer particle coating covering individual chalcopyrite particles. Encapsulation of chalcopyrite particles by secondary formed iron sulphate was observed and described in earlier bioleaching experimental studies. This outer sulphate layer is widely interpreted to represent a chemical barrier and hinder a complete dissolution of chalcopyrite in the leaching system due its acid resistance (Ahmadi et al., 2011; Klauber, 2008; Mejía et al., 2015; Schippers et al., 2014; Vera et al., 2013; Watling, 2014, 2006). Klauber (2008) suggested that during the leaching metal-deficient sulfides are formed by non-stoichiometric dissolution onto the chalcopyrite surface, which was not examined in detail in this study. The formation of a passivation

layer /film consisting of Cu-Fe sulphate around chalcopyrite particles was observed sporadically, but has been cited by Parker et al. (2003) to play an important role in the hindered dissolution of chalcopyrite, while Klauber (2008) stated that a true passivation of chalcopyrite does not occur.

## Chapter 5 Synopsis

The main objective of this study was to investigate mineralogical features of processing products from Kupferschiefer-type black shale ores comprising comminution products, flotation concentrates and tailings as well as bioleaching residues. Investigation methods were focused to mineral distribution analyses to reveal compositional distinctions as well as mineral liberation analyses were additionally used to trace mineralogical relationships of copper sulphides and their textural properties in terms of recoverability. Mineral distribution analyses served also for the assessment of the recovery of mainly individual copper and partially other base metal sulphides within applied mineral processing methods.

Ball mill products of three different black shales were investigated in detail. These black shale ores originated from one Polish (Rudna Mine) and two German (Mansfeld and Sangerhausen) localities. The comminution by ball milling delivered generally different products. While Rudna and Sangerhausen black shale showed consistent grain size distribution ( $D_{80}=45\ \mu\text{m}$ ), the ball mill product of Mansfeld black shale was decidedly finer-grained ( $D_{80}=20\ \mu\text{m}$ ). A main reason for the different particle size reduction is considered to be related to the grain size of rock-forming mineral constituents, which is apparently finer-grained in the Mansfeld black shale.

Mineral distribution analyses revealed that the composition of Rudna black shale was dominated by carbonate minerals, mainly dolomite, whereas Mansfeld black shale was mainly composed of quartz and dolomite. The main mineral constituents in Sangerhausen black shale were illite and quartz as well as a remarkable content of kerogen II-type organic matter (14.4%), which was moderately in Rudna black shale (7.2%) and low in Mansfeld black shale (2.4%). Due to the origin from a mine dump, Mansfeld black shale represents a low-grade ore (0.7% Cu), in which the copper mineralization is mainly caused by a low concentration of bornite (0.4%) and chalcocite (0.5%). Rudna and Sangerhausen black shales are marked by considerable increased amounts of copper sulphides so that the elevated copper content in Rudna black shale (3.6% Cu) is related to increased occurrence of mainly bornite (3.2%) and chalcocite (1.5%), whereas a dominating association of bornite (2.8%) and chalcopyrite (1.3%) mark the copper mineralization in Sangerhausen black shale.

Differences in the power consumption to reduce the particle size of the feed to a desired product size (Bond ball mill Work Index tests) were mainly caused by varying contents of organic matter in the various black shales. Sangerhausen black shale, extremely rich in organic matter, showed the most increased Bond-Index of 18.5 kWh/t, whereas the Bond Work Index for Mansfeld black shale, poor in organic carbon, was considerably lower (12.8 kWh/t).

Liberation analyses indicate that the particle reduction achieved by multi-stage comminution of final ball mill products was partly insufficient. While the more fine-grained ball mill product of Mansfeld black shale was marked by moderate to increased portions of liberated copper sulphides and middlings, liberation in Rudna black shale was generally low, whereas also the ball mill product of Sangerhausen black shale contained copper sulphides with moderate to increased degree of liberation. Increased liberation was achieved for bornite and chalcopyrite in ball mill products of Mansfeld and Sangerhausen black shale.

The grain size distribution of copper sulphides has shown, the particle size reduction by ball milling, in particular in the ball mill product of Rudna black shale, was not capable to meet grain sizes of copper sulphides in order to liberate them. Incomplete liberated copper sulphides were generally complexly (ternary+ locked) intergrown with illite, quartz and carbonates. The low portion of binary locked

copper sulphides in ball mill products was rather fine-grained, commonly  $-40\ \mu\text{m}$ , and marked by intergrowths among copper sulphides and pyrite. Here, chalcocite was associated generally with bornite, which was also predominantly intergrown with illite. Chalcopyrite in the ball mill of Sangerhausen black shale was mainly intergrown with bornite and pyrite. Depending on the dominant ore-texture in the feed, binary locked copper sulphides, which have been found to be partly related to liberated middlings, can occur in coarser-grained size fraction if they originate from vein-type ore, whereas fine-grained ( $-30\ \mu\text{m}$ ) binary locked copper sulphides represent rather middlings from the disseminated sulphides portion of the ore. According to the grain size distribution of binary locked copper sulphides, Mansfeld black shale feed contained mainly disseminated copper sulphides. However, a part of the copper mineralization in the Rudna black shale feed was hosted in a bornite-chalcocite vein-type association, whereas vein-type ore in Sangerhausen black shale feed was comparatively more complex containing an association of bornite, chalcocite, chalcopyrite and pyrite as well as gangue-type minerals such as barite and apatite.

Comminution of Mansfeld and Rudna black shale using the VeRo Liberator® impact crusher reveals extremely advanced particle size reduction ratios of 450-480 compared to other crusher types and achieved a product size, in which about 65% of the product is in the particle size range  $-100\ \mu\text{m}$ . This subproduct was generally coarser-grained than corresponding ball mill products. The mineral distribution of VeRo Liberator® products was generally similar to ball mill products, but the content of bornite (4.4%) and chalcocite (3.4%) was increased in VeRo Liberator® products of Rudna black shale. Generally, the grain size of chalcocite and chalcopyrite was consistent with ball mill products, whereas bornite was considerable finer-grained in VeRo Liberator® products of Rudna black shale ( $D_{80}=26.2\ \mu\text{m}$  vs.  $34.6\ \mu\text{m}$  ball mill) and coarser-grained in the VeRo Liberator® product of Mansfeld black shale ( $D_{80}=47.2\ \mu\text{m}$  vs.  $22.0\ \mu\text{m}$  ball mill).

Liberation of copper sulphides by VeRo Liberator® impact crushing of Mansfeld black shale was generally significantly lower than by ball milling, whereas VeRo Liberator® products of Rudna black shale showed considerable increased liberation in general and for bornite and chalcopyrite in particular. Consistently to ball mill products, the main part of locked copper sulphides was marked by complex (ternary+) intergrowths of illite and carbonates. However, besides increased content of liberated bornite and chalcocite, VeRo Liberator® products of Rudna black shale contained significantly increased portions of binary locked bornite and chalcocite. It has been shown that increased content of liberated copper sulphides is mainly related to the style of mineralization and rock matrix, in which copper sulphides occur. Due to the significant portion of vein-type ore and carbonate-dominated rock matrix in Rudna black shale feed, VeRo Liberator® impact crushing resulted in better liberation of copper sulphides by enhanced breakage between brittle carbonates and sulphides, whereas better liberation yields in VeRo Liberator® products of Mansfeld black shale were impeded by significantly increased portions of harder quartz and elastic-acting illite in the feed. Additionally, the proportion of carbonates in mineral associations of locked copper sulphide was generally lower in VeRo Liberator® product than in ball mill products and substantiates that breakage along grain boundaries of differently tenacity occur preferentially, which was apparently more enhanced realized between carbonates and sulphides.

Froth flotation tests carried out on ball mill products of Rudna and Sangerhausen black shale comprise a standard sulphide flotation, flotation with dextrin and flotation using dextrin and ethanol pre-treated feed. Standard flotation tests yield in high mass (50%) and copper recovery (75%) in the product, whereas flotation with dextrin was highly selective and yield in low mass recovery ( $< 10\%$ ) at

substantially decreased copper recovery. Flotation using dextrin and ethanol pre-treated feed achieved copper recovery rates comparable to standard sulphide flotation tests but coupled with a considerable decrease of the mass recovery (27% and 30%) in the concentrates that were marked by significantly increased copper contents (Rudna: 10.0%, Sangerhausen: 14.4%). Improved copper contents by flotation using dextrin and ethanol pre-treated feed were caused by enhanced recovery of copper sulphides (80%), in particular in the concentrate generated from Sangerhausen black shale feed, whereas the recoverability of copper sulphide from Rudna black shale feed was usually lower and deviated most pronounced for bornite. Mineral liberation data have shown, concentrates extracted by flotation using dextrin and ethanol pre-treated feed contain increased proportion of partly liberated middlings and moreover also locked copper sulphides. In particular bornite was finer-grained than in concentrates from flotation using solely dextrin, which is expressed by the generally enormous increase of the recovery of copper sulphides and provide evidence for their improved flotability caused by ethanol pre-treatment of the feed. It has been shown that the usage of dextrin promotes the selectivity to depress pyrite, galena and organic matter into the tailings, whereas ethanol pre-treatment of the feed causes increased flotability of copper target minerals. It was found that ethanol pre-treatment of the feed result in improved wettability of particle surfaces, on which flotation agents can enhanced adsorb. Additionally, ethanol wetted particle surfaces are capable to adsorb nanobubbles, on which larger air bubbles preferentially attach and entrain hydrophobic sulphides increasingly causing an enhancement of the flotability of copper sulphides.

Geochemical analyses have shown the increased recoverability is also reflected in the content of value trace metals (Ag, Co, Ni, Mo, V), which were generally more recovered in products from flotation using ethanol-pre-treated feed compared to flotation using solely dextrin. Although the recovery of trace metals by flotation of Rudna black was comparatively higher, concentrations were generally considerably increased in the concentrate from Sangerhausen black shale, especially in Co, Mo and V. Concentrates generated from feed containing mixed lithotypes in the processing plant in Lubin (Poland), investigated in relation to bioleaching residues, contained most increased concentrations of Ag and Co, which were primarily hosted in chalcocite (Ag) as well as cobaltite and pyrite (Co). Pyrite in concentrates of Sangerhausen black shale was carrier of Mo, which was also associated with cobaltite-gersdorffite.

Residues of bioleaching tests conducted on different Lubin concentrates and concentrates gained from the flotation using dextrin and ethanol pre-treated Sangerhausen as well as Rudna black shale were investigated by mineral distribution analyses focussing residual sulphides and process-related formed metal sulphates. Generally, the recovery of Cu was vastly enhanced by bioleaching compared to sterile control leaching but copper recovery rates were partly strong deviating mainly caused by the significantly distinct efficiency to dissolve chalcopyrite. While the copper recovery was about 80-90%, the dissolution rate of chalcopyrite was considerable different (49-78%). Chalcocite representing the most readily soluble phase among the copper sulphides, followed by bornite, whereas chalcopyrite and pyrite are decidedly more resistant regarding acid leaching. Mineral distribution analyses of residues sampled according defined process retention times within a 10 days lasting bioleaching test conducted on a Lubin concentrate have shown that nearly 90% of copper was dissolved within the first 4 days, which was basically promoted by the strong dissolution of chalcocite and bornite during the early stage of the bioleaching test, whereas the dissolution rate of chalcopyrite was substantial lower and decreased after day 4. Additionally was shown that the lowering of the dissolution rate of chalcopyrite is consistent with the increased occurrence of secondary formed metal sulphates, mainly

anglesite-like Pb sulphate, which occur widely as finest precipitates and have been found to form partly several  $\mu\text{m}$  thick coatings onto sulphide surfaces. It is considered to be the main mechanism observed in this study, which hinders the advanced dissolution of chalcopyrite, although Cu-sulphate layers onto chalcopyrite surfaces were observed additionally. SEM-observations of bioleaching residues reveal that apparently three “types” of chalcopyrite can be distinguished: a) completely dissolved chalcopyrite, b) remaining chalcopyrite marked by strong dissolution features and c) chalcopyrite exhibiting unaltered grain surface.

Besides improved copper recovery, bioleaching is partly capable to dissolve significantly portion of trace metals, which are mostly associated with cobaltite and pyrite. While Ag is not dissolved by bioleaching and accumulates in the residues, in particular Co and Mo are enhanced dissolved by bioleaching compared to sterile acid leaching. According to recovery associations it was shown that Co is dissolved from cobaltite in Lubin concentrates, whereas the Co recovery from the Sangerhausen concentrate is related to the dissolution of pyrite, which obviously also caused enhanced recovery of Mo. This is additionally indicated by a consistent recovery trend of pyrite, Co, Mo and Ni observed in the bioleaching tests with different retention times.

Finally, the combination of energy-saving extraction methods comprising modified approaches of sulphide flotation and bioleaching from ball mill products of Rudna and Sangerhausen black shale could be considered as a connected copper processing line (see Figure 5.1), in which an alternative recovery of copper from two different black shales with a complex ore mineralogy was experimentally simulated and characterized using EDS-based automated mineralogy. The comminution products were subjected to an ethanol pre-treatment prior processing via flotation. The pre-treatment of the black shale ore amplifies the copper recovery as well as the copper content in the flotation product. Thus, copper-rich concentrates with 10.0% and 14.4% Cu were produced, in which especially bornite and chalcopyrite from Sangerhausen ore as well as bornite and chalcocite from Rudna ore were enriched successfully in flotation products and pyrite was depressed into tailings. These copper concentrates were utilized as suitable feed for bioleaching tests. Bornite as well as chalcocite were nearly completely dissolved by bioleaching, but not in the residue of the sterile control leaching. Chalcopyrite shows lower solubility but is more efficiently dissolved in the concentrate from Rudna black shale and the chalcopyrite dissolution is mainly hindered by the substantial formation of Pb sulphate in both, bio- and abiotic leaching tests, but more pronounced in the bioleaching experiments. Further improvements of the bioleaching protocol is required especially for a complete dissolution of chalcopyrite. Although the composition of the feed in terms of gangue minerals and copper sulphide association was different, the total copper recovery achieved by combination of improved approaches of flotation and bioleaching is similar with 63.7% for Sangerhausen and 62.6% for Rudna black shale feed. Due to the partly low liberation of copper sulphides by ball milling, especially in the ball mill product of Rudna black shale, increase of the copper recovery is coupled to more advanced liberation of copper sulphides in general and the proportion of chalcopyrite as well as galena in the feed. While intergrowths of copper sulphides with minerals insoluble by acid leaching, such as illite and quartz, have to be unlocked by comminution to provide reactive copper sulphide surfaces for both, entrainment by flotation and oxidation by acidophilic bioleaching, galena has to be depressed into tailings by more selective flotation, because it causes amorphous to cryptocrystalline precipitates, which form insoluble coatings onto reactive copper sulphide grains. However, chalcopyrite dissolution can be more activated by slight increase of the operational leaching temperature from 42 to 50 °C at the bacterial growth phase (day 3), as developed and reported by Hedrich et al. (2018). However, this

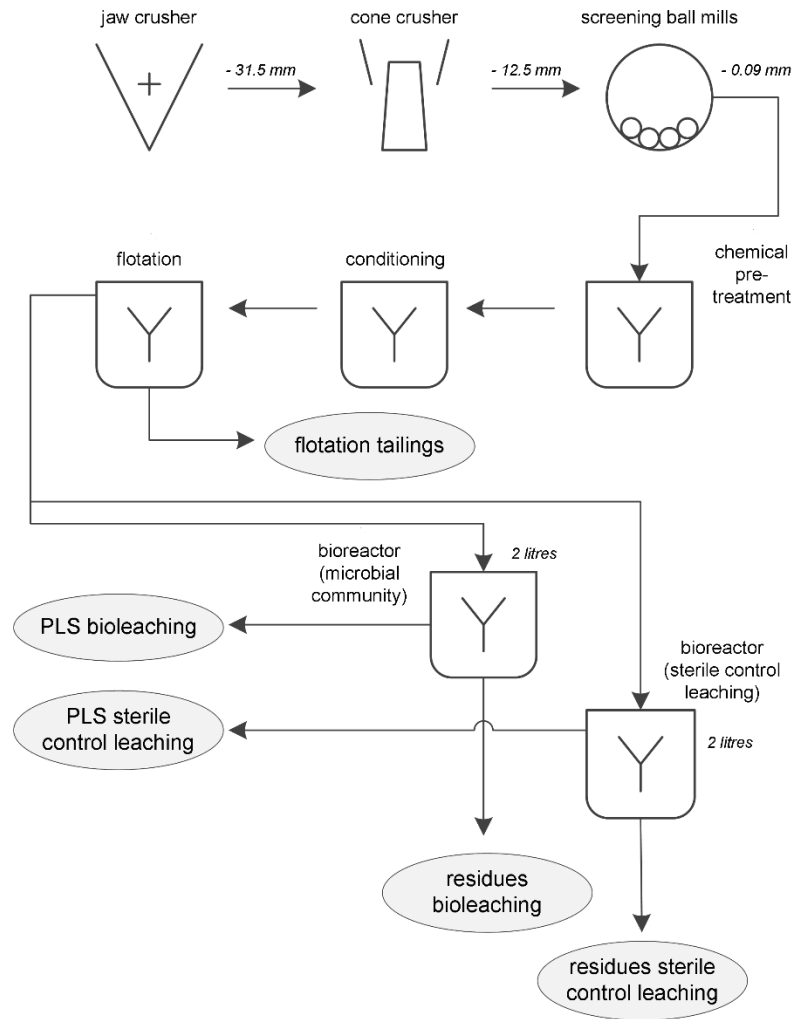


**Figure 5.1:** Processing scheme for the processing of Rudna and Sangerhausen black shale as applied in the frame of this study.

study has shown that improved flotation combined with bioleaching has the potential for the utilization to complex organic-rich ores. Wider implications of this methodology may allow an economic processing of Kupferschiefer-type ore in central Europe and other black shale ores worldwide and even replacing pyrometallurgy operations. Thus, energy-saving alternative mineral processing methods are to be considered to improve the metal recovery route economically and environmentally.

## REFERENCES

- Abd El-Rahiem, F.H., 2014. Recent Trends in Flotation of Fine Particles. *J. Min. World Express* 3, 63. <https://doi.org/10.14355/mwe.2014.03.009>
- Adach-Pawelus, K., Butra, J., Pawelus, D., 2018. The issue of determining the size of main excavations protective pillars in deep underground copper mines. *Arch. Min. Sci.* 63, 935–946. <https://doi.org/10.24425/ams.2018.124985>
- Ahmadi, A., Schaffie, M., Petersen, J., Schippers, A., Ranjbar, M., 2011. Conventional and electrochemical bioleaching of chalcopyrite concentrates by moderately thermophilic bacteria at high pulp density. *Hydrometallurgy* 106, 84–92. <https://doi.org/10.1016/J.HYDROMET.2010.12.007>
- Alderton, D.H.M., Selby, D., Kucha, H., Blundell, D.J., 2016. A multistage origin for Kupferschiefer mineralization. *Ore Geol. Rev.* 79, 535–543. <https://doi.org/10.1016/j.oregeorev.2016.05.007>
- Aletan, G., 1932. Untersuchungen zur Schwimmaufbereitung bituminöser Kupfererze vom Typ Niedermarsberg und Mansfeld. PhD-thesis, Technical University (Bergakademie) Clausthal.
- Anjum, F., Bhatti, H.N., Ambreen, A., 2009. Bioleaching of black shale by acidithiobacillus ferrooxidans. *Asian J. Chem.* 21, 5251–5266.
- Babiński, W., Madej, W., Bortel, R., 1978. Erfüllungsbericht betreffend den 1. Teil der Untersuchungen über die Entwicklung eines Aufbereitungsverfahrens für Kupfererze aus Feld 1 der Lagerstätte. Internal Report, Forschungsinstitut für Aufbereitung (FIA), Freiberg.
- Bechtel, A., Ghazi, A., Elliott, W., Oszczepalski, S., 2001. The occurrences of the rare earth elements and the platinum group elements in relation to base metal zoning in the vicinity of Rote Fäule in the Kupferschiefer of Poland. *Appl. Geochemistry* 16, 375–386. [https://doi.org/10.1016/S0883-2927\(00\)00035-4](https://doi.org/10.1016/S0883-2927(00)00035-4)
- Bellenfant, G., Guezennec, Anne-Gwenaëlle Bodéan, F., D’Hugues, P., Cassard, D., 2013. Reprocessing of mining waste: Combining environmental management and metal recovery? *Mine Clos.* 571–582.
- Bengtsson, M., Evertsson, C.M., 2008. Modelling of output and power consumption in vertical shaft impact crushers. *Int. J. Miner. Process.* 88, 18–23. <https://doi.org/10.1016/j.minpro.2008.04.005>
- Bengtsson, M., Evertsson, C.M., 2006. Measuring characteristics of aggregate material from vertical shaft impact crushers. *Miner. Eng.* 19, 1479–1486. <https://doi.org/10.1016/j.mineng.2006.08.003>
- Bennett, J.C., Tributsch, H., 1978. Bacterial leaching patterns on pyrite crystal surfaces. *J. Bacteriol.* 134, 310–317.
- Bond, F.C., 1952. The third theory of comminution. *Min. Eng.* 4, 484–494.
- Bonnici, N., 2012. The mineralogical and textural characteristics of copper-gold deposits related to mineral processing attributes. PhD Thesis. University of Tasmania.

- Borg, G., 1991. The significance of Rotliegend volcanics for the metal provinces of the Kupferschiefer basin. *Zentralblatt fuer Geol. und Palaeontol.* 4, 123–137.
- Borg, G., Frotzscher, M., Ehling, B., 2005. Metal content and spatial distribution of Au and PGE in the Kupferschiefer of the Mansfeld/Sangerhausen mining district, Germany, in: *Mineral Deposit Research: Meeting the Global Challenge*. Springer Berlin Heidelberg, Berlin, Heidelberg, pp. 885–888. [https://doi.org/10.1007/3-540-27946-6\\_225](https://doi.org/10.1007/3-540-27946-6_225)
- Borg, G., Piestrzynski, A., Bachmann, G.H., Püttmann, W., Walther, S., Fiedler, M., 2012. An Overview of the European Kupferschiefer Deposits. *SEG Spec. Publ.* 16, 455–486.
- Borg, G., Scharfe, F., Jimenez, P., Gomez, S., 2019. Energy-efficient comminution and coarse particle liberation of Au-Ag-Zn-Pb ores from Fresnillo's Cienega Mine, Mexico, by VeRo Liberator® technique, in: *Physical Separation 19*. pp. 0–11.
- Borg, G., Scharfe, F., Kamradt, A., Lempp, C., 2015a. Improved particle liberation of graphite and other complex ore minerals by high-velocity comminution - Introducing the new VeRo Liberator®. *World Min. - Surf. Undergr.* 67, 206–212.
- Borg, G., Scharfe, F., Lempp, C., 2017. Five Years of Innovative VeRo Liberator® Comminution – From Invention to Industrial-scale Pilot Phase Testing, in: *Physical Separation 2017*. Falmouth, Cornwall.
- Borg, G., Scharfe, O., Kamradt, A., 2015b. Breaking down comminution barriers -new dimensions of particle size reduction and liberation by VeRo Liberator®, in: Delgadillo, J.A. (Ed.), *International Comminution and Classification Congress 2015: Advances in Comminution and Classification*. San Luis Potosi, pp. 277–289.
- Brierley, C.L., 2008. How will biomining be applied in future? *Trans. Nonferrous Met. Soc. China* 18, 1302–1310. [https://doi.org/10.1016/S1003-6326\(09\)60002-9](https://doi.org/10.1016/S1003-6326(09)60002-9)
- Chander, S., 1978. Recent developments in floatability of fine particles-review. *Trans. INDIAN Inst. Met.* 31, 12--19.
- Chmielewski, T., 2015. Development of a hydrometallurgical technology for production of metals from kghm polska miedz S.A. concentrates. *Physicochem. Probl. Miner. Process.* 51, 335–350. <https://doi.org/10.5277/ppmp150120>
- Chmielewski, T., Kaleta, R., 2011. Galvanic Interactions of Sulfide Minerals in Leaching of Flotation Concentrate From Lubin Concentrator. *Probl. Miner. Process* 46, 21–34.
- Chmielewski, T., Konieczny, A., Drzymala, J., Kaleta, R., 2014. Development concepts for processing of Lubin- Glogow complex sedimentary copper ore, in: *Proceedings XXVII Int. Min. Process. Congress, IMPC 2014*. Santiago, Chile, pp. 20–24.
- Chmielewski, T., Luszczkiewicz, A., 2010. Leaching of gangue matter in technological flotation circuit of Polish copper ores, in: Harre, J. (Ed.), *Proceedings of Copper 2010*. GDMB, Hamburg, pp. 2655–2671.
- Chmielewski, T., Luszczkiewicz, A., Konopacka, Z., 2008. Acidic Pretreatment of Hard-to-treat Copper Ore Flotation Middlings to Facilitate Flotation Efficiency, in: Wang, D.D., Sun, C.Y., Wang, F.L., Zhang, L.C., Han, L. (Eds.), *XXIV International Mineral Processing Congress*. Beijing, pp. 1189–1200.

- Cox, D.P., Lindsey, D.A., Singer, D.A., Diggles, Michael, F., 2003. Sediment-hosted copper deposits of the world: deposit models and database, Open-File Report. <https://doi.org/10.3133/ofr2003107>
- Cropp, A., Goodall, W., 2013. The Influence of Rock Texture on Mineral Processing. Technical Report, MinAssist Carlton, Australia.
- Cropp, A.F., Goodall, W.R., Bradshaw, D.J., 2013. The Influence of Textural Variation and Gangue Mineralogy on Recovery of Copper by Flotation from Porphyry Ore – A Review. AusIMM GeoMet 2013 Proc.
- Curry, J.A., Ismay, M.J.L., Jameson, G.J., 2014. Mine operating costs and the potential impacts of energy and grinding. *Miner. Eng.* 56, 70–80. <https://doi.org/10.1016/j.mineng.2013.10.020>
- d'Hugues, P., Grotowski, A., Luszczkiewicz, A., Sadowski, Z., Farbiszewska, T., Sklodowska, A., Loukola-Ruskeeniemi, K., Langwaldt, J., Palma, J., Norris, P.R., Glombitza, F., Groudev, S.N., Pasava, J., Johnson, D.B., 2007. The Bioshale Project: Search for a Sustainable Way of Exploiting Black Shale Ores Using Biotechnology. *Adv. Mater. Res.* 20–21, 42–45. <https://doi.org/10.4028/www.scientific.net/AMR.20-21.42>
- d'Hugues, P., Norris, P.R., Johnson, B., Grotowski, A., Chmielewski, T., Luszczkiewicz, A., Sadowski, Z., Sklodowska, A., Farbiszewska, T., 2007. Presentation of the FP6 European project Bioshale: Exploitation of black shale ores using biotechnologies - Polish case studies. *Physicochem. Probl. Miner. Process.* 41, 373–385.
- Djordjevic, N., Shi, F.N., Morrison, R.D., 2003. Applying discrete element modelling to vertical and horizontal shaft impact crushers. *Miner. Eng.* 16, 983–991. <https://doi.org/10.1016/j.mineng.2003.08.007>
- Drzymala, J., Kapusniak, J., Tomasik, P., 2003. Removal of lead minerals from copper industrial flotation concentrates by xanthate flotation in the presence of dextrin. *Int. J. Miner. Process.* 70, 147–155. [https://doi.org/10.1016/S0301-7516\(02\)00156-4](https://doi.org/10.1016/S0301-7516(02)00156-4)
- Drzymala, J., Kowalczyk, P.B., Oteng-Peprah, M., Foszcz, D., Muszer, A., Henc, T., Luszczkiewicz, A., 2013. Application of the grade-recovery curve in the batch flotation of Polish copper ore. *Miner. Eng.* 49, 17–23. <https://doi.org/10.1016/j.mineng.2013.04.024>
- Dutrizac, J.E., Chen, T.T., Jambor, J.L., 1985. Mineralogical changes occurring during the ferric ion leaching of bornite. *Metall. Trans. B* 16, 679–693. <https://doi.org/10.1007/BF02667505>
- Evertsson, C.M., 2000. Cone Crusher Performance. PhD-thesis, Chalmers University of Technology, Goteburg.
- Filippov, L., Izart, C., Hejny, H., Hirsch, K.A., 2017. The BIOMore Project – A New Mining Concept for Extracting Metals from Deep Ore Deposits Using Biotechnology. *Min. Rep.* 153, 436–445.
- Foszcz, D., Drzymala, J., 2011. Differentiation of organic carbon, copper and other metals contents by segregating flotation of final Polish industrial copper concentrates in the presence of dextrin. *Physicochem. Probl. Miner. Process.* 47, 17–26.
- Gent, M., Menendez, M., Toraño, J., Torno, S., 2012. A correlation between Vickers Hardness indentation values and the Bond Work Index for the grinding of brittle minerals. *Powder Technol.* 224, 217–222. <https://doi.org/10.1016/j.powtec.2012.02.056>

- Gillitzer, G., 1935. Durch welche Bedingungen oder Einflüsse sind Metallanreicherungen im mitteldeutschen Kupferschiefer gebildet worden? *Met. und Erz* 22, 533–542.
- Gouin, J., 2008. Mode de genèse et valorisation des minerais de type black shales: cas du Kupferschiefer (Pologne) et des schistes noirs de Talvivaara (Finlande). Thesis. PhD-thesis, Université d'Orleans.
- Gouin, J., Auge, T., Bailly, L., D'Hugues, P., Disnar, J.R., Keravis, D., 2007. Organic and mineral characteristics of Kupferschiefer ore from Lubin mine (Poland): implications for bioleaching of the ore, in: Andrew, C.J. (Ed.), *Digging Deeper*. IAEG, Dublin, Ireland, pp. 269–272.
- Hammami, R., 1980. Beitrag zur Aufbereitung sehr fein verwachsener bitumenhaltiger Cu-Zn-Erze, Typ Kupferschiefer. PhD-thesis, Technical University Clausthal.
- Hampton, M.A., Nguyen, A. V., 2010. Nanobubbles and the nanobubble bridging capillary force. *Adv. Colloid Interface Sci.* 154, 30–55. <https://doi.org/10.1016/j.cis.2010.01.006>
- Hedrich, S., Guézennec, A.-G., Charron, M., Schippers, A., Jouliau, C., 2016. Quantitative Monitoring of Microbial Species during Bioleaching of a Copper Concentrate. *Front. Microbiol.* 07. <https://doi.org/10.3389/fmicb.2016.02044>
- Hedrich, S., Jouliau, C., Graupner, T., Schippers, A., Guézennec, A.G., 2018. Enhanced chalcopyrite dissolution in stirred tank reactors by temperature increase during bioleaching. *Hydrometallurgy* 179, 125–131. <https://doi.org/10.1016/j.hydromet.2018.05.018>
- Herbst, J.A., Lo, C.Y., Flintoff, B., 2003. Size Reduction and Liberation, in: Fuerstenau, M.C., Han, K.N. (Eds.), *Principles of Mineral Processing*. Society for Mining, Metallurgy, and Exploration, Inc. (SME), Littleton, Colorado, pp. 61–118.
- Hitzman, M., Kirkham, R., Broughton, D., Thorson, J., Selley, D., 2005. The Sediment-Hosted Stratiform Copper Ore System, in: Hedenquist, J.W., Thompson, J.F.H., Goldfarb, R.J., Richards, J.P. (Eds.), *Economic Geology - One Hundredth Anniversary Volume*. Society of Economic Geologists. <https://doi.org/doi.org/10.5382/AV100>
- Hitzman, M.W., Broughton, D., Selley, D., Woodhead, J., Wood, D., Bull, S., 2012. The Central African Copperbelt: Diverse Stratigraphic, Structural, and Temporal Settings in the World's Largest Sedimentary Copper District. *SEG Spec. Publ.* 16, 487–514.
- Hitzman, M.W., Selley, D., Bull, S., 2010. Formation of Sedimentary Rock-Hosted Stratiform Copper Deposits through Earth History. *Econ. Geol.* 105, 627–639. <https://doi.org/10.2113/gsecongeo.105.3.627>
- Hofmann, J., 2013. Geochemical constraints on the nature and effects of Kupferschiefer-related multi-stage metal enrichment in the Sangerhausen basin. MSc-thesis, Goethe University Frankfurt (Main).
- Holuszko, M.E., Franzidis, J.P., Manlapig, E. V., Hampton, M.A., Donose, B.C., Nguyen, A. V., 2008. The effect of surface treatment and slime coatings on ZnS hydrophobicity. *Miner. Eng.* 21, 958–966. <https://doi.org/10.1016/j.mineng.2008.03.006>

- Kamradt, A., Borg, G., Bois, M. du, Fiedler, M., Friedrich, B., Gorny, R., Kruse, S., Morgenroth, H., Romm, P., Schaefer, J., Wotruba, H., 2013. Innovative Gewinnung von Wertmetallen aus Kupferschiefer-Halden des ehemaligen Mansfelder Bergbaudistriktes, Sachsen-Anhalt, in: : Woidasky, Jörg; Ostertag, Katrin; Stier, C. (Ed.), *Innovative Technologien Für Ressourceneffizienz in Rohstoffintensiven Produktionsprozessen*. Fraunhofer Verlag, Stuttgart, pp. 52–67.
- Kamradt, A., Borg, G., Schaefer, J., Kruse, S., Fiedler, M., Romm, P., Schippers, A., Gorny, R., Bois, M. du, Bieligk, C., Liebetrau, N., Nell, S., Friedrich, B., Morgenroth, H., Wotruba, H., Merkel, C., 2012. An Integrated Process for Innovative Extraction of Metals from Kupferschiefer Mine Dumps, Germany. *Chemie Ing. Tech.* 84, 1694–1703. <https://doi.org/10.1002/cite.201200070>
- Kamradt, A., Schaefer, J., Schippers, A., Hedrich, S., 2017. Comparative bioleaching and mineralogical characterization of black shale-hosted ores and corresponding flotation concentrates, in: *Solid State Phenomena*. <https://doi.org/10.4028/www.scientific.net/SSP.262.139>
- Kamradt, A., Walther, S., Schaefer, J., Hedrich, S., Schippers, A., 2018. Mineralogical distribution of base metal sulfides in processing products of black shale-hosted Kupferschiefer-type ore. *Miner. Eng.* 119, 23–30. <https://doi.org/10.1016/j.mineng.2017.11.009>
- Kirkham, R. V., 1989. Distribution, settings, and genesis of sediment-hosted stratiform copper deposits. *Geol. Assoc. Canada Spec. Pap.* 36, 3–38.
- Klauber, C., 2008. A critical review of the surface chemistry of acidic ferric sulphate dissolution of chalcopyrite with regards to hindered dissolution. *Int. J. Miner. Process.* 86, 1–17. <https://doi.org/10.1016/j.minpro.2007.09.003>
- Kleiner, C., Ivanauskas, A., Bilsing, U., Sansoni, G., 1987. *Grundlagen der Kupferschieferflotation*. Internal Report, Forschungsinstitut für Aufbereitung (FIA), Freiberg.
- Knitzschke, G., 1995. Metall- und Produktionsbilanz für die Kupferschieferlagerstätte im südöstlichen Harzvorland, in: Jankowski, G. (Ed.), *Zur Geschichte Des Mansfelder Kupferschieferbergbaus*. GDMB-Informationsgesellschaft mbH, Clausthal-Zellerfeld, pp. 270–284.
- Knobloch, M., 2015. Mineralogisch-geochemische Untersuchungen und deren Vergleich zur in-situ Verwitterung an ausgewählten Kupferschieferhalden im ehemaligen Mansfelder Bergbaurevier, Sachsen-Anhalt. MSc-Thesis, Martin Luther University Halle-Wittenberg.
- Konieczny, A., Pawlos, W., Krzeminska, M., Kaleta, R., Kurzydło, P., 2013. Evaluation of organic carbon separation from copper ore by pre-flotation. *Physicochem. Probl. Miner. Process.* 49, 189–201. <https://doi.org/10.5277/ppmp130117>
- Kopp, J., Herrmann, S., Hoding, T., Simon, A., Ullrich, B., 2008. Die Kupfer-Silber-Lagerstätte Spremberg-Graustein (Lausitz, Bundesrepublik Deutschland) - Buntmetallanreicherungen an der Zechsteinbasis zwischen Spremberg und Weiswasser. *Z. Geol. Wiss* 36, 75–114.
- Kucha, H., Przyłowicz, W., 1999. Noble metals in organic matter and clay-organic matrices, Kupferschiefer, Poland. *Econ. Geol.* 94, 1137–1162. <https://doi.org/10.2113/gsecongeo.94.7.1137>
- Kutschke, S., Guézennec, A.G., Hedrich, S., Schippers, A., Borg, G., Kamradt, A., Gouin, J., Giebner, F., Schopf, S., Schlömann, M., Rahfeld, A., Gutzmer, J., D'Hugues, P., Pollmann, K., Dirlich, S., Bodéan, F., 2015. Bioleaching of Kupferschiefer blackshale - A review including perspectives of the Ecometals project. *Miner. Eng.* 75, 116–125. <https://doi.org/10.1016/j.mineng.2014.09.015>

- Kydros, K.A., Gallios, G.P., Matis, K.A., 1994. Modification of Pyrite and Sphalerite Flotation by Dextrin. *Sep. Sci. Technol.* 29, 2263–2275. <https://doi.org/10.1080/01496399408003178>
- Langeluettich, H.J., Mirsch, R., Knitzschke, G., Roloff, P., Spilker, M., Wordelmann, H., 1999. Bergbau auf Kupferschiefer, in: Bergbau-Museum, V.M.B.H. e. V. (Ed.), Mansfeld: Die Geschichte des Berg- und Huettenwesens. Deutsches Bergbau-Museum Bochum, p. 614.
- Liu, Q., Laskowski, J.S., 1989a. The role of metal hydroxides at mineral surfaces in dextrin adsorption, II. Chalcopyrite-galena separations in the presence of dextrin. *Int. J. Miner. Process.* 27, 147–155. [https://doi.org/10.1016/0301-7516\(89\)90012-4](https://doi.org/10.1016/0301-7516(89)90012-4)
- Liu, Q., Laskowski, J.S., 1989b. The role of metal hydroxides at mineral surfaces in dextrin adsorption, I. Studies on modified quartz samples. *Int. J. Miner. Process.* 26, 297–316. [https://doi.org/10.1016/0301-7516\(89\)90035-5](https://doi.org/10.1016/0301-7516(89)90035-5)
- Liu, Q., Zhang, Y., Laskowski, J.S., 2000. The adsorption of polysaccharides onto mineral surfaces: An acid/base interaction. *Int. J. Miner. Process.* 60, 229–245. [https://doi.org/10.1016/S0301-7516\(00\)00018-1](https://doi.org/10.1016/S0301-7516(00)00018-1)
- López Valdivieso, A., Celedón Cervantes, T., Song, S., Robledo Cabrera, A., Laskowski, J., 2004. Dextrin as a non-toxic depressant for pyrite in flotation with xanthates as collector. *Miner. Eng.* 17, 1001–1006. <https://doi.org/10.1016/j.mineng.2004.04.003>
- Luszczkiewicz, A., Chmielewski, T., 2008. Acid treatment of copper sulfide middlings and rougher concentrates in the flotation circuit of carbonate ores. *Int. J. Miner. Process.* 88, 45–52. <https://doi.org/10.1016/j.minpro.2008.06.003>
- Luszczkiewicz, A., Chmielewski, T., Konieczny, A., 2012. Leaching and Flotation of Concentrate and Middlings in Flotation Circuits of Carbonate - Shale Copper Ores, in: XXVI International Mineral Processing Congress (IMPC) 2012. New Dehli, India, pp. 3067–3075.
- Magwaneng, R.S., 2019. Recovery of Copper from Mine Tailing and Complex Carbonaceous Sulfide Ore by Flotation and High - Pressure Leaching. PhD-thesis, Akita University, Japan.
- Malewski, J., 2017. Production of Copper as a Complex Mining and Metallurgical Processing System in Polish Copper Mines of the Legnica-Głogów Copper Belt. *IOP Conf. Ser. Earth Environ. Sci.* 95, 042005. <https://doi.org/10.1088/1755-1315/95/4/042005>
- Malewski, J., 2016. Production Quality, Value and Revenue in Polish Copper Mines. *IOP Conf. Ser. Earth Environ. Sci.* 44, 052006. <https://doi.org/10.1088/1755-1315/44/5/052006>
- Mejía, E.R., Ospina, J.D., Osorno, L., Márquez, M.A., Morales, A.L., 2015. Mineralogical Characterization of Chalcopyrite Bioleaching, in: Fourier Transform - Signal Processing and Physical Sciences. *InTech*, pp. 197–213. <https://doi.org/10.5772/59489>
- Mejía, E.R., Ospina, Marquez, M.A., Morales, A.L., 2012. Bioleaching of Galena (PbS). *Fourier Transform - Mater. Anal.* 191–206. <https://doi.org/10.5772/35434>
- Menard, Y., 2011. Energy savings in comminution – Innovative routes for mineral ores embrittlement. Contribution to deliverable 4.4 – Promine project (FP7) BRGM/RP-60127-FR. Report, BRGM, Orleans.

- Mpongo, M., Siame, E., 2011. Effect of collector, frother and depressant addition on the copper recovery and concentrate grade of the nchanga underground scavenger circuit of konkola copper mine - Zambia. *African J. Sci. Technol.* 7, 8–11. <https://doi.org/10.4314/ajst.v7i1.55186>
- Mudd, G.M., Weng, Z., Jowitt, S.M., 2013. A Detailed Assessment of Global Cu Resource Trends and Endowments. *Econ. Geol.* 108, 1163–1183. <https://doi.org/10.2113/econgeo.108.5.1163>
- Oszczepalski, S., 1999. Origin of the Kupferschiefer polymetallic mineralization in Poland. *Miner. Depos.* 34, 599–613. <https://doi.org/10.1007/s001260050222>
- Oszczepalski, S., 1989. Kupferschiefer in southwestern Poland: sedimentary environments, metal zoning, and ore controls, in: *Sediment-Hosted Stratiform Copper Deposits*. pp. 571–600.
- Pacholewska, M., 2004. Bioleaching of galena flotation concentrate. *Physicochem. Probl. Miner. Process.* 38, 281–290.
- Pakostova, E., Grail, B.M., Johnson, D.B., 2017. Indirect oxidative bioleaching of a polymetallic black schist sulfide ore. *Miner. Eng.* 106, 102–107. <https://doi.org/10.1016/j.mineng.2016.08.028>
- Parker, A., Klauber, C., Kougianos, A., Watling, H.R., Van Bronswijk, W., 2003. An X-ray photoelectron spectroscopy study of the mechanism of oxidative dissolution of chalcopyrite. *Hydrometallurgy* 71, 265–276. [https://doi.org/10.1016/S0304-386X\(03\)00165-8](https://doi.org/10.1016/S0304-386X(03)00165-8)
- Paul, J., 2006. Der Kupferschiefer: Lithologie, Stratigraphie, Fazies und Metallogenese eines Schwarzschiefers [The Kupferschiefer: Lithology, stratigraphy, facies and metallogeny of a black-shale]. *Zeitschrift der Dtsch. Gesellschaft für Geowissenschaften* 157, 57–76. <https://doi.org/10.1127/1860-1804/2006/0157-0057>
- Pease, J.D., Young, M.F., Curry, D., Johnson, N.W., 2010. Improving fines recovery by grinding finer. *Miner. Process. Extr. Metall.* 119, 216–222. <https://doi.org/10.1179/037195510X12816242170852>
- Pesic, B., Olson, F.A., 1984. Dissolution of bornite in sulfuric acid using oxygen as oxidant. *Hydrometallurgy* 12, 195–215. [https://doi.org/10.1016/0304-386X\(84\)90034-3](https://doi.org/10.1016/0304-386X(84)90034-3)
- Piestrzyński, A., Sawłowicz, Z., 1999. Exploration for Au and PGE in the Polish Zechstein copper deposits (Kupferschiefer). *J. Geochemical Explor.* 66, 17–25. [https://doi.org/10.1016/S0375-6742\(99\)00020-5](https://doi.org/10.1016/S0375-6742(99)00020-5)
- Piestrzyński, A., Wodzicki, A., 2000. Origin of the gold deposit in the Polkowice-West Mine, Lubin-Sieroszowice Mining District, Poland. *Miner. Depos.* 35, 37–47. <https://doi.org/10.1007/s001260050004>
- Qin, W., Wei, Q., Jiao, F., Yang, C., Liu, R., Wang, P., Ke, L., 2013. Utilization of polysaccharides as depressants for the flotation separation of copper/lead concentrate. *Int. J. Min. Sci. Technol.* 23, 179–186. <https://doi.org/10.1016/j.ijmst.2013.04.022>
- Rahfeld, A., Kleeberg, R., Möckel, R., Gutzmer, J., 2018. Quantitative mineralogical analysis of European Kupferschiefer ore. *Miner. Eng.* 115, 21–32. <https://doi.org/10.1016/j.mineng.2017.10.007>
- Rappsilber, I., Stedingk, K., König, S., Heckner, J., Thomae, M., 2008. Geologisch-montanhistorische Karte Mansfeld-Sangerhausen 1: 50 000 - Geotourismus in den Kupferschieferrevieren. Landesamt für Geologie und Bergwesen Sachsen-Anhalt (LAGB), Halle (Saale).

- Rath, R.K., Subramanian, S., 1999. Adsorption, electrokinetic and differential flotation studies on sphalerite and galena using dextrin. *Int. J. Miner. Process.* 57, 265–283. [https://doi.org/10.1016/S0301-7516\(99\)00028-9](https://doi.org/10.1016/S0301-7516(99)00028-9)
- Refahi, A., Mohandesi, J.A., Rezai, B., 2009. Comparison between bond crushing energy and fracture energy of rocks in a jaw crusher using numerical simulation. *J. South. African Inst. Min. Metall.* 109, 709–717.
- Rentzsch, J., Franzke, H., Friedrich, G., 1997. Die laterale Verbreitung der Erzmineralassoziationen im deutschen Kupferschiefer. *ZEITSCHRIFT FUR Geol. WISSENSCHAFTEN* 25, 121–140.
- Rice, C.M., Atkin, D., Bowles, J.F.W., Criddle, A.J., 1979. Nukundamite, a new mineral, and idaite. *Mineral. Mag.* 43, 193–200. <https://doi.org/10.1180/minmag.1979.043.326.01>
- Safarzadeh, M.S., Li, J., Moats, M.S., Miller, J.D., 2012. Electrochimica Acta The stability of selected sulfide minerals in sulfuric acid and acidic thiocyanate solutions. *Electrochim. Acta* 78, 133–138. <https://doi.org/10.1016/j.electacta.2012.05.117>
- Saramak, D., Foszcz, D., Gawenda, T., Konieczny, A., Pawlos, W., 2016. Influence of type of lining in high-pressure grinding rolls on effectiveness of copper ore comminution. *Physicochem. Probl. Miner. Process.* 52, 182–192. <https://doi.org/10.5277/ppmp160116>
- Schippers, A., Glombitza, F., Sand, W., 2014. Geobiotechnology I: Metal-related Issues, *Advances in Biochemical Engineering/Biotechnology*. <https://doi.org/10.1007/978-3-642-54710-2>
- Schippers, A., Hedrich, S., Vasters, J., Drobe, M., Sand, W., Willscher, S., 2013. Biomining: Metal Recovery from Ores with Microorganisms, in: *Geobiotechnology I. Advances in Biochemical Engineering/Biotechnology*. pp. 1–47. [https://doi.org/10.1007/10\\_2013\\_216](https://doi.org/10.1007/10_2013_216)
- Sikamo, J., Mwanza, A., Mweemba, C., 2016. Copper mining in Zambia - History and future. *J. South. African Inst. Min. Metall.* 116, 491–496.
- Simubali, M.G., Chileshe, P.R.K., 2013. The impact of technology changes on production and performance of Konkola Copper Mines, Zambia, before and after privatization, in: *The Southern African Institute of Mining and Metallurgy Base Metals Conference 2013*. Johannesburg, pp. 75–88.
- Singer, D.A., 2017. Future copper resources. *Ore Geol. Rev.* 86, 271–279. <https://doi.org/10.1016/j.oregeorev.2017.02.022>
- Spolaore, P., Joulain, C., Guoin, J., Ibáñez, A., Augé, T., Morin, D., d'Hugues, P., 2009. Bioleaching of an organic-rich polymetallic concentrate using stirred-tank technology. *Hydrometallurgy* 99, 137–143. <https://doi.org/10.1016/j.hydromet.2009.07.011>
- Spolaore, P., Joulain, C., Guoin, J., Morin, D., D'Hugues, P., 2011. Relationship between bioleaching performance, bacterial community structure and mineralogy in the bioleaching of a copper concentrate in stirred-tank reactors. *Appl. Microbiol. Biotechnol.* 89, 441–448. <https://doi.org/10.1007/s00253-010-2888-5>
- Subramanian, S., Laskowski, J.S., 1993. Adsorption of Dextrin onto Graphite. *Langmuir* 9, 1330–1333. <https://doi.org/10.1021/la00029a029>

- Suchan, J., 2001. The stratabound Cu-Ag deposits of the Lubin Fore Sudetic Monocline, SW Poland, in: Kelly, J.G., Andrews, C.J., Ashton, J.H., Boland, M.B., Earls, G., Fusciardi, L., Stanley, G. (Eds.), *Europe's Major Base Metal Deposits Geology*. Irish Association for Economic Geology, pp. 239–252.
- Szubert, A., Guezennec, A.-G., Bodéan, F., Dirlich, S., Pawłowska, A., Grotowski, A., Sadowski, Z., Witecki, K., 2017. An update on possibilities of metals recovery from Polish copper ores by biotechnology. *Project Ecometals. E3S Web Conf.* 18, 01015. <https://doi.org/10.1051/e3sconf/201712301015>
- Uryga, A., Sadowski, Z., Grotowski, A., 2004. Bioleaching of Cobalt From Mineral Products. *Physicochem. Probl. Miner. Process.* 38, 291–299.
- Vaughan, D.J., Sweeney, M.A., Friedrich, G., Diedel, R., Haranczyk, C., 1989. The Kupferschiefer; an overview with an appraisal of the different types of mineralization. *Econ. Geol.* 84, 1003–1027. <https://doi.org/10.2113/gsecongeo.84.5.1003>
- Vera, M., Schippers, A., Sand, W., 2013. Progress in bioleaching: fundamentals and mechanisms of bacterial metal sulfide oxidation—part A. *Appl. Microbiol. Biotechnol.* 97, 7529–7541. <https://doi.org/10.1007/s00253-013-4954-2>
- Watling, H., 2014. Review of Biohydrometallurgical Metals Extraction from Polymetallic Mineral Resources. *Minerals* 5, 1–60. <https://doi.org/10.3390/min5010001>
- Watling, H.R., 2006. The bioleaching of sulphide minerals with emphasis on copper sulphides - A review. *Hydrometallurgy* 84, 81–108. <https://doi.org/10.1016/j.hydromet.2006.05.001>
- Wedepohl, K. h., 1964. Untersuchungen am Kupferschiefer in Nordwestdeutschland; Ein Beitrag zur Deutung der Genese bituminöser Sedimente. *Geochim. Cosmochim. Acta* 28, 305–364. [https://doi.org/10.1016/0016-7037\(64\)90109-7](https://doi.org/10.1016/0016-7037(64)90109-7)
- Whitney, D.L., Evans, B.W., 2010. Abbreviations for names of rock-forming minerals. *Am. Mineral.* 95, 185–187. <https://doi.org/10.2138/am.2010.3371>
- Whyte, R.M., Schoeman, N., Bowes, K.G., 2001. Processing of Konkola copper concentrates and Chingola refractory ore in a fully integrated hydrometallurgical pilot plant circuit. *J. South. African Inst. Min. Metall.* 101, 427–436.
- Wieniewski, A., Skorupska, B., 2016. Technology of Polish copper ore beneficiation – perspectives from the past experience. *E3S Web Conf.* 8, 01064. <https://doi.org/10.1051/e3sconf/20160801064>
- Wills, B.A., Atkinson, K., 1993. Some observations on the fracture and liberation of mineral assemblies. *Miner. Eng.* 6, 697–706. [https://doi.org/10.1016/0892-6875\(93\)90001-4](https://doi.org/10.1016/0892-6875(93)90001-4)
- Wills, B.A., Napier-Munn, T., 2005. Introduction, in: *Wills' Mineral Processing Technology*. Elsevier, pp. 1–29. <https://doi.org/10.1016/B978-0750644450-1/50003-5>
- Wodzicki, A., Piestrzyński, A., 1994. An ore genetic model for the Lubin—Sieroszowice mining district, Poland. *Miner. Depos.* 29, 30–43. <https://doi.org/10.1007/BF03326394>
- Zhang, X.H., Maeda, N., Craig, V.S.J., 2006. Physical properties of nanobubbles on hydrophobic surfaces in water and aqueous solutions. *Langmuir* 22, 5025–5035. <https://doi.org/10.1021/la0601814>

Zhao, X., Wang, R., Lu, X., Lu, J., Li, C., Li, J., 2013. Bioleaching of chalcopyrite by *Acidithiobacillus ferrooxidans*. *Miner. Eng.* 53, 184–192. <https://doi.org/10.1016/j.mineng.2013.08.008>

**other references**

Wills, B., 2012, MEI Blog 13.08.2012, <https://min-eng.blogspot.com/2012/08/return-to-nchanga-zambias-greatest.html>

## Appendix A - Comminution

**Table A.1:** Mineral distribution analysis of comminution products in wt.%.

Mineral [wt.%]	ball mill product			VeRo Liberator® product	
	Mansfeld	Rudna	Sangerhausen	Mansfeld	Rudna
albite	5.2%	1.0%	5.1%	7.1%	0.4%
anorthite	2.9%	2.6%	1.1%	1.6%	5.9%
anglesite	<0.05%	0.1%	0.2%	<0.05%	0.1%
anhydrite	1.1%	-	0.1%	0.4%	2.3%
ankerite	0.4%	2.5%	0.2%	0.1%	0.2%
apatite	0.1%	0.3%	1.0%	0.1%	0.7%
bornite	0.4%	3.2%	2.8%	0.8%	4.4%
barite	<0.05%	-	4.3%	-	-
biotite	0.8%	0.4%	0.7%	0.4%	<0.05%
calcite	1.9%	14.5%	2.1%	2.7%	9.4%
chalcopyrite	0.3%	0.6%	1.3%	0.2%	0.4%
cerussite	<0.05%	-	<0.05%	0.1%	-
chromite	1.0%	-	-	0.2%	-
clay	1.2%	0.1%	0.6%	0.3%	1.1%
cobaltite (Cu-Ni)	-	-	<0.05%	-	-
celestite	-	<0.05%	-	-	<0.05%
chalcocite	0.5%	1.5%	0.1%	0.6%	3.4%
covellite	-	<0.05%	<0.05%	<0.05%	<0.05%
dolomite	24.2%	19.5%	4.8%	24.3%	24.9%
feldspar	0.3%	0.1%	<0.05%	0.2%	<0.05%
Fe-Cu sulphate	<0.05%	-	<0.05%	<0.05%	<0.05%
(Fe) illite	-	-	0.1%	<0.05%	<0.05%
galena	0.4%	3.5%	1.5%	0.2%	0.3%
gypsum	0.5%	0.1%	0.6%	0.2%	0.4%
iron hydroxide	0.4%	-	0.1%	<0.05%	0.2%
iron oxide	0.2%	-	<0.05%	<0.05%	0.5%
idaite	0.1%	-	0.1%	<0.05%	<0.05%
illite	17.3%	19.5%	26.4%	12.9%	11.7%
jarosite	-	<0.05%	0.1%	<0.05%	-
K-feldspar	8.3%	4.7%	5.3%	8.1%	5.8%
kaolinite	<0.05%	0.1%	0.6%	<0.05%	0.1%
kutnahorite	-	-	-	<0.05%	-
langite	<0.05%	0.1%	0.1%	<0.05%	0.1%
millerite	-	-	<0.05%	-	-
muscovite	0.1%	<0.05%	0.1%	<0.05%	-
plagioclase	3.9%	0.2%	0.8%	3.7%	0.4%
pyrite	0.6%	2.3%	2.6%	0.6%	0.5%
quartz	23.3%	15.3%	21.4%	29.2%	18.5%
rutile	0.2%	0.2%	0.3%	0.2%	1.0%
serpentinite	<0.05%	-	-	-	-
smithsonite	-	-	-	<0.05%	-
sphalerite	1.7%	0.4%	0.4%	2.4%	-
tennantite	-	-	<0.05%	-	-

Mineral [wt.%]	ball mill product			VeRo Liberator® product	
	Mansfeld	Rudna	Sangerhausen	Mansfeld	Rudna
tetraedrite	-	-	<0.05%	-	-
unclassified	0.2%	0.1%	0.6%	0.6%	<0.05%
Zn sulphate	<0.05%	-	<0.05%	0.1%	-
zircon	-	-	-	<0.05%	0.1%
total organic carbon	2.4%	7.3	14.4%	2.4%	7.3

**Table A2:** Geochemical analyses of comminution products.

Method	Analyte	Unit	LOR	ball mill product			VeRo Liberator product	
				Mansfeld	Sangerhausen	Rudna	Mansfeld	Rudna
ME-ICP06	Al <sub>2</sub> O <sub>3</sub>	%	0.01	10.25	11.80	9.31	9.92	9.05
ME-ICP06	BaO	%	0.01	0.04	2.27	0.03	0.04	0.03
ME-ICP06	CaO	%	0.01	12.75	3.65	15.50	11.90	14.50
ME-ICP06	Cr <sub>2</sub> O <sub>3</sub>	%	0.01	0.16	0.03	0.03	0.07	0.02
ME-ICP06	Fe <sub>2</sub> O <sub>3</sub>	%	0.01	2.82	4.41	2.59	2.66	2.54
ME-ICP06	K <sub>2</sub> O	%	0.01	2.79	2.85	2.82	2.64	2.68
ME-ICP06	MgO	%	0.01	8.01	2.04	4.28	7.31	6.39
ME-ICP06	MnO	%	0.01	0.30	0.16	0.24	0.28	0.20
ME-ICP06	Na <sub>2</sub> O	%	0.01	0.82	0.72	0.41	0.81	0.44
ME-ICP06	P <sub>2</sub> O <sub>5</sub>	%	0.01	0.11	0.27	0.10	0.11	0.11
ME-ICP06	SiO <sub>2</sub>	%	0.01	34.9	37.9	26.7	34.4	27.3
ME-ICP06	SrO	%	0.01	0.01	0.09	0.04	0.01	0.03
ME-ICP06	TiO <sub>2</sub>	%	0.01	0.54	0.58	0.40	0.53	0.42
OA-GRA05	LOI	%	0.01	19.80	27.0	23.0	19.25	22.8
TOT-ICP06	Total	%	0.01	93.30	93.77	85.45	89.93	86.51
ME-ICP41a	Ag	ppm	1	>200	73	>200	70	>200
Ag-OG46	Ag	ppm	1	227		226		246
ME-ICP41a	Al	%	0.05	1.09	1.13	1.02	1.19	0.97
ME-ICP41a	As	ppm	10	40	400	120	40	60
ME-ICP41a	Ba	ppm	50	160	5720	120	180	130
ME-ICP41a	Be	ppm	5	<5	<5	<5	<5	<5
ME-ICP41a	Bi	ppm	10	10	<10	<10	<10	<10
ME-ICP41a	Ca	%	0.05	8.96	2.61	11.25	8.57	10.65
ME-ICP41a	Cd	ppm	5	44	7	<5	52	<5
ME-ICP41a	Co	ppm	5	48	743	137	54	88
ME-ICP41a	Cr	ppm	5	99	48	51	57	40
ME-ICP41a	Cu	ppm	5	6010	25400	3650 0	8290	>50000
Cu-OG46	Cu	%	0.001					5.51
ME-ICP41a	Fe	%	0.05	1.56	2.76	1.52	1.56	1.43

Method	Analyte	Unit	LOR	ball mill product			VeRo Liberator product	
				Mansfeld	Sangerhausen	Rudna	Mansfeld	Rudna
ME-ICP41a	<b>Ga</b>	ppm	50	<50	<50	<50	<50	<50
ME-ICP41a	<b>Hg</b>	ppm	5	<5	<5	8	7	<5
ME-ICP41a	<b>K</b>	%	0.05	0.52	0.53	0.59	0.53	0.54
ME-ICP41a	<b>La</b>	ppm	50	<50	<50	<50	<50	<50
ME-ICP41a	<b>Mg</b>	%	0.05	4.22	0.78	2.09	3.96	3.42
ME-ICP41a	<b>Mn</b>	ppm	30	2270	1240	1870	2170	1560
ME-ICP41a	<b>Mo</b>	ppm	5	95	368	300	129	204
ME-ICP41a	<b>Na</b>	%	0.05	0.09	0.14	0.16	0.07	0.17
ME-ICP41a	<b>Ni</b>	ppm	5	109	250	196	129	146
ME-ICP41a	<b>P</b>	ppm	50	530	1120	410	500	440
ME-ICP41a	<b>Pb</b>	ppm	10	8350	10200	4150 0	9200	4820
ME-ICP41a	<b>S</b>	%	0.05	1.82	3.96	2.63	2.01	2.78
ME-ICP41a	<b>Sb</b>	ppm	10	30	10	<10	30	<10
ME-ICP41a	<b>Sc</b>	ppm	5	<5	<5	<5	<5	<5
ME-ICP41a	<b>Sr</b>	ppm	5	162	484	372	166	265
ME-ICP41a	<b>Th</b>	ppm	100	<100	<100	<100	<100	<100
ME-ICP41a	<b>Ti</b>	%	0.05	<0.05	<0.05	<0.05	<0.05	<0.05
ME-ICP41a	<b>Tl</b>	ppm	50	<50	<50	<50	<50	<50
ME-ICP41a	<b>U</b>	ppm	50	<50	90	<50	<50	<50
ME-ICP41a	<b>V</b>	ppm	5	159	739	462	203	308
ME-ICP41a	<b>W</b>	ppm	50	<50	<50	<50	<50	<50
ME-ICP41a	<b>Zn</b>	ppm	10	10400	1260	380	13500	180

## Appendix B - Flotation

**Table B.1:** Mineral distribution of flotation concentrates and tailings from Rudna black shale in wt.%.

	Rudna black shale feed					
	standard flotation		flotation with dextrin		flotation with dextrin and ethanol pre-treatment	
	concentrate	tailings	concentrate	tailings	concentrate	tailings
albite	0.8%	0.7%	1.1%	0.7%	1.2%	2.3%
anorthite	4.2%	5.5%	3.2%	2.0%	3.2%	4.8%
anglesite	< 0.05%	< 0.05%	0.2%	0.2%	0.1%	-
ankerite	0.1%	< 0.05%	0.5%	0.1%	0.2%	0.2%
apatite	0.1%	1.3%	0.1%	< 0.05%	< 0.05%	0.3%
bornite	3.4%	1.8%	5.9%	1.4%	6.7%	1.9%
biotite	< 0.05%	< 0.05%	0.4%	0.1%	0.2%	0.2%
calcite	14.6%	18.7%	9.9%	17.7%	12.2%	18.3%
chalcopyrite	0.3%	0.2%	0.5%	0.1%	1.0%	0.2%
cerrusite	-	-	0.1%	-	< 0.05%	-
clay	0.6%	< 0.05%	0.1%	< 0.05%	0.1%	0.4%
celestite	< 0.05%	0.6%	-	< 0.05%	-	< 0.05%
cobalite	< 0.05%	-	0.1%	-	-	-
cobalite (Cu-Ni)	< 0.05%	-	-	-	-	-
chalcocite	3.9%	0.3%	9.6%	1.6%	11.0%	1.2%
covellite	-	< 0.05%	< 0.05%	< 0.05%	< 0.05%	-
dolomite	17.6%	18.8%	16.0%	23.7%	15.4%	21.6%
feldspar	< 0.05%	< 0.05%	< 0.05%	0.1%	< 0.05%	0.1%
Fe-Cu sulphate	< 0.05%	< 0.05%	< 0.05%	-	< 0.05%	-
illite (Fe)	-	< 0.05%	-	-	< 0.05%	< 0.05%
galena	2.6%	0.9%	4.5%	4.5%	8.5%	2.9%
gypsum	0.1%	0.3%	0.3%	0.1%	0.7%	1.1%
iron hydroxide	-	-	0.1%	0.1%	-	-
iron oxide	-	< 0.05%	-	-	-	-
idaite	< 0.05%	-	0.1%	< 0.05%	0.1%	< 0.05%
ilmenite	0.1%	-	-	-	-	-
illite	14.9%	14.5%	16.8%	17.5%	11.0%	13.0%
jarosite	< 0.05%	0.1%	0.1%	< 0.05%	0.1%	0.1%
K-feldspar	8.1%	7.8%	5.7%	6.6%	5.7%	6.6%
kaolinite	0.1%	0.1%	0.1%	< 0.05%	< 0.05%	< 0.05%
langite	-	-	< 0.05%	< 0.05%	< 0.05%	-
muscovite	0.1%	< 0.05%	0.1%	0.1%	< 0.05%	< 0.05%
plagioclase	0.3%	0.2%	0.2%	0.5%	0.1%	0.3%
pyrite	1.6%	0.7%	1.5%	0.6%	1.7%	1.9%
quartz	15.5%	21.3%	13.2%	15.8%	9.3%	15.9%
rutile	0.1%	0.1%	0.2%	0.4%	0.1%	0.2%
smithsonite	-	-	< 0.05%	-	-	-
sphalerite	< 0.05%	0.1%	< 0.05%	< 0.05%	< 0.05%	< 0.05%
tennantite	< 0.05%	-	-	-	-	-
unclassified	0.1%	0.1%	0.3%	0.1%	0.1%	0.1%

	Rudna black shale feed					
	standard flotation		flotation with dextrin		flotation with dextrin and ethanol pre-treatment	
	concentrate	tailings	concentrate	tailings	concentrate	tailings
Zn sulphate	-	-	< 0.05%	-	-	< 0.05%
zircon	-	< 0.05%	-	< 0.05%	-	-
TOC	11.6%	5.7%	8.7	5.9	11.2	6.3

Table B.2: Mineral distribution of flotation concentrates and tailings from Sangerhausen black shale in wt.%.

	Sangerhausen black shale feed					
	standard flotation		flotation with dextrin		flotation with dextrin and ethanol pre-treatment	
	concentrate	tailings	concentrate	tailings	concentrate	tailings
albite	5.4%	6.8%	3.3%	5.5%	3.0%	3.1%
anorthite	1.4%	2.9%	0.4%	2.5%	0.6%	1.9%
anglesite	0.1%	0.1%	< 0.05%	0.1%	0.3%	0.3%
anhydrite	-	-	-	-	< 0.05%	< 0.05%
ankerite	-	-	-	< 0.05%	-	0.1%
apatite	0.9%	0.2%	0.3%	0.4%	0.3%	0.4%
bornite	6.2%	1.6%	19.5%	3.3%	20.8%	2.2%
barite	3.3%	5.7%	4.1%	3.1%	1.2%	1.8%
biotite	0.6%	0.9%	0.2%	< 0.05%	0.8%	0.5%
calcite	1.7%	2.1%	2.1%	1.7%	2.6%	1.4%
chalcopyrite	1.5%	1.8%	6.9%	1.5%	10.5%	1.2%
cerussite	-	< 0.05%	0.2%	< 0.05%	0.2%	-
clay	0.3%	0.2%	0.1%	0.4%	0.3%	0.1%
celestite	-	-	-	< 0.05%	-	-
cobaltite	-	-	-	< 0.05%	-	-
cobaltite (Cu-Ni)	< 0.05%	-	< 0.05%	-	< 0.05%	-
chalcocite	0.1%	< 0.05%	0.6%	0.5%	1.7%	0.1%
covellite	< 0.05%	-	0.1%	-	0.1%	-
dolomite	6.3%	5.5%	4.6%	5.6%	3.7%	6.2%
feldspar	< 0.05%	< 0.05%	< 0.05%	< 0.05%	< 0.05%	0.1%
fahlore	< 0.05%	-	-	< 0.05%	< 0.05%	-
Fe-Cu sulphate	0.1%	< 0.05%	0.4%	< 0.05%	0.4%	0.2%
illite (Fe)	< 0.05%	0.1%	-	-	< 0.05%	0.1%
galena	2.4%	0.2%	8.0%	0.9%	8.6%	0.5%
gypsum	0.2%	0.5%	0.9%	1.8%	0.9%	1.5%
iron hydroxide	< 0.05%	< 0.05%	0.2%	0.1%	-	-
iron oxide	-	-	-	0.1%	< 0.05%	< 0.05%
idaite	-	< 0.05%	0.4%	0.2%	0.4%	< 0.05%
illite	18.4%	23.1%	14.5%	24.0%	15.8%	21.7%

	Sangerhausen black shale feed					
	standard flotation		flotation with dextrin		flotation with dextrin and ethanol pre-treatment	
	concentrate	tailings	concentrate	tailings	concentrate	tailings
jarosite	0.4%	0.6%	1.0%	2.4%	1.0%	1.3%
K-feldspar	5.2%	10.2%	3.3%	6.6%	5.4%	8.6%
kaolinite	0.7%	0.4%	0.2%	0.4%	0.3%	0.6%
langite	< 0.05%	< 0.05%	< 0.05%	< 0.05%	0.1%	-
millerite	-	-	-	< 0.05%	-	-
muscovite	< 0.05%	< 0.05%	< 0.05%	< 0.05%	< 0.05%	0.1%
plagioclase	0.3%	0.6%	1.2%	0.3%	0.6%	0.3%
pyrite	3.0%	2.4%	4.0%	4.9%	4.8%	8.1%
quartz	22.1%	22.3%	13.3%	17.7%	12.3%	15.5%
rutile	0.4%	0.1%	0.5%	0.2%	0.1%	0.2%
smithsonite	-	-	-	< 0.05%	-	-
sphalerite	0.5%	0.1%	2.3%	0.3%	3.2%	< 0.05%
tetraedrite	< 0.05%	-	< 0.05%	< 0.05%	0.1%	-
unclassified	0.2%	0.4%	0.4%	0.2%	0.1%	0.2%
Zn sulphate	-	-	0.1%	-	< 0.05%	-
zircon	< 0.05%	-	-	< 0.05%	< 0.05%	-
TOC	18.0%	11.0%	6.7%	15.1%	< 0.05%	22.0%

Table B.3: Mineral distribution of Lubin concentrates in wt.%.

	Lubin concentrate		
	LCA06	LC15a	LC15b
albite	0.4%	0.2%	0.3%
anorthite	0.1%	0.6%	0.8%
anglesite	1.2%	0.6%	0.4%
anhydrite	1.6%	0.2%	1.5%
ankerite	-	< 0.05%	< 0.05%
apatite	0.1%	0.1%	0.1%
bornite	8.0%	7.5%	5.2%
barite	-	< 0.05%	< 0.05%
biotite	1.2%	< 0.05%	-
calcite	0.3%	1.1%	1.4%
chalcopyrite	6.1%	15.6%	15.3%
cerussite	-	1.8%	0.8%
clay	< 0.05%	< 0.05%	0.1%
celestite	-	< 0.05%	-
cobaltite	-	0.1%	< 0.05%
cobaltite (Cu-Ni)	0.3%	0.6%	< 0.05%
chalcocite	5.9%	3.3%	3.2%

	Lubin concentrate		
	LCA06	LC15a	LC15b
<b>covellite</b>	1.5%	0.3%	0.5%
<b>dolomite</b>	0.7%	13.4%	16.2%
<b>feldspar</b>	-	< 0.05%	< 0.05%
<b>fahlore</b>	-	< 0.05%	0.1%
<b>Fe-Cu sulphate</b>	0.7%	0.3%	0.2%
<b>Fe-illite</b>	< 0.05%	-	-
<b>galena</b>	2.2%	2.3%	1.7%
<b>gypsum</b>	0.6%	0.2%	0.6%
<b>iron hydroxide</b>	0.1%	< 0.05%	0.3%
<b>idaite</b>	1.3%	1.0%	0.5%
<b>illite</b>	28.5%	14.8%	15.6%
<b>jarosite</b>	0.5%	0.3%	0.1%
<b>K-feldspar</b>	6.1%	5.4%	4.4%
<b>kaolinite</b>	0.3%	0.2%	0.3%
<b>langite</b>	1.8%	0.7%	0.4%
<b>muscovite</b>	< 0.05%	-	-
<b>plagioclase</b>	0.1%	< 0.05%	0.1%
<b>pyrite</b>	7.2%	9.2%	7.6%
<b>quartz</b>	10.2%	8.3%	-
<b>rutile</b>	0.2%	0.2%	0.2%
<b>serpentinite</b>	-	-	< 0.05%
<b>sphalerite</b>	0.8%	1.6%	1.8%
<b>tennantite</b>	0.6%	0.6%	1.0%
<b>unclassified</b>	0.7%	0.5%	0.8%
<b>Zn sulphate</b>	0.1%	< 0.05%	< 0.05%
<b>zircon</b>	0.2%	-	< 0.05%
<b>TOC</b>	10.3%	8.9%	8.5%

**Table B.4:** Geochemical data of flotation concentrates from Rudna black shale.

Method	Analyte	Unit	LOR	Rudna black shale feed		
				standard flotation	flotation + dextrin	flotation + dextrin + ethanol pre-treatment
ME-XRF15c	<b>SiO2</b>	%	0.01	24.9	24.2	22.2
ME-ICP61	<b>Ag</b>	ppm	0.5	>100	>100	>100
Ag-OG46	<b>Ag</b>	ppm	1	344	746	611
ME-ICP61	<b>Al</b>	%	0.01	4.87	4.71	4.38
ME-ICP61	<b>As</b>	ppm	5	176	289	277
ME-ICP61	<b>Ba</b>	ppm	10	180	220	160
ME-XRF15c	<b>Ba</b>	%	0.01	0.02	0.02	0.01

Method	Analyte	Unit	LOR	Rudna black shale feed		
				standard flotation	flotation + dextrin	flotation + dextrin + ethanol pre-treatment
ME-ICP61	Be	ppm	0.5	2.9	2.7	2.6
ME-ICP61	Bi	ppm	2	2	48	8
ME-ICP61	Ca	%	0.01	10.55	9.24	8.15
ME-ICP61	Cd	ppm	0.5	2.6	4.0	3.4
ME-ICP61	Co	ppm	1	234	282	301
ME-ICP61	Cr	ppm	1	191	177	171
ME-ICP61	Cu	ppm	1	>10000	>10000	>10000
Cu-OG46	Cu	%	0.001	5.50	11.40	10.00
ME-ICP61	Fe	%	0.01	2.21	2.23	2.40
ME-ICP61	Ga	ppm	10	10	10	10
ME-ICP61	K	%	0.01	2.41	2.30	2.15
ME-ICP61	La	ppm	10	20	20	20
ME-ICP61	Mg	%	0.01	2.59	2.23	2.04
ME-ICP61	Mn	ppm	5	1850	1610	1490
ME-ICP61	Mo	ppm	1	395	382	439
ME-ICP61	Na	%	0.01	0.21	0.21	0.18
ME-ICP61	Ni	ppm	1	384	331	400
ME-ICP61	P	ppm	10	480	460	440
ME-ICP61	Pb	ppm	2	>10000	>10000	>10000
ME-XRF15c	Pb	%	0.01	5.46	4.99	6.94
Pb-OG46	Pb	%	0.001	5.39	5.03	7.11
ME-ICP61	S	%	0.01	3.91	5.37	5.74
ME-XRF15c	S	%	0.01	3.84	5.15	5.53
ME-ICP61	Sb	ppm	5	<5	<5	<5
ME-ICP61	Sc	ppm	1	9	8	7
ME-ICP61	Sr	ppm	1	221	255	184
ME-ICP61	Th	ppm	20	20	20	<20
ME-ICP61	Ti	%	0.01	0.25	0.23	0.22
ME-ICP61	Tl	ppm	10	10	<10	<10
ME-ICP61	U	ppm	10	10	10	<10
ME-ICP61	V	ppm	1	1320	1240	1210
ME-ICP61	W	ppm	10	<10	<10	10
ME-ICP61	Zn	ppm	2	527	853	742
ME-XRF15c	Zn	%	0.01	0.06	0.09	0.07

**Table B.5:** Geochemical data of flotation tailings from Rudna black shale.

Method	Analyte	Unit	LOR	Rudna black shale feed		
				standard flotation	flotation + dextrin	flotation + dextrin + ethanol pre-treatment
ME-ICP06	Al <sub>2</sub> O <sub>3</sub>	%	0.01	9.99	9.25	9.53
ME-ICP06	BaO	%	0.01	0.03	0.03	0.03
ME-ICP06	CaO	%	0.01	16.95	16.10	16.90
ME-ICP06	Cr <sub>2</sub> O <sub>3</sub>	%	0.01	0.03	0.03	0.03
ME-ICP06	Fe <sub>2</sub> O <sub>3</sub>	%	0.01	2.41	2.54	2.31
ME-ICP06	K <sub>2</sub> O	%	0.01	3.01	2.79	2.88
ME-ICP06	MgO	%	0.01	4.65	4.46	4.63
ME-ICP06	MnO	%	0.01	0.26	0.25	0.25
ME-ICP06	Na <sub>2</sub> O	%	0.01	0.28	0.29	0.26
ME-ICP06	P <sub>2</sub> O <sub>5</sub>	%	0.01	0.11	0.10	0.08
ME-ICP06	SiO <sub>2</sub>	%	0.01	28.6	27.1	28.4
ME-ICP06	SrO	%	0.01	0.04	0.04	0.04
ME-ICP06	TiO <sub>2</sub>	%	0.01	0.42	0.40	0.39
OA-GRA05	LOI	%	0.01	24.6	23.6	23.4
TOT-ICP06	Total	%	0.01	91.38	86.98	89.13
ME-ICP41a	Ag	ppm	1	104	196	144
ME-ICP41a	Al	%	0.05	1.06	0.94	1.02
ME-ICP41a	As	ppm	10	80	110	90
ME-ICP41a	Ba	ppm	50	130	100	150
ME-ICP41a	Be	ppm	5	<5	<5	<5
ME-ICP41a	Bi	ppm	10	<10	<10	<10
ME-ICP41a	Ca	%	0.05	12.20	11.30	12.50
ME-ICP41a	Cd	ppm	5	<5	<5	<5
ME-ICP41a	Co	ppm	5	100	116	93
ME-ICP41a	Cr	ppm	5	55	47	51
ME-ICP41a	Cu	ppm	5	14100	27300	20500
ME-ICP41a	Fe	%	0.05	1.34	1.46	1.31
ME-ICP41a	Ga	ppm	50	<50	<50	<50
ME-ICP41a	Hg	ppm	5	<5	6	5
ME-ICP41a	K	%	0.05	0.60	0.54	0.58
ME-ICP41a	La	ppm	50	<50	<50	<50
ME-ICP41a	Mg	%	0.05	2.26	2.17	2.37
ME-ICP41a	Mn	ppm	30	1980	1880	1990
ME-ICP41a	Mo	ppm	5	258	273	251
ME-ICP41a	Na	%	0.05	0.05	0.07	0.05
ME-ICP41a	Ni	ppm	5	175	175	147
ME-ICP41a	P	ppm	50	430	410	340
ME-ICP41a	Pb	ppm	10	29300	40700	27500
ME-ICP41a	S	%	0.05	1.57	2.32	1.69

Method	Analyte	Unit	LOR	Rudna black shale feed		
				standard flotation	flotation + dextrin	flotation + dextrin + ethanol pre-treatment
ME-ICP41a	Sb	ppm	10	<10	<10	<10
ME-ICP41a	Sc	ppm	5	<5	<5	<5
ME-ICP41a	Sr	ppm	5	404	295	435
ME-ICP41a	Th	ppm	100	<100	<100	<100
ME-ICP41a	Ti	%	0.05	<0.05	<0.05	<0.05
ME-ICP41a	Tl	ppm	50	<50	<50	<50
ME-ICP41a	U	ppm	50	<50	<50	<50
ME-ICP41a	V	ppm	5	458	425	429
ME-ICP41a	W	ppm	50	<50	<50	<50
ME-ICP41a	Zn	ppm	10	260	350	340

**Table B.6:** Geochemical data of flotation concentrates from Sangerhausen black shale.

Method	Analyte	Unit	LOR	Sangerhausen black shale feed		
				standard flotation	flotation + dextrin	flotation + dextrin + ethanol pre-treatment
ME-XRF15c	SiO <sub>2</sub>	%	0.01	33.1	23.7	22.0
ME-ICP61	Ag	ppm	0.5	>100	>100	>100
Ag-OG46	Ag	ppm	1	99	624	452
ME-ICP61	Al	%	0.01	5.74	4.34	4.67
ME-ICP61	As	ppm	5	530	461	593
ME-ICP61	Ba	ppm	10	240	420	40
ME-XRF15c	Ba	%	0.01	1.62	1.48	1.20
ME-ICP61	Be	ppm	0.5	4.6	3.5	3.8
ME-ICP61	Bi	ppm	2	6	<2	<2
ME-ICP61	Ca	%	0.01	2.55	2.14	1.95
ME-ICP61	Cd	ppm	0.5	10.7	72.0	61.8
ME-ICP61	Co	ppm	1	1150	905	1040
ME-ICP61	Cr	ppm	1	188	142	153
ME-ICP61	Cu	ppm	1	>10000	>10000	>10000
Cu-OG46	Cu	%	0.001	3.90	12.35	14.40
ME-ICP61	Fe	%	0.01	4.18	5.71	6.60
ME-ICP61	Ga	ppm	10	20	10	10
ME-ICP61	K	%	0.01	2.28	1.66	1.83
ME-ICP61	La	ppm	10	20	20	10
ME-ICP61	Mg	%	0.01	1.17	0.88	0.85
ME-ICP61	Mn	ppm	5	1195	918	927
ME-ICP61	Mo	ppm	1	512	528	697
ME-ICP61	Na	%	0.01	0.38	0.27	0.26

Method	Analyte	Unit	LOR	Sangerhausen black shale feed		
				standard flotation	flotation + dextrin	flotation + dextrin + ethanol pre-treatment
ME-ICP61	Ni	ppm	1	472	352	386
ME-ICP61	P	ppm	10	1360	1050	1060
ME-ICP61	Pb	ppm	2	>10000	>10000	>10000
ME-XRF15c	Pb	%	0.01	1.88	5.98	7.11
Pb-OG46	Pb	%	0.001	1.965	6.17	7.43
ME-ICP61	S	%	0.01	5.15	>10.0	>10.0
ME-XRF15c	S	%	0.01	5.53	10.35	11.35
ME-ICP61	Sb	ppm	5	112	672	625
ME-ICP61	Sc	ppm	1	11	8	8
ME-ICP61	Sr	ppm	1	527	554	360
ME-ICP61	Th	ppm	20	<20	<20	<20
ME-ICP61	Ti	%	0.01	0.32	0.23	0.24
ME-ICP61	Tl	ppm	10	30	40	20
ME-ICP61	U	ppm	10	120	120	120
ME-ICP61	V	ppm	1	1980	1455	1620
ME-ICP61	W	ppm	10	<10	30	<10
ME-ICP61	Zn	ppm	2	2400	>10000	>10000
ME-XRF15c	Zn	%	0.01	0.24	1.48	1.32
Zn-OG46	Zn	%	0.001		1.495	1.360

**Table B.7:** Geochemical data of flotation tailings from Sangerhausen black shale.

Method	Analyte	Unit	LOR	Sangerhausen black shale feed		
				standard flotation	flotation + dextrin	flotation + dextrin + ethanol pre-treatment
ME-ICP06	Al <sub>2</sub> O <sub>3</sub>	%	0.01	13.30	12.50	12.00
ME-ICP06	BaO	%	0.01	3.83	2.76	2.06
ME-ICP06	CaO	%	0.01	3.66	3.57	3.27
ME-ICP06	Cr <sub>2</sub> O <sub>3</sub>	%	0.01	0.03	0.03	0.03
ME-ICP06	Fe <sub>2</sub> O <sub>3</sub>	%	0.01	3.59	4.29	5.07
ME-ICP06	K <sub>2</sub> O	%	0.01	3.20	3.02	2.97
ME-ICP06	MgO	%	0.01	2.10	2.07	2.00
ME-ICP06	MnO	%	0.01	0.17	0.16	0.15
ME-ICP06	Na <sub>2</sub> O	%	0.01	0.62	0.57	0.46
ME-ICP06	P <sub>2</sub> O <sub>5</sub>	%	0.01	0.27	0.28	0.28
ME-ICP06	SiO <sub>2</sub>	%	0.01	41.3	38.2	33.5
ME-ICP06	SrO	%	0.01	0.17	0.12	0.09
ME-ICP06	TiO <sub>2</sub>	%	0.01	0.64	0.62	0.58
OA-GRA05	LOI	%	0.01	21.7	26.5	32.3
TOT-ICP06	Total	%	0.01	94.58	94.69	94.76

Method	Analyte	Unit	LOR	Sangerhausen black shale feed		
				standard flotation	flotation + dextrin	flotation + dextrin + ethanol pre-treatment
ME-ICP41a	Ag	ppm	1	44	50	69
ME-ICP41a	Al	%	0.05	1.21	1.15	1.22
ME-ICP41a	As	ppm	10	350	410	440
ME-ICP41a	Ba	ppm	50	9450	5650	4650
ME-ICP41a	Be	ppm	5	<5	<5	<5
ME-ICP41a	Bi	ppm	10	10	<10	10
ME-ICP41a	Ca	%	0.05	2.72	2.56	2.33
ME-ICP41a	Cd	ppm	5	<5	5	7
ME-ICP41a	Co	ppm	5	561	728	886
ME-ICP41a	Cr	ppm	5	52	52	60
ME-ICP41a	Cu	ppm	5	15200	21000	20600
ME-ICP41a	Fe	%	0.05	2.09	2.57	3.25
ME-ICP41a	Ga	ppm	50	<50	<50	<50
ME-ICP41a	Hg	ppm	5	<5	<5	<5
ME-ICP41a	K	%	0.05	0.55	0.52	0.55
ME-ICP41a	La	ppm	50	<50	<50	<50
ME-ICP41a	Mg	%	0.05	0.82	0.78	0.74
ME-ICP41a	Mn	ppm	30	1330	1240	1140
ME-ICP41a	Mo	ppm	5	257	336	436
ME-ICP41a	Na	%	0.05	0.06	0.06	0.05
ME-ICP41a	Ni	ppm	5	197	246	317
ME-ICP41a	P	ppm	50	1210	1210	1180
ME-ICP41a	Pb	ppm	10	7420	10300	11300
ME-ICP41a	S	%	0.05	2.49	3.31	3.98
ME-ICP41a	Sb	ppm	10	30	50	20
ME-ICP41a	Sc	ppm	5	5	<5	<5
ME-ICP41a	Sr	ppm	5	771	552	475
ME-ICP41a	Th	ppm	100	<100	<100	<100
ME-ICP41a	Ti	%	0.05	<0.05	<0.05	<0.05
ME-ICP41a	Tl	ppm	50	<50	<50	<50
ME-ICP41a	U	ppm	50	100	100	110
ME-ICP41a	V	ppm	5	618	633	717
ME-ICP41a	W	ppm	50	<50	<50	<50
ME-ICP41a	Zn	ppm	10	830	1110	1210

**Table B.8:** Geochemical data of Lubin flotation concentrates.

Method	Analyte	Unit	LOR	Lubin concentrates	
				LC15a	LC15b
ME-XRF15c	SiO <sub>2</sub>	%	0.01	17.75	18.05
ME-ICP61	Ag	ppm	0.5	>100	>100
Ag-OG46	Ag	ppm	1	707	636
ME-ICP61	Al	%	0.01	3.84	3.78
ME-ICP61	As	ppm	5	4340	4230
ME-ICP61	Ba	ppm	10	180	170
ME-XRF15c	Ba	%	0.01	<0.01	0.01
ME-ICP61	Be	ppm	0.5	2.7	2.6
ME-ICP61	Bi	ppm	2	<2	<2
ME-ICP61	Ca	%	0.01	4.03	3.94
ME-ICP61	Cd	ppm	0.5	68.6	63.8
ME-ICP61	Co	ppm	1	1480	1480
ME-ICP61	Cr	ppm	1	134	131
ME-ICP61	Cu	ppm	1	>10000	>10000
Cu-OG46	Cu	%	0.001	14.35	13.65
ME-ICP61	Fe	%	0.01	9.92	9.76
ME-ICP61	Ga	ppm	10	10	10
ME-ICP61	K	%	0.01	1.88	1.83
ME-ICP61	La	ppm	10	20	20
ME-ICP61	Mg	%	0.01	1.77	1.77
ME-ICP61	Mn	ppm	5	1060	1045
ME-ICP61	Mo	ppm	1	375	361
ME-ICP61	Na	%	0.01	0.28	0.27
ME-ICP61	Ni	ppm	1	610	606
ME-ICP61	P	ppm	10	440	420
ME-ICP61	Pb	ppm	2	>10000	>10000
ME-XRF15c	Pb	%	0.01	4.19	4.05
Pb-OG46	Pb	%	0.001	4.59	4.51
ME-ICP61	S	%	0.01	>10.0	>10.0
ME-XRF15c	S	%	0.01	13.70	13.35
ME-ICP61	Sb	ppm	5	116	112
ME-ICP61	Sc	ppm	1	6	6
ME-ICP61	Sr	ppm	1	115	113
ME-ICP61	Th	ppm	20	<20	<20
ME-ICP61	Ti	%	0.01	0.24	0.23
ME-ICP61	Tl	ppm	10	30	20
ME-ICP61	U	ppm	10	<10	<10
ME-ICP61	V	ppm	1	792	766
ME-ICP61	W	ppm	10	<10	<10
ME-ICP61	Zn	ppm	2	>10000	>10000
ME-XRF15c	Zn	%	0.01	1.27	1.26
Zn-OG46	Zn	%	0.001	1.255	1.210

**Table B.9:** Geochemical data of Lubin concentrate LCA06.

Analyte	Unit	LOR	Lubin concentrate LCA06
Al <sub>2</sub> O <sub>3</sub>	%	0.2	5.5
CaO	%	0.1	4.2
Fe <sub>2</sub> O <sub>3</sub>	%	0.05	8.18
K <sub>2</sub> O	%	0.05	1.51
MgO	%	0.2	1.4
MnO	%	0.02	0.04
Na <sub>2</sub> O	%	0.2	< LQ
P <sub>2</sub> O <sub>5</sub>	%	0.05	0.1
SiO <sub>2</sub>	%	0.2	16.7
TiO <sub>2</sub>	%	0.05	0.28
LOI	%	0.1	32.9
<b>total</b>			70.81
As	ppm	20	2596
B	ppm	10	140
Ba	ppm	10	179
Be	ppm	2	2
Bi	ppm	10	< LQ
C (min.)	%	0.05	0.13
C (org.)	%	0.1	7.3
Cd	ppm	2	34
Ce	ppm	10	30
Cl-	%	0.01	0.067
Co	ppm	5	1059
Cr	ppm	10	132
Ct	%	0.1	7.67
Cu	%	0.01	14.7
Cu	ppm	5	148231
Fe	%	0.01	6.47
La	ppm	20	< LQ
Li	ppm	10	30
Mo	ppm	5	279
Nb	ppm	20	< LQ
Ni	ppm	10	455
Nt	%	0.01	0.16
Pb	ppm	10	28562
S	%	0.1	10.1
SO <sub>4</sub>	%	0.2	12.5
Sb	ppm	10	87
Sn	ppm	10	15
So	%	0.05	0.52
Sr	ppm	5	94

Analyte	Unit	LOR	Lubin concentrate LCA06
<b>St</b>	%	0.01	14.8
<b>V</b>	ppm	10	550
<b>W</b>	ppm	10	20
<b>Y</b>	ppm	20	< LQ
<b>Zn</b>	ppm	5	4394
<b>Zr</b>	ppm	20	66

## Appendix C - Bioleaching

**Table C.1:** Mineral distribution of (bio)leaching residues from Sangerhausen black shale and concentrate.

Mineral [wt.%]	Sangerhausen			
	black shale		concentrate	
	sterile control residues	bioleaching residues	sterile control residues	bioleaching residues
albite	5.5%	5.5%	5.9%	6.6%
anorthite	0.1%	0.2%	0.1%	< 0.05%
anglesite	0.9%	1.1%	5.7%	15.4%
anhydrite	0.3%	0.9%	0.1%	0.1%
apatite	0.2%	-	-	-
bornite	< 0.05%	-	5.8%	0.6%
barite	6.1%	4.7%	4.4%	7.5%
biotite	2.4%	0.4%	0.3%	0.2%
calcite	0.1%	0.2%	< 0.05%	-
chalcopyrite	0.6%	0.5%	6.6%	5.3%
cerussite	0.1%	< 0.05%	0.2%	< 0.05%
clay	0.3%	0.3%	0.4%	0.3%
celestite	< 0.05%	-	-	0.1%
cobaltite	< 0.05%	-	< 0.05%	-
cobaltite (Cu-Ni)	< 0.05%	-	< 0.05%	-
chalcocite	< 0.05%	-	0.2%	< 0.05%
covellite	-	-	0.6%	< 0.05%
dolomite	< 0.05%	-	-	< 0.05%
Fe-illite	0.6%	< 0.05%	-	0.3%
Fe-Cu sulphate	0.3%	< 0.05%	0.9%	0.4%
galena	1.0%	1.0%	4.3%	4.0%
gypsum	0.4%	1.1%	0.3%	0.2%
iron hydroxide	0.4%	0.4%	0.1%	0.7%
iron oxide	-	0.1%	-	0.1%
idaite	0.2%	-	3.8%	0.2%
illite	24.8%	35.4%	20.4%	26.0%
jarosite	1.2%	0.1%	1.6%	< 0.05%
K-feldspar	10.3%	9.4%	8.3%	6.9%
kaolinite	0.8%	0.6%	0.8%	1.9%
muscovite	0.1%	< 0.05%	< 0.05%	0.1%
plagioclase	< 0.05%	0.1%	0.3%	< 0.05%
pyrite	3.9%	0.8%	6.1%	0.7%
quartz	23.7%	21.7%	19.8%	20.5%
rutile	0.7%	0.5%	0.6%	0.2%
smithsonite	< 0.05%	-	-	0.1%
sphalerite	0.1%	< 0.05%	1.3%	1.4%
tetraedrite	< 0.05%	-	0.1%	-
unclassified	0.4%	0.6%	0.9%	0.1%
zircon	0.1%	< 0.05%	-	-
TOC	<b>14.4%</b>	<b>14.4%</b>	<b>&lt; 0.05%</b>	<b>&lt; 0.05%</b>

**Table C.2:** Mineral distribution of (bio)leaching residues from Rudna and Lubin concentrates.

Mineral [wt.%]	Rudna concentrate		Lubin concentrate		
			LC15a		LCA06
	sterile control residues	bioleaching residues	sterile control residues	bioleaching residues	bioleaching residues
albite	1.4%	1.9%	0.9%	0.7%	1.7%
anorthite	0.1%	0.1%	< 0.05%	0.1%	0.2%
anglesite	2.9%	4.6%	2.9%	3.5%	4.2%
anhydrite	7.4%	4.3%	2.5%	3.2%	0.8%
ankerite	< 0.05%	-	-	-	-
bornite	2.6%	-	2.2%	-	0.6%
barite	-	-	< 0.05%	-	< 0.05%
biotite	-	-	1.6%	8.4%	5.4%
calcite	0.2%	0.1%	0.1%	4.0%	0.1%
chalcopyrite	1.7%	0.3%	7.8%	6.7%	1.3%
cerussite	0.2%	0.1%	-	-	-
clay	< 0.05%	< 0.05%	< 0.05%	< 0.05%	< 0.05%
celestite	0.1%	-	-	< 0.05%	-
cobaltite	< 0.05%	-	0.1%	-	-
cobaltite (Cu-Ni)	-	-	0.5%	-	< 0.05%
chalcocite	2.6%	0.6%	0.4%	< 0.05%	0.3%
covellite	1.9%	< 0.05%	1.5%	0.1%	0.6%
dolomite	-	-	-	< 0.05%	< 0.05%
fahlore	-	-	< 0.05%	-	-
Fe-illite	-	-	< 0.05%	0.5%	0.4%
Fe-Cu sulphate	0.3%	< 0.05%	0.6%	0.3%	0.3%
galena	4.8%	5.3%	2.8%	1.8%	3.3%
gypsum	5.8%	5.6%	4.1%	0.4%	0.3%
iron hydroxide	< 0.05%	0.1%	< 0.05%	0.1%	0.3%
iron oxide	-	-	-	0.1%	< 0.05%
idaite	1.1%	< 0.05%	1.7%	0.1%	0.3%
illite	29.5%	37.6%	31.3%	34.3%	28.7%
jarosite	0.6%	0.1%	0.7%	0.8%	2.1%
K-feldspar	10.9%	12.1%	1< 0.05%	8.4%	17.0%
kaolinite	< 0.05%	< 0.05%	0.3%	0.3%	0.1%
muscovite	-	< 0.05%	0.1%	0.4%	0.1%
plagioclase	0.1%	< 0.05%	-	-	< 0.05%
pyrite	1.2%	1.1%	9.1%	2.6%	4.9%
quartz	12.6%	13.7%	9.2%	13.4%	13.1%
rutile	0.2%	0.1%	0.1%	0.1%	0.1%
smithsonite	-	< 0.05%	< 0.05%	< 0.05%	< 0.05%
sphalerite	0.1%	0.5%	1.3%	0.2%	0.2%
tetraedrite	-	-	0.5%	0.1%	0.1%
unclassified	0.3%	0.7%	0.1%	0.5%	3.2%
zircon	-	-	-	< 0.05%	< 0.05%

Mineral [wt.%]	Rudna concentrate		Lubin concentrate		
			LC15a		LCA06
	sterile control residues	bioleaching residues	sterile control residues	bioleaching residues	bioleaching residues
TOC	11.2%	11.2%	8.9%	8.9%	10.3%

**Table C.3:** Mineral distribution of bioleaching residues from Lubin concentrate LC15b taken after increasing retention time.

Mineral [wt.%]	concentrate LC15b				
	Day1	Day2	Day4	Day7	Day10
albite	0.7%	1.3%	1.0%	1.2%	1.4%
anorthite	< 0.05%	-	< 0.05%	0.1%	< 0.05%
anglesite	2.4%	2.2%	2.5%	3.8%	3.5%
anhydrite	14.4%	16.5%	5.3%	5.1%	8.3%
ankerite	-	-	-	< 0.05%	-
bornite	2.2%	1.0%	0.2%	< 0.05%	-
barite	< 0.05%	< 0.05%	0.1%	< 0.05%	-
biotite	-	-	< 0.05%	-	-
calcite	< 0.05%	< 0.05%	< 0.05%	0.1%	< 0.05%
chalcopyrite	14.1%	11.1%	7.4%	6.3%	6.8%
cerussite	0.1%	0.1%	0.5%	0.2%	-
clay	0.1%	< 0.05%	< 0.05%	-	-
cobaltite	< 0.05%	-	-	< 0.05%	-
cobaltite (Cu-Ni)	0.1%	< 0.05%	< 0.05%	-	-
chalcocite	0.4%	0.5%	0.5%	0.4%	< 0.05%
covellite	1.3%	0.7%	0.6%	0.2%	< 0.05%
fahlore	0.1%	0.1%	-	-	-
Fe-illite	< 0.05%	-	< 0.05%	0.1%	-
Fe-Cu sulphate	0.3%	0.3%	0.4%	0.3%	0.2%
galena	0.5%	1.2%	2.0%	2.0%	2.2%
gypsum	3.0%	2.9%	5.0%	5.9%	6.9%
iron hydroxide	0.1%	0.2%	0.2%	0.3%	0.1%
idaite	1.3%	1.3%	1.6%	0.5%	0.2%
illite	31.3%	28.4%	43.0%	45.9%	48.0%
jarosite	0.4%	0.7%	0.1%	< 0.05%	< 0.05%
K-feldspar	6.3%	10.8%	9.2%	9.9%	10.6%
kaolinite	0.3%	0.3%	0.1%	0.2%	0.4%
muscovite	< 0.05%	-	< 0.05%	< 0.05%	-
plagioclase	0.1%	-	< 0.05%	0.1%	< 0.05%
pyrite	7.0%	5.3%	2.5%	1.1%	0.7%
quartz	11.2%	13.1%	15.9%	14.3%	9.1%
rutile	0.2%	0.1%	0.2%	0.5%	0.3%
smithsonite	< 0.05%	< 0.05%	< 0.05%	0.1%	0.1%

Mineral [wt.%]	concentrate LC15b				
	Day1	Day2	Day4	Day7	Day10
sphalerite	0.9%	1.2%	0.9%	0.7%	0.5%
tetraedrite	0.3%	0.3%	0.1%	0.1%	-
unclassified	1.1%	0.3%	0.5%	0.4%	0.4%
zircon	-	-	< 0.05%	-	-

**Table C.4:** Geochemical data of leaching residues from Sangerhausen black shale and concentrate.

Analyte	Method	Unit	LOR	Sangerhausen			
				black shale		concentrate	
				bioleaching residues	sterile control residues	bioleaching residues	sterile control residues
Ag	ME-MS41	ppm	0.1	74.7	72.8	>100	>100
Ag	Ag-OG46	ppm	1			543	474
Al	ME-MS41	%	0.01	0.51	0.52	0.52	0.46
As	ME-MS41	ppm	0.1	116	377	250	349
Au	ME-MS41	ppm	0.02	<0.02	<0.02	<0.02	<0.02
B	ME-MS41	ppm	10	10	10	10	<10
Ba	ME-MS41	ppm	10	40	20	20	10
Be	ME-MS41	ppm	0.05	1.05	1.02	0.84	0.84
Bi	ME-MS41	ppm	0.01	2.53	2.37	9.02	7.91
Ca	ME-MS41	%	0.01	2.02	1.68	1.28	1.18
Cd	ME-MS41	ppm	0.01	0.34	1.49	25.9	32.7
Ce	ME-MS41	ppm	0.02	21	18.3	19.5	15.05
Co	ME-MS41	ppm	0.1	135	258	206	435
Cr	ME-MS41	ppm	1	28	31	27	25
Cs	ME-MS41	ppm	0.05	5.7	5.29	5.35	4.84
Cu	ME-MS41	ppm	0.2	1790	1560	>10000	>10000
Cu	Cu-OG46	%	0.001			2.14	7.1
Fe	ME-MS41	%	0.01	0.54	1.72	2.67	4.67
Ga	ME-MS41	ppm	0.05	2.09	2.33	2.28	2.2
Ge	ME-MS41	ppm	0.05	0.2	0.23	0.59	0.67
Hf	ME-MS41	ppm	0.02	0.52	0.58	0.54	0.65
Hg	ME-MS41	ppm	0.01	1.65	1.58	5.69	4.96
In	ME-MS41	ppm	0.005	0.028	0.048	0.122	0.132
K	ME-MS41	%	0.01	0.23	0.22	0.26	0.22
La	ME-MS41	ppm	0.2	6.7	5.5	5.4	4.4
Li	ME-MS41	ppm	0.1	10.4	10.8	10.4	8.8
Mg	ME-MS41	%	0.01	0.12	0.14	0.13	0.1
Mn	ME-MS41	ppm	5	29	87	35	99
Mo	ME-MS41	ppm	0.05	163	329	548	667
Na	ME-MS41	%	0.01	0.02	0.02	0.02	0.02

Analyte	Method	Unit	LOR	Sangerhausen			
				black shale		concentrate	
				bioleaching residues	sterile control residues	bioleaching residues	sterile control residues
<b>Nb</b>	ME-MS41	ppm	0.05	0.45	0.41	0.44	0.45
<b>Ni</b>	ME-MS41	ppm	0.2	70.8	80.8	93.4	111
<b>P</b>	ME-MS41	ppm	10	300	1190	400	270
<b>Pb</b>	ME-MS41	ppm	0.2	>10000	>10000	>10000	>10000
<b>Pb</b>	Pb-OG46	%	0.001	1.325	1.28	8.84	7.45
<b>Rb</b>	ME-MS41	ppm	0.1	18.4	16.9	17.9	16.1
<b>Re</b>	ME-MS41	ppm	0.001	3.58	3.36	5.16	4.34
<b>S</b>	ME-MS41	%	0.01	2.55	4.22	5.7	>10.0
<b>Sb</b>	ME-MS41	ppm	0.05	34.4	37.6	456	445
<b>Sc</b>	ME-MS41	ppm	0.1	1.5	3.3	1.6	1.6
<b>Se</b>	ME-MS41	ppm	0.2	48.6	64	194	230
<b>Sn</b>	ME-MS41	ppm	0.2	1.3	1.4	3.7	3.4
<b>Sr</b>	ME-MS41	ppm	0.2	304	228	186	122.5
<b>Ta</b>	ME-MS41	ppm	0.01	<0.01	<0.01	<0.01	<0.01
<b>Te</b>	ME-MS41	ppm	0.01	0.05	0.1	0.11	0.13
<b>Th</b>	ME-MS41	ppm	0.2	3.8	5.3	4.1	4.2
<b>Ti</b>	ME-MS41	%	0.005	0.008	0.008	0.007	0.007
<b>Tl</b>	ME-MS41	ppm	0.02	2.55	3.83	3.96	4.06
<b>U</b>	ME-MS41	ppm	0.05	52.6	80.9	56.4	74.1
<b>V</b>	ME-MS41	ppm	1	287	281	348	295
<b>W</b>	ME-MS41	ppm	0.05	0.66	0.79	17.7	16.5
<b>Y</b>	ME-MS41	ppm	0.05	5.97	7.22	5.53	5.93
<b>Zn</b>	ME-MS41	ppm	2	128	380	5340	7030
<b>Zr</b>	ME-MS41	ppm	0.5	24.4	25.7	24	26.7

**Table C.5:** Geochemical data of leaching residues from Rudna concentrate and Lubin concentrate LC15a.

Analyte	Method	Unit	LOR	Rudna		Lubin	
				concentrate		concentrate LC15a	
				bioleaching residues	sterile control residues	bioleaching residues	sterile control residues
<b>Ag</b>	ME-MS41	ppm	0.1	>100	>100	>100	>100
<b>Ag</b>	Ag-OG46	ppm	1	631	595	902	695
<b>Al</b>	ME-MS41	%	0.01	0.42	0.39	0.35	0.31
<b>As</b>	ME-MS41	ppm	0.1	66	219	961	3820
<b>Au</b>	ME-MS41	ppm	0.02	<0.02	<0.02	<0.02	<0.02
<b>B</b>	ME-MS41	ppm	10	10	10	10	10
<b>Ba</b>	ME-MS41	ppm	10	40	30	40	20

Analyte	Method	Unit	LOR	Rudna		Lubin	
				concentrate		concentrate LC15a	
				bioleaching residues	sterile control residues	bioleaching residues	sterile control residues
Be	ME-MS41	ppm	0.05	0.59	0.53	0.62	0.57
Bi	ME-MS41	ppm	0.01	0.68	0.58	9.19	6.73
Ca	ME-MS41	%	0.01	8.05	7.15	4.05	3.85
Cd	ME-MS41	ppm	0.01	2.11	2.06	24.1	44.7
Ce	ME-MS41	ppm	0.02	24.4	20.2	13.7	11.6
Co	ME-MS41	ppm	0.1	36.1	182.5	78.9	1060
Cr	ME-MS41	ppm	1	98	20	54	20
Cs	ME-MS41	ppm	0.05	15.3	13.2	10.1	7.64
Cu	ME-MS41	ppm	0.2	2820	>10000	>10000	>10000
Cu	Cu-OG46	%	0.001		6.12	2.06	6.39
Fe	ME-MS41	%	0.01	0.38	1.31	2.8	7.03
Ga	ME-MS41	ppm	0.05	1.97	1.94	2.08	2.25
Ge	ME-MS41	ppm	0.05	0.2	0.21	0.22	0.26
Hf	ME-MS41	ppm	0.02	0.31	0.32	0.28	0.32
Hg	ME-MS41	ppm	0.01	22.8	18.25	18.55	16.1
In	ME-MS41	ppm	0.005	0.036	0.041	0.099	0.141
K	ME-MS41	%	0.01	0.25	0.23	0.28	0.19
La	ME-MS41	ppm	0.2	9	7.6	5.6	4.8
Li	ME-MS41	ppm	0.1	10.4	8.8	7.2	6.2
Mg	ME-MS41	%	0.01	0.1	0.09	0.09	0.1
Mn	ME-MS41	ppm	5	26	40	39	187
Mo	ME-MS41	ppm	0.05	218	346	258	330
Na	ME-MS41	%	0.01	0.02	0.02	0.03	0.02
Nb	ME-MS41	ppm	0.05	0.4	0.3	0.33	0.27
Ni	ME-MS41	ppm	0.2	127	104.5	104.5	291
P	ME-MS41	ppm	10	140	100	250	130
Pb	ME-MS41	ppm	0.2	>10000	>10000	>10000	>10000
Pb	Pb-OG46	%	0.001	8.26	7.33	6.8	5.75
Rb	ME-MS41	ppm	0.1	21.8	19	18.1	14.2
Re	ME-MS41	ppm	0.001	1.23	1.05	5.83	4.5
S	ME-MS41	%	0.01	9.91	>10.0	8.75	>10.0
Sb	ME-MS41	ppm	0.05	1.35	1.53	73.9	69.3
Sc	ME-MS41	ppm	0.1	1.7	1	1.3	1.1
Se	ME-MS41	ppm	0.2	43.1	64	49.2	60.1
Sn	ME-MS41	ppm	0.2	1.2	1	3.5	2.8
Sr	ME-MS41	ppm	0.2	164	139.5	77.6	62.4
Ta	ME-MS41	ppm	0.01	<0.01	<0.01	<0.01	<0.01
Te	ME-MS41	ppm	0.01	0.04	0.07	0.13	0.12
Th	ME-MS41	ppm	0.2	2.9	2.5	3.1	2.8
Ti	ME-MS41	%	0.005	0.008	0.008	0.007	0.007

Analyte	Method	Unit	LOR	Rudna		Lubin	
				concentrate		concentrate LC15a	
				bioleaching residues	sterile control residues	bioleaching residues	sterile control residues
<b>Tl</b>	ME-MS41	ppm	0.02	0.46	0.92	3.84	2.77
<b>U</b>	ME-MS41	ppm	0.05	4.72	4.19	4.82	5.17
<b>V</b>	ME-MS41	ppm	1	190	181	142	119
<b>W</b>	ME-MS41	ppm	0.05	1.04	0.88	1.06	0.9
<b>Y</b>	ME-MS41	ppm	0.05	3.55	3.2	2.38	2.08
<b>Zn</b>	ME-MS41	ppm	2	497	516	3960	8670
<b>Zr</b>	ME-MS41	ppm	0.5	9.9	9.7	9.7	10.3

**Table C.6:** Geochemical data of leaching residues from Lubin concentrate LC15b.

Method	Analyte	Unit	LOR	bioleaching residues LC15b				
				day 1	day 2	day 4	day 7	day 10
ME-XRF15c	<b>SiO2</b>	%	0.01	20.9	23.6	27.4	28.3	28.8
ME-MS41	<b>Ag</b>	ppm	0.1	>100	>100	>100	>100	>100
Ag-OG46	<b>Ag</b>	ppm	1	721	799	876	914	922
ME-MS41	<b>Al</b>	%	0.01	0.32	0.34	0.34	0.37	0.34
ME-MS41	<b>As</b>	ppm	0.1	3820	2470	820	628	586
ME-MS41	<b>Au</b>	ppm	0.02	<0.02	<0.02	<0.02	<0.02	<0.02
ME-MS41	<b>B</b>	ppm	10	10	10	20	20	10
ME-MS41	<b>Ba</b>	ppm	10	30	30	30	40	40
ME-XRF15c	<b>Ba</b>	%	0.01	<0.01	<0.01	0.03	0.03	0.03
ME-MS41	<b>Be</b>	ppm	0.05	0.63	0.56	0.49	0.53	0.49
ME-MS41	<b>Bi</b>	ppm	0.01	6.79	6.05	6.57	6.93	7.21
ME-MS41	<b>Ca</b>	%	0.01	3.41	3.81	4.11	4.38	4.39
ME-MS41	<b>Cd</b>	ppm	0.01	53.8	48.4	33.3	26.6	25.1
ME-MS41	<b>Ce</b>	ppm	0.02	11.35	12.60	14.45	15.10	15.50
ME-MS41	<b>Co</b>	ppm	0.1	1025	689	105.0	72.3	60.9
ME-MS41	<b>Cr</b>	ppm	1	13	14	14	17	23
ME-MS41	<b>Cs</b>	ppm	0.05	5.80	6.06	6.38	6.50	6.11
ME-MS41	<b>Cu</b>	ppm	0.2	>10000	>10000	>10000	>10000	>10000
ME-XRF15c	<b>Cu</b>	%	0.01	8.83	5.67	4.11	3.04	2.84
Cu-OG46	<b>Cu</b>	%	0.001	8.99	5.47	3.87	2.95	2.69
ME-MS41	<b>Fe</b>	%	0.01	7.83	6.46	3.69	2.80	2.45
ME-MS41	<b>Ga</b>	ppm	0.05	2.51	2.54	2.03	2.00	1.81
ME-MS41	<b>Ge</b>	ppm	0.05	0.40	0.40	0.22	0.21	0.20
ME-MS41	<b>Hf</b>	ppm	0.02	0.29	0.27	0.26	0.25	0.25
ME-MS41	<b>Hg</b>	ppm	0.01	18.95	17.65	19.25	21.0	18.95
ME-MS41	<b>In</b>	ppm	0.005	0.207	0.150	0.117	0.101	0.093

Method	Analyte	Unit	LOR	bioleaching residues LC15b				
				day 1	day 2	day 4	day 7	day 10
ME-MS41	<b>K</b>	%	0.01	0.20	0.21	0.22	0.23	0.22
ME-MS41	<b>La</b>	ppm	0.2	4.6	5.0	5.7	6.1	6.3
ME-MS41	<b>Li</b>	ppm	0.1	5.6	5.8	5.1	5.6	5.1
ME-MS41	<b>Mg</b>	%	0.01	0.08	0.08	0.08	0.08	0.07
ME-MS41	<b>Mn</b>	ppm	5	157	152	66	36	24
ME-MS41	<b>Mo</b>	ppm	0.05	239	227	159.0	159.0	143.0
ME-MS41	<b>Na</b>	%	0.01	0.02	0.02	0.02	0.02	0.02
ME-MS41	<b>Nb</b>	ppm	0.05	0.27	0.31	0.30	0.30	0.31
ME-MS41	<b>Ni</b>	ppm	0.2	269	211	104.0	102.0	103.5
ME-MS41	<b>P</b>	ppm	10	110	170	190	220	180
ME-MS41	<b>Pb</b>	ppm	0.2	>10000	>10000	>10000	>10000	>10000
ME-XRF15c	<b>Pb</b>	%	0.01	3.85	5.07	6.33	6.65	6.75
Pb-OG46	<b>Pb</b>	%	0.001	5.07	5.54	6.08	6.44	6.52
ME-MS41	<b>Rb</b>	ppm	0.1	14.0	14.8	15.1	15.9	14.8
ME-MS41	<b>Re</b>	ppm	0.001	4.81	5.27	5.82	6.45	6.14
ME-MS41	<b>S</b>	%	0.01	>10.0	>10.0	>10.0	9.36	8.60
ME-XRF15c	<b>S</b>	%	0.01	15.80	14.80	11.85	9.93	9.21
ME-MS41	<b>Sb</b>	ppm	0.05	72.5	64.6	66.7	68.5	70.3
ME-MS41	<b>Sc</b>	ppm	0.1	1.2	1.2	1.0	1.1	1.0
ME-MS41	<b>Se</b>	ppm	0.2	55.1	51.2	48.6	46.3	44.6
ME-MS41	<b>Sn</b>	ppm	0.2	5.8	6.5	3.1	2.6	10.5
ME-MS41	<b>Sr</b>	ppm	0.2	64.2	70.6	76.8	82.0	82.5
ME-MS41	<b>Ta</b>	ppm	0.01	<0.01	<0.01	<0.01	<0.01	<0.01
ME-MS41	<b>Te</b>	ppm	0.01	0.13	0.09	0.08	0.09	0.08
ME-MS41	<b>Th</b>	ppm	0.2	2.9	3.1	3.6	3.8	3.6
ME-MS41	<b>Ti</b>	%	0.005	0.006	0.006	0.006	0.007	0.006
ME-MS41	<b>Tl</b>	ppm	0.02	2.46	2.14	0.96	0.85	0.80
ME-MS41	<b>U</b>	ppm	0.05	4.64	4.79	4.93	5.08	4.53
ME-MS41	<b>V</b>	ppm	1	116	125	127	137	133
ME-MS41	<b>W</b>	ppm	0.05	0.78	0.42	0.26	0.40	0.71
ME-MS41	<b>Y</b>	ppm	0.05	2.14	2.23	2.30	2.30	2.36
ME-MS41	<b>Zn</b>	ppm	2	>10000	9210	5700	4310	3760
ME-XRF15c	<b>Zn</b>	%	0.01	1.07	1.00	0.61	0.44	0.40
Zn-OG46	<b>Zn</b>	%	0.001	1.110	0.981			
ME-MS41	<b>Zr</b>	ppm	0.5	9.2	9.2	9.1	8.8	8.8

**Table C.6:** Geochemical data of leaching residues from Lubin concentrate LCA06.

Analyte	Unit	LOR	bioleaching residues LCA06
Al <sub>2</sub> O <sub>3</sub>	%	0.2	10.0
CaO	%	0.1	5.9
Fe <sub>2</sub> O <sub>3</sub>	%	0.05	5.72
K <sub>2</sub> O	%	0.05	2.79
MgO	%	0.2	1.0
MnO	%	0.02	< LQ
Na <sub>2</sub> O	%	0.2	< LQ
P <sub>2</sub> O <sub>5</sub>	%	0.05	0.33
SiO <sub>2</sub>	%	0.2	29.4
TiO <sub>2</sub>	%	0.05	0.45
Ag	ppm	0.2	1131
As	ppm	20	1452
B	ppm	10	218
Ba	ppm	10	286
Be	ppm	2	3
Bi	ppm	10	< LQ
Cd	ppm	2	23
Ce	ppm	10	46
Cl-	%	0.01	0.05
Co	ppm	5	168
Cr	ppm	10	169
Cu	ppm	5	12902
La	ppm	20	26
Li	ppm	10	53
Mo	ppm	5	382
Nb	ppm	20	< LQ
Ni	ppm	10	355
Pb	ppm	10	42046
S	%	0.1	1.8
SO <sub>4</sub>	%	%	15.5
Sb	ppm	10	79
Sn	ppm	10	10
So	%	0.05	1.6
Sr	ppm	5	131
St	%	0.01	8.6
V	ppm	10	760
W	ppm	10	< LQ
Y	ppm	20	< LQ
Zn	ppm	5	2600
Zr	ppm	20	86

## Appendix D – DIGITAL

Granulometric data

MLA-data comminution products

(bornite, chalcocite and chalcopyrite)

I declare that this thesis is my own work entirely and has been written without any help from other people. I used only the sources mentioned and included all the citations correctly both in word or content. All direct or indirect sources used are acknowledged as references.

Andreas Kamradt

## Lebenslauf

- 05/2018 – 12/2019      wissenschaftlicher Mitarbeiter/Haushalt
- 02/2018 – 04/2018      wissenschaftlicher Mitarbeiter/Drittmittel  
„Wirtschaftliche Gewinnung Seltener Erden aus monazithaltigem Sekundärrohstoff der Großregion Catalão, Brasilien“ innerhalb des BMBF-Förderprogramms „Client II - Internationale Partnerschaften für nachhaltige Innovationen“
- 02/2014 – 09/2017      wissenschaftlicher Mitarbeiter/Drittmittel  
Verbundprojekt “Innovative eco-efficient biohydrometallurgy process for the recovery of strategic and rare metals: primary and secondary resources, EcoMetals – Teilprojekt: Mineralogisch-geochemische Charakterisierung von Primärerzen und Prozessprodukten”, deutsch-französische Kooperation anlässlich des 50. Jahrestages des Élysée-Vertrages im Rahmen des BMBF-Programm "Wirtschaftsstrategische Rohstoffe für den Hightech-Standort Deutschland"
- 12/2012 – 01/2014      wissenschaftlicher Mitarbeiter/Drittmittel  
„Mineralogisch-petrologische Begleitforschung zur Entwicklung eines Prallzerkleinerers für primäre und sekundäre mineralische Rohstoffe“
- 10/2009 – 11/2012      wissenschaftlicher Mitarbeiter & Projektkoordinations-  
assistent/Drittmittel  
Verbundprojekt „Gewinnung von Metallen und mineralischen Produkten aus deponierten Reststoffen der ehemaligen Montanindustrie im Mansfelder Gebiet“, BMBF-Förderschwerpunkt r2 „Innovative Technologien für Ressourceneffizienz – rohstoffintensive Produktionsprozesse“
- 09/2008                      Diplom in Geologie/Paläontologie